Reassessment of the freshwater chondrichthyans from the Permian of France : systematics and palaeoecology

Vincent Luccisano

THESE de DOCTORAT DE
L'UNIVERSITE CLAUDE BERNARD LYON 1

Ecole Doctorale N° 341
Évolution, Écosystème, Microbiologie, Modélisation (E2M2)

Discipline : Paléontologie

Soutenue publiquement le 21/11/2022, par :
Vincent Luccisano

Révision des chondrichtyens d'eau douce du Permien français : systématique et paléoécologie

---

Devant le jury composé de:

Bourquin, Sylvie	DR CNRS Université de Rennes 1	Rapporteure
Hampe, Oliver	PD Dr Museum für Naturkunde Berlin	Rapporteur
Debiais-Thibaud, Mélanie	MCF Université de Montpellier	Examinatrice
Derycke, Claire	MCF Université de Lille	Examinatrice
Viriot, Laurent	PU Université Claude Bernard Lyon 1	Président du jury
Cuny, Gilles	PU Université Claude Bernard Lyon 1	Directeur de thèse
Pradel, Alan	MCF Muséum National d'Histoire Naturelle	Invité
Amiot, Romain	CR CNRS Université Claude Bernard Lyon 1	Invité

"You're Gonna Need a Bigger Boat"

Steven Spielberg (Jaws, 1975)

Remerciements

Réaliser cette thèse m'a amené à rencontrer et interagir avec de nombreuses personnes qui doivent être toutes remerciées pour l'aide qu'elles m'ont fourni.

Je tiens en premier lieu à remercier mes encadrants de thèse Gilles Cuny, Romain Amiot et Alan Pradel pour m'avoir fait confiance, il y a trois ans, pour entreprendre ce projet de recherche. Je les remercie d'avoir supporté mon anglais médiocre qui, je l'espère, s'est amélioré grâce à eux.

À Gilles, je souhaite te remercier pour m'avoir introduit au monde fascinant des requins. Je te remercie pour ta présence sans limite qui m'a permis d'avancer au-delà de ce que j'aurai pu espérer durant cette thèse. Que ce soit professionnel ou personnel, je suis chanceux d'avoir bénéficié de tes conseils et de ton sarcasme à toute épreuve. Bien évidemment, une mention spéciale à tes corrections de manuscrits, dire qu'elles étaient rapides serait un euphémisme. Bien que vilaines, je garderai précieusement tes figurines de xénacanthes.

À Romain, merci de m'avoir introduit à la géochimie, domaine que je connaissais à peine pour ne pas dire très peu. Que ce soit pour la chimie des phosphates ou pour le fonctionnement d'un spectromètre de masse, tu m'as énormément appris. Merci pour ta bonne humeur constante et pour tes blagues et tes références de film douteux. Les pauses du midi ont été une vraie bouffée d'oxygène bien qu'on ait dépassé le rouge plus d'une fois.

À Alan, merci d'avoir été présent malgré la distance depuis Paris. Merci pour m'avoir fourni les scans de neurocrânes d'Autun qui ont, sans aucun doute, embelli cette thèse. Les visites des collections du MNHN ont été un super moment dont je garde un agréable souvenir. Merci également de m'avoir accompagné dans la chaleur de Valencia pour mon premier congrès chez les grands du Paléozoïque.

Je souhaite remercier particulièrement deux personnes sans qui cette thèse n'aurait pas pu se dérouler aussi bien.

À Dominique Chabard, jeune retraité de la direction du Musée d'Histoire Naturelle d'Autun, merci infiniment pour l'accueil toujours chaleureux dont tu as fait preuve à Autun. Merci pour la mise à disposition des spécimens de Muse, pour les aller-retours à Lyon et pour ta passion et tes connaissances sur la paléontologie de la Saône-et-Loire. Merci infiniment pour l'organisation des fouilles de Muse de l'été 2021, le dégagement préalable du site ou encore

pour la fabuleuse conception du chevalet en bois pour scanner l'encombrant holotype d'*Orthacanthus buxieri*.

À Jean-Marc Pouillon, président de l'association Rhinopolis, merci d'avoir mis à disposition l'imposante collection de Buxières-les-Mines. Merci pour les balades sur les chemins paléontologiques de l'Allier qui ont commencé par ce déménagement hors norme des collections à l'été 2019. Merci pour ta disponibilité et ta passion, j'espère que tu ne regrettes pas trop tous ces aiguillons sacrifiés à la géochimie. Merci pour ma première expérience de fouilles dans les schistes de Bert, elle a été dans la lignée de la relation amicale de ces trois dernières années.

De nombreuses personnes ont également fourni le matériel nécessaire à cette thèse. Je remercie Georges Gand et Gaël de Ploëg pour les trois spécimens de *Triodus aeduorum* qui constituent mon premier article de thèse et la fierté d'avoir nommé une espèce. Merci à Christophe Bouix pour la préparation de nombreux spécimens de Buxières. Un remerciement tout à fait spécial à René Kindlimann, collectionneur passionné de requins en tout genre pour son accueil plus que chaleureux en Suisse. Mon séjour à Aarthal a été un des meilleurs souvenirs de ma thèse aussi bien la visite de ta fabuleuse collection que du musée de dinosaures. Merci à toi et à Marita pour votre accueil. Merci également d'avoir céder le matériel *d'Orthacanthus* de Buxières en ta possession au Muséum de Zurich. C'est un plaisir d'avoir pu publier ensemble.

J'ai eu la chance d'avoir pu réaliser quelques fouilles durant ces trois années parsemées de confinements. En mai 2021, en plus de Jean-Marc, je tiens à remercier Jean-Sébastien Steyer et Antoine Logghe du CR2P pour cette semaine forte en rencontre dans les sites de l'Allier. J'espère vous rejoindre très vite pour de nouvelles aventures à Buxières et à Franchesse. En août 2021, en plus de Dominique, la réouverture du site de Muse a été possible grâce à une équipe de passionnés qui m'ont fait passer deux superbes semaines de fouilles. Merci à la Société d'Histoire Naturelle d'Autun à travers David et Françoise Beaudoin, Patrick Baudinaud, Estelle Chabard, Alexandre Margueron, Guy Barnay, Nathalie Pégon, Bernard Arnoult et Robert Pillon.

De nombreuses personnes de nombreux laboratoires ont été d'une aide précieuse. Au LGL-TPE, merci à Arnauld Vinçon-Laugier pour ton aide à trouver les objets le plus improbables pour aider aux manips du R5 et pour le constant réapprovisionnement en capsules d'argent. Merci à Céline Salaviale et Nicolas Rinder pour votre aide à segmenter des fossiles décidément bien plats. Merci à Ghislaine Broillet pour l'accès à la salle de microscopie et pour les essais au MEB. Merci à Emmanuel Robert pour l'accès aux collections fossiles. Merci à

Claire Duchet, Éric Benech et à Nadine Brochet du LEHNA pour toutes les procédures administratives. Au LEHNA, merci à François Fourel pour ton aide sur tellement d'analyses géochimiques différentes et particulièrement sur celles du soufre dont les nombreuses pesées me font encore souffrir. Pour la même raison, je remercie Jean Goedert du CR2P pour ces conseils sur ce système isotopique si particulier et pour m'avoir accompagné de si nombreuses fois devant le spectromètre. Au CR2P, je remercie Séverin Morel pour la réalisation des lames minces d'aiguillons de xénacanthes. De l'INSA de Lyon, je remercie Jérôme Adrien et Joël Lachambre pour la réalisation des scans de xénacanthes.

Je tiens à remercier l'équipe enseignante de l'OSU de Lyon, en particulier les enseignants de Géosciences 1 et Véronique Gardien pour m'avoir donné de merveilleuses heures de TP pétrologie métamorphique dont je suis évidemment devenu un expert. Dans un registre différent, je remercie mon stagiaire de Poitiers Sylvain Leite pour ma première expérience d'encadrement de stage.

Je tiens à remercier particulièrement Sylvie Bourquin (Géosciences Rennes) pour m'avoir invité à présenter mes résultats lors de l'AG de l'AGPT 2022 mais également Mathilde Mercuzot (Géosciences Rennes), Camille Dusseaux (Chrono-Environnement) et Aude Gebelin (CEREGE) pour les discussions à propos de la géologie de la chaîne varisque.

Je remercie Jacky Royet et l'association Musique aux Champs pour m'avoir donné l'occasion de donner ma première conférence grand public. Je remercie aussi les organisateurs du BARCamp de la BU Science Lyon 1 pour cette autre expérience de vulgarisation filmée et en ligne.

Je remercie les membres de mon comité de suivi de thèse Sylvain Adnet (ISEM), Jean-Sébastien Steyer (CR2P), Jérémy Martin (LGL-TPE) et Manolo Gouy (LBBE) pour leurs suivis et conseils.

Je remercie les membres de mon jury de thèse, Sylvie Bourquin (Géosciences Rennes) et Oliver Hampe (Museum für Naturkunde Berlin), mes deux rapporteurs qui ont accepté d'évaluer ce travail, ainsi que mes examinatrices et examinateur Mélanie Debiais-Thibaud (ISEM), Claire Derycke (EEP) et Laurent Viriot (IGFL).

Bien que certains pensent qu'un bon doctorant est un doctorant déprimé, je me dois de remercier les nombreuses personnes qui m'ont aidé à sortir la tête de mes fossiles et à rigoler un bon coup.

Je tiens à remercier les doctorants du LGL-TPE, Thomas le dieu-MJ, Nicolas le chevalier bourrin, Yohan la giga boule de feu, Mickaël le sorceleur bancal, Gwendal le médecin

capitaliste et Hugo le prêtre qui parle trop avec qui je me suis embarqué dans une très longue aventure de jeu de rôle. Je tiens à dire que la ressemblance avec mon avatar, un barde peureux aux longs cheveux et qui entend des voix, est nulle et non avenue. En tout cas, je COMPTE bien finir cette aventure faite de longues séances pleines de saucissons et de chips, à ne faire que des 1 pour retrouver une charrette.

Merci à la team du R5 pour ces moments de convivialité pleines de vacheries et de rires. Merci à mon colloc de bureau Thomas pour son premier degré si exaspérant, ces sublîmes références à Kaamelott et nos longues discussions sur le seigneur des anneaux et le witcher. Merci à Yohan croco-boy qui pleurera, j'en suis sûre, des larmes de crocodiles pour la disparition de mon accent du sud. Merci à Nicolas, parisien en détachement constant, pour son aide sur les chimies, je n'oublierai pas l'échantillon 4 la prochaine fois. Merci à Thibaud et Ségolène pour leur mauvaise foi inébranlable et à moitié assumée. Merci à Arnauld pour les blagues et les vidéos douteuses. Merci à Jeanne pour son calme à toute épreuve face à l'avalanche de stupidités dites dans la salle de pause qui n'en demandait pas tant. Compagnon du R1, je tiens à remercier Nicolas cocco-boy pour ce fou-rire légendaire à base de comptage de nanomètres.

Pour finir je tiens à remercier mes proches pour leurs soutiens sans faille aux vues de ma passion plus qu'encombrante pour les fossiles et autres cailloux. Merci à mes parents pour avoir toujours cru en moi et m'avoir permis d'arriver là où j'en suis. Je ne compte pas les allers-retours de déménagements à Marseille, Poitiers, Montpellier et Lyon pour me permettre de suivre les études qui m'ont toujours passionnées. Merci à ma grande sœur Amélie et à mon beau-frère Sébastien pour le squattage en bonne et due forme de votre canapé parisien. Merci à eux pour leur présence bien que lointaine et leurs conseils dans les moments de doute. Je (ne) remercie (pas) Nala le cocker boudeur pour ses réveils tout en délicatesse. J'ai de la chance de tous vous avoir.

Enfin, j'ai une pensée toute particulière pour Émilie qui partage ma vie depuis bientôt 10 ans. Le confinement a été la meilleure période de ma thèse car j'ai pu revenir vivre avec toi à Montpellier comme avant. Merci pour ton soutien et ton amour indéfectible, tu as fait de moi un homme meilleur, je n'en serai pas là sans toi.

Résumé étendu

Introduction

Les Xénacanthiformes

Les Xénacanthiformes sont un ordre de chondrichtyens paléozoïques présent du début du Carbonifère jusqu'au Trias supérieur. Ils forment un groupe cosmopolite dont les restes se retrouvent en Amérique du Nord et du Sud, en Inde, en Australie et en Europe. Ils ont été découverts dans ce continent au cours du 19ème siècle et c'est dans cette région qu'ils connaîtront leur maximum de diversité au cours du Carbonifère terminal et du Permien basal. Ces animaux qui semblaient disparaître au cours du Permien moyen passeront la crise du Permien/Trias et ne s'éteindront qu'au Trias supérieur peu avant la crise du Trias/Jurassique.

Les xénacanthes sont morphologiquement caractérisés par un corps longiligne, évoquant une aiguille, à l'unique nageoire dorsale allongée et à la paire de nageoires anales unique chez les chondrichtyens. Leurs caractéristiques les plus diagnostiques et les plus abondamment trouvées dans le registre fossile sont leurs dents et aiguillons dorsaux. Le patron dentaire des xénacanthes est tricuspide avec deux cuspides latérales développées encadrant une cuspide médiane réduite. Leur aiguillon dorsale unique et non renouvelé au cours de la vie de l'animal est inséré superficiellement dans le derme à l'avant de la nageoire dorsale et tourné vers l'arrière. Ce dernier possède deux rangées de denticules et une faible ornementation. Les anatomies respectives des dents et aiguillons sont diagnostiques des deux familles actuellement établies. Les primitifs Diplodoselachidae possèdent des cuspides latérales compressées labio-lingualement, une cuspide médiane extrêmement réduite et un aiguillon de section circulaire où les denticules sont placés sur le bord ventral. Chez les Xenacanthidae, plus dérivés, les cuspides latérales sont de forme circulaire, la cuspide médiane est plus longue et l'aiguillon est compressé dorso-ventralement avec une rangée de denticule sur chaque bord latéral.

Une systématique et une écologie ambigües

De nombreuses questions portent sur l'histoire évolutive des xénacanthes ainsi que sur leur biologie. Tout d'abord leur systématique, initiée au cours du 19ème siècle a connu de nombreux changements et porte encore quelques interrogations. Par exemple, la validité du genre '*Expleuracanthus*' Heyler, 1969 qui est venu remplacer le genre historique '*Pleuracanthus*' préoccupé par un coléoptère. Cependant, ce remplacement nécessaire aux vues des contraintes du code international de nomenclature zoologique actuel est venu sans diagnose

précise ce qui limite sa définition et sa validité. Le '*Pleuracanthus*' étant en partie synonyme avec les genres *Xenacanthus* et *Triodus* (e.g. Ginter *et al.* 2010), l'emploi du terme '*Expleuracanthus*' est de ce fait problématique dans la systématique du groupe. Or, cette ambigüité empêche toute étude approfondie sur les relations de parenté et la paléobiogéographie de ce groupe.

Du point de vue de leur écologie, les xénacanthes ont été historiquement interprétés comme des marqueurs d'environnement d'eau douce du fait de leur apparente absence dans les sédiments marins. Cette interprétation a été récemment renforcée par des études géochimiques sur la composition isotopique de l'oxygène des phosphates de la bioapatite de leurs dents dans le registre européen et nord-américains. Dans les deux cas, les résultats montrent que les xénacanthes vivaient dans un environnement d'eau douce plus ou moins soumis à des événements d'assèchement. Cependant dans le même temps, des études portant sur l'histologie de leur aiguillon ont montré que leur schéma de croissance pourrait correspondance à des cycles tidaux liés au domaine marin. De plus, certaines localités ayant fournies des xénacanthes ont une sédimentologie qui laisserait penser à une potentielle influence marine.

Les bassins carbonifères et permiens du Massif central

Les problématiques précédemment évoquées se retrouvent chez les xénacanthes des bassins du Carbonifère et du Permien du nord du Massif central (France). Ils y sont connus depuis le 19ème siècle et ces bassins ont longtemps été interprétés comme d'anciens systèmes fluviatiles et lacustres d'eau douce intra-montagneux au sein de la chaîne hercynienne. De plus, les reconstitutions paléogéographiques de la région montrent des côtes à plusieurs centaines de kilomètres ce qui conforte l'éloignement au domaine marin. Mais, les récentes recherches paléontologiques dans cette région ont montré la présence de faunes extrêmement proches des autres bassins carbonifères et permiens européens ainsi que la présence de plusieurs taxa d'affinité marine ou pouvant supporter une large gamme de salinité. La ressemblance faunique pourrait être expliquée par des échanges via la Paléo-Téthys.

De ces bassins, deux ont livré une faune conséquente de xénacanthes : le bassin d'Autun (Saône-et-Loire) et le bassin de Bourbon-l'Archambault (Allier) tous deux datés du Permien basal. Parmi les différentes espèces décrites, certaines ont un caractère hautement ambigu. Dans le bassin d'Autun, la localité de Muse OSB présente une faune composée de '*Expleuracanthus*' *bonnardi* (initialement désigné comme '*Pygopterus*' *bonnardi*) et *Triodus* ?*frossardi* (initialement reporté en tant que '*Expleuracanthus*' *frossardi*). Ces deux espèces ont d'ailleurs été considérées comme synonyme. Cela démontre leur validité systématique comme étant

incertaine. De plus de nombreuses autres localités de ce bassin ont fourni les espèces de chondrichtyens *Bibractopiscis niger* (Symmoriiformes) et *Orthacanthus commailli* (Xenacanthiformes) sur la base de neurocrânes isolés. Leur préparation limitée et leur description succincte qui ne décrit qu'une infime partie de leur anatomie rendent leur attribution systématique ambigüe. Dans le bassin de Bourbon-l'Archambault, le xénacanthe *Orthacanthus buxieri* a été décrit dans la localité de Buxières-les-Mines. Là encore, sa préparation extrêmement limitée qui ne permet pas de visualiser les caractères diagnostiques questionne grandement la validité de cette espèce.

Objectifs de la thèse

En conséquence de ces questionnements, cette thèse a pour objectif de réviser la systématique et la paléoécologie des Xénacanthiformes, et plus globalement celles des chondrichtyens, du Permien inférieur des bassins d'Autun et de Bourbon-l'Archambault. À partir de la révision du matériel historique et de l'étude de nouveau matériel en partie par micro-tomographie à rayon X (µCT scan) et de la géochimie isotopique, les objectifs finaux sont de 1) fournir une liste faunique actualisée à la lumière des dernières données de la littérature et de 2) fournir une reconstitution paléoenvironnementale des sites de Muse OSB et de Buxières-les-Mines afin d'évaluer l'écologie des xénacanthes s'y trouvant.

Méthodes

La révision systématique a été effectuée selon plusieurs méthodes, en commençant par un inventaire et de nouvelles descriptions du matériel historique. Dans ce cas précis, certains spécimens, comme les neurocrânes isolés du bassin d'Autun, ne pouvaient être réétudiés aux vues de leur préparation. Cependant leur état de conservation dans des schistes bitumineux rendait impossible toute préparation mécanique supplémentaire sans risquer de les endommager. Pour pallier ce problème, il a été décidé d'utiliser le µCT scan afin de pouvoir avoir accès à l'ensemble de leur anatomie y compris les parties toujours incluses dans la roche. Afin de compléter ces nouvelles descriptions, de nombreux spécimens inédits ont également été pris en compte dans cette révision systématique. Dans leurs cas, certains ont pu être préparés mécaniquement et d'autres scannés au rayon X.

Afin de reconstituer l'environnement de vie et l'écologie des xénacanthes de Muse OSB et de Buxières-les-Mines une analyse multi-isotopique a été réalisée sur les aiguillons et sur les tissus minéralisés de la faune de vertébrés associés (aiguillons d'acanthodiens, écailles

d'actinoptérygiens et os de temnospondyles). Les aiguillons ont été privilégiés car leur croissance incrémentale continue sans remplacement permet de tracer l'évolution de la composition isotopique de la bioapatite (constituant majeur des tissus analysés) le long de la vie des individus. Les analyses ont porté sur les systèmes isotopiques suivants : l'oxygène des phosphates ($\delta^{18}O_p$) et des carbonates ($\delta^{18}O_c$), le carbone des carbonates ($\delta^{13}C_c$) et le soufre ($\delta^{34}S$) de la bioapatite des aiguillons. Ces systèmes isotopiques ont été choisi car ils constituent de bons marqueurs pour différencier les environnements d'eau douce et marins ($\delta^{18}O_p$ et $\delta^{34}S$) et pour tracer les milieux de nourrissage et les relations trophiques ($\delta^{13}C_c$).

Résultats

Révision systématique

Article 1 : Triodus *de Muse*

Trois squelettes partiels et inédits de xénacanthiformes du site de Muse OSB dans le bassin d'Autun ont été décrits. Leurs descriptions concluent à la présence d'une nouvelle espèce du genre *Triodus*, *T. aeduorum* n. sp., à ce jour endémique du bassin d'Autun. Cette espèce est principalement caractérisée par une combinaison inédite de caractères dentaires. Cette nouvelle espèce permet de discuter la validité systématique de l'ambigüe espèce '*Expleuracanthus*' *frossardi* de Muse OSB. L'holotype de cette espèce est un aiguillon dorsal isolé introuvable dans les collections du Muséum National d'Histoire Naturelle de Paris (MNHN). Or la systématique basée sur les aiguillons isolés de xénacanthes peut être hasardeuse du fait de la potentielle présence de caractères homoplasiques. Un autre spécimen de Muse OSB, plus complet, a été rapproché de cette espèce sous le nom *Triodus* ?*frossardi* et donc '*E.*' *frossardi* a été considéré comme appartenant au genre *Triodus*. La nouvelle espèce décrite permet de réviser la systématique de *T.* ?*frossardi* et de réattribuer ce dernier en tant que *Triodus* sp. car aucune diagnose au niveau spécifique ne peut être proposée. En conséquence, '*E.*' *frossardi*, du fait que l'espèce *frossardi* n'existe pas et qu'aucune diagnose ne peut être établie sur la base de son matériel, est proposé comme étant un *nomen dubium* sans affinité claire avec le genre *Triodus*. Cette étude permet de discuter le modèle évolutif du genre *Triodus* en Europe. Tous les bassins où il est présent présentent une espèce ou des espèces endémiques donc ne se retrouvant jamais dans plusieurs bassins. Cela suppose un taux de spéciation élevé.

Article 2 : les neurocrânes isolés du bassin d'Autun

Les neurocrânes isolés qui forment le matériel type du symmoriiforme *Bibractopiscis niger* et du xénacanthe *Orthacanthus commailli* du Carbonifère terminal du bassin d'Autun ont été scannés par μCT scan et reconstruits en 3 dimensions. Cela a permis de décrire l'entièreté de leur anatomie externe. Malheureusement, l'extrême compression des spécimens n'a pas permis d'accéder à leur anatomie interne. Afin de compléter les comparaisons, un spécimen inédit du Permien basal de Buxières-les-Mines a aussi été scanné et reconstruit.

Ces cinq spécimens permettent de réviser la validité de ces deux espèces de chondrichtyens. L'holotype et un paratype de *B. niger* sont identifiés en tant que cf. *Triodus* sp. avec le spécimen de Buxières-les-Mines ; un paratype de *B. niger* est identifié en tant que 'Ctenacanthiformes' indet. ; et l'holotype de *O. commailli* est identifié en tant que ?Xenacanthimorpha. Bien que la nouvelle systématique proposée soit moins précise que l'ancienne, cela permet de clairement définir *B. niger* et *O. commailli* comme des espèces non valides et de constater une plus grande diversité de chondrichtyens dans le bassin d'Autun que pensée précédemment.

Cette étude permet également de mieux comprendre les différences de distribution des xénacanthiformes entre les bassins d'Autun et de Bourbon-l'Archambault avec un questionnement sur de possibles différences de chaînes trophiques entre ces bassins. Buxières-les-Mines et par extension le bassin de Bourbon-l'Archambault correspondraient à la chaîne trophique aquatique type de vertébrés des autres bassins carbonifères et permiens européens : les grands xénacanthes type *Orthacanthus* en tant que top prédateur, suivi de grands temnospondyles, puis les petits xénacanthes type *Triodus* et enfin les petits vertébrés comme les acanthodiens et les actinoptérygiens. Le bassin d'Autun, quant à lui, pourrait être dépourvu de grands xénacanthes ou leur présence serait anecdotique et limitée à des individus de petite taille (voir Article 3). La niche des superprédateurs serait alors occupée par trois groupes de taille identique : les petit xénacanthes aquatiques, les temnonpondyles semi-aquatiques et les sphénacodontidés terrestres.

Le matériel révisé a été inclus dans une analyse phylogénétique et une analyse de morphométrie géométrique qui ont permis de discuter l'évolution morphologique des neurocrânes des xénacanthiformes et de leurs plus proches taxons. La morphométrie géométrique montre une discrimination claire entre Xenacanthiformes et 'Ctenacanthiformes' et confirme le caractère intermédiaire de ?Xenacanthimorpha déjà supposé par sa morphologie. L'analyse phylogénétique qui inclut un large spectre de chondrichtyens confirme la forte affinité entre Xenacanthiformes et 'Ctenacanthiformes' mais place ?Xenacanthimorpha plus proche des xénacanthes. La combinaison de la description anatomique, de la phylogénie et de

la morphométrie géométrique permet de discuter la transition morphologique du neurocrâne entre Xenacanthiformes et 'Ctenacanthiformes' : elle prend place dans la région ethmo-orbitaire et affecte l'orientation des processus pré-orbitaires et la forme de la fontanelle précérébrale.

*Article 3 : le matériel dentaire d'*Orthacanthus *de Buxières-les-Mines*

Orthacanthus buxieri a été érigé sur la base d'un spécimen très mal préparé dont la description anatomique est peu convaincante pour justifier son statut d'espèce à part entière. De plus, de nombreux auteurs ont supposé une synonymie avec l'espèce *Orthacanthus kounoviensis* largement distribuée en Allemagne, République Tchèque et Royaume-Uni au Carbonifère supérieur sur la base de ressemblances dentaires. Or aucune étude ne s'est attardée sur l'anatomie détaillée des dents d'*Orthacanthus* de Buxières-les-Mines.

Le but de cette étude a été d'identifier les dents et aiguillons isolés présumément appartenant à *Orthacanthus* et de discuter la systématique, l'ontogénie et la paléobiogéographie de ce genre en Europe à la transition Carbonifère-Permien. Les résultats supportent pour la première fois la présence de l'espèce *Orthacanthus kounoviensis* dans le Permien inférieur français. De plus, la présence de dents se distribuant en deux groupes en fonction de leur taille mais ayant des morphologies extrêmement semblables supportent la présence d'*Orthacanthus kounoviensis* sous forme juvénile et adulte à Buxières-les-Mines. Les quelques différences morphologiques rentrant dans la variabilité ontogénétique étaient déjà connues chez d'autres espèces de xénacanthes. *Orthacanthus kounoviensis* de Buxières-les-Mines est donc le dernier représentant de ce genre et l'un des derniers grands xénacanthes en Europe au Permien inférieur. La présence de juvéniles et d'adultes fait de Buxières-les-Mines une zone refuge pour les grands xénacanthes au Permien inférieur dont la diversité a été grandement impactée par la fragmentation des grands systèmes lacustres interconnectés de la fin de Carbonifère dû à des mouvements tectoniques à l'échelle européenne.

La découverte d'une dent attribuée à *Orthacanthus* cf. *kounoviensis* dans le site de Muse OSB est inattendue. Elle est la première occurrence de ce genre dans le bassin d'Autun et à Muse OSB où seulement le petit *Triodus* a été trouvé. Cela constitue un premier argument paléontologique pour une connexion des bassins carbonifères et permiens du nord du Massif central comme il avait été déjà proposé d'un point de vue sédimentologique.

Reconstitutions paléoenvironnementales et révision paléoécologique

Article 4 : géochimie isotopique de la faune de vertébrés de Muse OSB et Buxières-les-Mines

Les principaux résultats sont des valeurs de $\delta^{34}S$ bien inférieures à celles des eaux océaniques du Permien inférieur pour Buxières-les-Mines et Muse OSB. Le $\delta^{18}O_p$ indiquent clairement un environnement d'eau douce pour Buxières-les-Mines. Pour Muse OSB, les valeurs de $\delta^{18}O_p$ sont plus ambigües et peuvent correspondre à plusieurs environnements : soit à de l'eau douce soumise à de l'évaporation, soit au domaine marin. La reconstitution des paléotempératures en utilisant le $\delta^{18}O$ de l'eau de plusieurs environnements aquatiques actuels montre des températures viables pour un modèle de lac d'eau douce tropical profond pour Buxières-les-Mines (par exemple le Lac Matano en Indonésie). Pour Muse OSB, ce sont les modèles actuels de lacs tropicaux peu profond (par exemple le Lac Punta Laguna au Mexique) aux lacs tropicaux sous forte évaporation (par exemple le Lac Tanganyika en Afrique central) qui correspondent le mieux au paléoenvironnement de ce site. Pour Muse OSB, le domaine marin indique aussi des températures viables. La combinaison du $\delta^{18}O_p$ et du $\delta^{34}S$ permet de trancher en faveur d'un environnement d'eau douce subissant des épisodes d'assèchement pour le site de Muse OSB. Ces données ne valident pas l'hypothèse d'une influence marine dans les bassins du Massif central au Carbonifère-Permien.

Les hautes valeurs de $\delta^{13}C_c$ correspondent à l'enrichissement en carbone 13 mesuré dans tous les réservoirs à la limite Carbonifère-Permien. De plus, la présence de ces sites au sein de la chaîne hercynienne indique une forte productivité primaire due aux nutriments issus de l'altération des massifs montagneux environnants. Le $\delta^{13}C_c$ indique également des valeurs anormalement basses pour l'*Orthacanthus* de Buxières-les-Mines. Ces valeurs sont en vérité intermédiaires entre celles du *Triodus* et du temnonpondyle ce qui indiquerait qu'*Orthacanthus* ne nourrissait à la fois d'animaux purement aquatiques (*Triodus*) et semi-aquatiques (temnospondyles).

Les valeurs de $\delta^{18}O_p$ le long des aiguillons de xénacanthes et d'acanthodiens varie très peu à Buxières-les-Mines ce qui implique qu'ils vivaient dans un environnement stable. À Muse OSB, le $\delta^{18}O_p$ des aiguillons varie plus et suggère ainsi un environnement changeant. L'augmentation des valeurs indique que les organismes sont passés dans un environnement plus enrichi en oxygène 18 mais sans variation du $\delta^{34}S$. Cela correspondrait donc à des périodes d'assèchement comme précédemment supposé. Cette information permet d'établir deux stratégies chez les xénacanthes. Le grand *Orthacanthus* est absent des environnements peu profonds et à besoin d'environnement ouvert de taille conséquente pour se développer. *A contrario*, le petit *Triodus* est plus adaptatif se retrouvant à la fois dans de grands lacs et dans

des lacs ou marais peu profonds et peu oxygénés. Cette différence expliquerait en partie la baisse de diversité observée chez les grands xénacanthes au Permien basal où les grands systèmes lacustres du Carbonifère disparaissent alors que le genre *Triodus* effectue une radiation adaptative sans doute liée à sa plus grande tolérance écologique. Ces données contredisent l'hypothèse d'un comportement migratoire entre les domaines dulçaquicoles et marins chez les xénacanthes permiens du Massif central.

Conclusion

Ce travail de thèse a permis de mieux comprendre la diversité et l'écologie des xénacanthes permiens du Massif central. De nombreuses espèces historiques ont été révisées et réattribuées ce qui permet une meilleure compréhension de la systématique des xénacanthes européens. L'écologie des xénacanthes de Muse OSB et de Buxières-les-Mines est clairement dulçaquicole et aucune influence marine n'a pu être identifiée dans ces deux bassins. La combinaison des deux axes développés dans cette thèse permet de mieux comprendre la distribution de ce groupe à la limite Carbonifère-Permien.

Mots-clés : Xenacanthiformes, Massif central, Permien, systématique, géochimie isotopique stable, paléoécologie, paléobiogéographie

Abstract

The Xenacanthiformes are a Palaeozoic chondrichthyan order mainly present from the late Carboniferous to the early Permian deposits of the intra-mountainous basins of the European Hercynian Mountain Belt. This order is characterised by a tumultuous systematic history, resulting in various dubious species. At the same time, their palaeoecology is also debated. Historically considered as freshwater organisms, the questions of potential saltwater tolerance and migration patterns into the marine setting have recently been raised.

These questions are significant in two Carboniferous-Permian basins from the French Northern Massif central. The Autun Basin with the Muse OSB locality and the Bourbon-l'Archambault Basin with the locality of Buxières-les-Mines are known since the 19th century to have provided a rich collection of xenacanthiform and chondrichthyan remains as well as associated vertebrate faunas. However, several historical species are highly questionable from a systematic point of view. The palaeoenvironment of these basins is also ambiguous. While they were considered as freshwater environments, mainly based on the presence of Xenacanthiformes, recent studies argued for potential connections with marine settings during the late Carboniferous and early Permian.

In the light of these questions on the systematics and palaeoecology of the Xenacanthiformes from the early Permian of the Northern Massif central, this Ph.D. thesis initiated their revision. A first objective was to revise the systematics of historical species as well as the descriptions of unpublished specimens. X-ray computed microtomography technology was used for imaging unprepared specimens. Consequently, some historical species were invalidated whereas new species, forms and occurrences of known species were described. Phylogenetic and geometric morphometric analyses allowed to propose new hypotheses on the relationships of Xenacanthiformes among the chondrichthyans.

In parallel, a stable isotope geochemical analysis using the oxygen, carbon and sulfur isotope compositions of the phosphates, sulfates and carbonates of the bioapatite of xenacanthiform dorsal spines, and teeth, scales and bones of associated acanthodians, actinopterygians and temnospondyls were carried out to assess their palaeoecology. The main result is a clear freshwater ecology for the Permian Xenacanthiformes of the Northern Massif central. Furthermore, depending on the investigated localities, I was able to discriminate different ecology: the diplodoselachid *Orthacanthus* and xenacanthid *Triodus* from Buxières-

les-Mines lived in a large and stable freshwater lake whereas the small xenacanthid *Triodus* from the Muse OSB was able to live in more variable environment and to endure drying up.

These results allowed to discuss the palaeobiogeography of the Xenacanthiformes in the Northern Massif central and in Europe at the Carboniferous-Permian transition. The large xenacanthiforms evolved and diversified in large freshwater environments during the late Carboniferous and went nearly extinct during the early Permian with the disappearance of these settings. A few of them survived in refuge areas like the large lake of Buxires-les-Mines. The small xenacanthiforms were more adaptative and could survive in large lakes to shallow swamps like in the Muse OSB. This adaptability explains their high diversity in both the late Carboniferous and early Permian.

Keywords: Xenacanthiformes, Northern Massif central, Permian, systematics, stable isotope geochemistry, palaeoecology, palaeobiogeography

Figure captions

Figure 1. Global anatomy of Xenacanthiformes. **A**, *Triodus sessilis*, a xenacanthid. **B**, *Lebachacanthus seckenbergianus*, a diplodoselachid. Drawings not to scale (modified from Heidtke 2003).

Figure 2. Xenacanthiformes neurocranium in dorsal (**A**) and ventral (**B**) views. Drawings not to scale (modified from Schaeffer 1981).

Figure 3. Xenacanthiformes dental pattern in labila (**A**), lateral (**B**), lingual (**C**), basal (**D**) and oral (**E**) views. Drawings not to scale (modified from Schneider 1996).

Figure 4. Xenacanthiformes dorsal spine in lateral (**A**) and ventral (**B**, **D**) views and in cross section (**C**). Drawings not to scale (modified from Soler-Gijón 1999).

Figure 5. Morphological differences between the families Xenacanthidae and Diplodoselachidae. Drawings not to scale (modified from Soler-Gijón 1999; Hampe 2003; Heidtke 2003; Ginter *et al.* 2010). **Figure 6.** Supposed phylogenetic relationships within the Xenacanthiformes (modified from Turner & Burrow 2011).

Figure 7. Bransonelliformes teeth. **A-B**, *Bransonella* tooth in labial (**A**) and lingual (**B**) view. **C-D**, *Barclabornia* tooth in labial (**C**) and lingual (**D**) view (modified from Hampe & Ivanov 2007). Scale bar = 0.2 mm.

Figure 8. Xenacanthiformes and their potential origins. **A**, *Orthacanthus* tooth., **B**, *Leonodus* tooth. **C**, *Antarctilamna* tooth. **D**, *Phoebodus* tooth. The teeth are in labial view (top) and lingual view (bottom) except *Leonodus* which is in lateral view (bottom). **E**, *Orthacanthus* neurocranium. **F**, *Tamiobatis* neurocranium. **G**, *Cladodoides* neurocranium. The neurocrania are in dorsal view and not to scale (drawings from Ginter *et al.* [2010] for the teeth and from Schaeffer [1981] for the neurocranium). Scale bar = 5 mm, except 3 mm for A.

Figure 9. Hypothetical position of Xenacanthiformes within the chondrichthyan relationships. **A**, total group elasmobranch hypothesis. **B**, stem-chondrichthyan hypothesis.

Figure 10. Palaeobiogeography of the Xenacanthiformes through their evolutionary history. Palaeo-maps are modified from DeepTimeMaps™ (Colorado Plateau Geosystems, Inc., 2020).

Figure 11. Palaeobiogeography of the European Xenacanthiformes from the Late Carboniferous (Pennsylvanian) to the early Permian (Cisuralian). See the figure 25 for the caption of the geological map (modified from Roscher & Schneider 2006).

Figure 12. Schematic X-ray computed microtomography experimental device (modified from Landis & Keane 2010).

Figure 13. Evolution of the descriptions and illustrations of *Cladodoides wildungensis*. **A**, Photograph of the holotype (Maisey 2005). **B**, Reproduction of the original drawing of Gross (1937) (Maisey 2005). **C**, CT scan slides of the braincase (Maisey 2001). **D**, 3D renderings of the braincase (Maisey 2005). For **A**, **B** and **D** the dorsal view is left and ventral view is right.

Figure 14. Simplified water cycle (modified from Sharp 2007).

Figure 15. $\delta^{18}O_p$ values of the dental bioapatite of modern and fossil aquatic vertebrates. Modern data are from Iacumin *et al.* (1996) and Vennemann *et al.* (2001) and fossil data are from (Kolodny & Luz 1991; Fricke *et al.* 1998; Lécuyer *et al.* 2003a; Amiot *et al.* 2010; Goedert *et al.* 2018).

Figure 16. Calvin cycle and the C3 carbon fixation in plants. **Abbreviations**: **ADP**, adenosine diphosphate; **ATP**, adenosine triphosphate; **BPGA**, 1,3 bisphosphoaglycerate; **GAP**, Glyceraldehyde 3-phosphate; **NADPH***, oxydised nicotinamide adenine dinucleotide phosphate; **NADP**+, reduced nicotinamide adenine dinucleotide phosphate; **PGA**, trisphosphoglycerate; **Pi**, Pyruvate kinase; **RbBP**, Ribulose 1,5 bisphosphate; **Ru5P**, Ribulo5phosphate.

Figure 17. $\delta^{13}C$ variation among primary aquatic producers. Data are from Simenstad & Wissmar (1985), Fry & Sherr (1989), Hemminga & Mateo (1996), Benner *et al.* (1997), Cerling & Harris (1999) and Rau *et al.* (2001) (modified from Clementz & Koch 2001).

Figure 18. Isotopic fractionation on hard and soft tissues between modern primary producers, primary and secondary consumers (modified from Angst 2014).

Figure 19. Variation of the $\delta^{13}C$ over the Phanerozoic. Data from Katz *et al.* (2005) are sediment carbonate and organic carbon and those of Korte *et al.* (2005) are brachiopod shell carbonate (modified from Berner 2006).

Figure 20. Bioapatite $\delta^{34}S$ in modern vertebrate and their environmental distribution. Data and figure are modified from Goedert *et al.* (2020).

Figure 21. Variation of the $\delta^{34}S$ of the seawater sulfates over the Phanerozoic (Data are from Kampschulte & Strauss [2004] and the figure is modified from Berner [2006]).

Figure 22. Global morphology and histology of a xenacanth dorsal spine (modified from Beck *et al.* 2016).

Figure 23. $\delta^{18}O_p$ and $\delta^{18}O_c$ correlation in modern and fossil bioapatite samples (fossil and modern data from (Kolodny & Luz 1991; Iacumin *et al.* 1996; Fricke *et al.* 1998; Vennemann *et al.* 2001; Lécuyer *et al.* 2003a; Amiot *et al.* 2010; Goedert *et al.* 2018).

Figure 24. Potential diagenetic processes on carbonates of fossil bioapatite.

Figure 25. Palaeogeographical context. **A**, Palaeogeography of the Pangea in the late Carboniferous (Pennsylvanian, 300 Ma). **B-C**, The Hercynian Mountain, European component of the Central Pangea Mountain at the Carboniferous-Permian transition and the location of the continental sedimentary basins. White outlines are the past location of France in **B**. Red stars are the location of the investigated Autun and Bourbon-l'Archambault basins. **Abbreviation**: **AU**, Autun Basin; **BLG**, Blanice Graben; **BCG**, Boskovice Graben; **BU**, Bourbon-l'Archambault Basin; **CA**, Carpathian Basin; **CR**, Carnic Alps; **DB**, Donetsk Basin; **DÖ**, Döhlen Basin; **EB**, Erzgebirge Basin; **EBL**, Elbe Lineament; **FL**, Flechting Block; **FRL**, Franconian Lineament; **FR**, Franconian Basin; **GBFZ**, Golf of Biscay Fracture Zone; **GGF**, Great Glen Fault; **GMFZ**, Gibraltar Minas Fracture Zone; **GP**, Guardia Pisano Basin; **GSH**, Grand Sillon Houllier Fracture Zone; **HRF**,

Hunsrück Fracture; **IF**, Ilfeld Basin; **IS**, Intra Sudetic Basin; **KP**, Krkonoše Piedmont Basin; **LC**, Lu Caparoni Basin; **LO**, Lodève Basin; **MO**, Montceau les Mines Basin; **NGVC**, North German Vulcanite Complex; **NS**, North Sudetic Basin; **PBF**, Pays de Bray Fracture; **PD**, Perdasdefogu Basin; **PU**, Puertollano Basin; **RGL**, Rhein Graben Lineament; **SB**, Saale Basin; **SNB**, Saar–Nahe Basin; **ST**, St. Etienne Basin; **SV**, Salvan-Dorénaz Basin; **TF**, Thuringian Forest Basin; **TTFZ**, Tornquist–Teysseyre Fracture Zone; **WCB**, Western and Central Bohemian Basins; **WEI**, Weissig Basin; **ZÖ**, Zöbingen (modified from Roscher & Schneider 2006).

Figure 26. Formation of the Pangea and of the Hercynian Mountains. **A**, early Ordovician; **B**, middle Ordovician; **C**, early Silurian; **D**, late Silurian; **E**, early Devonian; **F**, middle Devonian; **G**, late Devonian; **H**, early Carboniferous. **Abbreviations**: **AR**, Armorica; **B**, Bohemia; **F**, Franconia; **FL**, Florida; **IB**, Iberian Peninsula; **PA**, Palaeo-Adria **PT**; Palaeo-tethys; **RHO**, Rheno-Hercynian Ocean; **STO**, Saxo-Thuringian Ocean; **T**, Thuringia (modified from Franke *et al.* 2017).

Figure 27. Distribution of the ice caps in the southern Gondwana during the Late Palaeozoic Ice Age (modified from Montañez & Poulsen 2013).

Figure 28. Climate curve at the Carboniferous-Permian transition. **Abbreviations**: **DGC I–IV**, Deglaciation Cycle 1–4 of the Gondwana Icecap; **PM-T**, Pietermaritzburg Transgression; **PCE**, Permian Chert Event (modified from Roscher & Schneider 2006).

Figure 29. Assumed correlations between the international chronostratigraphical stages and the continental 'stages' at the Carboniferous-Permian transition in Western and Central Europe (modified from Bercovici 2009).

Figure 30. Geological context of the Autun Basin. **A**, Location of the Carboniferous-Permian basins of the Northern Massif central, France. **B**, simplified geological map of the Autun Basin. The red line is the transect for the Figure 31 (modified from Elsass Damon 1977; Marteau 1983; Châteauneuf *et al.* 1992; Gand *et al.* 2007, 2011, 2015, 2017; Pellenard *et al.* 2017; Mercuzot 2020).

Figure 31. North-South geological section of the Autun Basin (see the Figure 30 for the location of the transect) (modified from Marteau 1983; Pellenard *et al.* 2017; Mercuzot 2020).

Figure 32. Simplified stratigraphy of the Autun Basin. **Abbreviation**: **C.**, Curgy Formation (200 m); **Steph**, 'Stephanian' (modified from Pellenard *et al.* 2017).

Figure 33. Stratigraphical section of the Muse OSB fossiliferous locality. **Abbreviation**: **GI to VIII**, Tonstein ('*Gore'* in French) (modified from Pellenard *et al.* 2017).

Figure 34. Geological context of the Bourbon-l'Archambault Basin. **A**, Location of the Carboniferous-Permian basins of the Northern Massif central, France. **B**, simplified geological map of the Bourbon-l'Archambault Basin. The red line is the transect for the Figure 35 (modified from Marteau 1983; Steyer *et al.* 2000).

Figure 35. West-East geological section of the Bourbon-l'Archambautl Basin (see the Figure 34 for the location of the transect) (modified from Mathis & Brulhet 1990).

Figure 36. Stratigraphical section of the Bourbon-l'Archambault Basins. **Abbreviation**: **Bx**, Buxières; **Clu**, Clusor Formation; **Post A**, Post Asselian; **Sax**, Saxonian; **T**, Trias (modified from Debriette 1992; Steyer *et al.* 2000).

Figure 37. Evolution of the palaeoenvironment during the lower Permian in the Bourbon-l'Archambault Basin (modified from Mathis & Brulhet 1990).

Figure 38. Stratigraphical section of the Buxières-les-Mines fossiliferous locality (modified from Steyer *et al.* 2000).

Figure 39. Structuring of a lake water column (modified from Kelts 1988).

Figure 40. Characteristics of lacustrine environment and their variation across latitudes (modified from Lewis Jr (1987).

Figure 41. Aquatic vertebrate samples used in the geochemical study. **A**, cf. *Triodus* dorsal spine. **B**, Temnospondyl bone. **C**, cf. *Acanthodes* fin spine. **D**, sub complete actinopterygian with ganoid scales. **E**, cf. *Orthacanthus* dorsal spine. **A** and **D** from the Muse OSB and **B**, **C** and **E** from Buxières-les-Mines. Scale bar: 1 cm.

Figure 42. Illustrated protocol for the chemical treatment of the carbonates in fossil bioapatite (adapted from Angst 2014).

Figure 43. Illustrated chemical protocol for the precipitation of silver phosphates from the fossil bioapatite (adapted from Angst 2014).

Figure 44. Pyrolysis setup of the VarioPyroCube for the analysis of the $\delta^{18}O_p$ of fossil bioapatite (modified from Lécuyer *et al.* 2007; Fourel *et al.* 2011; Angst *et al.* 2014).

Figure 45. Combustion setup of the VarioPyroCube for the analysis of the $\delta^{34}S$ of fossil bioapatite (modified from Fourel *et al.* 2014).

Figure 46. Geological context of the Muse oil-shale bed (OSB). **A**, Location of the Autun Basin in the Massif Central of France, and its simplified geological map in which the Muse OSB is represented by a black star. **B**, simplified stratigraphy of the Carboniferous-Permian deposits of the Autun Basin. **C**, simplified stratigraphy of the Muse OSB. **Abbreviations**: **C.**, Curgy formation (200 m); **G I to G VIII**, tonsteins (modified after Marteau 1983; Châteauneuf *et al.* 1992; Gand *et al.* 2007, 2011, 2015, 2017; Pellenard *et al.* 2017).

Figure 47. Holotype MHNA-PAL-2020-0001 of *Triodus aeduorum* sp. nov. from the Muse OSB, Autun Basin. Photo of the whole specimen as preserved (see Figs. 3–5 for details). **A**, photograph. **B**, Line drawing of **A**.

Figure 48. Details of the head region of the holotype MHNA-PAL-2020-0001 of *Triodus aeduorum* sp. nov. from the Muse OSB, Autun Basin. **A**, photograph. **B**, Line drawing of **A**.

Figure 49. Details of the dorsal spine of the holotype MHNA-PAL-2020-0001 of *Triodus aeduorum* sp. nov. from the Muse OSB, Autun Basin. **A**, photograph. **B**, details of the denticle. **C**, Line drawing of **A**.

Figure 50. Details of the left pectoral fin of the holotype MHNA-PAL-2020-0001 of *Triodus aeduorum* sp. nov. from the Muse OSB, Autun Basin. **A**, photograph. **B**, Line drawing of **A**.

Figure 51. Paratype of *Triodus aeduorum* sp. nov. specimen MHNA-PAL-2020-0002 from the Muse OSB, Autun Basin. **A**, photograph. **B**, Line drawing of **A**.

Figure 52. Paratype of *Triodus aeduorum* sp. nov. specimen MHNA-PAL-2020-0003 from the Muse OSB, Autun Basin. **A**, photograph. **B**, Line drawing of **A**.

Figure 53. Teeth of *Triodus aeduorum* sp. nov. specimens from the Muse OSB, Autun Basin. MHNA-PAL-2020-0001, (**A**, **D**, **H**, **L**, **M**, **P**); MHNA-PAL-2020-0002, (**B**, **E–F**, **I**, **Q**); MHNA-PAL-2020-0003, (C, G, J–K, N–O, R–S). **A–C**, photograph. **D–S**, line drawing. **A**, oral view. **B**, labial view. **C**, oral view. **D**, linguo-lateral oral view. **E–G**, lingual view. **H–J**, labial view. **K**, labio-lateral view. **L–O**, lateral view. **P**, labio-basal view. **Q–S**, basal view.

Figure 54. Revised Xenacanthiformes from the Muse OSB, Autun Basin. **A**, *Triodus* sp. (adapted from Soler-Gijón & Hampe 1998). **B**, '*Expleuracanhus*' *frossardi* (from Gaudry 1867). **C**, '*Expleuracanthus*' *frossardi* (from Gaudry 1883).

Figure 55. Stratigraphical and geographic distribution of the different *Triodus* species. Asterisk indicates potential marine occurrence. **Abbreviations: USA**, United States; **UK**, United Kingdom; **RF**, Russian Federation; **Aut**, Austria; **CR**, Czech Republic; **Br**, Brazil (modified after Hampe & Ivanov 2007b; Johnson & Thayer 2009; Pauliv *et al.* 2017).

Figure 56. Geological context. **A**, simplified geological map showing the location of the Autun and Bourbon-l'Archambault basins in the Northern Massif Central. **B**, simplified geological map of the Autun Basin. **C**, simplified geological map of the Bourbon-l'Archambault Basin. **D**, simplified stratigraphy of the Autun Basin. **E**, simplified stratigraphy of the Bourbon-l'Archambault Basin. **Abbreviations: C**, Curgy formation; **Post A**, Post Asselian; **Bx**, Buxières; **Clu**, Clusor formation; **Sax**, Saxonian; **T**, Trias (modified from Châteauneuf 1980; Marteau 1983; Châteauneuf & Farjanel 1989; Châteauneuf *et al.* 1992; Steyer *et al.* 2000; Gand *et al.* 2007, 2011, 2015, 2017; Pellenard *et al.* 2017).

Figure 57. Schematic outline of a xenacanthiform neurocranium showing the location of the 13 landmarks used in the geometric morphometric analysis (modified from Schaeffer 1981).

Figure 58. Neurocranium of 'Ctenacanthiformes' indet. from the Autun Basin. **A**, photograph of the specimen MHNH.F.AUT812. **B**, line drawing of the neurocranium of *Bibractopiscis niger* in ventral view following Heyler & Poplin (1982). **C–F,** 3D rendering and new interpretation drawings of MNHN.F.AUT812. **C, D** in dorsal view and **E, F** in ventral view. **C**, **E** are 3D surface rendering and **D**, **F** are line drawings. Bold lines are anatomical structures, slender lines are contours with no anatomical significance, dotted lines are supposed anatomical structures, black areas are foramina and grey areas are gaps in the 3D renderings. Scale bars = 1 cm.

Figure 59. Neurocranium of ?Xenacanthimorpha from the Autun Basin. **A**, photograph of the specimen MHNH.F.AUT813. **B**, line drawing of the neurocranium of *Orthacanthus commailli* following

Heyler & Poplin (1982). **C**–**F,** 3D rendering and new interpretation drawings of MNHN.F.AUT813. **C, D** in dorsal view and **E, F** in ventral view. **C**, **E** are 3D surface rendering and **D**, **F** are line drawings. Bold lines are anatomical structures, slender lines are contours with no anatomical significance, dotted lines are supposed anatomical structures, black areas are foramina and grey areas are gaps in the 3D renderings. Scale bars = 1 cm.

Figure 60. Isolated chondrichthyan neurocrania from the Autun and Bourbon-l'Archambault basins. **A,** MNHN.F.AUT811, holotype of *Bibractopiscis niger*. **B,** MNHN.F.AUT810 counter art impression of MNHN.F.AUT811. **C,** MNHN.F.AUT814, paratype of *B. niger*. **D,** MHNE.2021.9.1, specimen from Buxières-les-Mines; **A**, **B**, **D** in ventral view and **C** in dorsal view (modified from Heyler & Poplin [1982] except for **D**). Scale bars = 1 cm.

Figure 61. Neurocrania of cf. *Triodus* sp. from the Autun and Bourbon-l'Archambault basins. **A**–**D,** MNHN.F.AUT811 from an unknown locality of the Autun Basin. **E**–**H,** MNHN.F.AUT814 from La Comaille. **I–L,** MHNE.2021.9.1 from Buxières-les-Mines. **A**–**B**, **E**–**F**, **I**–**J** in dorsal view and **C**–**D**, **G**–**H**, **K**–**L** in ventral view. **A**, **C**, **E**, **G**, **I**, **K** are 3D surface rendering and **B**, **D**, **F**, **H**, **J**, **L** are line drawings. Bold lines represent anatomical structures, slender lines are contours with no anatomical significance, dotted lines are supposed anatomical structures, black areas are foramina and grey areas are gaps in the 3D renderings. Scale bars = 1 cm.

Figure 62. Strict consensus tree of the cladistic analysis obtained with PAUP from the two most parsimonious trees (MPTs) with the following characteristic: length [L] = 73 steps, Consistency Index [CI] = 0.548 and Retention Index [RI] = 0.790. Values in bold below branches are Bremer indices greater than 1 and letters indicate nodes mentioned in the text. Temporal distributions are represented by bold lines and follow Coates *et al.* 2017).

Figure 63. Principal Component Analysis (PCA) on Procrustes coordinates illustrating morphological variability of the ethmo-orbital region between neurocrania of 'Ctenacanthiformes' and Xenacanthiformes. **A,** Interspecific variation based on 13 landmarks. **B**, **C,** patterns of variation along PC1. **D**, **E,** patterns of variation along PC2. **F,** morphology of the ethmo-orbital region of the ?Xenacanthimorpha (MNHN.F.AUT813).

Figure 64. Comparison between Xenacanthiformes and 'Ctenacanthiformes' neurocrania. Line drawing are in dorsal view and not to scale. *Triodus sessilis* modified from Heidtke *et al.* (2004), *Orthacanthus* sp. modified from Schaeffer (1981), *Xenacanthus meisenheimensis* modified from Heidtke & Schwind (2004) *Tamiobatis vetustus* modified from Schaeffer (1981) and *Cladodoides wildungensis* modified from Maisey (2005). Bold lines represent anatomical structures, slender lines are contours with no anatomical significance, dotted lines are supposed anatomical structures, black areas are foramina and grey areas are gaps in the 3D renderings.

Figure 65. Hypothetical morphological transition between 'Ctenacanthiformes' and Xenacanthiformes neurocrania in the light of the Autun Basin fossil record. The relationships and the character changes follow those of the phylogeny of Figure 7. Each coloured text corresponds to coloured

parts on the line drawings, which are not to scale. Outline of *Tamiobatis* is from Schaeffer (1981). Bold lines represent anatomical structures, slender lines are contours with no anatomical significance, dotted lines are supposed anatomical structures, black areas are foramina and grey areas are gaps in the 3D renderings.

Figure 66. Geological context of the Buxières-les-Mines and Muse OSB localities. **A**, simplified geological map of the Carboniferous-Permian basins from the French Northern Massif central. **B**, simplified geological map of the Bourbon-l'Archambault basin and location of Buxières-les-Mines. **C**, simplified geological map of the Autun Basin and location of the Muse OSB (modified from Steyer *et al.* 2000; Pellenard *et al.* 2017; Luccisano *et al.* 2021b,c).

Figure 67. Stratigraphical context of the Buxières-les-Mines and Muse OSB localities. **A**, simplified stratigraphy of the Bourbon-l'Archambault basin with location of Buxières-les-Mines. **B**, simplified stratigraphy of the Buxières-les-Mines locality. **C**, simplified stratigraphy of the Autun Basin and location of the Muse OSB. **D**, simplified stratigraphy of the Muse OSB locality. **Abbreviations**: **Bog**, Boghead; **BX**, Buxières; **Conglo**, Conglomerate; **C**, Curgy formation **Clu**, Clusor; **Igor**, Igornay; **MP**, Mont Pelé; **PA**, post-Asselian; **Sax**, 'Saxonian'; **SB**, 'Stephanian B' (modified from Steyer *et al.* 2000; Pellenard *et al.* 2017; Luccisano *et al.* 2021a,c).

Figure 68. Dental nomenclature used in this work. **A**, labial. **B**, oral. **C**, basal. **D**, lateral view. **Abbreviations**: **bnf**, basal nutrient foramina; **bt**, basal tubercle; **bs**; button shaft; **cb**, coronal button; **H**, height; **L**, length; **lc**, lateral cusps; **lce**, lateral cutting edge; **lnf**; labial nutrient foramina; **mc**, median cusp; **onf**; oral nutrient foramina; **s**, serration; **tb**, tooth base; **W**, width (modified from Schneider 1985, 1996; Hampe 1994).

Figure 69. Isolated adult teeth of *Orthacanthus kounoviensis* from Buxières-les-Mines. **A–D**, MHNE.2021.14.18. **E–H**, MHNE.2021.14.19. **I–L**, MHNE.2021.14.22. **M–P**, MHNE.2021.14.23. **Q–T**, MHNE.2021.14.24. **U–X**, MHNE.2021.14.13. (**A**, **E**, **I**, **M**, **Q**, **U**) in basal view. (**B**, **F**, **J**, **N**, **R**, **V**) in labial view. (**C**, **G**, **K**, **O**, **S**, **W**), lateral. (**D**, **H**, **L**, **P**, **T**, **X**), oral view. Scale bar: 5 mm.

Figure 70. Isolated adult teeth of *Orthacanthus kounoviensis* from Buxières-les-Mines. **A–C**, MNHN.F.BU8. **D–F**, MHNE.2021.14.11. **G**, PIMUZ A/I 5131. **H–I**, PIMUZ A/I 5133. **J–K**, MHNE.2021.14.13. **J**, tooth base ornamentation. **K**, double serration pattern. (**A**, **D**, **I**), basal. (**B**, **E**, **H**), labial. (**C**, **F**), lateral. (**D**, **I**), oral view. Blue arrows are primary serration and red arrows are secondary serration. Scale bar: 5 mm (**A–I**), 1 mm for **J** and 500 µm for **K**.

Figure 71. Width-length biplot of *Orthacanthus kounoviensis* adult teeth from Buxières-les-Mines and comparisons with other European *Orthacanthus* species. *O. gibbosus* is from Hampe (2003), *O. kounoviensis* from the Saar-Nahe basin is from Hampe (1994), *Lebachacanthus seckenbergianus* is from Heidtke (1982), *O. gracilis* is from Hampe (1994) and *O. meridionalis* is from Soler-Gijón (1997a).

Figure 72. Isolated juvenile teeth of *Orthacanthus kounoviensis* from Buxières-les-Mines. **A–D**, MHNE.2021.14.10. **E–H**, MHNE.2021.14.5. **I**, MHNE.2021.14.9. **J**, MHNE.2021.14.12. **K**, MHNE.2021.14.4. **L–N**, PIMUZ A/I 513. **O**, tooth base ornamentation of MHNE.2021.14.7. **P**, double serration of MHNE.2021.14.3. (**A**, **E**, **I**, **L**), basal. (**B**, **F**, **J**, **M–N**), labial. (**C**, **G**, **K**), lateral. (**D**, **H**), oral view. Blue arrows are primary serration and red arrow is secondary serration. Scale bar: 5 mm (**A–M**), 2mm for **N**, 200 µm for **O** and 100 µm for **P**.

Figure 73. Tooth base thickness boxplot of juvenile and adult of *Orthacanthus* species. **A**, *Orthacanthus kounoviensis* from Buxières-les-Mines (this study). **B**, *Lebachacanthus seckenbergianus* from Heidtke (1982) and Hampe (1988a). **C**, *Orthacanthus donnelljohnsi* from Johnson & Thayer (2009).

Figure 74. *Orthacanthus* cf. *kounoviensis* tooth from the Muse OSB. **A–G**, MNHN.F.AUT892. **A–D**, tooth base. **E**, tooth base ornamentation. **F**, cusps. **G**, imprint of the serration of the lateral cutting edge. **A**, basal. **B**, labial. **C**, lateral. **D**, oral view. Blue arrows are primary serration and red arrows are secondary serration. Scale bar: 5 mm (**A–D**, **F**), 500 µm for **E** and 200 µm for **G**.

Figure 75. Isolated dorsal spine of *Orthacanthus* cf. *kounoviensis* from Buxières-les-Mines. (**A–C**, **E**), MHNE.2021.14.25. (**D**, **F–G**), MHNE.2021.14.26. **A–D**, entire dorsal spines. **E–G**, details of the denticles. **A**, lateral. **B**, dorsal view. **C–D**, ventral view. Scale bar: 1 cm (**A–D**) and 1 mm (**E–G**).

Figure 76. Linear regressions on total (**A**), adult (**B**) and juvenile (**C)** teeth of *Orthacanthus kounoviensis* from Buxières-les-Mines. For (**A–C**) the red line is the linear regression line, the blue lines are the confidence interval, and the brown lines are the prediction interval.

Figure 77. Temporal and geographic distribution of the European *Orthacanthus* species. *O. buxieri* is here restricted to the sole holotype (Heyler & Poplin 1989). Red lines are occurrences of the studied material. '?' refers to the fossil record gaps. *L. senckenbergianus s.l.* corresponds to the three *Lebacahacanthus* species from the Saar-Nahe basin as defined by Heidtke (2007), i.e. *L. senckenbergianus*, *L. pollichiae* and *L. colloseus*. Temporal and geographic distributions are from Heyler & Poplin (1989), Hampe (1994, 2003), Soler-Gijón (1997a), Heidtke (1998, 2007).

Figure 78. Geological context. **A,** simplified geological map showing the location of the Autun and Bourbon-l'Archambault basins in the Northern Massif Central. **B,** simplified geological map of the Autun Basin. **C,** simplified geological map of the Bourbon-l'Archambault Basin. **D,** simplified stratigraphy of the Muse OSB. **E,** simplified stratigraphy of Buxière-les-Mines (modified from Châteauneuf 1980; Marteau 1983; Châteauneuf & Farjanel 1989; Châteauneuf *et al.* 1992; Steyer *et al.* 2000; Gand *et al.* 2007, 2011, 2015, 2017; Pellenard *et al.* 2017).

Figure 79. Boxplot of the $\delta^{18}O_p$ values of the vertebrate faunas from the Muse OSB and Buxières-les-Mines. Data for the boxplot of *Lissodus* sp. are from Fischer *et al.* (2013).

Figure 80. Boxplot of the $\delta^{13}C_c$ values of the vertebrate faunas from the Muse OSB and Buxières-les-Mines.

Figure 81. Boxplot of the $\delta^{34}S$ values of the vertebrate faunas from the Muse OSB and Buxières-les-Mines. Red points are diagenetic altered samples in Buxières-les-Mines.

Figure 82. Evolution of the $\delta^{18}O_p$ (**A**) and $\delta^{13}C_c$ (**B**) values along the acanthodian fin spines.

Figure 83. Evolution of the $\delta^{34}S$ values along the acanthodian and xenacanthiform spines.

Figure 84. Evolution of the $\delta^{18}O_p$ (**A–B**) and $\delta^{13}C_c$ (**C**) values along the xenacanthiform dorsal spines.

Figure 85. Reconstruction of the palaeotemperatures in Buxières-les-Mines and the Muse OSB. **Abbreviations: Ice,** icehouse Earth; **Gre,** greenhouse Earth; **Mat,** Lake Matano; **Pun,** Lake Punta Laguna; **Tan,** Lake Tanganyika.

Figure 86. Oxygen isotope compositions of bioapatite ($\delta^{18}O_p$) from studied vertebrate taxa plotted against their corresponding oxygen isotope composition of carbonate ($\delta^{18}O_c$). Other points are extant and fossil referent samples from different aquatic environments. Additional extant data are from Iacumin *et al.* (1996) and Vennemann *et al.* (2001) and fossil data are from Kolodny & Luz (1991); Fricke *et al.* (1998); Lécuyer *et al.* (2003a); Amiot *et al.* (2010); Goedert *et al.* (2018).

Figure 87. Difference between the oxygen isotope compositions of bioapatite carbonate ($\delta^{18}O_c$) and phosphate ($\delta^{18}O_p$) plotted against the carbonate concentration.

Figure 88. The sulfur isotope composition ($\delta^{34}S$) plotted against the sulfur content (weight% SO_2).

Figure 89: Stuck *Orthacanthus* tooth in a temnospondyl dentary in Buxières-les-Mines. **A**, Photograph. **B**, interpretation drawing.

Figure 90. Environmental reconstruction of the Muse OSB and Buxières-les-Mines.

Figure 91. Anatomical comparisons between European (top) and American (bottom) xenacanthiforms. **A–B**, *Orthacanthus* with *O. gracilis* (**A**) and *O. donnelljohnsi* (**B**). **C–D**, *Xenacanthus* with *X. laevissimus* (**C**) and *X. slaughteri* (**D**). **E–F**, *Triodus* with *T. serratus* (**E**) and *T. elpia* (**F**) (modified from Hampe 1994, 2003; Johnson 1999; Johnson & Thayer 2009). The teeth are not in scale.

Figure 92. Dendrogram of the similarity of the xenacanth assemblages of the world.

Table captions

Contents

Introduction

1. Historical background of the study of the xenacanthiform systematics

The first report of the chondrichthyan order Xenacanthiformes dates to the middle of the 19th century with Agassiz's (1837) reference work "*Recherches sur les Poissons fossiles*" who erected the first species '*Pleuracanthus*' *laevissimus* (now *Xenacanthus laevissimus*, e.g. Ginter *et al.* 2010) based on an isolated dorsal spine, initially related to modern rays, from the late Pennsylvanian of England. The first xenacanthiform tooth was reported by Binney (1840) under the specific name '*Diplodus*' *gibbosus* (now *Orthacanthus gibbosus*, e.g. Ginter *et al.* 2010). During the second half of 19th century, the investigations on the xenacanthiforms enhanced the knowledge on this group thanks to numerous studies on the British (Owen 1867; Barkas 1873, 1874; Davis 1880, 1881, 1892; Stock 1880; Traquair 1881, 1882, 1888, 1903; Woodward 1889; Ward 1890; Woodward & Sherborn 1890), German and Czech (Jordan 1849; Kner 1867; Fritsch 1889, 1890; Koken 1889; Jaekel 1895, 1906) fossil records. In these studies, isolated teeth and dorsal spines as well as partial and sub-complete skeletons were described with a multiplication of erected new genera which are no longer considered valid (e.g. '*Aganodus*', '*Anodontacanthus*', '*Diplodus*', '*Dittodus*', '*Ochlodus*', '*Pleuracanthus*', '*Pternodus*') as well as still used ones (*Triodus, Xenacanthus*, *Orthacanthus*). Out of Europe, the Xenacanthiformes were first reported in North America by Cope (1888) and in India by Woodward (1889) and more recently in South America by Würdig-Maciel (1975) and in Australia by Turner (1982).

In France, the first report of xenacanthiform remains came from the Carboniferous-Permian basins of the Northern Massif central deposits and are attributed to Gaudry (1867, 1883) who erected the species '*Pleuracanthus*' *frossardi* based on isolated dorsal spines from the early Permian of the Muse OSB locality in the Autun Basin (Saône-et-Loire). The first sub-complete skeleton is attributed to '*Pleuracanthus*' *gaudryi* (Brongniart & Sauvage 1888) (now *Xenacanthus gaudryi*) from the late Carboniferous of Commentry (Allier). However, Agassiz (1833) actually made the first report of a French xenacanth with the species '*Pygopterus*' *bonnardi* that represents caudal and anal fins. He attributed it to a '*sauroïde'* fish (now Palaeonisciformes) without illustration. It was Woodward (1891) and Sauvage (1893) who first referred this specimen to the Xenacanthiformes.

As in the rest of Europe, the publications on the French xenacanthiforms from the Northern Massif central are quite non-existent in the first half of the 20th century (Hampe 2003). New studies were carried out in the 1960s (Heyler 1969) with an intensification of publications in the 1980s and 1990s (Heyler & Pacaud 1978; Heyler & Debriette 1986; Heyler & Poplin 1982, 1989, 1990; Poplin & Heyler 1989; Soler-Gijón & Hampe 1998). Recently, excavation campaigns have been made since 2010 in the Muse OSB of the Autun Basin (e.g. Gand *et al.* 2011, 2015) and since 1996 in the Buxières-les-Mines locality in the Bourbon-l'Archambault Basin (Allier; Steyer & Escuillié 1997; Steyer *et al.* 2000).

2. Systematic questions

As many other fossil groups originally defined in the 19th century, the systematics of the Xenacanthiformes was and is still debated. Indeed, the original fragmentary material (mainly isolated teeth and dorsal spines) and the inability to perform extensive comparisons with more complete specimens have produced erections of many genera and species, not necessarily valid in the light of the current systematic standards. For example, the first generic names '*Pleuracanthus*' and '*Diplodus*' were preoccupied by a coleopteran (Griffith *et al.* 1832) and an actinopterygian (Rafinesque-Schmaltz 1810) respectively. Many genera erected in the 19th century are in fact synonyms of current valid genera (see Ginter *et al.* [2010] for a recent synthesis): '*Diplodus*', '*Chilodus*', '*Ochlodus*', '*Didynodus*' and '*Lophocanthus*' are junior synonyms of *Orthacanthus*; '*Pleuracanthus*' (in part), '*Dittodus*' (in part), '*Pternodus*' and '*Compsacanthus*' are junior synonyms of *Xenacanthus*; '*Pleuracanthus*' (in part) is a junior synonyms of *Triodus*. Additionally, even more recent studies have induced systematic issues. Heyler (1969) proposed to change the genus of the specimens referred to '*Pleuracanthus*' into '*Expleuracanthus*' to correct the preoccupation of this generic name. But the formal definition of '*Expleuracanthus*' was not made, and it could refer to *Xenacanthus* and/or *Triodus* (e.g. Hampe 2003). Furthermore, *Bohemiacanthus* Schneider & Zajíc, 1994 is now synonymised with *Triodus* (e.g. Hampe 2003).

A look at the French Massif central fossil record shows the same thing. For example, the species *Orthacanthus buxieri* Heyler & Poplin, 1989 and *Orthacanthus commailli* (Heyler & Poplin, 1982) were erected on barely prepared specimens which question their systematic validity. In the Autun Basin, historical xenacanth species such as '*Expleuracanthus*' *frossardi* or '*Expleuracanthus*' *bonnardi* (previously '*Pygopterus*' *bonnardi*) are defined on isolated dorsal spines and not revised yet. Finally, the enigmatic species from the Autun Basin

Bibractopiscis niger Heyler & Poplin, 1982 is known by barely prepared isolated neurocrania and its systematic affinities are highly questionable. The French xenacanthiform systematics seems less well resolved compared to contemporaneous European areas, i.e. Germany (Hampe 1988a,b, 1989, 1991, 1993, 1994, 1995, 1997a,b; Heidtke 1982, 1998, 1999; Schneider *et al.* 2000), Bohemia (Schneider 1985, 1988, 1996; Schneider & Zajíc 1994; Schneider *et al.* 2000), Spain (Soler-Gijón 1997a,b, 1999, 2000; Schneider *et al.* 2000) and United Kingdom (Hampe 2003). It is all the more problematic as many xenacanth remains (from isolated parts to sub-complete specimens) were found in recent excavation campaigns but no publication with significative taxonomic updates has been done. Among these remains, several ones appear to be preserved in 3D dimensions, so they are good candidates for the use of X-ray computed microtomography (µCT scan), a powerful technique to investigate the hidden anatomy of fossils, still used on Palaeozoic chondrichthyans but less on Xenacanthiformes.

Consequently, a systematic reassessment of the French Permian Xenacanthiformes from the Northern Massif central is needed. The first axis of the Ph.D. work focuses on the xenacanthiform fauna of two localities from the early Permian of the French Massif central: Muse OSB in the Autun Basin (Saône-et-Loire) and Buxières-les-Mines in the Bourbon-l'Archambault Basin (Allier). The objectives are to reassess the systematics of already known species with a special emphasize on historical ones. This systematic reassessment will allow to discuss 1) the xenacanth diversity in each locality, 2) the palaeobiogeography of the French Permian Xenacanthiformes in the Massif central and with the other European Carboniferous-Permian basins and 3) to investigate their phylogenetic relationships within the Chondrichthyes. To perform this axis, classical comparative anatomy and biometric methods as well as scanned data from the µCT scan were used.

3. Palaeoecological questions

For a long time, the Xenacanthiformes were considered as strict freshwater chondrichthyans, evolving in lakes, river-channels and swamps. This interpretation was supported by the fact that they were found in non-marine sediments, their body shape evokes modern large freshwater fishes like pikes, garpikes, catfishes or sturgeon and they seem to tolerate low oxygenised water (Compagno 1990). This hypothesis was proposed early and not debated until recently.

In fact, the Xenacanthiformes are present all around the world, from North America to Australia since the beginning of their evolutionary history in the early Carboniferous. It seems

difficult to explain their global palaeobiogeography without marine migrations in a time when the Pangea was not yet formed. Furthermore, some of the sedimentary basins where they occured are supposed to have been influenced by marine incursions (e.g. Schultze 2009). Recent studies (Soler-Gijón 1999; Beck *et al.* 2016) investigated the histology and growth pattern of the dorsal spines of North American and European *Orthacanthus* of the late Carboniferous and suggested a potential migration behaviour between the freshwater and the marine settings.

However, the historical hypothesis of a full freshwater ecology was not abandoned in the recent studies. Above all, geochemical analyses on Carboniferous and Permian isolated teeth of North American and European Xenacanthiformes (Fischer *et al.* 2013, 2014b) support a freshwater living environment. Ambiguous results that could correspond to marine signals are interpreted as evaporation events and agree with their supposed ability to overcome low oxygenised water.

Consequently, the debate on the palaeoecology of the Xenacanthiformes is still open, especially for those which come from sedimentary basins with ambiguous palaeoenvironmental records like the Carboniferous-Permian basins of the Northern Massif central. In fact, the palaeoenvironment of some of these basins could be questionable. On one hand, their palaeogeography indicates that they are located several hundreds of kilometres away from the sea (e.g. Roscher & Schneider 2006). One the other hand, the study of their global fauna and flora and comparisons with contemporaneous European basins indicate some marine or brackish components like acritarchs or lungfishes (Schultze & Soler-Gijón 2004; Schultze 2009). Furthermore, the distribution of the genera *Orthacanthus*, *Xenacanthus* and *Triodus* indicates connections between the Massif central and other European basins and, consequently, questions the salinity tolerance to facilitate their dispersion.

Stable isotope analyses are a powerful tool to investigate the living environment of fossils. In the case of Xenacanthiformes, the previous geochemical analyses exclusively focused on their teeth, so punctual elements in their lifespan only dedicated to reconstructing the environment of their place of death. However, the xenacanthiforms possess an incrementally ever-growing dorsal spine that could trace their environment all along their lifespan, so more suitable to palaeoecological reconstructions during their entire life. Furthermore, the associated vertebrate fauna, including actinopterygians, acanthodians and temnospondyls, was never investigated to constrain the palaeoenvironment of the basins that have yielded Xenacanthiformes. The Autun and the Bourbon-l'Archambault basins are examples in which isolated dorsal spines of various xenacanthiforms and various associated aquatic vertebrate fauna are available.

Consequently, in addition to the systematic reassessment of the Xenacanthiformes from the Autun and the Bourbon-l'Archambault basins, their palaeoecology is also investigated. To do this, a second axis consists of geochemical analyses on their dorsal spines to trace their living environment and potential migrations during their lifespan, and on associated aquatic vertebrates (actinopterygians, acanthodians and temnospondyls) in order to reconstruct the palaeoenvironment of these basins. More precisely, this axis focuses on the stable isotope compositions of the oxygen and sulfur of phosphates and oxygen and carbon of carbonates of the bioapatite of the fossil samples.

4. Organisation of the manuscript

This present Ph.D. manuscript begins with a state-of-the-art section which exposes the general background on the evolutionary history of Xenacanthiformes, the principles of the X-ray computed microtomography and its applications to the Palaeozoic chondrichthyans and the principles of stable isotope geochemistry for the palaeoenvironemental study. The geological context as well as the material and methods used for the systematic and palaeoenvironmental studies represent one section respectively. The results and the discussions of the systematic and palaeoenvironmental studies are present under the form of published and submitted manuscripts to peer-reviewed journals. The manuscript ends with a general discussion, a presentation of unpublished or submitted data and a conclusion.

Chapter I – State-of-the-art

1. The order Xenacanthiformes

1.1. Anatomy

1.1.1. Overview

Xenacanthiformes constituted a chondrichthyan order characterised by a distinct elongated and eel-like body (Fig. 1). Their size ranges from less than 50 cm for the small *Triodus* to more than 3.5 m for the large *Lebachacanthus* (Hampe 2003). They possess an elongated dorsal fin which runs all along their back from the scapulocoracoid to the anal fins level. The presence of two anal fins is an autapomorphy. Initially, the second anal fin could be dedicated to form a heterocercal caudal fin like in the primitive *Diplodoselache* (Soler-Gijón 2004) or the lower lobe of the caudal fin isolated itself to give the second anal fin. In the more derived xenacanthiforms, the heterocercal caudal fin is lost with the development of a secondary dorsal fin (Soler-Gijón 2004). The pectoral and pelvic fins are large, well-developed. The xenacanthiforms possess a single dorsal spine, denticulated and inserted from the base of the neurocranium to the base of the dorsal fin. This order is also characterised by numerous cranial features like a long otico-occipital region or a rounded precerebral fontanelle. As many Palaeozoic chondrichthyans, the palatoquadrate has a distinct cleaver shape. Their teeth are unique with a lingually elongated base and a tricuspid pattern of the crown.

1.1.2. Neurocranium

The anatomy of the neurocranium was first extensively studied by Schaeffer (1981) based on the description of a few American neurocrania from the lower Permian (Fig. 2). The main characteristics of a xenacanthiform neurocranium are a long otico-occipital region that reaches more than half of its total length, a rounded and well-developed precerebral fontanelle and developed preorbital, postorbital and lateral otic processes. Following Schaeffer (1981), a rostrum is present in front of the precerebral fontanelle between the two nasal capsules. However, this structure is, most of the time, barely preserved and distinct from the regular rostrum of modern Elasmobranchii. The articular facet for the palatoquadrate is always situated on the dorsal margin of the postorbital processes. The otico-occipital region bears a pair of dorsal otic ridges that frame an elongated endolymphatic fossa. The otico-occipital crest is well-developed. Due to the high development of the lateral otic processes posteriorly, the

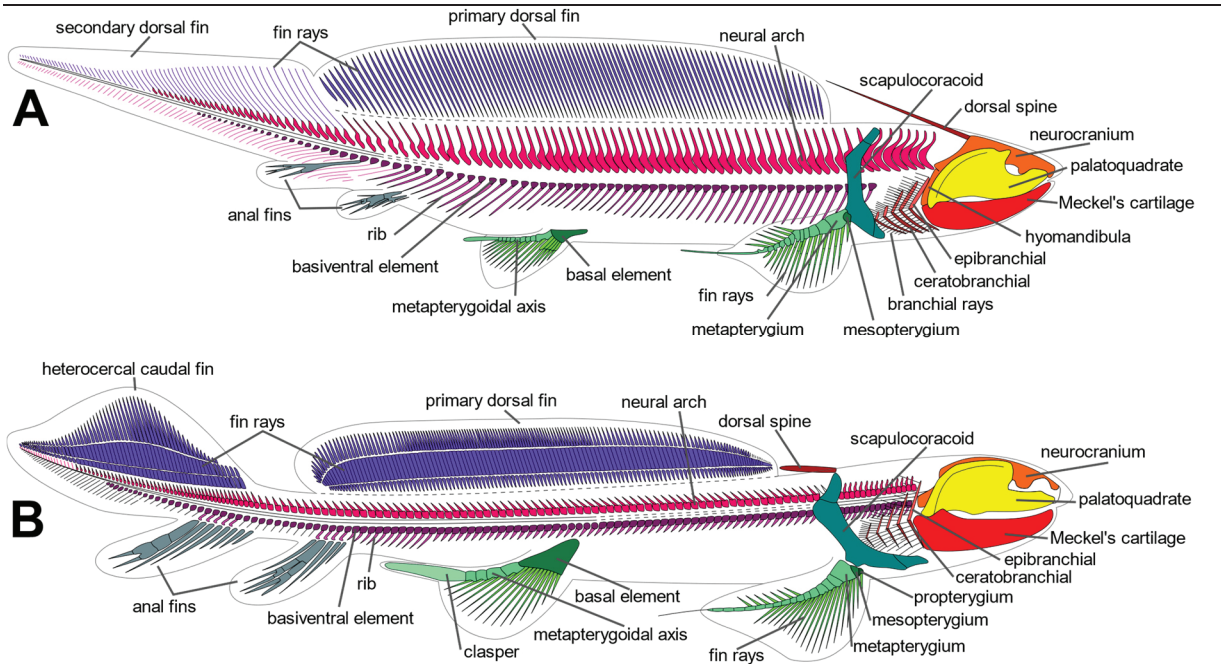

Figure 1. Global anatomy of Xenacanthiformes. **A**, *Triodus sessilis*, a xenacanthid. **B**, *Lebachacanthus seckenbergianus*, a diplodoselachid. Drawings not to scale (modified from Heidtke 2003).

occipital block is wedged between them. Its ventral side is characterised by the presence of two large foramina for lateral dorsal aorta. The lateral otic processes bear a wide articular surface for the hyomandibular.

1.1.3. Teeth

The teeth are the most abundant elements in the fossil record. They are arranged into multiple dental rows. They are easily recognisable from the other Palaeozoic chondrichthyans (Fig. 3): they are characterised by a distinct tricuspid pattern with two developed and large lateral cusps, sometimes serrated and/or ornamented. A reduced median cusp is present between them. A multiplication of the median cusp is frequently observed, which could be due to stuck food remains that altered the regular development of this cusp (Becker *et al.* 2000). The tooth bases present a developed lingual torus which gives them an labio-lingual extension. On the oral side of the base, there is a developed coronal button. The latter is articulated with the basal tubercle, on the basal side, of the following tooth in the dental row. The teeth are highly vascularised with the presence of numerous nutrient foramina on all the base sides. The heterodonty is present but underdeveloped in Xenacanthiformes. The median teeth are symmetric, and the following ones become more and more asymmetric. Usually, the last dental row exhibits reduced teeth without a median cusp. The size of the teeth can also be influenced by their position in the jaw, with an increase from the symphyseal to the first lateral teeth and

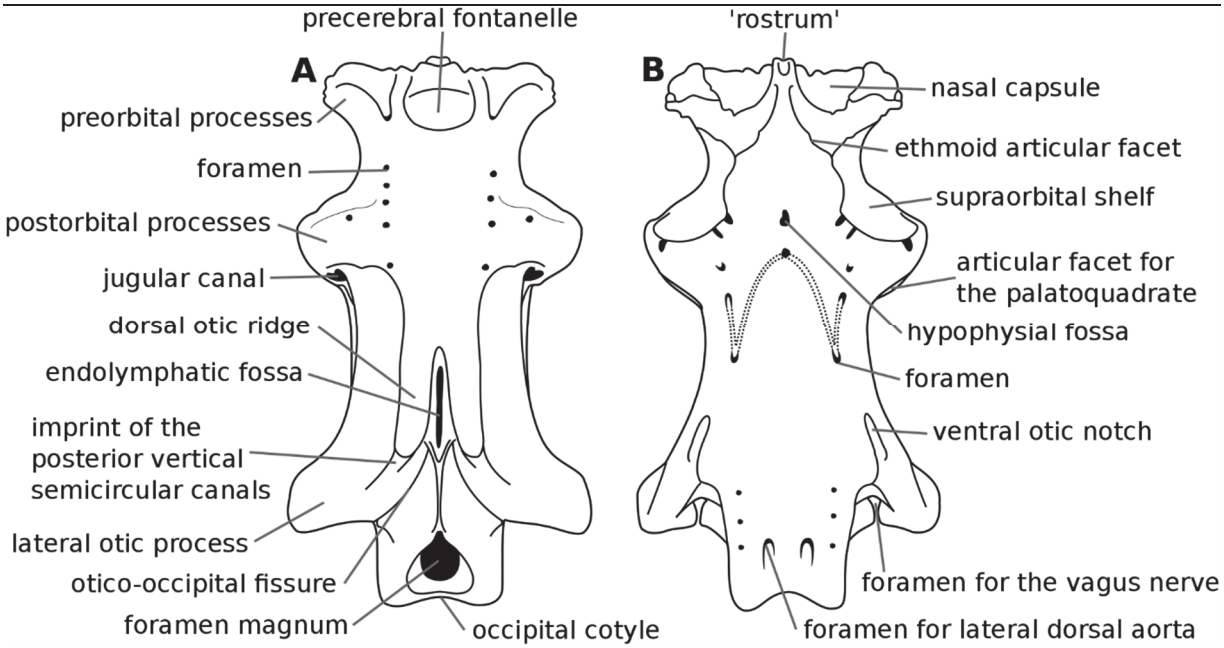

Figure 2. Xenacanthiformes neurocranium in dorsal (**A**) and ventral (**B**) views. Drawings not to scale (modified from Schaeffer 1981).

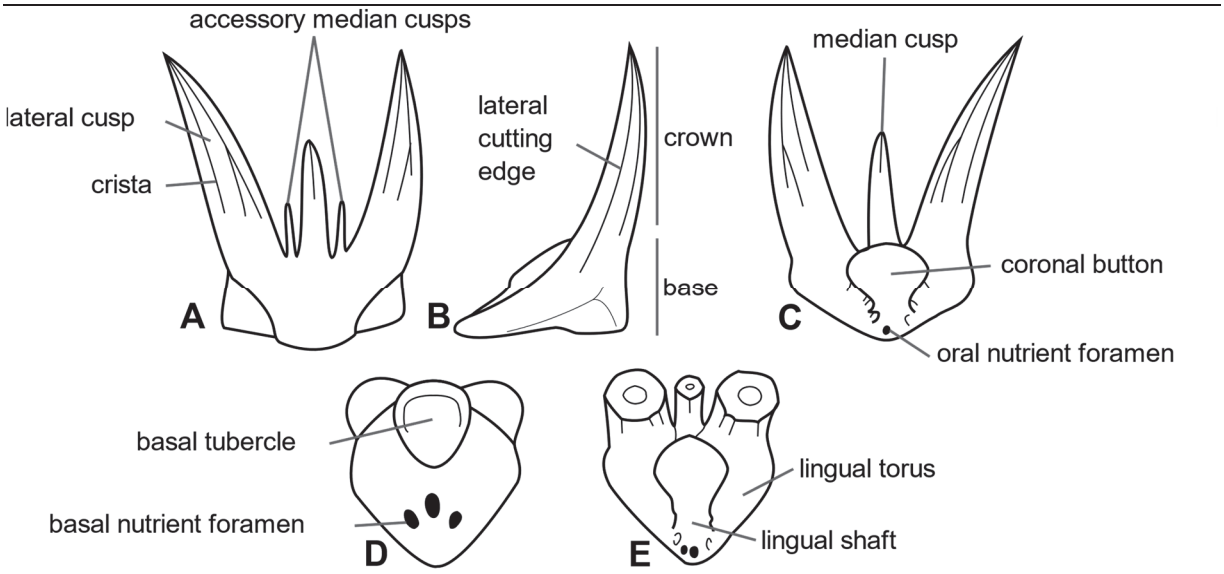

Figure 3. Xenacanthiformes dental pattern in labila (**A**), lateral (**B**), lingual (**C**), basal (**D**) and oral (**E**) views. Drawings not to scale (modified from Schneider 1996).

then a decrease to the last dental row. From a histological point of view, the xenacanthiform teeth are deprived of enameloid, an enamel-like tissue, and fully constituted of trabecular dentine and/or orthodentine.

1.1.4. Dorsal spine

The single denticulated dorsal spine is a main characteristic of Xenacanthiformes (Fig. 4). Its structure and growth pattern were studied by Soler-Gijón (1999). The dorsal spine originates and is superficially inserted into the dermis. It is an ever-growing structure, not replaced during the lifespan of an individual. Its insertion is primitively in front of the dorsal fin like in Diplodoselachidae, but it can also be at the base of the neurocranium for the derived Xenacanthidae. An intermediate position at the level of the scapulocorocoid is hypothesized for the diplodoselachid *Orthacanthus*. As for the teeth, the dorsal spine is made of dentine, mainly trabecular one. The denticles of the dorsal spine are dermal elements formed by a dermal papilla and secondarily attached to the spine by dentine (Soler-Gijón 1999). They increase in size until the sexual maturity of the individual and then stop growing. The dorsal spines always exhibit two distinct rows of denticles. They are positioned either on the ventral margin or on the lateral sides. The external ornamentation is not as pronounced as in other chondrichthyan order like Hybodontiformes or 'Ctenacanthiformes' but, usually, numerous longitudinal striations are present.

1.2. Systematics

The first described xenacanthiform remain was '*Pleuracanthus*' *laevissimus* (Agassiz 1837-1843), an isolated dorsal spine attributed to a ray. From this date to 1969, a systematic problem was the use of the genus '*Pleuracanthus*'. In fact, this name, preoccupied by the South American coeleopteran *Pleuracanthus sulcipennis* Griffith , Pidgeon & Gray, 1832 was usually used in the literature. Heyler (1969) proposed to replace the name '*Pleuracanthus*' by '*Expleuracanthus*' in order to fix this taxonomic conflict. However, '*Expleuracanthus*' is not a valid genus as some specimens have been demonstrated to belong to either *Triodus* or *Xenacanthus* (e.g. Hampe 2003). The first xenacanthiform tooth was described by Binney (1840) with the species '*Diplodus*' *gibbosus*. However, again, this name was preoccupied by a sparid actinopterygian *Diplodus annularis* Rafinesque-Schmaltz, 1810. '*Diplodus*' *gibbosus* was later attributed to the genus *Orthacanthus* erected by Agassiz (1843) on isolated dorsal spines.

The order Xenacanthiformes Berg, 1937 is usually divided into two families (e.g. Ginter *et al.* 2010). The Diplodoselachidae Dick, 1981 includes the most primitive genera with *Diplodoselache* Dick, 1981, *Dicentrodus* Traquair, 1888, *Lebachacanthus* Soler-Gijón, 1997b, *Orthacanthus* Agassiz, 1843, *Hagenoselache* Hampe & Heidtke, 1997, *Reginaselache* Turner & Burrow, 2011, *Taquaralodus* Chahud, Fairchild & Petri, 2010 and *Hokomata* Hodnett &

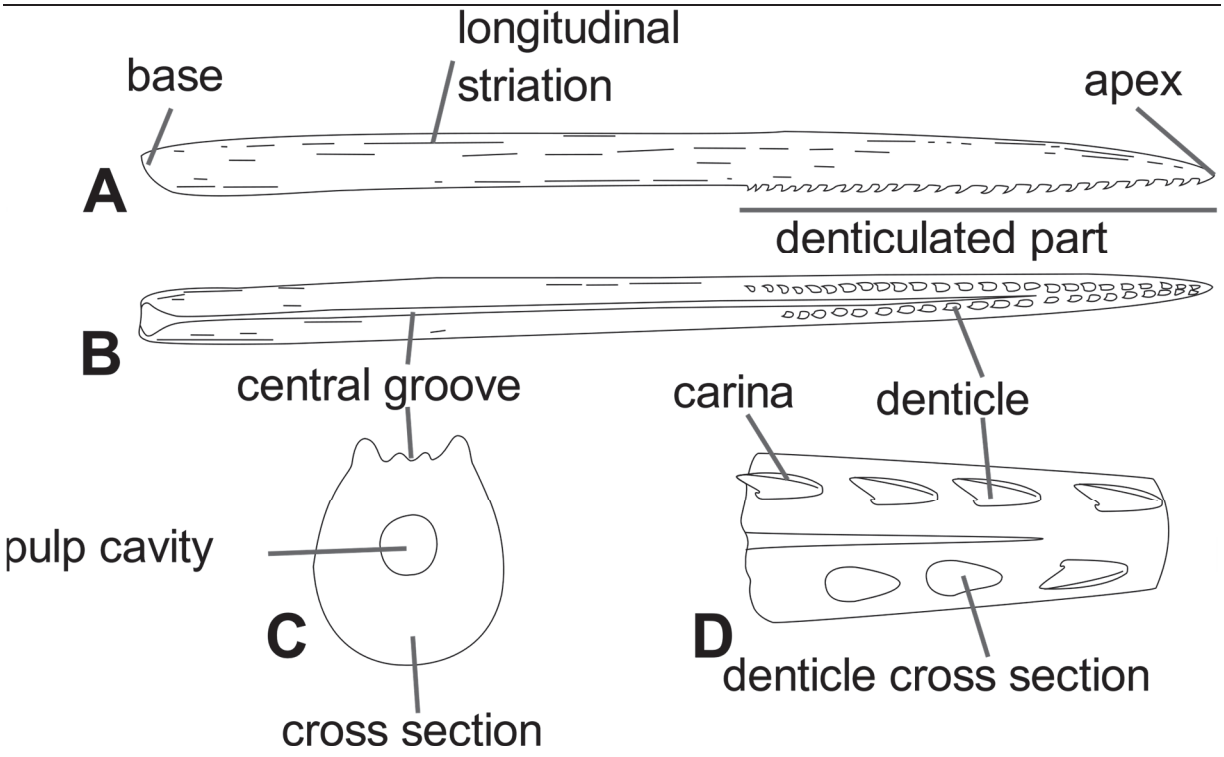

Figure 4. Xenacanthiformes dorsal spine in lateral (**A**) and ventral (**B**, **D**) views and in cross section (**C**). Drawings not to scale (modified from Soler-Gijón 1999).

Elliott, 2018. The derived xenacanthiforms form the family Xenacanthidae with the genera *Xenacanthus* Beyrich, 1848, *Triodus* Jordan, 1849, *Plicatodus* Hampe, 1993, *Wurdigneria* Richter, 2005 and *Mooreodontus* Hampe & Schneider, 2010 in Ginter *et al.* (2010, 168). The systematics of the genus *Tikiodontus* Bhat , Ray & Datta, 2018 remains ambiguous because of the absence of complete teeth with lateral cusps preserved.

The entire anatomy is not known for all the genera. Complete and sub-complete skeletons are known for the genera *Diplodoselache* (Dick 1981), in which the neurocranium lacks, *Lebachacanthus* (Soler-Gijón 1997a), *Xenacanthus* (e.g. Brongniart & Sauvage 1888; Schneider & Zajíc 1994) and *Triodus* (e.g. Fritsch 1890; Schneider & Zajíc 1994). Only the skeleton of an assumed juvenile of *Orthacanthus bohemicus* (Soler-Gijón 2004) was reported even if numerous cranial, branchial and post-cranial remains attributed to the putative *O. buxieri* are known from the lower Permian of France (Heyler & Poplin 1989; Heidtke 2003). Isolated dorsal spines are known in the genera *Diplodoselache* (Dick 1981), *Lebachacanthus* (Soler-Gijón 1997a), *Orthacanthus*, *Xenacanthus* and *Triodus* (e.g. Hampe 2003). *Anodontacanthus* Davis, 1881 was first described on isolated dorsal spines as a distinct genus. It is now regarded as a possible synonym of *Dicentrodus* (Ginter *et al.* 2010) even if its morphology clearly evokes a Xenacanthidae (Hampe 2003). *Hagenoselache* (Hampe & Heidtke 1997) is known from a

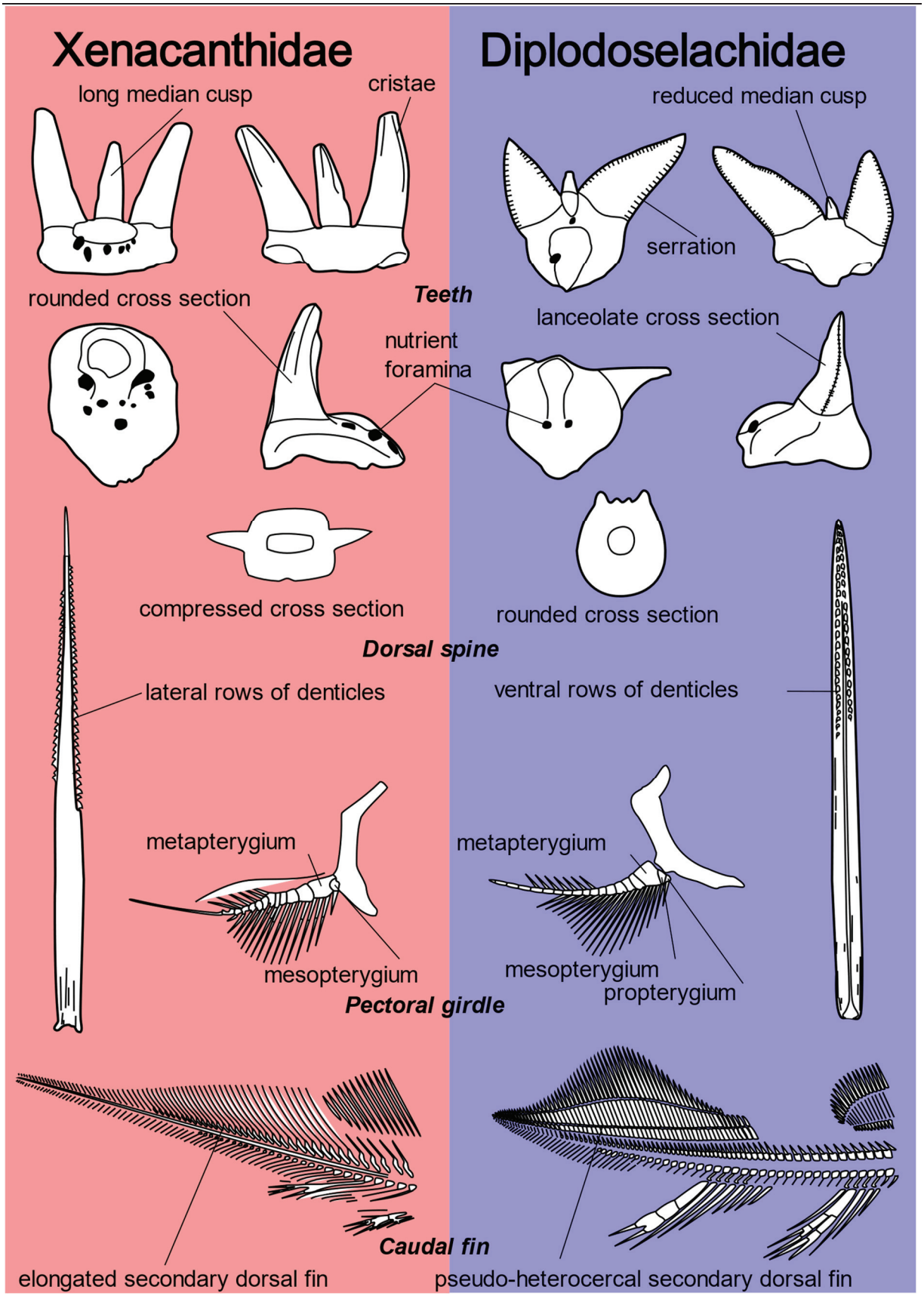

Figure 5. Morphological differences between the families Xenacanthidae and Diplodoselachidae. Drawings not to scale (modified from Soler-Gijón 1999; Hampe 2003; Heidtke 2003; Ginter *et al.* 2010).

partly preserved skeleton that does not preserve the dorsal spine. All the xenacanthiform genera are defined by their teeth, isolated, or recovered in position in the jaws (Ginter *et al.* 2010).

The distinction between the Xenacanthidae and Diplodoselachidae (Fig. 5) are mainly based on the morphology of their teeth and dorsal spines with the addition of some post-cranial differences (e.g. Ginter *et al.* 2010; Turner & Burrow 2011). Initially, the Diplodoselachidae exhibits a dental pattern with two labio-lingually compressed lateral cusps and a reduced number of nutrient foramina. The main cusp is reduced and reaches less than ¼ the size of the lateral ones. The cusps are usually not ornamented or serrated. This dental pattern is extremely variable within the Diplodoselachidae with a tendency to the serration in *Orthacanthus* and *Lebachacanthus*, a long median cusp in *Hagenoselache* or an asymmetric and labio-lingually compressed teeth in *Dicentrodus* (e.g. Ginter *et al.* 2010). The dorsal spine is rounded in cross section and the two rows of denticles are located on the ventral side (Dick 1981; Hampe 2003). Its insertion can vary between the genera. In *Diplodoselache* and *Lebachacanthus*¸ it occurs at the base and in front of the dorsal fin (Ginter et al., 2010). In this case, the global morphology is short and broad with a width/length ratio that does not exceed $^{1}/_{8}$. *A contrario*, in *Orthacanthus* (e.g. Heidtke 2003) the global morphology is long and slender with a width/length ratio around $^{1}/_{15}$. The insertion is supposed to occur far from the dorsal fin, in the shoulder region at the level of the scapulocoracoid even if no dorsal spine in anatomical connection was ever found for *Orthacanthus*. In the Diplodoselachidae, the pectoral girdle included an articulation between the fins and the scapulocoracoid with three elements (tribasal) (e.g. Hampe 2003): the propterygium, the mesopterygium and the metapterygium. The caudal fin is heterocercal in the primitive *Diplodoselache* (Dick 1981) contrary to *Lebachacanthus* or *Hagenoselache* in which it is pseudo-heterocercal with the development of a secondary dorsal fin (Soler-Gijón 2004).

The global morphology of the Xenacanthidae is not as variable as the Diplodoselachidae one. The dental pattern is characterised by rounded lateral cusps with a tendency to the ornamentation including vertical cristae (Ginter *et al.* 2010). Serration is lacking. The median cusp of the Xenacanthidae is higher than in most of the Diplodoselachidae and can reach more than half of the size of the lateral ones. There is a high number of nutrient foramina on the tooth base (Schneider & Zajíc 1994; Hampe 2003). The dorsal spine is usually inserted at the base of the neurocranium and possesses a dorso-ventrally compressed cross section two lateral rows of denticles (Schneider & Zajíc 1994). Its global morphology is long and slender and reaches $^{1}/_{6}$ of the total body length (e.g. Hampe 2003). The pectoral girdle is bibasal with only the

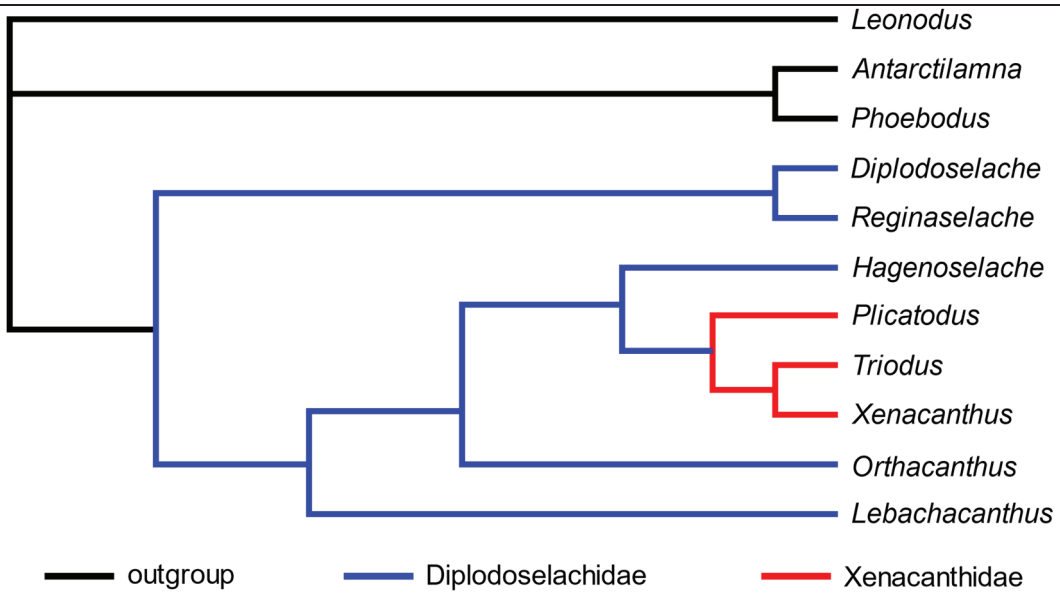

Figure 6. Supposed phylogenetic relationships within the Xenacanthiformes (modified from Turner & Burrow 2011).

metapterygium and the mesopterygium for the articulation between the fins and the scapulocoracoid (Hampe 2003). The caudal fin is elongated and composed of a secondary dorsal fin (Soler-Gijón 2004).

Since phylogenetic analyses on their internal relationships have been attempted (e.g. Soler-Gijón 2000; Hampe 2003; Heidtke *et al.* 2004), the Xenacanthidae have always been recovered monophyletic contrary to the Diplodoselachidae that appears paraphyletic as stem-group of the Xenacanthidae (Fig. 6; e.g. Turner & Burrow 2011). However, the Diplodoselachidae are always used as a valid family (e.g. Ginter *et al.* 2010). The erection of the genus *Lebachacanthus* (Soler-Gijón 1997a) introduced a new family, the Lebachacanthidae restricted to this genus, a new definition of Xenacanthidae that included *Xenacanthus*, *Triodus* and *Orthacanthus* and that restricted the Diplodoselachidae to the genus *Diplodoselache*. These relationships were no longer considered valid (e.g. Ginter *et al.* 2010; Turner & Burrow 2011) and the Xenacanthidae and Diplodoselachidae are currently used without clear argument to support the monophyly of the Diplodoselachidae. For example, the supposed monophyly of the Diplodoselachidae can be questioned by its high variation of dental and post-cranial morphology contrary to the Xenacanthidae. Furthermore, character states appear intermediate like the dorsal spine: broad and inserted at the base of the dorsal fin in *Diplodoselache*, slender and inserted in the shoulder region in *Orthacanthus* and slender and inserted at the base of the neurocranium in *Xenacanthus*.

1.3. Phylogenetic relationships within the Chondrichthyes

1.3.1. The superorder Xenacanthimorpha

Among the Chondrichthyes, the order Bransonelliformes Hampe & Ivanov, 2007 is seen as the sister-group of the Xenacanthiformes (Hampe & Ivanov 2007a) and form with them the superorder Xenacanthimorpha Berg, 1940. Morphologically, the Xenacanthimorpha are characterised by a distinct tricuspid pattern with two developed lateral cusps and a shorter median one. The tooth base is lingually extended into a lingual torus that bears a coronal button and a basal tubercle on the ventral side (Ginter *et al.* 2010).

The Bransonelliformes (Fig. 7) included two genera with *Bransonella* which is only known by isolated teeth. Its fossil record extends from the Visean of Russia to the early Permian of the USA. Putative fragmentary dental remains from the late Mississippian of China could belong to *Bransonella* (Hampe & Ivanov 2007a). The second genus, *Barclabornia*, is known by its teeth and a preserved incomplete palatoquadrate from the late Carboniferous to the early Permian of the USA (Zidek *et al.* 2003). The Bransonelliformes are distinct from the Xenacanthiformes by an inverted V-nested pattern of ornamentation on the labial margin of their cusps, labial foramina, and a central lingual foramen (Hampe & Ivanov 2007a). Ecologically, the Bransonelliformes differ from the Xenacanthiformes by occurring in the marine setting (e.g. Ginter *et al.* 2010). While *Bransonella* is interpreted as an analogous of modern catsharks, i.e. small predator feeding on the sea floor, *Barclabornia* possesses very reduced teeth (average height of 2 mm,) compared to the size of its palatoquadrate which reaches up to 45 cm. This size difference evokes a large animal, from 4.5 m to 5 m, and a potential filter feeding ecology like that of the Basking Shark or the Whale Shark (Zidek *et al.* 2003).

1.3.2. Position within the Chondrichthyes

The fossil record of the Xenacanthiformes begins in the lower Tournaisian of Russia with putative remains attributed to ?'*Diplodoselache*' *antiqua* (Lebedev 1996). The oldest clear report of a xenacanthiform is *Diplodoselache woodi* from the Visean of Scotland. *Diplodoselache* is the oldest and the more primitive xenacanthiform to date and its morphology, including its dental pattern, is clearly distinct from other Palaeozoic chondrichthyans. Bransonelliformes appears around the same time during the Visean, so the temporal origin of xenacanthiforms is still unknown.

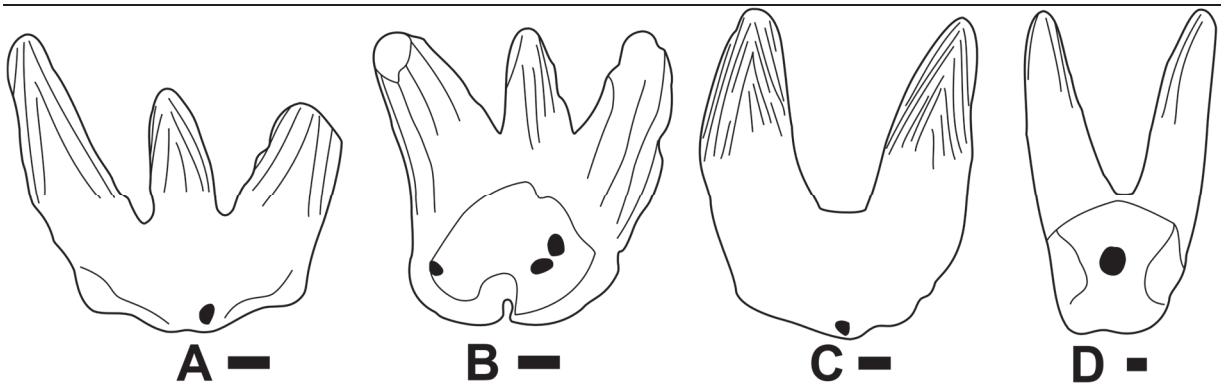

Figure 7. Bransonelliformes teeth. **A-B**, *Bransonella* tooth in labial (**A**) and lingual (**B**) view. **C-D**, *Barclabornia* tooth in labial (**C**) and lingual (**D**) view (modified from Hampe & Ivanov 2007). Scale bar = 0.2 mm.

Several authors have investigated this origin that could have occured during the middle to late Devonian in a group of marine chondrichthyans. Following Ginter (2004), three hypotheses can be considered to explain the origin of Xenacanthiformes (Fig. 8).

The first hypothesis is that of Mader (1986) and Long & Young (1995) who postulated an origin within the Antarctilamniformes or *Leonodus* descendants. It is supported by the very similar dental morphology of these groups, i.e. diplodont, compared to the Xenacanthiformes. This hypothesis minimises the morphological evolution of the teeth restricted to a few modifications of the base. However, Antarctilamniformes or *Leonodus* went extinct by the Frasnian, so potential origin of Xenacanthiformes must take place during the Famennian. The main issue is the absence in the fossil record of transitional form between them and true Xenacanthiformes in the Famennian.

The second hypothesis is an origin within a group of cladodont shark related to the 'Ctenacanthiformes'. The first mentions of this hypothesis were Schaeffer's (1981) work, followed by Young (1982) and Maisey (1984, 2001). The first study to support it with a phylogenetic analysis was that of Coates & Sequeira (2001a), until recent studies that supported close relationships between Xenacanthiforms and 'Ctenacanthiformes' (Coates *et al.* 2017, 2018). This hypothesis is supported by a similar neurocranial morphology between these two groups including a long otico-occipital region, a developed precerebral fontanelle and prominent dorsal otic ridges. However, this implies strong dental modifications to pass from a cladodont patten, i.e. a main central cusp and several smaller lateral ones, to a diplodont pattern with a reduced median cusp and developed lateral ones. This hypothesis supports the fact that, in chondrichthyans, the teeth represent a more adaptive signal than the other parts of the body like the neurocranium which could be a homologous and more conservative structure. However,

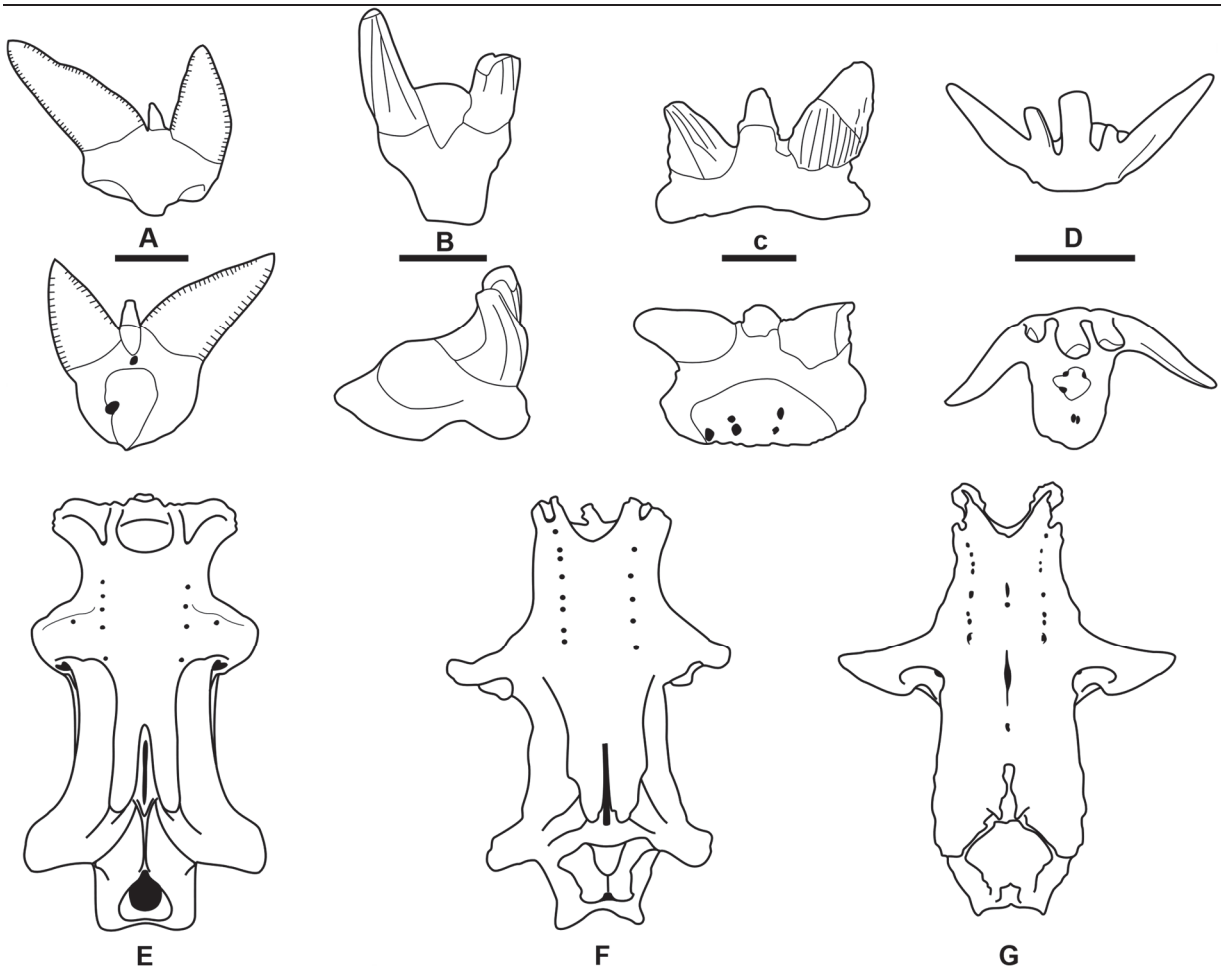

Figure 8. Xenacanthiformes and their potential origins. **A**, *Orthacanthus* tooth., **B**, *Leonodus* tooth. **C**, *Antarctilamna* tooth. **D**, *Phoebodus* tooth. The teeth are in labial view (top) and lingual view (bottom) except *Leonodus* which is in lateral view (bottom). **E**, *Orthacanthus* neurocranium. **F**, *Tamiobatis* neurocranium. **G**, *Cladodoides* neurocranium. The neurocrania are in dorsal view and not to scale (drawings from Ginter *et al.* [2010] for the teeth and from Schaeffer [1981] for the neurocranium). Scale bar = 5 mm, except 3 mm for A.

again, 'Ctenacanthiformes' related to Xenacanthiformes like *Tamiobatis* or *Cladodoides* are restricted to the upper Devonian and no intermediate form between them and Xenacanthiformes has ever been found in the late Devonian or in the early Carboniferous.

The third hypothesis supposes that the origin of Xenacanthiformes could be within the Phoebodontiformes. Phoebodontiformes are known from the Givetian to the end of the Devonian. This hypothesis is supported on dental arguments by Johnson (1979) and Ginter (2004), and in a certain way by Frey *et al.*'s (2019) phylogenetic analysis based on cranial and post-cranial elements. Phoebodontiformes does not possess the diplodont pattern of Xenacanthiformes but exhibits a tricuspid pattern with slender and curved cusps, a slightly

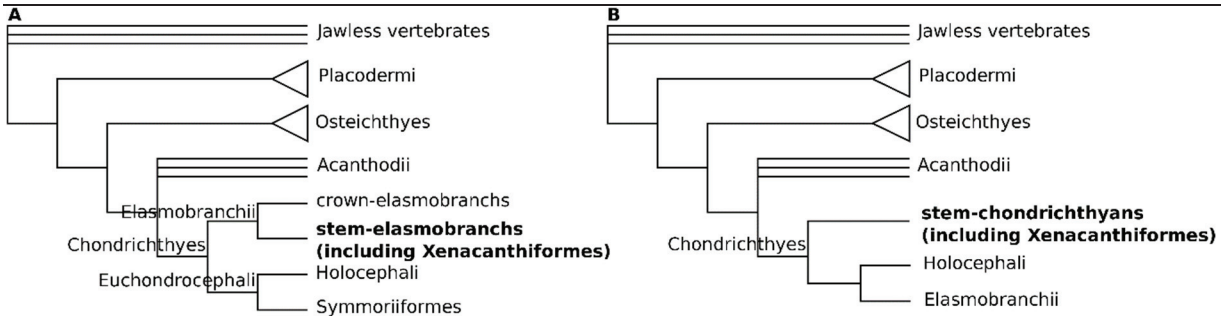

Figure 9. Hypothetical position of Xenacanthiformes within the chondrichthyan relationships. **A**, total group elasmobranch hypothesis. **B**, stem-chondrichthyan hypothesis.

reduced median cusp, a tendency to accessory median cusplets and a lingually developed base. This assumption is supported by the morphological evolution of the tooth base which becomes narrower during the late Devonian and close to a xenacanth-like shape. Even if the crown remains unchanged, this hypothesis is viewed as the most probable by Ginter (2004) to explain the appearance of Xenacanthiformes.

As the origin of Xenacanthiformes is still debated, their position within the Chondrichthyes is also changing (Fig. 9). Recent studies proposed two different hypotheses. On one hand, the Xenacanathiformes are within a total group Elasmobranchii, but not within the crown-elasmobranch (Coates *et al.* 2017, 2018; Frey *et al.* 2019, 2020). On the other hand, they could be out of the crown Chondrichthyes (Ginter *et al.* 2010; Pradel *et al.* 2011; Brazeau *et al.* 2020).

1.4. Palaeobiogeography

1.4.1. Global fossil record

The Xenacanthiformes were widely distributed around the world from the early Carboniferous to the upper Triassic (Fig. 10; e.g. Ginter *et al.* 2010). Fossils were reported in North and South America, Europe, India and Australia. Their top diversity occurred during the Carboniferous-Permian transition in the intra-mountainous basins of the Hercynian Mountain Belt in Europe (e.g. Hampe 2003; Heidtke 2007; Ginter *et al.* 2010). They seem to have disappeared before the Permian-Triassic mass extinction, but they are nevertheless known from the middle to the upper Triassic to finally disappeared during the Norian (e.g. Ginter *et al.* 2010).

Their origin area is difficult to define due to their poor fossil record at the beginning of their evolutionary history. Their oldest report is ?*Diplodoselache antiqua* from the Tournaisian of Russia (Lebedev 1996). However, as early as the Visean, they were present in Europe with

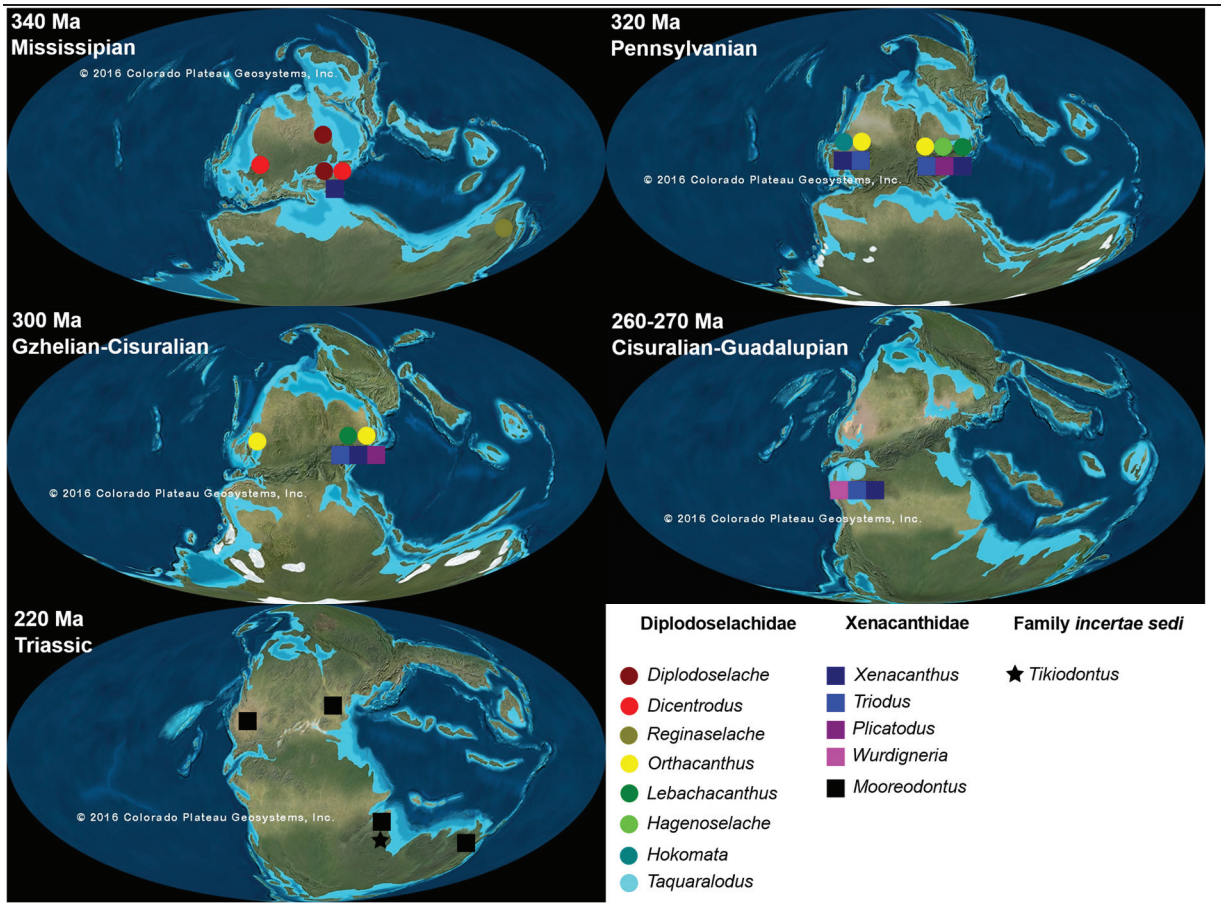

Figure 10. Palaeobiogeography of the Xenacanthiformes through their evolutionary history. Palaeomaps are modified from DeepTimeMaps™ (Colorado Plateau Geosystems, Inc., 2020).

Diplodoselache woodi (Dick 1981), in North America and Europe with *Dicentrodus* sp. (Hampe *et al.* 2006) and in Australia with *Reginaselache morrisi* (Turner & Burrow 2011). So, during the Tournaisian-Visean transition, even if their generic and specific diversity were not at their highest level, the Xenacanthiformes spread all around the world with a first diversification event of the basal Diplodoselachidae.

Their diversity remained low during the Mississippian with the presence in Europe of the genera *Diplodoselache* and *Xenacanthus* that is the first Xenacanthidae to appear (e.g. Hampe 2003), *Dicentrodus* in Europe and North America and *Reginaselache* in Australia. Their diversity increased quickly during the Pennsylvanian with the appearance of the genera *Orthacanthus*, *Triodus*, *Lebachacanthus*, *Plicatodus* and *Hagenoselache* (e.g. Fritsch 1879, 1889; Hampe 2003; Hampe & Heidtke 1997) in Europe and *Hokomata* in North America (Hodnett & Elliott 2018), while at the same time, the typical Mississippian genera *Diplodoselache*, *Dicentrodus* and *Reginaselache* disappear. Above all, the Pennsylvanian was a period of intense specific diversification for numerous genera, especially in Europe. The

genus *Orthacanthus* was represented by seven species in Europe and three species in North America, the genus *Xenacanthus* by seven species in Europe and one in North America, the genus *Triodus* with four species in Europe and one in North America (see Ginter *et al.* [2010] for the detailed specific list).

The Carboniferous-Permian transition was a time of generic turn over for the European Xenacanthiformes. The large *Orthacanthus* and *Lebachacanthus* almost disappeared with a single surviving species respectively. They disappeared at the Asselian/Sakmarian limit. *A contrario*, the genus *Triodus* performed a diversification event with the appearance of seven species during the Asselian (see Pauliv *et al.* [2017] for its distribution). The genus *Xenacanthus* remains poorly diversified in North America with one species (Johnson 1999) but maintains its specific diversity in Europe with four species (e.g. Ginter *et al.* 2010). At the same time, the genus *Plicatodus* (Fritsch 1879; Hampe 1995), appeared in the late Carboniferous with *P. plicatus* and the genus passed through the Carboniferous-Permian limit with the sole early Permian species *P. jordani* which quickly became extinct.

Interestingly, the great specific diversity of the European Xenacanthidae ends in the middle lower Permian. The genera *Xenacanthus* and *Triodus* disappear in the Sakmarian and Artinskian respectively. However, they survived in South America with *T. richterae* (Pauliv *et al.* 2017) and at least three potential *Xenacanthus* species (Ragonha 1984). Unfortunately, the latter were not published in peer-review journals, so it is hard to assess their systematic status. At the end of the lower Permian, the genera *Taquaralodus* (Chahud *et al.* 2010) and *Wurdigneria* (Richter 2005) appeared in Brazil. *Wurdigneria* and *Triodus* are the only xenacanthiforms reported in the Guadalupian and became extinct at the end of the Capitanian in South America.

No Xenacanthiformes is known in the Lopingian and the lower Triassic. Surprisingly, the order appears again in the fossil record during the middle Triassic with the genus *Tikiodontus* (Bhat *et al.* 2018) in India and especially *Mooreodontus*, initially identified as belonging to *Xenacanthus* (Woodward 1889), which is present in North America, Australia, India, and Europe (Ginter *et al.* 2010). While the group was mainly restricted to the intertropical belt from the Carboniferous to the middle Permian, Triassic representatives seems to colonise temperate regions of the southern hemisphere. This apparent diversification event could be more important because *Mooreodontus* has been extremely widely distributed around the world from the middle to upper Triassic. This genus could be a stratigraphic genus and the *Mooreodontus* species from different geographic areas could in fact belong to different genus.

The Xenacanthiformes became definitively extinct during the Norian before the Triassic-Jurassic mass extinction.

1.4.2. European Carboniferous-Permian record

The fossil record of the Xenacanthiformes in Europe covers all their evolutionary history from their earliest record with ?*Diplodoselache antiqua* of the Tournaisian of Russia to *Mooreodontus moorei* from the Carnian and Norian of the United Kingdom and Germany. It is in the Carboniferous-Permian intra-mountainous basins of the Hercynian Mountain Belt that the Xenacanthiformes reached their maximum diversity with the co-occurrence of five genera which are *Orthacanthus*, *Lebachacanthus*, *Xenacanthus*, *Triodus* and *Plicatodus* (Fig. 11).

As previously written, the fossil record of *Plicatodus* (e.g. Hampe 1995; Ginter *et al.* 2010) is restricted to the Kasimovian of Bohemia, Czech Republic (*P. plicatus*) and the Asselian of the Saar-Nahe Basin, Germany (*P. jordani*). *Lebachacanthus* (Heidtke 1998, 2007) is not widely distributed with *L. ventricosus* from the Moscovian-Kasimovian of Bohemia and *L. senckenbergianus* from the Kasimovian to the Asselian of the Saar-Nahe Basin. For the latter, Heidtke (2007) proposed to split *L. senckenbergianus* into three species (*L. senckenbergianus*, *L. pollichiae* and *L. colosseus*) based on morphometric differences of the palatoquadrate and the dorsal spine. Whether these species represent taxonomic or stratigraphic species, the diversity of this genus is restricted in space and time.

The genera *Orthacanthus*, *Xenacanthus* and *Triodus* represent most of the European Carboniferous-Permian diversity of Xenacanthiformes. *Orthacanthus* (see Ginter *et al.* [2010] for the list and age of the European species) appears in the Bashkirian of the United Kingdom (*O. denticulatus* and *O. cylindricus*) before to spread in Bohemia (*O. kounoviensis* and *O. bohemicus*), in the Saar-Nahe Basin, Germany (*O. kounoviensis* and *O. gracilis*), in the Puertollano Basin, Spain (*O. meridionalis*) and maybe in the Autun Basin, France (*O. commailli*). During the Carboniferous-Permian transition, almost all the species disappeared, the only survivor was *O. buxieri* (if this species is valid and not a junior synonym of *O. kounoviensis*; see the Systematic Reassessment section) in the Asselian-Sakmarian of the Bourbon-l'Archambault, France.

The European Xenacanthidae survived longer than the Diplodoselachidae. The genus *Triodus* (see Pauliv *et al.* [2017] for a stratigraphic occurrence of the European species) appeared in the Bashkirian-Moscovian of the United Kingdom (*T. serratus*) and spread in the Moscovian of Russia (*T. teberdaensis*), in the Kasimovian-Gzhelian of Saar-Nahe Basin (*T. lauterensis* and *T. palatinus*) and in the Gzhelian of Austria (*Triodus* sp. ZÖ). Contrary to

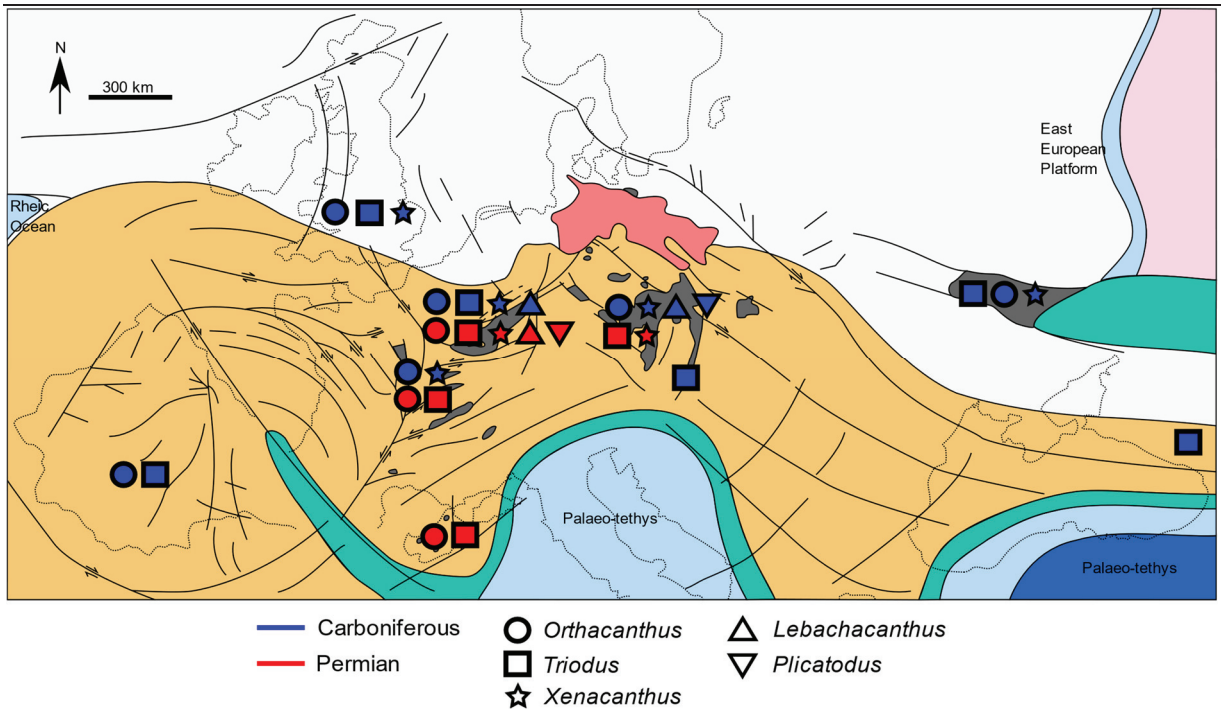

Figure 11. Palaeobiogeography of the European Xenacanthiformes from the Late Carboniferous (Pennsylvanian) to the early Permian (Cisuralian). See the figure 25 for the caption of the geological map (modified from Roscher & Schneider 2006).

Orthacanthus, the Carboniferous-Permian transition was a period of intense diversification with the occurrence of many species in the earliest Permian: in the Asselian of the Autun Basin (*T.* ?*frossardi*), the Asselian of the Saar-Nahe Basin (*T. palatinus*, *T. sessilis*, *T. obscurus*), the Asselian-Artinskian of the Saar-Nahe Basin (*T. kraetschmeri*).

The genus *Xenacanthus* (see Ginter *et al.* [2010] for the list and age of the European species) appeared in the late Mississippian of the United Kingdom (*X. elegans*) and diversified in the Bashkirian-Moscovian with *X. laevissimus* and *X. tenuis*. It spread in the other European basins in the Moscovian-Kasimovian of Bohemia (*X. parallelus*) in the Kasimovian-Gzhelian of the Commentry Basin, France (*X. gaudryi*), in the Gzhelian-Asselian of the Saar-Nahe Basin (*X. meisenheimensis* and *X. remigiusbergensis*), in the Asselian of the Saar-Nahe Basin (*X. humbergensis*) and in the Asselian-Sakmarian of Bohemia (*X. oelbergensis*).

The genera *Orthacanthus*, *Xenacanthus* and *Triodus* seem to appear in the early Pennsylvanian of the United Kingdom before to spread in numerous basins during the Pennsylvanian and are finally restricted to Western and Central Europe in the lower Permian. Remains of these three genera unidentified at the specific level are also known in the Carboniferous of Ukraine and in the Permian of Italy (e.g. Fischer *et al.* 2013). The distribution through space and time could be interpreted as resulting from the tectonic history of the intra-

mountainous basins during the Carboniferous-Permian transition (see Schneider [1996] for the detailed hypothesis of the distribution of European Carboniferous-Permian chondrichthyans). In the Carboniferous, the European basins could be connected by wide systems of lakes and river-channels. The latter have allowed the migration of the Xenacanthiformes from the Northern to the Western and Eastern basins. At the Carboniferous-Permian transition, the Francovian movements could have broken the inter-basin connections. The large Xenacanthiformes like *Orthacanthus* and *Lebachacanthus* were greatly affected and nearly disappeared in the lower Permian due to the fractionation of their environment. Smaller genus like *Xenacanthus* and especially *Triodus* were more adaptative by performing rapid speciations in the basins where they were present. However, even them did not survive longer and became extinct at the end of the Cisuralian. The reason of this first extinction in the European fossil record could be related to environment changes like the increase of the aridity during the middle and upper Permian (DiMichele & Phillips 1996). The origin of the Triassic xenacanthiform *Mooreodontus* from the Carnian of the United Kingdom and Germany (*M. moorei*) remains obscure. It is still hard to understand the real relationships with the North American, Indian and Australian species.

1.5. Palaeoecology

1.5.1. Historical hypothesis: strict freshwater adaptation

Xenacanthiformes were historically considered as chondrichthyans fully adapted to freshwater environment (e.g. Zangerl 1981). Indeed, their fossils are always found in non-marine sediments, even if pure freshwater environment is difficult to identify in the fossil record (Gray 1988; Schultze 2009). The rare cases where xenacanthiforms were found in putative marine environment are highly questionable. For example, two species of the genus *Triodus*, *T. elpia* (Johnson & Thayer 2009) and *T. teberdaensis* (Hampe & Ivanov 2007b) were supposedly found in marine sediments. However, for *T. elpia*, the co-occurrence of a typically freshwater lepospondyl amphibian makes this interpretation uncertain (Pauliv *et al.* 2017). For *T. teberdaensis*, the marine sediments of the Tolstiy Bugor Formation, Russia where it was found could be subjected to reworking or the teeth could have also been transported from freshwater to marine setting (Pauliv *et al.* 2017).

Anatomical arguments are in favour of a freshwater habitat for the xenacanthiforms. The morphological adaptation of the global body shape, e.g. short and broad fins and elongated body, does not evoke animals adapted to open marine environments but to more closed environments such as lakes and river-channels. Furthermore, Xenacanthiformes are supposed

to live in low oxygenised waters thanks to either low oxygen level tolerance or accessory airbreathing apparatus (Compagno 1990). In any case, low oxygenised waters are more likely to happen in freshwater than in marine environment (Compagno 1990).

The Xenacanthiformes are supposed to be fully adapted to freshwater setting, i.e. they spent all their lifespan in this environment. This assumption is supported by the presumed association of Xenacanthiformes with the egg capsule morphotype *Fayolia* (e.g. Renault & Zeiller 1888; Pruvost 1919, 1930; Fischer & Kogan 2008; Fischer *et al.* 2014a). This association is found from the lower Permian of the Saar-Nahe Basin (Heidtke 2007), in which the xenacanths are known since the late Carboniferous, to the middle-late Triassic of Madygen Formation, Kyrgyzstan (Fischer *et al.* 2011). This large stratigraphic occurrence implies a conservative ecology along their evolutionary history.

To assess the palaeoecology of the Xenacanthiformes, studies based on geochemical analyses of their teeth have been performed. The analyses concern two areas of two different ages, i.e. the early-middle Permian of southwestern USA (Fischer *et al.* 2014b) the late Carboniferous to early Permian of Western, Central and Eastern Europe (Fischer *et al.* 2013). In both analyses, the oxygen and strontium isotope compositions of their teeth postulated a freshwater environment for the xenacanthiforms, punctuated by evaporation events. This agrees with the previous palaeoecological assumption regarding their low oxygen tolerance.

1.5.2. Reinterpretation of the xenacanth palaeoecology: potential saltwater tolerance

Even if the historical hypothesis of a strict freshwater palaeoecology is supported by various arguments, a saltwater tolerance and potential migrations into the marine setting were also proposed for the Xenacanthiformes.

Firstly, a fully and strict adaptation to the freshwater environment is not common among the modern elasmobranchs (e.g. Helfman *et al.* 1997). Today, approximatively 5% of all elasmobranch species are reported to live in freshwater and brackish environments, with a small proportion which is exclusively freshwater adapted (Martin 2005). This represents four families, ten genera and 43 species, with only one subfamily, i.e. Potamotrygoninae, exclusively adapted to fresh waters (Carpenter *et al.* 2011). The reason to explain this distribution is the way the elasmobranchs perform osmoregulation. In the marine setting, they maintain osmotic status at a hyperosmotic level compared to seawater by urea retention. In a freshwater environment, they synthesise urea to counteract water absorption (Carpenter *et al.* 2011). This metabolism could be conservative through the elasmobranch evolutionary history, so also present in the xenacanthiforms if they are included within the Elasmobranchii. However, this

hypothesis could be criticised by the ambiguous position of the Xenacanthiformes among the chondrichthyans.

Studies on the dorsal spine growth pattern of Xenacanthiformes were the first to propose a partial to fully marine lifestyle based on direct biological arguments. In fact, the growth lines seem to be regularly deposited, so influenced by a monthly to seasonal cyclical pattern like the tides in a full marine to marine influenced environment (Soler-Gijón 1999). Furthermore, according to the number of major growth lines, so to different ontogenetic stages, *Orthacanthus platypternus* from the lower Permian of the USA is found in different environments (e.g. Beck *et al.* 2016): the smaller individuals come from shallow water (ponds and stream channels) whereas the larger specimens are found in marine limestones representing estuarine-lagoonal near-shore conditions. The distribution of assumed juveniles and adults in different environments, including marine influenced ones, contradict the full freshwater adaptation. In addition, sedimentological marine indicators in some supposedly freshwater basins containing xenacanthiforms have also been found. For example, in the Saar-Nahe Basin, marine bands with glauconite have been recognised as shark-bearing units (Krätschmer & Forst 2005; Schultze 2009).

Numerous basins, in which Xenacanthiformes are found, have ambiguous environmental records which do not exclude possible marine influences. For example, in the late Carboniferous Puertollano Basin (Spain; Soler-Gijón 1999) and Montceau-les-Mines (France; e.g. Schultze 2009), the presence of acritarchs seems to favour a marine influenced environment. In the Jogging Formation, Nova Scotia, Canada, the palaeoenvironment, firstly considered as freshwater, could correspond to brackish setting. Indeed, the presence of the stenohaline bivalve *Curvirimula*, brachiopods and echinoids indicate a marine palaeoenvironment (e.g. Falcon-Lang *et al.* 2006; Grey *et al.* 2011).

2. X-ray computed microtomography

2.1. How to explore the hidden anatomy of fossils?

Anatomical descriptions of fossils are traditionally made after mechanical or chemical preparation in order to extract them from their rock matrix (see Janvier 1996). However, in some cases, this preparation is limited or impossible due to the host sediment and fossil nature. In the present work, the fossils are preserved in oil-shale plates (see the Geological context section), a rock matrix that prevents any safe mechanical or chemical preparation, i.e. without risking a deterioration of the fossils. This fact is highly problematic with historical specimens

found in the 19th century (see the Material and Methods and Systematic Reassessment sections) and designed as holotypes: their true internal and external anatomy remains unavailable.

To overcome this issue, internal anatomy of fossil organisms was traditionally investigated thanks to the Solla's method of grinding sections (e.g. Stensiö 1927; Jarvik 1980). Important findings were made, e.g. the internal anatomy of osteostraceans (see Janvier 1996), but this destructive method requires species with an abundant material.

To avoid the destruction of fossils caused by the grinding sections method, the X-ray computed microtomography (µCT scan) was used to reassess the anatomy and systematics of historical species from the Carboniferous-Permian basins of the Northern Massif central for which the available material is limited to a few specimens. In fact, this technique allows to explore the internal anatomy, to access the hidden external anatomy without altering the physical integrity of the specimens and to share 3D reconstructions of the historical specimens with usual little visibility.

In the next paragraphs, the physical and experimental principles of the µCT scan will be explained. Then, some examples of the contributions of this technique to the study of Palaeozoic chondrichthyans will be presented to highlight the potential anatomical updates that could be acquired from the investigated specimens.

2.2. Principles of X-ray computed microtomography

µCT scan uses the ability of X-rays to pass through a large range of materials. Consequently, they allow to characterise the density of the penetrated material. It was Wilhelm Röntgen who discovered the X-rays (Röntgen 1896) and offered the possibility of visualising inner structures without the destruction of the analysed material.

2.2.1. Acquisition of data

The experimental device (Fig. 12) is composed of an X-ray source, a scintillator that converts X-rays to visible light, and a photodetector that records the visible light: a mirror reflects the light, and a lens focuses and magnifies it towards a camera. A computer allows to visualise the collected data. The acquisition phase consists of making multiple 2D radiographs of the specimen. To do this, X-rays pass through the specimen under different angular positions from 0 to 360°. Depending on the size of the specimen or that of the CT scan, the specimen or the X-ray source rotates.

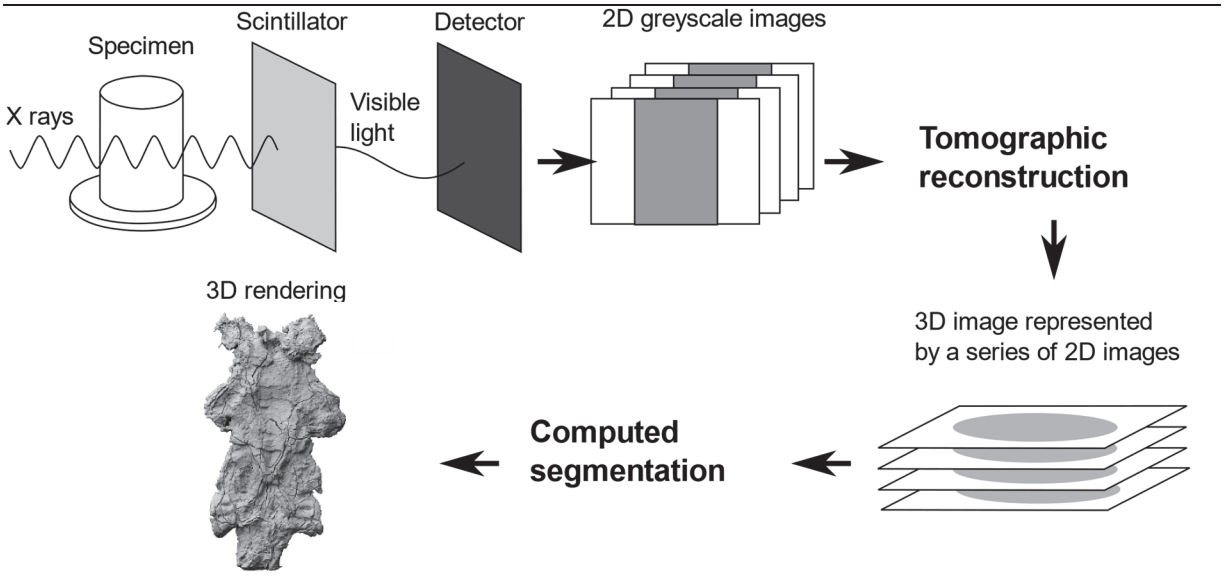

Figure 12. Schematic X-ray computed microtomography experimental device (modified from Landis & Keane 2010).

The microtomographic images are in greyscale mode and represent the X-ray absorption by the specimen materials. Usually, black areas represent no absorption, e.g. the air around the specimen, and white areas are those in which X-ray absorption is the highest. The X-ray absorption coefficient (Equation 1) increases with the thickness and density of the specimen and is defined by the Beer-Lambert's law for homogenous material:

Equation 1: $I = I_0 \times e^{-\mu x}$

With μ an image, I_0 the monochromatic intensity of the used beam, I the resulting attenuated intensity and x the thickness of the object.

Fossils are heterogenous material: the fossil density is expected to be different from that of the surrounding rock matrix. In this case, the Beer-Lambert's law (Equation 2) is:

Equation 2: $I = I_0 \times e^{-\int_0^L \mu(x)dx}$

With, in each coordinate [*0-L*] of the image μ, dx the thickness of the different materials.

2.2.2. Tomographic reconstruction

The tomographic reconstruction consists of generating a 3D image from a stack of 2D radiographs. The image resolution is expressed in voxel (Foley *et al.* 1996), which represents a

value on a regular grid in three-dimensional space. It is the pixel equivalent for 3D images which is typically between 30 and 100 µm for macroscopic palaeontological specimens. The voxel size depends on the way the detector magnifies the visible light and the size of its components.

The used X-ray beam is not perfectly homogenous due to imperfections within the different components of the experimental device (Moreau 2017). Consequently, artifacts that do not reflect the real inner structure of the fossils can appear. In order to minimise them, the 2D radiographs are corrected prior to any other treatment. The resulting images are called "flat flied" and are made from the 2D radiographs (raw images with the specimen and the X-ray beam), reference images (raw images without the specimen and with the X-ray beam) and black images (raw image without the specimen and the X-ray beam) (Moreau 2017). The reference images allow to correct the X-ray beam fluctuations and scintillator imperfections and the black images remove the imperfections of the camera (Moreau 2017). The correction consists of a logarithmic function (Equation 3):

Equation 3: $Flatflied = -ln\left\{\frac{[radiographs - blackimages]}{[referenceimages - blackimages]}\right\}$

The final step is the 3D reconstruction. Segmentation and 3D rendering are available from various computed programs. The two used in this work are Avizo v. 7.0 (© Thermo Fisher Scientific, Waltham, Massachusetts, USA) and MIMICS v. 20.0 software (© Materialise Inc. NV, Leuven, Belgium).

The µCT scan is a powerful tool to investigate the fossil inner structures without deteriorating them. However, as it was already mentioned concerning the needed corrections of raw data, several artifacts and limits of this method exist (e.g. Wils 2020). Something that cannot be predicted or corrected is the lack of difference in density between the fossil and its rock matrix. In this case, the X-ray absorption of the fossil and the matrix are equivalent, producing low-contrast 2D radiographs in which the limit between these materials is indefinable. Segmentation and 3D rendering are therefore impossible. Also, metallic structures or metal-enriched materials are highly absorbent and can affect the X-ray absorption of the nearby fossil. The latter could not be as visible as expected. Finally, the movement of the specimen caused by the scanner vibrations during the acquisition phase can duplicate the limit of the inner structures.

2.3. Application to the study of fossil chondrichthyans

μCT scan has been widely used in the field of palaeontological studies since the first 3D reconstruction of the therapsid *Thrinaxodon* by Rowe *et al.* (1992). Without establishing an exhaustive list of all the palaeontological publications that incorporated 3D models in their results, it could be interesting to note the contributions of this technique to certain studies of Palaeozoic chondrichthyans and their relatives to underline what can be expected in the present study on Xenacanthiformes.

2.3.1. Hidden anatomical parts of known species

Several Palaeozoic chondrichthyan species were discovered prior to the development of μCT scan in geological and biological studies. For example, the description of the upper Devonian 'ctenacanthiform' *Cladodoides wildungensis* (Jaekel, 1921) was for a long time restricted to its external and partly visible anatomy, mainly included in rock matrix. Maisey (2001) attempted to decipher its complete anatomy using CT scan and to describe its hidden inner anatomical parts. It was a few years later (Maisey 2005) that a detailed 3D rendering of *C. widungensis* was proposed with more detailed description of its inner neurocranial structures (Fig. 13).

Doliodus problematicus (Woodward, 1892) from the lower Devonian was first identified as a primitive chondrichthyan by teeth and then by an articulated specimen showing the neurocranium, the jaws and pectoral fins (Miller *et al.* 2003). The reconstruction of its braincase by Ginter & Maisey (2007) nuanced its phylogenetical position and questioned its chondrichthyan status. Contributions of μCT scan allowed the latest studies (e.g. Brazeau *et al.* 2020; Frey *et al.* 2020) to recover it as a stem-chondrichthyan.

2.3.2. μCT scan and the Palaeozoic chondrichthyan phylogeny

Since the first studies that have investigated the phylogenetic relationships of the Palaeozoic chondrichthyans, numerous hypothetic relationships were proposed. The latest phylogenies are different from the first ones in term of robustness. A way to understand this is the use of the μCT scan.

Before the use of the μCT scan, the phylogenetic studies on the Palaeozoic chondrichthyans included a few taxa. For example, Schaeffer (1981) only considered nine taxa, Maisey (1985) four taxa and Lund & Grogan (1997) 31 taxa. A first contributions of the μCT scan was the possibility to include a larger number of taxa. For example, in the latest studies, (Coates *et al.* (2018) considered 86 taxa and Frey *et al.* (2019, 2020) 60 and 63 respectively.

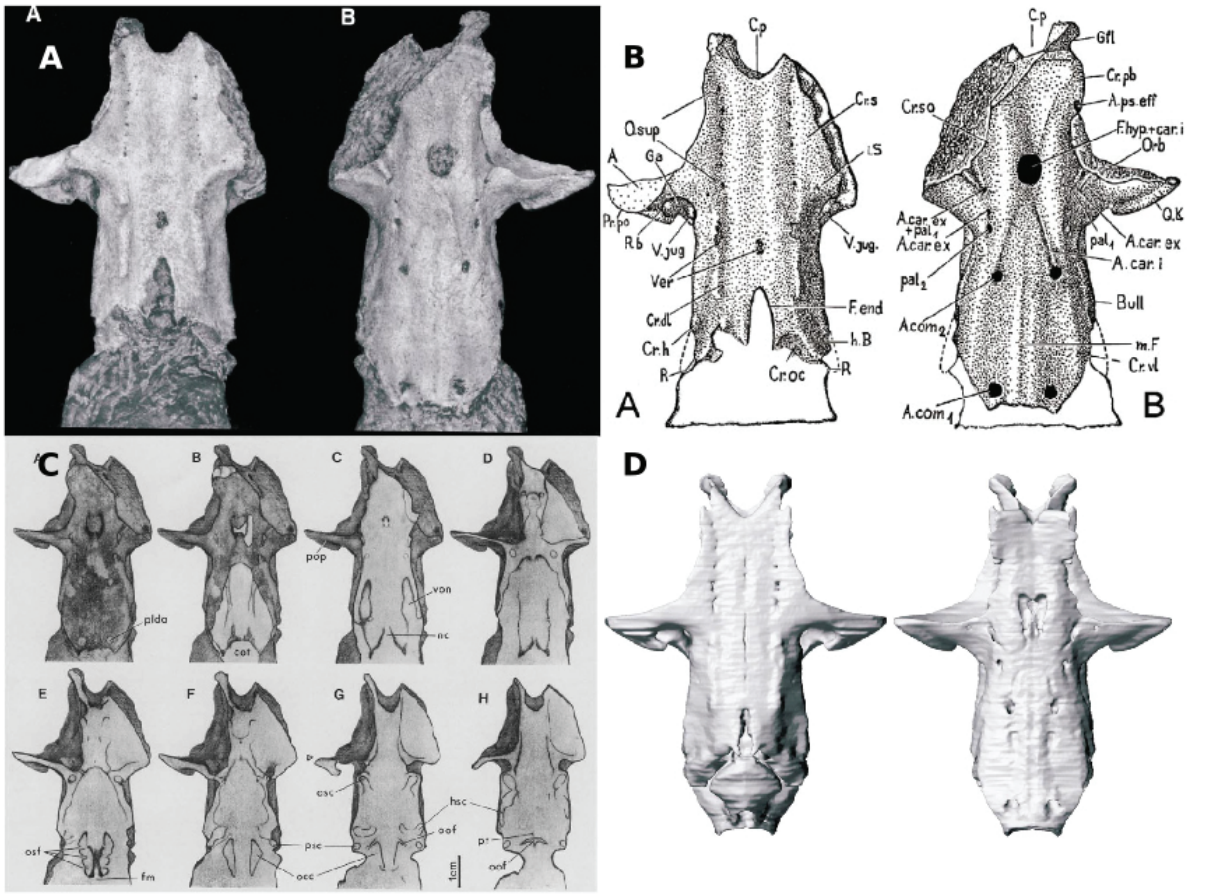

Figure 13. Evolution of the descriptions and illustrations of *Cladodoides wildungensis*. **A**, Photograph of the holotype (Maisey 2005). **B**, Reproduction of the original drawing of Gross (1937) (Maisey 2005). **C**, CT scan slides of the braincase (Maisey 2001). **D**, 3D renderings of the braincase (Maisey 2005). For **A**, **B** and **D** the dorsal view is left and ventral view is right.

The inclusion of additional taxa was possible thanks to the redescription of some species like *Gladbachus adentatus* Heidtke & Krätschmer, 2001 in which the Meckel's cartilage and the branchial region have not been described until the use of µCT scan. Another example is the Symmoriiformes that was only recently included within phylogenetic analyses. Numerous studies have allowed to describe their external (Maisey 2007; Pradel *et al.* 2011; Coates *et al.* 2017; Frey *et al.* 2019, 2020) and internal (Maisey 2007; Coates *et al.* 2017; Frey *et al.* 2019) anatomy.

With the multiplication of used taxa comes the multiplication of used characters. Prior to the use of the µCT scan, character matrices did not provide a large number of characters to discuss. For example, Schaeffer (1981) used 20 characters, Maisey (1985) 23 ones. Only Lund & Grogan (1997) performed an analysis with 92 characters on the cranial and post-cranial regions. Recently, phylogenetic analyses are routinely performed with more than 200

characters. For example, Coates *et al.* (2018) used 262 characters and Frey *et al.* (2019, 2020) 221 and 230 respectively. This character multiplication was possible thanks to the µCT scan that allowed to access numerous internal characters, inaccessible prior to the use of this technique. For example, the number of neurocranial characters increases from 11 out of 92 characters (~12%) in the Lund & Grogan (1997) matrix to 92 out of 262 (~35%) in Coates *et al.* (2018).

2.3.3. Palaeoecology

Another contribution of the use of the µCT scan is the inference of palaeoecology of Palaeozoic chondrichthyans. For example, in the phoebodontiform *Phoebodus saidselachus* Frey *et al.,* 2019, the description of the palatoquadrate and Meckel's cartilage concluded to a low bite force and a swift snapping feeding strategy close to that of the garpike (Frey *et al.* 2019). Exceptional braincase and brain preservation are also useful structures to infer the ecology. For example, Pradel *et al.* (2010) described the brain morphology of a sibyrhynchid Iniopterygian. The morphology of the small cerebellum, the enlarged mesencephalon and the horizontal semicircular canals suggest slow bottom-dweller ecology.

2.4. Potential contributions to the systematic reassessment of the chondrichthyans from the Carboniferous-Permian basins of the Northern Massif central

The potential contributions of the use of the µCT scan to the study of Palaeozoic chondrichthyans cover the description of the hidden anatomy as well as the resolution of phylogenetic relationships and palaeoecology inferences. Among the studied material of this work (see the Material and Methods and Systematic Reassessment sections), several specimens are type material of historical species. However, all of them are barely prepared and only a few parts of their anatomy are visible and describable. The µCT scan allows to reconstruct in three dimensions theses fossils and to fully describe them for the first time.

Their complete revised descriptions are applied to decipher the relationships of the Xenacanthiformes among the Chondrichthyes. In fact, the scanned specimens are isolated neurocrania and this anatomical structure was recently widely used to propose new relationships, e.g. between Xenacanthiformes and 'Ctenacanthiformes'. As in numerous studies (see the previous paragraphs on the contributions of the µCT scan to the chondrichthyan phylogeny), the µCT scan allows to identify new potential characters to propose new phylogenetic hypotheses.

3. Stable isotope geochemistry

Reconstructing the palaeoecology and palaeoenvironment of the xenacanthiforms from the Carboniferous-Permian basins of the Northern Massif central is one of the main objectives of this thesis. To do this, a geochemical analysis on the xenacanth dorsal spines and skeletal remains of the associated vertebrate fauna was carried out. This chapter introduces classical concepts of stable isotope geochemistry needed to perform a justified palaeoecological and palaeoenvironmental reconstructions.

3.1. Overview

3.1.1. Stable isotopes

The non-radioactive forms of atoms are called stable isotopes. The elements used in this work are oxygen, carbon and sulfur. Oxygen possesses three stable isotopes which are ^{16}O, ^{17}O and ^{18}O. For the carbon, they are ^{12}C and ^{13}C, and for the sulfur they are ^{32}S, ^{33}S, ^{34}S, ^{35}S and ^{36}S. For each of them, it is the lighter isotope, i.e. ^{16}O, ^{12}C and ^{32}S, that are the most abundant.

3.1.2. The delta notation δ

Inorganic and organic materials possess various proportions of stable isotopes which do not vary over the geological scale. The difference in isotopic ratio between several material is of the order of 10^{-4} to 10^{-5}, so a particular notation has been proposed to express them more conveniently: the delta notation (δ) (McKinney *et al.* 1950). This notation expresses isotopic ratio between the sample (sam) and that of an international standard (std) and is expressed in per mil (‰). In order to investigate the isotopic composition of the oxygen, carbon and sulfur content of the studied fossils, the following delta notation (δ, Equation 4) is considered:

Equation 4: $$\delta X^*_{sam}(‰) = \frac{\frac{X^*}{X}sam - \frac{X^*}{X}std}{\frac{X^*}{X}std} \times 1000$$

With *X** the number of heavy isotope and *X* the number of light one of a same element.

3.1.3. Isotopic fractionation

The isotopic fractionation is the mechanism during which two materials in contact with two different isotopic compositions exchange isotopes (Urey 1947). Consequently, after the exchange, the δ of each material will change: if one material is enriched in heavy isotope, so the other will be depleted. For two material *A* and *B*, if *a* and *b* are the stoichiometry coefficients and *1* and *2* the light and heavy isotopes respectively, the isotopic exchange (Equation 5) is:

Equation 5: $aA_1 + bB_2 = aA_2 + bB_1$

The equilibrium constant K (Equation 6) occurs when this exchange is under equilibrium conditions and is written:

Equation 6: $K = \frac{(A_2)^a (B_1)^b}{(A_1)^a (B_2)^b} = \frac{\left(\frac{A_2}{A_1}\right)^a}{\left(\frac{B_2}{B_1}\right)^b}$

This equilibrium constant depends on the equilibrium temperature and is correlated (Equation 7) with the fractionation factor α with n the number of exchanged atoms:

Equation 7: $\alpha = K^{\frac{1}{n}}$

If n=1, for a determined temperature, the fractionation factor (Equation 8) can be written as:

Equation 8: $\alpha_{A-B} = \frac{R_A}{R_B} = \frac{\left(\frac{X}{X}\right)A}{\left(\frac{X}{X}\right)B} = \frac{1000+\delta_A}{1000+\delta_B}$

The isotopic fractionation can be approximated to the following equation (Equation 9) if the difference between δ_A and δ_B does not exceed 10 (Criss 1999):

Equation 9: $1000 \times ln\alpha_{A-B} \approx \delta_A - \delta_B$

3.1.4. International standards

The measured oxygen, carbon and sulfur isotopic compositions of the fossil samples are not directly interpretable because they are relative measurements and must be calibrated against international standards which differ from one isotopic system to another.

The original standard for the $\delta^{18}O$ (isotopic ratio between ^{18}O and ^{16}O in a sample following the Equation 4) was the SMOW (Standard Mean Ocean Water) which correspond to the mean isotopic ratio of marine water. It was sampled far from the coast at depths between 500 and 2000 m in the Pacific, Atlantic and Indian Oceans (Craig 1961). It has been replaced by the V-SMOW (Vienna – Standard Mean Ocean Water) which is a water produced by the

IAEA (International Atomic Energy Agency) and which approximates the oxygen isotope ratio of the original SMOW. Its oxygen composition is defined as containing 99.76206% of ^{16}O, 0.03790% of ^{17}O and 0.020004% of ^{18}O. Consequently, the $^{18}O/^{16}O$ ratio is 0.00020052 (Baertschi 1976; Li *et al.* 1988).

The original standard for the $\delta^{13}C$ (isotopic ratio between ^{13}C and ^{12}C in a sample following the Equation 4) is the PDB (PeeDee Belemnite) which correspond to the carbon content of the calcium carbonate of a belemnite rostrum from the Cretaceous PeeDee Formation (South Carolina, USA) (Gonfiantini *et al.* 1995; Sharp 2007). As there is no more available material, it has been replaced by the V-PDB (Vienna – PeeDee Belemnite). The V-PDB is defined by the NBS-19 standard with a $^{13}C/^{12}C$ ratio of 0,0112372 close to the that of the PDB (less than 0.01‰ difference; Craig 1957).

The original standard for the $\delta^{34}S$ (isotopic ratio between ^{34}S and ^{32}S in a sample following the Equation 4) is the CDT (Canon Diablo Troilite) which correspond to a meteoritic sulfide sulfur (MacNamara & Thode 1950). As the $\delta^{34}S$ of this material is variable up to 0.4‰, it has been replaced by the V-CDT (Vienna – Canon Diablo Troilite) with the IAEA-S-1 standard which is a silver sulfide and whose $\delta^{34}S$ is -0.3‰ (IAEA 2020). The $^{32}S/^{34}S$ ration of the V-CDT is 22.6504 +/- 0.0020 (IAEA 2020).

The measured oxygen, carbon and sulfur isotopic compositions of the fossil samples were calibrated against other internal standards which are calibrated against these international standards. The corresponding table (Table 1) resumes them for the different considered isotopic systems and analyses.

The concepts of stable isotopes, delta notation and isotopic fractionation being introduced, the focus will be on the three isotopic systems used in this work: oxygen, carbon and sulfur. These elements come from the environment in which there are several parameters of variations. Then, some isotopic fractionation can occur when they are incorporated into the organisms.

Consequently, for each isotopic system, the environmental variations of the relative abundance of the stable isotopes are listed, then how they are incorporated in the vertebrate tissues and finally the fractionation equations needed to reconstruct the environment and ecology are presented.

Table 1. Used internal standards in this work (values are from (Hut, 1987; Lécuyer *et al.* 1993; IAEA 2020).

Standard	Description	Isotopes	δ (‰)	Applications
NBS-120c	Natural phosphorite	$^{18}O/^{16}O$	$21.7_{V\text{-}SMOW}$	Phosphate
NBS-127	Barium sulfate	$^{18}O/^{16}O$	$9.3_{V\text{-}SMOW}$	Phosphate
Carrara Marble	Calcite	$^{18}O/^{16}O$ and $^{13}C/^{12}C$	$-1.84_{V\text{-}PDB}$ and $2.03_{V\text{-}PDB}$	Carbonate
NBS-18	Calcite	$^{18}O/^{16}O$ and $^{13}C/^{12}C$	$-23.2_{V\text{-}PDB}$ and $-5.01_{V\text{-}PDB}$	Carbonate
IAEA-S-2	Silver sulfide	$^{34}S/^{32}S$	$22.62_{V\text{-}CDT}$	Sulfur
IAEA-SO-5	Barium sulfate	$^{34}S/^{32}S$	$0.5_{V\text{-}CDT}$	Sulfur
IAEA-SO-6	Barium sulfate	$^{34}S/^{32}S$	$-34.1_{V\text{-}CDT}$	Sulfur

3.2. $\delta^{18}O$

3.2.1. Variation of the $\delta^{18}O$ of the precipitations

The oxygen contained within the skeleton of aquatic vertebrates comes mainly from the environmental water. For freshwater environments, the origin of the latter is principally the precipitations. So, it is useful to understand what are the parameters that cause the variations of the $\delta^{18}O$ of the precipitations.

3.2.1.1. Water cycle

The main water reservoirs are the oceans, ice caps, groundwaters, lakes and rivers, vegetation and atmosphere. The oceans represent approximatively 96.5% of all the Earth waters, so its influence on the water cycle is predominant.

The $\delta^{18}O$ value of precipitation mainly comes from the evaporation/precipitation events from the oceanic to the continental environments and from the low to the high latitudes (Fig. 14). During evaporation events, the difference in mass between ^{16}O and ^{18}O will produce a diffusivity difference during which the light ^{16}O evaporates at higher rates than the heavy ^{18}O. Consequently, the $\delta^{18}O$ of clouds are depleted compared to the $\delta^{18}O$ seawater. According to the same process, the ^{18}O will precipitate more than the ^{16}O: the precipitation $\delta^{18}O$ is lower compared to the marine one. Following the Hadley model, the clouds migrate toward the high latitudes. The successive precipitation will produce $\delta^{18}O$ more and more negative due to diffusivity difference as described in the Rayleigh model (Dansgaard 1964; Hoefs 2009).

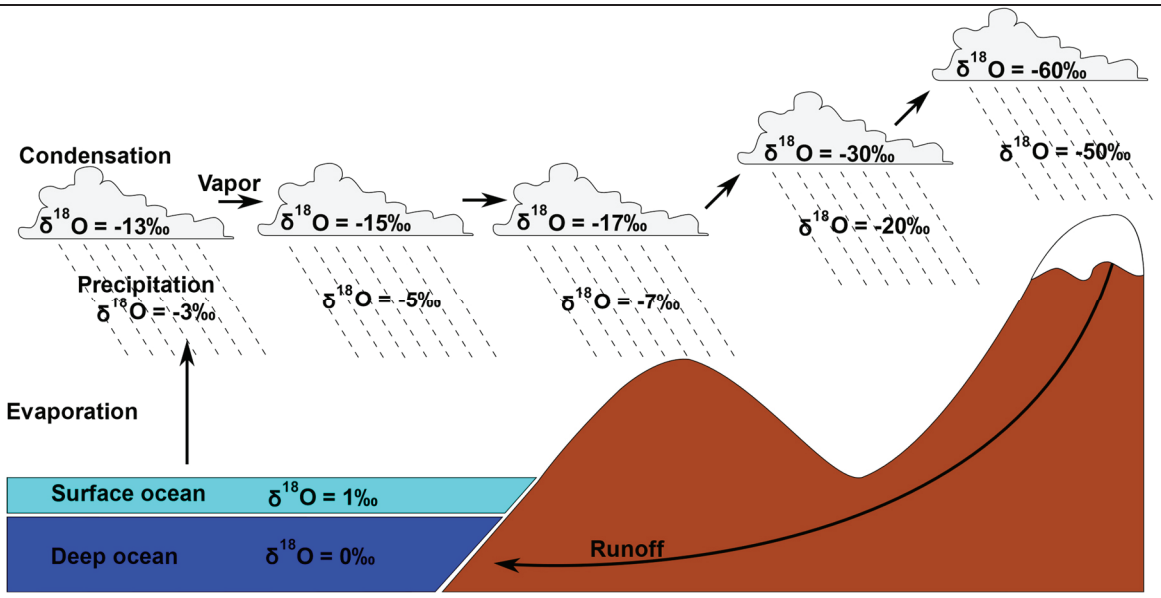

Figure 14. Simplified water cycle (modified from Sharp 2007).

The Rayleigh model works for a constant fractionation coefficient between vapor and liquid material at the equilibrium at a temperature of 25 °C. However, the temperature decreases when the clouds migrate toward the high latitude and the equilibrium is not always reached. Furthermore, direct measurements of the oxygen isotopic composition have demonstrated that factors like the altitude or humidity can impact the $\delta^{18}O$ of precipitation.

3.2.1.2. Effect of temperature, latitude and altitude on the $\delta^{18}O$ of the precipitations

With the increase of altitude and the migration toward high latitudes, the temperature decreases. Consequently, this will accentuate the condensation of water vapor. The resulting $\delta^{18}O$ value of the precipitations will be more and more negative. According to the Rayleigh model, the $\delta^{18}O$ decreases when the latitudes (Dansgaard 1964; Rozanski *et al.* 1993; von Grafenstein *et al.* 1996; Fricke & O'Neil 1999) and the altitude increase (Dansgaard 1964). It has been observed that the decrease of $\delta^{18}O$ with the altitude is about 0.28‰ per 100 m (Dansgaard 1964; Rozanski *et al.* 1993; Poage & Chamberlain 2001). It has also been observed that the decrease of $\delta^{18}O$ with the increase of latitudes in not linear, it is less marked at low than at high latitudes (see Fricke & O'Neil 1999).

3.2.1.3. Effect of the distance from the coast

As for the migration toward high latitudes and/or altitudes, the cloud migration from the coast to the inland decrease the $\delta^{18}O$ of the precipitation (Dansgaard 1964; Rozanski *et al.* 1993; Hoefs 2009). In fact, the clouds formed above ocean move away from the coast with the same

condensation/precipitation events. However, the clouds above the inlands are not supplied by newly evaporated water: the evaporation that comes from surface waters like the lakes or rivers is insignificant compared to the ocean. So, the fractionation produces $\delta^{18}O$ depletion of up to 3‰ per 1000 m in inland compared to the ocean (Sharp 2007).

3.2.1.4. Effect of the amount of precipitation at low latitudes

When the amount of precipitation increases, the $\delta^{18}O$ of the precipitation decreases, particularly at low latitudes (e.g. the monsoon; Kurita *et al.* 2009). Furthermore, according to the Rayleigh model, the precipitation is depleted in ^{18}O. So, the evaporation of the rain in the air and specific convection movements will deplete the residual cloud in heavy isotopes which continues to produce precipitations. So, the $\delta^{18}O$ of the precipitation will be even more depleted (Dansgaard 1964; Rozanski *et al.* 1993).

The variations of the $\delta^{18}O$ of environmental waters will be incorporated into vertebrate hard tissues. However, other parameters more related to the physiology of the organisms can influence the $\delta^{18}O$ of the skeletal remains.

3.2.2. Variation of the $\delta^{18}O$ in aquatic vertebrate tissues

The $\delta^{18}O$ values of bioapatite phosphate ($\delta^{18}O_p$) in vertebrates depends on the $\delta^{18}O$ of the body water that comes from the drinking water and the body temperature. In the studied ectothermic organisms, this temperature is directly related to that of the environment. The largest part of the oxygen contained in body water of aquatic vertebrates comes from the ingested water which can be either environmental water or food water without fractionation (Langlois *et al.* 2003; Koch *et al.* 2007) for the incoming flux. *A contrario*, the water from the dejection is the outgoing flux which is not impacted by fractionation (Schoeller *et al.* 1986; Wong *et al.* 1988).

Among the studied taxonomic groups, none of them is a plant-eater, so the food water comes from the water of prey. Prey oxygen comes from the prey body water which is contained in the body fluids (e.g. blood, plasma) and tissues (e.g. muscle, bone). If the prey is herbivorous, the oxygen comes from the drinking water and the food, i.e. plants. Freshwater aquatic plant oxygen comes from the environment, so from the precipitations (depleted in ^{18}O). There is no fractionation when the plant incorporates oxygen from the environment (Dawson & Ehleringer 1993) except for brackish ones (Lin & Sternberg 1993). If the prey is carnivorous, the oxygen

comes from the tissues, so the muscles mainly made of proteins. Consequently, carnivores have lower $\delta^{18}O$ values than herbivores.

To reconstruct the palaeoecology and the palaeoenvironment of fossil organisms based on the $\delta^{18}O$ of their mineralized tissues, the incorporation of environmental and biological processes is needed. These terms are united into fractionation equations that allow to interpret the $\delta^{18}O$ data of the investigated specimens.

3.2.3. Fractionation equation

A large number of fractionation equations relating the $\delta^{18}O$ of bioapatite phosphate, environmental water and body/environmental temperature have been calculated for vertebrate groups, mainly mammals (Longinelli 1984; Luz *et al.* 1984; Luz & Kolodny 1985; Levinson *et al.* 1987; d'Angela & Longinelli 1990; Bryant *et al.* 1994; Chillón *et al.* 1994; Iacumin & Longinelli 2002; Longinelli *et al.* 2003; Amiot *et al.* 2004; Navarro *et al.* 2004; Daux *et al.* 2008). This apparent multiplication of case studies is justified by the fact that these equations depend on the ecology and physiology of the different groups. For example, when the environmental water is incorporated in the body, a fractionation occurs, and it depends on the body temperature, the evapotranspiration, and feces (Bryant & Froelich 1995). This fractionation will increase the $\delta^{18}O$ of the body water for terrestrial vertebrates which renew their body water by drinking. *A contrario*, aquatic organisms, less influenced by evapotranspiration (Bocherens *et al.* 1996; Zazzo *et al.* 2004; Amiot *et al.* 2010), do not enrich the ^{18}O of their body water.

A large number of fractionation equations were made for a large number of vertebrate groups (see Longinelli 1984; Luz *et al.* 1984; Luz & Kolodny 1985; Levinson *et al.* 1987; d'Angela & Longinelli 1990; Ayliffe *et al.* 1992; Bryant *et al.* 1994; Chillón *et al.* 1994; Kohn 1996; Barrick *et al.* 1999; Iacumin & Longinelli 2002; Longinelli *et al.* 2003; Amiot *et al.* 2004, 2007; Navarro *et al.* 2004; Daux *et al.* 2008; Royer *et al.* 2013 for more details). The present studied taxonomic groups (xenacanthiforms, acantodians and temnospondyls) do not belong to modern groups for which an equation was made. Their ecology and physiology could be different from their closest modern relatives. However, numerous studies have demonstrated that oxygen fractionation occurs in the same way in aquatic ectothermic vertebrates and invertebrates without air breathing (Longinelli & Nuti 1973; Kolodny *et al.* 1983; Lécuyer *et al.* 1993, 2003a, 2013). Xenacanthiformes could be air-breathing (Compagno 1990), but no clear evidence support this assumption. Consequently, the equation of Lécuyer *et al.* (2013)

was used (Equation 10). It was established based on modern brachiopods and sharks (closest xenacanth relatives) and was already tested in numerous studies on diverse modern and fossils vertebrates (e.g. Rey *et al.* 2016; Séon *et al.* 2020; Goedert *et al.* 2018, 2020):

Equation 10: $T_{body}(°C) = 117.4(\pm 9.8) - 4.5(\pm 0.43) \times \left(\delta^{18}O_{PO_4} - \delta^{18}O_{H_2O}\right)$

The $\delta^{18}O$ of the precipitation depends on temperature and is related to it by fractionation equations (Dansgaard 1964). In the fossil record, the reconstruction of the palaeotemperature is possible for known $\delta^{18}O$ of the precipitation (Dansgaard 1964). As the studied taxonomic groups (xenacanthiforms, actinopterygians and temnospondyls) are supposed to be ectothermic, their body temperature is equivalent to the ambient one. So, for a viable temperature range, it is also possible to reconstruct the palaeo-$\delta^{18}O$ of the environment water. The phosphate (bioapatite)-drinking water fractionation equation mainly uses the $\delta^{18}O$ of the phosphate group of the bioapatite to relate environmental water ^{18}O and body/environmental temperature.

3.2.4. Use of the $\delta^{18}O$ of biopatite phosphate ($\delta^{18}O_p$) as a proxy of ingested environmental water

Modern marine environments typically exhibit a mean $\delta^{18}O$ between -2 and 2‰. The freshwater $\delta^{18}O$ is generally lower compared to marine one except in dry tropical environment submitted to evaporation (e.g. Amiot *et al.* 2010). Consequently, the freshwater vertebrate $\delta^{18}O_p$ is lower than that of marine vertebrates. Recent analyses on modern vertebrates have shown that the $\delta^{18}O_p$ is a good environmental proxy, especially in ectothermic organisms (Fig. 15; Goedert *et al.* 2020).

In the fossil record, numerous studies (e.g. Kolodny & Luz 1991; Amiot *et al.* 2010; Fischer *et al.* 2013, 2014b; Goedert *et al.* 2018) have investigated the palaeoenvironment using the vertebrate $\delta^{18}O_p$, especially in aquatic organisms. The $\delta^{18}O$ of the ocean over the geologic time is unknown but it is supposed to significatively vary from the current known values (e.g. Veizer & Prokoph 2015). In the late Palaeozoic, comparisons with the $\delta^{18}O_p$ of known marine organisms, such as conodonts (Sweet & Donoghue 2001), allow to establish a marine referential (Joachimski *et al.* 2006). In fact, conodonts never exhibit $\delta^{18}O_p$ values lower than 18‰. So, lower $\delta^{18}O$ values are interpreted as coming from freshwater environment (e.g. Fischer *et al.* 2013). Furthermore, in modern marine environments with a $\delta^{18}O$ of about 0‰, the temperature variation from 1°C to 30°C in the Equation 10 results in $\delta^{18}O_p$ values that never reach more than 18‰.

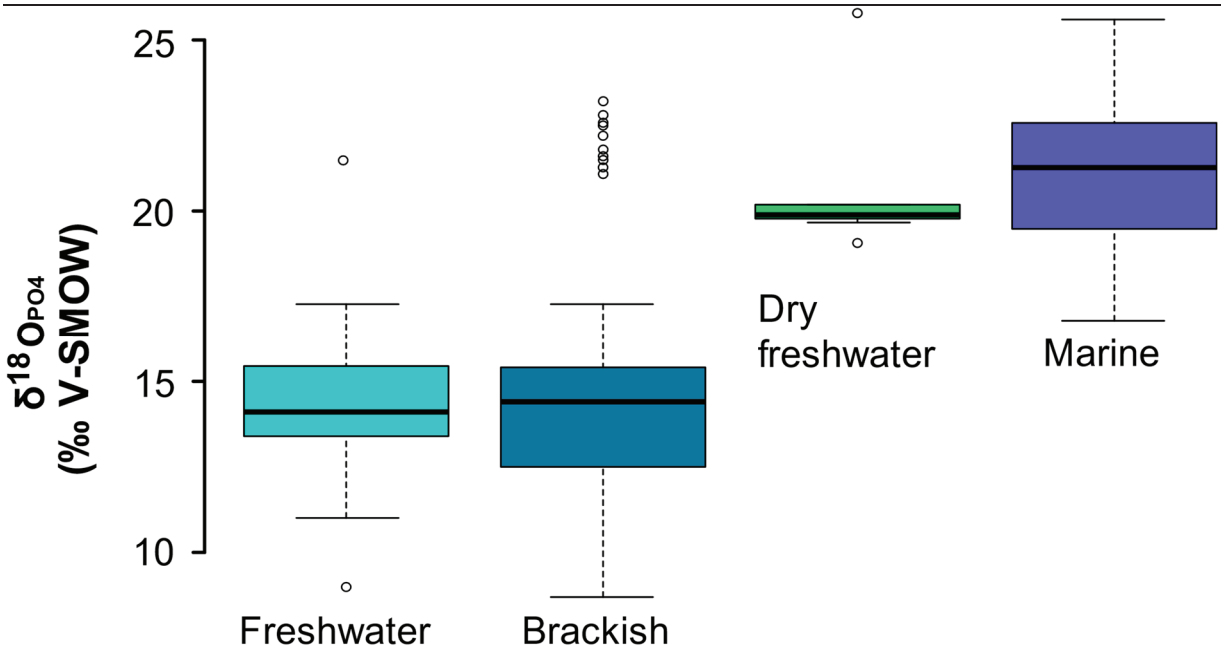

Figure 15. $\delta^{18}O_p$ values of the dental bioapatite of modern and fossil aquatic vertebrates. Modern data are from Iacumin *et al.* (1996) and Vennemann *et al.* (2001) and fossil data are from (Kolodny & Luz 1991; Fricke *et al.* 1998; Lécuyer *et al.* 2003a; Amiot *et al.* 2010; Goedert *et al.* 2018).

3.3. $\delta^{13}C$

3.3.1. Carbon cycle

In the aquatic environment, the $\delta^{13}C$ of water comes from the $\delta^{13}C$ of the bicarbonates (HCO_3^-) (approximately at 0‰, Hemminga & Mateo 1996) which is derived from the atmospheric $\delta^{13}C$. The dissolved CO_2 contained in the ocean exhibits a $\delta^{13}C$ of -9‰. The oceanic dissolved CO_2 of the ocean is the primary source for the phytoplankton. The later exhibits more negative $\delta^{13}C$ compared to the positive one of ambient bicarbonate because of the preferential use of ^{12}C in their metabolism.

The variations of environmental $\delta^{13}C$ are less pronounced than the $\delta^{18}O$. However, the variations caused by biological factors are important at different stages.

3.3.1.1. Incorporation of carbon into plants

Carbon is incorporated within plants and algae thanks to the photosynthetic CO_2-fixation. There are several modes of CO_2-fixation including the C_3 (Fig. 16), C_4 and CAM metabolisms. C_4 and CAM metabolism appeared in the Cenozoic (Kohn 2010) whereas the C_3 metabolism is present within aquatic and terrestrial plants, algae, and some bacteria since the Palaeozoic (Osborne & Beerling 2006). To discuss, the incorporation of carbon into plants, the

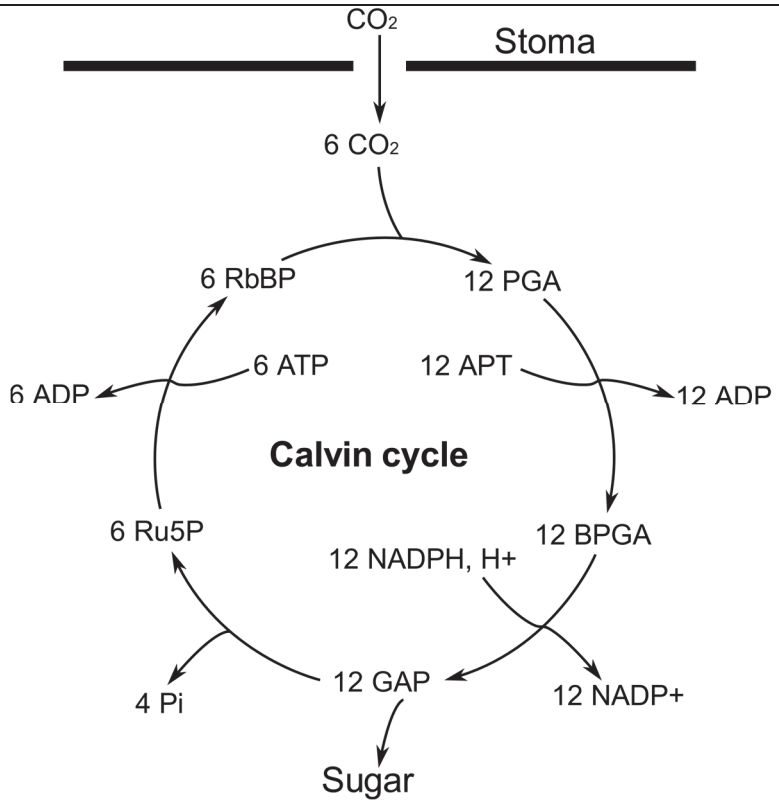

Figure 16. Calvin cycle and the C3 carbon fixation in plants. **Abbreviations**: **ADP**, adenosine diphosphate; **ATP**, adenosine triphosphate; **BPGA**, 1,3 bisphosphoaglycerate; **GAP**, Glyceraldehyde 3-phosphate; **NADPH***, oxydised nicotinamide adenine dinucleotide phosphate; **NADP**+, reduced nicotinamide adenine dinucleotide phosphate; **PGA**, trisphosphoglycerate; **Pi**, Pyruvate kinase; **RbBP**, Ribulose 1,5 bisphosphate; **Ru5P**, Ribulo5phosphate.

focus will only be done on the C_3 metabolism which were present in the aquatic plants (embryophytes like ginkgophytes, pteridophytes, sphenophytes, spermatophytes, tracheophytes) and algae from the late Carboniferous and early Permian of the investigated basins.

In terrestrial C_3 plants, the atmospheric CO_2 is assimilated by photosynthetic cells thanks to its diffusion from the air to the stomatal pores with a fractionation of about 4.4‰ (Marshall *et al.* 2007). In aquatic environments, the CO_2 diffusion is much slower than in terrestrial ones. Compared to the terrestrial plants, a magnitude difference of up to 4 orders is observed in aquatic plants (Hemminga & Mateo 1996). The presence of epiphytes is also a factor that reduces the CO_2 diffusion in aquatic plants (Sand-Jensen *et al.* 1985).

Then, the carbon is incorporated into the Calvin cycle (Fig. 16) thanks to the Ribulose-1,5-bisphosphate carboxylase-oxygenase (RuBisCO) which preferentially incorporates the ^{12}C with a fractionation of -29‰ (Marshall *et al.* 2007). The low $\delta^{13}C$ values of terrestrial plants is

due to the diffusion which does not significatively affect the carbon supply (Hemminga & Mateo 1996) and to the high fractionation of the ^{12}C incorporation. In aquatic plants, the RuBisCO discriminates the ^{13}C less than terrestrial ones, so the $\delta^{13}C$ is less negative (Hemminga & Mateo 1996).

3.3.1.2. Variation of the $\delta^{13}C$ of aquatic primary producers

Usually, the productivity, dissolved CO_2 concentration and bicarbonate use have been proposed as source of variation in $\delta^{13}C$ value of aquatic primary producers (Fry & Sherr 1989; Clementz & Koch 2001).

Following Fry & Wainright (1991), marine phytoplankton $\delta^{13}C$ value of carbonate is influenced by the temperature. Higher temperatures seem to favour the incorporation of ^{13}C, so the $\delta^{13}C$ increases with the temperature. The growth rate is also reported to be positively correlated with the $\delta^{13}C$ value of marine phytoplankton. This is linked to the apparent increase of $\delta^{13}C$ from the offshore to the nearshore setting (Clementz & Koch 2001): the nutrients are more abundant next to the coastline, producing a higher growth rate. *A contrario*, a raise in the lipid content of the marine water seems to decrease the $\delta^{13}C$ of phytoplankton (Fry & Wainright 1991). For marine plants, the dissolved CO_2 is the primary carbon source. However, depending on the considered plants, the $\delta^{13}C$ can be higher if the bicarbonate-derived inorganic carbon from the marine HCO_3^- is also used (Hemminga & Mateo 1996): the difference between dissolved CO_2 and marine bicarbonate is 9‰.

In freshwater plants, the ability of using HCO_3^- was also reported to be a significant factor of $\delta^{13}C$ variation (Osmond *et al.* 1981). MacLeod & Barton (1998) have demonstrated that the metabolic activity of freshwater plants influences the $\delta^{13}C$ variations more than their position in the water column. The metabolism is positively correlated to the temperature and light intensity. The increase of these parameters also increases the $\delta^{13}C$ value of freshwater plants. However, the water layer around the freshwater plants can still influence their $\delta^{13}C$: a high rate of water flow favours the diffusion of the CO_2 into the stomata and lowers their $\delta^{13}C$ (MacLeod & Barton 1998).

These parameters do not operate in the same way in marine, freshwater, and terrestrial environment and plant $\delta^{13}C$ has been proposed as an environmental proxy (Fig. 17). However, plant consumers can exhibit similar $\delta^{13}C$ even if there are two different carbon sources. For example, offshore-foragers $\delta^{13}C$ can be close to that of C_3 plant-eaters or marine plant-eaters can resemble terrestrial C_4 plant-consumers (Clementz & Koch 2001).

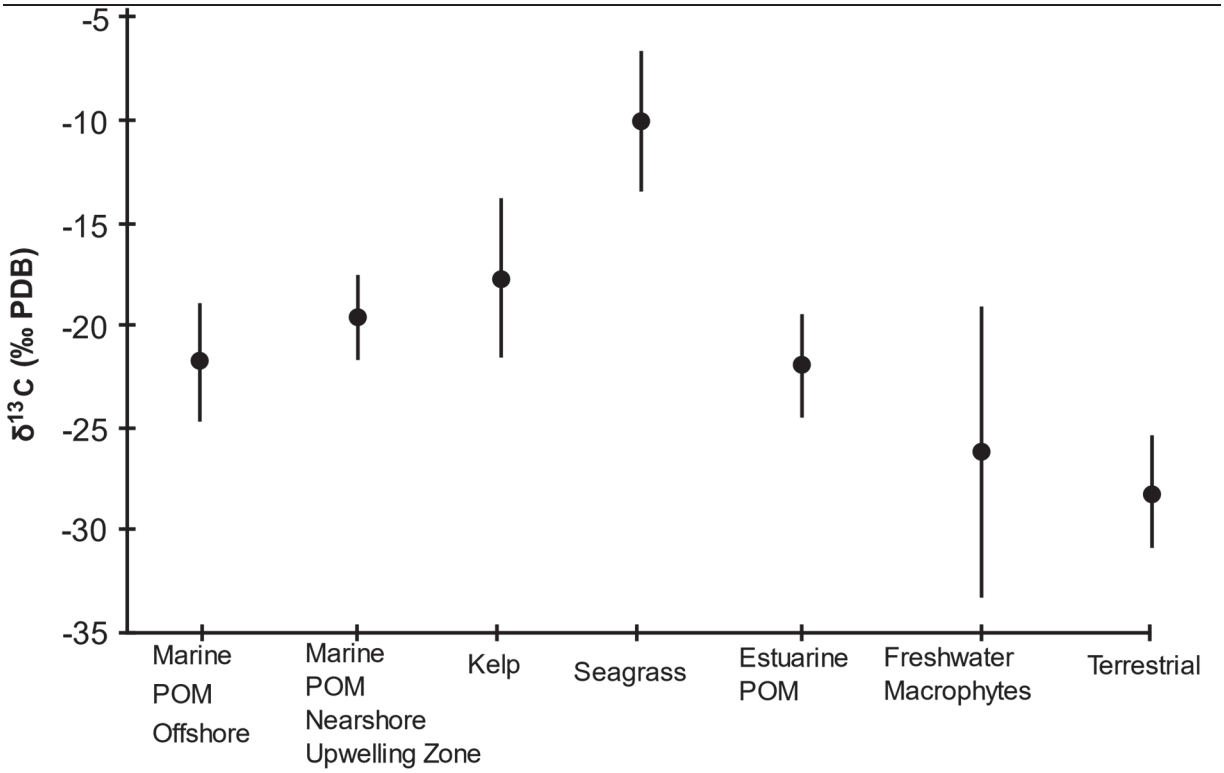

Figure 17. $\delta^{13}C$ variation among primary aquatic producers. Data are from Simenstad & Wissmar (1985), Fry & Sherr (1989), Hemminga & Mateo (1996), Benner *et al.* (1997), Cerling & Harris (1999) and Rau *et al.* (2001) (modified from Clementz & Koch 2001).

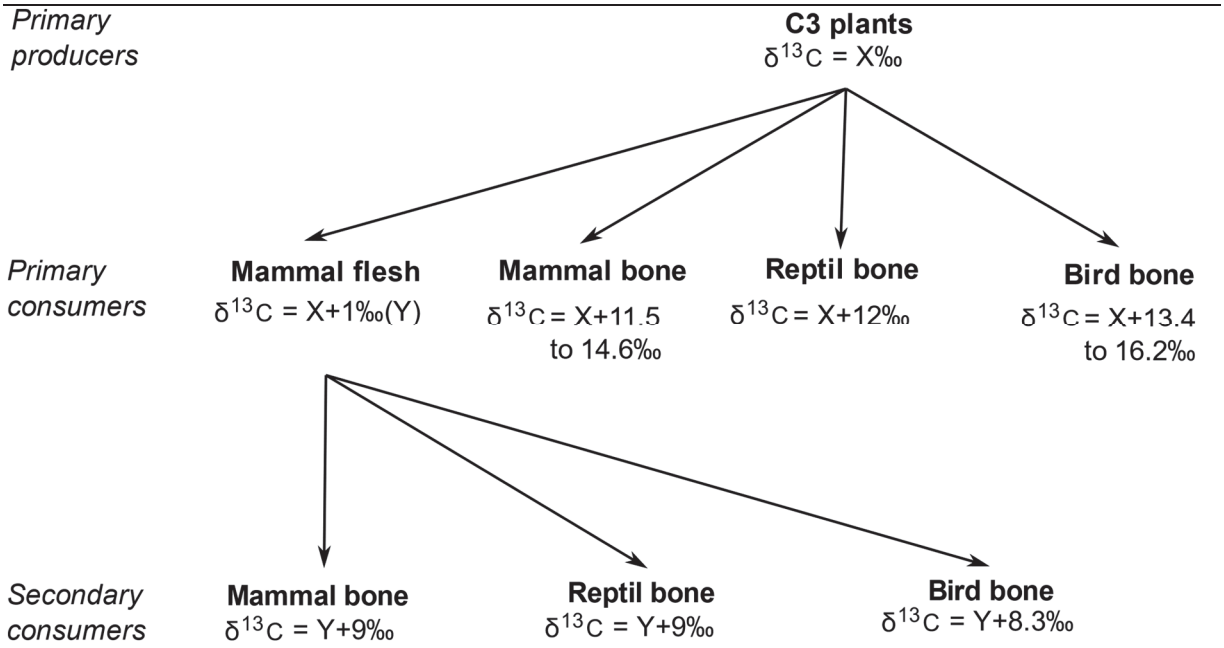

Figure 18. Isotopic fractionation on hard and soft tissues between modern primary producers, primary and secondary consumers (modified from Angst 2014).

3.3.2. Carbon fractionation in food web

The isotopic fractionation processes within food webs were established for terrestrial ecosystems. However, the same processes could also occur in aquatic environments.

Isotopic fractionations occur within food webs with a ^{13}C-enrichment between the primary producers and the last consumers (Fig. 18). Depending on the considered tissues and the digestive physiology ecologic orders, the fractionation will not be the same (Ambrose & Norr 1993; Passey *et al.* 2005). Between the primary producers and the primary consumers, the bone fractionation ranges from 11.5 to 16.2‰ (see Lee-Thorp *et al.* 1989; Tieszen & Fagre 1993; Sillen & Lee-Thorp 1994; Johnson *et al.* 1998; Koch 1998; Cerling & Harris 1999; Kelly 2000; Passey *et al.* 2005; Amiot *et al.* 2010; Angst *et al.* 2014). The secondary or tertiary consumers will preferentially feed on the primary consumer flesh. The enrichment between them and the secondary consumers bone apatite will be around 9‰ (see Stanton 2006; Angst *et al.* 2014). Vennemann *et al.* (2001) observed almost the same ^{13}C-enrichment, i.e. 11‰ to 12‰, in modern sharks, reinforcing the fact that the processes occurring in terrestrial ecosystems could also occur into aquatic ones.

The present review of the carbon cycle within the hydrosphere and the biosphere is mainly based on experiments on modern organisms. However, parameters that regulate the carbon cycle were not constant in the past geological record and it is useful to describe its specificities during the late Carboniferous and early Permian.

3.3.3. Carbon cycle at the Carboniferous-Permian transition

The Carboniferous-Permian transition is characterised by a strong primary productivity (e.g. Wilson *et al.* 2017), so a massive ^{12}C capture by plants. Consequently, the other reservoirs like atmosphere or ocean, are depleted in ^{12}C. On the other hand, this strong primary productivity also captures atmospheric CO_2 and releases O_2. So, this period records the lowest CO_2 atmospheric pressure (pCO_2) ever measured (Berner & Kothavala 2001). Moreover, Bouttes *et al.* (2011) have shown that during icehouse period, the pCO_2 also decreases and is negatively correlated with the $\delta^{13}C$ of the ocean. In the Carboniferous-Permian transition, multiple phased glaciations are reported (Isbell *et al.* 2003). All these parameters generated higher global $\delta^{13}C$ values in the different reservoirs compared to those of the present-day (Fig. 19). For example, in brachiopod shells, the $\delta^{13}C$ is enriched by 2 to 4‰ compared to modern ones (see the synthesis of Berner 2006). For this period, even if the recorded $\delta^{13}C$ of the hard

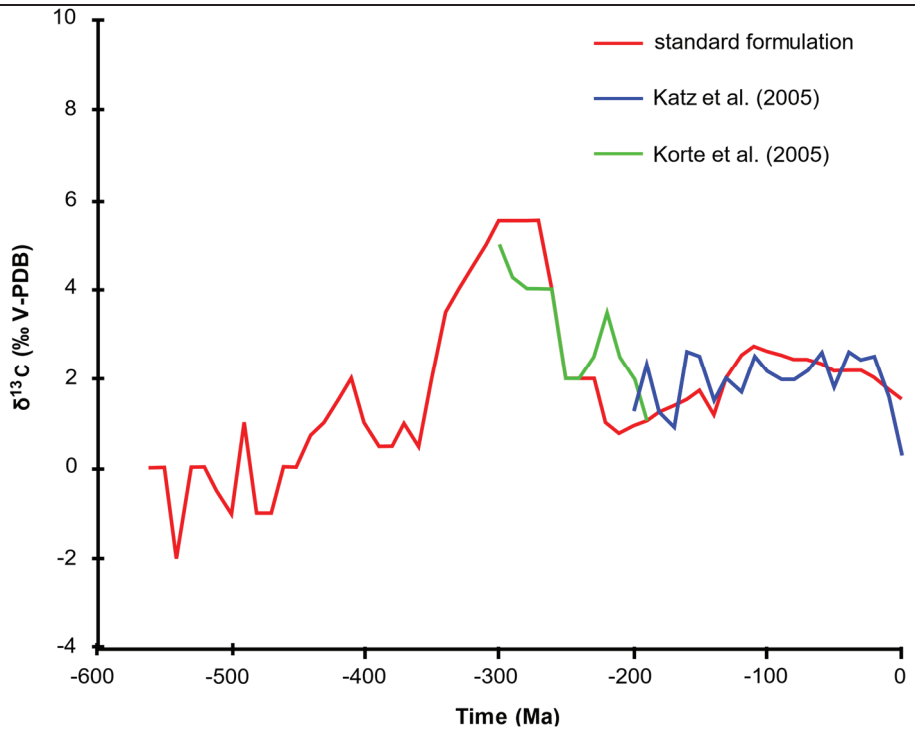

Figure 19. Variation of the $\delta^{13}C$ over the Phanerozoic. Data from Katz *et al.* (2005) are sediment carbonate and organic carbon and those of Korte *et al.* (2005) are brachiopod shell carbonate (modified from Berner 2006).

mineralized tissues of the xenacanthiforms and the associated vertebrate fauna is also enriched in ^{13}C, assumptions about the organisation of the food web could also be possible.

3.4. $\delta^{34}S$

3.4.1. Sulfur cycle in vertebrate tissue

3.4.1.1. Inorganic reservoirs of the sulfur

Sulfur mainly occurs under inorganic form in the environment: dissolved sulfate in the hydrosphere, evaporitic sulfate and iron sulfide in oceanic lithosphere, it can also be found under dihydrogen sulfide and sulfur dioxide in the atmosphere (Jones *et al.* 2016). Numerous bacteria are able to perform anaerobic photosynthesis. In this case, the dihydrogen sulfide is used to reduce the environmental CO_2 with light energy and produce elementary sulfur. Anaerobic photosynthesis can also use elementary sulfur to produce sulfates ions. The latter can be used in the synthesis of organic sulfur molecules during assimilative reduction of sulfate (Goedert 2017).

3.4.1.2. Organic sulfur in the biosphere reservoir

Cysteine and methionine are the two amino acids containing sulfur within the biosphere that are incorporated into proteins. In plants, they are produced by the reduction of sulfate ions from the substrate to the plant cells, i.e. assimilative reduction of sulfate. In plants, the cysteine is produced first and then used to produce methionine. Animals cannot produce cysteine and methionine by assimilation of environmental sulfate ions. The whole methionine comes from their diet. An important part of the animal cysteine comes from their diet too, but it can be synthetised from methionine too (e.g. Saito 2004).

3.4.1.3. Sulfur content of vertebrate fluids

Within vertebrate fluids, e.g. blood, sulfate ions come from the oxidation of the cysteine and the methionine. This corresponds to an endogenous source. These sulfate ions come from the primary assimilative reduction of sulfur by bacteria or plants and from a secondary oxidation. They can also be used in various anabolic reactions (Goedert 2017). Feeding can also provide to the organism free sulfate ions that correspond to the first exogen source. In herbivores, sulfate ions come from ingested plants. The latter usually come from environmental free sulfate ions. However, in carnivores, sulfate ions have three possible origins: oxidation of the cysteine and methionine (endogenous source), feeding (first exogenous source) and environmental water (second exogenous source) in which the free sulfate ions are assimilated through intestinal wall (Goedert 2017). Marine water has relatively constant sulfur concentration of 28 mm/L (Morris & Riley 1966) whereas freshwater setting exhibits lower and more variable concentrations from 0 to 6.3 mm/L (UNEP 1990).

3.4.2. Isotopic fractionation between environmental and animal and vegetal fluid sulfur

The assimilative reduction of sulfur process occurring in plants produces sulfide under the form of cysteine from environmental sulfates. Small fractionation occurs between environmental and organic $\delta^{34}S$ in this case, between 1 and 3‰ (Krouse 1989; Trust & Fry 1992; Monaghan *et al.* 1999; Oduro *et al.* 2012; Tcherkez & Tea 2013). This is caused by unidirectional transport of sulfate ions to the roots and the absence of exchange with external setting which totally oxides the sulfates and limits the fractionation (Goedert 2017).

A small isotopic fractionation of 0.5 +/- 2.4‰ has been measured between primary or secondary consumers tissues and their diet (Nehlich 2015). This is explained by the fact that diet sulfur is under cysteine or methionine reduced form and it is incorporated within primary/secondary consumers under the same form. So, no oxidation change is reported

(Goedert 2017). Thanks to these apparent small isotopic fractionation processes, the $\delta^{34}S$ has been used as an environmental proxy (Nehlich 2015 and references within).

3.4.3. Isotopic fractionation and the variations of the $\delta^{34}S$ in vertebrate bioapatite

Recent investigations (Goedert 2017; Goedert *et al.* 2018, 2020) of modern and fossil vertebrates from a broad phylogenetic context have demonstrated that the isotopic fractionation between the $\delta^{34}S$ of the bioapatite and the environmental $\delta^{34}S$ is negligible. An enrichment of 0.8‰ in bioapatite $\delta^{34}S$ is measured and the equation relating these terms (Equation 11; Goedert *et al.* 2020) is:

Equation 11: $\delta^{34}S_{environment} = -1.24(\pm 1.87) + 1.08(\pm 0.19) \times \delta^{34}S_{apatite}$

The current seawater $\delta^{34}S$ is close to 21‰ (Böttcher *et al.* 2007) and the $\delta^{34}S$ from freshwater environments, e.g. rivers, lakes, swamps or precipitations, ranges from -20‰ to 20‰ (Krouse 1980; Kaplan 1983; Nehlich 2015). Bioapatite $\delta^{34}S$ is therefore a good environmental proxy and allow to discriminate vertebrates living in a marine or freshwater/terrestrial setting (Fig. 20; Goedert 2017; Goedert *et al.* 2018, 2020) applicable to fossil vertebrates. The $\delta^{34}S$ of vertebrate bioapatite living in a strict marine environment is supposed to be almost equal to the marine $\delta^{34}S$ (currently 21.2 +/- 0.8‰). Their $\delta^{34}S$ actually range from 7.2‰ to 22.9‰ with a mean of 17.25‰ (Goedert *et al.* 2018). On the other hand, the vertebrates living, at least partially, in freshwater environment exhibit $\delta^{34}S$ values that range from 3.3‰ to 21.9‰ with a mean of 10.36‰ (Goedert *et al.* 2020). Variations might be due to still misunderstood mechanisms relative to their ecology and/or physiology which could influence sulfur incorporation from the environment to the bioapatite.

As for the carbon, the sulfur geochemistry was not constant during the geological time. As the main objective is to discriminate marine to freshwater environment, it is important to understand the variation of the $\delta^{34}S$ of the seawater to clearly establish a marine reference for environmental interpretations.

3.4.4. Seawater $\delta^{34}S$ variations over geological time

Currently, the $\delta^{34}S$ of the marine biota is around 21.2 +/- 0.8‰, that of dissolved seawater sulfate is 20.9+/- 0.5‰ (Kampschulte & Strauss 2004) and that of global average seawater is 21 +/- 0.1‰ (Rees *et al.* 1978). This is in good agreement with the $\delta^{34}S$ from the

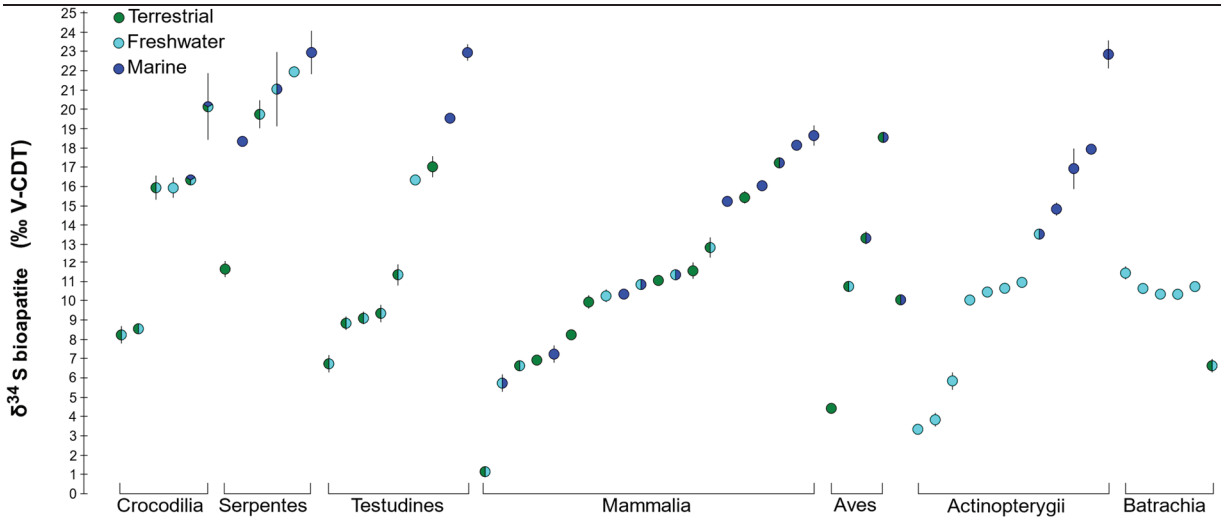

Figure 20. Bioapatite $\delta^{34}S$ in modern vertebrate and their environmental distribution. Data and figure are modified from Goedert *et al.* (2020).

Figure 21. Variation of the $\delta^{34}S$ of the seawater sulfates over the Phanerozoic (Data are from Kampschulte & Strauss [2004] and the figure is modified from Berner [2006]).

marine vertebrate bioapatite. However, the $\delta^{34}S$ of seawater has varied over geological time (Fig. 21) as demonstrated by many data (e.g. analyses on marine evaporitic sulfate deposits and pyrite by Claypool *et al.* [1980] and Strauss [1993], on marine barite by Paytan *et al.* [1998, 2004] and on carbonate associated sulfate by Ohkouchi *et al.* [1999] and Kampschulte *et al.* [2001]).

The marine $\delta^{34}S$ is influenced by the proportion of sulfate (oxidised form) and sulfide (reduced form) which have not the same $\delta^{34}S$ (Bottrell & Newton 2006). For example, inputs from river runoff will drain gypsum and pyrite with $\delta^{34}S$ values of 0 to 10‰, so lower than that of seawater (Krouse 1980). Volcanic inputs are characterised by a $\delta^{34}S$ of 0‰ (Paytan *et al.* 2020). Another mechanism is the deposition of sulfate within minerals with a $\delta^{34}S$ close to that of seawater and of sulfide of -15‰ (Krouse 1980; Kaplan 1983). At the Carboniferous-Permian transition, the seawater $\delta^{34}S$ was of about 12‰ (Paytan *et al.* 2020).

The isotopic relative abundance of the oxygen, carbon and sulfur are determined in the skeletal remains of Xenacanthiformes and their associated aquatic to semi-aquatic fauna. However, prior to any analysis, it is essential to understand how the biological material grows and mineralises. The various investigated tissues do not possess the same growth pattern, so knowing them will allow to understand what kind of temporal record is being measured.

3.5. Analysed tissues and mineralisation timing

3.5.1. Bioapatite within vertebrate hard tissues

Collagen and bioapatite are the two main components of vertebrate skeletons (Pasteris *et al.* 2008). The collagen is quicky deteriorated after the animal death (e.g. Hare 1980), and only the bioapatite can be preserved in the fossil record. The latter is a calcium hydroxyphosphate. Its chemical formula is $Ca_5(PO_4)_3OH$ and Pan & Fleet (2002) have demonstrated that numerous substitutions can occur. Among them, the phosphate group PO_4^{3-} and the hydroxyl OH^- can be replaced by carbonate group CO_3^{2-} and/or sulfate group SO_4^{2-}. Carbonate content in vertebrate bioapatite is typically between 2 and 13.4% (Brudefold & Soremark 1967; Rink & Schwarcz 1995; Vennemann *et al.* 2001; Goedert *et al.* 2018). These multiple substitutions allow to analyse the isotopic composition of several elements including the oxygen from the phosphate and carbonate group, the carbon from the carbonate group and the sulfur from the sulfate group.

3.5.2. Xenacanth dorsal spines

The xenacanth dorsal spine is an ever-growing structure like those of fossil and modern chondrichthyans (Maisey 1978, 1979; Soler-Gijón 1999; Clarke *et al.* 2002; Ramos 2007; Tovar-Ávila *et al.* 2008; Barnett *et al.* 2009). Soler-Gijón (2004) proposes that this structure is homologous to the Euselachii fin-spine having a structure close to that of modern selachimorphs, with the exception of the absence of an ornamented mantle. Maisey (2009)

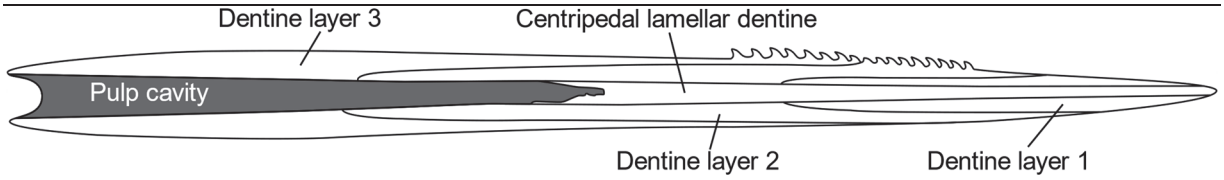

Figure 22. Global morphology and histology of a xenacanth dorsal spine (modified from Beck *et al.* 2016).

argued that the xenacanth dorsal spine develops from the dorsal-fin module, under the regulation of *Hox* and *Tbx* genes like in modern selachimorphs.

Primitive xenacanths, i.e. *Diplodoselache*, *Lebachacanthus*, exhibit a dorsal spine inserted in front of the dorsal fin (Dick 1981; Heidtke 1982, 2007). *A contrario*, more derived taxa, such as *Orthacanthus*, *Xenacanthus*, *Triodus* and *Plicatodus*, show an insertion next to the neurocranium occipital region. However, the juveniles of these taxa also have their dorsal spine inserted in front of the dorsal fin (Soler-Gijón 2004): this secondary location comes from the differential growth of the most proximal part of the dorsal spine.

Xenacanth dorsal spines are made of dentine layers. Dentine is a tubular tissue composed at 75% of bioapatite, 20% of collagen and 5% of lipids. It is firstly produced by mesenchymal cells, or odontoblasts, and secondly mineralized as bioapatite (Francillon-Vieillot *et al.* 2009; Jerve 2016). Soler-Gijón's (1999) detailed histological study of *Orthacanthus* dorsal spine has demonstrated how this structure is formed and developed: the dorsal spine is superficially inserted in the dermis and solely composed of successive dentine layers. The first type of layer to form is the centripetally growing lamellar dentine directly around the pulp cavity. Then, when the dorsal spine is in the dermis, a layer of trabecular dentine forms. When the dorsal spine moves to a more superficial location, the trabecular dentine is surrounded by a centrifugally growing lamellar dentine layer. The denticles are independent elements formed by a dermal papilla and secondarily attached by dentine to the dorsal spine (Soler-Gijón 1999).

The growth of the different dentine layers is not constant (Fig. 22). The thickness of each layer decreases from the proximal to the distal part of the dorsal spine. So, at the apex, only the older dentine layers are visible whereas near the base the youngest and sometimes the whole set of dentine layers is still present (Soler-Gijón 1999). Therefore, the sampling strategy is to sample, from the apex to the base of each dorsal spine, when possible, only the outermost dentine layers. This allows to access to the first ontogenetic stage of each individual next to the apex, and to progress through the lifetime in direction to the base. Furthermore, when the dorsal spine grows and moves to the superficial skin section and then out of the body, it stops to record

the isotopic composition of its environment. So, the most distal part of each dentine layer corresponds to juvenile ontogenetic stage and the most proximal one to adult stage. Consequently, with the overall arrangement of the dentine layers within the dorsal spine, the proposed sampling allow to access all the ontogenetic stages of each individual.

3.5.3. Acanthodian fin spines

The fin spines are divided into inner lamellar basal layer, middle thicker trabecular layer and outer dentine ornament (Denison 1979; Burrow *et al.* 2015; Jerve 2016). Recent studies (Jerve 2016; Jerve *et al.* 2017) have demonstrated that Silurian acanthodian fin spine growth is similar to that of modern chondrichthyans (e.g. *Callorhinchus* and *Squalus*; Jerve 2016). The most noticeable difference is that internal growing layer can be made of dentine or bone (Gross 1971; Denison 1979; Jerve 2016). However, no detailed histological study was made on the fin spine of Permian *Acanthodes* species. Beznosov (2009) figured that *A. lopatini* fin spines from the Carboniferous of Russia are entirely made of dentine. Such an internal structure is only found in *A. fritschi* and *Acanthodes* sp. from the Carboniferous of the Czech Republic (Zajíc 1985, 1998).

As the acanthodian fin spine growth is similar to that of chondrichthyans, the sampling strategy is the same as for xenacanth dorsal spines, from the apex (early ontogenetic stage) to the base (late ontogenetic stage).

3.5.4. Temnospondyl bones

In vertebrates having a low metabolism, i.e. amphibians or lepidosaurians, the skeleton is mostly made up of lamellar bone. This structure is poorly vascularised, and each skeletal element is composed of a succession of bioapatite layers deposited from the core to the periphery. The layering is discontinuous because of environmental, e.g. temperature, or metabolic variations (Hota 1994; Kumbar & Pancharatna 2004). Consequently, in lamellar bones, the peripheric layer records the end of life. The bone core could record the earliest ontogenetic stage but can also be affected by compaction or secondary ossification.

In Buxières-les-Mines, temnospondyls were sampled, and it can be assumed that they possessed the same bone structure as modern amphibians (e.g. Steyer *et al.* 2004). So, sampling was done at the periphery of the bones to minimise potential compaction or secondary ossification.

3.5.5. Actinopterygian ganoid scales

Ganoid scales of palaeoniscoid fishes are composed of three layers: covering well-mineralised ganoine, dentine and a bony plate (e.g. Sasagawa *et al.* 2013). Ganoine originates from the basal epidermal layer (Sire *et al.* 1986, 1987; Sire 1994). The growth is cyclic outward with a succession of isopedine (compact primary bone) and dentine layers in palaeoniscoid fishes (Schultze 2018). Ganoid scales sampled for this study come from sub-complete specimen (Muse) or isolated scales (Buxières-les-Mines).

3.6. Estimating the potential effect of diagenesis of fossil bioapatite samples on the primary preservation of stable isotope compositions

The aim of the next paragraphs is to present the methods to estimate the effect of potential diagenesis for the analyses on the oxygen and sulfur of the phosphates and of the oxygen and carbon of the carbonates of the fossil bioapatite.

3.6.1. Definition

Diagenesis is a set of physico-chemical processes that affect the sediments and that are caused by water-rock interactions, microbial activity, increase of pressure and temperature and compaction of their deposition (e.g. Marshak & Werner 2013). Fossils are typical results of diagenetic processes that affect the proportions of organic and inorganic components (e.g. bioapatite) of plant or animal remains (e.g. Hedges 2002). In this part, only the diagenetic processes affecting the isotopic compositions of fossils are discussed.

Diagenesis can affect the stable isotope composition of buried organism and erase the biological and environemental signal recorded during the life of the organism. There are two types of diageneses, which affect the isotopic composition differently. Early diagenesis occurs directly after the surface burial of the specimen by surficial sediments. The physico-chemical alterations reflect the characteristics of the living environment or the environment where the specimen died. In this case, the modified isotopic composition can be considered close to the initial one and the measured values can be interpreted (e.g. Lécuyer *et al.* 2003b). However, in the case of organisms with a significant migratory pattern, the isotopic signal from the different living environments is altered by the one in which the specimen died. The second type of diagenesis is the late diagenesis. This occurs long after the specimen is buried, so during the fossilisation process. The resulting isotopic composition should not reflect those of the living environment of the specimen, but potentially the maturation temperature of the sediment under

high pressures and/or the isotopic composition of diagenetic fluids. Consequently, it could reflect a significantly different environment depending on the more or less complex tectonic history of the study area. In this case, the measured isotopic composition of the fossil bioapatite should not be considered as interpretable. Regarding the different used isotopic proxies, several ways to assess the effect of diagenesis on the stable isotope record were proposed.

3.6.2. Observation of thin section

A first step to assess the diagenesis is to observe thin section of the considered fossil samples. A direct observation is sufficient to see if the specimen is entirely recrystallised, so subject to diagenetic processes. This method can be useful during the selection step of the specimen to analyse. However, it is not sufficient to clearly assess the real alteration in the specimen and other methods are required.

3.6.3. $\delta^{18}O_p$ and $\delta^{18}O_c$ relationships in fossil bioapatite

Within the mammal skeletal tissues, it has been demonstrated that the phosphates and carbonates precipitate close to an isotopic equilibrium from the body water. Thus, a positive correlation with a slope close to 1 between the $\delta^{18}O_p$ and $\delta^{18}O_c$ of a same sample is observed in modern mammals (Figure 23; Bryant *et al.* 1996; Iacumin *et al.* 1996). The same is also observed in modern sharks (e.g. Kolodny & Luz 1991; Vennemann *et al.* 2001). In the fossil record, the observation of the same $\delta^{18}O_p$-$\delta^{18}O_c$ relationship can be considered as evidence for the preservation of the initial isotopic composition (e.g. Kolodny & Luz 1991; Amiot *et al.* 2010; Goedert *et al.* 2018). So, the oxygen isotopic composition of the phosphates can be interpreted.

3.6.4. Carbonate percentage in fossil bioapatite

In bioapatite, the abnormally high weight percentage of the carbonate can be interpreted as evidence of dissolution-recrystallisation processes. Weight percentage of carbonate in modern vertebrate is between 2 and 13.4‰ (Brudefold & Soremark 1967; Rink & Schwarcz 1995; Vennemann *et al.* 2001). If these values are higher in treated samples than in modern vertebrates, so secondary carbonates were added during diagenetic processes (Figure 24). So, the oxygen and carbon isotopic composition of carbonates are not initially preserved and not interpretable. Furthermore, it must be noted on the figure 24 that the increase of the carbonate concentration could also originate from the addition of calcite that was not removed by the chemical treatment. In this case too, the data will not be interpretable.

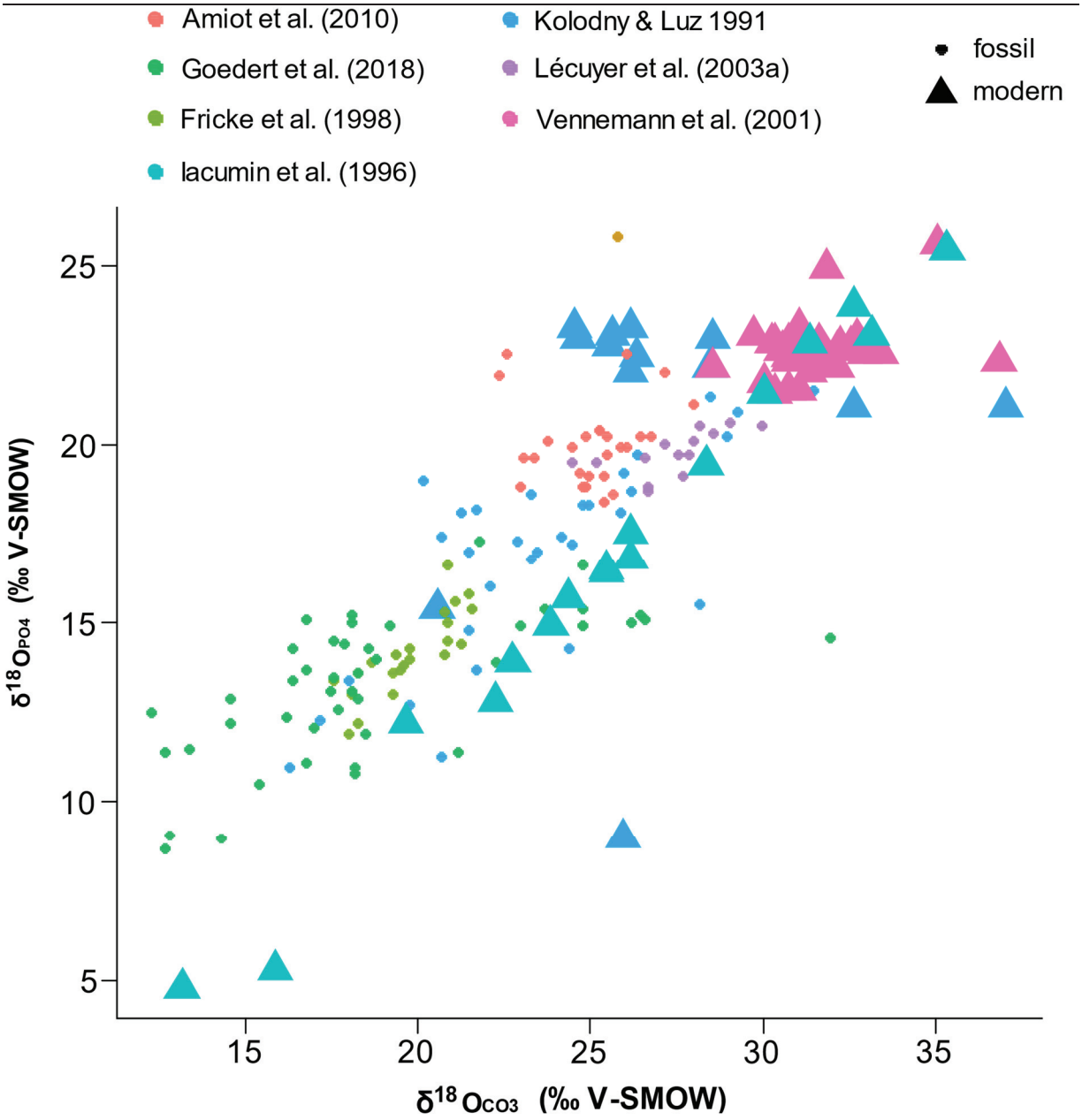

Figure 23. $\delta^{18}O_p$ and $\delta^{18}O_c$ correlation in modern and fossil bioapatite samples (fossil and modern data from (Kolodny & Luz 1991; Iacumin *et al.* 1996; Fricke *et al.* 1998; Vennemann *et al.* 2001; Lécuyer *et al.* 2003a; Amiot *et al.* 2010; Goedert *et al.* 2018).

3.6.5. Sulfur concentration in fossil bioapatite

$\delta^{34}S$ is a good proxy for discriminating environment. There are several ways to assess the diagenesis of the sulfur content in fossil bioapatite. In modern vertebrates, the sulfur concentration in bone is usually 0.6 weight% SO_2 (wt%). It has been demonstrated that diagenetic processes can increase the sulfur weight concentration by the addition of pyritc within the sample and this increase is more marked in dentine and bone than in enamel. The

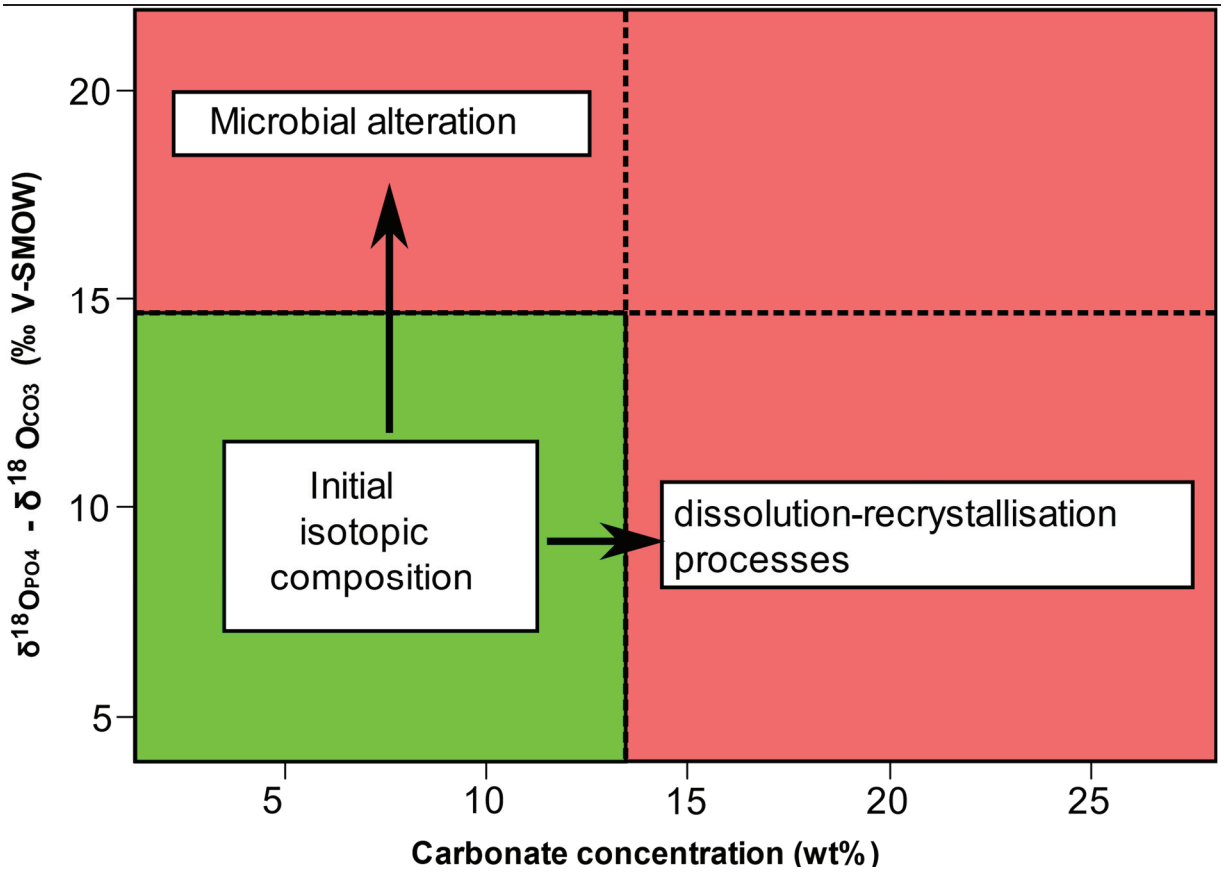

Figure 24. Potential diagenetic processes on carbonates of fossil bioapatite.

enamel is less porous, so less sensitive to secondary precipitation of sulfur minerals. So, a linear correlation between the measured $\delta^{34}S$ and the wt% sulfur concentration is assumed to be evidence of diagenesis.

Even if the diagenesis has a significant impact on the sulfur concentration of fossil bioapatite (up to 2%), the initial environmental signal would not be replaced by the diagenetic signal. Environmental sulfur is incorporated in plants in the form of methionine and cysteine, then incorporated in vertebrate tissues without isotopic fractionation. Sulfur alteration occurs mainly from endogen pyritization of the organic matter. However, the latter does not imply a change in sulfur oxidation state (methionine and pyrite are at -2), so a significative isotopic fractionation is unlikely. Consequently, diagenetic pyrite should have the same isotopic composition as the original sulfur content in bioapatite.

Chapter II – Geological context

1. The Hercynian Mountains

1.1. Overview

The Central Pangean Mountains was a mountain belt whose relics can be currently found in North America and Europe. During the Carboniferous-Permian transition, it stretched over 10,000 km and was divided into three mountain systems: the Appalachians in North America, the Hercynian Mountain Belt in Europe (Fig. 25) and the Mauritanides Belt in North Africa and Ural Mountains (e.g. McCann 2008). It was formed by the collision of two continents: Laurussia in the North and Gondwana in the South, together forming the supercontinent Pangea (McCann 2008).

In Europe, the Hercynian Mountain Belt (Fig. 2.1) can be observed from Portugal to Poland and the preservation of the Carboniferous-Permian basins occurs nearby the magmatic and metamorphic basement (Faure *et al.* 2005; Baptiste 2016). It exhibits a double-overthrust fan structure. Thrusts are oriented to the North at its north margin and to the South at its south margin (Franke 2000). Within it, there are several oceanic sutures underlined by ophiolites and ultra-high-pressure metamorphic rocks (Matte 2001). The deformation forming this mountain belt is at its maximum during the Devonian and the Carboniferous (Matte 2001).

1.2. Formation

Franke *et al.*'s (2017) hypothesis (Fig. 26) is followed in this work to explain the formation of the Hercynian Mountain Belt. These authors proposed a scenario for the evolution of the location of all the tectonic plates included in this process and that begins in the Ordovician until the Carboniferous. During the early Ordovician, the split between Avalonia and Gondwana opened the Rheic Ocean and closed the Iapetus Ocean. The Rheic Ocean was closed during the Caledonian orogeny with the collision between Avalonia and Baltica and between Avalonia-Baltica and Laurussia. The northern margin of Gondwana splitted and the Galice-Moldanubian Ocean opened. During the Silurian, the Saxo-Thurungian Ocean opened thanks to the complete split of the Northern margin of Gondwana and the Rheic Ocean was reduced. The Galice-Moldanubian Ocean and Gondwana subducted under Armorica. During the late Devonian, the Saxo-Thuringian and the Rheic oceans closed: it is the variscan phase and the initiation of the

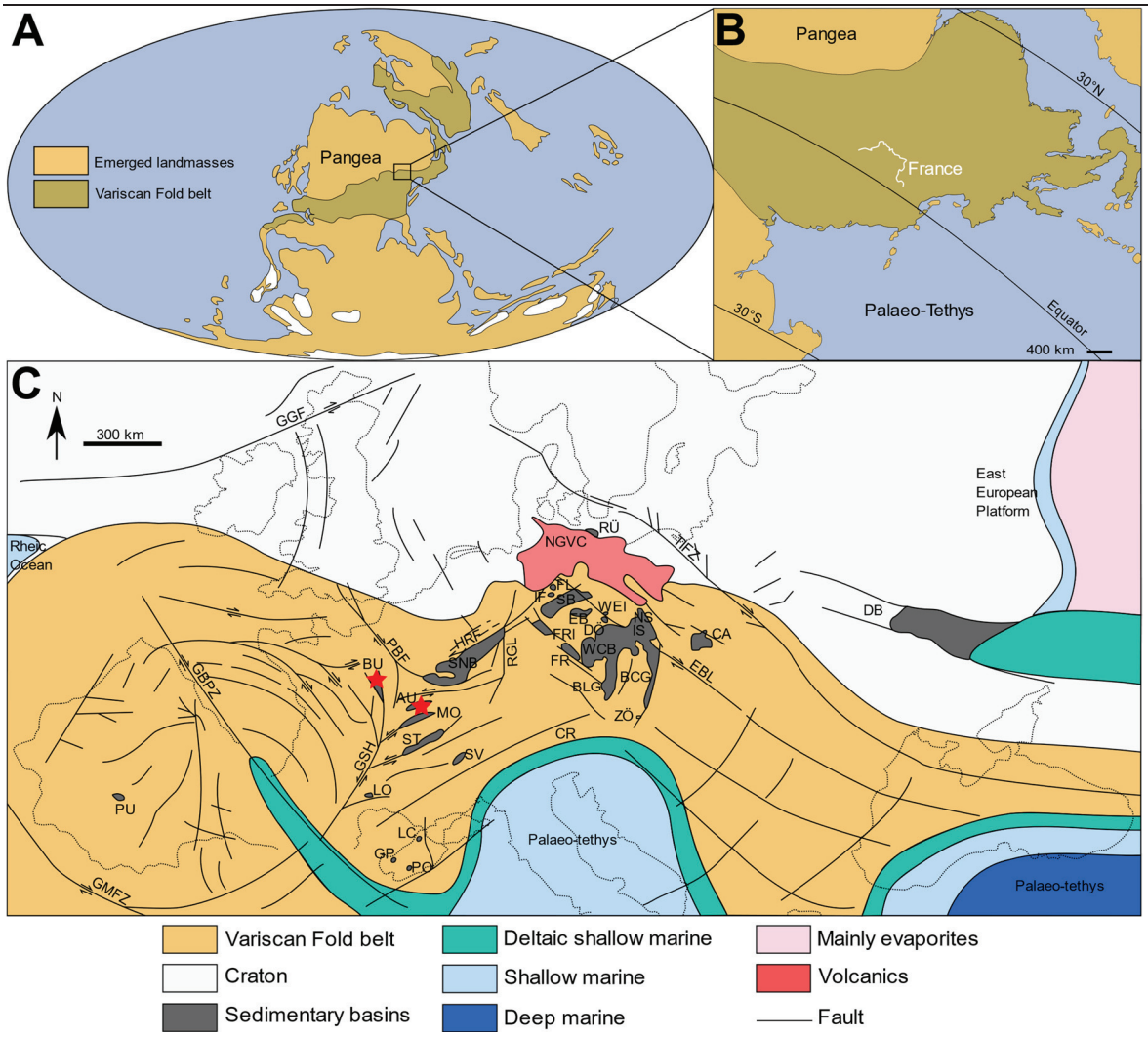

Figure 25. Palaeogeographical context. **A**, Palaeogeography of the Pangea in the late Carboniferous (Pennsylvanian, 300 Ma). **B-C**, The Hercynian Mountain, European component of the Central Pangea Mountain at the Carboniferous-Permian transition and the location of the continental sedimentary basins. White outlines are the past location of France in **B**. Red stars are the location of the investigated Autun and Bourbon-l'Archambault basins. **Abbreviation**: **AU**, Autun Basin; **BLG**, Blanice Graben; **BCG**, Boskovice Graben; **BU**, Bourbon-l'Archambault Basin; **CA**, Carpathian Basin; **CR**, Carnic Alps; **DB**, Donetsk Basin; **DÖ**, Döhlen Basin; **EB**, Erzgebirge Basin; **EBL**, Elbe Lineament; **FL**, Flechting Block; **FRL**, Franconian Lineament; **FR**, Franconian Basin; **GBFZ**, Golf of Biscay Fracture Zone; **GGF**, Great Glen Fault; **GMFZ**, Gibraltar Minas Fracture Zone; **GP**, Guardia Pisano Basin; **GSH**, Grand Sillon Houllier Fracture Zone; **HRF**, Hunsrück Fracture; **IF**, Ilfeld Basin; **IS**, Intra Sudetic Basin; **KP**, Krkonoše Piedmont Basin; **LC**, Lu Caparoni Basin; **LO**, Lodève Basin; **MO**, Montceau les Mines Basin; **NGVC**, North German Vulcanite Complex; **NS**, North Sudetic Basin; **PBF**, Pays de Bray Fracture; **PD**, Perdasdefogu Basin; **PU**, Puertollano Basin; **RGL**, Rhein Graben Lineament; **SB**, Saale Basin; **SNB**, Saar–Nahe Basin; **ST**, St. Etienne Basin; **SV**, Salvan-Dorénaz Basin; **TF**, Thuringian Forest Basin; **TTFZ**, Tornquist–Teysseyre Fracture Zone; **WCB**, Western and Central Bohemian Basins; **WEI**, Weissig Basin; **ZÖ**, Zöbingen (modified from Roscher & Schneider 2006).

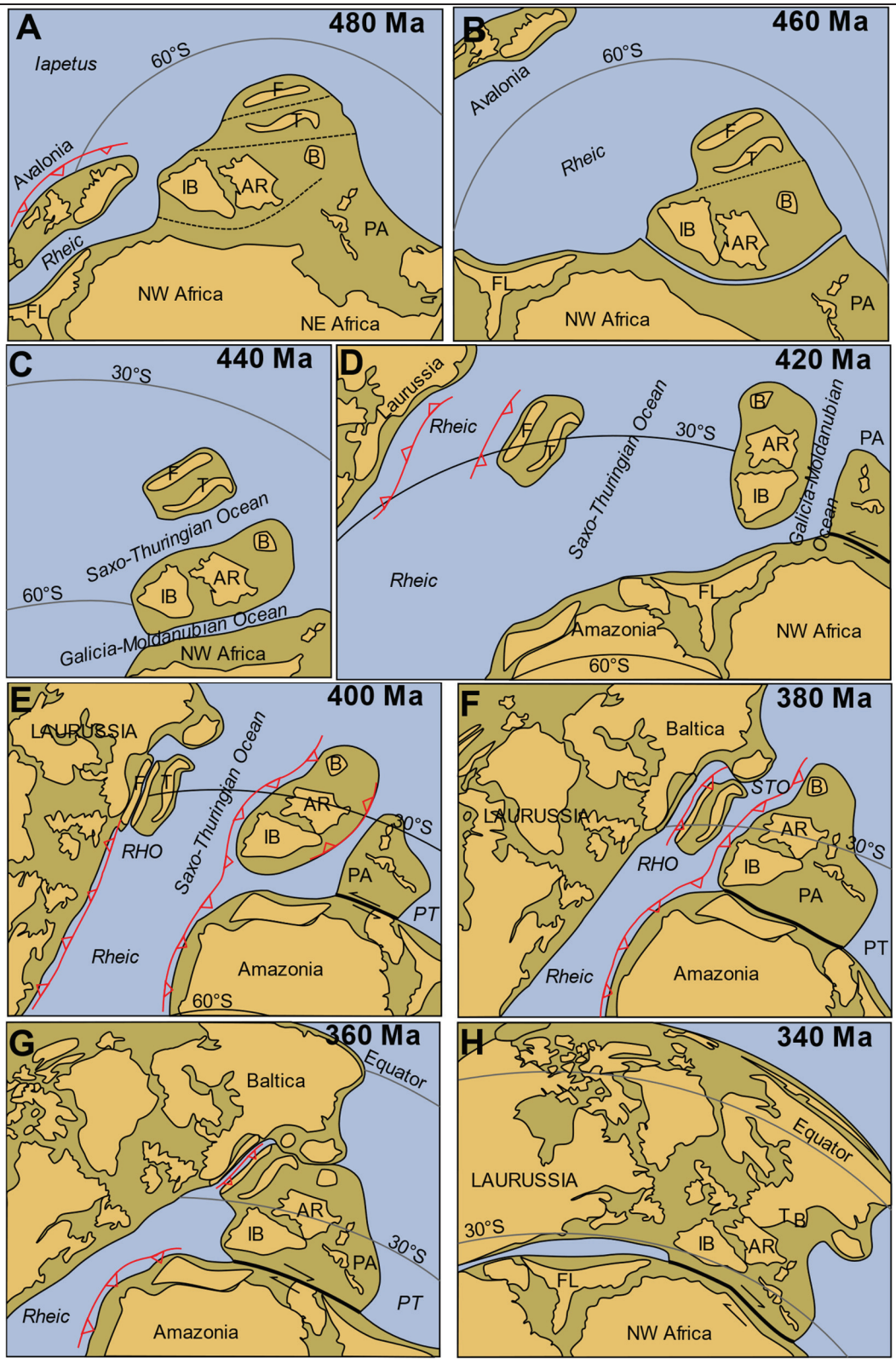

Figure 26. Formation of the Pangea and of the Hercynian Mountains. **A**, early Ordovician; **B**, middle Ordovician; **C**, early Silurian; **D**, late Silurian; **E**, early Devonian; **F**, middle Devonian; **G**, late Devonian; **H**, early Carboniferous. **Abbreviations**: **AR**, Armorica; **B**, Bohemia; **F**, Franconia; **FL**, Florida; **IB**, Iberian Peninsula; **PA**, Palaeo-Adria **PT**; Palaeo-tethys; **RHO**, Rheno-Hercynian Ocean; **STO**, Saxo-Thuringian Ocean; **T**, Thuringia (modified from Franke *et al.* 2017).

hercynian reliefs. During the Carboniferous, the Rheic Ocean ended its closure with the collision between Laurussia and Gondwana and the formation of the Pangea.

2. Climatic setting

2.1. Global tendency: the late Palaeozoic Ice Age

The end of the Palaeozoic era is characterised by an icehouse climate known as the late Palaeozoic Ice Age (LPIA). The latter started at the end of the Devonian and lasted for 50 to 90 Ma (Crowell 1978; Frakes *et al.* 1992; Bishop *et al.* 2010; Montañez & Poulsen 2013). The late Carboniferous and the early Permian constitute its climax (e.g. Fielding *et al.* 2008; Montañez & Poulsen 2013). This glacial event is unique by its duration, i.e. the longest of the Phanerozoic (Mercuzot 2020), and by the co-development of large intertropical forests without equivalent in the modern ecosystems (Cleal & Thomas 2005).

The origin of this icehouse settings was favoured by multiple cause such as the formation of the Pangea which modified the atmospheric circulation and concentrated large arid areas at high latitudes (Isbell *et al.* 2008), the formation of the Great Pangean Mountains which initiated a CO_2 sink through silicate alteration (Goddéris *et al.* 2017), the CO_2 sequestration through development of large forest systems resulting in low atmospheric CO_2 pressure similar to the current one (e.g. Foster *et al.* 2017) and the intense explosive volcanism which produced sulfate aerosols inducing cold climatic conditions (Sur *et al.* 2015).

As the majority of landmasses were situated in the southern hemisphere, traditional views reconstructed a unique ice cap in the southern pole (Veevers 1994; Ziegler 1996; Hyde *et al.* 1999; Scotese *et al.* 1999). However, more recent studies argued for multiple small ice caps (Fig. 27) in the southern Gondwana (e.g. Isbell *et al.* 2003, 2012; Tabor & Poulsen 2008). The ice caps were not constant, and three phases of increase interspersed by decreases are recognised (Isbell *et al.* 2003): from the Frasnian to the Tournaisian, from the Bashkirian to the Moscovian and from the Gzhelian to the Sakmarian/Artinskian.

2.2. Climate at the Carboniferous-Permian transition

The Carboniferous-Permian transition was the most intense period of the LPIA. The atmospheric CO_2 concentration was low (Berner & Kothavala 2001) and progressive turn over from an icehouse to a greenhouse climate began (e.g. Roscher & Schneider 2006). This turn-over came with alternations of aridification and wet periods that occurred from the late Moscovian to the early Artinskian (Roscher & Schneider 2006). These events are particularly

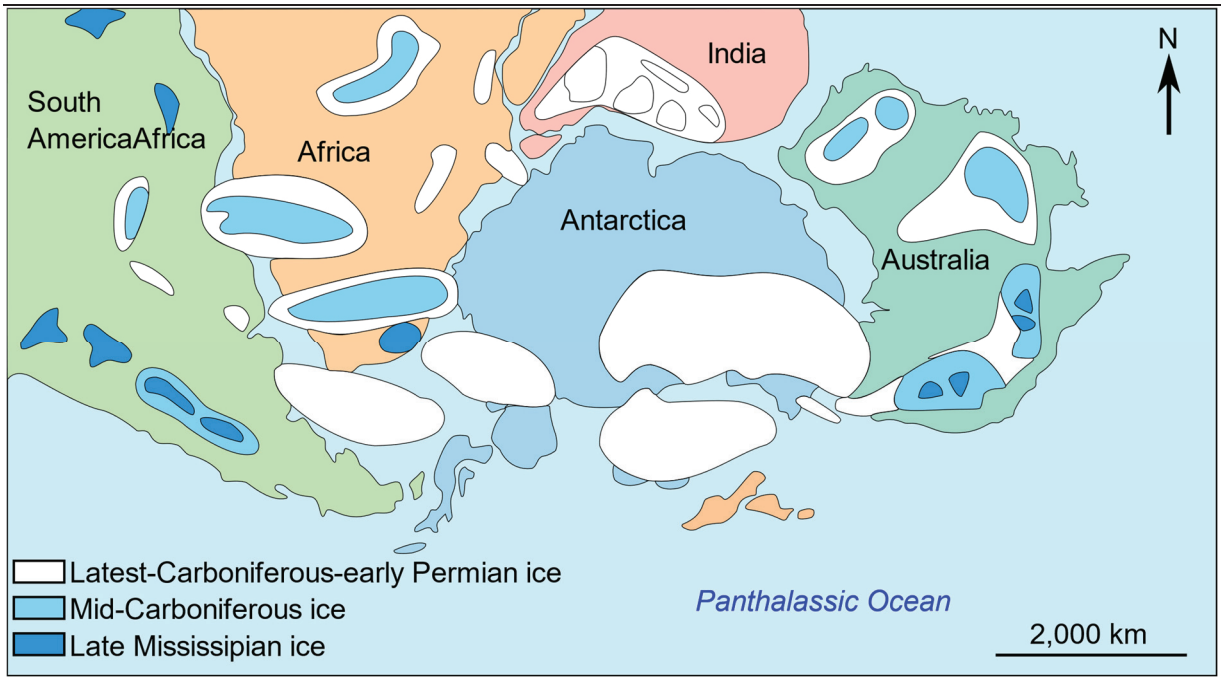

Figure 27. Distribution of the ice caps in the southern Gondwana during the Late Palaeozoic Ice Age (modified from Montañez & Poulsen 2013).

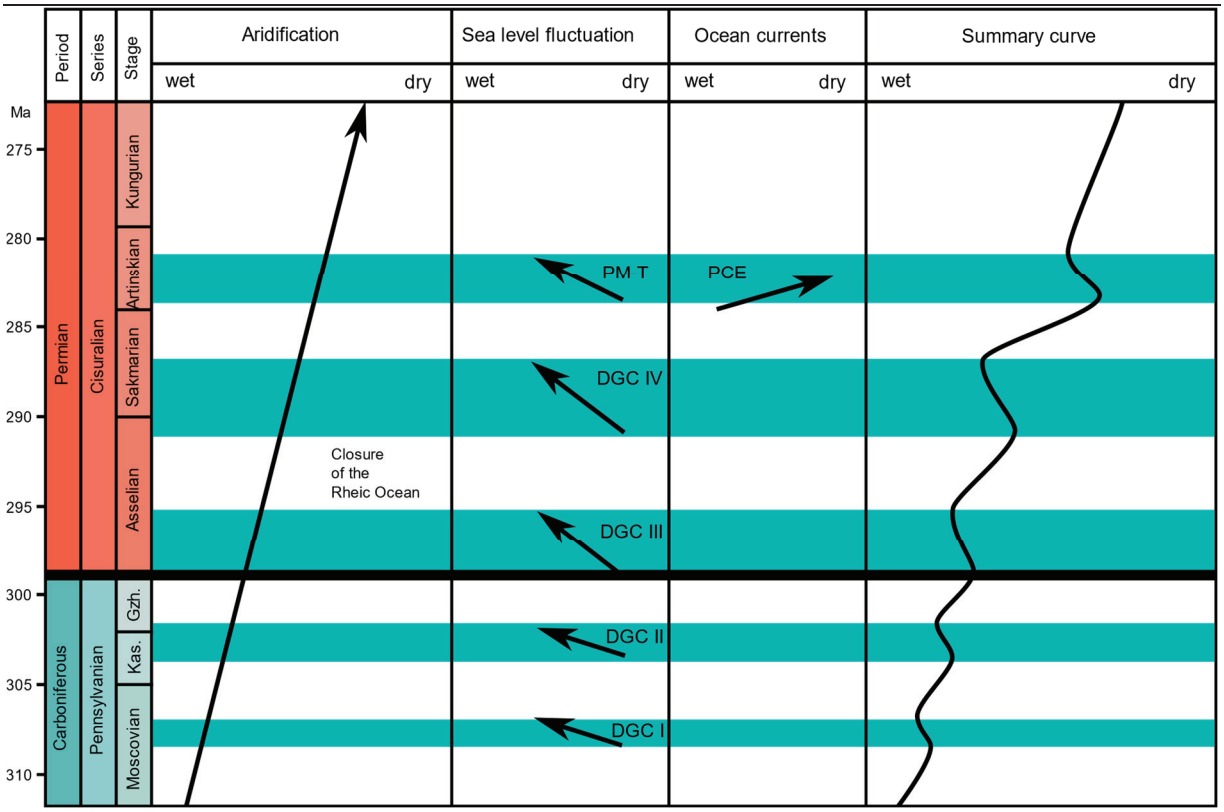

Figure 28. Climate curve at the Carboniferous-Permian transition. **Abbreviations**: **DGC I–IV**, Deglaciation Cycle 1–4 of the Gondwana Icecap; **PM-T**, Pietermaritzburg Transgression; **PCE**, Permian Chert Event (modified from Roscher & Schneider 2006).

well-recorded in the African and European Carboniferous-Permian basins including the Autun and the Bourbon-l'Archambault basins (Roscher & Schneider 2006).

The different wet events (Fig. 28) seem to have been caused by the decrease of the ice caps: the increase of the sea level could be the main factor for the development of wet climate in the northern Pangea (Mercuzot 2020). Regarding the different climatic areas, the eastern Pangea was characterised by a tropical setting with a monsoon system whereas an arid one occurs in its western part. In the highest latitudes, there is a cold temperate climate (Scotese 2002).

3. Stratigraphical correlations of the Carboniferous and Permian deposits of Western and Central Europe

The continental Carboniferous-Permian sedimentary sequences are divided into continental 'stages' ('Westphalian', 'Stephanian', 'Autunian', 'Saxonian', 'Thuringian', 'Rotliegend') which do not correspond to the referent stages of the International Chronostratigraphical Chart (Mercuzot 2020). These 'stages' have a significant importance for the geology of the Western and Central Europe because a few of them, like the 'Autunian' (*sensu* Gand *et al.* 2017), were used to define local continental stratotype. However, the definition of these 'stages' is geographically ambiguous: they are mainly defined on micro- and macrofloristic assemblages. Consequently, their limits are more influenced by environmental changes than evolutionary ones, and they can significatively vary from one region to another. The correlations between the different European basins are thus difficult and must be limited to nearby basins (Fig. 29). Their use must also be limited to describe facies without precise dating.

4. The Autun Basin

4.1. Overview

The Autun basin (Saône-et-Loire, France) is located in the Northern Massif central (Fig. 30; Elsass Damon 1977). It is a half-graben that measures 30 km from the West to the East and 13 km from the North to the South (Marteau 1983; Châteauneuf & Farjanel 1989). Lying on Devonian-Carboniferous magmatic basement (Fig. 31), its inner synclinal structure was caused by post-permian compressive tectonic movements (Elsass Damon 1977; Marteau 1983). Its highest altitude reaches 458 m. It constitutes a part of the drainage basin of the Arroux river (Mercuzot 2020).

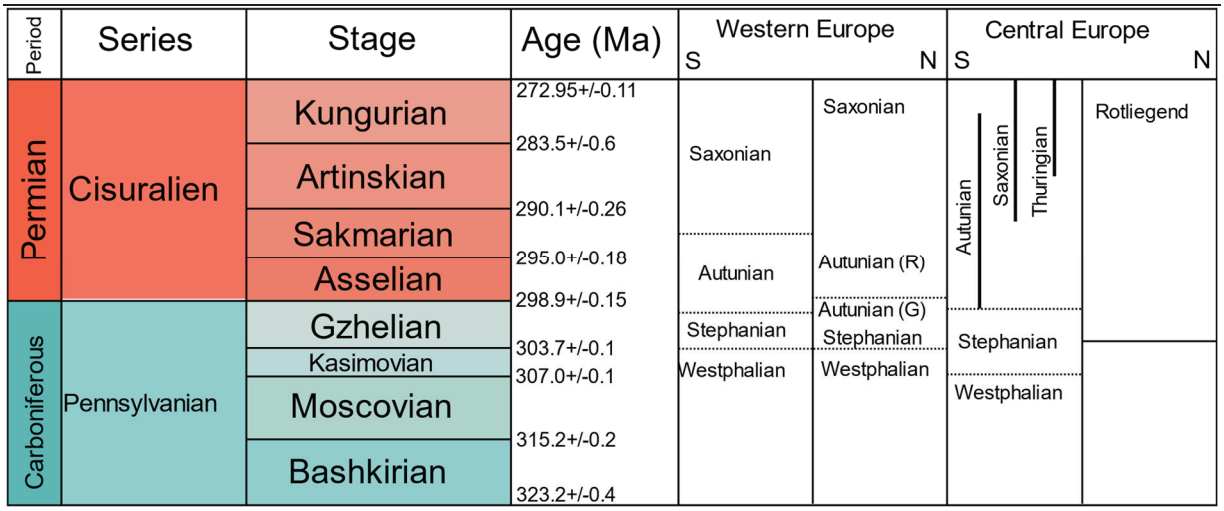

Figure 29. Assumed correlations between the international chronostratigraphical stages and the continental 'stages' at the Carboniferous-Permian transition in Western and Central Europe (modified from Bercovici 2009).

At its northern margin, it is in unconformity with the Visean volcano-sedimentary rocks of the Lucenay-Lévèque complex (Marteau 1983). At its southern margin, its straight rocks, showing a high dip of 70°, come from the syn-sedimentary Autun fault (Choulet *et al.* 2012). The latter produces an unconformity between the Carboniferous-Permian sediments and the Carboniferous granite. Its western margin ends with the Visean Saint-Honoré-les-Bains volcanic tuffs. At its eastern margin, Mesozoic rocks cover the basin-basement contact (Mercuzot 2020). At some points, Pliocene-Pleistocene lacustrine formations, up to 20 m, covers the Carboniferous-Permian rocks (Châteauneuf & Farjanel 1989).

4.2. Stratigraphy and sedimentology

The Autun Basin is divided into four formations (Fig. 32; Pruvost 1942; Marteau 1983): the Igornay and Muse Formations correspond to the lower 'Autunian' and the Surmoulin and Millery Formations correspond to the upper 'Autunian'. This stratigraphical sequence could reach between 1,100 and 1,200 m of thickness at the center of the basin. Below these formations, the 'Stephanian' is represented by the Epinac coal beds and the Mont Pelé Formation, a disconformity separating the 'Stephanian' from the 'Autunian'. Above them, detritic deposits from the Triassic is present, also separating by a dsconformity (Bourquin *et al.* 2011).

The present description of the stratigraphy (Fig. 32) of the Autun Basin is essentially based on Pellenard *et al.*'s (2017) work. The 'Stephanian' Epinac sector, in the eastern part of

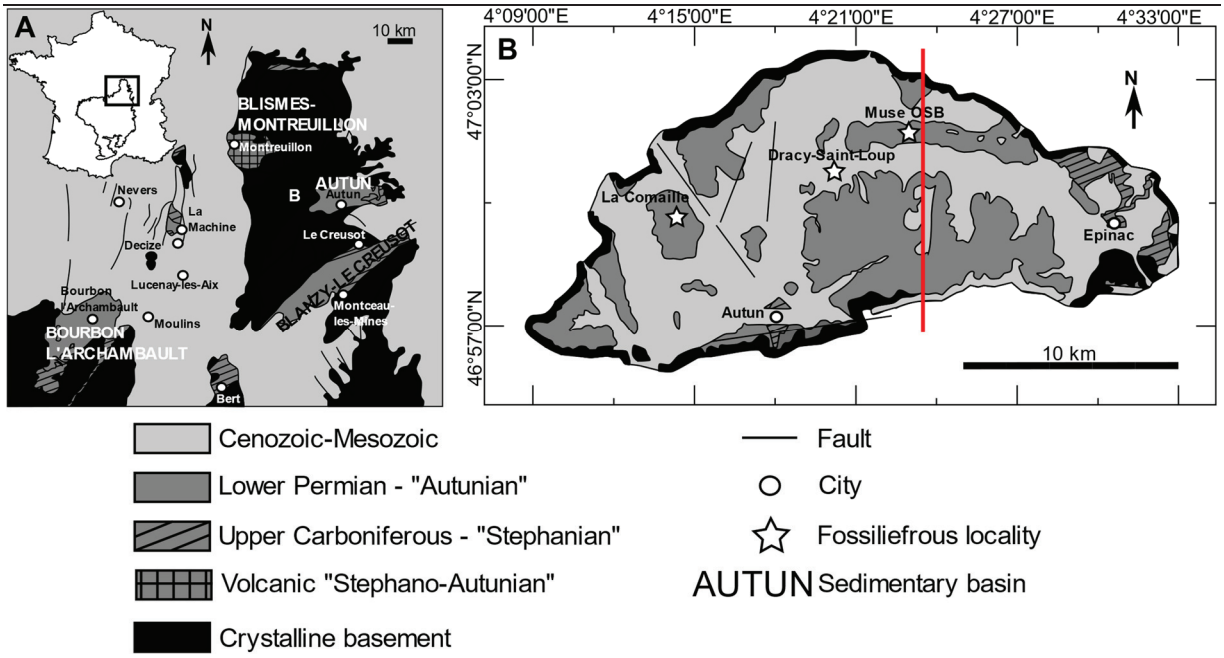

Figure 30. Geological context of the Autun Basin. **A**, Location of the Carboniferous-Permian basins of the Northern Massif central, France. **B**, simplified geological map of the Autun Basin. The red line is the transect for the Figure 31 (modified from Elsass Damon 1977; Marteau 1983; Châteauneuf *et al.* 1992; Gand *et al.* 2007, 2011, 2015, 2017; Pellenard *et al.* 2017; Mercuzot 2020).

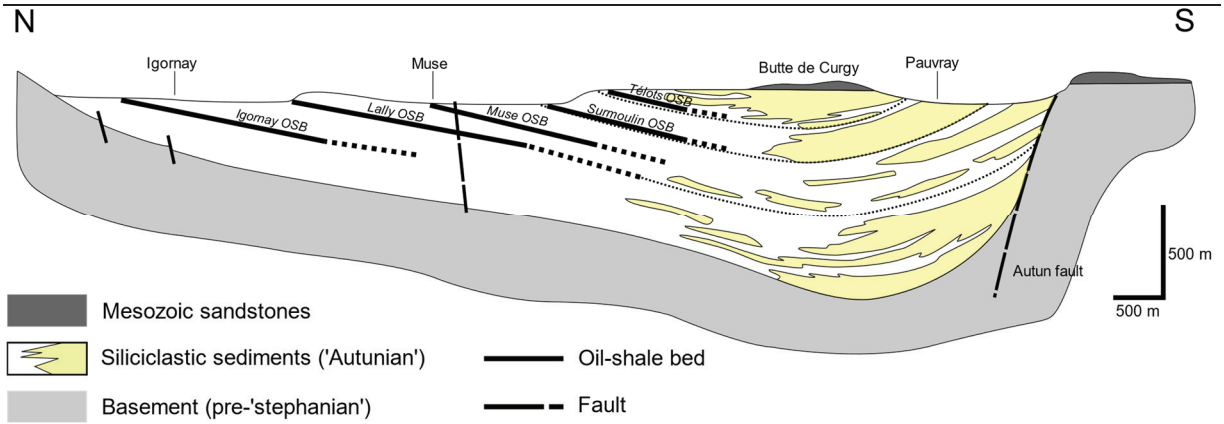

Figure 31. North-South geological section of the Autun Basin (see the Figure 30 for the location of the transect) (modified from Marteau 1983; Pellenard *et al.* 2017; Mercuzot 2020).

the basin, is constituted by the Epinac coal beds (alternation of sandstone/conglomerates and coal seams), the Mont Pelé Formation (sandstone and conglomerates) and the Grand Moloy coal bed at the base of the 'Autunian' rocks. The Igornay Formation (200 to 250 m) contains the Moloy coal bed and the Igornay oil-shale beds. Above them, there is a sandstone/claystone member, then the Lower Lally Sandstones. The Muse Formation (300 to 400 m) is constituted by the Upper Lally Sandstones, including the Lally oil-shale beds, a sandstone/conglomerate

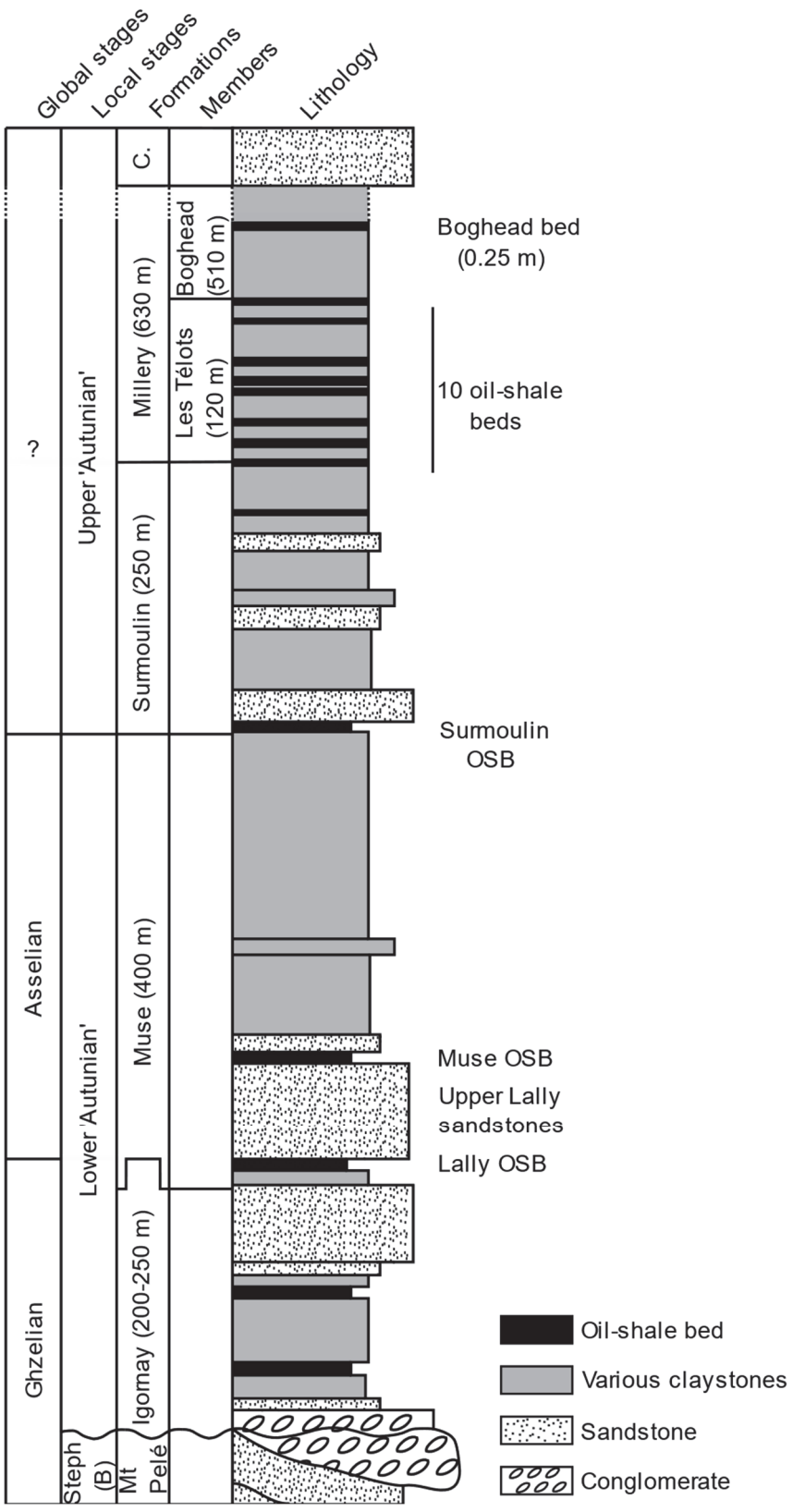

Figure 32. Simplified stratigraphy of the Autun Basin. **Abbreviation**: **C.**, Curgy Formation (200 m); **Steph**, 'Stephanian' (modified from Pellenard *et al.* 2017).

member with coal levels and the Muse oil-shale beds. The Surmoulin Formation (250 m) is mainly constituted by claystones with the Surmoulin oil-shale bed at its base. The Millery Formation (200 to 250 m) is represented by claystones and the Télots oil-shale beds. Above, there is a boghead coal with several claystone and carbonate levels. The top of the formation is characterised by redden claystones and alternations of sandstones levels. (see Pellenard *et al.* [2017] for a more detailed description of the stratigraphy of the Autun Basin).

4.3. Formation

Around the Epinac sector, the first filing phase occurred with the thin late Kasimovian-Gzhelian ('Stephanian') coal series and ended with a second filing event with the thick Gzhelian-Asselian formations ('Autunian'). They could have been caused by two subsidence phases of two different intensity directly related with the thickness of the deposits (Marteau 1983; Châteauneuf & Farjanel 1989).

The formation of a basin in the Epinac sector took place with an extensive phase based on a subsident block between two strike-slip movements. The Autun fault may be the first and an oriented NNE-SSO fault, not directly visible, may be the second one. The folding of the Epinac coal series may have been caused by a Gzhelian ('Stephanian C') compressive phase.

The half-graben shape of the Autun basin may have been acquired by a second tectonic event with an extensive phase caused by the activity of the Autun fault. The latter was diachronic from the East to the West, its eastern part was first active with the coal deposits.

4.4. Palaeoenvironment

The first attempt to reconstruct the palaeoenvironment of the Autun Basin was proposed by Marteau (1983). This study attributed the fine-grained laminated sediments and oil-shale beds to palustrine and/or lacustrine environments and the medium to coarse-grained sediments (sandstones and conglomerates) to a fluvial environment.

Recent studies (Mercuzot 2020; Mercuzot *et al.* 2022) have investigated numerous cores and outcrops section and re-interpreted the Autun Basin as mainly lacustrine: deep facies are prominent in the Gzhelian with the association of laminated levels and oil-shale beds corresponding to periods of dysoxia and/or anoxia of the bottom water. During the early Asselian, the facies become more proximal with an acme at the Gzhelian/Asselian transition. In all cases, the palaeoenvironment of the Autun Basin is always seen as freshwater without marine influence.

4.5. The Muse OSB fossiliferous locality

The lowermost Permian fauna of the Muse OSB contains a rich aquatic vertebrate assemblage including chondrichthyans (Xenacanthiformes; Agassiz 1833-43; Gaudry 1883; Sauvage 1893; Heyler 1969, 1987; Heyler & Pacaud 1978; Heyler & Poplin 1982, 1989; Heyler & Debriette 1986; Poplin & Heyler 1989; Soler-Gijón & Hampe 1998), acanthodians (Heyler 1969), actinopterygians (Aeduelliformes and Paramblypteriformes) (Heyler 1969, 2000; Poplin & Dutheil 2005) and temnospondyls (Schoch 1992; Steyer *et al.* 1997; Werneburg & Steyer 1999). Historical findings come from the fossiliferous layer called the "fish layer" (locally called "*couche à poisson*") that have provided numerous remains of the actinopterygian *Aeduella blainvillei* (e.g. Brignon 2014) at the base of the serie. From 2010, scientific excavation campaigns have been organised in order to complete the fauna and flora lists and to clarify the taphonomic and stratigraphic context (Gand *et al.* 2011, 2015).

The Muse OSB fossiliferous locality is situated in the northern part of the Autun Basin and correlated with the Muse OSB in the Muse Formation (Gand *et al.* 2007, 2011, 2015, 2017; Pellenard *et al.* 2017). The stratigraphic series (Fig. 33) was detailed by Pellenard *et al.* (2017): it is made of 3.5 m of black to grey claystones to siltstones with some thin sandstone levels. Within the stratigraphic series, ten volcanic layers, probably ashfall deposits, locally named '*gores'* and more commonly named tonsteins, are found. They are ochre clayey layers intercalated with claystones and siltstones. A recent study by Pellenard *et al.* (2017) has radiochronologically dated two tonsteins within the Muse OSB locality at 298.05 ± 0.39 Ma and 298.57 ± 0.38 Ma. So, this locality represents the lowermost Permian in the Autun Basin, just above the Carboniferous-Permian limit.

The palaeoenvironmental reconstruction of the Muse OSB is ambiguous, depending on the method used to reconstruct it. The facies characterisation indicates a deep lake with dysoxia/anoxia in the bottom water (Mercuzot 2020; Mercuzot *et al.* 2022) whereas the isotopic and elemental geochemistry on the organic matter seems to indicate a lacustrine coastal zone without significative depth (Mercuzot 2020).

5. The Bourbon-l'Archambault Basin

5.1. Overview

The Bourbon-l'Archambault Basin is located in the Northern Massif central, southeast to the Autun Basin (Fig. 34; Châteauneuf 1980; Châteauneuf & Farjanel 1989). Structurally, this basin is divided into two sub-basins by the central granitic horst named the 'Gipcy-Bourbon

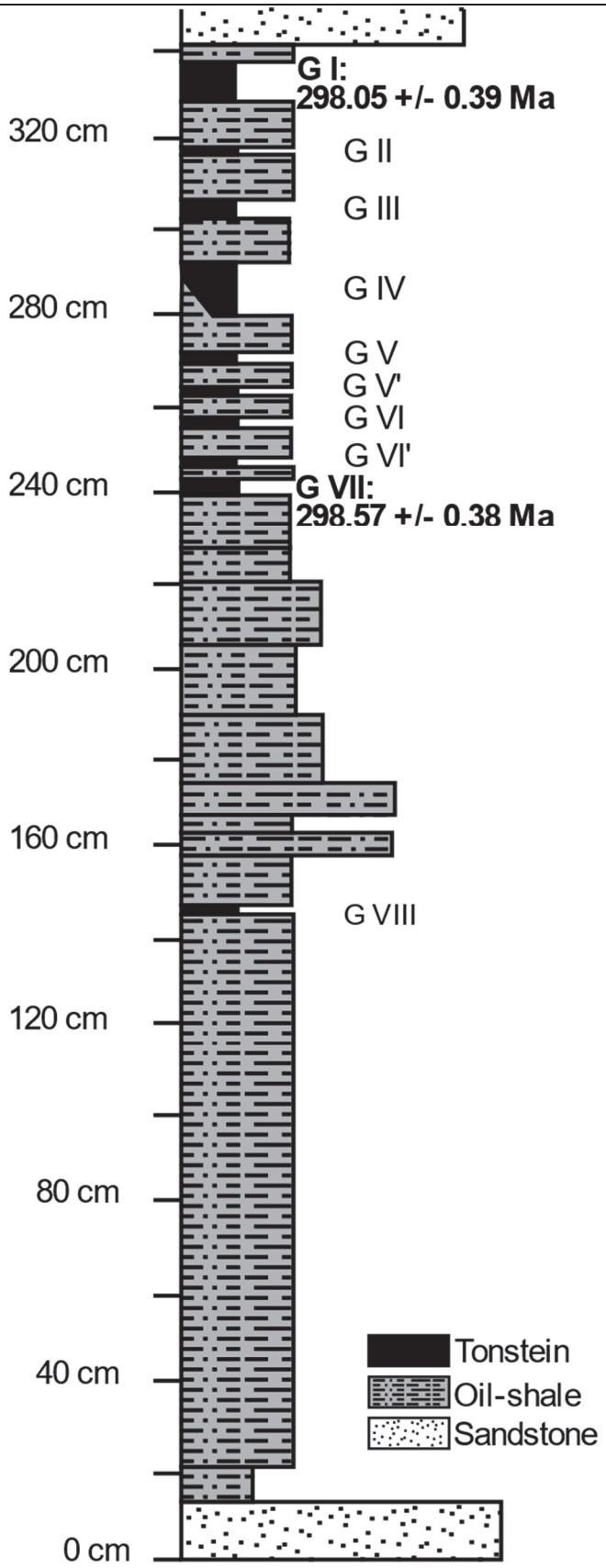

Figure 33. Stratigraphical section of the Muse OSB fossiliferous locality. **Abbreviation**: **GI to VIII**, Tonstein ('*Gore'* in French) (modified from Pellenard *et al.* 2017).

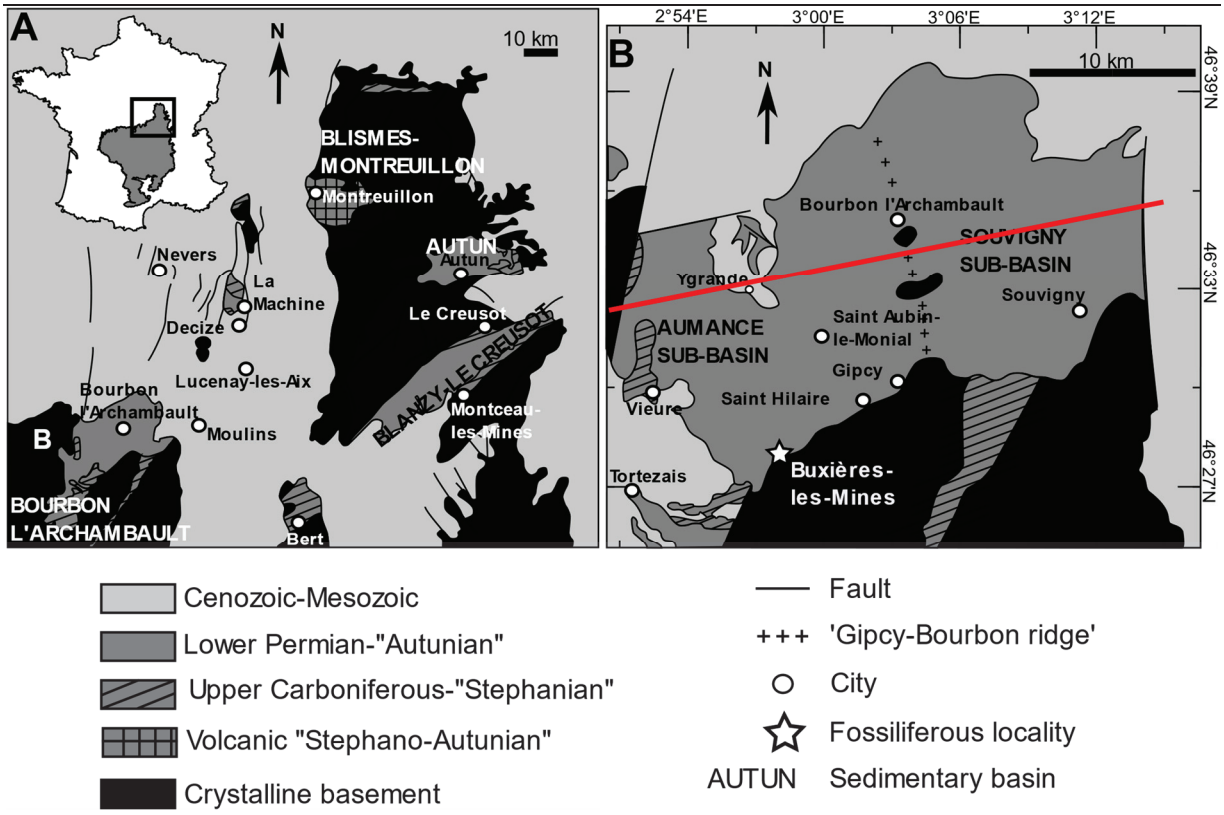

Figure 34. Geological context of the Bourbon-l'Archambault Basin. **A**, Location of the Carboniferous-Permian basins of the Northern Massif central, France. **B**, simplified geological map of the Bourbon-l'Archambault Basin. The red line is the transect for the Figure 35 (modified from Marteau 1983; Steyer *et al.* 2000).

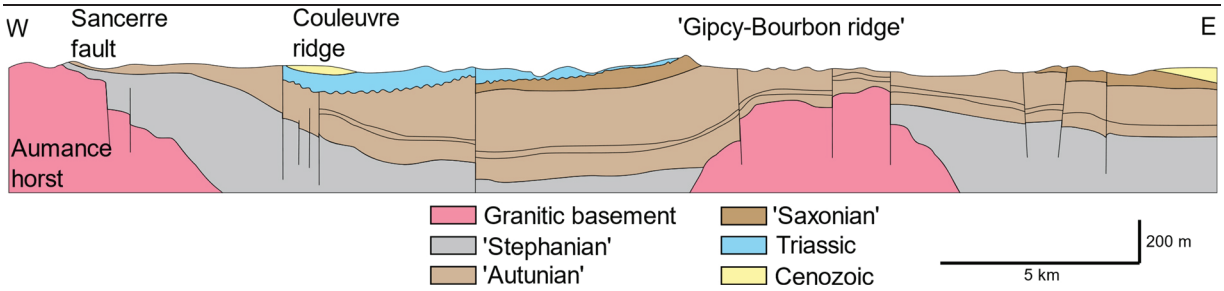

Figure 35. West-East geological section of the Bourbon-l'Archambautl Basin (see the Figure 34 for the location of the transect) (modified from Mathis & Brulhet 1990).

ridge': the western part is the Aumance sub-basin, and the eastern part is the Souvigny sub-basin (Mathis & Brulhet 1990). Its mean altitude reaches 300 m. It constitutes a part of the drainage basin of the Aumance river (Mercuzot 2020).

The Bourbon-l'Archambault is situated between the Aumance granitic horst to the West and the Montmarault granitic complex to the east (Fig. 35). Its northern margin is limited by the Mesozoic deposits of the southern margin of the Paris Basin. At its southern margin, there

are Cenozoic deposits Separated by a disconformity. The majority of the basin represents 'Autunian' deposits even if some 'Stephanian' rocks are present in its southern part (Mercuzot 2020).

5.2. Stratigraphy and sedimentology

Bougnieres (1961) and Paquette (1980) described the stratigraphy and sedimentology of the Bourbon-l'Archambault Basin (Fig. 36). It is divided into four formations that extend from the 'Stephanian' with the Inférieure Formation to the lower 'Autunian' with the Mouillère and Buxières formations and the upper 'Autunian' with the Renière Formation.

The Inférieure Formation (500 m) is composed of conglomerates with alternations of claystones and siltstones with a pronounced dip of 40° to 45°. The Mouillière Formation (200 m) represents the first deposits of the 'Autunian', separated from the 'Stephanian' by lithological and palynological criteria. Its base corresponds to an unconformity, and it is mainly composed of conglomerates. The Buxières Formation (350 m) contains oil-shale beds and coal levels. Even if this formation is considered as lower 'Autunian', there are still ambiguities due to the presence of potential 'stephanian'-related flora. Numerous tonsteins are reported and among them two are of particularly importance: the 'Lien Blanc' and the 'Lien Vert'. These two tonsteins were tentatively dated at 294.6+/- 3.2 Ma and 295 Ma respectively (Ducassou *et al.* 2018; S. Bourquin, pers. comm., 2022). This putative dating confirms a lower Permian age and excludes a 'Stephanian' age. At the top of this formation, there are dolomites associated with tonsteins. Some of them are tentatively related to microbial deposits. The Renière Formation (500 m) corresponds to coarse sandstones and conglomerates with alternations of claystones/siltstones and carbonates/black claystones. Above the Renière Fomation, the 'Saxonian' is visible in the northern margin of the basin. Above it, there are Triassic sandstones.

5.3. Evolution of the palaeoenvironment

The palaeoenvironment (Fig. 37; see Paquette [1980] for details on the environment and the corresponding facies) of the Bourbon-l'Archambault Basin has evolved following the different steps of its formation (see Mathis & Brulhet 1990). During the 'Stephanian', the filling of the basin had just begun thanks to the erosion of the relief at the West and the deposits were controlled by active faults. In this context, the aquatic environment was limited to swamps with coarse sediments and plant debris at the bottom of scree slopes.

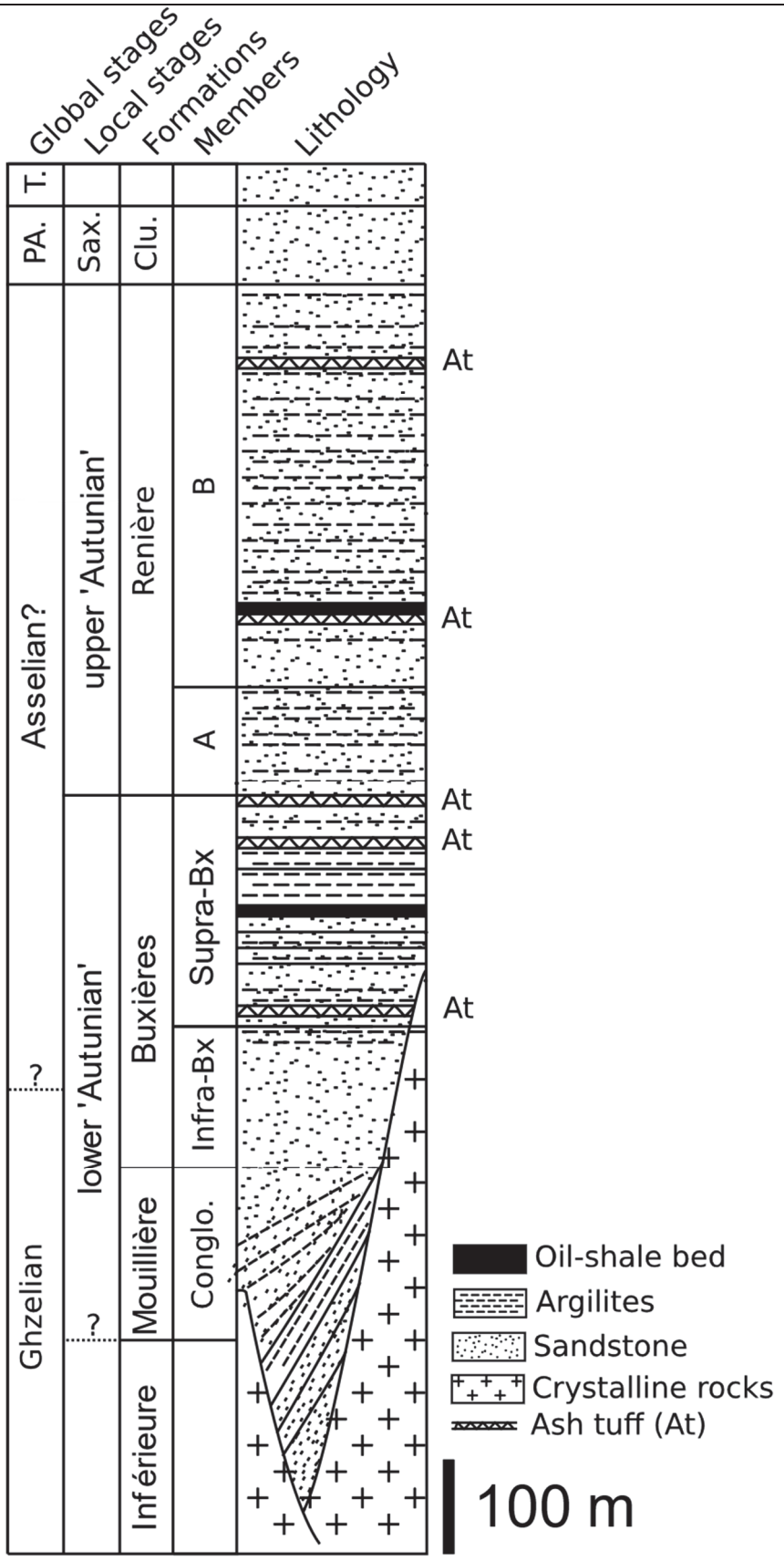

Figure 36. Stratigraphical section of the Bourbon-l'Archambault Basins. **Abbreviation**: **Bx**, Buxières; **Clu**, Clusor Formation; **Post A**, Post Asselian; **Sax**, Saxonian; **T**, Trias (modified from Debriette 1992; Steyer *et al.* 2000).

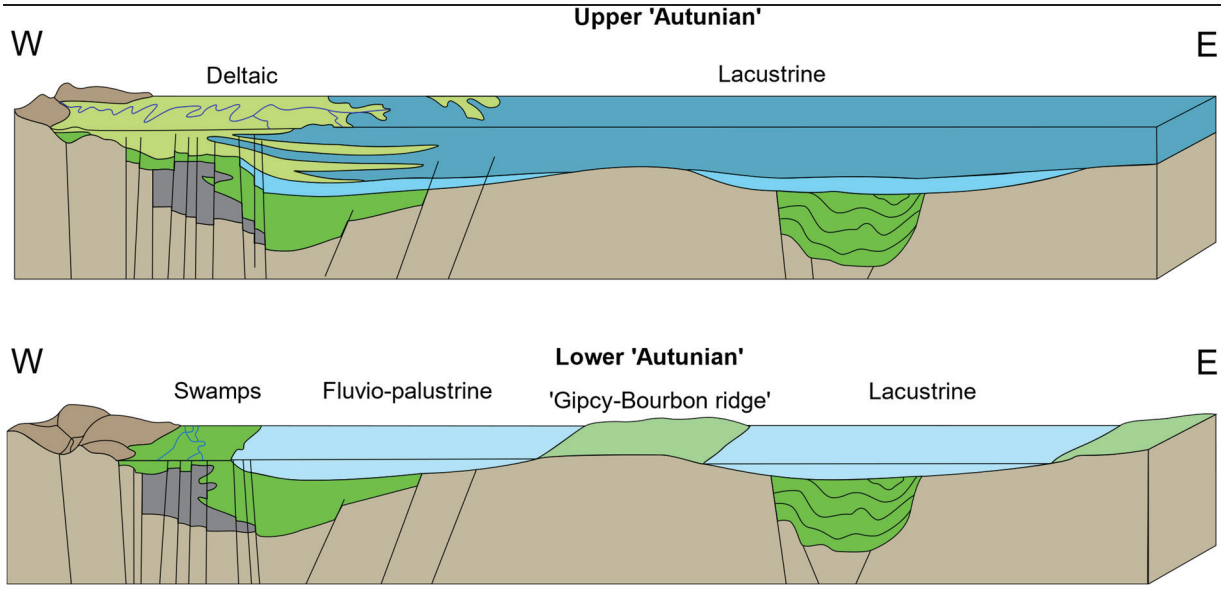

Figure 37. Evolution of the palaeoenvironment during the lower Permian in the Bourbon-l'Archambault Basin (modified from Mathis & Brulhet 1990).

During the lower 'Autunian', extensive movements have allowed the development of the basin to the East. The western part of the basin was therefore characterised by fluvio-palustrine environment with sandstones to coarse conglomerates. The coal levels and associated carbonates with animal and plant debris are characteristic of pure palustrine facies. In the eastern part, a lacustrine environment with laminated or bituminous claystones associated with vertebrate debris is reported. The two geographical sectors are separated by the 'Gipcy-Bourbon ridge'. During the upper 'Autunian', the 'Gipcy-Bourbon ridge' was drowned and the whole basin corresponds to a large lacustrine environment associated with deltaic inputs.

5.4. Buxières-les-Mines

The former open-cast coal mine of Buxières-les-Mines is a fossiliferous locality that have provided a diversified aquatic vertebrate fauna including chondrichthyans (Xenacanthiformes, Hybodontiformes; e.g. Steyer *et al.* 2000), acanthodians (Heyler 1984; Heyler & Poplin 1990), actinopterygians (Palaeonisciformes; Štamberg 1998, 2018) and temnospondyls (Steyer *et al.* 2000). Palaeontological investigations are occasionally reported from the 19th century to the 1950s (de Launay 1888; Berthoumieu 1903; Letourneur 1953; Guillot 1958; Bougnieres 1961). From the 1990s, excavation campaigns have been organised to complete the faunal and flora taxonomic lists (Steyer & Escuillié 1997; Steyer *et al.* 2000).

This fossiliferous locality is located in the southern part of the Bourbon-l'Archambault Basin within the Buxières Formation. The presence of the two tonsteins 'Lien Blanc' and 'Lien

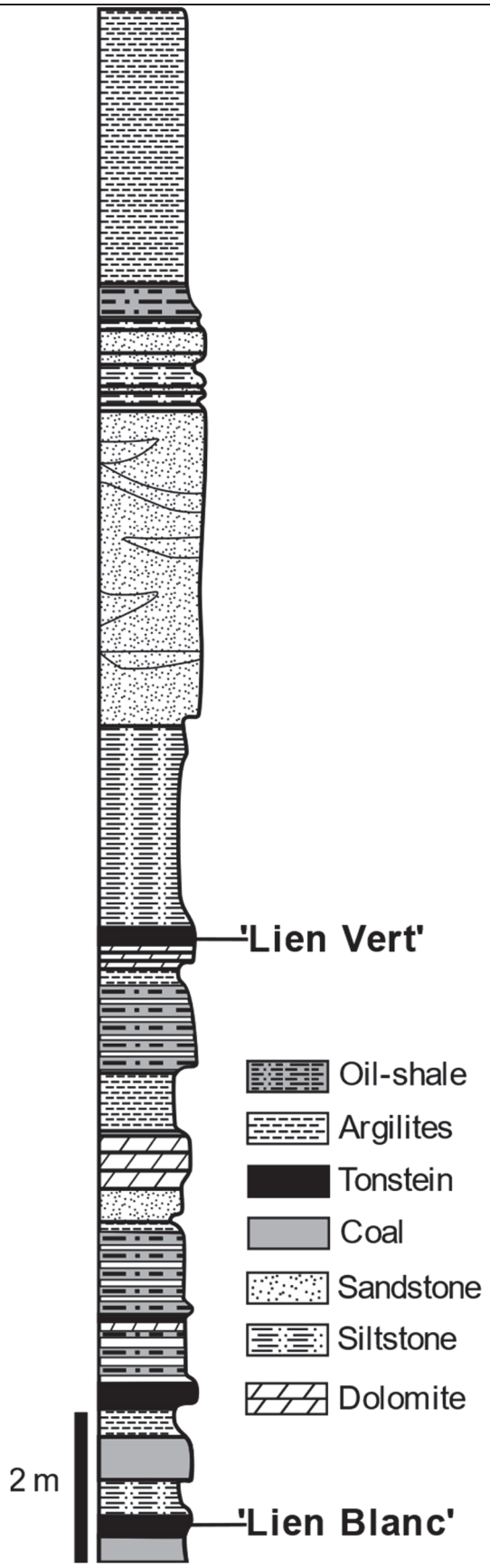

Figure 38. Stratigraphical section of the Buxières-les-Mines fossiliferous locality (modified from Steyer *et al.* 2000).

Vert' indicates a late Asselian to early Sakmarian age. The stratigraphical section (Fig. 38) is mainly composed of oil-shale, claystone and siltstone levels that contain the majority of the fossils found to date. Coal beds are reported at the base of the stratigraphic section and sandstones occur in the upper half (Steyer *et al.* 2000). The palaeoenvironment of Buxières-les-Mines has been seen as lacustrine to palustrine (Steyer *et al.* 2000) with potential periods of drying up (Kaulfuß 2003).

6. Hypothesis of marine influences in the continental European Carboniferous-Permian basins

The European Carboniferous-Permian basins have been traditionally interpreted as freshwater environment. The reasons are the absence of clear sedimentological evidence of a marine influence and palaeogeographical reconstructions that situated the sea far away, more than 200 km in several cases.

However, recent studies (Schultze & Soler-Gijón 2004; Schultze 2009) have questioned this interpretation and proposed that marine influences could have occurred in these basins. The arguments are the presence of several taxa which are typically marine components. For example (see Schultze [2009] and Table 2 for the detailed list), there are acritarchs in the Puertollano Basin (Spain) and in Montceau-les-Mines (France), myxinoids in Montceau-les-Mines, some polychaetes in Montceau-les-Mines and Eurypterids in the Saar-Nahe Basin and in Bohemia. Furthermore, in many European basins, the presence of many saltwater-tolerant taxa such as acanthodians, lungfishes, palaeonisciforms, osteolepiforms, actinistians, conchostracans, syncharids, ostracods and limulids is also seen as evidence of at least brackish environment. Finally, the faunal lists of several European basins are similar (Table 2). Following Schultze & Soler-Gijón (2004) and Schultze (2009) the most parsimonious explanation for these similarities are migrations through marine settings, implying connections to the sea, despite their absence in palaeogeographical reconstructions.

Regarding the Autun and the Bourbon-l'Archambault basins, and more precisely the Muse OSB and Buxières-les-Mines fossiliferous localities, their faunal lists do not allow to clearly support a marine influence. The late Carboniferous ('Stephanian') Montceau-les-Mines Basin is not contemporaneous and typical marine marker like myxinid (Poplin *et al.* 2001) lacks in the early Permian localities of the Muse OSB and Buxières-les-Mines. Furthermore, geochemical analyses of shark teeth from Buxières-les-Mines agree with a freshwater

Table 2. Faunal composition of some European Carboniferous-Permian basins. * indicates marine and brackish to euryhaline fauna (modified from Schultze 2009).

Taxa	**Puertollano (Spain)**	**Montceau-les-Mines (France)**	**Saar-Nahe (Germany)**	**Central Germany**	**Bohemia (Czech Republic)**
Acritarchs*	x	x			
Medusae		x	x	x	x
Anthraconaia		x	x	x	
Polychaeta*		x			
Microconchids		x	x	x	x
Onychophoran		x			
Arthropleura		x	x	x	x
Euthycarcinoid		x			
Limulid		x	x		x
Eurypterid			x		x
Conchostracans*	x	x	x	x	x
Ostracodes*		x	x	x	x
Syncarids*		x	x		x
Isopods		x			
Arachnids		x			x
Scorpions		x			x
Myriapods		x	x		x
Insects		x	x	x	x
Brachiopods					
Echinoderms					
Myxinids*		x			
Petromyzontids					
Xenacanths	x	x	x	x	x
Euselachians	x		x	x	x
Palaeoxyris			x	x	x
Acanthodians	x	x	x	x	x
Palaeonisciformes	x	x	x	x	x
Haplolepiforms		x			x
Platysomids	x				
Lungfish*		x (Autun)	x		x
Coelacanth*			x		

Taxa	Puertollano (Spain)	Montceau-les-Mines (France)	Saar-Nahe (Germany)	Central Germany	Bohemia (Czech Republic)
Osteolepiforms*			x		
Branchiosaurs		x	x	x	x
Amphibamids					x
Temnospondyls	x	x	x	x	x
Aïstopods		x			x
Lepospondyls	x	x	x		x

environment influenced by evaporations, as indicated by the reconstructed sedimentological setting (Kaulfuß 2003). However, some authors (Mercuzot 2020; Mercuzot *et al.* 2022) have argued in favour of a connection between the Carboniferous-Permian basins from the Northern Massif central. In this case, the question of marine influences, still not recovered in the Autun and Bourbon-l'Archambault basins must be investigated.

7. Lacustrine environment

Buxières-les-Mines and the Muse OSB have been interpreted as potential lacustrine environments. It is therefore informative to understand their peculiarities.

7.1. Definition

The most general definition of a lake could be an inland water body within a topographic depression in the Earth's crust, larger than a pond, and in which sedimentation or water stratification occurs (Kelts 1988; Touchard 2000). The viable condition for its maintenance is a positive hydrological balance between the inputs (precipitations, river systems) and the outputs (evaporation) which depend on the climatic (atmospheric convection), the geographic (altitude, continentality) and the orbital settings (Street-Perrott & Harrison 1984; Kutzbach & Street-Perrott 1985; Kelts 1988). Depending on its formation a lake can contain freshwater, brackish water or saltwater. Its waters are stagnant contrary to the streams or rivers (Forel 1901; Touchard 2000). It is also independent from the marine environment without direct water exchange (Touchard 2000).

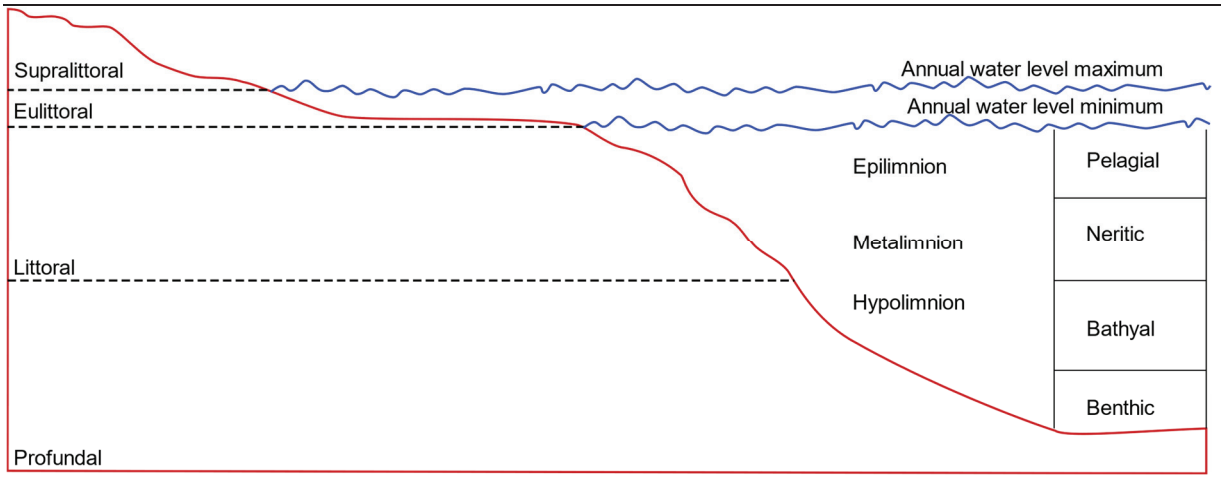

Figure 39. Structuring of a lake water column (modified from Kelts 1988).

7.2. Structure

A lake is characterised by a water stratification (Fig. 39) producing different physico-chemical zonings within the water column. The epilimnion is the surface water, in contact with the atmosphere and delimited at its base by the thermocline. The biological productivity is at its maximum and concentrates the oxygen (e.g. Hutchinson 1957). The metalimnion is the transition zone between superficial and deep water and could be interpreted as the thermocline or the chemocline. Finally, the hypolimnion corresponds to the deep water with a constant temperature. The oxygen level is at its minimum in the hypolimnion, allowing a good preservation of the organic matter (e.g. Hutchinson 1957).

As for the marine environment, the lacustrine water column can also be divided into a pelagic zone under the influence of the tide, a well-oxygenised neritic zone and a deep bathyal zone that makes the transition with the benthic zone on the bottom of the lake (Kelts 1988).

The coast of a lake can be divided into the supralittoral zone, which is always above the annual water level maximum, the eulittoral zone which is between the annual water level maximum and minimum, the littoral zone whose lower limit is the metalimnion-hypolimnion transition and the profundal zone which is under the influence of the hypolimnion (Kelts 1988).

In some case, this water stratification can be removed, and the top and bottom waters mix. This happens when the thermal gradient becomes negligible, for example during the winter when the superficial water is cold and dense (Mercuzot 2020). An amictic lake never mix its waters, a monomictic lake mixes its waters once per year, a dimictic one mixes twice per year and a polymictic lake mixes its waters several time per year.

7.3. Formation

There are numerous mechanisms for the formation of lakes (see Hutchinson [1957] for the details and Kelts [1988] for an abridged version). Some lakes are formed by short term processes, i.e. the event lake, including meteorite and volcanic craters, landslides, glacial lakes, karst sink-holes, groundwater lakes and rivers meanders. When depressions occur in the marine coastline, paralic lakes can be formed with their water level controlled by the sea level fluctuation. Tectonic lakes correspond to those formed by crustal warps, foreland deeps, intermountain basins, rift and strike slip. Following Biddle & Christie-Blick (1985), the fast subsidence and the long history of tectonic lake made them more likely to be preserved in the geological record.

7.4. Geochemistry

Lake pH could range from 1 to 11 (Kelts 1988). The geochemical content of a lake is expressed by the Total Dissolved Solids (TDS) which represents all the suspended inorganic and organic particles. It ranges to depleted oligosaline environment as the Cameron Crater Lakes (around 50 ppm TDS) to the hypersaline Qarhan Lake (around 500,000 ppm TDS; see Kelts [1988] and the reference within). Nutrients, principally orthophosphate, come from drainage basin geology by precipitations, river systems and wind (Kelts 1988). The nutrient content ranges from 5-10 µg/L for oligosaline lakes to 100 µg/L for hypersaline ones (Wetzel 1983).

7.5. Characteristics of tropical lakes

The palaeolatitudes of Buxières-les-Mines and the Muse OSB indicated a tropical to equatorial context.

Lewis Jr (1987) reported numerous features that seem to significatively vary between lakes from low and high latitudes (Fig. 40). Tropical lakes are characterised by a high annual solar irradiance throughout the year. They do not record the highest solar irradiance values and they exhibit the lowest differences between the annual maximum and minimum. Furthermore, the water temperature in tropical lakes is constant with a few variations of the superficial water and a few differences between the top and the bottom lake. They also show little differences in the variation of daily irradiance between the seasons. At low latitudes, the Coriolis effect is at its minimum, so the currents in the superficial waters are less disturbing than in higher latitudes. Consequently, the water stability, i.e. the thermal ability to homogenise the water column, is also at its minimum under low latitudes. The lower the mixed water thickness, i.e. the

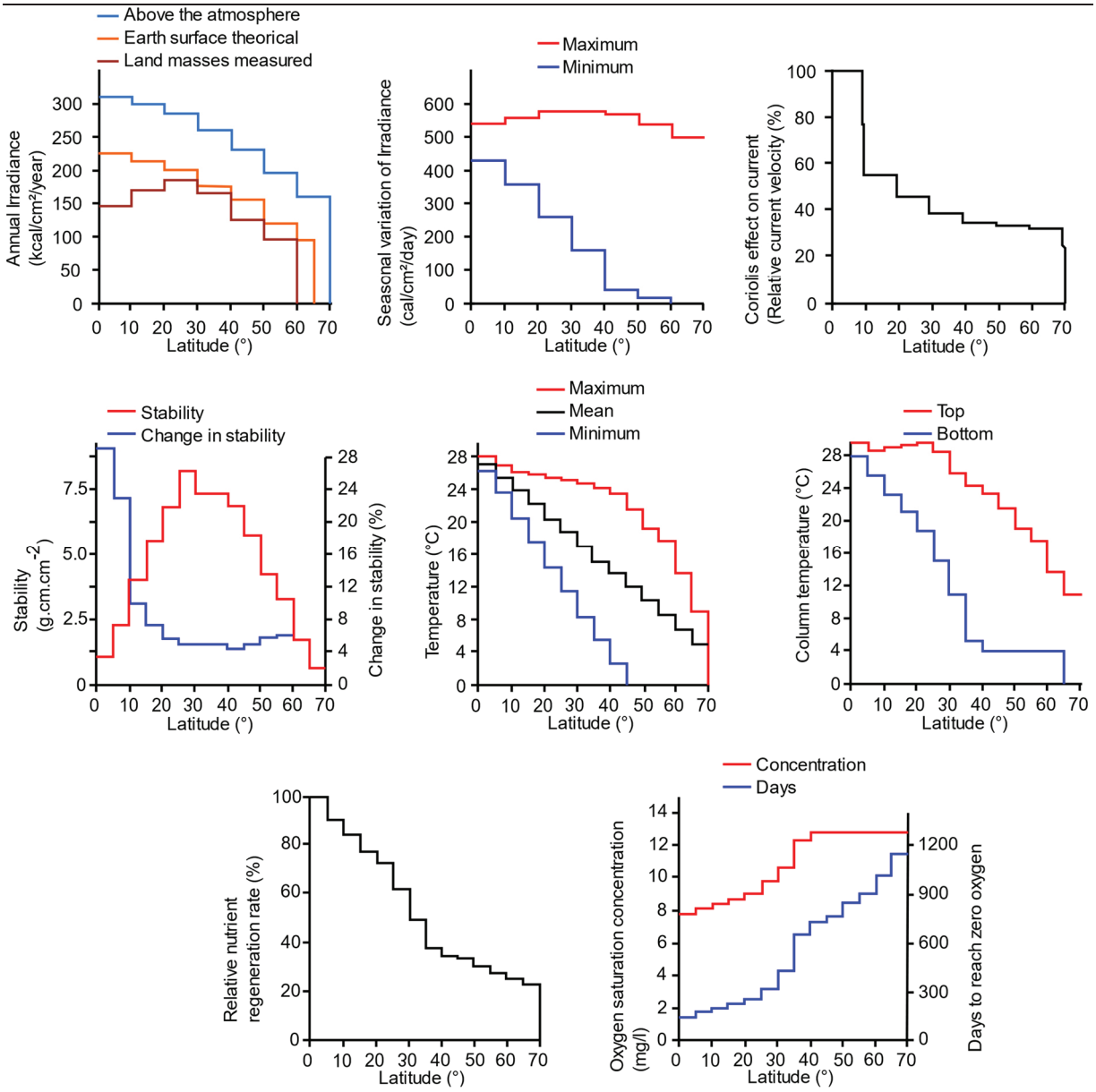

Figure 40. Characteristics of lacustrine environment and their variation across latitudes (modified from Lewis Jr (1987).

epilimnion, is, the higher the primary productivity. The mixed water thickness is reported to vary more than in temperate lakes without reaching the highest or the lowest values recorded in temperate lakes. So, the primary production in tropical water is as important as in temperate settings, but the ability to recycling the nutrient within the water column is more important. Finally, the oxygen decrease in the hypolimnion is more accentuated than in high latitudes lakes.

Chapter III – Material and methods

1. Systematic study

All the details about the provenance of the studied fossils, inventory numbers, morphometric analyses, scan parameters and character matrix for the phylogenetic analysis are also provided in the Material and Methods sections of the three related published papers.

1.1. Material from the Autun Basin

Almost all the investigated material from the Autun Basin come from the lowermost Permian Muse OSB locality. This locality has preserved three partial skeletons of Xenacanthidae in anatomical connection, always including the neurocranium, the jaws, the dorsal spine and the teeth and in one specimen the scapulocoracoid, the pectoral fin and the anterior part of the vertebral column. These specimens were recently discovered during the excavation campaigns organised between 2010 and 2014 (Gand *et al.* 2011, 2015) by the *Société d'Histoire Naturelle et des Amis du Muséum d'Autun* (SHNA, France) and the *Muséum d'Histoire Naturelle d'Autun* (MHNA, France) and are not yet published. I describe them all. They come from different layers including the historical fossiliferous "fish layer" and are currently hosted in the MHNA.

Four isolated neurocrania come from the different localities of the Autun Basin and were found in the second half of the 19th century. The Darcy-Saint-Loup and La Comaille localities are correlated with the Lally OSB in the Muse Formation. They are uppermost Carboniferous in age following the dating of the Lally OSB at 298.91+/- 0.16 Ma by Pellenard *et al.* (2017). They were first published by Heyler & Poplin (1982) who erected two species: the symmoriiform *Bibractopiscis niger* and the xenacanthiform *Orthacanthus commailli*. However, these specimens are not well prepared, and their external anatomy is only partially available. They are currently hosted in the *Muséum National d'Histoire Naturelle de Paris* (MNHN, France). Thanks to μCT scan acquisitions, I entirely redescribe these specimens.

Isolated xenacanthiform dental material is abundant in the Muse OSB but the teeth are usually barely preserved with, in most cases, only an imprint of the fossil available. So, they are not very useful for systematic study. However, a single large tooth, mentioned and briefly described by Heyler (1969) was found during an excavation campaign in 1958. I entirely

redescribe this tooth. Its location within the Muse OSB stratigraphy is not precisely known but it could come from the base near the fossiliferous "fish layer" even if this assumption must be proposed with caution. It is currently hosted in the MNHN.

1.2. Material from Buxières-les-Mines

Isolated material is abundant in Buxières-les-Mines and come from excavation campaigns organised by the *Rhinopolis* Association between 1996 and 2005 (Steyer & Escuillié 1997; Steyer *et al.* 2000). Despite this abundance, a few specimens have been prepared for systematic study due to lack of time and funds. I describe the investigated material that is represented by one neurocranium, two dorsal spines and 40 teeth. The material is hosted in different collections including the MNHN, the *Muséum d'Histoire Naturelle et d'Ethnographie de Colmar* (MHNE, France) and the Palaeontological Institute and Museum at the University of Zurich (PIMUZ, Switzerland). The location of the fossils within the Buxières-les-Mines stratigraphy was reported during the excavation campaigns and they come from oil-shale levels between the two volcanic tuffs "*Lien Blanc*" and "*Lien Vert*". The attempted dating of these levels (Ducassou *et al.* 2018) indicate an Asselian-Sakmarian age.

1.3. Scanning

Neurocrania from the Autun and Bourbon-l'Archambault basins were scanned by X-ray computed microtomography in order to access to their entire external anatomy. The flattened aspect of the fossils does not allow an investigation of the internal structures. The specimen from Buxières-les-Mines was scanned at the microtomographic platform of the *Étude Recherches Matériaux* Society (Poitiers, France) with a X8050-16 Viscom tomograph. The obtained resolution is 95 µm. The material from the Autun Basin was scanned at the tomographic platform AST-RX of the MNHN with a v|tome|x L240-180 model. The obtained resolution is between 35 and 79 µm. Prior to the 3D reconstruction, the resulting slides were converted from 16 bits to 8 bits images by the software Image J v.1.4.3.67 (Rasband 1997-2022). I segment the 3D models with the softwares Avizo v. 7.0 (© Thermo Fisher Scientific, USA) for the specimen from Buxières-les-Mines and with MIMICS v. 20.0 (© Materialise Inc, Belgium) for the specimens from the Autun Basin. The scan parameters are available in the supplementary material of paper 2.

1.4. Morphometric analyses

Standard biometric analyses include measurements of teeth (length, width, height, crown-base angle). These measurements complete the anatomical description and are used in linear regression models performed in R v. 4.0.2 (R Core Team 2020) for the material from Buxières-les-Mines.

Geometric morphometrics were performed on the 3D models of the scanned neurocrania to quantify the shape of the ethmoidal region of Xenacanthiformes. The investigated specimens and some 'Ctenacanthiformes' were included in this analysis. Only manually placed landmarks were used. The placement of the landmarks, the Generalized partial Procrustes Analysis (pGPA) and the principal component analysis on the pGPA were performed with the package geomorph v. 3.3.1 (Adams & Otarola-Castillo 2013) in R v. 4.0.2.

1.5. Phylogenetic analysis

Relationships between Xenacanthiformes and 'Ctenacanthiformes' based on the morphology of their neurocrania was attempted thanks to a cladistic analysis performed in PAUP v. 4.0a168 (Swofford 2003).The taxa-character matrix includes 22 taxa and 33 external neurocranial characters. Taxa are divided into an outgroup (Placodermi, Acanthodii and stem-chondrichthyans), Euchondrocephali (Holocephali and Symmoriiformes) and Elasmobranchii (Euselachii, Phoebodontiformes, 'Ctenacanthiformes' and Xenacanthiformes). 19 characters came from previous studies (Schaeffer 1981; Lund & Grogan 1997; Coates & Sequeira 1998, 2001a,b; Maisey 2001; Brazeau 2009; Pradel *et al.* 2011; Davis *et al.* 2012; Zhu *et al.* 2013; Brazeau & Friedman 2014; Coates *et al.* 2018; Frey *et al.* 2019; Brazeau *et al.* 2020) and 14 new characters were added (see the supplementary material of paper 2 for details of the taxa, characters and analysis parameters).

1.6. Systematic notes

The systematic scheme of Palaeozoic chondrichthyans retained in this work follows the Ginter *et al.*'s (2010) synthesis. For Xenacanthiformes, I added informations from the latest studies (Heidtke 1998; Hampe 2003; Johnson & Thayer 2009; Pauliv *et al.* 2017), but we do not follow Heidtke (2007) concerning the division of *Lebachacanthus seckenbergianus* into three different species (*L. seckenbergianus*, *L. colosseus*, *L. pollichiae*) as I consider it could correspond to stratigraphic species without clear anatomical difference. Bengtson's (1988) recommendations are followed concerning potential invalid taxa as well as taxa in open

nomenclature. Following Heyler (1969), all the material referred to '*Pleuracanthus*' belong to '*Expleuracanthus*' even if it was not explicitly mentioned in previous works.

The description of xenacanthiform teeth follows Schneider's (1985, 1996; Fig. 3) nomenclature and the description of neurocranium follows Schaeffer (1981) (Fig. 2).

2. Geochemical study

2.1. Investigated vertebrate groups

The systematic attribution of xenacanthiforms (Figure 41 and Table 3) dorsal spines is limited to the family level. Ten dorsal spines are attributed to the Xenacanthidae due to their dorso-ventral compression and their two lateral rows of denticles. Buxières-les-Mines has provided a chondrichthyan fauna composed of three xenacanthiforms species (Steyer *et al.* [2000]; see the results section for a discussion of the *Orthacanthus* species present in Buxières-les-Mines): the diplodoselachid *Orthacanthus kounoviensis* and *Orthacanthus buxieri* and the xenacanthid *Triodus* sp. In the Muse OSB, *Triodus aeduorum*, *Triodus* sp., '*Expleuracanthus*' *frossardi* and '*Expleuracanthus*' *bonnardi* belong to the Xenacanthidae, but only the genus *Triodus* can be considered as valid (e.g. Ginter *et al.* 2010). As no generic diagnostic character has been formally identified in the investigated dorsal spines, they could refer to cf. *Triodus* sp. I consider that the three diplodoselachid dorsal spines from Buxières-les-Mines, which exhibits rounded cross section, two posterior rows of denticles and a long and slender morphology could belong to cf. *Orthacanthus* sp.

The acanthodian fauna is composed of numerous isolated, curved and laterally flattened spines that are attributed to *Acanthodes* sp. in Buxières-les-Mines (Steyer *et al.* 2000) or to *Acanthodes bonni* in the Muse OSB (Heyler 1969). *A. bourbonensis* from the Lower Permian of La Queue d'Étang in the Bourbon-l'Archambault Basin was also described by Heidtke & Dürkheim (1996). As specific attribution of isolated spines is hazardous and no generic diagnostic character can be identified on them, I choose to refer the different fin spines to cf. *Acanthodes* sp.

In Buxières-les-Mines, only isolated actinopterygian scales that exhibit a distinct ganoid pattern were sampled. Most of the actinopterygians found in this locality belong to the Paramblypteriformes, Aeduelliformes or Palaeonisciformes (Heyler 1969; Steyer *et al.* 2000). Isolated scales are not well suited for precise systematic identification, so we left this material in open nomenclature as Actinopterygii indet. In the Muse OSB, isolated ganoid scales come from five sub-complete actinopterygian specimens. Heyler (1969) only described Aeduellidae

Table 3. Investigated taxa and biological tissues for the geochemical analyses.

Systematics		**Tissues**	**Localities**
Xenacanthiformes	cf. *Triodus* sp.	Dentine	Muse, Buxières-les-Mines
Xenacanthiformes	cf. *Orthacanthus* sp.	Dentine	Buxières-les-Mines
Acanthodii	cf. *Acanthodes* sp	Dentine	Muse, Buxières-les-Mines
Actinopterygii	Actinopterygii indet.	Ganoid	Buxières-les-Mines
Actinopterygii	?Aeduellidae	Ganoid	Muse
Temnospondylii	Temnospondylii indet.	Bone	Buxières-les-Mines

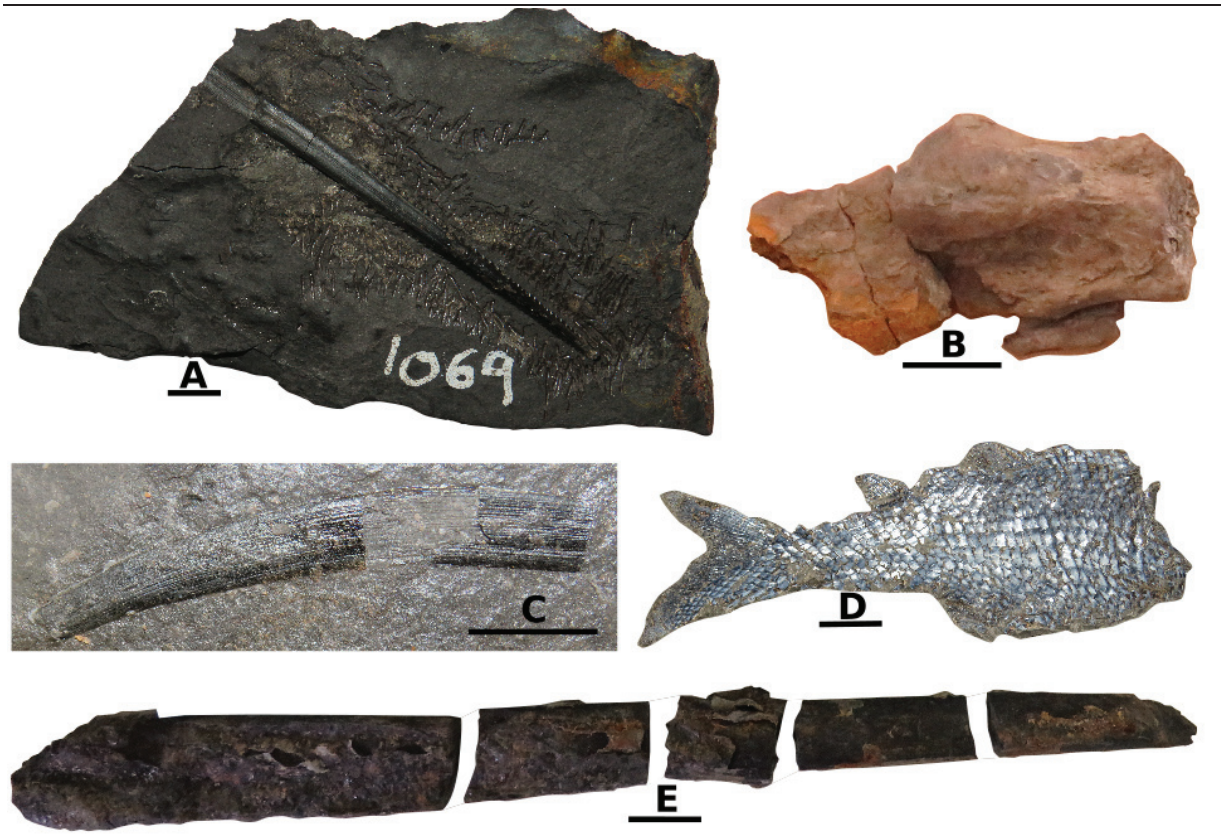

Figure 41. Aquatic vertebrate samples used in the geochemical study. **A**, cf. *Triodus* dorsal spine. **B**, Temnospondyl bone. **C**, cf. *Acanthodes* fin spine. **D**, sub complete actinopterygian with ganoid scales. **E**, cf. *Orthacanthus* dorsal spine. **A** and **D** from the Muse OSB and **B**, **C** and **E** from Buxières-les-Mines. Scale bar: 1 cm.

from this locality, so we tentatively assign them to the ?Aeduellidae, as the revision of the actinopterygian fauna of the Muse OSB is out of the scope of this work.

Tetrapods are extremely rare in the Muse OSB, only *Onchiodon frossardi* (Gaudry, 1867) *sensu* Werneburg & Steyer (1999) was reported. Unfortunately, there is no remain suitable for geochemical analyses. In Buxières-les-Mines, three temnospondyls were reported

(Steyer *et al.* 2000): *Onchiodon*, *Melanerpeton* and *Cheliderpeton*. The studied bone samples consist of isolated and fragmented elements of the tarsus of supposedly several individuals. According to their incomplete aspect, it has not been possible to identify them, so I left them in open nomenclature as Temnospondylii indet. for the time being. However, their size, up to 2 cm for the most complete phalange, indicates a medium to large animals which could correspond to *Onchiodon* or *Cheliderpeton*.

2.2. Analytical techniques

2.2.1 Chemical treatment for the analysis of the oxygen and carbon isotopic composition of the carbonate group in fossil bioapatite

The objectives of this treatment are to remove 1) potential remaining organic matter in the sample powder and 2) secondary calcite that would have potentially precipitated. The used protocol (Figure 42) follows that of Koch *et al.* (1997):

- Day 1: 1) Weigh approximately 10-20 mg of powder per sample in 15 ml centrifuge tubes; 2) add 0.04 ml of 3.5% NaClO per mg of powder; 3) put the tubes in an ultrasonic tank for 10-15 mn to enhance the contact between powder and solution and wait 24 hours.
- Day 2: 1) Remove the supernatant using a 1 ml micropipette; 2) add 2 ml of distilled water to each tube, centrifuge for 5 minutes at 2500 rounds per minute (rpm); 3) repeat steps 1 and 2 three times; 4) add 0.04 ml of 0.1M $C_2H_4O_2$ per mg of powder; 4) put the tubes in an ultrasonic tank for 10-15 mn and wait 24h.
- Day 3: 1) Remove the supernatant using a 1 ml micropipette; 2) add 2 ml of distilled water to each tube, centrifuge for 5 minutes at 2500 rpm; 3) repeat steps 1 and 2 three times; 4) leave the tubes in a dry-oven at 50° C until the powders have completely dried.

2.2.2. Chemical protocol for the analysis of the oxygen isotopic composition of the phosphate group in fossil bioapatite

The objective of this chemical protocol is to isolate the phosphate group (PO_4^{3-}) and to precipitate it into silver phosphate Ag_3PO_4. This transformation is necessary to solely analyse the oxygen isotope composition of the phosphate group in bioapatite and not that of the carbonates group. The used protocol (Figure 43) follows that of Crowson *et al.* (1991) which was modified by Lécuyer *et al.* (1993):

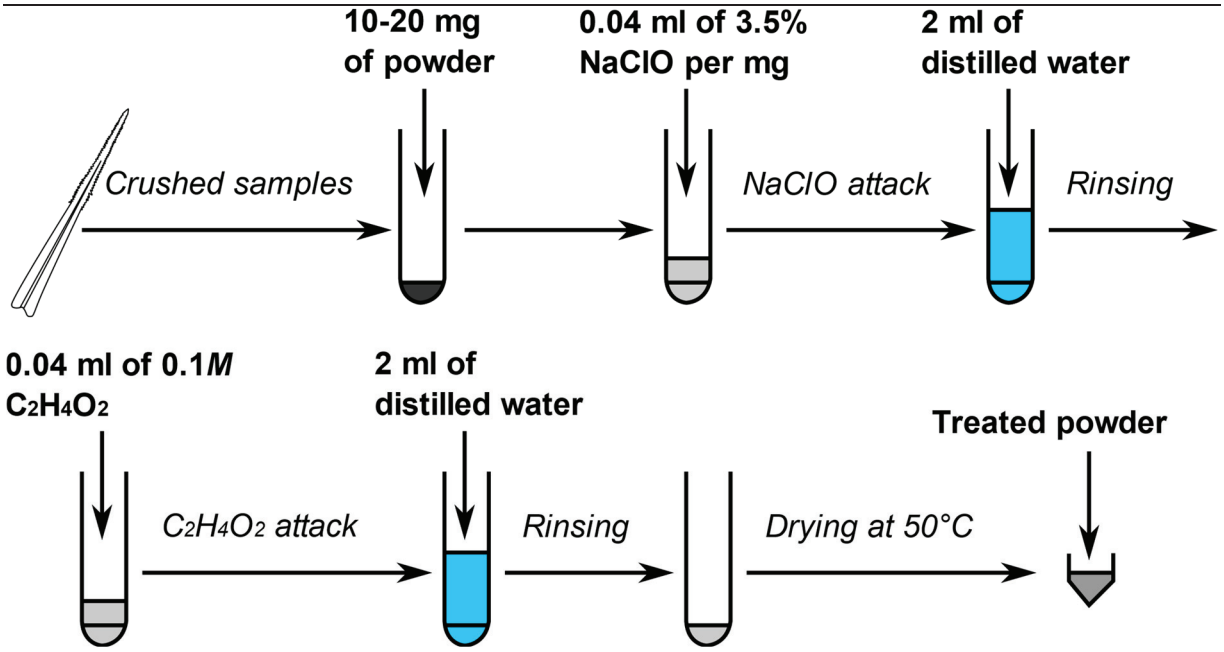

Figure 42. Illustrated protocol for the chemical treatment of the carbonates in fossil bioapatite (adapted from Angst 2014).

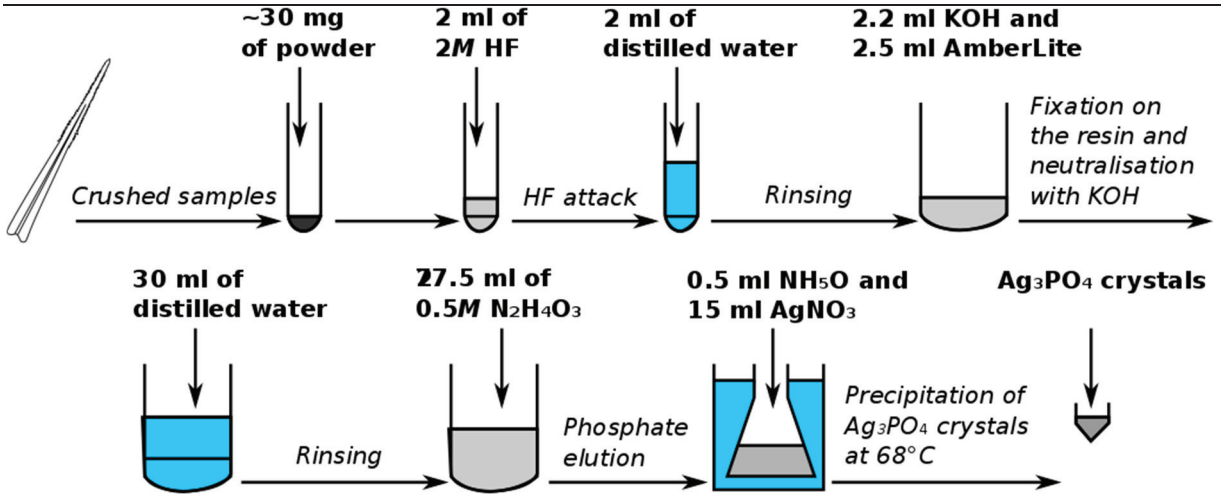

Figure 43. Illustrated chemical protocol for the precipitation of silver phosphates from the fossil bioapatite (adapted from Angst 2014).

- Day 1: 1) Weigh 10 to 30 mg of powder per sample in 15 ml centrifuge tubes. 2) Add 2 ml of 2M HF in each tube to dissolve all the ions including the phosphate ones; 3) put the tubes in an ultrasonic tank to enhance the reaction and wait 24 hours.
- Day 2: 1) Centrifuge each 15 ml tubes for 5 minutes at 2500 rpm and transfer the supernatant in 50 ml tubes; 2) Add 2 ml of distilled water in each 15 ml tubes; 3) repeat steps 1 and 2 twice; 4) Add 2.2 ml of KOH in each 50 mL tubes to neutralise the solution; 5) Add 2.5 ml of AmberLite® MB (ion-exchange resin) in each 50 ml tubes

to perform the ion exchange process; 6) Gently shake the tubes for 24 hours using a tube shaker.

- Day 3: 1) Remove the solution and rinse the resin by adding 30 ml of distilled water; 2) repeat 4 times and remove the liquid solution; 3) Add 27.5 ml of 0.5M $N_2H_4O_3$ to elute the phosphate; 4) Shake the tubes for 4 hours; 5) Separate the resin from the liquid solution into Erlenmeyer flasks with a 63 µm stainless steel sieve; 6) Add 0.5 ml of NH_5O and 15 ml of $AgNO_3$ in each flasks to precipitate the silver phosphate; 7) Put each flask into thermostatic tank at 68°C; 8) Add 1-2 ml of distilled water per 15 minutes to maintain a constant solution volume in the Erlenmeyer flasks.
- Day 4: 1) Filter the liquid solution to recover the Ag_3PO_4 crystals on acetate filters; 2) Dry them in a dry-oven at approximately 50° C for 4 hours until the powders have completely dried.

2.3. Stable isotope measurements

2.3.1. Measurement of the oxygen isotopic composition of the phosphate group of the fossil bioapatite

A VarioPyroCube elemental analyser in pyrolysis mode (Figure 44) interfaced in continuous flow mode with an Isoprime™ isotope ratio mass spectrometer (IRMS) is used to measure $\delta^{18}O_p$ values of bioapatite samples. The analyses follow the method of Lécuyer *et al.* (2007) and Fourel *et al.* (2011). Precipitated Ag_3PO_4 crystals from fossil bioapatite samples were weighed at 300 µg with 400 µg of pure graphite powder in a silver foil capsule. 5 aliquots were prepared for each sample. The VarioPyroCube performs the pyrolysis of each capsule at 1450°C, recombining oxygen atoms of silver phosphates and carbon into carbon monoxide (CO). The CO is isolated thanks to a temperature-controlled 'purge-and- trap' chromatography device and transferred to an Isoprime mass spectrometer that will calculate the $\delta^{18}O_p$ value. The obtained $\delta^{18}O_p$ values are calibrated against the NBS120c (natural Miocene phosphorite from Florida) and the NBS127 (barium sulfate) standards. The accepted $\delta^{18}O$ value of the NBS 120c is 21.7‰ (V-SMOW; Lécuyer *et al.* 1993) and the certified $\delta^{18}O$ value of NBS127 is 9.3‰ V-SMOW (Hut 1987) for correction of instrumental mass fractionation during CO isotopic analysis. Additionally, the silver phosphate samples precipitated from NBS120c along with the apatite samples were also analysed along with the silver phosphate from fossil samples to ensure that no isotopic fractionation occurred during the chemistry procedure. Data are reported as $\delta^{18}O_p$ values versus V-SMOW (in ‰ δ units).

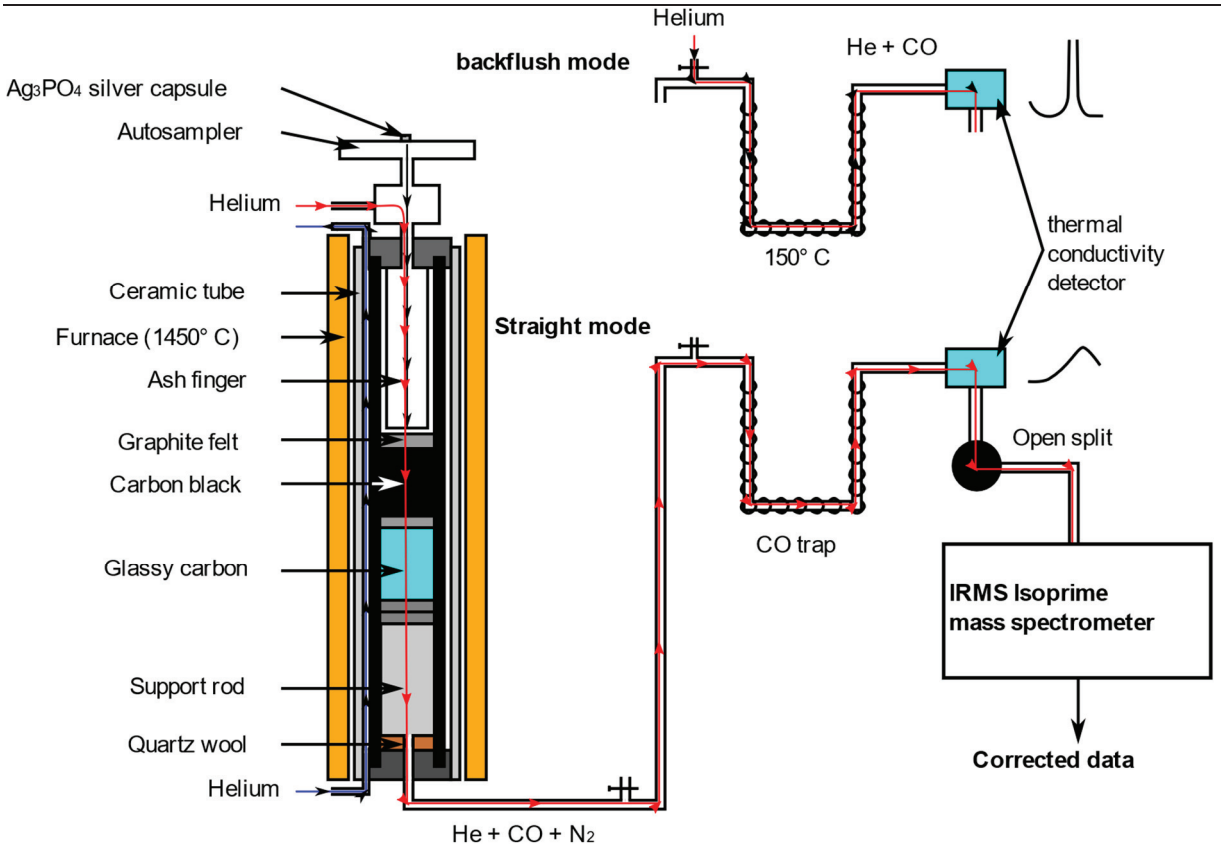

Figure 44. Pyrolysis setup of the VarioPyroCube for the analysis of the $\delta^{18}O_p$ of fossil bioapatite (modified from Lécuyer *et al.* 2007; Fourel *et al.* 2011; Angst *et al.* 2014).

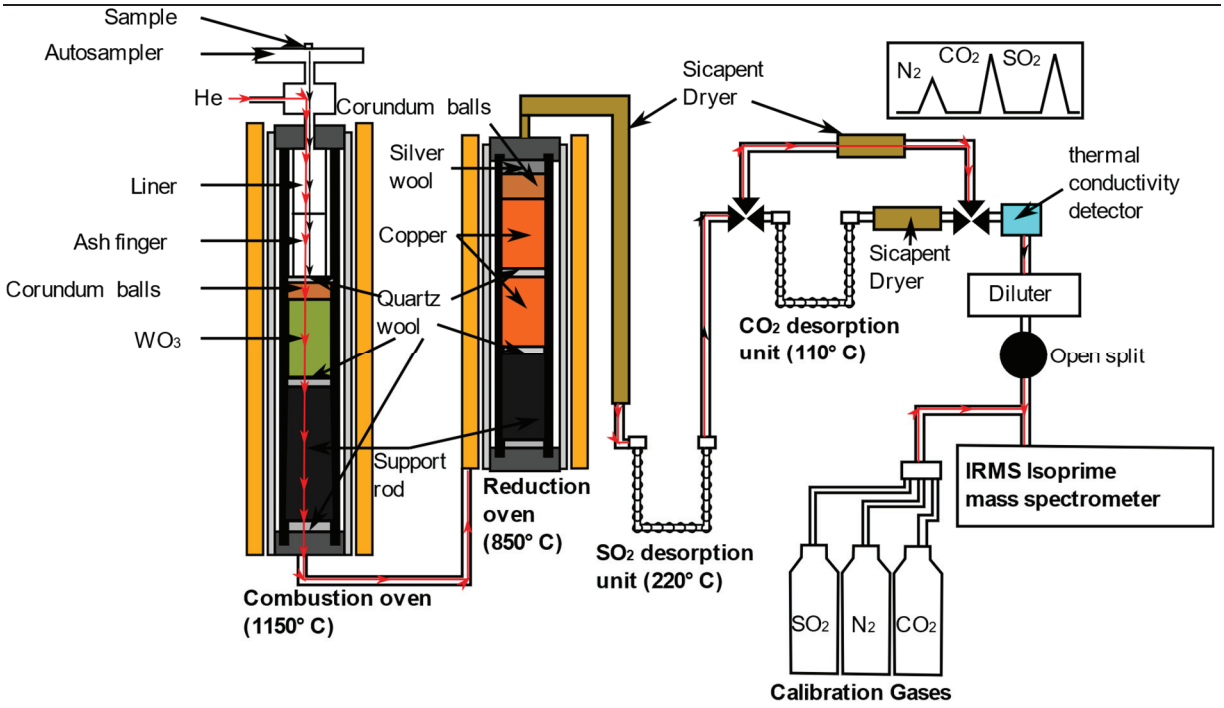

Figure 45. Combustion setup of the VarioPyroCube for the analysis of the $\delta^{34}S$ of fossil bioapatite (modified from Fourel *et al.* 2014).

2.3.2. Analysis of the sulfur isotopic compositions of the fossil bioapatite

A VarioPyroCube elemental analyser in NCS combustion mode (Figure 2.18) interfaced in continuous-flow mode with an Isoprime 100™ isotope ratio mass spectrometer (IRMS) is used to analyse $\delta^{34}S$ from bioapatite samples. Analyses follow Fourel *et al.*'s (2014) setup and Goedert *et al.*'s (2016) method. Each fossil bioapatite samples were weighed at 5 mg with 15 mg of tungsten trioxide (WO_3) powder in a tin foil capsule. 3 aliquots were prepared for each sample. The VarioPyroCube performs combustion (which produces SO_2 and SO_3) and reduction (reduction of SO_3 into SO_2 using copper oxydation) of each capsule at 1050°C and 850°C respectively, transforming bioapatite samples into SO_2 only. The SO_2 is transferred to an Isoprime mass spectrometer which calculate the $\delta^{34}S$. The obtained values are calibrated against IAEA-S-2, IAEA-SO-5 and IAEA-SO-6 international standards. The IAEA-S-2 is fixed at 22.62‰, the IAEA-SO-5 at 0.5‰ and the IAEA-SO-6 at -34.1‰ (Coplen 2001) for correction of instrumental mass fractionation. Data are reported as $\delta^{34}S$ vs. V-CDT. The VarioPYROcube elemental analyser was also used to measure the sulfur content of samples. This setup is suitable for the analysis of low concentration sulfur in bioapatite (less than 1%; Fourel *et al.* 2015)

2.3.3. Measurement of the oxygen and carbon isotopic composition of the carbonate group of the fossil bioapatite

An isoFlow system connected online in continuous flow mode to a precisION mass spectrometer is used to analyse the $\delta^{18}O_c$ and $\delta^{13}C_c$ of carbonates ($\delta^{18}O_c$ and $\delta^{13}C_c$) from treated fossil bioapatite samples (Fig. 45). The bioapatite samples were reacted with anhydrous phosphoric acid at a regulated temperature of 90°C. The acid attack produces CO_2 that is transferred to the mass spectrometer via the centrION interface. Monitoring gas is calibrated CO_2. An acid fractionation factor α (CO_2–apatite carbonate) of 1.00773 determined for the NBS120c standard was selected (Passey *et al.* 2007). Each treated fossil bioapatite samples were weighed at 1-2 mg in 3.7 mL soda glass vials. 3 aliquots were made for each sample. The obtained $\delta^{18}O_c$ and $\delta^{13}C_c$ values are calibrated against the Carrara marble, the NBS18 and the NBS120c standards. The Carrara marble $\delta^{18}O_c$ and $\delta^{13}C_c$ are fixed at -1.84‰ V-SMOW and 2.03‰ V-PDB respectively, the NBS18 $\delta^{18}O_c$ and $\delta^{13}C_c$ at -23.2‰ V-SMOW and -5.01‰ V-PDB respectively and the NBS120c $\delta^{18}O_c$ and $\delta^{13}C_c$ at 1.13‰ V-SMOW and -6.27‰ V-PDB respectively (e.g. Coplen 2001; Coplen *et al.* 2002). Isotopic compositions are quoted in the standard δ notation relative to V-SMOW for oxygen and V-PDB (Vienna Pee Dee belemnite) for carbon.

Chapter IV – Systematic reassessment

Paper 1: A new *Triodus* shark species (Xenacanthidae, Xenacanthiformes) from the lowermost Permian of France and its paleobiogeographic implications

Vincent Luccisano, Alan Pradel, Romain Amiot, Georges Gand, Jean.-Sébastien Steyer, and Gilles Cuny

Published in Journal of Systematic Paleontology

Luccisano, V., Pradel, A., Amiot, R., Gand, G., Steyer, J. S., & Cuny, G. (2021). A new Triodus shark species (Xenacanthidae, Xenacanthiformes) from the lowermost Permian of France and its paleobiogeographic implications. **Journal of Vertebrate Paleontology**, 41(2), e1926470.

A new *Triodus* shark species (Xenacanthidae, Xenacanthiformes) from the lowermost Permian of France and its paleobiogeographic implications

Vincent Luccisano,[*,1] Alan Pradel,[2] Romain Amiot,[1] Georges Gand,[3, 4] Jean.-Sébastien Steyer,[2, 4] and Gilles Cuny [5]

[1]Univ Lyon, UCBL, ENSL, UJM, CNRS, LGL-TPE, F-69622, Villeurbanne, France;
[2]CR2P - Centre de Recherche en Paléontologie - Paris ; Muséum National d'Histoire Naturelle - Centre National de la Recherche Scientifique- Sorbonne Université. France ;
[3]Biogéosciences, Univ. Bourgogne Franche-Comté, 21000 Dijon, France ;
[4]Société d'Histoire Naturelle et des Amis du Muséum d'Autun, France ;
[5]Univ Lyon, Université Claude Bernard Lyon 1, CNRS, ENTPE, UMR 5023 LEHNA, F-69622, Villeurbanne, France.

Abstract

The Xenacanthiformes from Central and Eastern European deposits have been extensively studied, but the systematic of the species from the French Carboniferous-Permian Autun Basin (Saône-et-Loire) remains debated. Numerous xenacanthiform remains are still identified under the doubtful genus '*Expleuracanthus*', and many of them consist of isolated dorsal spines which are difficult to identify. Numerous well-preserved specimens are still undescribed and the diversity of the xenacanthiform fauna from the Autun Basin is poorly understood. For example, specimens of the genus *Triodus* from the Muse oil-shale bed (OSB) of the Autun Basin have no specific attribution, whereas this genus is widely distributed across European Carboniferous-Permian basins. In this study, we describe new specimens of *Triodus* from the lowermost Permian of the Muse OSB. They allow the erection of a new species, *Triodus aeduorum* sp. nov., and to discuss the validity of several species from the same locality: '*Expleuracanthus*' *frossardi* is considered as a *nomen dubium* and other *Triodus* specimens need for the time being to be left in open nomenclature as *Triodus* sp. These results highlight the endemism of the *Triodus* species in each European Carboniferous-Permian basin and raise the question of how they migrated from one to another.

Introduction

Xenacanthiformes form an order of Paleozoic elasmobranchs (Coates *et al.* 2017, 2018; Frey *et al.* 2019) or stem-chondrichthyans (Ginter *et al.* 2010; Pradel *et al.* 2011). They are principally found in lacustrine deposits (Zangerl 1981; Compagno 1990; Kriwet *et al.* 2008), but also in marine sediments (Hampe 2003; Hampe & Ivanov 2007b; Johnson & Thayer 2009). Their first occurrence in the fossil record is in the Tournaisian of Russia (lower Mississippian, Lower Carboniferous; Lebedev 1996). They are divided into two families (see Ginter *et al.* [2010] for the latest synthesis): the Diplodoselachidae, including *Diplodoselache*, *Dicentrodus*, *Hagenoselache*, *Orthacanthus* and *Lebachacanthus*, and the Xenacanthidae, including *Xenacanthus*, *Triodus*, *Plicatodus*, *Wurdigneria* and *Mooreodontus*. Their maximum diversity occurs in the European Carboniferous-Permian lacustrine basins, where five genera (*Lebachacanthus*, *Orthacanthus*, *Xenacanthus*, *Triodus* and *Plicatodus*) are present (e.g. Hampe 2003; Heidtke 2007; Ginter *et al.* 2010).

The genus *Triodus* Jordan, 1849 *sensu* Ginter, Hampe and Duffin (2010) is known worldwide: most of the species are coming from Europe (e.g. Hampe 1989, 2003; Ginter *et al.* 2010) and range from the lowermost Bashkirian (lower Pennsylvanian, Upper Carboniferous; Davis 1892) to the Artinskian (upper Cisularian, Lower Permian; Hampe 1989). Several *Triodus* teeth, undetermined at the species level, come from the lower Pennsylvanian to the Upper Permian of the Mediterranean border (Soler-Gijón 1993a,b, 1994, 1995; Schindler & Hampe 1996; Ginter *et al.* 2010; Fischer *et al.* 2013). The genus is also known from the Bashkirian of North America (Johnson & Thayer 2009) and from the Middle Permian (Capitanian) of South America (Pauliv *et al.* 2017).

In France, *Triodus* has been reported in the Muse oil-shale bed (OSB) of the Carboniferous-Permian Autun Basin (Saône-et-Loire; Fig. 46) from a sub-complete specimen attributed to *T.* ?*frossardi* Soler-Gijón & Hampe, 1998 (Asselian, Lower Permian; France; Soler-Gijón & Hampe 1998; Heidtke *et al.* 2004). The Muse OSB is known since the 19th century for having yielded fossil vertebrates (see Brignon [2014] for history). Many studies have investigated the xenacanth fauna from the Muse OSB (Agassiz 1833-1843; Gaudry 1883; Sauvage 1893; Heyler 1969, 1987; Heyler & Pacaud 1978; Heyler & Poplin 1982, 1989; Heyler & Debriette 1986; Poplin & Heyler 1989; Soler-Gijón & Hampe 1998), and three species have been identified: *'Expleuracanthus' frossardi* ('*Pleuracanthus*' *frossardi* in Gaudry [1867, 1883] and in Brongniart & Sauvage [1888]); *'Expleuracanthus' bonnardi* (*Pygopterus*

bonnardi in Agassiz [1833-1843] , *'Pleuracanthus' bonnardi* in Sauvage [1893]), and *Triodus* ?*frossardi* (Soler-Gijón & Hampe 1998; Heidtke *et al.* 2004). Several other specimens, mainly isolated teeth and dorsal spines have been associated with the genus *'Expleuracanthus'* (e.g. Heyler 1969).

The genus *'Expleuracanthus'* was erected by Heyler (1969) to replace the genus name *'Pleuracanthus'* because the latter was already attributed to a South American coleopteran (*Pleuracanthus sulcipennis*; Griffith *et al.* 1832), and is regarded as a junior synonym (Schneider & Zajíc 1994; Hampe 2003) of either *Triodus* or *Xenacanthus*, or possibly both. *T.* ?*frossardi* was originally referred to as *'Expleuracanthus' frossardi* ('*Pleuracanthus*' *frossardi* in Soler-Gijón & Hampe [1998]), the holotype of which being an isolated spine figured by Gaudry (1883). However, *T.* ?*frossardi* does not display a well-preserved spine, preventing a comparison with the holotype of *'E'. frossardi*, so that no definite attribution to this species can be made as emphasized by Soler-Gijón & Hampe (1998). Furthermore, Heidtke *et al.* (2004) and Ginter *et al.* (2010) attributed the species *'Expleuracanthus' frossardi* (Gaudry 1883) to the genus *Triodus* but no diagnostic character of *Triodus* has been demonstrated to be present in the holotype of *'E'. frossardi*.

Consequently, the systematic of the xenacanthiforms from the Autun Basin is poorly understood, even if it has been extensively studied, and needs a global revision to better understand the real diversity of this group in this basin. It is all the more true as 1) the age of the Autun Basin corresponds to that of the maximum diversity of the European Xenacanthiformes, including that of the genus *Triodus* (Hampe & Ivanov 2007b; Pauliv *et al.* 2017), and 2) recent international excavation campaigns led by two of us (GG and JSS) in the Muse OSB of the Autun basin yielded interesting new xenacanthiform sub-complete specimens. We describe some of these new specimens of *Triodus* here. These specimens will allow to determine 1) if *T.* ?*frossardi* is the unique species present in France, 2) if *'E'. frossardi* can be related to the genus *Triodus*, and 3) to discuss the paleobiogeography of the genus *Triodus* in the European Carboniferous-Permian basins.

Geological Setting

The Autun Basin (Fig. 46A) is a half-graben basin oriented West-East (30 km × 15 km), located in the Northern Massif Central (Saône-et-Loire, France) and is mainly composed of siliciclastic sediments intercalated with oil-shale beds (Fig. 1B; Manès 1844, 1847; Roche 1881; Delafond 1889; Pruvost 1942; Marteau 1983; Gand *et al.* 2015; Pellenard *et al.* 2017; see Gand *et al*. [2017] for historical review). The basin is interpreted as representing fluvio-

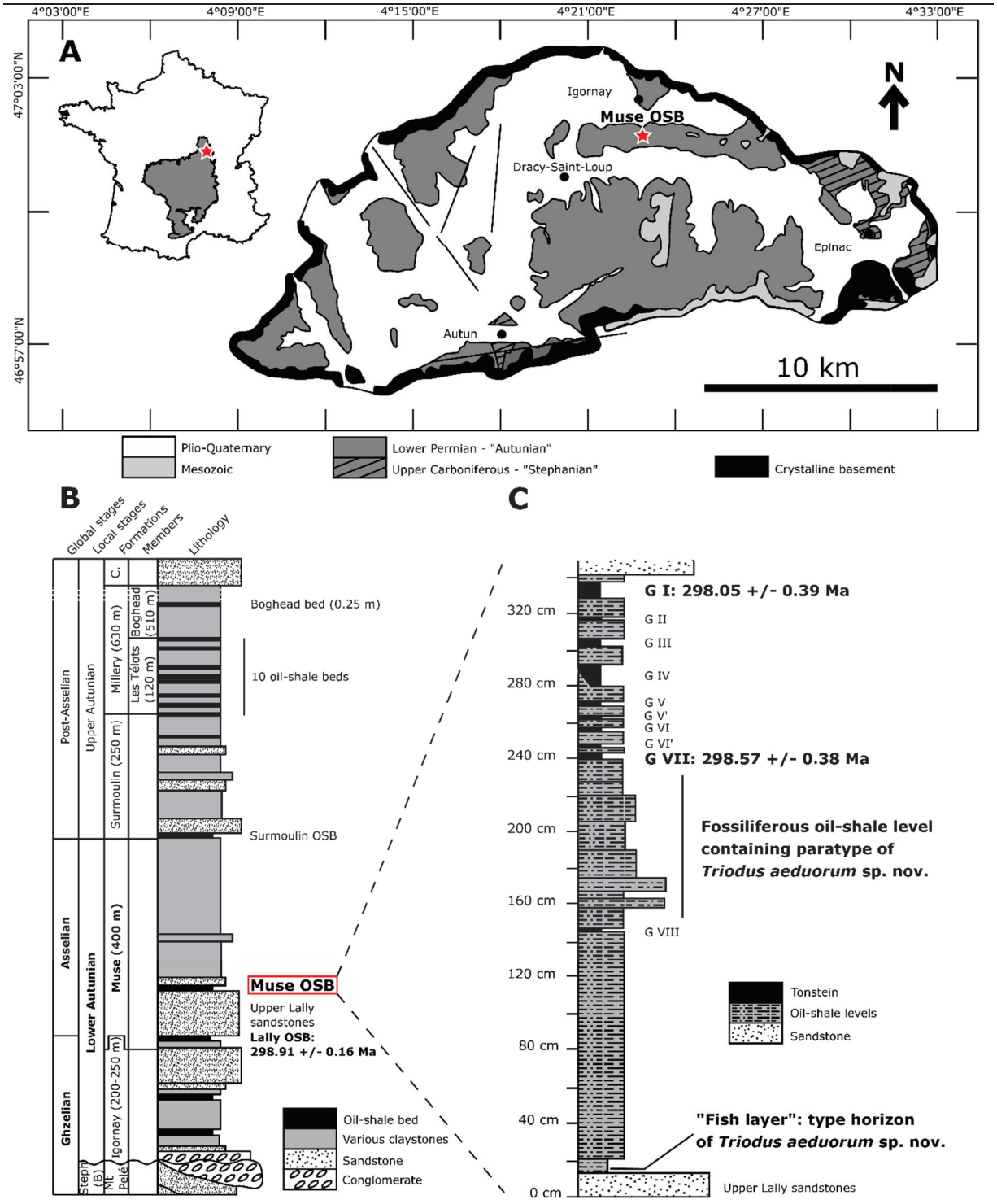

Figure 46. Geological context of the Muse oil-shale bed (OSB). **A**, Location of the Autun Basin in the Massif Central of France, and its simplified geological map in which the Muse OSB is represented by a black star. **B**, simplified stratigraphy of the Carboniferous-Permian deposits of the Autun Basin. **C**, simplified stratigraphy of the Muse OSB. **Abbreviations**: **C.**, Curgy formation (200 m); **G I to G VIII**, tonsteins (modified after Marteau 1983; Châteauneuf *et al.* 1992; Gand *et al.* 2007, 2011, 2015, 2017; Pellenard *et al.* 2017).

lacustrine environments (Pruvost 1942; Marteau 1983). It is divided into four formations (Fig. 46B): Igornay and Muse formations constitute the lower 'Autunian' (upper Gzhelian to lower Asselian), and Surmoulin and Millery formations correspond to the upper 'Autunian' (post-Assselian) (Fig. 46B; Pruvost 1942).

The Muse OSB is located in the Muse Formation above the Upper Lally sandstones (Fig. 46B; e.g. Gand *et al.* 2007, 2011, 2015, 2017; Pellenard *et al.* 2017). The stratigraphy (Fig. 46C) of the Muse OSB was studied by Gand *et al.* (2007, 2011, 2015) and Pellenard *et al.* (2017): it is limited at its base by the Upper Lally sandstone and at its top by a sandstone layer. It is mainly composed of oil-shale beds with intercalations of volcanic tonsteins (locally called "*gore*"). Two tonsteins were dated by radiochronology at 298.05 +/- 0.39 Ma and 298.57 +/- 0.38 Ma (Fig. 46C; G I and G VII, upper part of the Muse OSB stratigraphy in Pellenard *et al.* [2017]). One tonstein from the Lally OSB situated directly under the Upper Lally sandstone (Fig. 46B) was dated at 298.91 +/- 0.16 Ma (Pellenard *et al.* 2017). The Muse OSB is therefore dated as lower Asselian (lowermost Permian) in age, just above the Carboniferous-Permian boundary.

Materials and Methods

Material

The new specimens described in this work (Figs. 47–53) were found during excavation campaigns between 2010 and 2014 organized by the SHNA and the MHNA. Specimens are flattened by post-sedimentary compression and preserved on oil-shale plates. They are currently housed in the collections of the MHNA.

At the base of the Muse OSB, there is a fossiliferous layer called the "fish layer" ("*couche à poissons*"; Fig. 46C), which has provided a great number of fossil actinopterygians (*Aeduella blainvillei*; see Brignon [2014] for an historical account). This "fish layer" has also provided a large number of fossil chondrichthyans, such as isolated teeth, dorsal spines, skin fragments and portions of neurocrania (Gand *et al.* 2011, 2015). Historical specimens of '*Expleuracanthus*' studied by Gaudry (1867, 1883) Brongniart & Sauvage (1888) Sauvage (1893) and Heyler (1969) and the holotype of the new *Triodus* species, MHNA-PAL-2020-0001, come from this "fish layer". Concerning the other new material of *Triodus*, MHNA-PAL-2020-0002 comes from the fossiliferous oil-shale level between the tonsteins G VII and G VIII

(Fig. 46C), and MHNA-PAL-2020-0003 comes from the Muse OSB but no specific oil-shale level was reported.

Systematic

We follow Schneider's (1985, 1996) nomenclature for describing xenacanthiform teeth, Schaeffer's (1981) one for describing xenacanthiform neurocranium, and Ginter *et al.* (2010) for the systematic of the Xenacanthiformes, with additional information on the genus *Triodus* from recent studies (Johnson & Thayer 2009; Pauliv *et al.* 2017). As proposed by Heyler (1969) the genus *'Expleuracanthus'* replaces the genus *'Pleuracanthus'*. So, '*Expleuracanthus*' *frossardi* replaces '*Pleuracanthus*' *frossardi* Gaudry, 1883. Consequently, following recommendations by Bengtson (1988), the use of the genus name between inverted commas highlight the fact that this genus could be valid, but no diagnosis has been established for now.

Abbreviations

Institutional Abbreviations—**MNHN**, Muséum National d'Histoire Naturelle de Paris; **MHNA**, Muséum d'Histoire Naturelle d'Autun; **RMH/PP**, Roemer- und Pelizaeus Museum, Hildesheim, Germany; **SHNA**, Société d'Histoire Naturelle et des Amis du Muséum d'Autun.

Anatomical Abbreviations—**ags**, actinopterygian ganoid scales; **an**, unidentified anterior part of neurocranium; **be**, basiventral elements; **br**, branchial rays; **dcpq**, dorsal crest of palatoquadrate; **d**, denticles; **dor**, dorsal otic ridges; **ds**, dorsal spine; **ema**, elements of metapterygial axis; **erpf**, elements of right pectoral fin; **hpa**, hypertrophic neural arch; **lch**, left ceratohyal; **lhm**, left hyomandibular; **llop**, left lateral otic process; **lmc**, left Meckel's cartilage; **lpop**, left postorbital process; **lpq**, left palatoquadrate; **lprp**, left preorbital process; **ls**, longitudinal striation; **lscp**, left scapulocoracoid; **mes**, mesopterygium; **met**, metapterygium; **mg**, median ventral groove; **n**, neurocranium; **oc**, occipital condyle; **occ**, occipital crest; **pf**, precerebral fontanelle; **plpq**, palatine part of left palatoquadrate; **por**, postaxial radials; **prpq**, palatine part of right palatoquadrate; **prr**, preaxial radials; **r**, rostrum; **rc**, ridge covering posterior vertical semi-circular canal; **rch**, right ceratohyal; **rdf**, radials of dorsal fin; **rlop**, right lateral otic process; **rmc**, right Meckel's cartilage; **rpop**, right postorbital process; **rpq**, right palatoquadrate; **rprp**, right preorbital process; **rscp**, right scapulocoracoid; **t**, teeth; **ube**, Unidentified branchial elements; **uc**, unidentified cartilage; **v**, vertebral remains; **vg**, proximal ventral groove.

Systematic Palaeontology

Class Chondrichthyes Huxley, 1880
Order Xenacanthiformes Berg, 1937
Family Xenacanthidae Fritsch, 1889
Genus *Triodus* Jordan, 1849

Expleuracanthus Heyler, 1969:25, fig. 1.
Bohemiacanthus Schneider & Zajíc 1994:122, figs. 19–22.

Type Species—Triodus sessilis Jordan, 1849.

Type Locality—Lebach, Southwest Germany; upper Oderheim Subformation, Saar-Nahe Basin, lower Sakmarian, lower Cisuralian, Lower Permian (following Ginter *et al.* 2010; Voigt *et al.* 2019).

Included Species—Triodus elpia Johnson & Thayer, 2009 from the Bashkirian of the United States; *T. serratus* (Davis, 1892) from the Bashkirian and Moscovian of the United Kingdom; *T. teberdaensis* Hampe & Ivanov, 2007b from the Moscovian of Russia; *T. lauterensis* Hampe, 1989 from the Kasimovian and Gzhelian of Germany; *T. palatinus* Hampe, 1989 from the Gzhelian and Asselian of Germany; *T. carinatus* (Fritsch, 1890) from the Asselian of Austria; *T. obscurus* Hampe, 1989 from the Asselian of Germany; *T. kraetschmeri* Hampe, 1989 from the Asselian to the Artinskian of Germany; *T. richterae* Pauliv *et al.,* 2017 from the Capitanian of Brazil; and *T. aeduorum* sp. nov. from the Asselian of France.

Diagnosis (following Hampe [2003])—Tricuspid teeth with cusps of rounded to polygonal cross-section; long median cusp in some species reaching almost the same length as the laterals; surface of the cusps equipped with variable number of always straight vertical cristae; cristae can split dichotomously below the apex of a cusp or in a more proximal position; both crown and base constructed of orthodentine (except the coronal button which is made of trabecular dentine); length of spine less than one-sixth of total body length.

Remarks—Triodus sp. ZÖ is considered by Schindler & Hampe (1996) as a distinct morphotype, but without clearer systematic attribution. Following Hampe (2003), *Bohemiacanthus* Schneider & Zajíc, 1994 is a junior synonym of *Triodus*. The species *Triodus carinatus* and *T. sessilis* were erroneously attributed to the genus *'Expleuracanthus'* by Poplin & Heyler (1989). Heidtke *et al.* (2004) and Ginter *et al.* (2010) consider that *'Expleuracanthus' frossardi* (Gaudry, 1883) from the Asselian of the Autun Basin is a representative of the genus *Triodus* without providing any morphological comparison.

***Triodus aeduorum* sp. nov.**
(Figs. 47–53)

Etymology—Genitive of Aedui, a Gallic tribe that occupied the Saône-et-Loire department (France) from the late Iron Age to the Roman period, where the holo- and para- types were found.

Holotype—Specimen MHNA-PAL-2020-0001 (Figs. 47–50, 53), anterior half of an individual preserving the neurocranium, the jaws, the dorsal spine, teeth, anterior vertebral remains, proximal part of the left scapulocoracoid and the pectoral fin all in connection; paleontological collection of the MHNA.

Paratypes—Specimen MHNA-PAL-2020-0002 (Figs. 51, 53) preserving the neurocranium, the jaws, the dorsal spine, and teeth; Specimen MHNA-PAL-2020-0003 (Figs. 52–53) preserving the incomplete neurocranium, the jaws, the broken dorsal spine and teeth; paleontological collection of the MHNA.

Type Locality—Excavation site of Muse (Path of the Poil Fou/Les Echars), Dracy-Saint-Loup Municipality, Saône-et-Loire, France.

Type Horizon—Bottom of the Fish layer, Muse OSB, Muse formation, Autun Basin, Northern Massif Central, lowermost Asselian, Cisuralian, lower Permian (Pellenard *et al.* 2017).

Diagnosis—Triodus species defined by the following combination of characters. For the teeth: a maximum height of 2 mm, a rounded to rhomboid base, median cusps between ½ and $^{2}/_{3}$ the size of the lateral ones, three to five vertical cristae on the labial side and one or none vertical

Figure 47. Holotype MHNA-PAL-2020-0001 of *Triodus aeduorum* sp. nov. from the Muse OSB, Autun Basin. Photo of the whole specimen as preserved (see Figs. 3–5 for details). **A**, photograph. **B**, Line drawing of **A**.

crista on the lingual side of the cusps, few irregular bifurcation pattern, rounded cross-section of the cusps that becomes polygonal toward the apex, angle of 110°-130° between the crown and the base in mesial or distal view, rounded to oval coronal button always with a lingual shaft; up to 8 oral nutrient foramina and up to 11 basal nutrient foramina and median cusps not labially displaced. For the dorsal spine: dorso-ventrally compressed with lateral hook-shaped denticles, wide proximal ventral groove that almost reaches the apex, numerous fine proximal longitudinal striations and a width/length ratio of $^{1}/_{13}$.

Description

Preservation—The specimen MHNA-PAL-2020-0001 (Figs. 47–50) represents a 19.5 cm long half-individual. The specimen shows several proximal vertebral remains and the proximal part of the left scapulocoracoid (Fig. 47). The highly compressed 4.9 cm long neurocranium and jaws (Fig. 48), the 8.1 cm long dorsal spine (Fig. 49) and a 6.3 cm long pectoral fin (Fig. 50) are also preserved. MHNA-PAL-2020-0002 (Fig. 51) shows a 5.7 cm long neurocranium, the jaws and an incomplete 7.7 cm long dorsal spine in a good preservation state. MHNA-PAL-2020-0003 (Fig. 52) consists of a poorly preserved individual showing part of the neurocranium, the jaws and the dorsal spine. The teeth (Fig. 53) of the specimens are variously preserved: few teeth are visible in MHNA-PAL-2020-0002 with only one in basal view, MHNA-PAL-2020-0001 shows at least 30 teeth, but mostly incomplete, and MHNA-PAL-2020-0003 shows at least 50 worn teeth.

Neurocranium—The neurocrania (Figs. 48, 51–52) are mainly visible in dorsal view. The otico-occipital region represents more than half of the entire neurocranial length. The preorbital process is rectangular in shape and is antero-laterally oriented. There is an apparently short rostrum and a precerebral fontanelle which is flared U-shaped (Fig. 51). Due to the distortion of the neurocranium, the precerebral fontanelle can appear laterally compressed with a V shape (Figs. 48, 52). The border of the supraorbital shelf is concave. The postorbital process is pointed in dorsal view, and slightly longer than the preorbital and lateral otic processes. The articular surface for the palatoquadrate is situated on the posterior side of the postorbital process. The border of the otic region is concave. The two dorsal otic ridges are well developed and curved (Figs. 48, 51). The lateral otic processes are also well developed, with a broad pointed shape. They are oriented laterally (Fig. 48) or postero-laterally (Fig. 51). On the holotype (Fig. 48), the articular surface for the otic process of the palatoquadrate is visible. The anterior part of the occipital block is wedged between the otic capsules, from the level of the lateral otic processes anteriorly. Then, it extends on a considerable distance beyond the rear of the lateral otic processes posteriorly. The ethmoid region (Fig. 51–52) shows distinct tessellated calcified cartilage that suggests an adult growth state according to the ontogeny of current neoselachians (Benzer 1944). The holotype (Fig. 48) possesses few tesserae on the ethmoid region that indicate a more juvenile growth state. The state of preservation does not allow to observe whether multiple tessellated calcified cartilage is present like in *Orthacanthus* (Schaeffer 1981; Pradel *et al.* 2011).

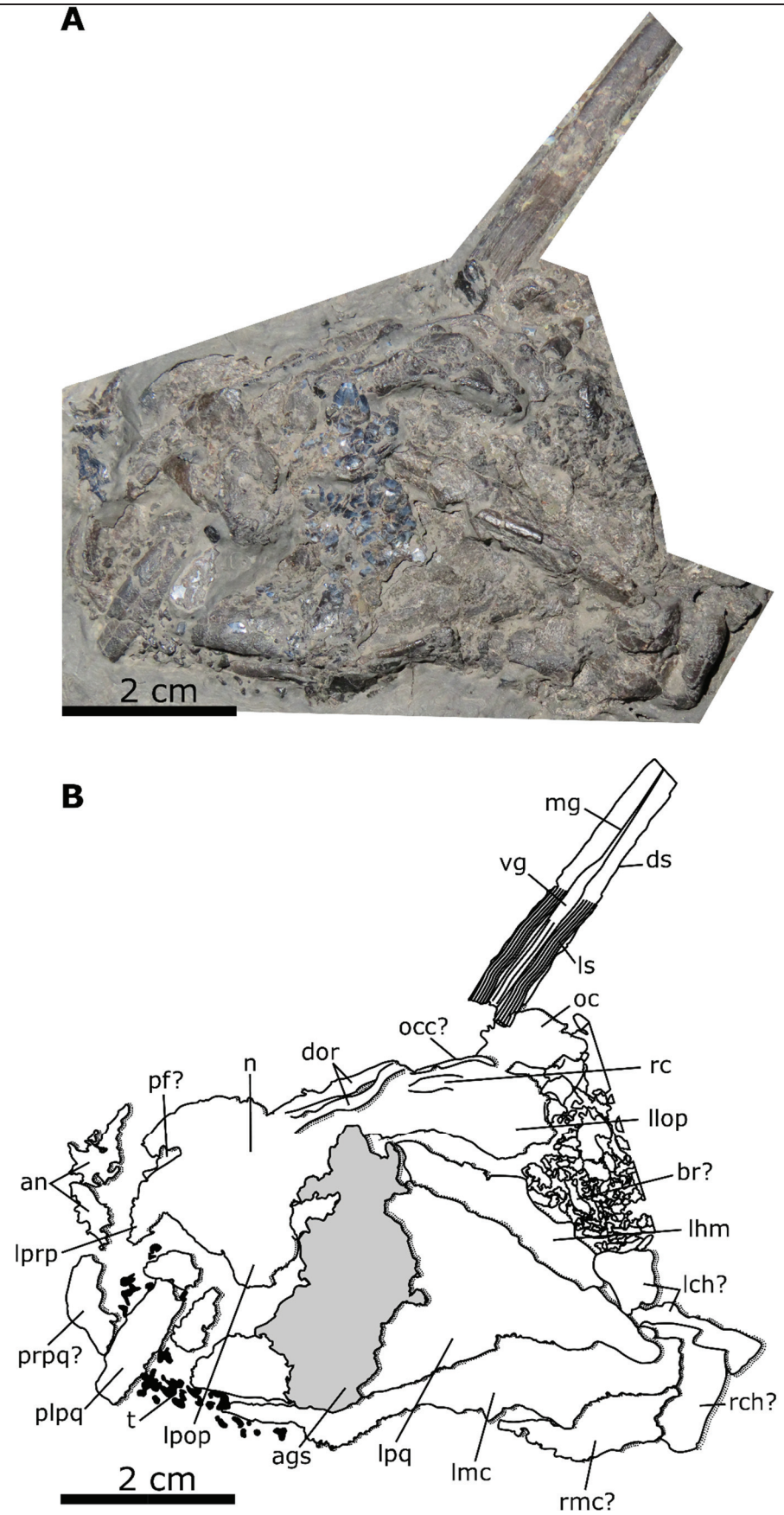

Figure 48. Details of the head region of the holotype MHNA-PAL-2020-0001 of *Triodus aeduorum* sp. nov. from the Muse OSB, Autun Basin. **A**, photograph. **B**, Line drawing of **A**.

Palatoquadrate—The palatoquadrate (Figs. 48, 51–52) has a distinct cleaver-shape with a slender palatine part and a broad quadrate part. The palatine part is not very curved. On a paratype (Fig. 51), the ethmoid process is connected to the preorbital process. The palatine part is slightly shorter than the quadrate one. The angle between the palatine and quadrate parts is 90°. The posterior border of the quadrate part is arc-shaped, and a broad dorsal crest is present along it. The articular process for the Meckel's cartilage is small. The ventral border of the palatoquadrate is sigmoid.

Meckel's Cartilage—The Meckel's cartilage (Figs. 48, 51–52) is articulated with the palatoquadrate at the level of its articular process. It is articulated with the ceratohyal at its distal extremity in the holotype (Figs. 47–48). As the left and right Meckel's cartilages are not visible together, the symphysis cannot be observed, but the Meckel's cartilages may not be fused together.

Hyoid Arch—The hyomandibular, and probably the ceratohyal (Fig. 48), are greatly altered. Both might still be in connection. The hyomandibular is situated posteriorly to the palatoquadrate, but it does not contact the lateral otic process. The ceratohyal might be situated next to the Meckel's cartilage and is probably connected to its more distal part.

Dorsal Spine—Only the holotype (Fig. 49) has a well and entirely preserved dorsal spine. The spine on one paratype (Fig. 51) is almost complete but its denticles are still hidden in the matrix. In the other paratype (Fig. 52), only the proximal part of the spine is preserved, without the denticles. Contrary to the two others, its cross-section is visible, and it is dorso-ventrally compressed. The spines are straight, and their base presents thin longitudinal striations in ventral side. It is 8.1 cm long in the type specimen (Fig. 49) and 7.7 cm in the paratype (Fig. 51), which is not complete. The width/length ratio is $^{1}/_{13}$ (Fig. 49), with a maximum width at its base. The proximal part of the spine has fine longitudinal striations that disappear distally, and a ventral groove. The latter is broad next to the base and reaches almost the apex (Fig. 49). There is no dorsal groove. The denticles are situated on each lateral side of the spine, along the distal half. They are hook-shaped and closely set, but do not touch each other. The apex of the most proximal denticles tends to be parallel to the spine surface (Fig. 49). The most proximal denticles are almost of the same size (Fig. 49), which, following Soler-Gijón (2004), indicate that this specimen can be interpreted as a sub-adult specimen.

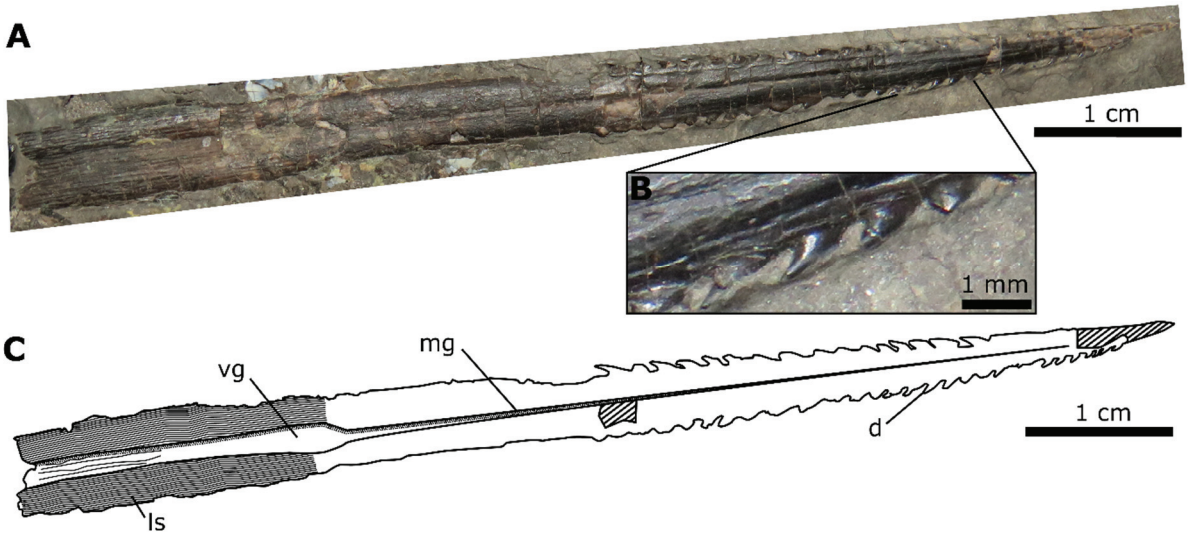

Figure 49. Details of the dorsal spine of the holotype MHNA-PAL-2020-0001 of *Triodus aeduorum* sp. nov. from the Muse OSB, Autun Basin. **A**, photograph. **B**, details of the denticle. **C**, Line drawing of **A**.

Teeth—The height of the teeth (Fig. 53) does not exceed 2 mm. They have two main lateral cusps, and a slender but quite long median cusp that reaches ½ to $^{2}/_{3}$ the size of the lateral cusps. The median cusps are broken in many teeth but always present. Three to five vertical cristae are located on the labial side of the lateral cusps. The vertical cristae do not reach at the apex and can reach half the height of the lateral cusps. Very few bifurcations are visible, but if they are present, they are irregular. On the lingual side of the cusps, one or no vertical crista is present. Some teeth have a developed vertical crista on each lateral side of the cusps, which resembles a lateral cutting edge as in *Xenacanthus* (e.g. Ginter *et al.* 2010). The cross-section of the cusps is rounded at their base, and polygonal at their apex because of the presence of the cristae. On the oral face, the coronal button is rounded to oval, and has always a lingual shaft. Three to eight nutrient foramina are present on the lateral and posterior sides of the coronal button. The angle between the crown and the base of the teeth is always greater than 110° and can reaches 130° in mesial or distal view. The median cusp is not labially displaced. In basal view, the base of the tooth is rounded to rhomboid, sometimes elliptic and labio-lingually compressed. In MHNA-PAL-2020-0003, the smaller teeth tend to be more rhomboid. The basal tubercle always has a depression in its center and no lingual shaft. It is mainly prominent in mesial or distal view compared to the ventral border of the base. The basal face has between four and 11 nutrient foramina behind the basal tubercle.

Scapulocoracoid—The distal part of the scapulocoracoid (i.e. coracoid and articular process for the pectoral fin) is missing and only its outline is visible (Figs. 47–50). The articular process

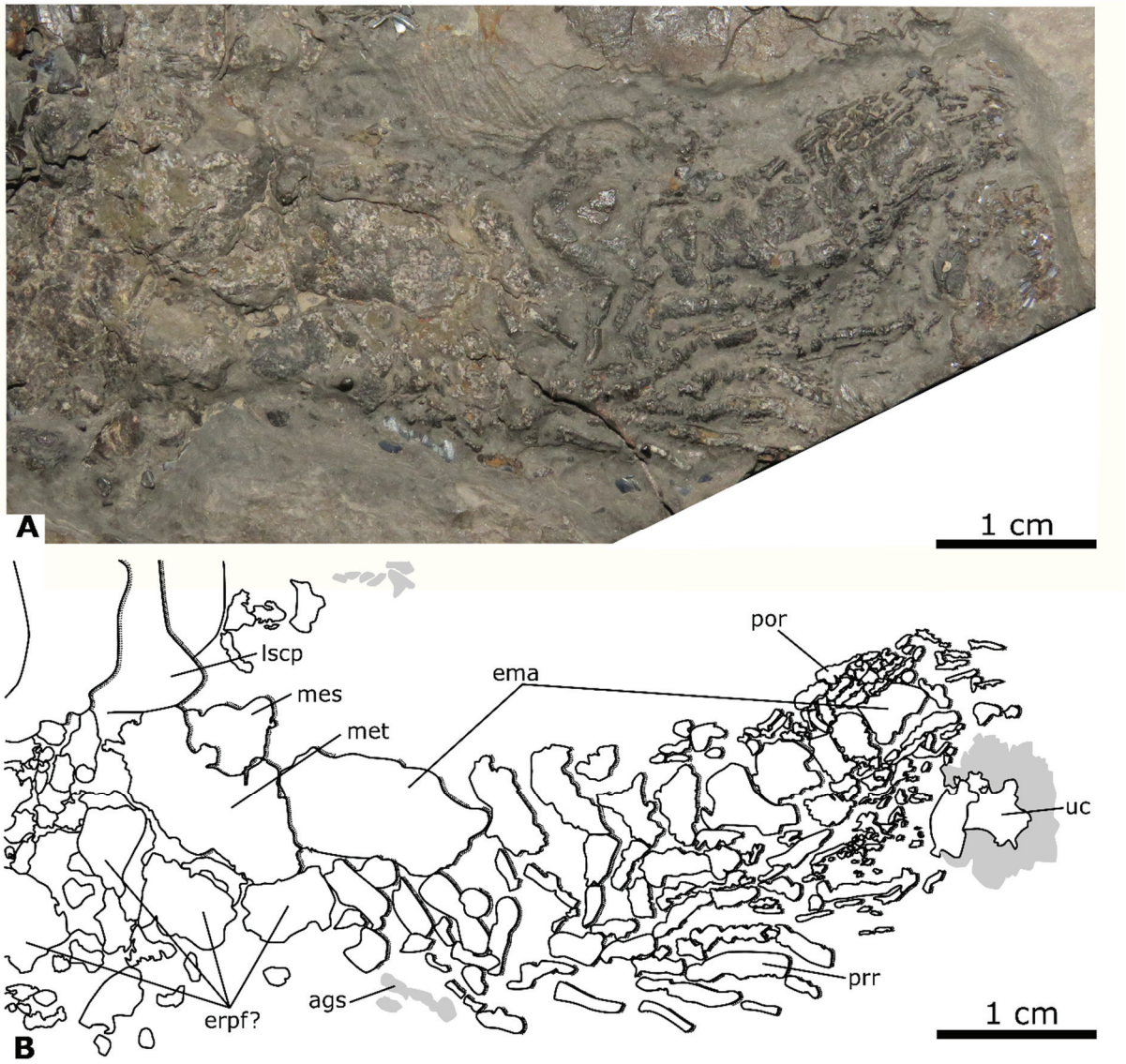

Figure 50. Details of the left pectoral fin of the holotype MHNA-PAL-2020-0001 of *Triodus aeduorum* sp. nov. from the Muse OSB, Autun Basin. **A**, photograph. **B**, Line drawing of **A**.

for the pectoral fin is rounded and well-developed. The suprascapular cartilage is long and pointed. The scapula forms a well-pronounced angle in its proximal part, i.e. 120°.

Branchial Region—The branchial region is poorly preserved with no identifiable element. Few pieces of cartilages can be parts of the branchial elements (Fig. 47).

Vertebral Column—The vertebral column is visible (Fig. 47). The hypertrophic neural arches are characterized by an elongated and broad shape. Below them, smaller and less elongated elements are interpreted as the basiventral elements. Dorsally, there are numerous slender and elongated elements which are the radials of the dorsal fin (Fig. 47).

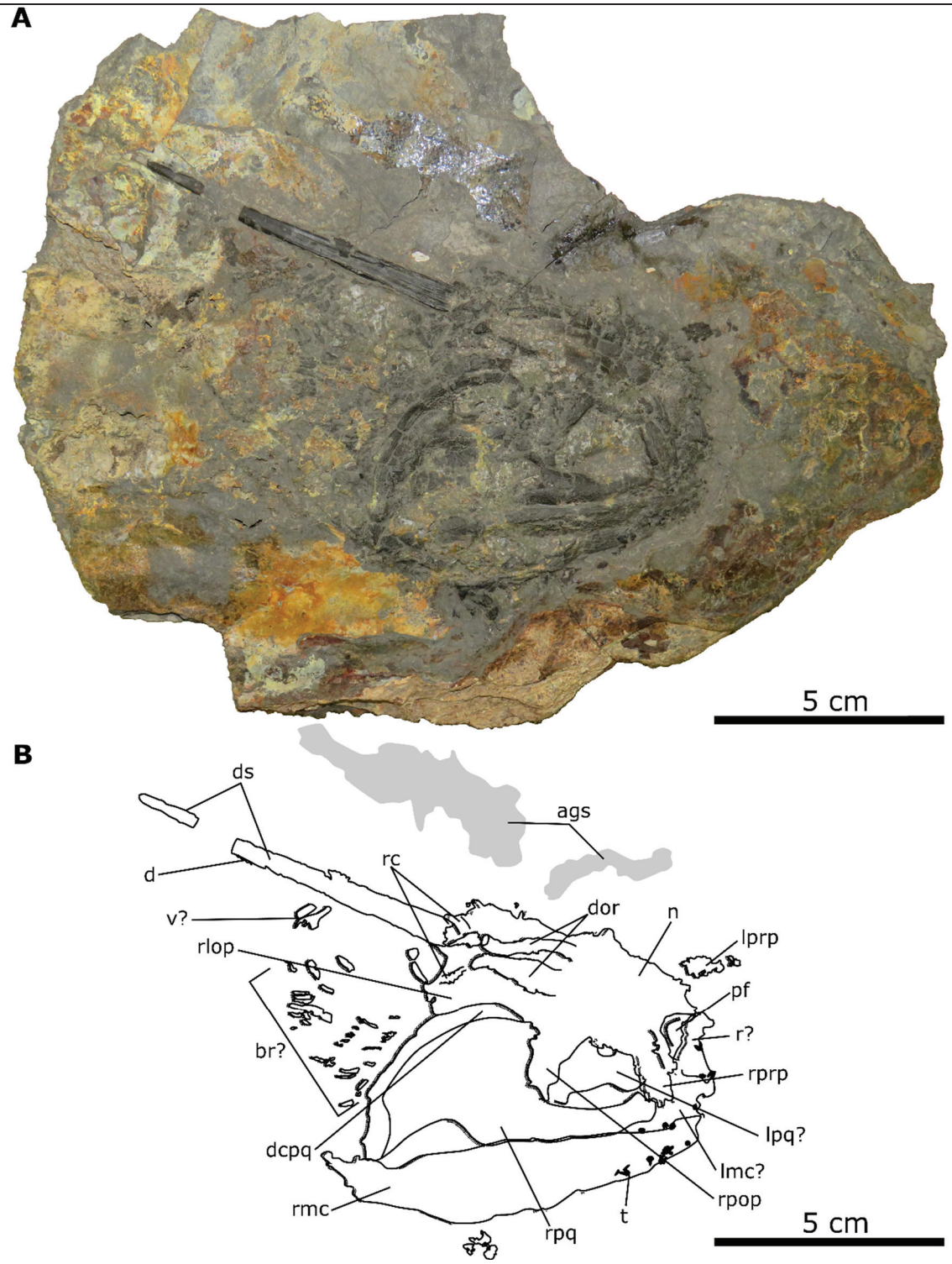

Figure 51. Paratype of *Triodus aeduorum* sp. nov. specimen MHNA-PAL-2020-0002 from the Muse OSB, Autun Basin. **A**, photograph. **B**, Line drawing of **A**.

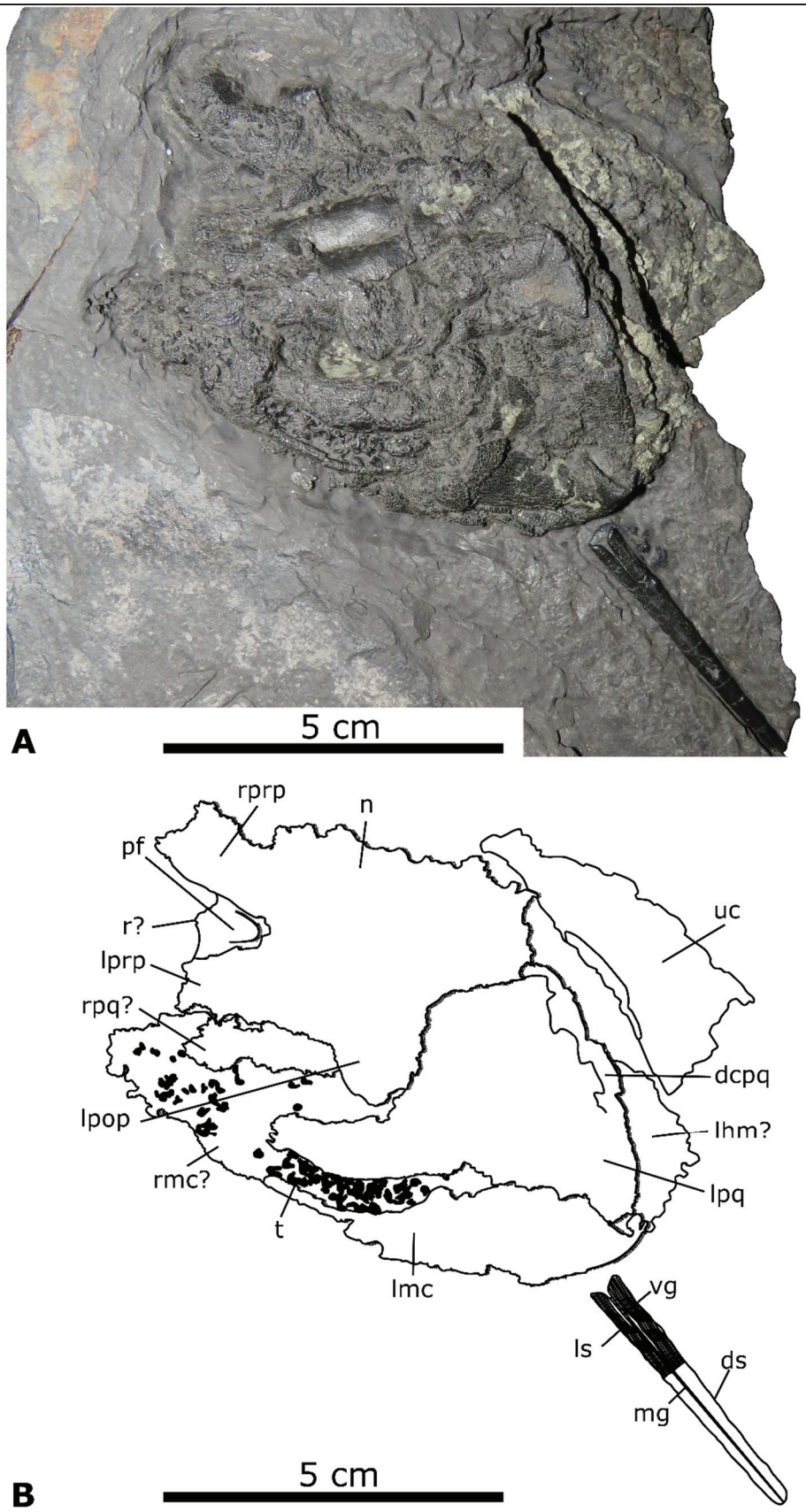

Figure 52. Paratype of *Triodus aeduorum* sp. nov. specimen MHNA-PAL-2020-0003 from the Muse OSB, Autun Basin. **A**, photograph. **B**, Line drawing of **A**.

Pectoral Fin—The pectoral fin (Fig. 50) is composed of a long and broad metapterygium which articulates with a stocky mesopterygium. Both articulates with the articular process of the scapulocoracoid. The propterygium is absent. At least 10 axial elements constituting the metapterygial axis are visible, and the more proximal one is longer than the others. The most distal and slender elements are not present. The preaxial radials are longer than the postaxial ones and inserted on the anterior side of every elements of the metapterygial axis. The posterior radials are inserted on the posterior side of these elements restricted to the distal part of the fin.

Comparisons

The two lateral rows of denticles on the flattened dorsal spine and the small teeth with rounded cross-section and a long median cusps that reaches $^{2}/_{3}$ the size of the lateral ones exclude the Diplodoselachidae (e.g. Ginter *et al.* 2010) and clearly refer to the Xenacanthidae (e.g. Ginter *et al.* 2010).

Teeth—The teeth (Fig. 53) display lateral cusps with a circular cross-section, devoid of lateral cutting edge and few nutrient foramina at the base: this differs from the teeth of *Xenacanthus* which display lateral cusps with a lanceolate to subcircular cross-section, with a lateral cutting edge and a large number of nutrient foramina at the base (e.g. Heidtke & Schwind 2004; Ginter *et al.* 2010). The teeth (Fig. 53) also differ from those of *Plicatodus* (e.g. Hampe 1995; Ginter *et al.* 2010) by their symmetrical aspect, their long median cusps, their circular cross-section at the base of the cusps and their vertical cristae restricted to the upper part of the cusps. The teeth of *Wurdigneria* from the Guadalupian of Brazil (e.g. Richter 2005; Ginter *et al.* 2010) have lanceolate cusps, and numerous nutrient foramina on the base. Those of *Mooreodontus* from the Middle and Upper Triassic of India, North America and Europe (Ginter *et al.* 2010) have a triangular base in basal view. On the other hand, the teeth of the Muse OSB specimens (Fig. 53) are reminiscent to those of *Triodus* (e.g. Hampe 1989; Ginter *et al.* 2010) because they have a long and slender median cusps, a circular to polygonal cross-section of the cusps devoid of lateral cutting edge, vertical cristae restricted to the upper half of the cusps and a reduced height in lateral view (less than 2 mm).

Triodus Species—The small but well-developed rectangular preorbital process, antero-laterally oriented (Figs. 48, 51), is reminiscent to that of *T. sessilis* (Jordan 1849; Schwind 1991; Heidtke *et al.* 2004), *T. carinatus* (Schneider & Zajíc 1994) and *T.* sp. (Soler-Gijón & Hampe 1998; Heidtke *et al.* 2004). Specimens from the Muse OSB (Figs. 48, 51) have a broad and pointed

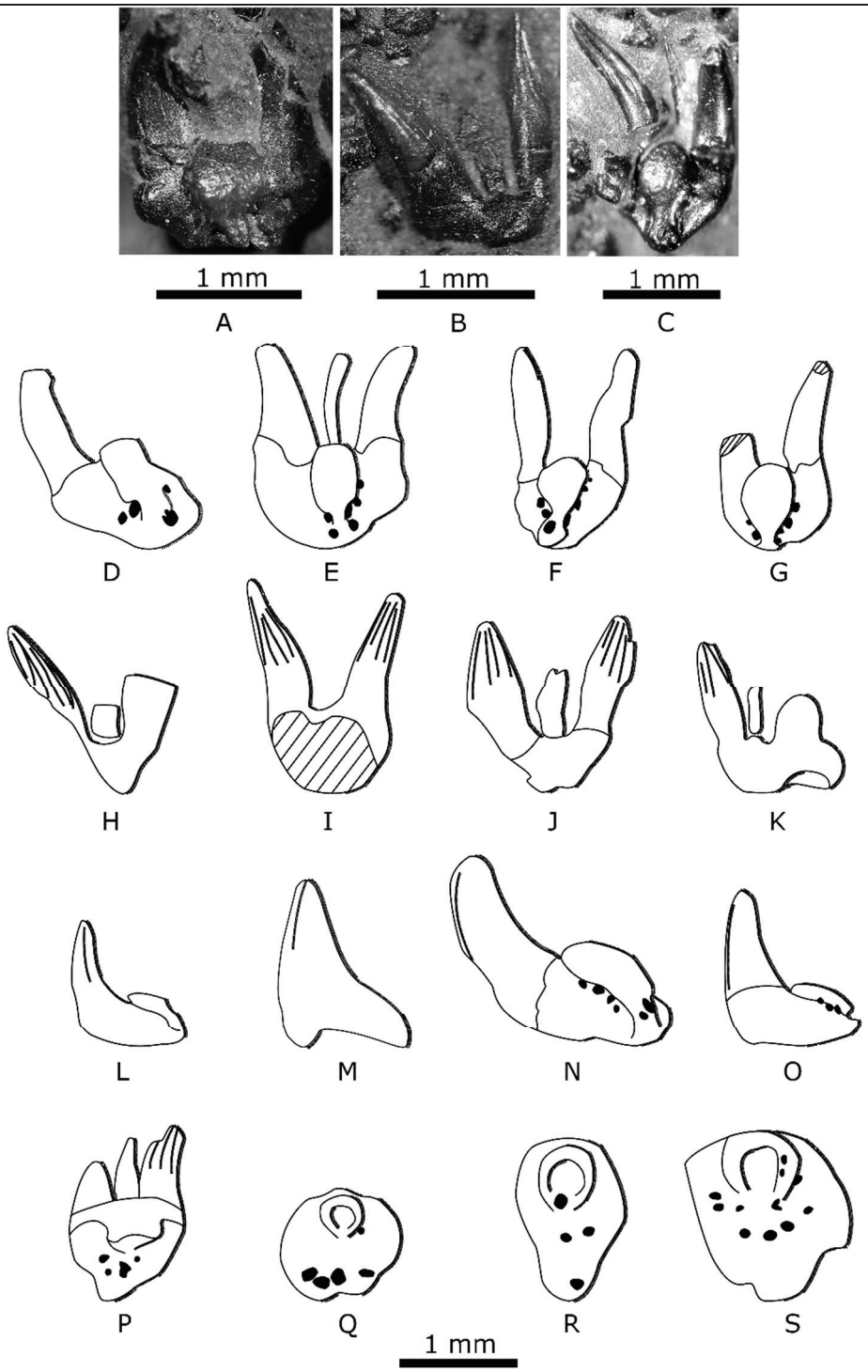

Figure 53. Teeth of *Triodus aeduorum* sp. nov. specimens from the Muse OSB, Autun Basin. MHNA-PAL-2020-0001, (**A**, **D**, **H**, **L**, **M**, **P**); MHNA-PAL-2020-0002, (**B**, **E–F**, **I**, **Q**); MHNA-PAL-2020-0003, (C, G, J–K, N–O, R–S). **A–C**, photograph. **D–S**, line drawing. **A**, oral view. **B**, labial view. **C**, oral view. **D**, linguo-lateral oral view. **E–G**, lingual view. **H–J**, labial view. **K**, labio-lateral view. **L–O**, lateral view. **P**, labio-basal view. **Q–S**, basal view.

lateral otic process, postero-laterally or laterally oriented. This morphology is similar to that of *T. sessilis*, *T. carinatus* and *T.* sp. The outline of the otic part of the neurocranium is concave (Figs. 48, 51), as in *T.* sp. (Soler-Gijón & Hampe 1998) *T. carinatus* (Fritsch 1890; Schneider & Zajíc 1994), but not in *T. sessilis* (Schwind 1991; Heidtke *et al.* 2004) where this outline is straight and posteriorly flared.

The palatoquadrate (Figs. 48, 51–52) is similar to that of *T. carinatus* (Fritsch 1890; Schneider & Zajíc 1994) that has a well curved palatine part, an elongated ovoid quadrate part and a strong articular process. This morphology is observed in *T. sessilis* (Jordan 1849; Heidtke *et al.* 2004) except for the articular process that is more developed and identical to the one of *T.* sp. (Soler-Gijón & Hampe 1998; Heidtke *et al.* 2004).

The dorsal spine (Fig. 49) has hook-shaped denticles contrary to that of *T. serratus* which has trapezoid denticles (Hampe 2003) and a width/length ratio of $^{1}/_{13}$ contrary to that of *T. sessilis* with a ratio of $^{1}/_{11}$ (Jordan 1849; Heidtke *et al.* 2004) or that of *T. carinatus* with a ratio of $^{1}/_{16}$ (Schneider & Zajíc 1994). The denticles of *T. sessilis* and *T. carinatus* are narrowly spaced, i.e. they can touch each other, which is not the case here (Fig. 49). The dorsal spine of *T. carinatus* has a triangular cross-section (Fritsch 1890; Schneider & Zajíc 1994; Hampe 2003) contrary to the dorso-ventrally compressed one of the paratype (Fig. 52). In *?T. pulchellus* (Davis 1880; Hampe 2003), $^{2}/_{3}$ of the length bears denticles. In *T.* sp., the cross-section is dorso-ventrally compressed (Soler-Gijón & Hampe 1998). The dorsal spine (Fig. 49) has a long ventral groove stretching along most of the entire length of the spine.

The combination of tooth characters (Fig. 53) excludes the attribution to many of the *Triodus* species: *T. elpia* (lower Bashkirian of the United States; Johnson & Thayer 2009) has asymmetrical tooth base and a coronal button; *T. serratus* (lower Bashkirian to Moscovian of the United Kingdom; Davis 1892; Hampe 2003) has higher teeth, up to 5 mm and a distinctly concave basal face; *T. teberdaensis* (Moscovian of Russia; Heidtke *et al.* 2004; Hampe & Ivanov 2007b) shows an angle from 90° to 100° between the crown and the base and its teeth are much smaller (less than 1 mm), with few but developed oral nutrient foramina and a median foramen between their cusps. The teeth of *T. palatinus* (lower Gzhelian to upper Asselian of Germany; Hampe 1989; Heidtke *et al.* 2004) differ from those of the specimens from the Muse OSB by the numerous vertical cristae (six to nine) and bifurcations, and their possible asymmetrical tooth base. Those of *T. sessilis* (Asselian of Germany; Jordan 1849; Hampe 1989; Heidtke *et al.* 2004) have a Y-shaped bifurcation pattern of the vertical cristae, a constant angle of 90° between the crown and the base, a constant number of six vertical cristae on each face of each cusp and a median cusp greater than $^{2}/_{3}$ the size of the lateral cusps. The teeth of *T.*

obscurus (Asselian of Germany; Hampe 1989; Heidtke *et al.* 2004) have between two and four oral nutrient foramina and no vertical crista on the lingual face of the cusps. *T. kraetschmeri* teeth (upper Asselian to Artinskian of Germany; Hampe 1989; Heidtke *et al.* 2004) are different because of their small height (less than 1 mm), a constant angle of 100° between the crown and the base and a labially displaced median cusp. The teeth of *T. richterae* (Capitanian of Brazil; Pauliv *et al.* 2017) have long vertical cristae, down to the base of the cusps and a concave basal face. The tooth morphotype of *T.* sp. ZÖ (Schindler & Hampe 1996) has a rounded cross-section at the apex of the cusps and only four oral nutrient foramina (against eight in the specimens from the Muse OSB). The *Triodus* teeth from the Puertollano basin (Soler-Gijón 1993a,b, 1994, 1995) are different by the presence of an occasional oral nutrient foramen between the cusps and the coronal button, more vertical cristae on the lingual side of the cusps, and the oval to circular cross-section of the cusps.

Triodus species whose tooth morphology reminds that of the Muse OSB specimens (Fig. 53) are *T. lauterensis* (Kasimovian to Gzhelian of Germany; Hampe 1989; Heidtke *et al.* 2004) and *T. carinatus* (Asselian of Czechia; Fritsch 1890; Schneider & Zajíc 1994).The teeth of *T. lauterensis* only differs by a smaller angle (100° to 110°) between the crown and the tooth base. Those of *T. carinatus* only differ by their height (up to 4 mm), but several characters, like the cross-section of the cusps are not known for this species.

The scapulocoracoid (Fig. 47) shares with the genus *Triodus* (*T. sessilis* in Heidtke *et al.* [2004], and *T. carinatus* in Schneider & Zajíc [1994]) a well-developed and pointed suprascapula cartilage. The articular process with the pectoral fin is more rounded (Fig. 50) than in *T. sessilis* (Heidtke *et al.* 2004). The metapterygium (Fig. 50) is not entirely preserved but its dimensions seem to be like those of *T. sessilis* (Heidtke *et al.* 2004). Contrary to *T. sessilis*, the first element of the metapterygial axis is very long (Fig. 50).

***Triodus* sp.**

(Figs. 54A)

Triodus ?*frossardi* Soler-Gijón & Hampe 1998:336, figs. 1–4.

Triodus ?*frossardi* Heidtke, Schwind and Krätschmer, 2004:45, fig. 20.

Triodus frossardi Ginter *et al.* 2010:53.

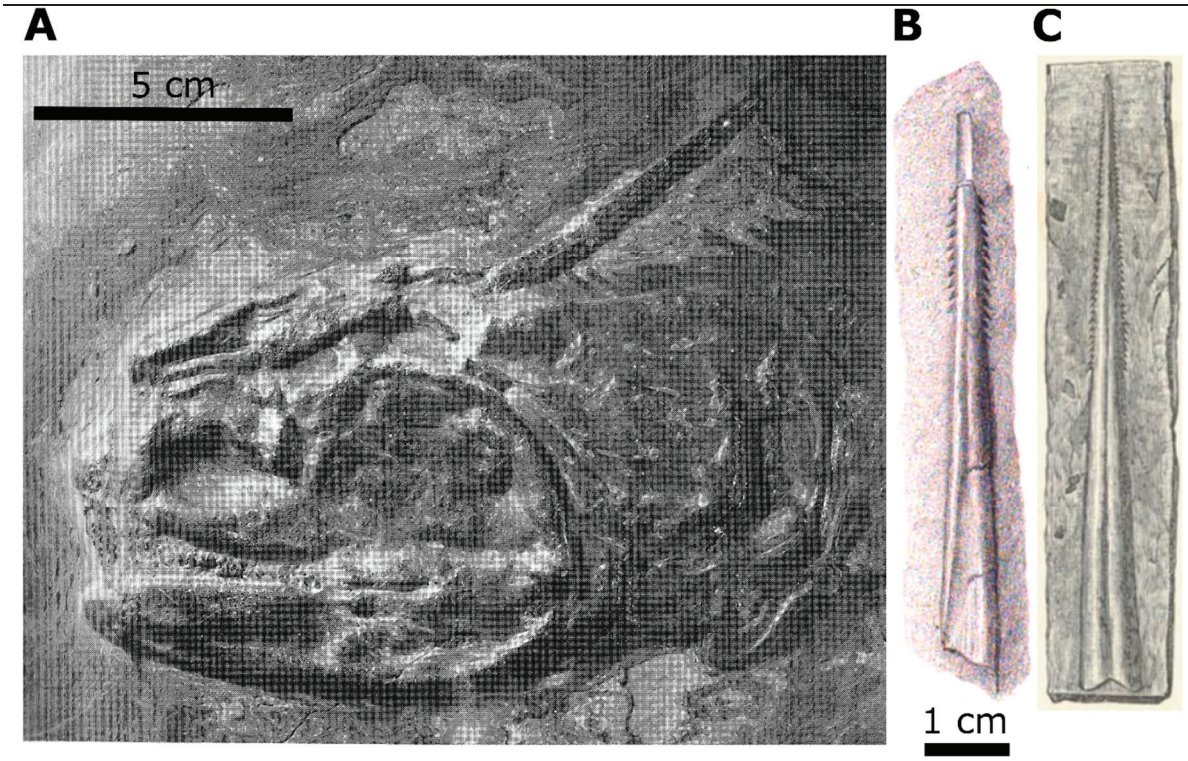

Figure 54. Revised Xenacanthiformes from the Muse OSB, Autun Basin. **A**, *Triodus* sp. (adapted from Soler-Gijón & Hampe 1998). **B**, '*Expleuracanhus*' *frossardi* (from Gaudry 1867). **C**, '*Expleuracanthus*' *frossardi* (from Gaudry 1883).

Referred Material—Specimen RMH/PP 51, anterior part of an individual showing neurocranium, jaws, dorsal spine, teeth, scapulocoracoid and anterior part of vertebral column; paleontological collection of the RMH/PP.

Occurrence—Excavation site of Muse (Path of the Poil Fou/Les Echars), Dracy-Saint-Loup Municipality, Saône-et-Loire, France.

Horizon—Undetermined oil-shale level of the Muse OSB, Muse formation, Autun Basin, Northern Massif Central, lowermost Asselian, Cisuralian, lower Permian (following Soler-Gijón & Hampe 1998).

Description

The specimen RMH/PP 51 (Fig. 54A) was described in detail by Soler-Gijón and Hampe (1998). The teeth have a long median cusp, six to nine labial vertical cristae on each cusp but a lower number on the lingual side, a Y-shaped and irregular bifurcation of the vertical cristae below the apex, a lingual shaft on the coronal button, few oral nutrient foramina, a basal tubercle

with a concave articular depression, about four basal nutrient foramina and an angle comprised between 90° and 95° between the crown and the base. The dorsal spine has an elliptic cross-section and fine proximal longitudinal striations. In addition, *Triodus* sp. shows a neurocranium with narrow preorbital processes, postorbital processes with semi-triangular outline, an otico-occipital region that reaches $^{2}/_{3}$ of the entire length, and parallel dorsal otic ridges that are perpendicular to the postorbital process. The palatoquadrate has a cleaver-shape, a low and slightly curved palatine part and a deep quadrate part with a dorso-posterior crest.

Comparisons

We follow Soler-Gijón & Hampe (1998) in considering that RMH/PP 51 belongs to the genus *Triodus* based on similarities of its neurocranium with that of *T. sessilis*, and on its tooth morphology, typical of *Triodus*. Soler-Gijón & Hampe (1998:344) listed tooth diagnostic characters based on Hampe (1989). These differences in tooth morphology allow to distinguish *T.* sp. from the other known species of this genus (Soler-Gijón & Hampe 1998). All the teeth of *Triodus aeduorum* sp. nov. (Fig. 53) can also be separated from those of *T.* sp. by a median cusp that reaches $^{2}/_{3}$ the size of the lateral ones, three to five vertical cristae, few irregular bifurcations of the vertical cristae and an angle of 110° to 130° between the crown and the base. Despite the resemblances of their neurocranium and palatoquadrate, these differences in tooth morphology confirm that *T.* sp. is different from *T. aeduorum* sp. nov.

Soler-Gijón & Hampe (1998) justified their attribution to *T.* ?*frossardi* by the fact that its dorsal spine is too poorly preserved to be compared with that of '*Expleuracanthus*' *frossardi* (Gaudry, 1883) from the same locality. On the contrary, Heidtke *et al.* (2004) considered '*E*'. *frossardi* and *T.* ?*frossardi* as synonyms. We follow Soler-Gijón & Hampe (1998) who did not synonymize *T.* sp. with '*E*'. *frossardi*. We propose to change the nomenclature from *Triodus* ?*frossardi* to *Triodus* sp. pending the discovery of new specimens.

'*Expleuracanthus*' *frossardi* (Gaudry, 1883) *nomen dubium*
(Figs. 54B–9C)

Pleuracanthus frossardi(Gaudry, 1867:39, fig. 3.
Pleuracanthus frossardi Gaudry, 1883:222, fig. 221.
Pleuracanthus frossardi Brongniart & Sauvage, 1888:33, fig. 14.
Pleuracanthus bonnardi Sauvage, 1893:32, pl. I.

Holotype—Specimen MNHN 1888.8.2, an isolated dorsal spine figured by Gaudry (1883); paleontological collections of the MNHN.

Type Locality—Dracy-Saint-Loup, Autun Basin, Saône-et-Loire, France.

Type Horizon—Lally OSB, Muse formation, Autun Basin, Northern Massif Central, uppermost Gzhelian, Pennsylvanian, Upper Carboniferous (following Pellenard *et al.* 2017).

Occurrence—Muse OSB, Autun Basin, Saône-et-Loire.

Remarks—Many authors (e.g. Ginter *et al.* [2010] and references therein) consider that the holotype of *'Expleuracanthus' frossardi* is the isolated dorsal spine from Dracy-Saint-Loup figured by Gaudry (Fig. 54C; 1883). But the original name *'Pleuracanthus' frossardi* appeared in Gaudry (Fig. 54B; 1867) with an illustration of an isolated and incomplete dorsal spine that comes from the "fish layer" of the Muse OSB, without detailed description and apparently of a different shape than that of Gaudry (1883). Sauvage (1893) synonymized the *'Expleuracanthus' frossardi* specimens mentioned by Gaudry (1867, 1883) with *'Expleuracanthus' bonnardi* (*Pygopterus bonnardi* in Agassiz [1833-1843] and '*Pleuracanthus*' *bonnardi* in Sauvage [1893]). According to Hampe (2003), a lot of characters of the dorsal spine are shared among the genera *Triodus* and *Xenacanthus*. So, apart from rare Xenacanthidae species in which the dorsal spine displays an autapomorphy, like the triangular cross-section of *T. carinatus*, an isolated dorsal spine cannot be diagnostic at species level without associated teeth.

Description

Following the illustration of Gaudry (1867:39, 1883:222), this species is characterized by a long ventral groove in the spine, the denticles occupy the distal half of the total length and there can be fine longitudinal striations at the base of the spine according to Gaudry (Fig. 54A; 1867) but not figured in Gaudry (Fig. 54B; 1883).

Comparisons

Among the Xenacanthidae, the two genera with known dorsal spines are *Triodus* and *Xenacanthus*. Following Hampe (2003), the difference between them is the relative length of the spine compared to the body length: ¼ in *Xenacanthus* and $^{1}/_{6}$ in *Triodus*. *'E'. frossardi*

(Figs. 54B–54C; Gaudry 1867, 1883) shares several characters with other xenacanthiforms: a serrated distal half is also present in many *Triodus* and *Xenacanthus* species (e.g. Hampe 2003), and two lateral rows of denticles are also known in Xenacanthidae (e.g. Hampe 2003; Ginter *et al.* 2010). The absence of proximal longitudinal striations may be characteristic of *'E'. frossardi* according to Gaudry (Fig. 54C; 1883: 222), but such striations appear on Gaudry's (Fig. 54B; 1867: 39) figure and this character is common to many xenacanthiforms (e.g. Schneider & Zajíc 1994; Hampe 2003). Consequently, no diagnostic character based on the dorsal spine of '*E*'. *frossardi* allows a distinction between *Xenacanthus* and *Triodus contra* Heidtke *et al.* (2004) and Ginter *et al.* (2010) who included '*E*'. *frossardi* into the genus *Triodus*. The dorsal spines of *T. aeduorum* sp. nov. (Figs. 47, 51–52) and *'E'. frossardi* (Figs. 54B–54C) share a long ventral groove, but this character is also present in the type species *T. sessilis* (Heidtke *et al.* 2004) and in all the known *Triodus* dorsal spines (Schneider & Zajíc 1994; Hampe 2003). There is no character relating *T. aeduorum* sp. nov. to *'E'. frossardi*. A diagnosis of '*E*'. *frossardi*, based only on the morphology of the dorsal spine, appears therefore impossible to come up with for now. Consequently, '*E*'. *frossardi* is considered as a *nomen dubium* and Gaudry's (1867, 1883) historical material needs to be exhaustively revised, which it is out of the scope of the present work.

Discussion

Chondrichthyan Diversity of the Muse Oil-shale Bed

The erection of *Triodus aeduorum* sp. nov. and the reassessment of *T.* sp. and '*Expleuracanthus*' *frossardi* permit to better understand the chondrichthyan diversity of the Muse OSB. Another form of the doubtful genus '*Expleuracanthus*' is present in the Muse OSB: *'Expleuracanthus' bonnardi* refers to *Pygopterus bonnardi* described by Agassiz (1833-1843) and to specimens described and figured by Sauvage as *'Pleuracanthus' bonnardi* in 1893 (see Sauvage [1893] for the list of synonyms). No tooth was described or mentioned by Agassiz (1833-1843) or Sauvage (1893). The insertion of the dorsal spine at the base of the neurocranium, similar to that of the genera *Triodus* and *Xenacanthus*, suggests that '*E*'. *bonnardi* is a Xenacanthidae even if the denticles and the dorsal spine cross-section are not visible. Even if Sauvage (1893) considered '*E*'. *bonnardi* and *'E'. frossardi* as synonymous, we cannot formally consider '*E*' *bonnardi* as an invalid or valid species until a complete revision of all the existing associated material is done, which is out of the scope of this work.

As two specimens appear to belong to the same adult growth stage, another possibility would be that *Triodus aeduorum* sp. nov. and *T.* sp. represent sexual morphs of the same species. Few studies have investigated the sexual dimorphism among xenacanthiforms: they focused on morphometric analyses of *Orthacanthus platypternus* dorsal spines from the Sakmarian of the United States (Donelan & Johnson 1997; Johnson & Thayer 2009; Johnson 2012; Beck *et al.* 2016) and morphological differences of the pelvic and anal fins between *Xenacanthus*, *Triodus* and *Orthacanthus* (Schneider & Zajíc 1994; Schneider 1996; Heidtke & Schwind 2004). No sexual dimorphism within the xenacanthiform has been detected based on tooth morphology so far. The three new specimens from the Muse OSB (Figs. 47, 51–52) are not sufficient to perform similar morphometric analysis to eventually detect a sexual dimorphism. New material, especially associated with pelvic fins, which are absent here, is necessary to make progress on this matter.

Paleobiogeographic Remarks about the European *Triodus* Species

The Autun Basin (Fig. 46A) belongs to a group of Carboniferous-Permian basins located in the Northern Massif Central (e.g. Gand *et al.* 2015, 2017). Based on their paleontological contents, these French basins were connected, at least partially and temporarily to others from Europe, such as the basins of Saar-Nahe (Western Germany) Thuringia (Eastern Germany), Bohemia (Czechia) and Puertollano (Spain) (Boy & Schindler 2000; Steyer *et al.* 2000, 2012; Schultze & Soler-Gijón 2004; Schultze 2009). The connections between basins are inferred from the presence of many common vertebrate and "invertebrate" taxa (see Schultze [2009] for a synthesis), but also from possible marine influences (Schultze & Soler-Gijón 2004; Steyer *et al.* 2012) or river channels (Schneider & Zajíc 1994; Schneider *et al.* 2000; Štamberg *et al.* 2016) which would have facilitated the movement of these faunas throughout Western and Central Europe.

Among the vertebrates present in these basins, *Triodus* is widely distributed (Fig. 55): the genus is present in the basins of Autun (*T. aeduorum* and *T.* sp.; Soler-Gijón & Hampe 1998; Heidtke *et al.* 2004; this work), Saar-Nahe and Thuringia (*T. sessilis, T. lauterensis*, *T. palatinus*, *T. obscurus* and *T. kraetschmeri*; Jordan 1849; Hampe 1989; Heidtke *et al.* 2004), Bohemia (*T. carinatus*; Fritsch 1890; Schneider & Zajíc 1994) and Puertollano (*Triodus* teeth; Soler-Gijón 1993a,b, 1994, 1995) but also in other localities (Schneider & Zajíc 1994; Fischer *et al.* 2013), whose connections with the Carboniferous-Permian basins of Western and Central Europe have not been discussed (*T. serratus* from the United Kingdom and *T. teberdaensis* from Russia; Davis 1892; Hampe 2003; Hampe & Ivanov 2007b). The study of the new material

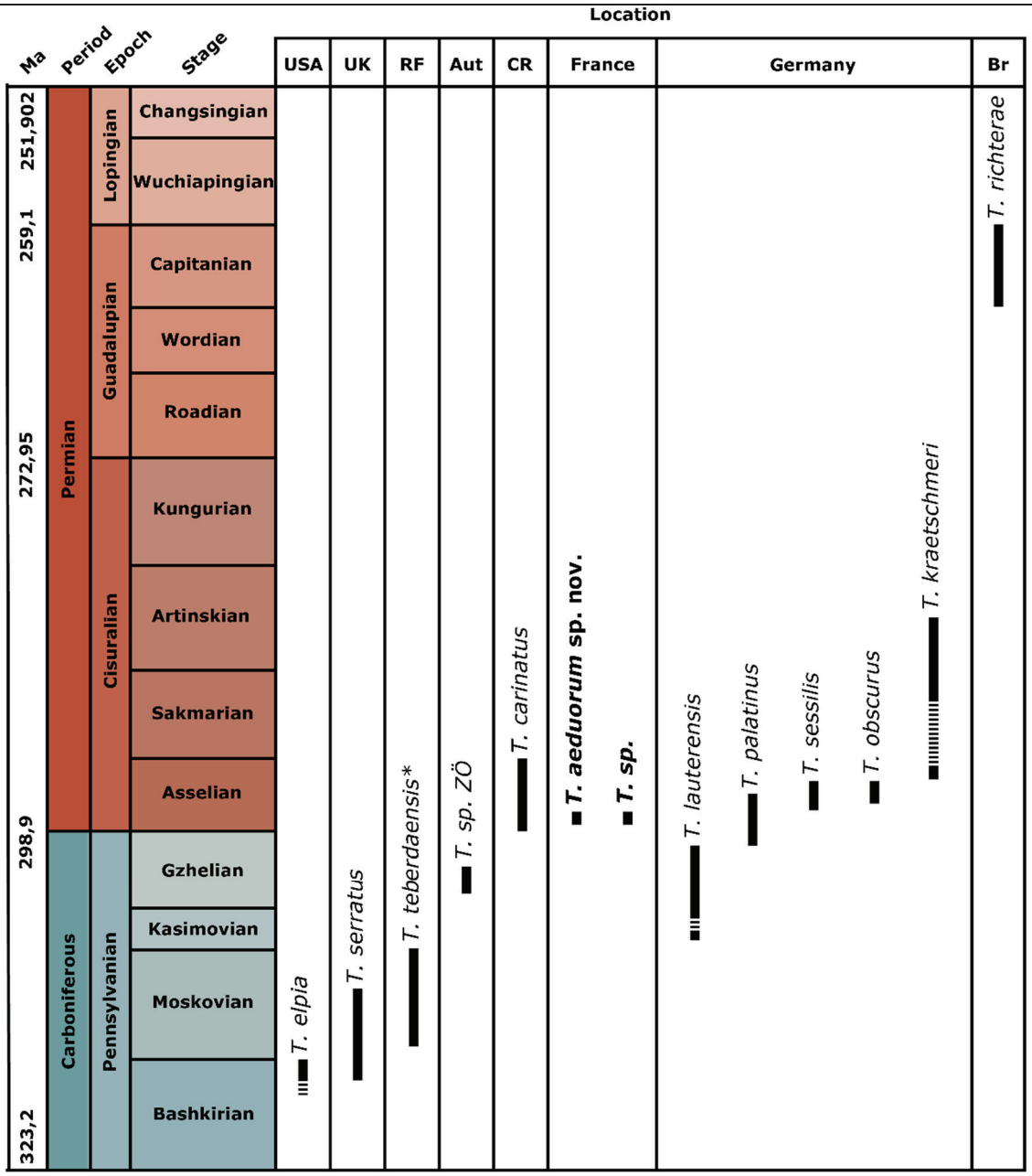

Figure 55. Stratigraphical and geographic distribution of the different *Triodus* species. Asterisk indicates potential marine occurrence. **Abbreviations: USA**, United States; **UK**, United Kingdom; **RF**, Russian Federation; **Aut**, Austria; **CR**, Czech Republic; **Br**, Brazil (modified after Hampe & Ivanov 2007b; Johnson & Thayer 2009; Pauliv *et al.* 2017).

from the Muse OSB suggests that each *Triodus* species present in these basins is endemic to it: each basin housing its own *Triodus* species. This suggests that the evolution rate within the *Triodus* genus is relatively strong.

Triodus was also considered as an obligate freshwater chondrichthyan (e.g. Zangerl 1981), i.e. living in eutrophic lakes and rivers (Schneider 1996). It was also interpreted as an

ambush predator (Hampe 2003). These characteristics raise the question of migration patterns of this genus across Western and Central Europe. The migrations of the aquatic fauna between these basins would have taken place *via* the coastal waters of the Palaeotethys (Schultze 2009) and /or the North Sea (Steyer *et al.* 2012), which bordered the basins to the south and the north respectively. *Triodus teberdaensis* (Hampe & Ivanov 2007b) has been found in marine sediments in Russia, even if the autochthonous character of these species in these marine sediments has never been discussed (Pauliv *et al.* 2017). Some authors (Schultze & Soler-Gijón 2004; Hampe *et al.* 2006; Carpenter *et al.* 2011; Beck *et al.* 2016) consider xenacanthiforms to be saltwater tolerant and euryhaline. Euryhalinity has also been proposed in contemporaneous temnospondyl amphibians (e.g. Steyer 2002; Laurin & Soler-Gijón 2006); which could therefore live in fresh, brackish and/or marine waters (e.g. Steyer 2014). This would suggest that marine migrations between European basins were indeed possible through coastal waters.

Schneider *et al.* (2000) and Štamberg *et al.* (2016) considered the xenacanthids as rather freshwater and their migrations mostly favored by interconnected river channels. This is also consistent with a geochemical study of shark teeth (Fischer *et al.* 2014b) suggesting both freshwater and shallow marine modes of life. Yet this study is based on a small North American sample, and it needs to be tested on a larger European sample. However, faunal exchanges between river mouths via coastal waters cannot be completely excluded.

As mentioned before, Xenacanthiformes, such as *Triodus*, are also interpreted as ambush predators (Hampe 2003); therefore, as bad swimmers, rather confined in their living environment. Among extant actinopterygians, pikes (*Esox*, Esocidae) are also ambush predators (e.g. Juanes *et al.* 2002), spending most of their time inactive (Diana 1980) and using only fast-start swimming temporarily (Harper & Blake 1990). Sedentary fishes are bad swimmers which can migrate on short distances only, from freshwaters to brackish environments during the spawning season (Johnson & Muller 1978; Karas & Lehtonen 1993; Rosell & MacOscar 2002). An example of ambush predator within marine chondrichthyans is Pacific Angel Sharks (*Squatina californica*) (Fouts & Nelson 1999). They are dorso-ventrally flattened body shark with large pectoral and pelvic fins (e.g. Walsh & Ebert 2007). A study of Gaida (1997) has demonstrated that the populations of Pacific Angel Shark from the California Channel Islands have no migratory behavior: the different populations are confined to their living environment, i.e. shallow marine water around islands, resulting in genetic divergences. The author argued that the deep-water column between the islands and the submarine topography are barriers that this species cannot cross. The biogeography of these populations goes in the sense of a restricted environment for an ambush chondrichthyan, like *Triodus* could be. However, differences in

body morphologies between *Squatina* and *Triodus* certainly limit the value of such a comparison. Furthermore, among obligate freshwater tetrapods, the Chinese giant salamander (*Andrias davidianus*) is an ambush predator (Browne *et al.* 2014) that is also restricted to a confined living environment (Zheng & Wang 2010) even if they are semi-terrestrial animal. These three examples of ambush aquatic predators which live in restricted environment are consistent with the observed endemism of the xenacanthiform *Triodus* in the different European basins.

On the contrary, the European eel (*Anguilla anguilla*) is a good long-distance swimmer with long spawning migration patterns between freshwater and marine environments (e.g. Aarestrup *et al.* 2009). Eels use undulatory swimming (e.g. Müller *et al.* 2001). Xenacanthiformes have often been described as possessing an eel-like body, but contrary to eels, they show developed pelvic and anal fins like the Angel Shark (e.g. Walsh & Ebert 2007). The swimming-type of the xenacanthiforms is still unknown but it could be different from that of eels. Xenacanthiformes might have shown an ecology more similar to that of pikes or angel sharks, which would be consistent with their observed endemism in each European basin.

New studies are needed for a better understanding of the paleoecology of the xenacanthiforms as, for example, geochemical analyses on mineralized parts of their skeleton, like the dorsal spine, which could investigate their living environment along their life cycle to determine if marine migrations were possible.

Conclusions

The description of new specimens of *Triodus* from the Muse OSB of the Autun Basin allows the erection of the new species *T. aeduorum* sp. nov. This new species is mainly characterized by a significantly different tooth patterning compared to the other *Triodus* species comprising tooth size, number of cristae on the crown, number of nutrient foramina on the base, angle between the crown and the base and the shape of the base. It makes possible a revision of the systematics of some xenacanthiform species from the Muse OSB: '*Expleuracanthus*' *frossardi* (Gaudry, 1883) cannot be formally related to the genus *Triodus* and must be considered as a *nomen dubium*. Consequently, *T.* ?*frossardi* should not be considered as a relative of '*E*'. *frossardi* but as *Triodus* sp., a species different from *Triodus aeduorum* sp nov. The study of the new remains of *Triodus* from the Muse OSB emphasizes the need to revise the historical species of xenacanthiforms (e.g. '*E*'. *frossardi*, *'E*'. *bonnardi*), in order to better understand the diversity of Xenacanthidae in the Autun Basin.

Triodus aeduorum sp. nov. confirms the observed endemism of the *Triodus* species in each European Carboniferous-Permian basin in which the genus is present. This endemism is likely to be linked to an ambush predator mode of life rather than to a strict adaptation to freshwater environments.

The description of the new xenacanth material from the Muse OSB encourages the systematic revision of doubtful *Triodus* specimens and new sieving campaigns where *Triodus* was already found to recover isolated teeth in order to better understand how the genus extended its geographic distribution across European basins during the Carboniferous and the Permian.

Acknowledgments

The authors are grateful to the SHNA and MHNA for having co-organized the excavation campaigns between 2010 and 2014 during which the studied specimens were found. We thank particularly the Gevrey, Barnay, and Jacquemard families, G. Grillot and S. Kunz (Dracy-Saint-Loup Municipality) for their help, D. Chabard (MHNA) for access to the palaeontological collections, D. Beaudoin, P. Baudinaud and R. Pillon (SHNA), and G. de Ploëg for the long mechanical preparation of the specimens. For their precious help on the field, we also thank B. Blanc (Marine), E. Chenal (Éducation Nationale), C. Delhaye (CNRS), I. van Waveren and her students (Naturalis, Leiden), J. Fortuny (ICP, Barcelona), S. Hervet (PaléOvergne), J. Galtier (Montpellier), A. Bercovici (Manchester University), F. Prost (Dijon University), S. Giner (Var Département), K. Rey (ex-BPI), and O. Béthoux, G. Cousin, G. Odin, L. Anseaume, J. Barbier, M. Sanders, D. Perez, J. Falconnet, D. Germain and V. Rouchon (MNHN). We thank the two anonymous reviewers for their remarks that have helped to greatly improve this manuscript. The first author was funded by the Docotoral School ED 341 - E2M2 Évolution Écosystème Microbiologie Modélisation, Université Claude Bernard Lyon 1, France.

Paper 2: Phylogenetic implications of the systematic reassessment of Xenacanthiformes and 'Ctenacanthiformes' (Chondrichthyes) neurocrania from the Carboniferous-Permian Autun Basin (France)

Vincent Luccisano[1,2], Mizuki Rambert-Natsuaki, Gilles Cuny, Romain Amiot, Jean-Marc Pouillon and Alan Pradel

Published in Journal of Systematic Palaeontology

Luccisano, V., Rambert-Natsuaki, M., Cuny, G., Amiot, R, Pouillon, J-M. & Pradel, P. (2021). Phylogenetic implications of the systematic reassessment of Xenacanthiformes and 'Ctenacanthiformes' (Chondrichthyes) neurocrania from the Carboniferous–Permian Autun Basin (France). **Journal of Systematic Palaeontology**, 19(23), 1623-1642.

Phylogenetic implications of the systematic reassessment of Xenacanthiformes and 'Ctenacanthiformes' (Chondrichthyes) neurocrania from the Carboniferous-Permian Autun Basin (France)

Vincent Luccisano[1,2], Mizuki Rambert-Natsuaki, Gilles Cuny, Romain Amiot, Jean-Marc Pouillon and Alan Pradel

[1]Univ Lyon, UCBL, ENSL, UJM, CNRS, LGL-TPE, F-69622, Villeurbanne, France;
[2]Univ Lyon, Université Claude Bernard Lyon 1, CNRS, ENTPE, UMR 5023 LEHNA, F-69622, Villeurbanne, France;
[3]CR2P - Centre de Recherche en Paléontologie - Paris; Muséum National d'Histoire Naturelle - Centre National de la Recherche Scientifique- Sorbonne Université. France;
[4]Rhinopolis Association, 179 rue des Plattières 38300 Nivolas Vermelle/BP 39 03800 Gannat, France

Abstract

Four complete isolated neurocrania excavated during the 19th century in the Autun Basin (Saône-et-Loire, France) were used by Heyler & Poplin (1982) to erect two species: the symmoriiform *Bibractopiscis niger* and the xenacanthiform *Orthacanthus commailli*. However, the specimens have not been mechanically prepared and only a portion of their anatomy is available, complicating their systematic attribution. We revise their systematic status by using X-ray computed microtomogaphy and new comparative material from the Bourbon-l'Archambault Basin (Allier, France). This method allows access to the hidden anatomy of the specimens and new systematic revision: we propose *O. commailli* to be left in open nomenclature as ?Xenacanthimorpha. The specimens attributed to *B. niger* encompass two distinct morphologies: the holotype, one paratype and a neurocranium from the Bourbon-l'Archambault Basin are identified as cf. *Triodus* sp. The last paratype is left in open nomenclature as 'Ctenacanthiformes' indet. We included these neurocrania in geometric morphometric and cladistic analyses of a large sample of Palaeozoic chondrichthyans. Based on the results we propose an evolutionary scenario for the neurocranial transition between the orders 'Ctenacanthiformes' and Xenacanthiformes. This transition mostly affects the ethmo-

orbital region. The revision of the diversity of these chondrichthyan faunas questions potential differences in trophic structures between the different European Carboniferous-Permian basins.

Introduction

The fossil record of Paleozoic chondrichthyans is mostly composed of teeth and dorsal spines due to the highly calcified nature of these elements (Zangerl 1981; Ginter *et al.* 2010). In contrast, other cranial and post-cranial remains are rare because they are made of tessellated calcified cartilage (e.g. Zangerl 1981; Maisey *et al.* 2020) which is more difficult to fossilize. Among these cartilaginous remains, complete neurocrania are only known from a few taxa (see Zangerl [1981] and references within).

Consequently, complete neurocrania were less studied than teeth (e.g. Schaeffer 1981). Furthermore, only a single side of the braincase is often visible (e.g. Williams 1985), and it is not always preserved in three dimensions (e.g. Poplin & Heyler 1989). However, technologies newly applied to fossils, such as X-ray computed microtomography (µCT Scan), allow both external (e.g. Maisey 2001, 2005; Ginter & Maisey 2007; Maisey *et al.* 2009) and internal (e.g. Pradel *et al.* 2009, 2011; Coates *et al.* 2017; Frey *et al.* 2019) explorations of anatomy.

The erection of two chondrichthyan species from the French Carboniferous-Permian Autun Basin (Saône-et-Loire) based on isolated braincases occurred before the use of µCT Scan in palaeontology: the ‘cladodont’ (currently assigned to Symmoriiformes) *Bibractopiscis niger* Heyler & Poplin, 1982 was erected based on the description of three isolated neurocrania, and the xenacanthiform *Orthacanthus commailli* (Heyler & Poplin, 1982) was erected based on the description of a unique braincase. For these two species, the neurocrania were not entirely visible, so that the original descriptions were incomplete. Consequently, the original hypothesis that *Bibractopiscis niger* and *Orthacanthus commailli* are two valid species can be considered doubtful, as suggested by Schultze & Soler-Gijón (2004), requiring a systematic reappraisal. As the specimens are preserved in three dimensions (Heyler & Poplin 1982), they are good candidates for the use of X-ray computed microtomography to describe their hidden morphology and assess their previous systematic attribution.

A recent study (Luccisano *et al.* 2021a) of material from the Muse oil-shale bed (OSB) of the Autun Basin has revealed that some historical species of Xenacanthiformes are not valid and need a global systematic reassessment. Furthermore, the distribution of the taxa comprising

this fauna across the different European Carboniferous-Permian basins that have provided chondrichthyan fossils is not fully understood.

We propose a new description of the material of *Bibractopiscis niger* and *Orthacanthus commailli* and a description of an isolated neurocranium from the Bourbon-l'Archambault Basin in the light of µCT Scan analyses that reveal their hidden external anatomy. This reassessment will allow 1) an assessment of the original attribution of Heyler & Poplin (1982); 2) a better understanding of the diversity pattern of these Palaeozoic chondrichthyans in the Carboniferous-Permian basins and 3) a discussion of the morphological evolution between 'Ctenacanthiformes' and Xenacanthiformes.

Geological setting

The Autun Basin is located in the Northern Massif Central (Fig. 56A, B; Saône-et-Loire) and is part of a group of Carboniferous-Permian basins (Fig. 56A; Gand *et al.* 2015, 2017). It is divided (Fig. 56D) between the Igornay and Muse formations (lower 'Autunian'; Pruvost 1942) on the one hand, which extend from the late Gzhelian to the early Asselian (Pellenard *et al.* 2017), and Surmoulin and Millery formations (upper 'Autunian'; Pruvost 1942) on the other hand, which are post-Asselian in age (Pellenard *et al.* 2017). The Dracy-Saint-Loup and La Comaille localities (Fig. 56B) are correlated to the Lally OSB in the Muse Formation (Fig. 56D). Pellenard *et al.* (2017) dated the Lally OSB by radiochronology at 298.91 +/- 0.16 Myr, which corresponds to the uppermost Gzhelian, just below the Carboniferous-Permian boundary.

The Bourbon-l'Archambault Basin is also located in the Northern Massif Central (Fig. 56A, C; Allier), West of the Autun Basin (e.g. Châteauneuf 1980; Châteauneuf & Farjanel 1989). It is divided into the Souvigny and the Aumance sub-basins (Fig. 56C; e.g. Steyer *et al.* 2000). The Bourbon-l'Archambault Basin has been considered to extend from the upper 'Stephanian' to the 'Autunian' (Fig. 56E; e.g. Debriette 1992). Following Pellenard *et al.* (2017), these local stages (*sensu* Gand *et al.* 1997a,b) represent geological records from the upper Pennsylvanian to the middle Cisuralian. Buxières-les-Mines locality is situated in the Aumance sub-Basin and corresponds to the lower 'Autunian', more precisely to the early Asselian (e.g. Steyer *et al.* 2000).

Material and methods

Scanning

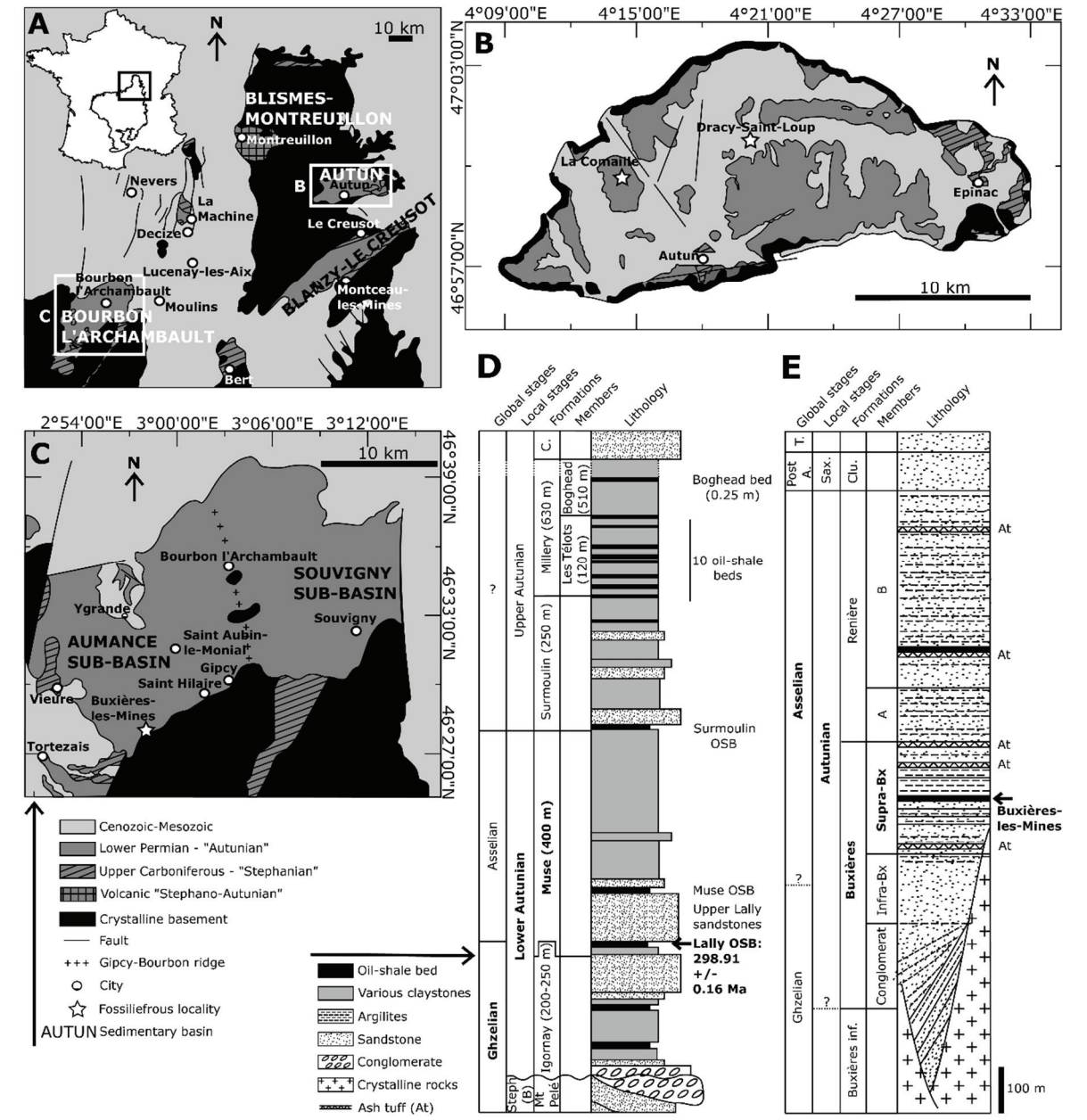

Figure 56. Geological context. **A**, simplified geological map showing the location of the Autun and Bourbon-l'Archambault basins in the Northern Massif Central. **B**, simplified geological map of the Autun Basin. **C**, simplified geological map of the Bourbon-l'Archambault Basin. **D**, simplified stratigraphy of the Autun Basin. **E**, simplified stratigraphy of the Bourbon-l'Archambault Basin. **Abbreviations: C**, Curgy formation; **Post A**, Post Asselian; **Bx**, Buxières; **Clu**, Clusor formation; **Sax**, Saxonian; **T**, Trias (modified from Châteauneuf 1980; Marteau 1983; Châteauneuf & Farjanel 1989; Châteauneuf *et al.* 1992; Steyer *et al.* 2000; Gand *et al.* 2007, 2011, 2015, 2017; Pellenard *et al.* 2017).

The specimens from the Autun Basin were imaged using the tomographic platform AST-RX of the *Muséum National d'Histoire Naturelle* (MNHN, Paris, France) with a v|tome|x

L240-180 tomograph. The specimen from Buxières-les-Mines was imaged using the microtomographic platform of the ERM Society (*Études Recherches Matériaux*; Poitiers, France) with a X8050-16 Viscom model. Scan parameters are given in Supplemental material (Supplemental material I). Reconstructed slices were converted from 16 bits to 8 bits in order to reduce the data size for 3D processing with the software ImageJ v.1.4.3.67 (Rasband 1997-2020). Segmentation and 3D rendering were performed with MIMICS v.20.0 software (© Materialise Inc. NV, Leuven, Belgium) for specimens from the Autun Basin, and with Avizo v.7.0 (© Thermo Fisher Scientific, Waltham, Massachusetts, USA) for the specimen from Buxières-les-Mines. 3D renderings are available from the MorphoMuseuM repository (Luccisano *et al.* 2021b).

Geometric morphometric analysis

We performed a geometric morphometric analysis of the shape of the ethmo-orbital region in dorsal view of the neurocranium of some Xenacanthiformes and 'Ctenacanthiformes' (Table 4). We did not include MNHN.F. AUT814 from the Autun Basin in our analysis because of the incomplete preservation of the ethmo-orbital region of this specimen.

To quantify the variation in shape, we digitized a set of thirteen 2D landmarks on the braincases in dorsal view (Fig. 57) using the package geomorph v.3.3.1 (Adams & Otarola-Castillo 2013) of the R software package v.4.0.2 (R Core Team 2020). Landmarks 1 and 8 are situated in the middle of the extremity of the preorbital processes, indicating the orientation of the latter. Landmarks 2 and 7 are situated at the most internal point of the supraorbital shelf. Landmarks 3 and 6 are situated at the extremity of the postorbital processes. Landmarks 4 and 5 are situated at the posterior extremity of the postorbital processes. Landmarks 9 and 13 are situated at the anterior extremities of the precerebral fontanelle. Landmark 11 is situated at the posterior extremity of the precerebral fontanelle. Landmarks 10 and 12 are situated between the landmarks 11 and 9/13 and correspond to the change of curvature between these landmarks.

We used the package geomorph v.3.3.1 in R (Adams & Otarola-Castillo 2013) to perform Generalized partial Procrustres Analysis (pGPA) following Claude (2008). Then we performed a Principal Component Analysis (PCA, Pearson type) on the Procrustes coordinates, resulting from the pGPA. Data and script are available in Supplemental material II and III.

Cladistic analysis

We performed a cladistic analysis including Symmoriiformes, Holocephali, Euselachii, Phoebodontiformes, 'Ctenacanthiformes' and Xenacanthiformes (see the Supplemental

Table 4. List of the specimens used in the geometric morphometric analysis.

Order	Species	Reference	Examined material
Xenacanthiformes	*Triodus sessilis* Jordan, 1849	Heidtke *et al.* (2004)	Reconstruction
Xenacanthiformes	*Triodus carinatus* Fritsch, 1890	Schneider & Zajíc (2004)	Specimen from the collection of René Kindlimann (Aathal, Switzerland)
Xenacanthiformes	*Xenacanthus humbergensis* Hampe, 1994	Heidtke & Schwind (2004)	Reconstruction
Xenacanthiformes	*Xenacanthus meisenheimensis* Hampe, 1994	Heidtke & Schwind (2004)	Reconstruction
Xenacanthiformes	*Orthacanthus* sp.	Schaeffer (1981)	MCZ 13388 and a composite specimen
Xenacanthiformes	cf. *Triodus* sp.	This study	MNHN.F.AUT811 and MHNE.2021.9.1
?	Xencanthimorpha?	This study	MNHN.F.AUT813
'Ctenacanthiformes'	*Tamiobatis vetustus* Eastman, 1897	Schaeffer (1981)	NMNH 1717
'Ctenacanthiformes'	*Tamiobatis* sp. Eastman, 1897	Schaeffer (1981)	AMNH 2140
'Ctenacanthiformes'	*Cladodoides wildungensis* Jaekel, 1921	Maisey (2005)	Surface rendering of the specimen P2468
'Ctenacanthiformes'	'Ctenacanthiformes' indet.	This study	MNHN.F.AUT812

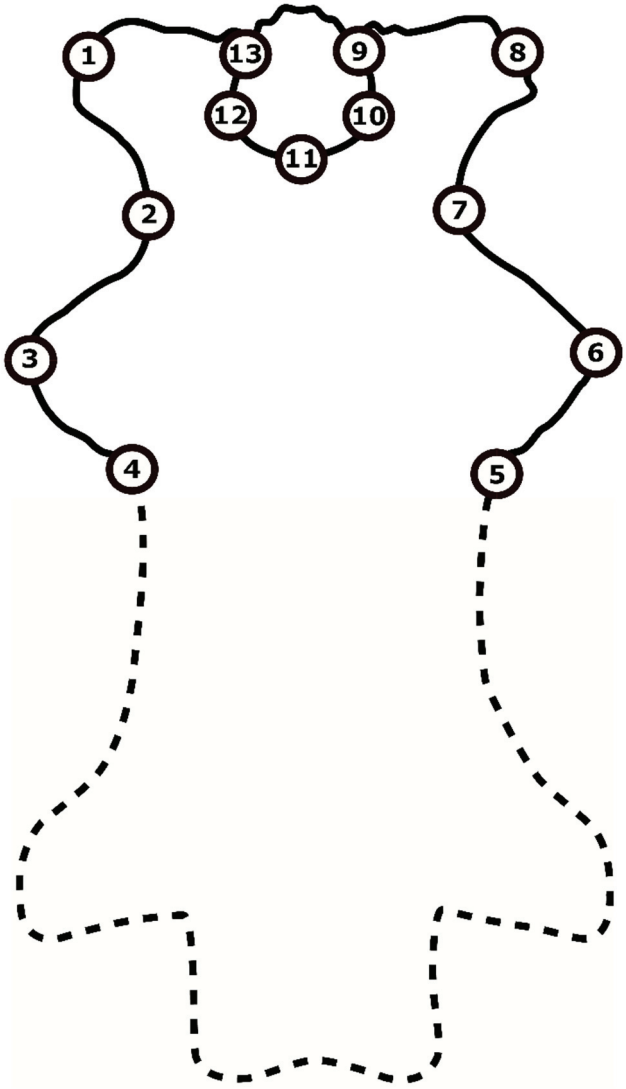

Figure 57. Schematic outline of a xenacanthiform neurocranium showing the location of the 13 landmarks used in the geometric morphometric analysis (modified from Schaeffer 1981).

material IV for a detailed list of the specimens used). The chosen outgroups comprise the placoderm *Dicksonosteus arcticus*, the 'acanthodian' *Acanthodes bronni* and the stem-chondrichthyan *Doliodus problematicus*, following several recent studies that resolved the latter as sister groups to all other euchondrichthyans (*sensu* Zhu *et al.* 2013) (e.g. Coates *et al.* 2017, 2018; Frey *et al.* 2019, 2020; Brazeau *et al.* 2020).

The cladistic analysis was used to validate the systematic attribution of the material from the Autun and Bourbon-l'Archambault basins and to discuss the morphological transition of the neurocranium between 'Ctenacanthiformes' and Xenacanthiformes, whose close relationships are supported by many recent phylogenetic analyses (e.g. Coates *et al.* 2017, 2018; Frey *et al.* 2019, 2020; Brazeau *et al.* 2020). However, our dataset was not designed to reassess

general relationships among Chondrichthyes. Symmoriiformes, Holocephali and Euselachii are only included to structure the resulting trees.

To investigate the phylogenetic signal of the isolated braincases, we used 33 external morphological characters of the neurocranium. Their descriptions are mostly derived from several recent studies for 19 of them, and we added 14 new characters (see the character list and description in the Supplemental material V and VI and the references within). We ran the analysis including all 22 taxa with PAUP v.4.0a168 (Swofford 2003) (see the Supplemental material VII for the parameters). Bremer supports were manually calculated in PAUP. In the resulting phylogeny, we described characters showing a unique evolutionary history, even if they are convergent, as 'unambiguous'. We reserved the term 'synapomorphy' for the ones that exclusively define a clade.

Material

Bibractopiscis niger (Figs 58, 60, 61) and *Orthacanthus commailli* (Fig. 59) consist of four neurocrania from different localities of the Autun Basin (Saône-et-Loire, France) that are housed in the MNHN. The holotype of *O. commailli* MNHN.F.AUT813 (Fig. 59A) was discovered in 1882 in La Comaille (Fig. 56B). The geographic origin of the holotype of *B. niger* MNHN.F.AUT811 (Fig. 60A) and its counterpart MNHN.F.AUT810 (Fig. 60B), discovered in 1879, is unknown, but the surrounding matrix suggests that it comes from the same group of Carboniferous–Permian basins as the other neurocrania. The paratype of *B. niger* MNHN.F.AUT812 (Fig. 58A) was discovered in 1881 and comes from Dracy-Saint-Loup (Fig. 56B). The paratype of *B. niger* MNHN.F.AUT814 (Fig. 60C) was discovered in 1882 and comes from La Comaille (Fig. 56B). The isolated neurocranium from Buxières-les-Mines, MHNE.2021.9.1 (Fig. 60D), was found during excavation campaigns of the Association 'Rhinopolis' (Allier, France) in 1995 and is housed in the MHNE (*Musée d'Histoire Naturelle et d'Ethnographie de Colmar*).

Systematic notes

We use Schaeffer's (1981) nomenclature for neurocranium descriptions. We follow recent phylogenetic analyses in considering the genus *Cladoselache* as a symmoriiform and *Akmonistion* as a valid genus (e.g. Coates *et al.* 2017, 2018; Frey *et al.* 2019, 2020; Brazeau *et al.* 2020). Concerning the validity of the 'Ctenacanthiformes', several authors considered it as valid (e.g. Duffin & Ginter 2006; Ginter *et al.* 2010; Hodnett *et al.* 2012, 2021), but results of recent studies recover this Order as a para- or polyphyletic group (e.g. Coates *et al.* 2017, 2018;

Frey *et al.* 2019, 2020; Brazeau *et al.* 2020). The validity of 'Ctenacanthiformes' is out of the scope of this work, so we use the classification of Ginter *et al.* (2010) for convenience, but we follow the recommendations of Bengtson (1988) by using inverted commas to specify the possible invalidity of this Order.

Abbreviations

Institutional abbreviations—**ERM**, Étude Recherche Matériaux; **MHNE**, Musée d'Histoire Naturelle et d'Ethnographie de Colmar; **MNHN,** Muséum National d'Histoire Naturelle de Paris.

Anatomical abbreviations—**afh,** articular facet for the hyomandibula; **afp,** articular facet for the palatoquadrate; **afppp,** articular facet of the preorbital process for the palatine part of the palatoquadrate; **am,** allochthonous material; **avsc,** anterior vertical semicircular canal; **cjv,** canal for jugular vein; **dor,** dorsal otic ridge; **ef,** endolymphatic fossa; **fbpn,** foramen for branch of palatine nerve; **fica,** foramen for internal carotid artery; **foa,** foramen for orbital artery; **fson,** foramen for superficial ophthalmic nerve; **fvn,** foramen for vagus nerve; **glda,** groove for lateral dorsal aorta; **hf,** hypophysial fossa; **lda,** lateral dorsal aorta; **lop,** lateral otic process; **lor,** lateral otic ridge; **n,** notch; **nc,** nasal capsule; **ob,** occipital block; **oc,** occipital crest; **oco,** occipital cotyle; **oof,** otico-occipital fissure; **pf,** precerebral fontanelle; **pop,** postorbital process; **pp**, parachordal plate; **prp,** preorbital process; **pvsc,** posterior vertical semicircular canal; **r,** rostrum or internasal plate; **rpe**, raised posterior edge of the precerebral fontanelle; **snc,** separate nasal calcification; **ss,** supraorbital shelf; **von,** ventral otic notch.

Systematic palaeontology

Class Chondrichthyes Huxley, 1880

'Ctenacanthiformes' indet.

(Fig. 58)

1982 *Bibractopiscis niger* Heyler & Poplin: 17, pl. 2, fig. 3.

Referred material—MNHN.F.AUT812, shortened to AUT812 below, isolated neurocranium in ventral view.

Occurrence—Dracy-Saint-Loup, Autun Basin, Saône-et-Loire, France.

Horizon—Lally OSB, Muse formation, Autun Basin, Northern Massif Central, uppermost Gzhelian, upper Pennsylvanian, upper Carboniferous (Pellenard *et al.* 2017).

Comparative description

This neurocranium (Fig. 58) shares with 'ctenacanthiforms' and xenacanthiforms a long otico-occipital region that reaches at least half the length of the neurocranium.

The ethmo-orbital region is well calcified. In dorsal view (Fig. 58C, D), the precerebral fontanelle has a V-shape like the 'ctenacanthiforms' *Cladodoides* (e.g. Maisey 2001, 2005) and *Tamiobatis* (e.g. Romer 1964; Schaeffer 1981; Williams 1998), and is different from all known xenacanthiform neurocrania, which possess a U-shaped precerebral fontanelle.

The preorbital processes are not entirely preserved and the right one is more complete than the left one. They appear to be short, pointed and anteriorly directed as shown by the right one. AUT812 possesses more pointed preorbital processes than *Cladodoides* (e.g. Maisey 2001, 2005), *Tamiobatis* (e.g. Romer 1964; Schaeffer 1981; Williams 1998) and some *Xenacanthus* species (Schwind 1991; Schneider & Zajíc 1994; Heidtke & Schwind 2004). *Orthacanthus* (Heidtke 1982, 1998, 2007) possesses more laterally oriented preorbital processes than AUT812.

Four foramina for the superficial ophthalmic nerves are present on the dorsal surface of the ethmo-orbital region: two on the right side, and two on the left side. The supraorbital shelf, not laterally extended as in *Cladodoides* (e.g. Maisey 2001, 2005), has a sigmoid-shaped rim.

A distinct ventral articular facet for the palatoquadrate is visible on the right postorbital process, similar to that of *Tamiobatis* (e.g. Romer 1964; Schaeffer 1981; Williams 1998) and different from the more dorsally oriented one of xenacanthiforms (e.g. Schaeffer, 1981).

In ventral view (Fig. 58E, F), at the level of the postorbital processes, there are two pairs of foramina interpreted as foramina of the orbital aorta for the anterior process and foramina of palatine nerve or orbital artery for the posterior one. The disposition of the two foramina for the orbital artery or the palatine nerve in AUT812 and *Cladodoides* (Maisey 2005) is in a more central position than in *Orthacanthus* (Schaeffer 1981). Posteriorly to them, the foramen for the internal carotid artery is visible (fica, Fig. 58E, F).

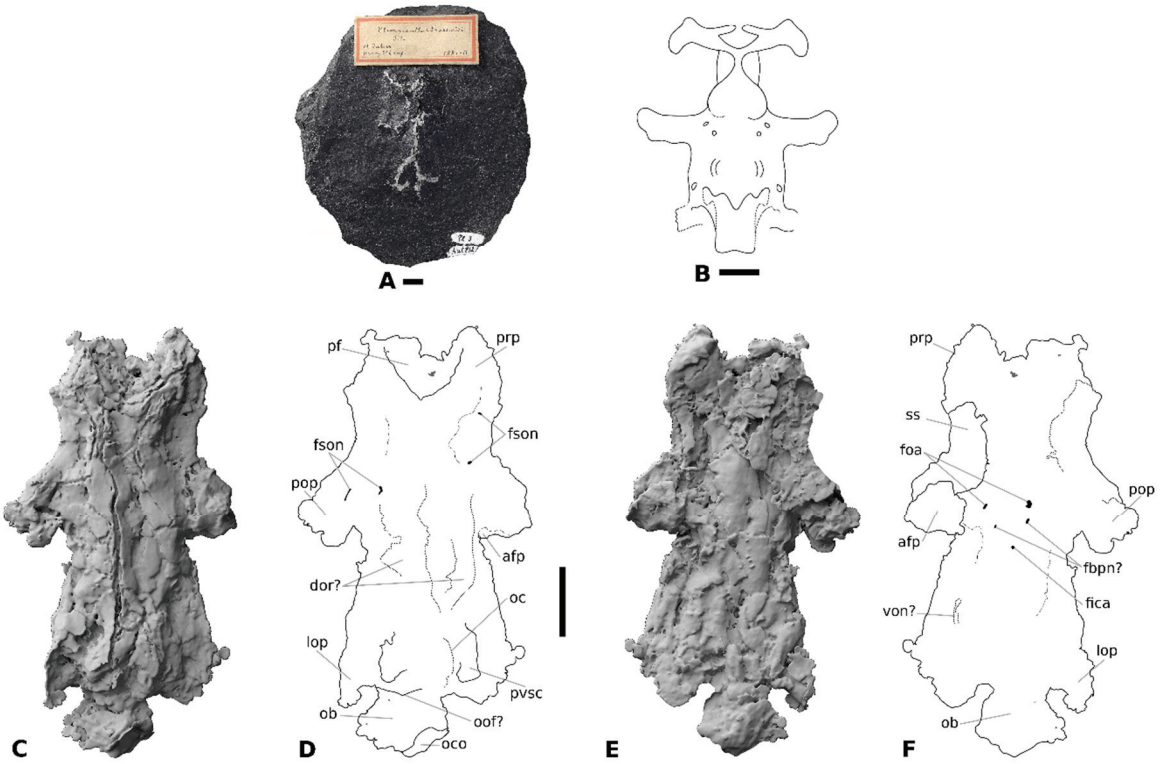

Figure 58. Neurocranium of 'Ctenacanthiformes' indet. from the Autun Basin. **A**, photograph of the specimen MHNH.F.AUT812. **B**, line drawing of the neurocranium of *Bibractopiscis niger* in ventral view following Heyler & Poplin (1982). **C**–**F,** 3D rendering and new interpretation drawings of MNHN.F.AUT812. **C, D** in dorsal view and **E, F** in ventral view. **C**, **E** are 3D surface rendering and **D**, **F** are line drawings. Bold lines are anatomical structures, slender lines are contours with no anatomical significance, dotted lines are supposed anatomical structures, black areas are foramina and grey areas are gaps in the 3D renderings. Scale bars = 1 cm.

In dorsal view, the lateral outline of the otico-occipital region is slightly convex. The lateral otic processes are posteriorly oriented and do not seem to be entirely preserved, especially the right one.

Posterior to the dorsal otic ridges, two structures are interpreted as the outline of the posterior vertical semicircular canals. They are wide and extend from the dorsal otic ridges to the posterior side of the lateral otic processes. Between them, the observed longitudinal structure could be the occipital crest. Next to the left posterior vertical semicircular canal, the otico-occipital fissure is visible. Its orientation in AUT812 resembles that of *Tamiobatis* (Schaeffer 1981), and is different from that of *Orthacanthus* (e.g. Schaeffer 1981) and *Triodus* (e.g. Heidtke *et al.* 2004) in which it is more antero-posteriorly oriented.

The occipital block is not completely preserved but the rounded occipital cotyle is visible on its posterior side. The occipital block is wedged between the two lateral otic processes. In ventral view (Fig. 58E, F), next to the right lateral otic process, there is a furrow possibly indicating a ventral otic notch. No ventral otic foramen could be identified.

?Xenacanthimorpha

(Fig. 59)

1982 '*Expleuracanthus*' c*ommailli* Heyler & Poplin: 23, fig. 3, pl. 2, fig. 4.
1989 *Orthacanthus commailli* Heyler & Poplin: 73, fig. 1.

Referred material—MNHN.F.AUT813, shortened to AUT813 below, isolated neurocranium in dorsal view.

Occurrence—La Comaille, Autun Basin, Saône-et-Loire, France.

Horizon—Lally OSB, Muse formation, Autun Basin, Northern Massif Central, uppermost Gzhelian, upper Pennsylvanian, upper Carboniferous (Pellenard *et al.* 2017).

Comparative description

The ethmo-orbital region appears to be well calcified. In dorsal view below the precerebral fontanelle, an incomplete rostrum (*sensu* Schaeffer 1981) or a narrow internasal plate is present, but anteriorly displaced. AUT813 (Fig. 59C, D) and AUT812 share a V-shaped precerebral fontanelle, as in 'Ctenacanthiformes', and contrasting with the U-shaped one of Xenacanthiformes (e.g. Schaeffer 1981; Heidtke 1982, 1998, 2007; Heidtke *et al.* 2004).

The preorbital processes are angular and directed more antero-laterally than anteriorly. Their orientation is similar to those of *Orthacanthus* and *Triodus* (e.g. Schaeffer 1981; Heidtke *et al.* 2004) but more laterally displaced than in *Tamiobatis* (e.g. Romer 1964; Schaeffer 1981; Williams 1998).

The supraorbital shelf, between the preorbital and postorbital processes, is sigmoid. The postorbital processes are rounded and bear an articular facet for the quadrate part of the palatoquadrate on their postero-dorsal side. AUT813 shares with *Orthacanthus* and *Lebachacanthus* (Heidtke 1982, 1998, 2007) broad and short postorbital processes that are

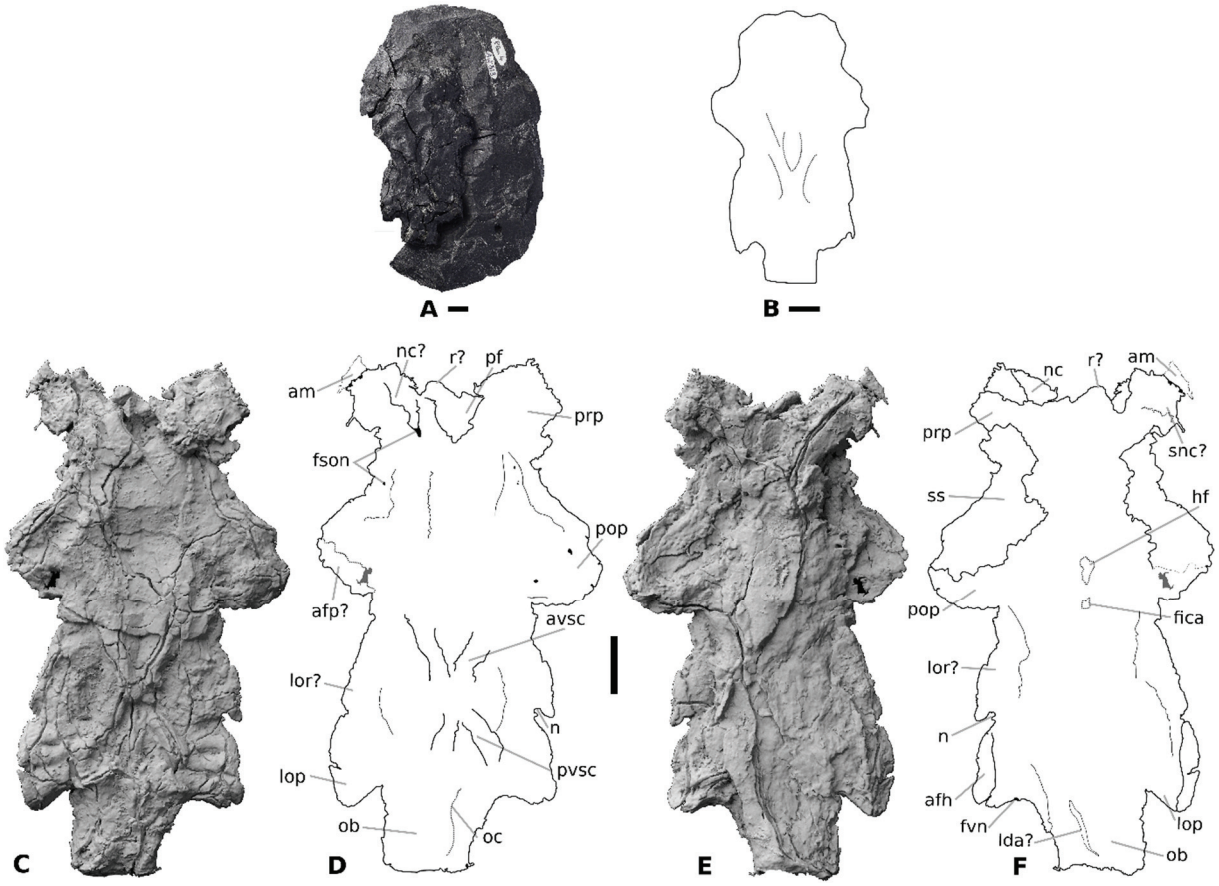

Figure 59. Neurocranium of ?Xenacanthimorpha from the Autun Basin. **A**, photograph of the specimen MHNH.F.AUT813. **B**, line drawing of the neurocranium of *Orthacanthus commailli* following Heyler & Poplin (1982). **C**–**F,** 3D rendering and new interpretation drawings of MNHN.F.AUT813. **C, D** in dorsal view and **E, F** in ventral view. **C**, **E** are 3D surface rendering and **D**, **F** are line drawings. Bold lines are anatomical structures, slender lines are contours with no anatomical significance, dotted lines are supposed anatomical structures, black areas are foramina and grey areas are gaps in the 3D renderings. Scale bars = 1 cm.

different from the pointed and more slender ones of *Tamiobatis*. Foramina for superficial ophthalmic nerves are visible on the supraorbital shelf.

In ventral view (Fig. 59E, F), the incomplete rostrum is still visible, and it seems to be forked. There is a putative separate nasal calcification between the nasal capsules and the preorbital processes.

In ventral view, the hypophysial fossa is situated at the level of the postorbital processes and behind it there is a foramen for the internal carotid artery. AUT813 seems to possess a hypophysial fossa in front of a single foramen for the internal carotid artery contrary to *Cladodoides* and *Tamiobatis vetustus* in which two foramina are present within the anterior border of a well-developed hypophysial fossa (e.g. Schaeffer 1981; Maisey 2005).

In the otico-occipital region, in dorsal view, the lateral outline between the postorbital and lateral otic processes is slightly convex. It differs from the concave outline of *Xenacanthus meisenheimensis* and *X. decheni* and the straight one of *Triodus sessilis*.

The left lateral otic process is entirely preserved. It has a pointed shape and is posteriorly oriented, as in *Orthacanthus* and *Lebachacanthus* (Heidtke 1982, 1998, 2007). The lateral otic processes are more developed than in *Cladodoides* (e.g. Maisey 2001, 2005) and they are broader and more posteriorly oriented than in *Tamiobatis* (e.g. Romer 1964; Schaeffer 1981; Williams 1998).

There is a notch at mid-length of the lateral edge of the otic region. This notch is very pronounced on the right side, smaller on the left. Its presence has never been reported in any 'ctenacantiforms', nor xenacanthiforms.

The endolymphatic fossa is not visible. There is no dorsal otic ridge contrary to known 'Ctenacanthiformes' and Xenacanthiformes but the outline of the anterior and posterior horizontal semicircular canals is visible. The shape of the anterior and posterior canals forms a 'X'.

The occipital crest is present and is as long as those of *Orthacanthus* and *Lebachacanthus* (Heidtke 1982, 1998, 2007). It is more developed in AUT813 than in *Cladodoides* and *Tamiobatis*. The occipital crest extends posteriorly almost to the rear of the occipital block. The latter has a broad square shape different from the slenderer one of *X. meisenheimensis*.

In ventral view (Fig. 59E, F), the two foramina for the lateral dorsal aorta in the occipital block seem to be absent, contrary to *Orthacanthus*. However, there is a deep longitudinal sulcus in the location corresponding to these foramina on the left side, whereas, on the right side, foramina could be masked by compression. The occipital block is wider in *T. sessilis* than in AUT813 (Fig. 59). The lateral otic ridge seems to be delimited by lateral depressions. At their posterior extremities, there are articular facets for the hyomandibula. The left foramen for the vagus nerve is visible.

Order Xenacanthiformes Berg, 1937

Family Xenacanthidae Fritsch, 1889

cf. *Triodus* sp.

(Figs 60, 61)

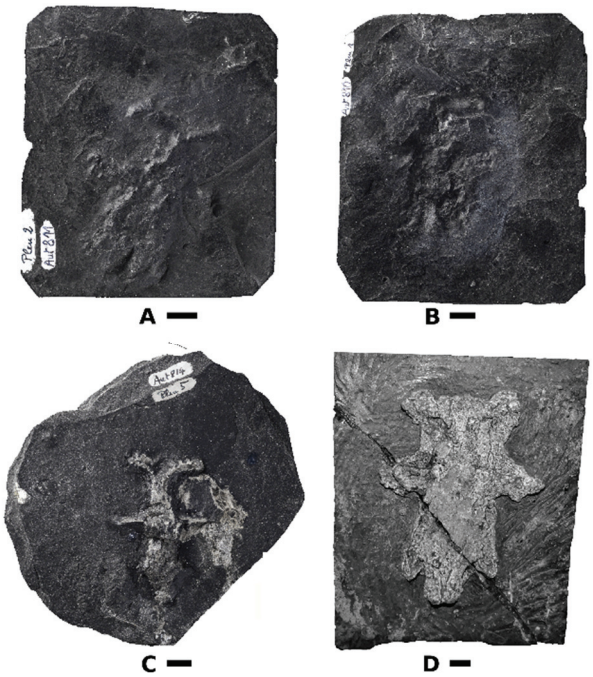

Figure 60. Isolated chondrichthyan neurocrania from the Autun and Bourbon-l'Archambault basins. **A,** MNHN.F.AUT811, holotype of *Bibractopiscis niger*. **B,** MNHN.F.AUT810 counter art impression of MNHN.F.AUT811. **C,** MNHN.F.AUT814, paratype of *B. niger*. **D,** MHNE.2021.9.1, specimen from Buxières-les-Mines; **A**, **B**, **D** in ventral view and **C** in dorsal view (modified from Heyler & Poplin [1982] except for **D**). Scale bars = 1 cm.

1982 *Bibractopiscis niger* Heyler & Poplin: 17, figs 1, 2, pl. 1, figs 1, 2, pl. 2, figs 1, 2.

Referred material—MNHN.F.AUT811, shortened to AUT811 below, isolated neurocranium in ventral view; MNHN.F.AUT810, counter impression of MNHN.F.AUT811 without cartilaginous remains; MNHN.F.AUT814, shortened to AUT814 below, isolated neurocranium in dorsal view; MHNE.2021.9.1, isolated neurocranium in ventral view.

Occurrences—La Comaille and an unknown locality of the Autun Basin, Saône-et-Loire, France; Buxières-les-Mines, Bourbon-l'Archambault Basin, Allier, France.

Horizons—Lally OSB, Muse formation, Autun Basin, Northern Massif Central, uppermost Gzhelian, upper Pennsylvanian, upper Carboniferous (Pellenard *et al.* 2017); Supra-Buxières member, Buxières formation, lower Asselian, lower Cisuralian, lower Permian (Steyer *et al.* 2000).

Comparative description

The ethmo-orbital region appears to be well-calcified. In dorsal view, the preorbital processes are well-developed and roughly square-shaped, although more elongated in AUT814 (Fig. 61E, F) than in AUT811 (Fig. 61A, B) and MHNE.2021.9.1 (Fig. 61I, J). They are antero-laterally oriented. The three specimens (Fig. 6) share with *Triodus sessilis*, *T. carinatus* and *T. aeduorum* rectangular and anteriorly to antero-laterally oriented preorbital processes. In the genera *Orthacanthus* and *Lebachacanthus* (Heidtke 1982, 1998, 2007), the preorbital processes have a similar shape but they are less developed than in the three specimens. Compared to *Cladodoides* (e.g. Maisey 2001, 2005) and *Tamiobatis* (Romer 1964; Schaeffer 1981; Williams 1998), the preorbital processes (Fig. 61) have a more rectangular shape and are antero-laterally oriented.

The precerebral fontanelle has a flared U-shape with a well-developed raised posterior edge on the posterior side (Fig. 61). Only the xenacanthiforms (e.g. Schaeffer 1981; Heidtke *et al.* 2004; Heidtke & Schwind 2004) possess a U-shaped precerebral fontanelle, and the latter has a V-shape in *Cladodoides* and *Tamiobatis.*

Between the preorbital and the postorbital processes, the border of the supraorbital shelf is sigmoid. The supraorbital shelf is well-developed but does not exceed the width of the pre- and postorbital processes.

Two appendices in AUT811 and a broad structure in AUT814 and MHNE.2021.9.1 are located in front of the precerebral fontanelle. They are interpreted as being part of a larger rostrum (*sensu* Schaeffer 1981) or an internasal plate that is not entirely preserved.

Small portions of the nasal capsules are preserved. The size of the nasal capsules associated with the anterior appendices seems to indicate that the most anterior part of the ethmoid region is not entirely preserved in AUT811 and AUT814. The interorbital space is smooth without foramen.

The anterior outline of the postorbital processes is more rounded than the posterior edge, and the extremities of the postorbital processes are rounded in AUT811 and more pointed in AUT814 and MHNE.2021.9.1. The three specimens (Fig. 61) share with *T. sessilis*, *T. carinatus* and *T. aeduorum* small rounded to pointed postorbital processes. The postorbital processes are more pointed in MHNE.2021.9.1, but in AUT811 and AUT814 the shape is similar to that of *Orthacanthus* and *Lebachacanthus*. The postorbital processes of *Cladodoides* and *Tamiobatis* are long and pointed, contrary to those of the three specimens (Fig. 61). They are less developed in *Xenacanthus decheni* and they are broader and less rounded in *X. humbergensis* and *X. meisenheimensis.*

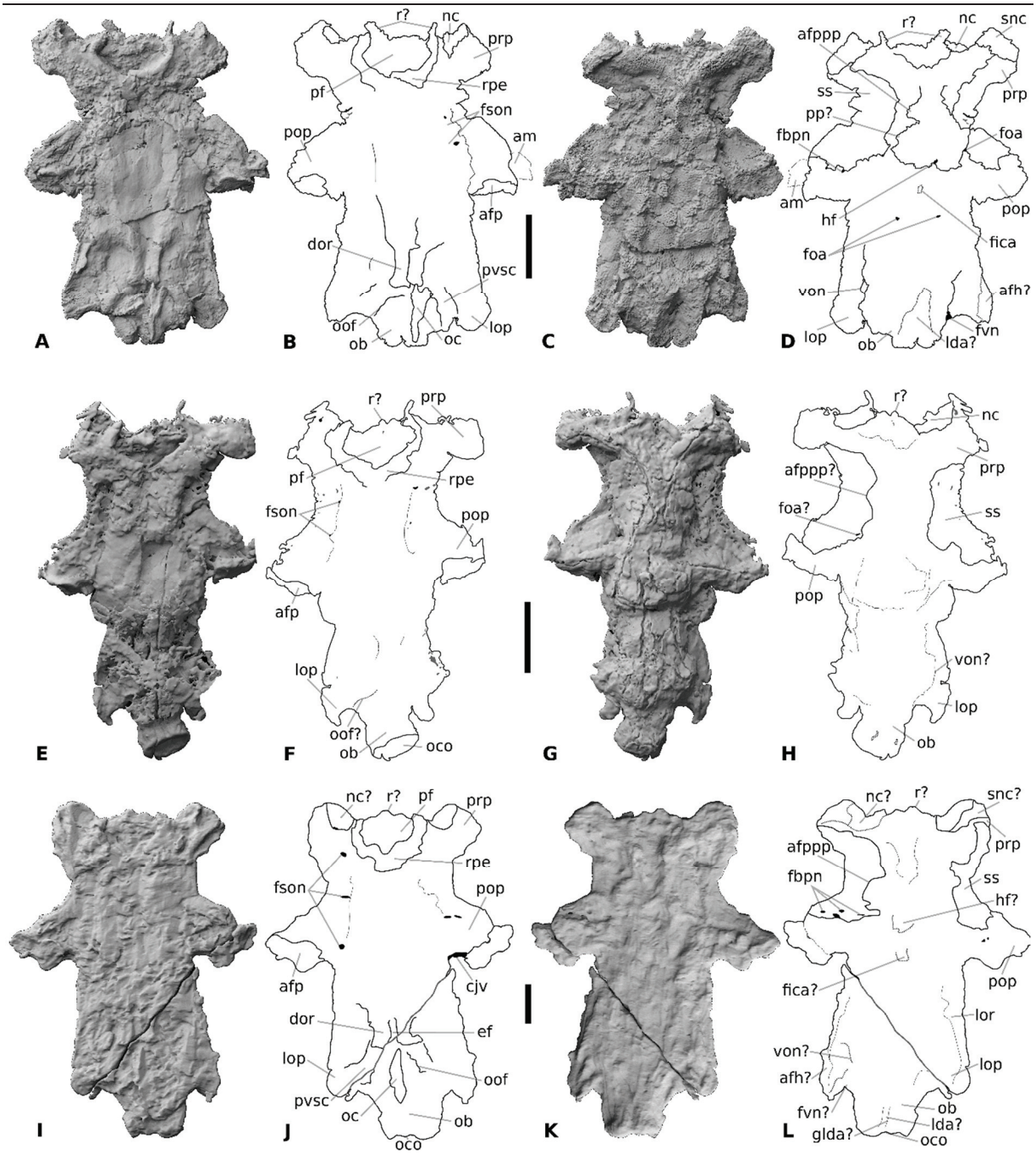

Figure 61. Neurocrania of cf. *Triodus* sp. from the Autun and Bourbon-l'Archambault basins. **A**–**D,** MNHN.F.AUT811 from an unknown locality of the Autun Basin. **E**–**H,** MNHN.F.AUT814 from La Comaille. **I–L,** MHNE.2021.9.1 from Buxières-les-Mines. **A**–**B**, **E**–**F**, **I**–**J** in dorsal view and **C**–**D**, **G**–**H**, **K**–**L** in ventral view. **A**, **C**, **E**, **G**, **I**, **K** are 3D surface rendering and **B**, **D**, **F**, **H**, **J**, **L** are line drawings. Bold lines represent anatomical structures, slender lines are contours with no anatomical significance, dotted lines are supposed anatomical structures, black areas are foramina and grey areas are gaps in the 3D renderings. Scale bars = 1 cm.

At the level or in front of the postorbital process, foramina for superficial ophthalmic nerves are visible in AUT811, AUT814 and MHNE.2021.9.1 (Fig. 61). The articular facet for the quadrate part of the palatoquadrate is situated on the postero-dorsal side of the postorbital processes and is well-developed all along it.

In ventral view, the ethmo-orbital region of AUT811, AUT814 and MHNE.2021.9.1 (Fig. 61C, D, G, H, K, L), shows the articular facet of the preorbital process for the palatine part of the palatoquadrate on each side of the neurocrania. Between these facets, there is a longitudinal depression. Between the postorbital processes and in front of the hypophysial fossa, there is an inverted heart-shaped structure in AUT811 and MHNE.2021.9.1 that could correspond to a flattened parachordal plate. One foramen for a branch of the palatine nerve is visible under the right postorbital process in AUT811 (Fig. 61C, D). The hypophysial fossa is represented by a small, single hole and the single foramen for the internal carotid artery is behind it, whereas in *Tamiobatis* sp. there is an anterior and a posterior foramen for the internal carotid artery.

The otico-occipital region of AUT814 is less well-preserved than AUT811 and MHNE.2021.9.1. In dorsal view, the lateral outlines of the otico-occipital region are almost straight in AUT811 and MHNE.2021.9.1. The latter (Fig. 61) share with *T. sessilis*, *T. carinatus* and *T. aeduorum* a straight lateral outline of the otico-occipital region. The anterior part of the otico-occipital region in *Orthacanthus* and *Lebachacanthus* is slenderer than the posterior part, whereas the two parts have the same width in the three specimens (Fig. 61). The lateral outline of the otico-occipital region is concave in *X. decheni* and *X. meisenheimensis* while it is almost straight in the three specimens (Fig. 61).

The lateral otic processes are well-developed, posteriorly oriented with a bulbous shape, but are probably not completely preserved in AUT811 and MHNE.2021.9.1 (Fig. 61). They are more posteriorly oriented than in *T. carinatus* (Schneider & Zajíc 1994), *T.* sp. (Soler-Gijón & Hampe 1998; Luccisano *et al.* 2021a), *T. aeduorum* (Luccisano *et al.* 2021a), *Orthacanthus* and *Lebachacanthus*. They are also more developed (Fig. 61) than in *Cladodoides* (e.g. Maisey 2001, 2005) and *X. decheni*. Compared to *Tamiobatis* (Romer 1964; Schaeffer 1981; Williams 1998), they have a more massive and rounded shape (Fig. 61).

The most posterior part of the dorsal otic ridges are present in AUT811 and MHNE.2021.9.1. They are more posteriorly situated in AUT811 than in MHNE.2021.9.1. Their small dorsal otic ridges (Fig. 61) are similar to those of *T. sessilis* (Jordan 1849; Schwind 1991; Heidtke *et al.* 2004) and *T. carinatus* (Schneider & Zajíc 1994) but seem to be smaller than in *T. aeduorum* (Luccisano *et al.* 2021a) and *T.* sp. (Soler-Gijón & Hampe 1998; Luccisano *et al.*

2021a). *Cladodoides* (e.g. Maisey 2001, 2005) possesses a foramen in front of the dorsal otic ridges, which is absent in the three specimens (Fig. 61).

An anteroposteriorly elongated endolymphatic fossa is present between the dorsal otic ridges in MHNE.2021.9.1 (Fig. 61I, J). Behind these ridges, there is a straight occipital crest not visible in AUT814 (Fig. 61E, F). It reaches the dorsal otic ridges anteriorly and it extends until the posterior side of the occipital block posteriorly. On the lateral sides of the occipital crest, there is the otico-occipital fissure that delimits the posterior outlines of the posterior semicircular canals. The latter begin next to the dorsal otic ridges and end at the level of the anterior part of the occipital block. The occipital block is more complete in MHNE.2021.9.1 than in AUT811 and it is almost complete in AUT814. It has an elongated shape in AUT814 and seems broader in AUT811 and MHNE.2021.9.1. It is wedged between the lateral otic processes. The occipital cotyle is visible in AUT814 (Fig. 61E, F) at the posterior side of the occipital block.

In ventral view, behind the hypophysial fossa, there is a foramen for the internal carotid artery in AUT811 (Fig. 61C, D) and MHNE.2021.9.1 (Fig. 61K, L). Behind it, one of the paired foramina for the orbital artery is present in AUT811 (Fig. 61C, D). The ventral otic notch is visible next to the lateral otic processes on both specimens. At the extremities of the lateral otic processes in AUT811 and MHNE.2021.9.1, articular facets for the hyomandibula might be present. On the posterior side of the right lateral otic process in AUT811 and on the left one in MHNE.2021.9.1, a depression indicates the position of a foramen for the vagus nerve.

A single foramen for the lateral dorsal aorta seems to be present on the occipital block in AUT811 and MHNE.2021.9.1. In all Xenacanthiformes (e.g. Schaeffer 1981; Heidtke *et al.* 2004; Heidtke & Schwind 2004), there are always two foramina for lateral dorsal aorta, suggesting a possible preservation bias. The occipital block is not as slender as in *Orthacanthus* (Schaeffer 1981), nor *X. meisenheimensis* (Heidtke & Schwind 2004), but it is similar to those of *T. sessilis* (Jordan 1849; Schwind 1991; Heidtke *et al.* 2004) and *T. carinatus* (Schneider & Zajíc 1994).

Phylogenetic analysis

A strict consensus tree (Fig. 62) was computed for the two most parsimonious trees (MPTs; length [L] = 73 steps, Consistency Index [CI] = 0.548, Retention Index [RI] = 0.790) of the PAUP analysis (see the Supplemental material VIII for the complete list of apomorphies). The relationships within Xenacanthiformes and between *Akmonistion zangerli*, *Cladoselache kepleri* and Holocephali are unresolved, resulting in polytomies.

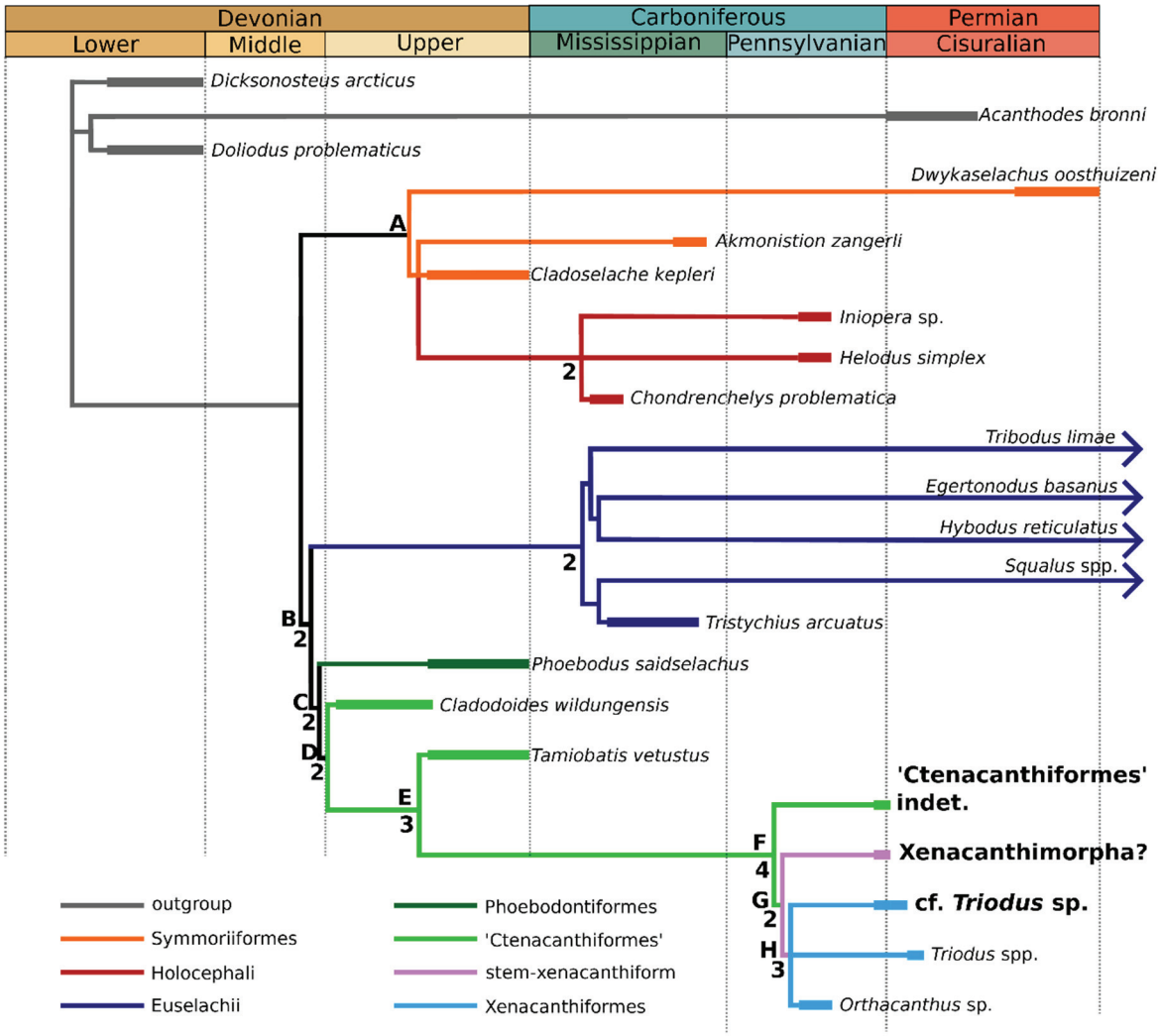

Figure 62. Strict consensus tree of the cladistic analysis obtained with PAUP from the two most parsimonious trees (MPTs) with the following characteristic: length [L] = 73 steps, Consistency Index [CI] = 0.548 and Retention Index [RI] = 0.790. Values in bold below branches are Bremer indices greater than 1 and letters indicate nodes mentioned in the text. Temporal distributions are represented by bold lines and follow Coates *et al.* (2017).

The Euchondrocephali (Fig. 62, node A) are supported by two unambiguous characters: the orbits are larger than the otic capsule (ch. 12^1) and the postorbital processes and arcade are wider than the braincase (ch. 13^1).

Our analysis supports close relationships between the crown elasmobranchs and a clade composed of Phoebodontiformes, 'Ctenacanthiformes' and Xenacanthiformes. This elasmobranch total group (Fig. 62, node B,) is supported by one unambiguous character: the presence of a precerebral fontanelle (ch. 1^1); and by one synapomorphy: the presence of a rostral bar (ch. 7^1).

The sister group of the crown elasmobranchs (Fig. 62, node C) is supported by two unambiguous characters: the presence of dorsal otic ridges forming a crest (ch. 21^1) and the presence of an elongated endolymphatic fossa (ch. 23^1); and one synapomorphy: the presence of an antero-posteriorly elongated occipital crest (ch. 25^1).

The ['Ctenacanthiformes'+?Xenacanthimorpha+Xenacanthiformes] clade (Fig. 62, node D) is supported by two unambiguous characters: the wide postorbital processes and arcade (ch. 13^1) and the otico-occipital region reaching 50% or more of the neurocranium length (ch. 33^1).

The clade E excluding *Cladodoides wildungensis* (Fig. 62, node E) is well-supported by two unambiguous characters: the entrance of internal carotids through separate openings flanking the hypophysial fossa (ch. 10^1) and the presence of a developed articular facet for the hyomandibular on the lateral otic processes (ch. 19^1); and one synapomorphy: the presence of a sub-otic occipital fossa (ch. 20^1).

The clade F excluding *Tamiobatis vetustus* (Fig. 62, node F) is well-supported by four unambiguous characters: the foramen or foramina for the internal carotid artery situated below the hypophysial fossa (ch. 11^1), the massive postorbital process and arcade (13^2) and the postorbital process expanded anteroposteriorly (ch. 15^0); and one synapomorphy: the lateral otic process is posteriorly oriented (ch. 18^2).

The [?Xenacanthimorpha+Xenacanthiformes] clade (Fig. 62, node G) is supported by one unambiguous character: the postero-dorsal articular facet of the palatoquadrate on the postorbital process (ch. 16^0); and two synapomorphies: the antero-laterally orientation of the preorbital process (ch. 6^1) and the maximum width of the neurocranium at the level of the pre- and postorbital processes (ch. 32^1).

The Xenacanthiformes (Fig. 62, node H) are well-supported by two unambiguous characters: the U-shaped precerebral fontanelle (ch. 2^0) and the presence of an ethmoidal articulation (ch. 8^1); and two synapomorphies: the presence of a raised posterior edge of the precerebral fontanelle (ch. 4^1) and an antero-posteriorly oriented otico-occipital fissure (ch. 28^1).

Following our phylogenetic analysis, cf. *Triodus* sp. is included in the Xenacanthiformes (Bremer Index of 3). 'Ctenacanthiformes' indet. and ?Xenacanthimorpha are recovered as stem-Xenacanthiformes and 'Ctenacanthiformes' appears as a paraphyletic assemblage.

Morphometric analysis

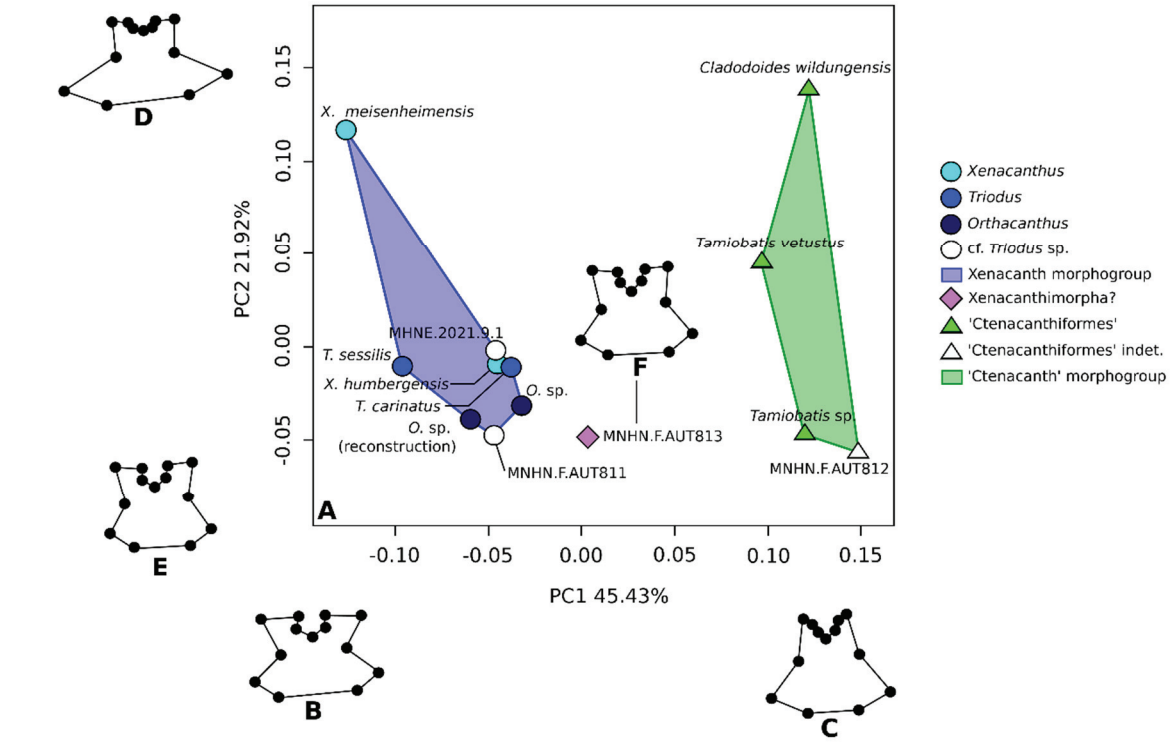

Figure 63. Principal Component Analysis (PCA) on Procrustres coordinates illustrating morphological variability of the ethmo-orbital region between neurocrania of 'Ctenacanthiformes' and Xenacanthiformes. **A,** Interspecific variation based on 13 landmarks. **B**, **C,** patterns of variation along PC1. **D**, **E,** patterns of variation along PC2. **F,** morphology of the ethmo-orbital region of the ?Xenacanthimorpha (MNHN.F.AUT813).

Figure 63A represents the projection of the specimens on the first factorial plane that comes from the pGPA. PC1 (45.43% of the variance) clearly separates Xenacanthiformes from 'Ctenacanthiformes'. PC1 highlights the morphological differences in term of shape of the precerebral fontanelle and orientation of the preorbital processes: U-shaped and antero-laterally oriented for the xenacanthiforms (Fig. 63B) and V-shaped and anteriorly oriented for the 'ctenacanthiforms' (Fig. 63C). PC2 (21.92% of the variance) shows variation in shape, in each order, between forms with elongated postorbital processes (Fig. 63D) and forms with short ones (Fig. 63E). Variability in the shape of the postorbital processes only concerns inter-specific variations that does not allow genera in each order to be distinguished. AUT811 and MHNE.2021.9.1 are included in the xenacanthiform morphogroup, whereas AUT812 is within the 'Ctenacanthiformes'. AUT813, attributed to ?Xenacanthimorpha, is included neither in the morphospace of Xenacanthiformes nor in that of 'Ctenacanthiformes'. It is intermediate between the two following PC1, while remaining closer to Xenacanthiformes than to 'Ctenacanthiformes' (Fig. 63F).

Discussion

Reassessment of the systematics of *Bibractopiscis niger* and *Orthacanthus commailli*

The symmoriiform *Bibractopiscis niger* (Fig. 58B) is not valid as it encompasses two distinct neurocranial morphotypes, neither corresponding to a symmoriiform due to the absence of large orbits and a small otico-occipital region. AUT812 (Fig. 58) belongs to the order 'Ctenacanthiformes' because of the presence of a long otico-occipital region, anteriorly oriented preorbital processes and a V-shaped precerebral fontanelle.

AUT811 and AUT814 (Fig. 61) are assigned to the order Xenacanthiformes because of the presence of a long otico-occipital region, antero-laterally oriented preorbital processes and a U-shaped precerebral fontanelle. Comparisons with a new specimen from Buxières-les-Mines (MHNE.2021.9.1) allow these to be related to the genus *Triodus*: the genus *Xenacanthus* possesses different shapes for the precerebral fontanelle and for the pre- and postorbital processes (Fig. 64). The neurocrania of *Orthacanthus* and *Triodus* have a similar morphology, but AUT811, AUT814 and MHNE.2021.9.1 display preorbital processes and an anterior part of the otico-occipital region not laterally compressed that are closer to *Triodus* than to *Orthacanthus*. Furthermore, the apparent small size of the neurocrania, between 5 and 10 cm long, which belong to adult specimens as indicated by the well-calcified ethmoid region according to Benzer (1944), corresponds to adult *Triodus* and not to the 30-cm long neurocranium of adult *Orthacanthus*.

Orthacanthus commailli (Fig. 59B) is not a xenacanthiform. AUT813 (Fig. 60) exhibits a long otico-occipital region together with both a 'ctenacanthiform' V-shaped precerebral fontanelle, and xenacanthiform antero-laterally oriented preorbital processes. Comparisons with known 'ctenacanthiform' and xenacanthiform neurocrania (Fig. 64) support its closer relationship with Xenacanthiformes. The retention of 'ctenacanthiform' characters together with autapomorphies like the absence of dorsal otic ridges and a pronounced notch next to the lateral otic processes exclude it from the xenacanthiform clade.

In our geometric morphometric analysis, no familial or generic attribution of the studied specimens can be made within the xenacanth morphogroup: *Xenacanthus* is distributed all along PC2 because the length of the postorbital processes can be developed or not within a same genus. Concerning *Orthacanthus*, the composite specimen *O.* sp. (reconstruction) was based on the morphology of the real specimen *O.* sp. in the Figure 63A, so it is logical that these two specimens are close to each other. Taking into account the observed variation among *Triodus*

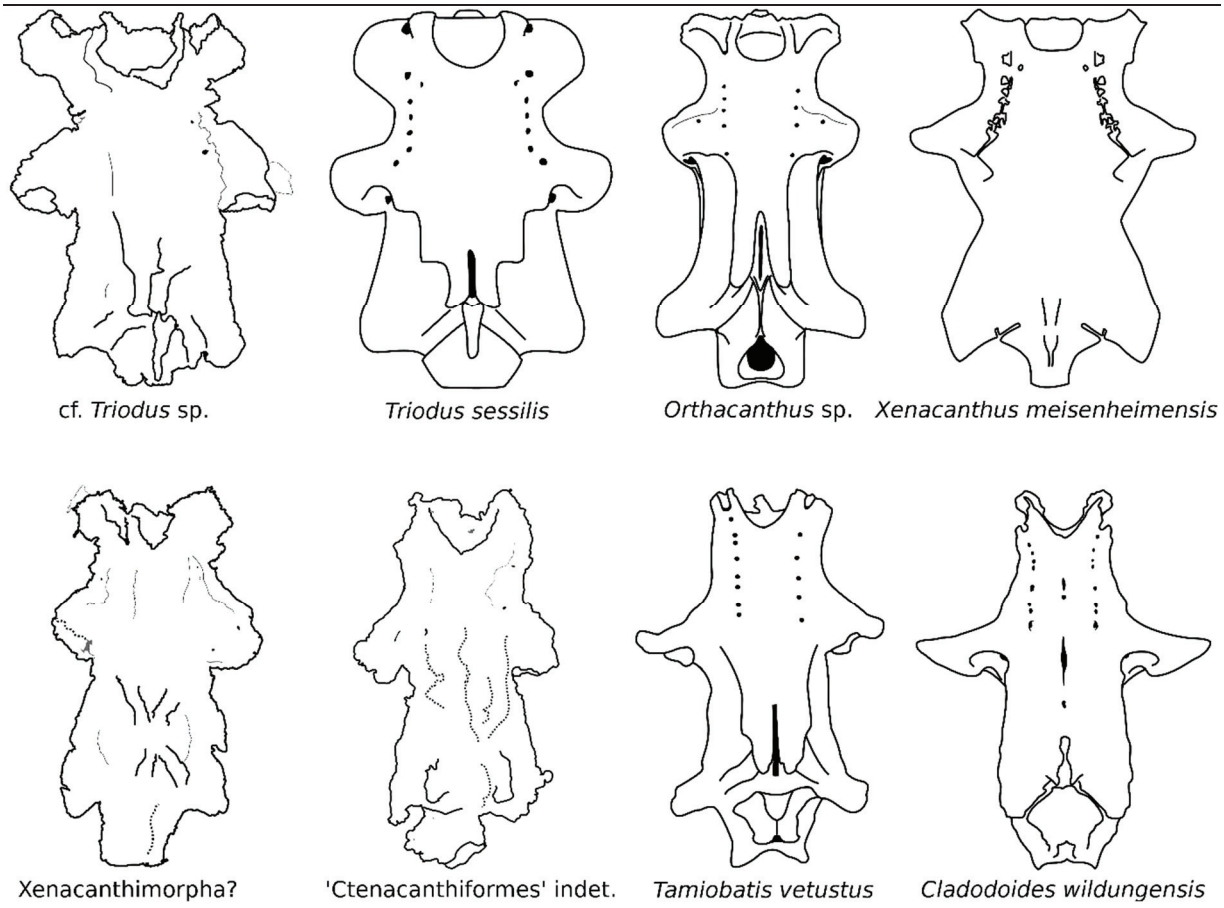

Figure 64. Comparison between Xenacanthiformes and 'Ctenacanthiformes' neurocrania. Line drawing are in dorsal view and not to scale. *Triodus sessilis* modified from Heidtke *et al.* (2004), *Orthacanthus* sp. modified from Schaeffer (1981), *Xenacanthus meisenheimensis* modified from Heidtke & Schwind (2004) *Tamiobatis vetustus* modified from Schaeffer (1981) and *Cladodoides wildungensis* modified from Maisey (2005). Bold lines represent anatomical structures, slender lines are contours with no anatomical significance, dotted lines are supposed anatomical structures, black areas are foramina and grey areas are gaps in the 3D renderings.

and *Xenacanthus,* we do not interpret the distribution of the studied specimens along PC2 like a discrimination criteria of the genus *Orthacanthus* compared to the other genera.

However, geometric morphometric results are congruent with our new anatomical interpretations of specimens from the Autun Basin. cf. *Triodus* sp., ?Xenacanthimorpha and 'Ctenacanthiformes' indet. fall within three different morphogroups in agreement with their systematic reassessment. This confirms the first identification of a 'ctenacanthiform' in the Late Carboniferous of the French Massif Central and reveals a higher chondrichthyan diversity than previously identified in the Autun Basin.

Phylogenetic position of fossils from the Autun and Bourbon-l'Archambault basins

Our phylogenetic analysis (Fig. 62) is congruent with previous studies (Coates *et al.* 2017, 2018; Frey *et al.* 2019, 2020) in recovering two main chondrichthyan clades: Euchondroncephali (node A, Fig. 62) and elasmobranch total group (node B, Fig. 62). This global chondrichthyan organisation contradicts the hypotheses of Ginter *et al.* (2010), Pradel *et al.* (2011), Brazeau *et al.* (2020) that supported a position of Xenacanthiformes, 'Ctenacanthiformes' and Symmoriiformes out of the crown-chondrichthyan clade.

This recovered elasmobranch total group agrees with Coates *et al.* (2017, 2018) but is different from Frey's *et al.* (2019, 2020) latest studies. Phoebodontiformes, 'Ctenacanthiformes' and Xenacanthiformes are united into a monophyletic clade (Fig. 62, node C) that is the sister-group of the crown-elasmobranchs, but not as stem-elasmobranchs. Although our analysis supports the close relationship between Phoebodontiformes and ['Ctenacanthiformes'+Xenacanthiformes] previously proposed by dental analyses of Ginter (2004) and Ginter *et al.* (2010), their position within the elasmobranch sister-group is still ambiguous. The monophyly of 'Ctenacanthiformes' is not supported, and they appear as a paraphyletic group, contrary to the hypotheses of Frey *et al.* (2019, 2020) but in agreement with Coates *et al.* (2017, 2018) and Brazeau *et al.* (2020).

The addition of the specimens from the Autun Basin to the phylogenetic analysis proposes for the first time that some non-xenacanthiform specimens could be more closely related to xenacanthiforms than *Tamiobatis*, contrary to numerous recent studies (Pradel *et al.* 2011; Coates *et al.* 2017, 2018; Frey *et al.* 2019, 2020; Brazeau *et al.* 2020). The systematics of 'Ctenacanthiformes' indet. and ?Xenacanthimorpha remains difficult to assess. Following Ginter *et al.* (2010), the sister-group of Xenacanthiformes is Bransonelliformes, both united into the superorder Xenacanthimorpha. As the neurocranium of bransonelliforms remains unknown, the position of 'Ctenacanthiformes' indet. and ?Xenacanthimorpha in the proposed phylogeny (Fig. 62, nodes F and G) can correspond to several phylogenetic scenarios. They could indeed belong to bransonelliforms, basal xenacanthimorphs, stem-xenacanthimorphs or 'ctenacanthiforms' more related to Xenacanthiformes than *Tamiobatis.*

Neurocranial evolution between Xenacanthiformes and 'Ctenacanthiformes'

Geometric morphometric results (Fig. 63) show that differences between xenacanthiform and 'ctenacanthiform' neurocrania encompass the shape of the precerebral fontanelle and the orientation of the preorbital processes. This interpretation is reinforced by the intermediate status of ?Xenacanthimorpha in the geometric morphometric analysis as well as in the comparative description. Our phylogenetic analysis (Fig. 62) could also support this

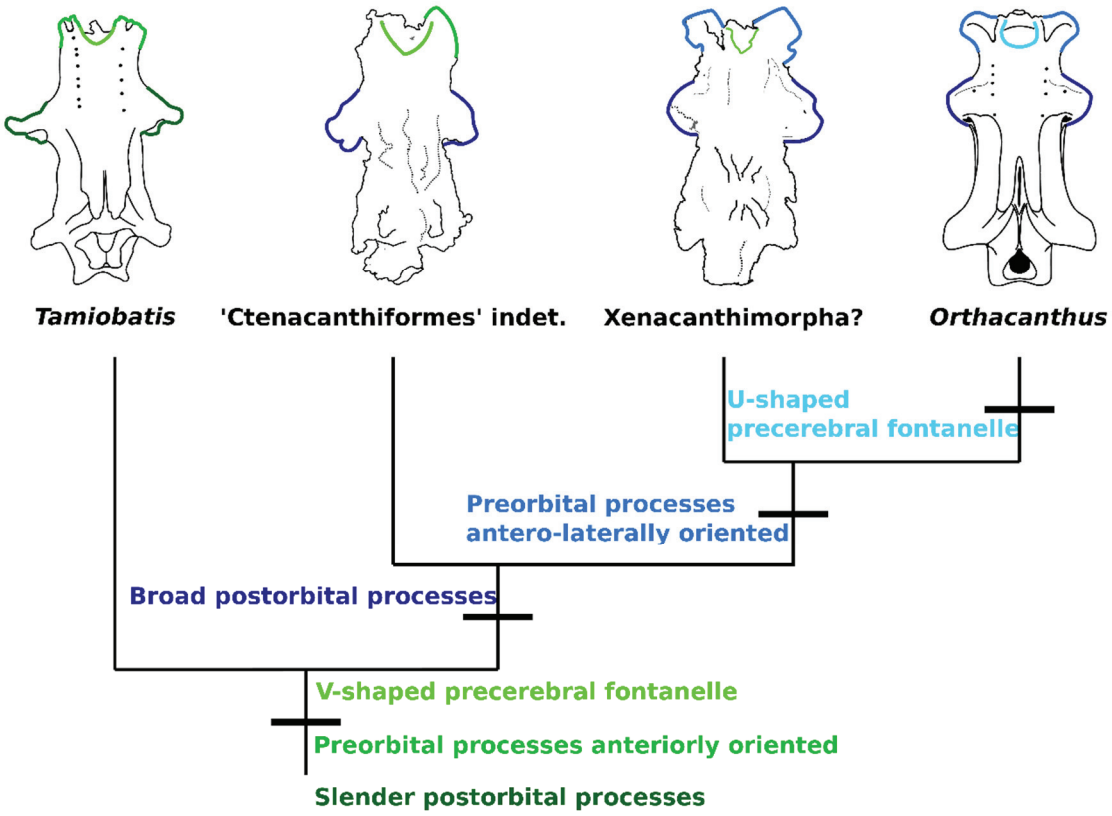

Figure 65. Hypothetical morphological transition between 'Ctenacanthiformes' and Xenacanthiformes neurocrania in the light of the Autun Basin fossil record. The relationships and the character changes follow those of the phylogeny of Figure 7. Each coloured text corresponds to coloured parts on the line drawings, which are not to scale. Outline of *Tamiobatis* is from Schaeffer (1981). Bold lines represent anatomical structures, slender lines are contours with no anatomical significance, dotted lines are supposed anatomical structures, black areas are foramina and grey areas are gaps in the 3D renderings.

hypothesis because ?Xenacanthimorpha is also retrieved in an intermediate position between 'Ctenacanthiformes' and Xenacanthiformes. The associated character transformations are anterior (ch. 6^0) to antero-laterally oriented preorbital processes (ch. 6^1) from 'Ctenacanthiformes' indet. to ?Xenacanthimorpha (Fig. 62, node G), and V-shaped (ch. 2^1) to U-shaped precerebral fontanelle (ch. 2^0) from ?Xenacanthimorpha to Xenacanthiformes (Fig. 7, node H).

However, some character states, supposedly derived in the proposed phylogeny, are also found in the outgroup *Doliodus problematicus*, for example ch. 2^0 in the clade H. *Dicksonosteus arcticus* and *Acanthodes bronni*, which represent more remote outgroups than *D. problematicus* (Coates *et al.* 2017, 2018; Frey *et al.* 2019, 2020; Brazeau *et al.* 2020), do not possess these character states. They can therefore be seen as convergences between the primitive *D. problematicus* and the derived Xenacanthiformes. Our phylogenetic (Fig. 62) and geometric

morphometric (Fig. 63) analyses still provide a clarification of the morphological transition between 'Ctenacanthiformes' and Xenacanthiformes that affects the ethmo-orbital region of the neurocranium (Fig. 65).

Trophic structures of the Autun and Bourbon-l'Archambault basins

As a result of our analysis, the trophic structure of the Autun Basin may be different from that of the other European Carboniferous-Permian basins. Following Soler-Gijón (1995), Boy & Schindler (2000) and Kriwet *et al.* (2008), the Carboniferous–Permian freshwater environments of Europe were dominated by large predators such as the xenacanthiform *Orthacanthus*, like *O. buxieri* in the Bourbon-l'Archambault Basin. The latter appears, however, to be absent from the Autun Basin and taxa like cf. *Triodus* sp., 'Ctenacanthiformes' indet. and ?Xenacanthimorpha are smaller chondrichthyans according to the size of their neurocrania, i.e. between 5 and 9 cm long. They could correspond to small third level consumers as proposed by Kriwet *et al.* (2008). Their size does not reach that of adult *Orthacanthus* (see above) which was a large third level consumer at the top of the foodchain (Kriwet *et al.* 2008).

In the Carboniferous–Permian of the Autun Basin, Eryopoidea and Sphenacodontoidea were reported (Table 5). Most of them can reach up to 1.5 metres long like the longest *Triodus*. As 'Ctenacanthiformes' indet. and ?Xenacanthimorpha possess neurocranium of similar size, they could also reach about the same body size. Consequently, the top predator trophic level could have been occupied by these three vertebrate groups which hunted each other (Table 5), as already supposed in the Texas red beds (Zoehfeld *et al.* 2014), even if no data from other European basins has confirmed this hypothesis. Such a trophic structure has been proposed by Falconnet (2015) for the lower Permian Viala Formation of the Lodève Basin (Southern France) in which large xenacanthiforms are also unknown. However, it is surprising that the trophic structures of the Autun and Bourbon-l'Archambault basins are so different considering they are geographically close and represent almost the same temporal records (Gand *et al.* 2015, 2017). Furthermore, our work supports the presence of the genus *Triodus* in these two basins, pointing to a possible communication between them even if it was discontinuous or brief. This questions the migration pattern of the xenacanthiforms in the Northern Massif Central, and whether these patterns are the same between large and small xenacanthiforms.

Table 5. Occurrences of supposed top predators, i.e. Xenacanthidae, Sphenacodontoidea and Eryopoidea, in the Carboniferous-Permian Autun Basin.

Formation	Locality	Systematics		References
Millery	Margenne	Sphenacodontoidea	*Callibrachion gaudryi*	Boule & Glangeaud (1893)
Millery	Margenne	Xenacanthidae	'*Expleuracanthus*' *bonnardi*	Sauvage (1893)
Millery	Les Télots	Sphenacodontoidea	*Haptodus baylei*	Gaudry (1886)
Millery	?	Eryopoidea	*Onchiodon* sp.	Werneburg (1997)
Surmoulin	?	Xenacanthidae	'*Expleuracanthus*'	Heyler (1969)
Muse	Muse OSB	Eryopoidea	*Onchiodon frossardi*	Werneburg & Steyer (1999)
Muse	Muse OSB	Xenacanthidae	'*Expleuracanthus*' *frossardi nomen dubium*	Gaudry (1867, 1883)
Muse	Muse OSB	Xenacanthidae	'*Expleuracanthus*' *bonnardi*	Agassiz (1833)
Muse	Muse OSB	Xenacanthidae	*Triodus* sp.	Soler-Gijón & Hampe (1998)
Muse	Muse OSB	Xenacanthidae	*Triodus aeduorum*	Luccisano *et al.* (2021)
Muse	La Comaille, Dracy-Saint-Loup	Xenacanthidae	cf. *Triodus* sp.	Present study
Muse	Dracy-Saint-Loup	'Ctenacanthiformes'	'Ctenacanthiformes' indet.	Present study
Muse	La Comaille	?	Xenacanthimorpha?	Present study
Igornay	?	Sphenacodontoidea	*Stereorachis dominans*	Falconnet (2014)
Igornay	?	Eryopoidea	*Onchiodon*	Heyler (1969)
Igornay	?	Xenacanthidae	'*Expleuracanthus*' *bonnardi*	Sauvage (1893)

Conclusions

X-ray computed microtomography allows enhanced descriptions of several historical isolated neurocrania from the Autun and Bourbon-l'Archambault basins. They demonstrate the invalidity of the species *Bibractopiscis niger* and *Orthacanthus commailli*. The holotype and a paratype of *B. niger*, together with a new neurocranium from the Bourbon-l'Archambault Basin are attributed to cf. *Triodus* sp. The second paratype of *B. niger* is related to the ambiguous order 'Ctenacanthiformes' without more precise attribution. The holotype of *O. commailli* does not belong to a xenacanthiform proper but is more closely related to Xenacanthiformes than to any other Palaeozoic chondrichthyan orders and is left in open nomenclature as ?Xenacanthimorpha.

Phylogenetic and geometric morphometric analyses allow a better understanding of the morphological transitions in the neurocranium between 'Ctenacanthiformes' and Xenacanthiformes. The main morphological shift occurs in the ethmoidal region where the orientation of the preorbital processes becomes more laterally oriented and the precerebral fontanelle changes from a V-shape to a U-shape from 'Ctenacanthiformes' to Xenacanthiformes.

The revised faunal lists of the chondrichthyans from the Autun and Bourbon-l'Archambault basins raise the question of their trophic structures that appear potentially different. The Bourbon-l'Archambault Basin corresponds to the structure found in other European Carboniferous-Permian basins, whereas the Autun Basin seems to be devoid of large xenacanths as top predators.

Acknowledgements

The authors thank the Rhinopolis Association, the Gannat Town hall and the Conseil Départemental de l'Allier for having funded the excavation campaigns in the Buxières-les-Mines locality during which the specimen MHNE.2021.9.1 was found, and for providing storage space in which the Buxières-les-Mines fossils are housed. We thank René Kindlimann (Aathal, Switzerland) for access to his collection. We thank Florent Goussard (MNHN) and Céline Salaviale (LGL-TPE) for their help in the 3D reconstructions, and Philippe Loubry (MNHN) for the photographs of the specimens from the Autun Basin. We thank two anonymous reviewers and the associate editor, Martin Brazeau, for their remarks that have

greatly helped to improve this manuscript. The first author was funded by the Doctoral School ED 341 - E2M2 Évolution Écosystème Microbiologie Modélisation, Université Claude Bernard Lyon 1, France.

Supplementary material

A) Scan parameters

Table S1. Scan parameters for the whole set of described neurocrania

	MNHN.F.AUT 811	**MNHN.F.AUT 812**	**MNHN.F.AUT 813**	**MNHN.F.AUT 814**	**MHNE.2021.9.1**
Voxel x.y.z (µm)	34.6343	79.6788	56.14744	63.31675	95.82
Voltage (kV)	130	150	150	150	140
Current (µA)	270	310	360	310	350

B) Script for geometric morphometric analysis in R

```
install.packages("geomorph")#install the package geomorph
library(geomorph)#open the package geomorph
fileslist<-list.files(getwd())#create a R object with all the neurocranium image files
digitize2d(fileslist,nlandmarks=13,scale=1,tpsfile = "neuro",MultScale = FALSE,verbose = FALSE)#digitalize the 2D landmarks and create a file with the Procruste coordinates
mydata<-readland.tps("neuro", specID="ID")#create a R object with the Procruste coordinates
Y<-gpagen(mydata)#make the Generalized partial Procrustes Analysis on the Procrustes coordinates
pca<-gm.prcomp(Y$coords)#make the Principal Component Analysis (PCA)
spec.names <- names(Y$Csize)#create a R object with the names of each point
d<-plot(pca)#create a R object for the graphic representation of the PCA
d#make the graph of the PCA
text(pca$x[,1:2], spec.names, pos = 3, offset = 0.5)#add the names of each point on the graph d
picknplot.shape(d)#determine the shape of a point in the graph
```

C) Procrustres coordinates for the geometric morphometric analysis

LM=13
46.5910675245173 499.733100131176
86.5420950715221 389.392166906115
15.2009744518707 308.53889687051
86.5420950715221 263.831794615529
282.492373040165 257.173290024361
354.784708601412 288.563383097008
269.17536385783 401.757961146855
303.419101755262 498.781885189581
215.90732712849 500.684315072771
213.053682303704 473.099081766506
175.00508463989 455.025997876194
118.883403085764 477.855156474483
138.858916859267 501.635530014367
SCALE=0.0102066709000538
ID=AUT_811.jpg

LM=13
95.5992066962335 599.967993003935
73.3923855331377 459.324792304329
11.001792741583 351.463089512149
83.967062277469 336.658542070086
265.851502279968 322.911462302455
336.701836466987 346.175751139984
274.311243675433 477.301742769692
235.184939721407 620.059878818165
217.207989256044 596.795589980636
204.518377162846 552.381947654444
167.507008557686 528.060191142482
140.012849022425 551.324479980011
122.035898557062 579.876107189706
SCALE=0.010060163662254
ID=AUT_812.jpg

LM=13
38.7180086201511 565.677231557249
69.3558998063589 474.751877069149
11.0450746455118 381.849884440003
79.2390905115872 323.539059279156
257.136523205697 321.56242113811
322.365581860204 365.048460241114
245.276694359423 477.716834280717
256.148204135174 557.770678993066
190.919145480667 563.700593416203
182.024273845962 535.039340371041
164.234530576551 503.413130114311
142.491511025048 524.16783059529
126.678405896683 550.852445499407
SCALE=0.0158096716597143
ID=AUT_813.jpg

LM=13
68.279361609095 501.178487101006
88.7979449059904 383.662964582422
2.06029733275042 289.464013992129
96.2592479230433 258.686139046786
279.993834717971 266.147442063839
374.192785308264 309.982597289025
287.455137735024 392.989593353739
320.098338434631 495.582509838216
239.889331001312 492.784521206821
216.572759073022 462.93930913861
187.660209881941 428.43078268474
144.757717533887 458.275994752951
146.62304328815 486.2558810669
SCALE=0.0167531059540553
ID=MHNE.2021.9.1.jpg

LM=13
184.295383846586 611.631232431757
173.282203760385 502.600749578362
4.78054844150177 385.861040664626
155.661115622462 317.579324130177
357.20231119995 316.478006121557
509.184196389531 388.063676681866
339.581223062028 499.296795552502
330.770678993066 605.023324380036
293.325866699981 605.023324380036
279.008732587919 586.300918233494
256.982372415516 568.679830095571
233.854694234493 584.098282216253
218.436242113811 605.023324380036
SCALE=0.0100889216594508
ID=Cladodoides wildungensis.jpg

LM=13
42.4612405521895 534.923605471922
73.9069898182274 451.068274095821
11.9683927790619 375.789056155912
74.8598913111376 328.1439815104
241.617652570429 322.426572552939
299.744643637954 378.647760634643
231.135736148417 452.974077081642
260.675682428634 533.970703979012
178.726154038353 534.923605471922
187.302267474546 509.195265163346
152.997813729777 480.608220376039
118.693359985009 504.430757698794
127.269473421201 531.111999500281
SCALE=0.0338524650828392
ID=Orthacanthus sp. reconstruction.jpg

LM=13
86.2946530076832 547.032594165782
90.0455431319883 459.824398775689
15.0277406458867 392.308376538197
80.6683178212256 314.477406458867
244.769760759573 294.785233306265
315.098950590293 342.609082391155
244.769760759573 440.132225623087
292.593609844462 520.776363295646
207.260859516522 515.150028109189
199.759079267912 481.392016990443
161.312455493785 458.886676244612
138.807114747954 487.0183521769
151.935230183022 524.527253419951
SCALE=0.0380861977085
ID=Orthacanthus sp.jpg

LM=13
54.0927665688051 739.425373227559
116.001005684303 549.74906615029
10.6252795302643 433.835767380848
144.979330376663 375.879117996127
382.074714223249 431.201374226997
486.133243800362 515.501955150228
355.73078268474 591.899356611906
392.612286838653 723.619014304454
266.161415453807 728.887800612156
270.113005184584 689.371903304391
224.011124992192 657.75918545818
170.006065338247 680.151527265913
170.006065338247 724.936210881379
SCALE=0.0130410818943194
ID=Triodus carinatus.JPG

LM=13
67.487594478106 594.749778249735
123.310756449497 457.928302829658
17.137291523518 363.795127740646
107.986751202449 304.688250359173
393.669991879568 304.688250359173
482.330307951777 369.267986757449
370.683984008995 468.874020863264
423.223430570304 596.938921856456
299.536816790555 630.870647760635
299.536816790555 576.142057592604
250.281085639328 542.210331688425
197.741639078019 570.669198575801
190.079636454494 625.397788743832
SCALE=0.00736773604460865
ID=Triodus sessilis.jpg

LM=13
117.818583296896 674.003223186957
94.3080579673935 534.115597476419
23.7764819788869 424.791654694234
120.169635829846 351.909026172778
300.025154600537 344.855868573927
403.471466050347 413.036392029483
335.29094259479 542.344281341745
304.727259666438 671.652170654007
261.232787806859 649.31717159098
243.599893809732 621.104541195577
208.334105815479 596.4184895996
187.174633018927 619.929014929102
170.717265288275 646.96611905803
SCALE=0.0223863900145709
ID=Tamiobatis sp.jpg

LM=13
135.604722343682 572.604972203136
117.845336997939 452.235804859766
6.355862327441 365.412143169467
118.831969517147 304.240926978575
295.439190455369 320.027047285902
386.2093822225 356.532450496596
300.372353051409 457.168967455806
287.546130301705 567.671809607096
246.107564494972 562.738647011056
238.214504341308 538.072834030858
208.61552876507 512.420388531451
177.043288150416 535.112936473234
164.217065400712 558.792116934224
SCALE=0.0266723313506939
ID=Tamiobatis vetustus.jpg

LM=13
81.4174651758387 577.039015553751
109.130876382035 439.537859953776
12.1339371603474 354.265825473171
104.867274658005 299.904903491786
330.838166031607 300.970803922793
423.571503529265 357.463526766194
325.50866387657 443.801461677806
358.551577237804 583.434418139796
272.213642326192 574.907214691736
270.081841464176 540.798400899494
218.918620775814 518.414491848335
166.689499656443 546.127903054532
166.689499656443 574.907214691736
SCALE=0.0167531059540553
ID=Xenacanthus humbegensis.jpg

LM=13
123.220019988756 568.184046473858
144.399731401087 464.302604784808
32.4498282216253 388.660778312199
98.0060778312199 352.352701605347
398.556268349054 351.344143919045
463.103960272347 385.635105253295
353.171172465488 468.336835530014
376.367999250421 564.149815728652
291.649153601099 556.081354238241
288.623480542195 531.875969767006
249.289730776438 515.739046786183
211.973096383284 530.867412080704
206.930307951777 556.081354238241
SCALE=0.0170950849361644
ID=Xenacanthus meisenheimensis.jpg

D) Taxa for the phylogenetic analyses

Placodermi

Dicksonosteus arcticus Goujet, 1975
Temporal and geographical distribution: Lower Devonian, Europe.
Origin of examined material: Dicksonland, Spitsberg, Norway.
Reference: Goujet (1975, 1984).

Stem-chondrichthyan

Acanthodes bronni Agassiz, 1833
Temporal and geographical distribution: Lower Permian, Europe.
Origin of examined material: Saar-Nahe Basin, Germany.
Reference: Davis *et al.* (2012), Brazeau & de Winter (2015).

Doliodus problematicus Miller *et al.* 2003
Temporal and geographical distribution: Lower Devonian, North America.
Origin of examined material: Campbellton Formation in New Brunswick, Canada.

Reference: Maisey *et al.* (2009).

Holocephali

Chondrenchelys problematica (Traquair, 1888)

Temporal and geographical distribution: Lower Mississippian, Europe.

Origin of examined material: Glencartholm Volcanic Beds, Scotland.

Reference: Finarelli & Coates (2014).

Helodus simplex Agassiz, 1838

Temporal and geographical distribution: upper Pennsylvanian, Europe.

Origin of examined material: Knowles Ironstone, United Kingdom.

Reference: Moy-Thomas (1936).

Iniopera sp.

Temporal and geographical distribution: upper Pennsylvanian, North America.

Origin of examined material: Stranger Formation, Kansas, USA.

Reference: Pradel (2010).

Symmoriiformes

Akmonistion zangerli Coates & Sequeira, 2001b

Temporal and geographical distribution: upper Mississippian, Europe.

Origin of examined material: Manse Burn Formation of Bearsden, near Glasgow, Scotland.

Reference: Coates & Sequeira (2001b).

Cladoselache kepleri (Newberry, 1889)

Temporal and geographical distribution: Upper Devonian, North America.

Origin of examined material: Cleveland Shales, Ohio, USA.

Reference: Maisey (2007).

Dwykaselachus oosthuizeni Oelofsen, 1986

Temporal and geographical distribution: upper Cisuralian, South Africa.

Origin of examined material: Prince Albert Formation, Ecca Group, Karoo Superroup, South Africa

Reference: Coates *et al.* (2017).

‘Ctenacanthiformes’

Tamiobatis vetustus (Eastman, 1897)

Temporal and geographical distribution: Upper Devonian, North America.

Origin of examined material: eastern Powel County, Kentucky, USA.

Reference: Romer (1964), Schaeffer (1981).

Cladodoides wildungensis (Jaekel 1921)

Temporal and geographical distribution: Upper Devonian, Europe

Origin of examined material: Wildungen Limestone, Wildungen, Germany.

Reference: Maisey (2005).

‘Ctenacanthiformes’ indet.

Temporal and geographical distribution: upper Gzhelian, Europe.

Origin of examined material: Autun Basin, France.

Reference: this work.

Xenacanthimorpha

?Xenacanthimorpha

Temporal and geographical distribution: upper Gzhelian, Europe.

Origin of examined material: Autun Basin, France.

Reference: this work.

Xenacanthiformes

cf. *Triodus* sp.

Temporal and geographical distribution: upper Gzhelian to lower Asselian, Europe.

Origin of examined material: Autun and Bourbon-l’Archambault basins, France.

Reference: this work.

Triodus spp.

Triodus sessilis Jordan, 1849

Temporal and geographical distribution: lower Asselian, Europe.

Origin of examined material: Saar-Nahe Basin, Germany.

Reference: Heidtke *et al.* (2004).

Triodus carinatus (Fritsch, 1890)

Temporal and geographical distribution: lower Asselian, Europe.

Origin of examined material: Podkrkonoske Basin, Czech Republic.

Reference: Schneider & Zajíc (1994).

Orthacanthus sp.

Temporal and geographical distribution: middle Pennsylvanian, North America

Origin of examined material: Texas, USA.

Reference: Schaeffer (1981).

Euselachii

Hybodus reticulatus Agassiz, 1837

Temporal and geographical distribution: Lower Jurassic, Europe.

Origin of examined material: Lyme Regis, United Kingdom.

Reference: Maisey (1987).

Egertonodus basanus (Egerton, 1845)

Temporal and geographical distribution: Lower Cretaceous, Europe.

Origin of examined material: Southeastern England, United Kingdom.

Reference: Maisey (1983).

Tribodus limae Brito & Ferreira, 1989

Temporal and geographical distribution: Lower Cretaceous, South America.

Origin of examined material: Santana Formation, Northeastern Brazil.

Reference: Lane (2010).

Tristychius arcuatus Agassiz, 1837

Temporal and geographical distribution: Mississippian, Europe.

Origin of examined material: Wardie Beach, Edinburgh, Scotland.

Reference: Coates & Tietjen (2018).

Squalus spp.

Squalus acanthias Linnaeus, 1758

Temporal and geographical distribution: Current, North and South America, Europe, Australia.
Origin of examined material: worldwide.
Reference: Schaeffer (1981).

Squalus margaretsmithae de F. L. Viana *et al.*, 2018
Temporal and geographical distribution: Current, Southern Africa.
Origin of examined material: South Africa.
Reference: de F. L. Viana *et al.* (2018).

Phoebodontiformes

Phoebodus saidselachus Frey *et al.,* 2019
Temporal and geographical distribution: Famennian, North Africa.
Origin of examined material: Maïder region, Morocco.
Reference: Frey *et al.,* (2019).

E) Characters for the phylogenetic analyses

New characters are in bold.

1. Precerebral fontanelle (Schaeffer 1981; Lund & Grogan 1997; Coates & Sequeira 1998, 2001a,b; Maisey 2001; Brazeau 2009; Pradel *et al.* 2011; Davis *et al.* 2012; Zhu *et al.* 2013; Brazeau & Friedman 2014; Coates *et al.* 2018; Frey *et al.* 2019; Brazeau *et al.* 2020)
   0 absent
   1 present

2. **Shape of the precerebral fontanelle** (We define the U-shaped state present in Xenacanthiformes or Hybodonthiformes in which the precerebral has symmetric rounded outline. The V-shaped corresponds to the state present in some 'Ctenacanthiformes' in wich the precerebral fontanelle has a pointed posterior extremity. The elongated state corresponds to the state present in some Euselachii in which the precerebral fontanelle has a rounded extremity with straight lateral sides)
   0 U-shaped
   1 V shaped
   2 elongated

3. **Size of the precerebral fontanelle** (We define state 0 and 1 according to the maximum width and length of the precerebral fontanelle. State 0 corresponds to Xenacanthiformes, 'Ctenacanthiformes' and Hybodonthiformes and state 1 corresponds to the Euselachii.)
   0 width and length of almost equal size
   1 length superior to the width

4. **Raised posterior edge of the precerebral fontanelle** (State 1 corresponds to the raised surface of the internasal space present in Xenacanthiformes, positioned directly behind the precerebral fontanelle.)
   0 absent
   1 present

5. Prominent preorbital process (Brazeau 2009; Davis *et al.* 2012; Zhu *et al.* 2013; Coates *et al.* 2018; Brazeau *et al.* 2020)
   0 absent
   1 present

6. **Orientation of the preorbital process** (The orientation is indicated by the direction of the longest axis of the preorbital processes compared to the antero-posterior axis of the neurocranium.)
   0 anteriorly oriented, i.e. between 80) and 90°.
   1 antero-laterally oriented, i.e. between 45° and 80°.
   2 laterally oriented, i.e. lower than 45°.

7. Rostral bar (Maisey 1985; Coates *et al.* 2017, 2018)
   0 absent
   1 present

8. Ethmoidal articulation (Maisey 2001; Pradel *et al.* 2011)
   0 absent
   1 present

9. Supraorbital shelf broad with convex lateral margin (Coates & Sequeira 1998; Brazeau 2009; Davis *et al.* 2012; Zhu *et al.* 2013; Coates & Tietjen 2018; Brazeau *et al.* 2020)
   0 absent
   1 present

10. Entrance of internal carotids (Schaeffer 1981; Coates & Sequeira 1998; Brazeau 2009; Davis *et al.* 2012; Zhu *et al.* 2013; Coates *et al.* 2018; Frey *et al.* 2019)
    0 through a common opening at the central midline of the basicranium
    1 through separate openings flanking the hypophyseal opening or recess

11. **Position of the foramen or foramina for internal carotid artery** (In the case in which the hypophysial fossa and foramina for internal carotid artery are clearly different openings like in Xenacanthiformes and 'Ctenacanthiformes', we consider states 1. In the case in which the hypophysial fossa and foramina for internal carotid artery passes by the same opening or if the distinction between them is too tenuous, we consider the state 0.)
    0 next to the hypophysial fossa
    1 clearly below the hypophysial fossa

12. Orbit larger than otic capsule (Lund & Grogan 1997; Coates *et al.* 2017, 2018; Frey *et al.* 2019)
    0 absent
    1 present

13. **Postorbital process and arcade** (modified from Coates *et al.*(2018) and Frey *et al.* (2019) with the addition of the state 3)
    0 short and deep - width not more than maximum braincase width (excluding arcade)
    1 process and arcade wide - width exceeds maximum width of braincase, and anteroposteriorly narrow
    2 process and arcade massive
    3 absent

14. Postorbital process downturned, with anhedral angle relative to basicranium (Coates *et al.* 2018; Frey *et al.* 2019)

0 absent

1 present

15. Postorbital process expanded anteroposteriorly (Coates *et al.* 2018; Frey *et al.* 2019)

0 present

1 absent

16. **Position of the articular facet of the palatoquadrate on the postorbital process** (modified from Coates & Tietjen, 2018. In most of the Palaeozoic chondrichthyans, the palatoquadrate is articulated with the postorbital processes of the neurocranium. Most of the time, the articular facet is positioned on the posterior side of the postorbital processes, so we distinguish state 0 in which it is almost entirely visible in dorsal view and state 1 in which it is almost entirely visible in ventral view.)

0 postero-dorsal side

1 postero-ventral side

2 anterior

17. **Shape of the lateral otic process** (We describe here the shape of the extremity of the lateral otic processes. Rounded state corresponds to broad extremity and pointed state to narrower one.)

0 absent

1 rounded

2 pointed

18. **Orientation of the lateral otic process** (The orientation is indicated by the direction of the longest axis of the lateral otic processes compared to the antero-posterior axis of the neurocranium)

0 postero-laterally oriented, i.e. between 45° and 80°.

1 posteriorly oriented, i.e. between 80° and 90°.

19. **Articulation facet for the hyomandibular on the lateral otic process** (We consider the presence of this structure in the Xenacanthiformes and in some 'Ctenacanthiformes')

0 absent

1 present

20. Sub-otic occipital fossa (Coates *et al.* 2018; Frey *et al.* 2019)
    0 absent
    1 present

21. Dorsal otic ridges forming crests (adapted from Coates & Sequeira 1998, 2001b; Maisey 2001; Davis 2002; Davis *et al.* 2012; Zhu *et al.* 2013; Brazeau & Friedman 2014; Coates *et al.* 2018; Frey *et al.* 2019; Brazeau *et al.* 2020) (We consider here the state 1 only for taxa, e.g. *Orthacanthus*, in which the dorsa otic ridges are well developed in posterior crests.)
    0 absent
    1 present

22. Endolymphatic fossa (Pradel *et al.* 2011; Coates *et al.* 2018; Frey *et al.* 2019)
    0 absent
    1 present

23. Endolymphatic fossa elongate (slot-shaped), dividing dorsal otic ridge along midline (Coates *et al.* 2017, 2018; Frey *et al.* 2019)
    0 absent
    1 present

24. Metotic fissure (ventral otic notch) (Schaeffer 1981; Janvier 1996; Coates & Sequeira 1998; Maisey 2001; Davis 2002; Brazeau 2009; Pradel *et al.* 2011; Davis *et al.* 2012; Zhu *et al.* 2013; Coates *et al.* 2018; Frey *et al.* 2019; Brazeau *et al.* 2020)
    0 absent
    1 present

25. Occipital crest anteroposteriorly elongate, and extends from the roof of the posterior tectum (Coates *et al.* 2018; Frey *et al.* 2019)
    0 absent
    1 present

26. Occipital block (Schaeffer 1981; Coates & Sequeira 1998; Maisey 2001; Brazeau 2009; Pradel *et al.* 2011; Davis *et al.* 2012; Coates *et al.* 2017, 2018; Frey *et al.* 2019; Brazeau *et al.* 2020)
    0 entirely posterior to otic capsules
    1 wedged between otic capsules

27. Dorsal part of the adult otico-occipital fissure (Schaeffer 1981; Coates & Sequeira 1998, 2001b; Maisey 2001; Brazeau 2009; Pradel *et al.* 2011)
    0 open
    1 closed

28. Orientation of the otico-occipital fissure (this character is only considered when the dorsal part of the otico-occipital fissure is open and correspond to the position of the fissure relative to the antero-posterior axis of the neurocranium)
    0 laterally oriented, almost at 45° to the antero-posterior axis of the neurocranium.
    1 antero-posteriorly oriented, almost parallel to the antero-posterior axis of the neurocranium.

29. Outline of the otico-occipital region in dorsal view (We describe here the shape of the otico-occipital region of the neurocranium in dorsal view. We consider state 1 or 2 only if the curvature of the lateral outline is pronounced.)
    0 convex
    1 concave
    2 straight

30. Multilayered prismatic calcification in the outer wall of the neurocranium (Maisey 2001, 2005; Pradel *et al.* 2011)
    0 absent
    1 present

31. Palatoquadrate fused to the neurocranium (Maisey 2001; Pradel *et al.* 2011; Coates *et al.* 2018; Frey *et al.* 2019; Brazeau *et al.* 2020)
    0 absent
    1 present

32. Maximum width of the neurocranium at the level of: (We consider here the state 0 for the species with small or anteriorly oriented preorbital processes)

0 the postorbital processes only

1 the pre- and post-orbital processes

33. Proportion of the otico-occipital region (State 1 is characterizing Xenacanthiformes and 'Ctenacanthiformes' which exhibits elongated otico-occipital region)

0 length less than 50% of the neurocranium entire length

1 equal or more than 50 % of the neurocranium entire

F) Character matrix

Acanthodes bronni

0 - - - 0 - ? 1 0 0 0 0 2 0 0 ? 0 - 0 ? 0 0 ? 1 ? 0 ? ? 2 0 0 0 1

Akmonistion zangerli

0 - - - 0 2 0 0 1 0 0 1 1 0 1 1 1 0 0 0 0 1 0 1 0 0 0 0 2 0 0 0 0

cf. *Triodus* sp.

1 0 0 1 0 1 1 1 0 1 1 0 2 0 0 0 1/2 1 1 ? 1 1 1 1 1 1 0 1 2 ? 0 0 1

Chondrenchelys problematica

0 - - - 0 - 0 0 1 0 ? 1 3 - - - 0 - 0 0 0 1 0 0 0 0 1 - 2 0 1 0 0

Cladodoides wildungensis

1 1 0 0 ? ? ? 0 0 0 0 0 1 0 1 0 ? ? 0 0 1 1 1 1 ? ? 0 0 2 0 0 0 1

Cladoselache kepleri

? ? ? ? ? ? ? ? 0 1 0 0 1 1 0 1 1 0 - 0 0 0 ? ? 1 ? 0 0 ? 0 0 0 0 0

'Ctenacanthiformes' indet.

1 1 0 0 0 0 ? 0 0 1 1 0 2 0 0 1 2 1 ? ? 1 ? ? 1 ? 1 0 0 0/2 ? 0 0 1

Dicksonosteus arcticus

0 - - - 0 - 0 0 0 ? ? 0 0 0 0 - 0 - 0 0 0 0 - 0 0 0 ? ? 0 0 0 0 0

Doliodus problematicus

1 0 0 0 0 - 0 0 0 0 0 0 2 0 0 0 0 - 0 0 0 0 - 1 0 0 0 0 2 0 0 0 0

Dwykaselachus oosthuizeni

0 - - - 0 2 0 0 0 0 0 1 1 0 1 1 0 - 0 0 0 1 0 1 0 0 0 0 2 0 0 0 0

Egertonodus basanus

1 0 1 0 0 - 1 0 0 1 1 0 0 1 0 2 1 0 1 0 0 1 1 0 0 0 1 - 2 0 0 0 0

Helodus simplex

0 - - - 0 - 0 0 1 0 0 1 3 - - - 0 - 0 0 0 1 0 0 0 0 1 - 2 0 1 0 0

Hybodus reticulatus

1 0 1 0 0 - 1 0 0 0 0 0 0 1 0 2 1 0 0 0 0 1 1 0 0 0 1 - 2 0 0 0 0

Iniopera sp.

0 - - - 0 - 0 0 1 0 0 1 3 - - - 0 - 0 0 1 0 - 0 0 0 1 - 2 0 1 0 0

Orthacanthus sp.

1 0 0 1 0 1 1 1 0 1 1 0 2 0 0 0 1/2 0/1 1 1 1 1 1 1 1 1 0 1 1 1 0 1 1

Phoebodus saidselachus

? ? ? ? ? ? ? ? 0 ? ? 0 0 0 1 ? 0 - ? 0 1 1 1 1 1 0 1 - 2 0 0 ? 0

Tamiobatis vetustus

1 1 0 0 0 0 1 1 0 1 0 0 1 0 1 1 2 0 1 1 1 1 1 1 1 1 0 0 2 0 0 0 1

Triodus spp.

1 0 0 1 0 1 1 1 0 1 1 0 2 0 0 0 1/2 0 1 ? 1 1 1 1 1 1 0 1 1/2 1 0 1 1

Squalus spp.

1 2 1 0 1 - 1 0 0 0 0 1 0 0 1 - 0 - 0 0 0 1 0 0 0 0 1 - 1 0 0 1 0

Tribodus limae

1 2 1 0 0 - 1 0 0 0 0 0 0 1 0 - 1 0 0 0 0 1 0 0 0 0 1 - 2 0 0 0 ?

Tristychius arcuatus

1 2 1 0 1 - 1 0 0 0 0 0 0 1 1 1 0 - 0 0 1 1 0 0 0 0 1 - 1 0 0 0 1

?Xenacanthimorpha

1 1 0 0 0 1 1 0 0 1 1 0 2 0 0 0 2 1 1 ? 0 ? ? ? 1 1 0 0 0/2 ? 0 1 1

G) PAUP Display Buffer for the cladistic analysis

P A U P * Version 4.0a (build 169) for 32-bit Microsoft Windows (built on Feb 10 2021 at 22:12:44)
Fri Jan 14 17:48:21 2022
Microsoft Windows

Data matrix has 22 taxa, 33 characters
Valid character-state symbols: 01234
Missing data identified by '?'
Gaps identified by '-'
2 taxa transferred to outgroup
Total number of taxa now in outgroup = 3
Number of ingroup taxa = 19

Heuristic search settings:

Optimality criterion = parsimony
Character-status summary:
Of 33 total characters:

All characters are of type 'unord'

All characters have equal weight

All characters are parsimony-informative

Gaps are treated as "missing"

Multistate taxa interpreted as uncertainty

Starting tree(s) obtained via stepwise addition

Addition sequence: random

Number of replicates = 1000

Starting seed = generated automatically

Number of trees held at each step = 1

Branch-swapping algorithm: tree-bisection-reconnection (TBR) with reconnection limit = 8

Steepest descent option not in effect

Initial 'Maxtrees' setting = 100

Branches collapsed (creating polytomies) if maximum branch length is zero

'MulTrees' option in effect

No topological constraints in effect

Trees are unrooted

Heuristic search completed

Total number of rearrangements tried = 6091240

Score of best tree(s) found = 73

Number of trees retained = 2

Time used = 7.09 sec (CPU time = 1.61 sec)

H) Apomorphy list of the PAUP analysis

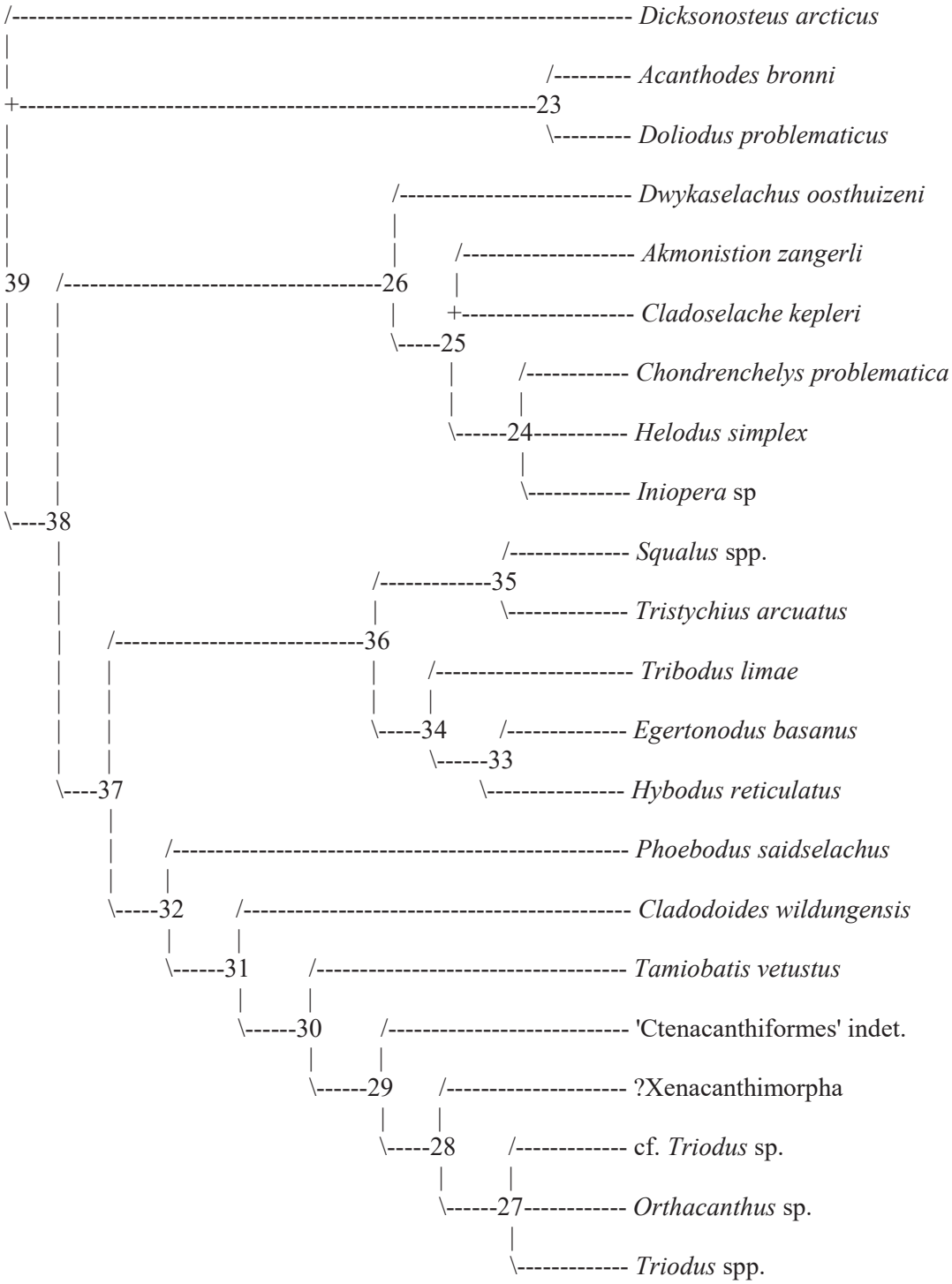

Apomorphy lists:

Branch	Character	Steps	CI	Change
node_39 --> Dicksonosteux arcticus				
	24 (Metotic fissure (ventral otic)	1	0.333	1 ==> 0
	29 (outline of the otico-occipital)	1	0.500	2 ==> 0
node_39 --> node_23				
	13 (Postorbital process and arcade)	1	0.600	0 ==> 2
node_23 --> Acanthodes bronni				
	8 (Ethmoidal articulation)	1	0.333	0 ==> 1
	33 (Proportion of the otico-occipi)	1	0.333	0 ==> 1
node_23 --> Doliodus problematicus				
	1 (precerebral fontanelle bis)	1	0.500	0 ==> 1
node_39 --> node_38				
	2 (Shape of the precerebral fontan)	1	0.500	0 --> 1
	15 (Postorbital process expanded a)	1	0.333	0 ==> 1
	16 (Position of the articular face)	1	0.500	0 --> 1
	22 (Endolymphatic fossa)	1	0.500	0 ==> 1
node_38 --> node_26				
	6 (Orientation of the preorbital p)	1	1.000	0 --> 2
	12 (Orbit larger than otic capsule)	1	0.500	0 ==> 1
	13 (Postorbital process and arcade)	1	0.600	0 ==> 1
node_26 --> node_25				
	9 (Supraorbital shelf broad with c)	1	1.000	0 ==> 1
node_25 --> Akmonistion zangerli				
	17 (Shape of the lateral otic proc)	1	0.667	0 ==> 1

node_25 --> node_24

13 (Postorbital process and arcade) 1 0.600 1 ==> 4

24 (Metotic fissure (ventral otic) 1 0.333 1 ==> 0

27 (Dorsal part of the adult otico) 1 0.333 0 ==> 1

31 (Palatoquadrate fused to the ne) 1 1.000 0 ==> 1

node_24 --> Iniopera sp

21 (Dorsal otic ridge) 1 0.250 0 ==> 1

22 (Endolymphatic fossa) 1 0.500 1 ==> 0

node_25 --> Cladoselache kepleri

29 (outline of the otico-occipital) 1 0.500 2 ==> 0

node_38 --> node_37

1 (precerebral fontanelle bis) 1 0.500 0 ==> 1

7 (Rostral bar) 1 1.000 0 ==> 1

27 (Dorsal part of the adult otico) 1 0.333 0 --> 1

node_37 --> node_32

21 (Dorsal otic ridge) 1 0.250 0 ==> 1

23 (Endolymphatic fossa elongate () 1 0.500 0 ==> 1

25 (Occipital crest anteroposterio) 1 1.000 0 ==> 1

node_32 --> node_31

13 (Postorbital process and arcade) 1 0.600 0 ==> 1

17 (Shape of the lateral otic proc) 1 0.667 0 --> 2

26 (Occipital block) 1 1.000 0 --> 1

27 (Dorsal part of the adult otico) 1 0.333 1 --> 0

33 (Proportion of the otico-occipi) 1 0.333 0 ==> 1

node_31 --> node_30

10 (Entrance of internal carotids) 1 0.500 0 ==> 1

19 (Articulation for the hyomadibu) 1 0.500 0 ==> 1

20 (Sub-otic occipital fossa) 1 1.000 0 ==> 1

node_30 --> node_29

11 (Position of the foramen or for) 1 0.500 0 ==> 1

13 (Postorbital process and arcade) 1 0.600 1 ==> 2

15 (Postorbital process expanded a) 1 0.333 1 ==> 0

18 (Orientation of the lateral oti) 1 0.500 1 ==> 0

30 (Multilayered prismatic calcifi) 1 1.000 0 --> 1

node_29 --> node_28

6 (Orientation of the preorbital p) 1 1.000 0 ==> 1

16 (Position of the articular face) 1 0.500 1 ==> 0

32 (Maximum width of the Neurocran) 1 0.333 0 ==> 1

node_28 --> node_27

2 (Shape of the precerebral fontan) 1 0.500 1 ==> 0

4 (Posterior bead of the precerebr) 1 1.000 0 ==> 1

8 (Ethmoidal articulation) 1 0.333 0 ==> 1

28 (Orientation of the orico-occip) 1 1.000 0 ==> 1

node_27 --> cf. Triodus sp.

32 (Maximum width of the Neurocran) 1 0.333 1 ==> 0

node_27 --> Orthacanthus sp.

29 (outline of the otico-occipital) 1 0.500 2 ==> 1

node_27 --> Triodus spp.

18 (Orientation of the lateral oti) 1 0.500 0 ==> 1

node_28 --> ?Xenacanthimorpha

21 (Dorsal otic ridge) 1 0.250 1 ==> 0

node_30 --> Tamiobatis vetustus

8 (Ethmoidal articulation) 1 0.333 0 ==> 1

node_31 --> Cladodoides wildungensis

16 (Position of the articular face) 1 0.500 1 ==> 0

node_37 --> node_36

2 (Shape of the precerebral fontan) 1 0.500 1 --> 2

3 (Size of the precerebral fontane) 1 1.000 0 ==> 1

14 (Postorbital process downturned) 1 0.500 0 --> 1

24 (Metotic fissure (ventral otic) 1 0.333 1 ==> 0

node_36 --> node_34

15 (Postorbital process expanded a) 1 0.333 1 ==> 0

16 (Position of the articular face) 1 0.500 1 --> 2

17 (Shape of the lateral otic proc) 1 0.667 0 ==> 1

node_34 --> node_33

2 (Shape of the precerebral fontan) 1 0.500 2 --> 0

23 (Endolymphatic fossa elongate () 1 0.500 0 ==> 1

node_33 --> Egertonodus basanus

10 (Entrance of internal carotids) 1 0.500 0 ==> 1

11 (Position of the foramen or for) 1 0.500 0 ==> 1

19 (Articulation for the hyomadibu) 1 0.500 0 ==> 1

node_36 --> node_35

5 (Prominent preorbital processes) 1 1.000 0 ==> 1

29 (outline of the otico-occipital) 1 0.500 2 ==> 1

node_35 --> Squalus spp.

12 (Orbit larger than otic capsule) 1 0.500 0 ==> 1

14 (Postorbital process downturned) 1 0.500 1 --> 0

32 (Maximum width of the Neurocran) 1 0.333 0 ==> 1

node_35 --> Tristychius arcuatus

21 (Dorsal otic ridge) 1 0.250 0 ==> 1

33 (Proportion of the otico-occipi) 1 0.333 0 ==> 1

I) Bootstrap analysis with PAUP

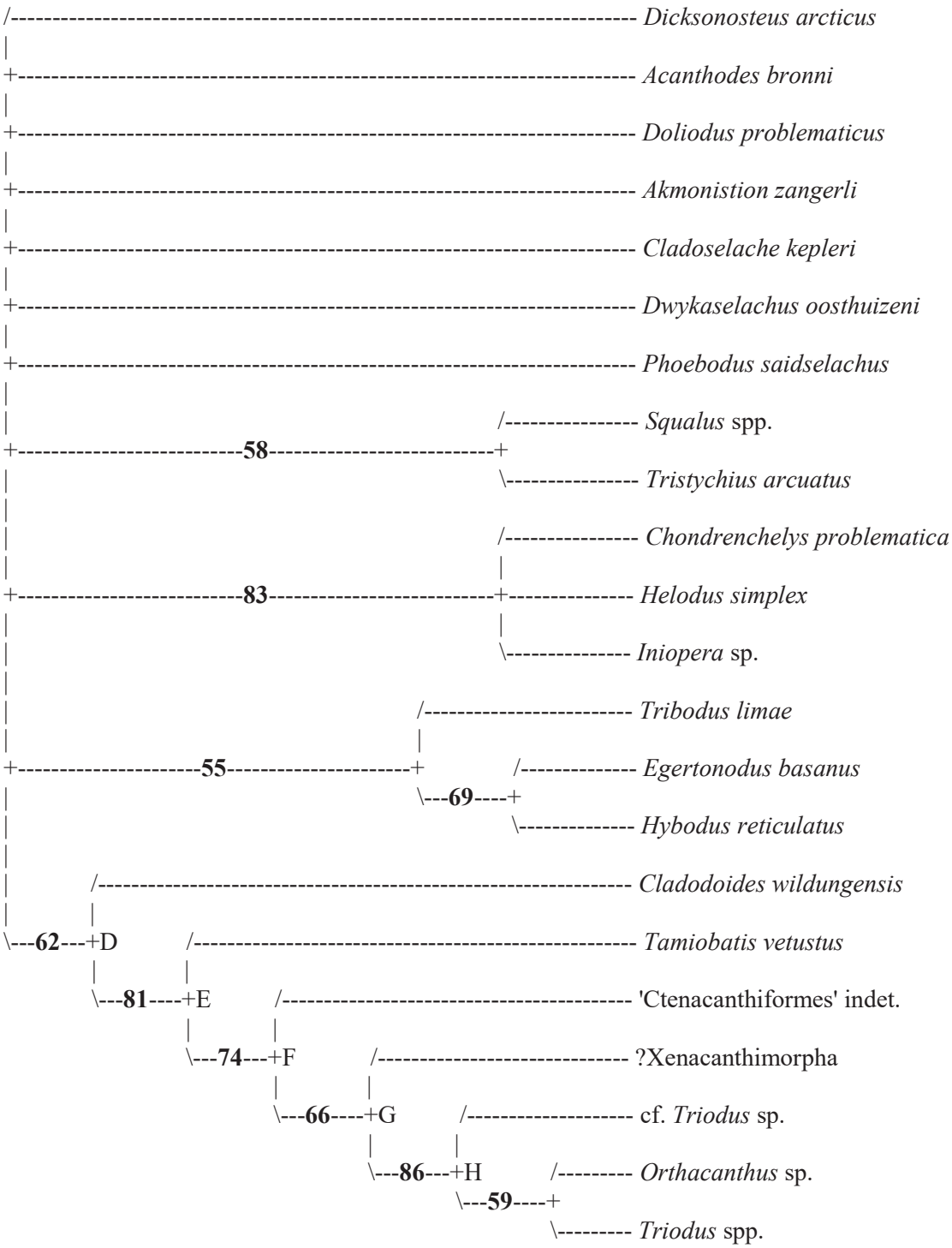

Figure S1. Bootstraps analysis with 1000 replicates from the same character matrix. Bootstrap 50% majority-rule consensus tree (Length = 79 steps, CI = 0.421, RI = 0.650). In this analysis, Euselachii, Holocephali, Symmoriiformes and *Phoebodus saidselachus* are not recovered as monophyletic, resulting in an important polytomy between them and the Ctencanthiformes-Xenacanthiformes clade (D). However, the Xenacanthiformes are better resolved with *Orthacanthus* sp. and *Triodus* spp. more

related with each other than with cf. *Triodus* sp., but with a low value (59). Despite low resolution, the clades E, F, G and H are recovered with the same diagnostic characters than in the previous heuristic research analysis (see the Apomorphy list) with relative high values. The clade D is defined by the same diagnosic characters minus Ch. 13^1 but with the addition of other characters (1^1, 2^1, 21^1, 23^1). Consequently, the same neurocranial transition between 'Ctenacanthiformes 'and Xenacanthiformes is also supported by the bootstrap analysis with PAUP. Letters denominating the clades are the same than in the figure 7 in the main text and the numbers are bootstrap values.

PAUP Display Buffer for the bootstrap analysis

P A U P * Version 4.0a (build 169) for 32-bit Microsoft Windows (built on Feb 10 2021 at 22:12:44)

Sun Jan 16 09:50:32 2022

Microsoft Windows

Data matrix has 22 taxa, 33 characters

Valid character-state symbols: 01234

Missing data identified by '?'

Gaps identified by '-'

2 taxa transferred to outgroup

Total number of taxa now in outgroup = 3

Number of ingroup taxa = 19

Bootstrap method with heuristic search:

Number of bootstrap replicates = 1000

Starting seed = generated automatically

Number of characters resampled in each replicate = 33

Optimality criterion = parsimony

Character-status summary:

Of 33 total characters:

All characters are of type 'unord'

All characters have equal weight

All characters are parsimony-informative

Gaps are treated as "missing"

Multistate taxa interpreted as uncertainty

Starting tree(s) obtained via stepwise addition

Addition sequence: random

Number of replicates = 1000

Starting seed = generated automatically

Number of trees held at each step = 1

Branch-swapping algorithm: tree-bisection-reconnection (TBR) with reconnection limit = 8

Steepest descent option not in effect

Initial 'Maxtrees' setting = 100

Branches collapsed (creating polytomies) if maximum branch length is zero

'MulTrees' option in effect

No topological constraints in effect

Trees are unrooted

1000 bootstrap replicates completed

Time used = 11:26:11 (CPU time = 11:25:42.2)

Paper 3: Systematics, ontogeny and palaeobiogeography of the genus *Orthacanthus* (Diplodoselachidae, Xenacanthiformes) from the lower Permian of France

Vincent Luccisano, Alan Pradel, Romain Amiot, Jean-Marc Pouillon, René Kindlimann, Jean-Sébastien Steyer, Gilles Cuny

Published in Papers in Palaeontology

Luccisano, V., Pradel, P., Amiot, R., Pouillon, J.-M., Kindlimann, R., Steyer, J.-S. & Cuny, G. (2022). Systematics, ontogeny and palaeobiogeography of the genus *Orthacanthus* (Diplodoselachidae, Xenacanthiformes) from the lower Permian of France. **Papers in Palaeontology**, 8(6), e1470.

Systematics, ontogeny and palaeobiogeography of the genus *Orthacanthus* (Diplodoselachidae, Xenacanthiformes) from the lower Permian of France

by Vincent Luccisano[1,2*], Alan Pradel[3], Romain Amiot[1], Jean-Marc Pouillon[4], René Kindlimann[5], Jean-Sébastien Steyer[3], Gilles Cuny[2]

[1]Univ Lyon, UCBL, ENSL, UJM, CNRS, LGL-TPE, F-69622, Villeurbanne, France; vincent.luccisano@univ-lyon1.fr.com, romain.amiot@univ-lyon1.fr

[2]Univ Lyon, Université Claude Bernard Lyon 1, CNRS, ENTPE, UMR 5023 LEHNA, F-69622, Villeurbanne, France; vincent.luccisano@gmail.com, gilles.cuny@univ-lyon1.fr

[3]CR2P - Centre de Recherche en Paléontologie - Paris ; Muséum National d'Histoire Naturelle - Centre National de la Recherche Scientifique- Sorbonne Université, France; alan.pradel@mnhn.fr, jean-sebastien.steyer@mnhn.fr

[4]Rhinopolis Association, 179 rue des Plattières 38300 Nivolas Vermelle/BP 39 03800 Gannat, France; jmpdb@wanadoo.fr

[5] Shark Museum, Zuerichstrasse 58, CH-8607 Aathal, Switzerland; mad_design@gmx.ch

*Corresponding authors

Abstract

The erection of *Orthacanthus buxieri* Heyler & Poplin from the lower Permian locality of Buxières-les-Mines (Allier, France) was based on a poorly prepared specimen displaying a few parts of its anatomy. The supposedly related teeth have been regarded as possibly belonging to *O. kounoviensis*, a species already known from the Carboniferous-Permian of Germany and Czech Republic. The holotype of *O. buxieri* requires extensive preparation work to be revised, but the description of *Orthacanthus* isolated teeth and dorsal spines from Buxières-les-Mines nevertheless provides useful information, especially since no precise description of this material has been provided so far. The aim of this description is to better understand the evolutionary history of the French *Orthacanthus* and its relationships with the other European species. The studied material is assigned to *O. kounoviensis*. This is the latest occurrence of this genus in Europe and the presence of both juvenile and adult teeth indicate that Buxières-les-Mines was probably one of the last suitable environments for its reproduction. We also identify

Orthacanthus cf. *kounoviensis* from the Muse oil-shale bed, the first record of this genus in the Autun Basin. It questions the relationships between the different Carboniferous-Permian basins of the Northern Massif Central that could still have been in connection during the lower Permian contrary to the central European basins that seem to be more isolated from each other.

Introduction

Xenacanthiformes are an order of Palaeozoic chondrichthyans (e.g. Zangerl 1981; Ginter *et al.* 2010). They appear during the early Carboniferous in Europe (Lebedev 1996) and rapidly spread worldwide (Hampe *et al.* 2006). They reach their top diversity around the Carboniferous-Permian transition in North America and Europe (e.g. Fritsch 1889, 1890; Schneider & Zajíc 1994; Johnson 1999; Hampe 2003), before diversifying in India and Australia during the late Permian and early Triassic (Richter 2005; Ginter *et al.* 2010). Their last record dates from the Norian of North America and India (Ginter *et al.* 2010). They are traditionally divided into two families (Ginter *et al.* 2010): Diplodoselachidae, including the most primitive Xenacanthiformes with a dorsal spine showing a rounded cross section with two posterior rows of denticles, and non-diphycercal, inequilobate caudal fin (Dick 1981); and the derived Xenacanthidae showing a dorso-ventrally flattened cross section of the dorsal spine with two lateral rows of denticles and a pseudo-diphycercal caudal fin (Schneider & Zajíc 1994) (see, however, Turner & Burrow [2011] for different phylogenetic relationships).

The Carboniferous-Permian fossils records of European Xenacanthiformes is composed of five genera (e.g. Schneider & Zajíc 1994): the diplodoselachid *Lebachacanthus* and *Orthacanthus*; and the xenacanthid *Xenacanthus*, *Triodus* and *Plicatodus*. They are encountered in supposed freshwater basins and are ecologically divided into the top predator diplodoselachids and the meso predator xenacanthids (e.g. Kriwet *et al.* 2008). Among the Diplodoselachidae, the different European species of *Lebachacanthus* and *Orthacanthus* are unequally distributed from the Bashkirian to the Sakmarian (Table 6; Ginter *et al.* 2010).

Among these *Orthacanthus* species, *Orthacanthus buxieri* Heyler & Poplin, 1989 from the Bourbon-l'Archambault Basin is not currently considered as valid (Hampe 2003; Ginter *et al.* 2010). Indeed, the holotype consists of a specimen mostly unprepared with a few parts of its anatomy being visible (Heyler & Poplin 1989). Based on isolated teeth and spines that have never been fully described yet (e.g. Heidtke 1998; Steyer *et al.* 2000), several authors have considered *O. buxieri* as a possible synonyme of *O. kounoviensis* from Germany and the Czech

Table 6. Occurrences of the Carboniferous-Permian *Lebachacanthus* and European *Orthacanthus*.)

Species	Age	Occurrences	References
Lebachacanthus senckenbergianus	Kasimovian-Asselian	Saar-Nahe Basin, Germany	Heidtke (2007)
Lebachacanthus ventricosus	Kasimovian	Kounova, Czech Republic	Heidtke (1998)
Orthacanthus cf. kounoviensis	Asselian	Autun, France	This work
Orthacanthus buxieri	Asselian-Sakmarian	Bourbon-l'Archambault Basin, France	Heyler & Poplin (1989)
Orthacanthus meridionalis	Gzhelian	Puertollano, Spain	Soler-Gijón (1997)
Orthacanthus gracilis	Moscovian-Gzhelian	Saar-Nahe Basin, Germany; Hagley, United Kingdom	Giebel (1848), Hampe (1994, 2003)
Orthacanthus kounoviensis	Moscovian-Sakmarian	Saar-Nahe Basin, Germany; Kounova, Czech Republic; Ardwick, United Kingdom; Bourbon-l'Archambault, France.	Fritsch (1889), Hampe (1994, 2003), this work
Orthacanthus bohemicus	Moscovian	Plzen Basin, Czech Republic	Fritsch (1889)
Orthacanthus denticulatus	Bashkirian-Moscovian	West Yorkshire, Northumberland and Lancashire, United Kingdom	Hampe (2003)
Orthacanthus gibbosus	Bashkirian-Moscovian	Glasgow, Greater Manchester, Tyne & Wear, West Midlands and West Yorkshire, United Kingdom	Hampe (2003)
Orthacanthus cylindricus	Bashkirian-Moscovian	Unknown, United Kingdom	Agassiz (1843)

Republic (Hampe 2003; Ginter *et al.* 2010). Furthermore, *Orthacanthus* remains from the French Carboniferous-Permian are sparse: in the lowermost Permian of the Muse oil-shale beds (OSB) of the Autun Basin, a single tooth has been described by Heyler (1969), which is redescribed here. Moreover, *Orthacanthus* remains have been tentatively mentioned during recent excavation campaigns (Gand *et al.* 2015) but these fossils may rather belong to the genus *Triodus*. So, little is known about the distribution of *Orthacanthus* in the Northern Massif central. In this study, we propose to describe *Orthacanthus* material from Buxières-les-Mines (Bourbon-l'Archambault Basin) and Muse (Autun Basin) to test the presence of *O. kounoviensis* in the lower Permian of France.

Geological setting

The Bourbon-l'Archambault Basin is located in the Northern Massif Central (Fig. 66A; Allier, France; Châteauneuf 1980; Châteauneuf & Farjanel 1989) is part of a large set of Carboniferous-Permian non-marine basins (Gand *et al.* 2015, 2017). It extends approximately on 30 km x 20 km. It is structurally divided into two sub-basins (Fig. 66B; Châteauneuf & Farjanel 1989; Steyer *et al.* 2000): the Aumance sub-basin on the West and the Souvigny sub-basin on the East, separated from each other by the 'Gipcy-Bourbon ridge'. The sedimentary deposits, which are mostly composed of conglomerates, alluvial arkoses, palustrine coal seams and bituminous black shales, fluvial sandstones and thin pyroclastic horizons (Roscher & Schneider 2006) extend stratigraphically from the late Carboniferous to the Triassic (e.g. Steyer *et al.* 2000). However, the most geologically and palaeontologically investigated parts of this basin are dated from the late Pennsylvanian (upper Carboniferous) to the middle Cisuralian (lower Permian). According to some authors (Steyer *et al.* 2000; Roscher & Schneider 2006), the Bourbon-l'Archambault Basin was deposited in a freshwater setting, even if potential marine influences have sometimes been suggested (Schultze & Soler-Gijón 2004; Schultze 2009).

The former open-cast coal mine of Buxières-les-Mines is located in the southern part of the Aumance sub-basin (Fig.66B; Steyer *et al.* 2000). Stratigraphically, Buxières-les-Mines is situated in the Supra-Buxières Member in the upper part of the Buxières Formation of the Bourbon-l'Archambault Basin (Fig. 67A; Steyer *et al.* 2000). Even if the Carboniferous-Permian transition is barely known in the Bourbon-l'Archambault Basin, the Buxières-les-Mines locality has been considered as early Permian in age (Fig. 67A; e.g. Steyer *et al.* 2000; Roscher & Schneider 2006). Correlated with the lower 'Autunian' local age (Debriette 1992; Steyer *et al.* 2000), the Buxières Formation is supposed to extend from the latest Asselian to the middle Sakmarian, inducing a Sakmarian age for the Supra-Buxières Member (Roscher & Schneider 2006; Schneider & Werneburg 2006; but see Steyer [2000] for methodological problems). Recently, the volcanic tuffs 'Lien Blanc' was dated to 294.6 +/-3.2 Ma (Fig. 67B; Ducassou *et al.* 2018) and the 'Lien Vert' to 295 Ma (S. Bourquin, pers. comm. [2022]), which implies a late Asselian to early Sakmarian age for this locality. The palaeoenvironment of Buxières-les-Mines is interpreted as a lacustrine and/or palustrine environment interspersed by several period of drying up (Kaulfuß 2003) without direct evidence of marine influences contrary to Schultze & Soler-Gijón's (2004) opinion.

The Muse OSB is located in the Autun Basin, East of the Bourbon-l'Archambault Basin (Fig. 66C). Some xenacanth remains from this locality have recently been revised (Luccisano.

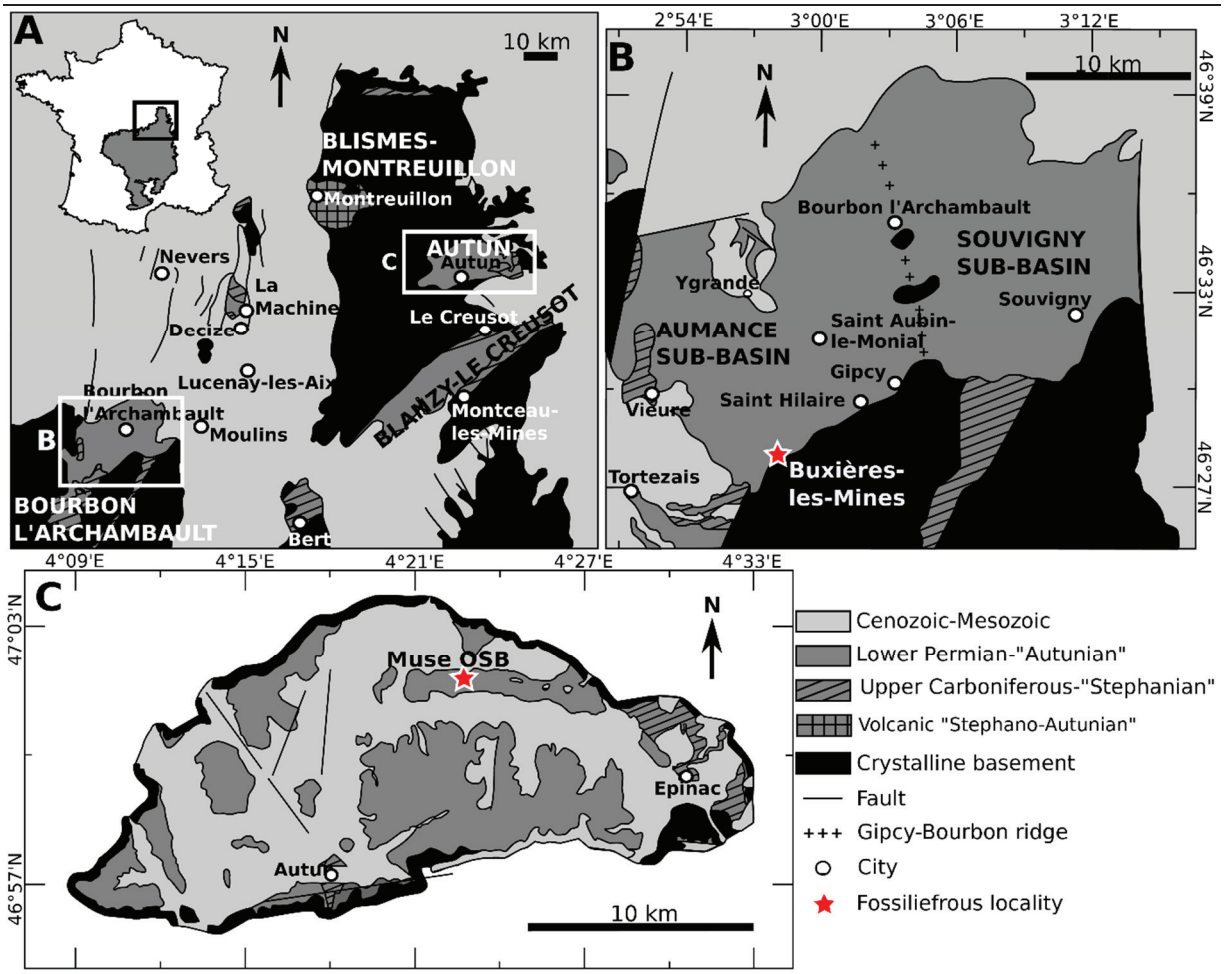

Figure 66. Geological context of the Buxières-les-Mines and Muse OSB localities. **A**, simplified geological map of the Carboniferous-Permian basins from the French Northern Massif central. **B**, simplified geological map of the Bourbon-l'Archambault basin and location of Buxières-les-Mines. **C**, simplified geological map of the Autun Basin and location of the Muse OSB (modified from Steyer *et al.* 2000; Pellenard *et al.* 2017; Luccisano *et al.* 2021b,c).

2021a). Two volcanic layers were dated to 298.05 +/- 0.39 Ma and 298.57 +/- 0.38 Ma (Fig. 67D; Pellenard *et al.* 2017), indicating a lowermost Permian age for the Muse OSB. A recent sedimentological study has postulated that this locality represents a marginal lacustrine environment (Mercuzot 2020; Mercuzot *et al.* 2022).

Material and methods

Material

Most of the isolated teeth and the two dorsal spines considered in this work were found in the Buxières-les-Mines open-cast coal mine between 1996 and 2005, during excavation

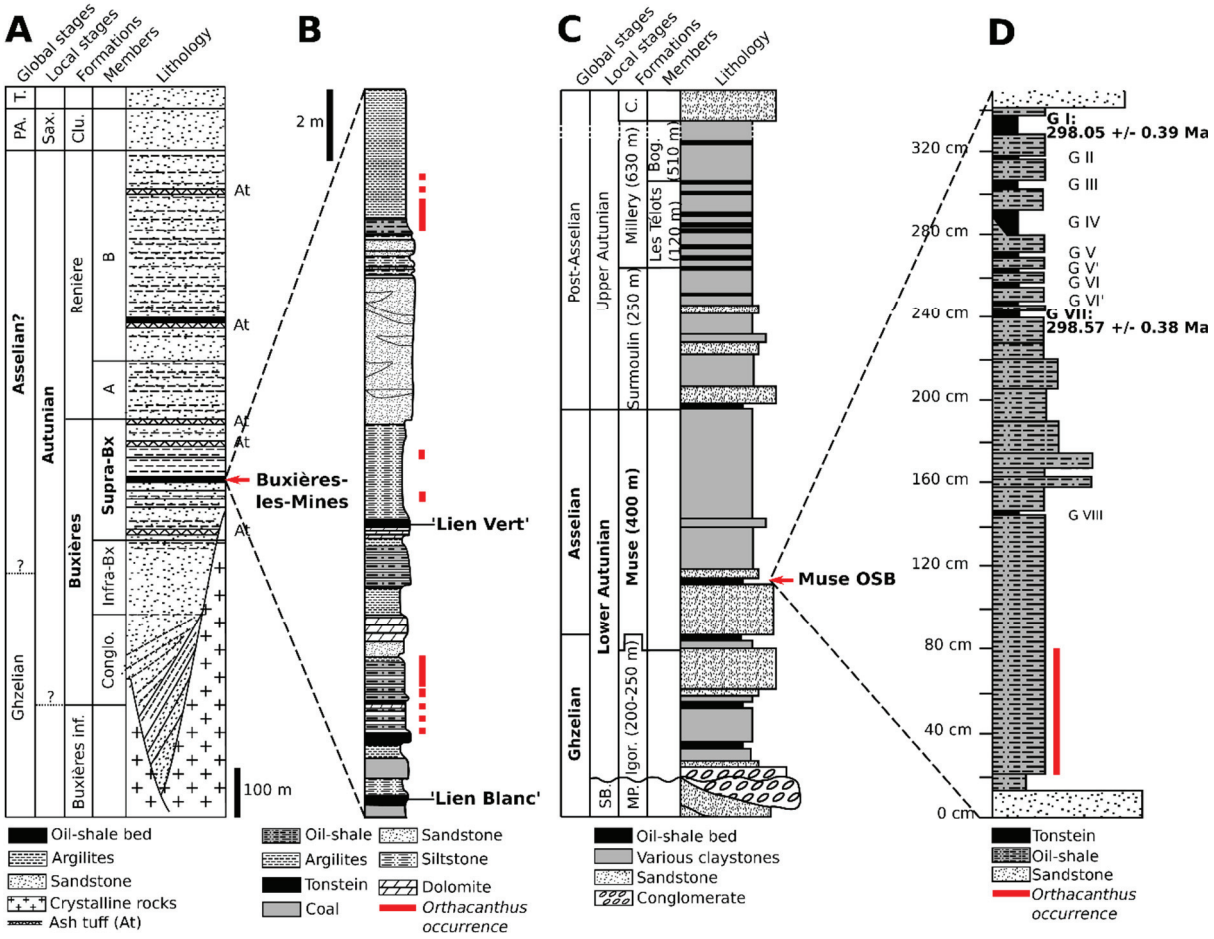

Figure 67. Stratigraphical context of the Buxières-les-Mines and Muse OSB localities. **A**, simplified stratigraphy of the Bourbon-l'Archambault basin with location of Buxières-les-Mines. **B**, simplified stratigraphy of the Buxières-les-Mines locality. **C**, simplified stratigraphy of the Autun Basin and location of the Muse OSB. **D**, simplified stratigraphy of the Muse OSB locality. **Abbreviations**: **Bog**, Boghead; **BX**, Buxières; **Conglo**, Conglomerate; **C**, Curgy formation **Clu**, Clusor; **Igor**, Igornay; **MP**, Mont Pelé; **PA**, post-Asselian; **Sax**, 'Saxonian'; **SB**, 'Stephanian B' (modified from Steyer *et al.* 2000; Pellenard *et al.* 2017; Luccisano *et al.* 2021a,c).

campaigns of the Rhinopolis Association headed by two of us (JMP and JSS). This material is currently housed in the *Muséum d'Histoire Naturelle et d'Ethnographie de Colmar* (MHNE, France). Other teeth come from the *Muséum National d'Histoire Naturelle* (MNHN, Paris, France) and from the Palaeontological Institute and Museum at the University of Zurich (PIMUZ, Switzerland).

The stratigraphic origin of most of the specimens from Buxières-les-Mines was recorded during the excavation process (Fig. 67B; Steyer & Escuillié 1997; Steyer *et al.* 2000). Most of the chondrichthyan material, including those considered here, was found between the volcanic tuffs 'Lien Blanc' and 'Lien Vert' (JMP, pers. obs. [2021]; Fig. 67B). The material from Muse

redescribed here, which consist of a single large tooth, comes from the historical collections of the MNHN and its stratigraphic position was less constrained. However, recent stratigraphical investigations and datings of this locality (Pellenard *et al.* 2017) allow to cautiously locate this specimen at the base of the Muse series (Fig. 67D).

Nomenclature

We follow Schneider's nomenclature (1985, 1996) to describe Xenacanthiformes teeth (Fig. 68). We follow the Xenacanthiformes systematics established by Ginter *et al.* (2010) with additional information from Hampe (2003) and Johnson & Thayer (2009) for the genus *Orthacanthus* and from Heidtke (1998) for *Lebachacanthus*.

The fractions ($^{x}/_{y}$) used in the description part correspond to the occurrences of the considered character (x) out of the total observed (y).

Institutional abbreviations

MHNE, Muséum d'Histoire Naturelle et d'Ethnographie de Colmar, MNHN, Muséum National d'Histoire Naturelle, PIMUZ, Palaeontological Institute and Museum at the University of Zurich.

Systematic palaeontology

Class Chondrichthyes Huxley, 1880
Order Xenacanthiformes Berg, 1937
Family Diplodoselachidae Dick, 1981
Genus *Orthacanthus* Agassiz, 1843

Type Species—Orthacanthus cylindricus Agassiz, 1843 (a junior synonym of *O. gibbosus* (Binney 1840) following Hampe [2003]).

Type Locality—Unknown for *O. cylindricus* (following Hampe 2003). For *O. gibbosus*: Silverdale, Staffordshire, United-Kingdom; Coal Measures, Moscovian, Pennsylvanian, Carboniferous (following Hampe 2003).

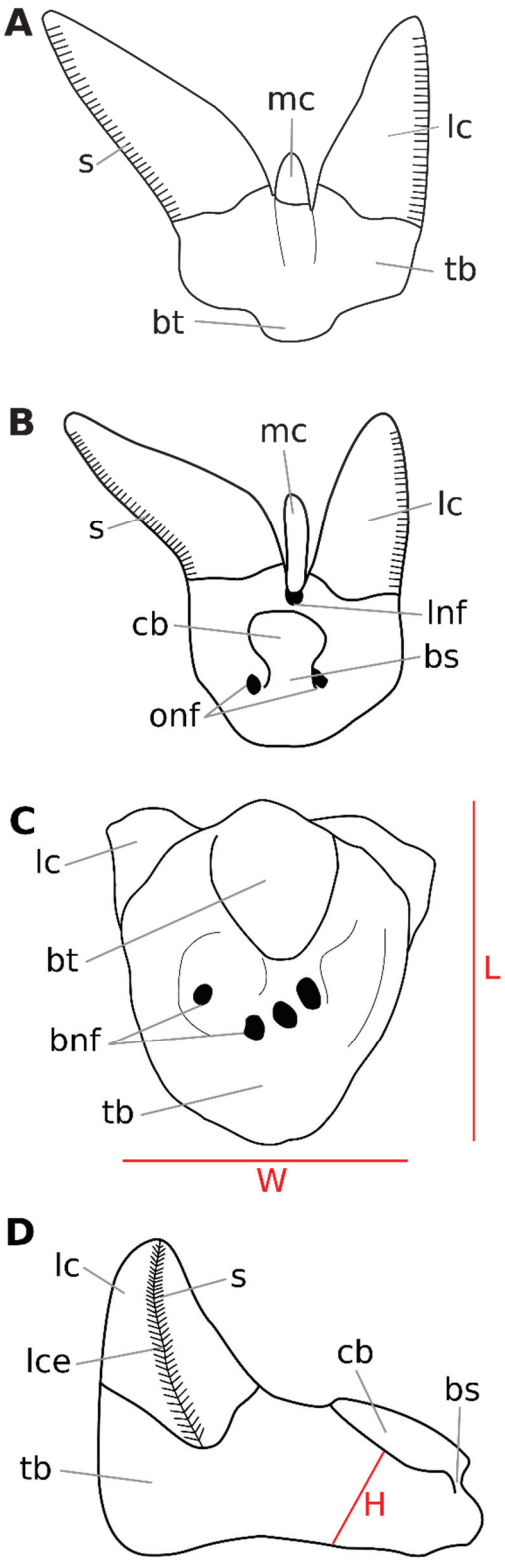

Figure 68. Dental nomenclature used in this work. **A**, labial. **B**, oral. **C**, basal. **D**, lateral view. **Abbreviations**: **bnf**, basal nutrient foramina; **bt**, basal tubercle; **bs**; button shaft; **cb**, coronal button; **H**, height; **L**, length; **lc**, lateral cusps; **lce**, lateral cutting edge; **lnf**; labial nutrient foramina; **mc**, median cusp; **onf**; oral nutrient foramina; **s**, serration; **tb**, tooth base; **W**, width (modified from Schneider 1985, 1996; Hampe 1994).

Included Species—European species: *O. denticulatus* Davis, 1880; *O. kounoviensis* Fritsch, 1889; *O. gracilis* (Giebel, 1848); *O. bohemicus* Fritsch, 1879; *O. meridionalis* (Soler-Gijón, 1997a; *O. buxieri* Heyler & Poplin, 1989. Species from the United States: *O. donnelljohnsi* Johnson & Thayer, 2009; *O. compressus* (Newberry, 1856); *O. huberi* Zidek, 1992; *O. texensis* (Cope, 1888); *O. platypternus* (Cope, 1884).

Diagnosis (following Hampe 2003)—Teeth tricuspid, characterised by large lateral cusps and consistently minute median cusp; at least serration on the lanceolate, dagger-shaped lateral cusps; median foramen on the upper side in front of the median cusp; basal tubercle without concave depression; histological structure: cusps constructed of orthodentine; dorsal spine straight and slender.

Remarks—Current *Lebachacanthus* species were considered as belonging to *Orthacanthus* (Fritsch 1889). Soler-Gijón (1997b) erected the genus *Lebachacanthus* and the family Lebachacanthidae based on dental, cranial and non-cranial characters. Even if the Lebachacanthidae is not considered as valid, the short and wide dorsal spine justifies the validity of *Lebachacanthus* (Ginter *et al.* 2010) contrary to Heidtke's opinion (1998) who considered it as a sub-genus of *Orthacanthus*.

Orthacanthus commailli (Heyler & Poplin, 1982) was based on a poorly preserved neurocranium. A recent revision (Luccisano *et al.* 2021c) has demonstrated that the specimen does not belong to the Xenacanthiformes.

***Orthacanthus kounoviensis* Fritsch, 1889**

(Figs. 69–73; Tables 7–9)

1997 *Orthacanthus buxieri* Steyer & Escuillié, p. 17.
1998 *Orthacanthus* (*Orthacanthus*) *buxieri* Heidtke, p. 141, fig. 6.
2000 *Orthacanthus* (*Orthacanthus*) *buxieri* Steyer *et al.*, p. 243, pl. 1B.
2010 *Orthacanthus kounoviensis* Ginter *et al.*, p. 48.

Syntype—The entire original material in Fritsch (1889); pl. 83, fig. 1, pl. 86, fig. 4, pl. 87, figs. 1–2, 5; Národni Muzeum, Prague, Czech Republic.

Referred Material—Isolated teeth: MHNE.2021.14.1, MHNE.2021.14.2, MHNE.2021.14.3.1, MHNE.2021.14.3.2, MHNE.2021.14.3.3, MHNE.2021.14.3.4, MHNE.2021.14.4, MHNE.2021.14.5, MHNE.2021.14.6, MHNE.2021.14.7, MHNE.2021.14.8, MHNE.2021.14.9, MHNE.2021.14.10, MHNE.2021.14.11, MHNE.2021.14.12, MHNE.2021.14.13, MHNE.2021.14.14, MHNE.2021.14.15, MHNE.2021.14.16, MHNE.2021.14.17, MHNE.2021.14.18, MHNE.2021.14.19, MHNE.2021.14.20, MHNE.2021.14.21, MHNE.2021.14.22, MHNE.2021.14.23, MHNE.2021.14.24, MNHN.F.BU7, MNHN.F.BU8, PIMUZ A/I 5121, PIMUZ A/I 5122, PIMUZ A/I 5123, PIMUZ A/I 5124, PIMUZ A/I 5125, PIMUZ A/I 5126, PIMUZ A/I 5127, PIMUZ A/I 5128, PIMUZ A/I 5129, PIMUZ A/I 5130, PIMUZ A/I 5131, PIMUZ A/I 5132, PIMUZ A/I 5133, PIMUZ A/I 5134.

Type locality—Kounová, Pilsen basin, Czech Republic.

Type horizon—Kounová layer, Gzhelian (‘Stephanian B’), Pennsylvanian, Carboniferous.

Other occurrence—Saar-Nahe Basin, Germany (Hampe 1994); Former open-cast coal mine of Buxières-les-Mines, Allier, France (this study).

Horizon—Most of the material studied here come from between the ‘Lien Blanc’ and the ‘Lien Vert’ volcanic tuffs, which are late Asselian to early Artinskian, Cisuralian, Permian (Ducassou *et al.* 2018).

Emended diagnosis based on teeth only—Total height between 5 and 23 mm; height of the median cusp less than $^1/_5$ that of lateral cusps; often with a blunt top; accessory median cusp relatively frequent; lateral cusps with lanceolate cross-section and edges showing a double serration; simple or complex secondary serration pattern; lack of serration on the median cusp; outline of the base penta- or hexagonal; upper side of the base showing a relatively small, nearly heart-shaped coronal button and tiny nutrient foramina; basal side slightly convex with strongly extended basal tubercle without concave depression and two to six nutrient foramina, partially placed on the periphery, away from the basal tubercle.

Remark—Orthacanthus buxieri from Buxières-les-Mines was erected by Heyler & Poplin (1989) based on an unprepared and almost disarticulated specimen, partially showing the

neurocranium, the scapulocoracoid and the palatoquadrate. Heidtke (1998) described another specimen with articulated neurocranium, jaws, branchial and scapular regions and dorsal spine. As no tooth was described (Steyer *et al.* [2000] only illustrated one tooth) and no diagnostic character has been defined for the genus *Orthacanthus* on other anatomical parts, this species is considered as doubtful and synonymized with *O. kounoviensis* by Hampe (2003) and Ginter *et al.* (2010).

Description

Adult teeth—The teeth (Figs 69–70) are tricuspid with two high lateral cusps and a small median cusp that reaches from $^{1}/_{5}$ to less than $^{1}/_{6}$ of the height of the lateral ones. Their tooth base size ranges approximatively from 10 to 20 mm (Fig. 71), and their height reaches 16.5 mm for those which have complete cusps (Table 7). The lateral cusps are labio-lingually compressed and have a blunt apex. The cusps have a lanceolate cross-section that forms developed lateral cutting edges, but the median one can be oval at its base. The median cusp can form a labial bulging. The posterior lateral cusp can be more or less curved toward the posterior edge depending on its position on the jaw. A serration is present on the lateral cusps but never seen on the median cusp. The serration always occurs on the external cutting edge and sometimes (4 out of 18 teeth) on the internal one. The serration extends all along the cusps and a distinct pattern of double serration can be present ($^{8}/_{19}$). This double pattern is complex with double secondary serrations between two primary serrations (Fig. 70L). At the base of the cusps of the largest teeth in labial view, small depressions formed by their pronounced lanceolate cross-section can occur ($^{10}/_{19}$). The angle between the crown and the base of the teeth is between 95° and 120°. In oral view, the coronal button is rectangular to heart-shaped and is positioned on the lingual part of the lingual torus, not in contact with the cusps. Between the cusps and the coronal button, a pronounced fossa is present, and it can be developed into a foramen. There are between 2 and 4 oral nutrient foramina always situated on the lingual side of the coronal button. In a few teeth, the slightly elongated shape of the coronal button can produce a very small lingual shaft. In basal view, the tooth base has a pentagonal and asymmetric shape. The basal tubercle never displays a central depression and is always situated on the labial side of the base. The basal tubercle can be more or less rounded depending on the degree of wear of the tooth. In lateral view, it is labially displaced, forming an angulous labial edge between the crown and the tooth base. On the lingual side of the basal tubercle, a weak lingual shaft is present. On each side of this lingual shaft, depressions are present. The more the depressions are developed, the more the lingual shaft is pronounced. There are usually between 2 and 6

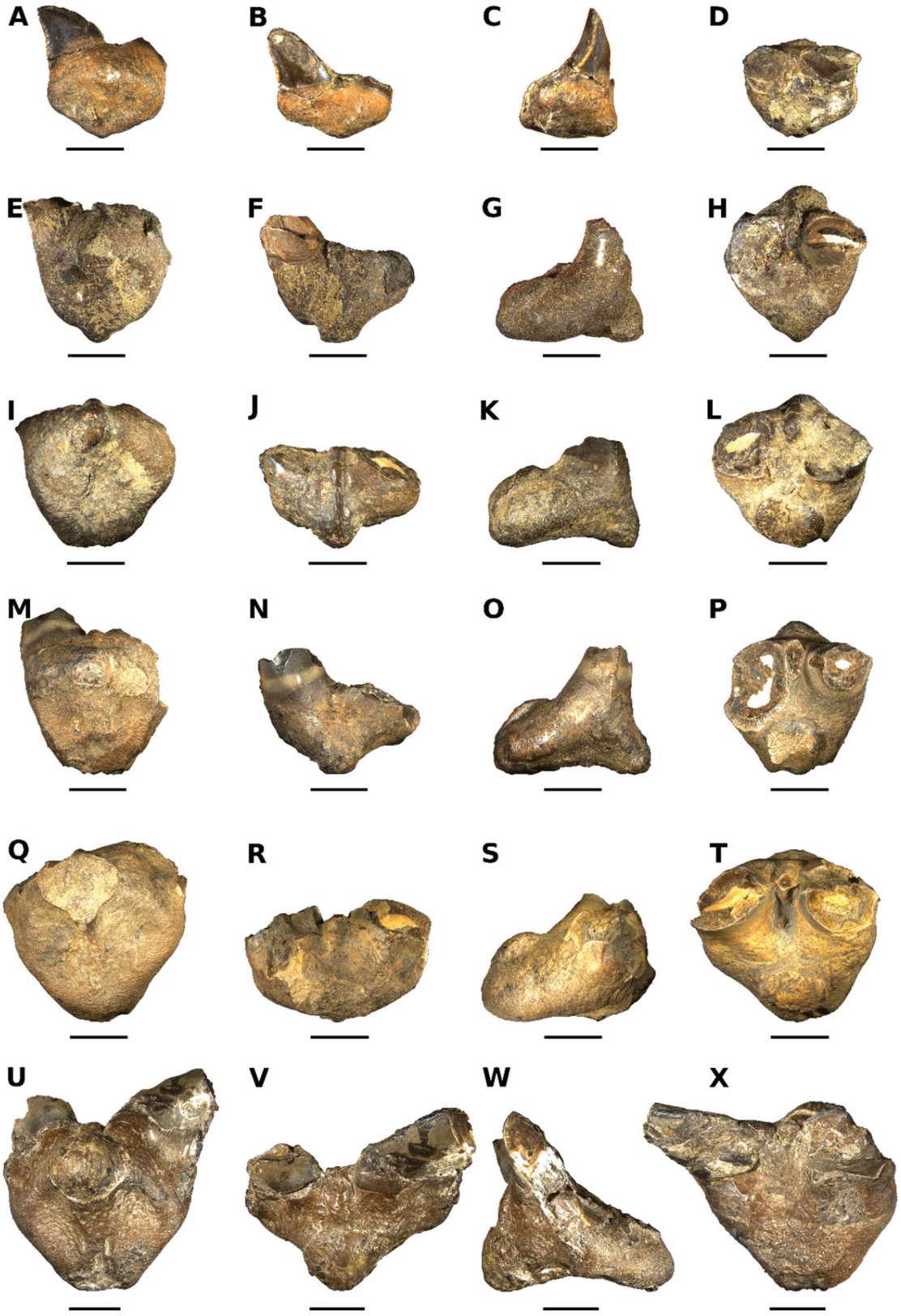

Figure 69. Isolated adult teeth of *Orthacanthus kounoviensis* from Buxières-les-Mines. **A–D**, MHNE.2021.14.18. **E–H**, MHNE.2021.14.19. **I–L**, MHNE.2021.14.22. **M–P**, MHNE.2021.14.23. **Q–T**, MHNE.2021.14.24. **U–X**, MHNE.2021.14.13. (**A**, **E**, **I**, **M**, **Q**, **U**) in basal view. (**B**, **F**, **J**, **N**, **R**, **V**) in labial view. (**C**, **G**, **K**, **O**, **S**, **W**), lateral. (**D**, **H**, **L**, **P**, **T**, **X**), oral view. Scale bar: 5 mm.

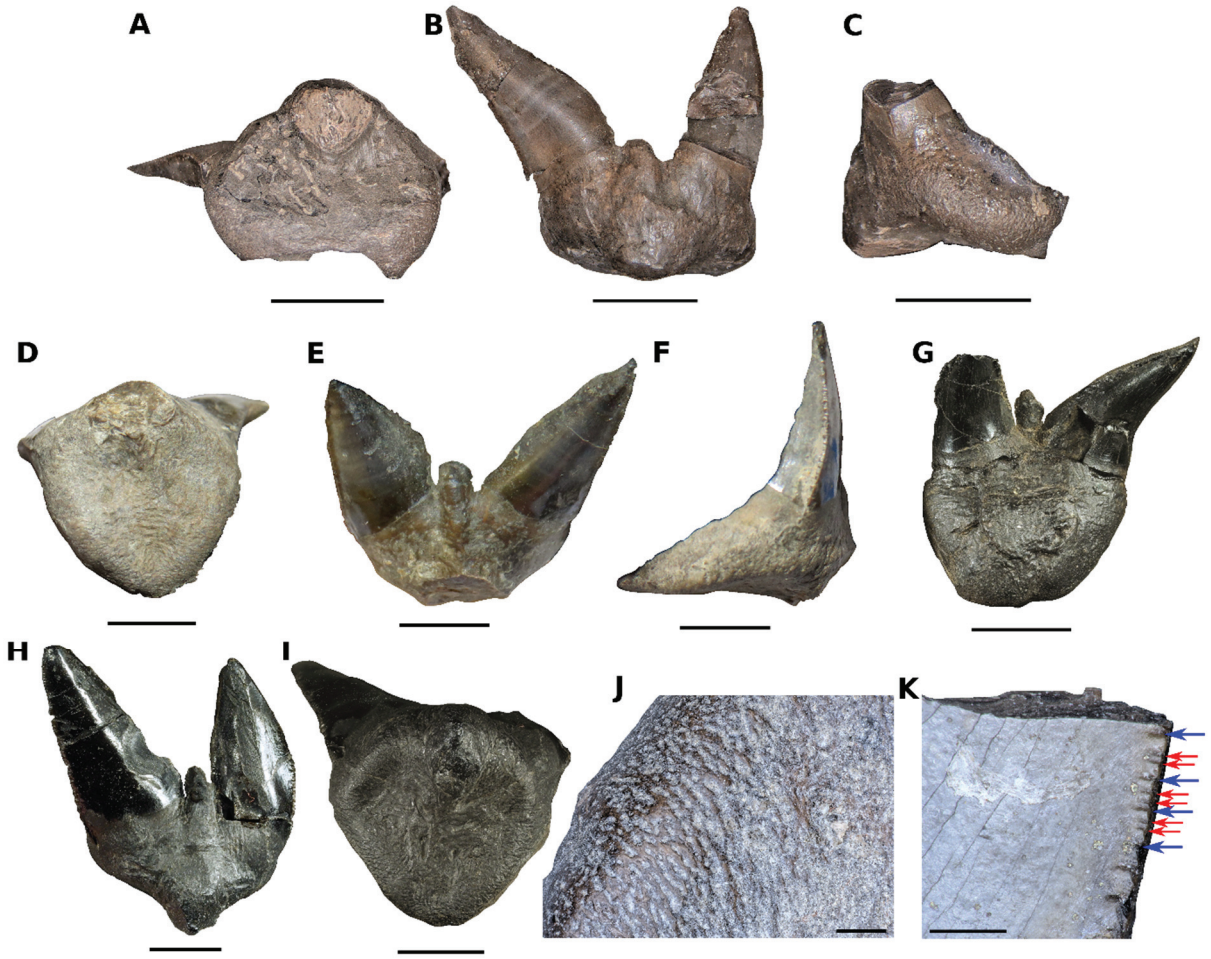

Figure 70. Isolated adult teeth of *Orthacanthus kounoviensis* from Buxières-les-Mines. **A–C**, MNHN.F.BU8. **D–F**, MHNE.2021.14.11. **G**, PIMUZ A/I 5131. **H–I**, PIMUZ A/I 5133. **J–K**, MHNE.2021.14.13. **J**, tooth base ornamentation. **K**, double serration pattern. (**A**, **D**, **I**), basal. (**B**, **E**, **H**), labial. (**C**, **F**), lateral. (**D**, **I**), oral view. Blue arrows are primary serration and red arrows are secondary serration. Scale bar: 5 mm (**A–I**), 1 mm for **J** and 500 µm for **K**.

basal nutrient foramina situated on the lingual side of the tooth base for the largest ones or in the middle of the tooth base for the smallest ones. A thin spotted and sometimes elongated ornamentation ($^{14}/_{19}$) is visible on the tooth base outline, on the basal tubercle, on the coronal button and in the middle of the tooth base in basal view (Fig. 70K). This ornamentation is more pronounced in the largest teeth.

Juvenile teeth—The teeth (Fig. 72) have small median cusp that reaches $^{1}/_{5}$ or less of the size of the lateral ones. One tooth has a median cusp divided in three (Fig. 72N). One tooth (Fig. 72E–H) has a labial bulging formed by the median cusp. The serration occurs on the external cutting edge but not on the internal one. Two teeth do not show serration. A double serration is

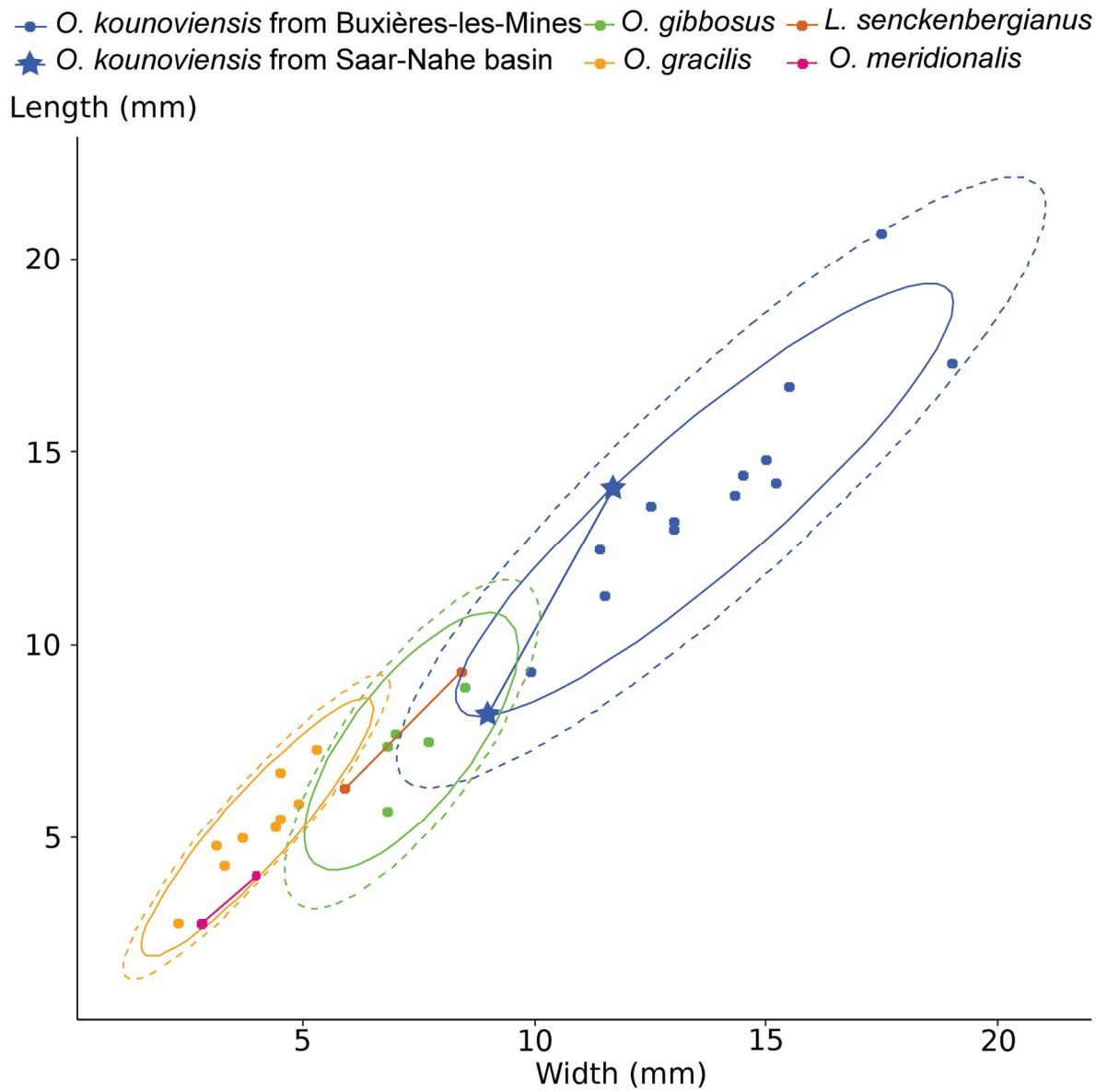

Figure 71. Width-length biplot of *Orthacanthus kounoviensis* adult teeth from Buxières-les-Mines and comparisons with other European *Orthacanthus* species. *O. gibbosus* is from Hampe (2003), *O. kounoviensis* from the Saar-Nahe basin is from Hampe (1994), *Lebachacanthus seckenbergianus* is from Heidtke (1982), *O. gracilis* is from Hampe (1994) and *O. meridionalis* is from Soler-Gijón (1997a).

Table 7. Measurements (in mm) of adult and juvenile teeth of *Orthacanthus kounoviensis* from Buxières-les-Mines.

	Adult teeth					Juvenile teeth				
	n	**Min**	**Mean**	**Max**	**sd**	**n**	**Min**	**Mean**	**Max**	**sd**
Length	14	9.3	14.2	20.7	0.28	15	3.8	5.5	6.6	0.09
Width	18	8.7	13.3	19.0	0.26	15	3.5	5.3	6.2	0.07
Height	6	7.2	13.2	16.5	0.38	14	3.7	5.6	7.5	0.14
Thickness	11	2.8	4.8	6.7	0.1	8	1.0	1.4	1.7	0.02

Abbreviations: n, number of samples; sd, standard deviation.

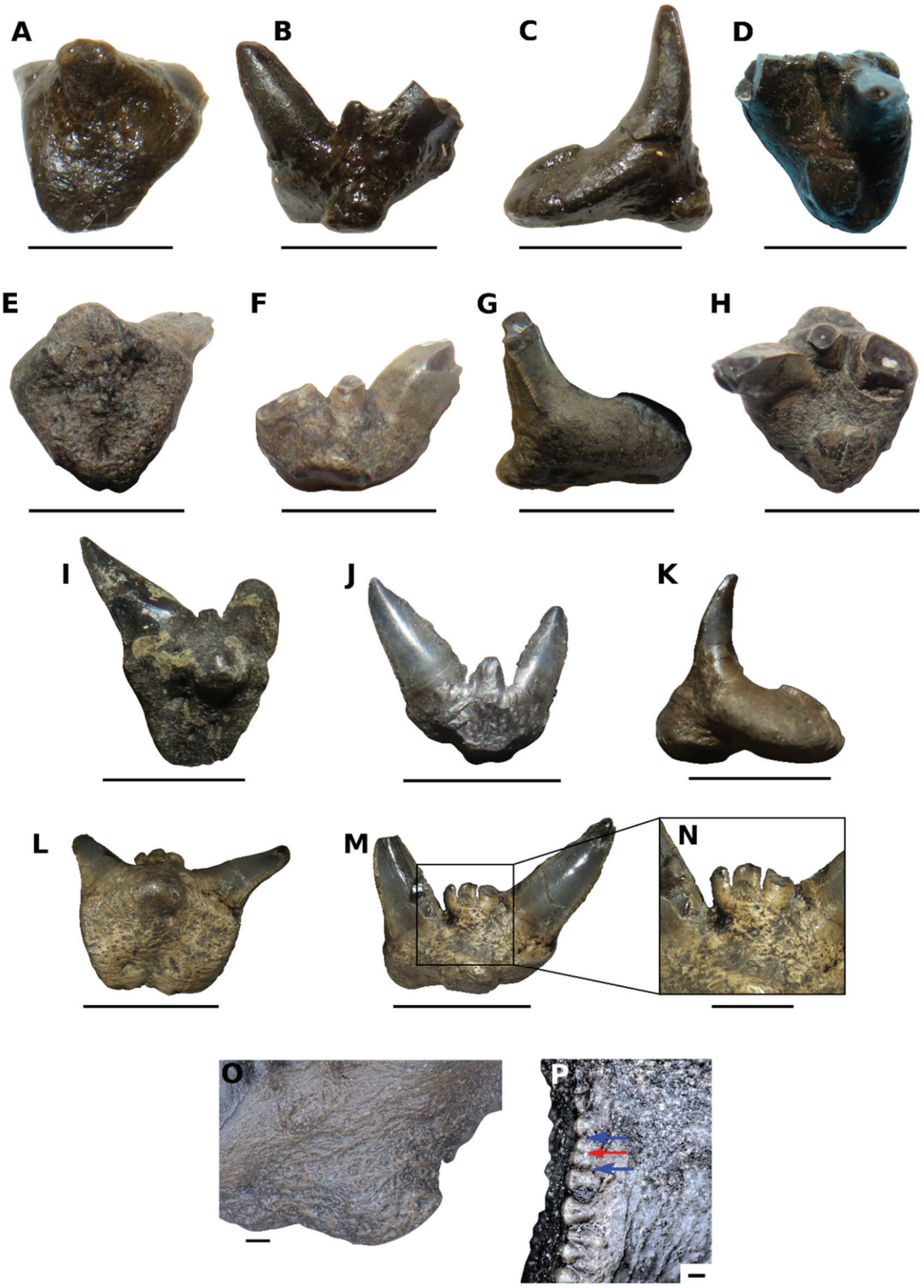

Figure 72. Isolated juvenile teeth of *Orthacanthus kounoviensis* from Buxières-les-Mines. **A–D**, MHNE.2021.14.10. **E–H**, MHNE.2021.14.5. **I**, MHNE.2021.14.9. **J**, MHNE.2021.14.12. **K**, MHNE.2021.14.4. **L–N**, PIMUZ A/I 513. **O**, tooth base ornamentation of MHNE.2021.14.7. **P**, double serration of MHNE.2021.14.3. (**A**, **E**, **I**, **L**), basal. (**B**, **F**, **J**, **M–N**), labial. (**C**, **G**, **K**), lateral. (**D**, **H**), oral view. Blue arrows are primary serration and red arrow is secondary serration. Scale bar: 5 mm (**A–M**), 2mm for **N**, 200 µm for **O** and 100 µm for **P**.

present ($^{6}/_{21}$): this double pattern is simple with a single secondary serration between two primary serrations (Fig. 72P). In oral view, the coronal button is oval to heart-shaped and positioned on the lingual part of the lingual torus. Between the cusps and the coronal button, a foramen can be present ($^{2}/_{21}$). There are between 4 and 8 oral nutrient foramina situated on the lingual and lateral sides of the coronal button. In basal view, the tooth base has a pentagonal, sometimes rhomboid, and asymmetric shape. The basal tubercle can be labially displaced ($^{5}/_{21}$), forming an angular labial edge between the crown and the tooth base. On the lingual side of the basal tubercle, a weak lingual shaft can be present. There are usually between 3 and 12 basal nutrient foramina. Few are situated on the lingual side of the base for the largest ones, and numerous small ones occur in the middle of the tooth next to the basal tubercle. A spotted ornamentation ($^{13}/_{21}$) is visible on the tooth base, mainly on the outlines.

Comparisons

Adult teeth—The tricuspid lanceolate teeth (Figs. 69–70) associated with a developed lingual torus that bears a coronal button are characteristic of Xenacanthiformes (e.g. Ginter *et al.* 2010). The labio-lingually compressed lanceolate cusps, the minute median cusps and the serration of the lateral cutting edges of the lateral cusps clearly evokes the genera *Orthacanthus* and *Lebachacanthus* (e.g. Ginter *et al.* 2010).

Orthacanthus and *Lebachacanthus* possess heterodont dentition (Hampe 1988a; Soler-Gijón 1997a,b). The material from Buxières-les-Mines is likely represented by posterolateral teeth due to the asymmetric shape of their base and the presence of a median cusp. The teeth of *Orthacanthus* and *Lebachacanthus* are very similar (Hampe 2003; Ginter *et al.* 2010). These genera are usually differentiated by their dorsal spine, which is near the cranial region, elongated and long in *Orthacanthus*; whereas it is near the scapular region, broad and short in *Lebachacanthus* (Heidtke 1998; Ginter *et al.* 2010). The only dental difference between them relies in the cusp of lateral teeth which is straight, pointed and dagger-shaped in *Lebachacanthus* (Ginter *et al.* 2010), whereas it has a blunt apex and a tendency to be curved in posterior teeth in *Orthacanthus* (Hampe 2003). The teeth from Buxières-les-Mines correspond to those of *Orthacanthus* by their blunt apex and the curvature of the posterior lateral cusp.

Among the genus *Orthacanthus*, the type species *O. cylindricus* (Agassiz 1843) and the species *O. denticulatus* (Davis 1880) and *O. huberi* (Zidek 1992) are known by isolated dorsal spines only. *O. buxieri* is known by more material: neurocrania, palatoquadrates,

scapulocoracoids and dorsal spines (Heyler & Poplin 1989; Heidtke 1998) and a figured tooth (Steyer *et al.* 2000). Among the species known by their teeth, *O. platypternus* (e.g. Johnson 1999, 2018) and *O. donnelljohnsi* (Johnson & Thayer 2009) differ from the present material by their absence of serration on the lateral cutting edges. The small median cusp and the shape of the pentagonal tooth base of the studied material are different from those of *O. texensis* (e.g. Johnson 1999), *O. compressus* (e.g. Johnson 1999, 2012), *O. gracilis* (Hampe 1994) and *O. gibbosus* (Hampe 2003), where the tooth base is rounded, oval or rhomboid but never pentagonal. *O. meridionalis* (Soler-Gijón 1997b) differs by its rhomboid coronal button and its low angle of almost 90° between the crown and the base, contrary to the heart-shaped coronal button and the crown-base angle that ranges from 95° to 120° in our specimens. *O. bohemicus* (Fritsch 1889) is different by its high median cusp that usually reaches $^1/_3$ of the size of the lateral cusps and by the more frequent presence of a lingual shaft on the coronal button. Ornamentation of the tooth base seems to vary within *Orthacanthus*. Hampe (2003) notes that *O. gibbosus* possesses a unique and primitive scarred surface of the base. However, a thin spotted ornamentation is visible in *O. kounoviensis* (Ginter *et al.* 2010) and a similar pattern is observed in the material from Buxières-les-Mines.

Among *Orthacanthus* species, *O. kounoviensis* (Fritsch 1889; Hampe 1994) is the only one that possesses a double serration pattern, simple or complex, on the lateral cutting edges. *Lebachacanthus* can sometimes possess a double serration pattern, only on the largest lateral teeth and restricted near the cusp base. Furthermore, *O. kounoviensis* possesses very high adult teeth relative to the other *Orthacanthus* species (Hampe 2003). The size of the base of the adult material studied here is similar to that of *O. kounoviensis* (Fig. 71, Table 7). The thickness of the base of the studied teeth is as developed as in *O. kounoviensis* (Fig. 73A; Hampe 2003). Unfortunately, as most of the lateral cusps are broken, the extreme curvature of the posterior lateral cusps of large lateral teeth of *O. kounoviensis* (Fritsch 1889; Hampe 1994) is rarely observed in the studied material, even if a few teeth show a curvature of the posterior lateral cusp similar to that of the latter species. Comparisons with the known *Orthacanthus* teeth suggest therefore that the material from Buxières-les-Mines belongs to *O. kounoviensis*.

Juvenile teeth—The juvenile teeth (Fig. 72) from Buxières-les-Mines share with the adult ones a minute median cusp that reaches $^1/_5$ or less of the size of the lateral ones, lanceolated cusps, serration, sometimes complex, on the external cutting edge, a heart-shaped coronal button, a possible lingual shaft in the case of an elongated coronal button, a pentagonal tooth base, a rounded basal tubercle that can be labially displaced ($^5/_{20}$), a spotted ornamentation of the tooth

base and a similar crown-base angle. Within these shared features, only the presence of a double serration is diagnostic of *O. kounoviensis* (Hampe 1994, 2003) in which the pattern can be complex or simple (Fritsch 1889) like in the juveniles from Buxières-les-Mines.

The juvenile teeth from Buxières-les-Mines differ from the adult ones by a number of significant characters (Table 8): the double serration is rarely present ($^{6}/_{20}$). The number of oral nutrient foramina, between 4 and 8, is higher than in the adult ones (Fritsch 1889; Hampe 1994). Furthermore, they can be placed on the lateral side of the coronal button and not only on its lingual side as is the case in the adult teeth. In these juvenile teeth, even if the lingual shaft is present, the depressions at the tooth base are also less expressed and even absent. Their tooth base thickness is reduced, not as thick as in the adult teeth (Fig. 73A). In the juvenile teeth, 3 to 12 basal nutrient foramina are mostly situated in the centre of the tooth base, near the lingual side of the basal tubercle. This relatively high number seems to be linked with a multiplication of small foramina in juveniles compared to the adult teeth. The labial bulging formed by the median cusps is often absent compared to the adult teeth in which it often occurs. At least, the ornamentation of the tooth base is less pronounced than in adults.

Orthacanthus* cf. *kounoviensis
(Figs. 74–75)

1969 *Expleuracanthus* Heyler, p. 28.

Referred Material—MNHN.F.AUT892, shortened to AUT892 below, a single large isolated tooth in two parts, the cusps being separated from the tooth base; MHNE.2021.14.25 and MHNE.2021.14.26, isolated sub-complete dorsal spines.

Occurrence—Excavation site of Muse, Path of the Poil Fou/Les Echars, Dracy-Saint-Loup Municipality, Saône-et-Loire, France for AUT892; Former open-cast coal mine of Buxières-les-Mines, Allier, France for MHNE.2021.14.25 and MHNE.2021.14.26.

Horizon—Muse oil-shale bed (OSB), Muse Formation, Autun Basin, Northern Massif Central, lowermost Asselian, Cisuralian, Lower Permian (Pellenard *et al.* 2017) for AUT892; First bituminous shale sequence between the ‘Lien Blanc’ and the ‘Lien Vert’ volcanic tuffs (Fig. 2B), which are late Asselian to early Artinskian, Cisuralian, Permian (Ducassou *et al.* 2018) for MHNE.2021.14.25 and MHNE.2021.14.26.

Table 8. Comparison of morphological characters between adult and juvenile teeth of *Orthacanthus kounoviensis* from Buxières-les-Mines.

Characters	Adult teeth	Juvenile teeth
Relative length of the median cusp	$<^1/_5$ to $^1/_5$ lateral cusps	$<^1/_5$ to $^1/_5$ lateral cusps
Serration on the lateral cutting edges	Yes ($^{17}/_{19}$), no ($^0/_{19}$), unknown ($^2/_{19}$)	Yes ($^{17}/_{21}$), no ($^2/_{21}$), unknown ($^2/_{21}$)
Serration of the serration	Yes ($^8/_{19}$), no ($^{11}/_{19}$)	Yes ($^6/_{21}$), no ($^{15}/_{21}$)
Coronal button shape	Rectangular to heart-like	Oval to heart-like
Coronal button shaft	No or a few	No or a few
Number of oral foramina	1 to 4	4 to 8
Labial oral foramen	Yes	Yes
Basal tubercle shaft	No or less expressed	No or less expressed
Basal tubercle shape	Smooth and rounded	Smooth and rounded
Number of basal foramina	2 to 6	3 to 12
Tooth base shape	Rhomboid to pentagonal	Rhomboid to pentagonal
Tooth base thickness	Thick	Thin
Tooth base-crown angle	110° to 120°	95° to 120°
Ornamentation of the tooth base	Yes ($^{14}/_{19}$), no ($^2/_{19}$), unknow ($^3/_{19}$)	Yes ($^{13}/_{21}$), no ($^8/_{21}$)

Remarks—AUT892 was briefly described but not illustrated by Heyler (1969: 28–29) as “une dent trouvée en fouille à Muse en 1958 (qui) présente une taille extraordinaire” (a tooth found during the excavations at Muse in 1958 (which) presents an extraordinary size). The Muse locality refers stratigraphically to the Muse OSB. Heyler (1969) identified this tooth (historical inventory number 2FMu) as belonging to the genus *Expleuracanthus*. However, he noted that this attribution could be erroneous and suggested that it could represent a different genus or species compared to the other *Expleuracanthus* material he mentioned.

Tooth

Description—Its tooth base measures 8.7 mm in length labio-lingually and 8.7 mm in width mesio-distally. The lateral cusps have a pointed apex. The median one is oval and antero-posteriorly compressed. The posterior lateral cusp is curved toward the posterior edge with a sigmoid shape whereas the anterior cusp is almost straight. Consequently, this is a lateral tooth. A distinct pattern of double serration, with a simple secondary serration, is present. The angle between the crown and the base of the teeth ranges from 110 to 115°. In oral view, the coronal button is rectangular and antero-posteriorly compressed. There are two pronounced oral nutrient foramina on the lingual side of the coronal button. In basal view, the tooth base is pentagonal and almost symmetric. In lateral view, the basal tubercle is labially displaced, forming an angular labial edge between the crown and the tooth base. There are 3 basal nutrient foramina

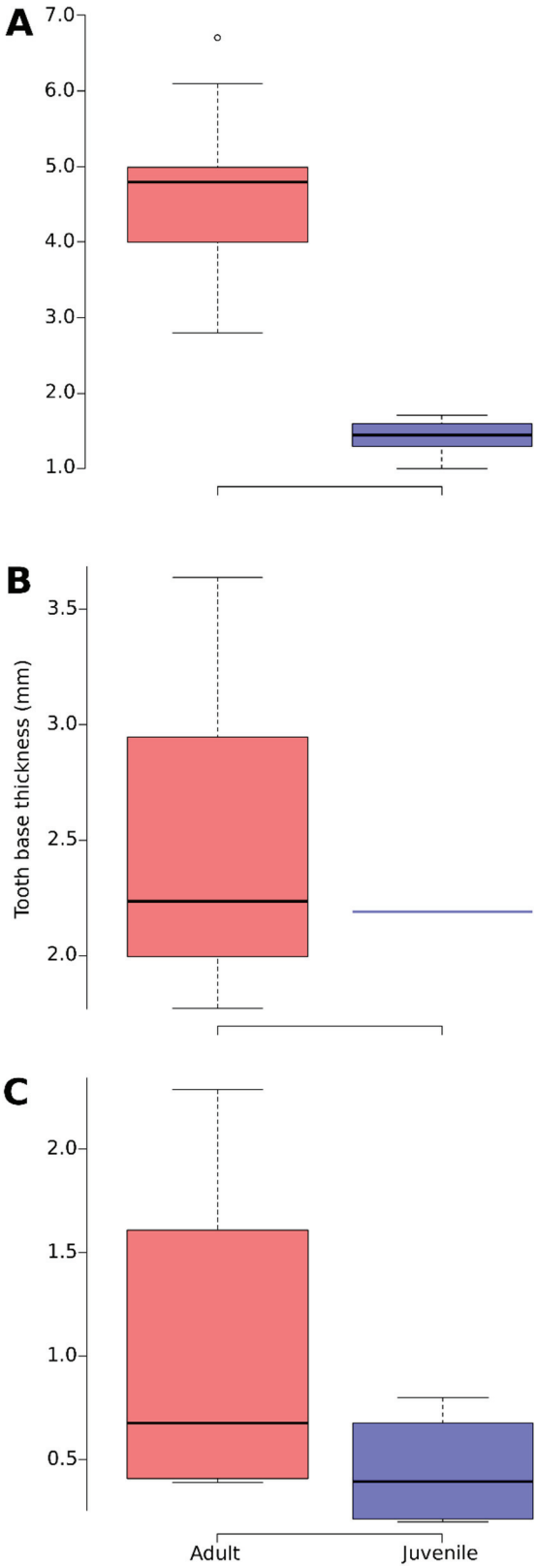

Figure 73. Tooth base thickness boxplot of juvenile and adult of *Orthacanthus* species. **A**, *Orthacanthus kounoviensis* from Buxières-les-Mines (this study). **B**, *Lebachacanthus seckenbergianus* from Heidtke (1982) and Hampe (1988a). **C**, *Orthacanthus donnelljohnsi* from Johnson & Thayer (2009).

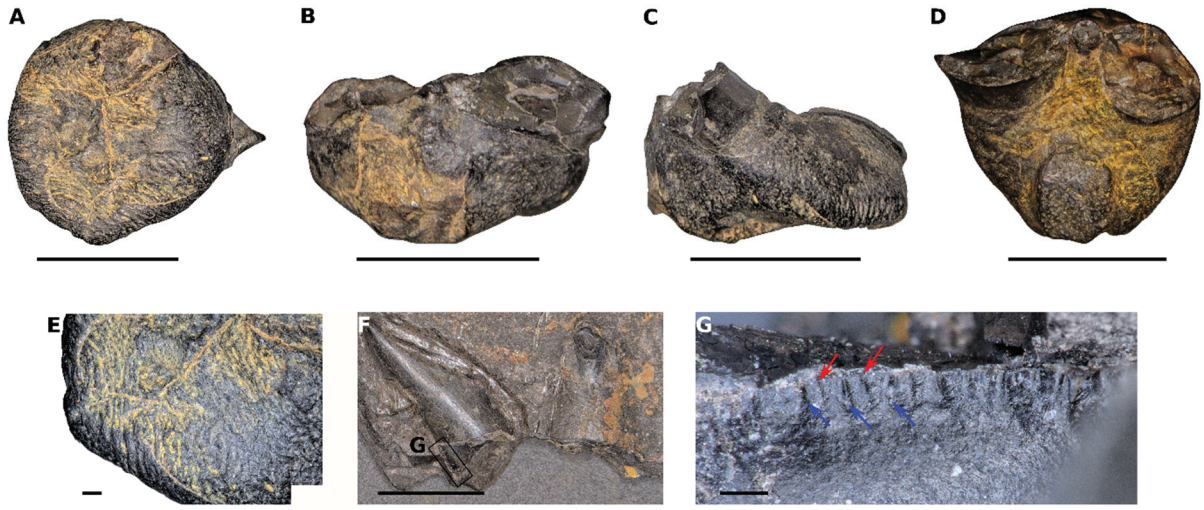

Figure 74. *Orthacanthus* cf. *kounoviensis* tooth from the Muse OSB. **A–G**, MNHN.F.AUT892. **A–D**, tooth base. **E**, tooth base ornamentation. **F**, cusps. **G**, imprint of the serration of the lateral cutting edge. **A**, basal. **B**, labial. **C**, lateral. **D**, oral view. Blue arrows are primary serration and red arrows are secondary serration. Scale bar: 5 mm (**A–D**, **F**), 500 µm for **E** and 200 µm for **G**.

mainly situated on the lingual side of the base. The outlines of the tooth base present a thin spotted to elongated ornamentation.

Comparisons—The coronal button shape of *O. bohemicus* (Hampe 2003) and *O. kounoviensis* (Fritsch 1889; Hampe 1994) might be different from the antero-posteriorly compressed one of AUT892. Furthermore, the lateral cutting edge seems to be less developed in AUT892 than in *O. bohemicus* and *O. kounoviensis*.

However, AUT892 possesses a double serration pattern on the external cutting edge, like in *O. kounoviensis* (Fig. 74G). This tooth also shares with those of *O. kounoviensis* from Buxières-les-Mines a possible antero-posteriorly compressed median cusp, a low number of oral and basal nutrient foramina, and a labial fossa between the cusps and the coronal button. The elongated spotted ornamentation of AUT892 can also be seen in teeth of *O. kounoviensis* from Buxières-les-Mines. Its oval coronal button resembles that of juvenile teeth of *O. kounoviensis*. The base of AUT892 is less concave than that of the adult teeth from Buxières-les-Mines but more concave than that of the juveniles from Buxières-les-Mines. So, AUT892 is morphologically close to *O. kounoviensis* from Buxières-les-Mines by its pentagonal tooth base, double serration, low number of oral and basal nutrient foramina and developed fossa between the cusps, coronal button and tooth base ornamentation. However, as there are significant intraspecific variations in the tooth pattern of *O. kounoviensis* from Buxières-les-

Mines, the description of a sole tooth is insufficient to make a clear systematic attribution. Consequently, this specimen can be related to the material from Buxières-les-Mines as *O.* cf. *kounoviensis*.

Dorsal spines

Description—The two sub-complete dorsal spines (Fig. 75) measure 13 to 19 cm in length and 1.1 to 1.5 cm in maximum width next to the base. MHNE.2021.14.25 possesses a distinct curvature, ventrally oriented (Fig. 10A), whereas MHNE.2021.14.26 is almost straight. In both spines, the cross section varies along the length. It is dorso-ventrally compressed in the most proximal part, rounded in the mid-length, and slightly laterally compressed distally. At mid-length, MHNE.2021.14.25 seems to be more angular in cross section than MHNE.2021.14.26. In both spines, fine but distinct longitudinal striations run along the dorsal side, from the base to the apex. Along the ventral side, the striations are present except near the apex between the two rows of denticles. These two rows of denticles are distally situated on the ventral side (Fig. 75C-D). They occupy 28% to 37% of the preserved length. When preserved, the number of denticles is 3 to 4 in MHNE.2021.14.25 and 5 to 6 in MHNE.2021.14.26 per cm. No denticle is entirely preserved in MHNE.2021.14.25, but in MHNE.2021.14.26 four complete ones are visible (Fig. 75F-G): these denticles are proximally recurved and some of them present a cutting edge (Figs. 75E, G). Their base has an oval cross section that becomes more rounded in the most distal part. The space between the denticle rows is relatively flat except in the most proximal part where a central groove seems to be present in MHNE.2021.14.25. This central groove is well-marked in MHNE.2021.14.26. The distance between the denticles is equivalent to the width of the denticle base in MHNE.2021.14.25 but it is highly reduced in MHNE.2021.14.26. This space increases toward the apex.

Comparison—MHNE.2021.14.25 and MHNE.2021.14.26 (Fig. 75) can be assigned to the genus *Orthacanthus* following the combination of the following characters (Ginter *et al.* 2010): the two rows of denticles are situated on the ventral side and the cross section of the dorsal spine is rounded, i.e. not dorso-ventrally compressed. These characters are those of a Diplodoselachidae (Ginter *et al.* 2010). The ratio width/length is less than $^{1}/_{15}$ contrary to *Lebachacanthus* or *Diplodoselache* in which it is approximatively $^{1}/_{10}$ and $^{1}/_{8}$ respectively.

The two specimens show a similar morphology: both have posteriorly recurved denticles with a fine cutting edge (Fig. 75E–G) and an oval to rounded cross section at their base. They also exhibit a surface with fine longitudinal striations on dorsal and ventral sides and a cross

Figure 75. Isolated dorsal spine of *Orthacanthus* cf. *kounoviensis* from Buxières-les-Mines. (**A–C**, **E**), MHNE.2021.14.25. (**D**, **F–G**), MHNE.2021.14.26. **A–D**, entire dorsal spines. **E–G**, details of the denticles. **A**, lateral. **B**, dorsal view. **C–D**, ventral view. Scale bar: 1 cm (**A–D**) and 1 mm (**E–G**).

section rounded at mid-length and more compressed at the base and at the apex. Yet MHNE.2021.14.25 is more curved than MHNE.2021.14.26, its denticles are more distant from each other, and the central groove between its denticle rows is less pronounced. However, as MHNE.2021.14.26 is not entirely preserved, we cannot ascertain that its most distal part is not curved, and the space between denticle is known to be variable within the same species, like in *Orthacanthus huberi* (Zidek 1992).

Orthacanthus huberi (Zidek 1992) differs from MHNE.2021.14.25 and MHNE.2021.14.26 by its higher number of denticles per cm, almost 11, and the more laterally displaced rows of denticles. *O. gibbosus*, including *O. cylindricus* following Hampe (2003), is different from our specimens by the fact that the denticles touch each other and have a massive shape, and by the invariable rounded cross section not compressed at the base or at the apex. *O. denticulatus* (Davis 1880; Hampe 2003) also differs from our specimens by its slenderer denticles, always rounded cross section of the dorsal spine, higher number of denticles per cm,

i.e. 8, and the large space between the denticles reaching half the width of the dorsal spine. *O. bohemicus* (Fritsch 1889; Heidtke 1998) differs from our specimens by a constant rounded cross section, higher number of denticles per cm, i.e. 6 to 11, more laterally displaced rows of denticles and by the fact that the denticles touch each other. *O. platypternus* (Beck *et al.* 2016) is also different from MHNE.2021.14.25 and MHNE.2021.14.26 by its more laterally displaced denticle rows and sub-triangular cross section of the dorsal spine, yet it possesses a cutting edge on the denticles as in the two studied specimens.

O. meridionalis (Soler-Gijón 1997b) differs from MHNE.2021.14.25 and MHNE.2021.14.26 by the postero-lateral orientation of the denticle rows and by the fact that the proximal denticles are more spaced from each other than the distal ones. It shares with our specimens a fine cutting edge on the denticles, a well-marked central groove at the most proximal part of the denticulated region, a fine longitudinal striation that is well-marked except between the denticle rows, and possible supplementary knobs on or next to the denticle rows. The cross section of the dorsal spine of *O. meridionalis*, which is dorso-ventrally compressed at the base, rounded in the mid-length and slightly laterally compressed at its apex, is similar to our specimens but it is generally less angular at mid-length (Soler-Gijón 1997b). The two specimens (Fig. 9) are morphologically close to *O. meridionalis* as already proposed by Steyer *et al.* (2000).

O. kounoviensis (Fritsch 1889; Hampe 1994) differs from MHNE.2021.14.25 and MHNE.2021.14.26 by its small ridge between the denticle rows and the small number of denticle per cm, i.e. 2. The cross section of its dorsal spine varies from dorso-ventrally compressed at the base to rounded at mid-length and angular at the apex because of strong striations on its dorsal side. MHNE.2021.14.25 also shows a rather angular cross section at mid-length but without strong striations. A curvature is observed in both MHNE.2021.14.25 and *O. kounoviensis*. However, in *O. kounoviensis* it is present only in the distal quarter whereas in MHNE.2021.14.25 the curvature is along the entire length. Even if the two studied specimens are not complete, their denticulated regions do not seem to reach more than half the length of the spine, as in *O. kounoviensis* (Fritsch 1889; Hampe 1994).

In Buxières-les-Mines, all the teeth are attributed to *Orthacanthus kounoviensis*, so it would be surprising that another species could only be represented by isolated dorsal spines. Two different *Orthacanthus*/*Lebachacanthus* species in the same locality were already reported (see the distribution of these genera in Ginter *et al.* [2010]), but with two distinct groups of dental morphologies which is not the case here. A diagnosis solely based on the dorsal spine should be avoided because many character states like longitudinal striations, shape of the

denticles, ventral central groove or cutting edge on the denticles can be shared by several *Orthacanthus* species (Heidtke 1998). The same issue was reported in Hybodontiformes (Maisey 1987). Moreover, the temporal and geographic intraspecific variations are barely known in *O. kounoviensis*. We reported dental variability between the material from Buxières-les-Mines and the type material from Kounová and it was also highlighted by Hampe (2003) between *O. kounoviensis* and *O.* cf. *kounoviensis* from the United Kingdom. The same thing could occur on the dorsal spines. Finally, *O. meridionalis* (Soler-Gijón 1997b), anatomically close to *Orthacanthus* cf. *kounoviensis* (Fig. 75), is only known from the Kasimovian of the Puertollano Basin, whereas *O. kounoviensis* is known from the Moscovian to the Gzhelian of Germany, Czech Republic and United Kingdom (*O.* cf. *kounoviensis* in Hampe [2003]). For all these reasons, and without formal diagnostic character, the isolated dorsal spines from Buxières-les-Mines are attributed to *O.* cf. *kounoviensis.*

Discussion

Is *Orthacanthus buxieri* a valid species?

Several authors (e.g. Hampe 2003; Ginter *et al.* 2010) have questioned the validity of *O. buxieri* and suggested a possible synonymy with either *O. kounoviensis* based on dental characters or with *O. meridionalis* (Steyer *et al.* 2000) based on neurocranial and dorsal spine characters. The present study of isolated teeth from Buxières-les-Mines highlights the presence of *O. kounoviensis* in this locality. Based on the original description of Heyler & Poplin (1989), no diagnostic character can be identified for *O. buxieri*. Consequently, we propose to restrict the species *O. buxieri* to the sole holotype. Future works need to focus on the reassessment of the holotype of *O. buxieri* in order to validate or not this species.

Dental ontogeny of *Orthacanthus kounoviensis*

Ontogeny of the teeth of *Orthacanthus* has been unequally studied between the North American and the European species. *O. donnelljohnsi* and *O. platypternus* have similar juvenile and adult teeth (Johnson 1999, 2018; Johnson & Thayer 2009). *O. compressus* displays a relatively longer juvenile tooth base than the adult one, and without serration on the crown (Johnson 1999, 2012). *O. bohemicus* juvenile teeth lack serration and possess longer median cusp than adult teeth (Hampe 2003). *O. gibbosus* can lack serration on juvenile teeth (Hampe 2003). On the contrary, the genus *Lebachacanthus* always displays serration on juvenile teeth

even if the global shape of these teeth evokes the genus *Xenacanthus* (Hampe 2003). Furthermore, juvenile *Orthacanthus* are supposed to possess thinner tooth base compared to adult specimens (Figure 73B–C; Johnson 2012, 2018).

In juvenile *Orthacanthus kounoviensis* teeth from Buxières-les-Mines (Fig. 72), characters as the possible absence of serration and thinner base of the teeth (Fig. 73) correspond to known differences between juvenile and adult teeth of other species. Furthermore, the presence of a double serration in both juvenile and adult *O. kounoviensis* teeth within the known variation of the type material from Kounová (Fritsch 1889) reinforces the hypothesis that they belong to the same species at different ontogenetic stages. The size difference (Fig. 76A) between them is greater than the adult variation of other *Orthacanthus* species (Fig. 71), so it reinforces again this hypothesis of teeth belonging to both juvenile and adult individuals. Xenacanthiformes, which produced egg-capsules (see Fischer & Kogan 2008; Fischer *et al.* 2014a), also show a strong size difference between neonates and adults. Furthermore, the comparison between the linear regression of juvenile and adult *O. kounoviensis* teeth (Fig. 76B–C) reveals none or just a minor statistical influence of the ontogeny on teeth length/width ratio (Table 9), which is congruent with a juvenile-adult model as demonstrated by Johnson & Thayer (2009).

Even if the global shape of the tooth base and crown is similar between juvenile and adult teeth of *O. kounoviensis*, some differences are reported (Table 8) which are congruent with modern chondrichthyans (e.g. Reif 1976). However, the apparent multiplication of both oral and basal nutrient foramina was usually used to differentiate *Orthacanthus* species, which appears to contradict the juvenile-adult model hypothesis. As present-day chondrichthyans grow fast during their early life (e.g. Irvine *et al.* 2006), the nutrient foramina on the tooth base could be more numerous in juveniles than in adults to favour this strong growth with a higher rate of tooth replacement (e.g. Wass 1973). Following this hypothesis, the multiplication of nutrient foramina could be an ontogenetic difference, not yet reported within the genus *Orthacanthus*.

Palaeobiogeography of the European *Orthacanthus* in the Carboniferous-Permian basins

The genus *Orthacanthus* is known in European basins, from the Bashkirian of United Kingdom (e.g. Hampe 2003) to the Asselian-Sakmarian of France, with at least eight species. (Ginter *et al.* 2010). On the contrary, *Lebachacanthus*, with two species only (Ginter *et al.* 2010), is restricted from the Moscovian of Bohemia to the Asselian of Germany (e.g. Ginter *et al.* 2010). The *Orthacanthus* and *Lebachacanthus* diversity was greatly affected by the

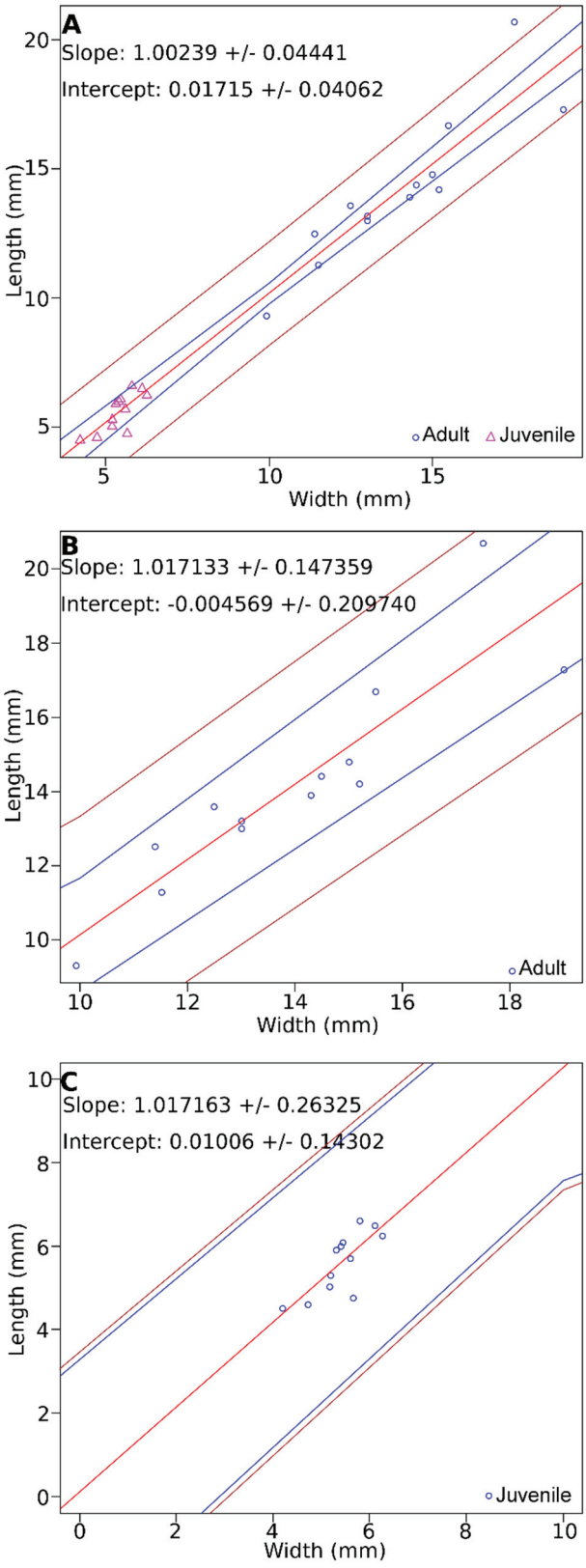

Figure 76. Linear regressions on total (**A**), adult (**B**) and juvenile (**C**) teeth of *Orthacanthus kounoviensis* from Buxières-les-Mines. For (**A–C**) the red line is the linear regression line, the blue lines are the confidence interval, and the brown lines are the prediction interval.

Table 9. Analyses of Variance Table of the total *Orthacanthus kounoviensis* teeth from Buxières-les-Mines for the two linear models including width, length and ontogeny.

	Linear model: Width~Length+Ontogeny+Length*Ontogeny				
	Df	Sum Sq	Mean q	F value	Pr(>F)
Width	1	5.4587	5.4587	556.5333	<2e-16***
Ontogeny	1	0.0002	0.0002	0.0207	0.8869
Width:Ontogeny	1	0.0000	0.0000	0.0000	0.9993
Residuals	21	0.2060	0.0098		
	Linear model: Length~Width+Ontogeny+Width*Ontogeny				
	Df	Sum Sq	Mean q	F value	Pr(>F)
Width	1	5.2350	5.2350	701.4010	<2e-16***
Ontogeny	1	0.0385	0.385	5.1559	0.3381*
Width:Ontogeny	1	0.0025	0.0025	0.3366	0.56799
Residuals	21	0.1567	0.0075		

Abbreviations: Df, degree of freedom; Sum q, sum of squares; Mean q, mean of the sum of squares; F value, test statistic for the F test; Pr(>F), p-value of the F-statistic.

Carboniferous-Permian transition, and only *L. senckenbergianus* from the Saar-Nahe Basin (Heidtke 2007) and *O. kounoviensis* from Buxières-les-Mines and maybe Muse (*Orthacanthus* cf. *kounoviensis*) are found in the early Permian deposits (Fig. 77). Thus, Buxières-les-Mines is the latest occurrence of *Orthacanthus* in Europe and could be a refuge zone for this genus, like the Meisenheim Formation of the Saar-Nahe Basin for the genus *Lebachacanthus*. In addition, the presence of both juvenile and adult *Orthacanthus kounoviensis* teeth at Buxières-les-Mines indicates a suitable environment for the development of this species all along its lifespan.

Comparisons between the teeth of the European *Orthacanthus* and *Lebachacanthus* separate the 'gracile' species (with rounded tooth base, rounded coronal button with a predominant lingual shaft, positioned in the centre of the oral face and that does not reach more than 10 mm in width and length) from the 'robust' species (with angular tooth base, angular to heart-shaped coronal button with a rare lingual shaft, displaced in the lingual margin of the oral face and that can reach more than 10 mm in tooth base width and length). According to the distribution of the European *Orthacanthus* and *Lebachacanthus* (Fig. 77), only the large and robust species crossed the Carboniferous-Permian transition, whereas the small and gracile species are restricted to the Carboniferous deposits only.

The Carboniferous-Permian transition in Europe is characterized by tectonic Franconian movements that were supposed to have halted the interconnectivity between several sedimentary basins of central Europe in which Xenacanthiformes had dispersed (Schneider

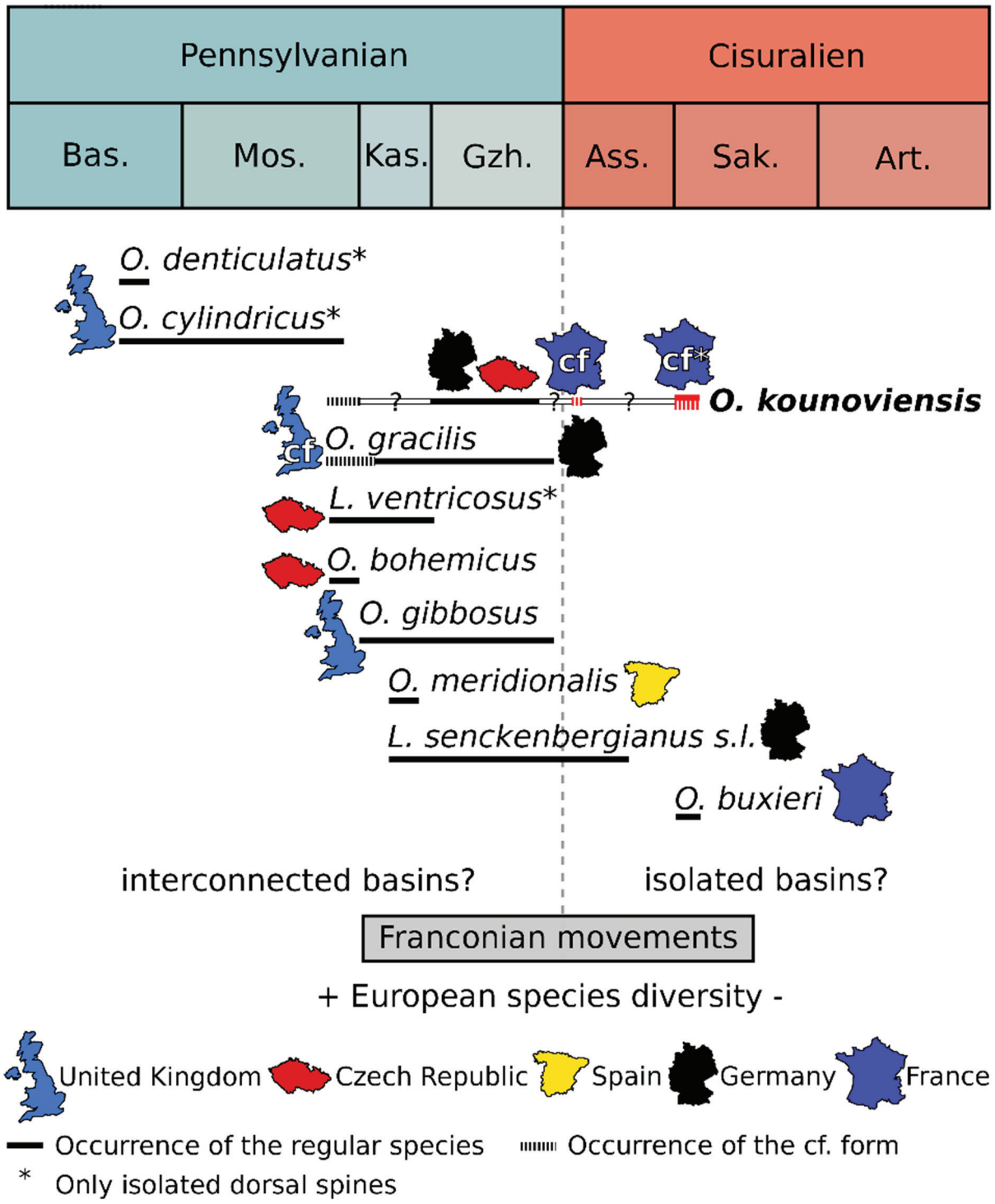

Figure 77. Temporal and geographic distribution of the European *Orthacanthus* species. *O. buxieri* is here restricted to the sole holotype (Heyler & Poplin 1989). Red lines are occurrences of the studied material. '?' refers to the fossil record gaps. *L. senckenbergianus s.l.* corresponds to the three *Lebacahacanthus* species from the Saar-Nahe basin as defined by Heidtke (2007), i.e. *L. senckenbergianus*, *L. pollichiae* and *L. colloseus*. Temporal and geographic distributions are from Heyler & Poplin (1989), Hampe (1994, 2003), Soler-Gijón (1997a), Heidtke (1998, 2007).

1996). *Orthacanthus* and *Lebachacanthus* are large apex predators in their ecosystems (e.g. Kriwet *et al.* 2008) and are therefore susceptible to get extinct quickly in response to environmental changes. Consequently, it is not surprising that their diversity decreases at the Carboniferous-Permian transition, in response to the Franconian movements. The surviving of the largest species could be explained by their ability to spread more efficiently than the smallest ones and, thus, to occupy potential refuge zones like Buxières-les-Mines in the Bourbon-l'Archambault Basin.

Orthacanthus cf. *kounoviensis* from the lowermost Permian Muse OSB (Fig. 74) is the first concrete report of this genus in the Autun Basins and enhances our understanding of its palaeobiogeography in the Northern Massif central and the relationships between the different basins. Mercuzot (2020) has proposed that the Carboniferous-Permian basin of the Northern Massif central could be widely connected. This assumption was mainly based on sedimentological observations. Similar assumptions have already been proposed by Poplin (1999) and Štamberg & Steyer (2021) based on the actinopterygian distribution in various basins. Contrary to Schneider (1996) who argued for the stoppage of connections between central European basins in the Permian, this interconnectivity could have continued in the lower Permian in the Northern Massif central, assuming a possible different tectonic history in Western Europe.

The dispersion patterns of *Orthacanthus* species are different from those of other European Xenacanthiformes like the genus *Triodus*. Each European *Triodus* species have been supposed to endemically evolve in each Carboniferous-Permian basin in which they were present with no species present in several basins (Luccisano *et al.* 2021a). On the contrary, some species like *O. kounoviensis* and *O. gracilis* seem to be present in different basins and a same basin can possess more than one *Orthacanthus* species (e.g. Hampe 2003). Such different dispersion patterns might be related to different ecological status. Xenacanth dispersal patterns have been supposed to occur both through river channels between distant sedimentary basins (e.g. Schneider & Zajíc 1994) or through the marine environment of the Paleotethys (Schultze & Soler-Gijón 2004). *O. kounoviensis* being present in different basins (Fig. 77), its migration could preferentially occur through the river channels. Indeed, the palaeogeographical reconstruction of the European intra-mountainous basins at the Carboniferous-Permian transition (e.g. Roscher & Schneider 2006) assumed numerous fault systems between the French Massif central and the German and Czech basins. These faults could correspond to rivers and lakes which allowed the migration of the xenacanthiforms from Germany to France (Boy & Schindler 2000). Furthermore, no unambiguous sedimentological or palaeontological

evidence of a potential marine influence has been found in the basins where *O. kounoviensis* has been described. As *O. kounoviensis* juveniles and adults are found in Buxières-les-Mines, this species could live in a constant environment all along its lifespan, therefore without a migrator behavior in the marine environment.

Conclusions

Morphological and biometric study of isolated *Orthacanthus* teeth from the Buxières-les-Mines (Bourbon-l'Archambault basin) indicates the presence of *O. kounoviensis* in the lower Permian of France. The studied material represents the latest record of this genus in Europe and Buxières-les-Mines can be seen as a refuge zone for the latest French Diplodoselachidae in a way similar to that of the Meisenheim Formation in Germany.

The description of *Orthacanthus* cf. *kounoviensis* from the lowermost Permian of Muse (Autun basin) extends the distribution of this genus in the French Permian. It suggests that connections between the different Carboniferous-Permian basins of the Northern Massif central still occurred during the lower Permian.

The presence of *Orthacanthus kounoviensis* in Buxières-les-Mines strongly questions the validity of *Orthacanthus buxieri* and agrees with previous studies that consider it like a temporal and geographical population of *O. kounoviensis*. *O. buxieri* should be restricted to its holotype and further investigations regarding it are needed to clarify its systematic status, in order to fully describe all the *Orthacanthus* material from Buxières-les-Mines and to understand the diversity and dispersion of European *Orthacanthus.*

Acknowledgements

The authors thank the Rhinopolis Association, the Gannat Municipality and the Conseil Départemental de l'Allier for having funded the excavation campaigns at Buxières-les-Mines during which the specimens were found, and for providing storage space in which the Buxières-les-Mines fossils were housed. We thank all the workers who excavated at Buxières-les-Mines, including Guy Sesia and Jacques Rival (Rhinopolis Association) for the fine preparation of the specimens. The authors thank the two reviewers Michał Ginter and Oliver Hampe, the scientific editor Sally Thomas and the editor Lionel Cavin for their remarks that have greatly helped to improve this manuscript. The first author was funded by the Doctoral School ED 341 - E2M2

Évolution Écosystème Microbiologie Modélisation, Université Claude Bernard Lyon 1, France. JSS was funded by regular annual credits given to his lab by the MESR.

Supplementary material

Table S2. Detailed measurements (in mm) of the dental material of *Orthacanthus kounoviensis* from Buxières-les-Mines.

Specimen number	Length (mm)	Width (mm)	Height (mm)	Ontogeny
MNHE.2021.14.1	4,5	4,2	3,7	Juvenile
MNHE.2021.14.2	3,8	?	4	Juvenile
MNHE.2021.14.3.1	4,9	?	?	Juvenile
MNHE.2021.14.3.2	6	5,4	?	Juvenile
MNHE.2021.14.3.3	5,7	5,6	?	Juvenile
MNHE.2021.14.3.4	13,9	14,3	?	Adult
MNHE.2021.14.4	6,5	?	6,4	Juvenile
MNHE.2021.14.5	5,9	5,3	?	Juvenile
MNHE.2021.14.6	20,7	17,5	?	Adult
MNHE.2021.14.7	?	3,5	3,4	Juvenile
MNHE.2021.14.8	?	10,4	10,1	Adult
MNHE.2021.14.9	5,3	5,2	5,8	Juvenile
MNHE.2021.14.10	6,5	6,1	7,1	Juvenile
MNHE.2021.14.11	12,5	11,4	16,1	Adult
MNHE.2021.14.12	?	4,6	5,2	Juvenile
MNHE.2021.14.13	17,3	19	?	Adult
MNHE.2021.14.14	16,7	15,5	?	Adult
MNHE.2021.14.15	?	13,6	16,5	Adult
MNHE.2021.14.16	14,2	15,2	?	Adult
MNHE.2021.14.17	?	?	?	Adult
MNHE.2021.14.18	8,5	10	?	Adult
MNHE.2021.14.19	13,6	12,5	?	Adult
MNHE.2021.14.20	14,4	14,5	?	Adult
MNHE.2021.14.21	?	12	?	Adult
MNHE.2021.14.22	13	13	?	Adult
MNHE.2021.14.23	13,2	13	?	Adult
MNHE.2021.14.24	14,8	15	?	Adult
MNHN.F.BU7	11,27	11,52	?	Adult
MNHN.F.BU8	9,3	9,92	13,7	Adult
PIMUZ A/I 5122	?	8,72	7,15	Adult
PIMUZ A/I 5123	4,76	5,66	5,05	Juvenile
PIMUZ A/I 5124	5,03	5,18	6,43	Juvenile
PIMUZ A/I 5125	?	5,97	6,73	Juvenile
PIMUZ A/I 5127	6,24	6,26	7,5	Juvenile
PIMUZ A/I 5128	4,6	4,72	4,22	Juvenile
PIMUZ A/I 5130	6,6	5,8	5,3	Juvenile
PIMUZ A/I 5131	6,09	5,45	6,75	Juvenile

Synthesis of the systematic reassessment of the chondrichthyan fauna from the Carboniferous-Permian Autun and Bourbon-l'Archambault basins

The present systematic reassessment concludes that some species must be considered as invalid or restricted to their type material. In the Autun Basin, *Triodus* ?*frossardi* must be considered as a *nomen dubium*, the type material of *Bibractopiscis niger* correspond to at least two morphologies related to Xenacanthiformes and 'Ctenacanthiformes' and *Orthacanthus commailli* must no longer be considered as a xenacanthiform, although closely related to them. Finally, in Buxères-les-Mines, the presence of *O. kounoviensis* questions the validity of *O. buxieri* and the latter species must be restricted to its sole holotype.

These studies allow to report for the first time a 'ctenacanthiform' in these presumed freshwater basins. From a palaeobiogeographic point of view, the fossil record of the Autun and Bourbon-l'Archambault basins highlights differences between small and large xenacanthiforms. *Triodus* seems to possess a high rate of evolution with numerous speciation events around the Carboniferous-Permian boundary. Its distribution is endemic with a single species in each basin where this genus is present, and no basin shares the same species. On the contrary, the large *Orthacanthus* and *Lebachacanthus* can be present in several basins and their diversity decreases at the Carboniferous-Permian boundary.

This systematic reassessment shows the scientific importance of the Autun and Bourbon-l'Archambault basin in the resolution of global chondrichthyan relationships. The specimen to a ?Xenacanthimorpha shows for the first time that some chondrichthyans could be more closely related to xenacanthiforms than 'ctenacanthiforms' or phoebodontiform are supposed to be. As in several recent hypotheses the xenacanthiform, 'ctenacanthiform' and/or phoebodontiform position can vary, the incorporation of taxa like the ?Xenacanthimorpha from the Autun Basin could be helpful to resolve some phylogenetic questions.

Furthermore, the observed different distribution patterns between small and large xenacanthiform genera, typically between *Triodus* and *Orthacanthus*, allow to better understand the effect of global environmental changes on intra-mountainous aquatic organisms, like those occurring at the Carboniferous-Permian boundary in Europe. *Triodus* seems to easily pass through this boundary with a multiplication of species, whereas the majority of *Orthacanthus* went extinct in the early Permian. This could be explained by a better adaptation of small xenacanths to global changes and by their ability to spread more efficiently between basins. Large xenacanthiforms, even if also present in a variety of European Carboniferous

basins, seem to only survive in a restricted number of Permian localities, between Western and Central Europe. This survival could be the result of particular environmental settings in these 'refuge' areas. Consequently, it will be interesting to investigate the environmental conditions of the early Permian basins, in localities like Muse or Buxières-les-Mines, to better understand the reasons behind the survival of large xenacanthiformes.

Chapter V – Palaeoenvironmental and palaeoecological study

Paper 4: Stable isotope compositions ($\delta^{18}O$, $\delta^{13}C$, $\delta^{34}S$) of vertebrate aquatic faunas from the early Permian intra-mountainous basins of the French Massif central: ecological and environmental implications

Vincent Luccisano, Kathleen Lachat, Gilles Cuny, Alan Pradel, François Fourel, Christophe Lécuyer, Jean-Marc Pouillon, Romain Amiot

In preparation for submission to **Palaeogeography, Palaeoclimatology, Paleoecology**

Stable isotope compositions ($\delta^{18}O$, $\delta^{13}C$, $\delta^{34}S$) of vertebrate aquatic faunas from the early Permian intra-mountainous basins of the French Massif central: ecological and environmental implications

Vincent Luccisano[1,2*], Kathleen Lachat[1], Gilles Cuny[2], Alan Pradel[3], François Fourel[2], Christophe Lécuyer[1], Jean-Marc Pouillon[4], Romain Amiot[1]

[1]Univ Lyon, UCBL, ENSL, UJM, CNRS, LGL-TPE, F-69622, Villeurbanne, France;
[2]Univ Lyon, Université Claude Bernard Lyon 1, CNRS, ENTPE, UMR 5023 LEHNA, F-69622, Villeurbanne, France;
[3]CR2P - Centre de Recherche en Paléontologie - Paris ; Muséum National d'Histoire Naturelle - Centre National de la Recherche Scientifique- Sorbonne Université. France;
[4]Rhinopolis Association, 179 rue des Plattières 38300 Nivolas Vermelle/BP 39 03800 Gannat, France

RH: Isotopic compositions of French Permian freshwater fauna

*Corresponding author. Email: vincent.luccisano@gmail.com

Abstract

The palaeoecology of the Xenacanthiformes has been heavily debated. Historically considered as freshwater organisms, hypotheses of euryhaline ecology and migratory behaviour were recently proposed based on the histology of their dorsal spines. However, recent studies still argued for a full freshwater ecology based on the stable isotope compositions of their teeth. The ecology of xenacanthiforms coming from the environmentally ambiguous lower Permian intra-mountainous localities of Buxières-les-Mines (Bourbon-l'Archambault Basin, Allier) and the Muse oil-shale bed (OSB; Autun Basin, Saône-et-Loire) from the French Massif central is particularly important to investigate. These two localities were interpreted as freshwater settings, but the possibility of marine influences have been proposed. To assess the palaeoenvironment of the two French localities of Buxières-les-Mines and Muse OSB; and the palaeoecology of their xenacanthiforms, we have analysed the stable isotope compositions ($\delta^{18}O_p$, $\delta^{18}O_c$, $\delta^{13}C_c$ and $\delta^{34}S$) of the bioapatite of their vertebrate fauna. Buxières-les-Mines vertebrates exhibit $\delta^{18}O_p$ values always lower than the contemporaneous marine vertebrates

whereas the Muse OSB shows higher $\delta^{18}O_p$ values. $\delta^{34}S$ values of Buxières-les-Mines and the Muse OSB vertebrates are always lower than those of the seawater $\delta^{34}S$ value of the Permian. $\delta^{13}C_c$ values in Buxières-les-Mines and the Muse OSB, are higher than the co-occurring $\delta^{13}C$ values of marine sediments and invertebrates. Buxières-les-Mines is interpreted as a large and deep freshwater lake that shares similarities with the modern Indonesian Lake Matano whereas the Muse OSB is seen as a shallow tropical lake with drying up events, equivalent to the Amazonian Lake Punta Laguna or the African Lake Tanganyika. The oxygen isotope compositions of the xenacanth dorsal spines of Buxières-les-Mines are constant from the apex to the base. This implies no migration pattern for these early Permian European specimens. The apparent ability of small xenacanthiforms to endure drying up, as showing by the variations of the isotope composition of the Muse OSB specimens, contrary to the largest ones, could explain their palaeobiogeography in the early Permian during which Carboniferous xenacanthiforms occurring in large lake and river systems disappeared.

Introduction

Xenacanthiformes is an order of Palaeozoic chondrichthyans characterised by an eel-like body, diplodont teeth and an ever-growing dorsal spine (e.g. Zangerl 1981; Ginter *et al.* 2010). They are divided into two families (e.g. Ginter *et al.* 2010): the Diplodoselachidae which exhibit a rounded dorsal spine with two posterior rows of denticles, and the Xenacanthidae that have a dorso-ventral compressed dorsal spine which bears two lateral rows of denticles. Their top diversity occurred between the late Carboniferous and the early Permian of Europe and North America (se Hampe 2003; Heidtke 2007; Ginter *et al.* 2010).

Most of the time they have been discovered in ancient lacustrine or palustrine deposits (Zangerl 1981; Compagno 1990; Kriwet *et al.* 2008). Consequently, some authors (e.g. Schneider *et al.* 2000; Fischer *et al.* 2013, 2014b; Štamberg *et al.* 2016) have interpreted them as a good proxy for freshwater environments. However, numerous studies (Schultze 1985, 1995, 1998, 2009, 2013; Olson 1989; Soler-Gijón 1993b; Johnson 1999; Soler-Gijón & Moratalla 2001; Schultze & Soler-Gijón 2004; Hampe *et al.* 2006; Laurin & Soler-Gijón 2010; Carpenter *et al.* 2011; Beck *et al.* 2016) started to question their full freshwater-adaptation and argued in favour of a possible euryhaline ecology.

To test the different hypotheses of their living environment, recent studies have investigated the phosphate oxygen isotope composition ($\delta^{18}O_p$) of the teeth of some

Carboniferous and Permian xenacanthiforms from North America and Europe (Fischer *et al.* 2013, 2014b). Xenacanthiforms were thus interpreted as full freshwater organisms living in environments submitted to significative drying up events. However, other studies (Schultze 1985, 1995, 1998, 2009, 2013; Olson 1989; Soler-Gijón 1993b; Johnson 1999; Soler-Gijón & Moratalla 2001; Schultze & Soler-Gijón 2004; Hampe *et al.* 2006; Laurin & Soler-Gijón 2010; Carpenter *et al.* 2011) plead for an euryhaline behaviour, reinforced by the conclusions of Soler-Gijón (1999) and Beck *et al.* (2016) who focused on the histological structure of the dorsal spine of American and European *Orthacanthus* and who supported an euryhaline ecology with diadromous and catadromous migrations. These conflicting views of the palaeoecology of the xenacanthiforms emphasise the need to provide new investigations on this topic.

This is all the more true for xenacanthiforms from environmentally ambiguous basins like the Bourbon-l'Archambault Basin (Allier, France) in the French Massif central. Fischer *et al.* (2013) measured $\delta^{18}O_p$ values of teeth and dorsal spines of *Orthacanthus buxieri* from the Buxières-les-Mines locality in agreement with a freshwater living environment. However, Schultze & Soler-Gijón (2004) and Schultze (2009) listed faunal components of nearby localities from the French Massif central that could indicate a probable marine influence. In addition, the palaeoenvironment of the nearby Autun Basin (Saône-et-Loire, France) has been widely investigated by Mercuzot (2020) and Mercuzot *et al.* (2022) from a sedimentological point of view. Doubts persist for the fossiliferous locality of the Muse oil-shale bed (OSB) which has also provided xenacanthiform remains. Depending on the used methods, the Muse OSB can be considered as a distal or coastal freshwater lake, but none of these hypotheses have been tested by geochemical analyses on xenacanthiform hard tissues.

In this work, we propose to test the hypothesis of a strict freshwater living environment of the Xenacanthiformes from Buxières-les-Mines and the Muse OSB. We investigate the phosphate oxygen ($\delta^{18}O_p$), carbonate oxygen and carbon ($\delta^{18}O_c$ and $\delta^{13}C_c$) and the sulfur isotope composition ($\delta^{34}S$) of the bioapatite along their dorsal spines in order to define 1) their living environment and 2) its potential changes during their lifetime. To better constraint the environmental reconstruction, we also investigated the whole associated aquatic vertebrate fauna composed of acanthodian fin spines, actinopterygian scales and temnospondyl bones.

Geological context

The Bourbon-l'Archambault Basin is located in the Northern Massif Central (Fig. 78C; Allier, France; Châteauneuf 1980; Châteauneuf & Farjanel 1989) and is part of a large set of

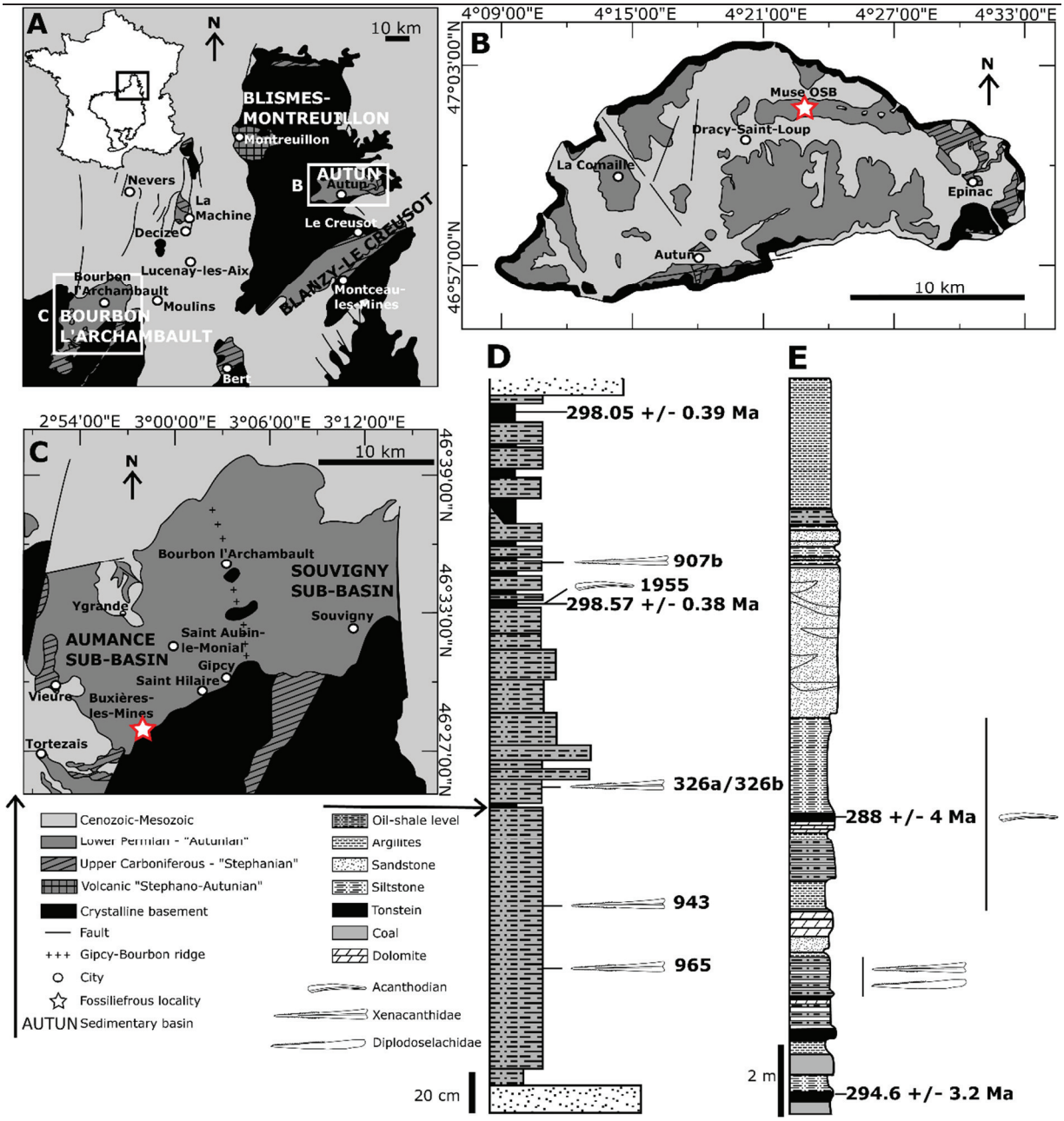

Figure 78. Geological context. **A,** simplified geological map showing the location of the Autun and Bourbon-l'Archambault basins in the Northern Massif Central. **B,** simplified geological map of the Autun Basin. **C,** simplified geological map of the Bourbon-l'Archambault Basin. **D,** simplified stratigraphy of the Muse OSB. **E,** simplified stratigraphy of Buxière-les-Mines (modified from Châteauneuf 1980; Marteau 1983; Châteauneuf & Farjanel 1989; Châteauneuf *et al.* 1992; Steyer *et al.* 2000; Gand *et al.* 2007, 2011, 2015, 2017; Pellenard *et al.* 2017).

Carboniferous-Permian non-marine basins (Fig. 78A; Gand *et al.* 2015, 2017). It extends approximately on 30 km × 20 km. It is structurally divided between two sub-basins (Châteauneuf & Farjanel 1989; Steyer *et al.* 2000): the Aumance sub-basin on the West and the Souvigny sub-basin on the East, both separated by the 'Gipcy-Bourbon ridge'. The sedimentary

deposits that are mostly composed of conglomerates, alluvial arkoses, palustrine coal seams, bituminous black shales, fluvial sandstones and thin pyroclastic horizons (Roscher & Schneider 2006) extend stratigraphically from the late Carboniferous to the Triassic (e.g. Steyer *et al.* 2000). The most sedimentologically and paleontologically investigated parts of this basin are dated from the uppermost Gzhelian (Pennsylvanian, Carboniferous) to the Sakmarian (Cisuralian, Permian). For some authors (Steyer *et al.* 2000; Roscher & Schneider 2006), the Bourbon-l'Archambault Basin is characteristic of a freshwater environment, even if some doubts remain about potential marine influences (Schultze & Soler-Gijón 2004; Schultze 2009).

The former open-cast coal mine of Buxières-les-Mines is a fossiliferous locality located in the southern part of the Aumance sub-basin (Steyer *et al.* 2000). Stratigraphically (Fig. 78D), Buxières-les-Mines is situated in the Supra-Buxières Member in the upper part of the Buxières Formation (Steyer *et al.* 2000). Even if the Carboniferous-Permian transition is badly known in this basin, the Buxières-les-Mines locality has always been considered as early Permian deposits (Steyer *et al.* 2000; Roscher & Schneider 2006; Schneider & Werneburg 2006). Correlated with the lower 'Autunian' local age (Debriette 1992; Steyer *et al.* 2000), the Buxières Formation extends from the latest Asselian to the middle Sakmarian, (Roscher & Schneider 2006; Schneider & Werneburg 2006). The volcanic tuffs "Lien Blanc" and "Lien Vert" are dated to 294.6 +/-3.2 Ma (Ducassou *et al.* 2018) and to 295 Ma (S. Bourquin, pers. comm., 2022) respectively, which implies a late Asselian to early Sakmarian age for this locality. The palaeoenvironment of Buxières-les-Mines could represent lacustrine or palustrine environments affected by several drying up events (Kaulfuß 2003) without direct evidence of marine influences, contrary to Schultze & Soler-Gijón's (2004) and Schultze's (2009) opinions for all the basins of the Northern Massif Central.

The Autun Basin is a half-graben basin, oriented West-East (30 km × 15 km), located in the Northern Massif Central (Fig. 78B; Saône-et-Loire, France; Gand *et al.* 2015, 2017). It is divided into four formations: Igornay and Muse formations that constitute the lower 'Autunian' (upper Gzhelian to lower Asselian), and Surmoulin and Millery formations that correspond to the upper 'Autunian' (post-Assselian) (Pruvost 1942). The basin is interpreted as representing fluvio-lacustrine environments (Pruvost 1942; Marteau 1983; Mercuzot 2020; Mercuzot *et al.* 2022).

The Muse OSB is located in the Muse Formation (Gand *et al.* 2007, 2011, 2015, 2017; Pellenard *et al.* 2017). It is mainly composed of oil-shale beds with intercalations of volcanic tonsteins locally named "*gore*" (Fig. 78E). Two tonsteins were dated by radiochronology at 298.05 +/- 0.39 Ma and 298.57 +/- 0.38 Ma (upper part of the Muse OSB stratigraphy in

Pellenard *et al.* [2017]). The Muse OSB is therefore dated as lower Asselian (lowermost Permian) in age, just above the Carboniferous-Permian limit. Mercuzot (2020) proposed that this locality could be characterised by a palustrine environment that corresponds to a coastal freshwater lake.

Material and methods

Material

All the material comes from the Buxières-les-Mines and the Muse OSB localities. We choose to investigate the dorsal spines of Xenacanthiformes because they are hard-mineralized structures composed of dentine (Reif 1978). which is known for being able to well-preserve isotope compositions (e.g. Fischer *et al.* 2013). Furthermore, they are non-replaced structures with a continuous incremental growth (Soler-Gijón 1999; Beck *et al.* 2016) that allow to trace variations of the isotope composition during the lifespan of these organisms.

The systematic attribution of the xenacanthiform dorsal spines is limited to the family level. Ten dorsal spines are attributed to the Xenacanthidae due to their dorso-ventral compression and their two lateral rows of denticles. Buxières-les-Mines has provided a chondrichthyan fauna composed of three xenacanthiform species (Steyer *et al.* 2000): the diplodoselachid *Orthacanthus kounoviensis* (Luccisano et al., 2022), the putative *O. buxieri* and the xenacanthid *Triodus* sp. (e.g. Steyer *et al.* 2000). For the Muse OSB, *Triodus aeduorum*, *Triodus* sp., "*Expleuracanthus*" *frossardi* and "*Expleuracanthus*" *bonnardi* belong to the Xenacanthidae (e.g. Luccisano *et al.* 2021a), but only the genus *Triodus* can be considered as valid (see Ginter *et al.* 2010). As no generic diagnostic character has been formally identified in the investigated dorsal spines, the material is referred to cf. *Triodus* sp. For the same reason, we consider that the three diplodoselachid dorsal spines from Buxières-les-Mines, which exhibits rounded cross section, two posterior rows of denticles and a long and slender morphology could belong to the genus *Orthacanthus*.

The acanthodian fauna is composed of numerous isolated, curved and laterally flattened spines that are attributed to *Acanthodes* sp. from Buxières-les-Mines (Steyer *et al.* 2000) or to *A. bonni* in the Muse OSB (Heyler 1969). *A. bourbonensis* from the Lower Permian of La Queue d'Étang in the Bourbon-l'Archambault Basin was also described by Heidtke & Dürkheim (1996). As the specific attribution based on isolated spines is hazardous and no

generic diagnostic character can be identified on them, we choose to refer the different fin spines to cf. *Acanthodes* sp.

In Buxières-les-Mines, only isolated actinopterygian scales that exhibit a distinct ganoid pattern were sampled. Most of the actinopterygians already found in this locality belong to the Paramblypteriformes, Aeduelliformes or Palaeonisciformes (Heyler 1969; Steyer *et al.* 2000). Isolated scales are not well suited for systematics, so we left this material under the open nomenclature as Actinopterygii indet. In the Muse OSB, isolated ganoid scales come from five sub-complete actinopterygian specimens. Heyler (1969) only described Aeduellidae from this locality, so we tentatively assign them to the ?Aeduellidae.

Tetrapods are extremely rare in the Muse OSB, only *Onchiodon frossardi* (Gaudry, 1867) *sensu* Werneburg & Steyer (1999) was reported. Unfortunately, no remain suitable for geochemical analyses are available. In Buxières-les-Mines, three temnospondyls were reported (Steyer *et al.* 2000): *Onchiodon*, *Melanerpeton* and *Cheliderpeton*. The studied bone samples encompass isolated and fragmented elements of the tarsus of supposedly several individuals. Because of their incomplete aspect, it has not been possible to identified them, so we left them under open nomenclature as Temnospondylii indet. for the time being. However, their size, up to 2 cm for the most complete phalange, indicates a medium to large animals which could correspond to *Onchiodon* or *Cheliderpeton*.

$\delta^{18}O_p$ analysis

Bioapatite samples were treated following a previously described wet chemistry protocol (Crowson *et al.* 1991; Lécuyer *et al.* 1993). This protocol consists of the isolation of phosphate ions (PO_4^{3-}) from bioapatite as silver phosphate (Ag_3PO_4) crystals, using acid dissolution and anion-exchange resin. For each sample, between 10 and 30 mg of biological tissues powder were dissolved in 2 ml of 2 M HF during 24h. The CaF_2 residue was separated by centrifugation and the solution was neutralized by adding 2.2 ml of 2 M KOH. Amberlite™ IRN 78 anion-exchange resin (2.5 ml) was added to the solution to separate the PO_4^{3-} ions. After 24 h, the resin was rinsed with deionized water and eluted with 27.5 ml of 0.5 M NH_4NO3. After 4 h, 0.5 ml of NH_4OH and 15 ml of an ammoniacal solution of $AgNO_3$ were added and the samples were placed in a thermostated bath at 68 °C for 7 h, allowing the slow and quantitative precipitation of Ag_3PO_4 crystals. Oxygen isotope compositions were measured using a high-temperature pyrolysis technique involving a VarioPYROcube™ elemental analyser (Elementar GmbH) interfaced in continuous flow mode to an Isoprime™ Isotopic Ratio Mass Spectrometer (Elementar Uk Ltd; Fourel *et al.* 2011; The EA-Py-CF-IRMS

technique was performed at the Plateforme d'Écologie Isotopique du Laboratoire d'Écologie des Hydrosystèmes Naturels et Anthropisés [LEHNA] – UMR5023, Université Claude Bernard Lyon 1). For each sample, 5 aliquots of 300 µg of Ag_3PO_4 were mixed with 400 µg of pure graphite powder and loaded in silver foil capsules. Pyrolysis was performed at 1450°C. Measurements were calibrated against NBS120c (natural Miocene phosphorite from Florida) and NBS127 (barium sulfate, $BaSO_4$: $\delta^{18}O = 9.3$ ‰). The value of NBS120c was fixed at 21.7‰ (VSMOW; Lécuyer *et al.* 1993) and that of NBS127 set at the certified value of 9.3‰ (V-SMOW; (Hut 1987; Halas & Szaran 2001) for correction of instrumental mass fractionation during CO isotopic analysis. Silver phosphate samples precipitated from standard NBS120c were repeatedly analysed ($\delta^{18}O_p = 21.7$‰; $1\sigma = 0.2$; $n = 20$) along with the silver phosphate samples derived from fossil bioapatites to ensure that no isotopic fractionation occurred during the wet chemistry. Data are reported as $\delta^{18}O_p$ values versus V-SMOW (in ‰).

$\delta^{18}O_c$ and $\delta^{13}C_c$ analyses

To remove potential organic contaminants and secondarily precipitated calcite, bioapatite samples were pre-treated following the protocol of Koch *et al.* (1997). About 10 mg of bioapatite powder was washed with a 2% NaOCl solution, followed by a 0.1 M $C_2O_2H_4$ solution. Each treatment lasted for 24 h and samples were rinsed 5 times with distilled water between each one. Pre-treated powders were collected after 24 h of air-dried at 40°C. Carbon and oxygen isotope compositions were measured using an isoFLOW system connected on-line in continuous flow mode to a precisION mass spectrometer (Elementar UK). For each sample, three aliquots of 1 to 2 mg of pre-treated bioapatite powder were loaded in LABCO Exetainer® 3.7 ml soda glass vials, round bottomed with Exetainer caps (LABCO UK), and reacted with anhydrous phosphoric acid. The reaction took place at 90°C in a temperature regulated sample tray. The CO_2 gas generated during the acid digestion of the carbonate sample was then transferred to the mass spectrometer via the centrION interface. Calibrated CO_2 gas was used as the monitoring gas. For bioapatite, the acid fractionation factor α (CO_2–apatite carbonate) of 1.00773 determined for the NBS120c phosphate rock reference material was used (Passey *et al.* 2007). The calibrated materials used were Carrara marble ($\delta^{18}O = -1.84$‰ V-PDB, $\delta^{13}C = +2.03$‰ V-PDB [Fourel *et al.* 2016]), NBS18 ($\delta^{18}O = -23.2$‰ V-PDB, $\delta^{13}C = -5.01$‰ V-PDB) and NBS120c ($\delta^{18}O = -1.13$‰ V-PDB, $\delta^{13}C = -6.27$‰ V-PDB) (Passey *et al.* 2007). Isotopic compositions are quoted in the standard δ notation relative to V-SMOW for oxygen and V-PDB (Vienna Pee Dee belemnite) for carbon.

$\delta^{34}S$ analysis

Sulfur isotope compositions of bioapatite samples were measured using a VarioPYROcube™ elemental analyser in NCS combustion mode interfaced in continuous-flow mode with an Isoprime 100 isotope ratio mass spectrometer. Bioapatite samples were analysed by weighing 3 aliquots of 5 mg in tin foil capsules mixed with 15 mg of pure tungsten oxide (WO_3) powder. Tungsten oxide is a powerful oxidant that ensures the full thermal decomposition of bioapatite sulfate into sulfur dioxide (SO_2) gas (Goedert *et al.* 2016). Measurements were calibrated against S2 (silver sulfide, Ag_2S), IAEA-SO-5 and IAEA-SO-6 international standards. For each analytical run of bioapatite samples, we have also analysed BCR32 samples as a compositional and isotopic standard (S% = 0.72, certified value; $\delta^{34}S$ = 18.4‰; Lécuyer *et al.* 1993; Goedert *et al.* 2016) to ensure that analytical conditions were optimal to perform sulfur isotope analyses on samples with low-sulfur content. The standard deviation of $\delta^{34}S$ measurements was better than 0.2‰. Data are reported as $\delta^{34}S$ vs. V-CDT. The VarioPYROcube™ elemental analyser was also used to measure the sulfur content of samples.

Palaeotemperature

As Xenacanthiformes, Acanthodii and Actinopterygii are primarily non-air-breathing vertebrates, it is assumed that their body temperature (T_b) is similar to that of their surrounding water (T_w). Furthermore, their $\delta^{18}O$ body water ($\delta^{18}O_{BW}$) value is considered to be equal to the $\delta^{18}O$ of ambient environment ($\delta^{18}O_w$) (Kolodny *et al.* 1983). In order to investigate the T_b, we use the equation of Longinelli & Nuti (1973), updated by Lécuyer *et al.* (2013) that has proven to be valid for a large range of invertebrates and vertebrates:

$$T_w(°C) = T_b(°C) = 117.4(\pm 9.8) - 4.5(\pm 0.43) \times \left(\delta^{18}O_{\mathrm{p}} - \delta^{18}O_{\mathrm{w}}\right)$$

Sampling

The xenacanthiform dorsal spine growth pattern has been discussed by Soler-Gijón (1999) and Beck *et al.* (2016). They showed that the growth occurred by the addition of new proximal dentine layers. Thus, the oldest part of the dorsal spine is the apex, i.e. the inner distal part. As the pattern of the different growth layers of the xenacanthiforms dorsal spines was not well-preserved and in order to have sufficient quantity of material for the geochemical process, we sampled *Triodus* dorsal spines by cutting small sections all along the length of each spine.

For *Orthacanthus* dorsal spine, we sampled in the same way but with focus on the most external growth layer to avoid mixing of several growth layers.

Following Jerve *et al.* (2017) the growth model of the acanthodian fin spines is more related to chondrichthyans than to osteichthyans. However, no study has identified dentine growth layers like in some extant (e.g. Maisey 1979; Burrow *et al.* 2015, 2016) and extinct (e.g. Maisey 1978, 1982; Soler-Gijón 1999; Beck *et al.* 2016) chondrichthyans. The acanthodian fin spine grows by implementation of new dentine material from the apex to the base. Consequently, the distal part of the fin spine is older than the base.

Results

$\delta^{18}O_p$, $\delta^{18}O_c$, $\delta^{13}C_c$ and $\delta^{34}S$ values

The oxygen, carbon and sulfur isotope compositions of bioapatite phosphates and carbonates are reported in Table 10 (see Table S3 for the detailed values along the acanthodian and xenacanthiform spines length). In the Muse OSB, the $\delta^{18}O_p$ values ranges from 17.3‰ to 25.1‰, the $\delta^{18}O_c$ from 21.2‰ to 23.1‰, the $\delta^{13}C_c$ from 3.3‰ to 5.9‰ and the $\delta^{34}S$ from 1.2‰ to 6.9‰. In Buxières-les-Mines, the $\delta^{18}O_p$ values ranges from 14.0‰ to 18.7‰, the $\delta^{18}O_c$ from 19.3‰ to 23.8‰, the $\delta^{13}C_c$ from -2.7‰ to 5.7‰ and the $\delta^{34}S$ from -20.3‰ to 8.0‰ (Figs. 79-81). Compared to Buxières-les-Mines, for the whole dataset and within a same taxonomic group, the Muse OSB has relatively higher $\delta^{18}O_p$ and $\delta^{18}O_c$ values whereas the differences in $\delta^{13}C_c$ and $\delta^{34}S$ are less marked. Between the taxonomic groups, the temnospondyls from Buxières-les-Mines have the lowest $\delta^{18}O_p$ (15.1‰ +/- 0.6) and $\delta^{13}C_c$ (-2.6‰ +/- 0.1).

Isotopic variations along the spines

Along a same fin spine, the acanthodians from the Muse OSB and Buxières-les-Mines (Fig. 82) do not show significant variations of their $\delta^{18}O_p$, $\delta^{18}O_c$, $\delta^{13}C_c$ and $\delta^{34}S$ values (Fig. 83), i.e. less than 1‰. The only exception is the specimen (1024) from the Muse OSB in which the $\delta^{18}O_p$, $\delta^{13}C_c$ and $\delta^{34}S$ values decrease from the apex to the base.

$\delta^{18}O_p$ values of xenacanthid dorsal spines from the Muse OSB range from 17.3‰ to 25.1‰ (Fig. 84). There are different observed tendencies in the $\delta^{18}O_p$ values along the dorsal spine. One dorsal spine (965a) shows no significative evolution in the $\delta^{18}O_p$ values. For the other three ones, there is an increase in $\delta^{18}O_p$ values between the apex and the base. Specimen

Table 10. Systematics, skeletal tissue, location, and age are given along with oxygen, carbon and sulfur isotopic compositions of bioapatite phosphate and carbonate samples. The numbers in bracket correspond to the number of specimens used for $\delta^{18}O_c$, $\delta^{13}C_c$ and $\delta^{34}S$ analyses.

Specimen	Skeletal tissue	Taxon	Locality name	Age	n	δ18Op (%V-SMOW)	sd (δ18Op)	δ18Oc (%V-SMOW)	sd (δ18Oc)	δ13Cc (%V-PDB)	sd (δ13Cc)	δ34S (%V-CDT)	sd (δ34S)
MU1	ganoid scale	?Aeduellidae	Muse OSB	early Asselian	1	17.9		21.3		4.9		6.4	
MU2	ganoid scale	?Aeduellidae	Muse OSB	early Asselian	1	17.8		21.5		4.5		6.1	
MU3	ganoid scale	?Aeduellidae	Muse OSB	early Asselian	1	17.6		21.2		3.3		3.6	
MU4	ganoid scale	?Aeduellidae	Muse OSB	early Asselian	1	18.1		21.3		5.9		6.9	
MU5	ganoid scale	?Aeduellidae	Muse OSB	early Asselian	1	18.6		21.3		5.3		7.0	
1924	fin spine	cf. *Acanthodes* sp.	Muse OSB	early Asselian	3	20.6	0.6	22.5	0.9	4.5	1.1	2.2	1.3
1955	fin spine	cf. *Acanthodes* sp.	Muse OSB	early Asselian	8	19.5	0.2						
943	dorsal spine	cf. *Triodus* sp.	Muse OSB	early Asselian	5	18.3	0.6						
907b	dorsal spine	cf. *Triodus* sp.	Muse OSB	early Asselian	2	21.3	2.5						
965a	dorsal spine	cf. *Triodus* sp.	Muse OSB	early Asselian	6	19.2	0.2						
326a/326b	dorsal spine	cf. *Triodus* sp.	Muse OSB	early Asselian	6	24.1	1.3						
BXT	ganoid scale	Actinopterygii indet.	Buxières-les-Mines	Asselian-Sakmarian	1	16.3		20.8		2.1		-3.8	0.2
BX39	ganoid scale	Actinopterygii indet.	Buxières-les-Mines	Asselian-Sakmarian	1	16.7		20.5		0.7			
D062	ganoid scale	Actinopterygii indet.	Buxières-les-Mines	Asselian-Sakmarian	1	16.9		20.1		1.3			
D20-1	ganoid scale	Actinopterygii indet.	Buxières-les-Mines	Asselian-Sakmarian	1	16.8		20.1		1.6			
D20-2	ganoid scale	Actinopterygii indet.	Buxières-les-Mines	Asselian-Sakmarian	1	16.4		20.4		2.0			
0-20-04-97-2	ganoid scale	Actinopterygii indet.	Buxières-les-Mines	Asselian-Sakmarian	1							7.1	
BX-12-03-96-2	fin spine	cf. *Acanthodes* sp.	Buxières-les-Mines	Asselian-Sakmarian	1							4.6	
NN5	fin spine	cf. *Acanthodes* sp.	Buxières-les-Mines	Asselian-Sakmarian	3	17.4	0.1						
NN9	fin spine	cf. *Acanthodes* sp.	Buxières-les-Mines	Asselian-Sakmarian	9 (4)	17.3	0.2	21.3	0.3	6.8	0.3		
BJM2	fin spine	cf. *Acanthodes* sp.	Buxières-les-Mines	Asselian-Sakmarian	3 (1)	17.1	0.2	19.3	1.0	2.4	0.6		
BJM3	fin spine	cf. *Acanthodes* sp.	Buxières-les-Mines	Asselian-Sakmarian	5 (4)	17.4	0.1	21.1	0.2	3.4	0.1		
BXA86	fin spine	cf. *Acanthodes* sp.	Buxières-les-Mines	Asselian-Sakmarian	4	18.6	0.1						
BX28	dorsal spine	cf. *Triodus* sp.	Buxières-les-Mines	Asselian-Sakmarian	3	16.9	0.3						
D07	dorsal spine	cf. *Triodus* sp.	Buxières-les-Mines	Asselian-Sakmarian	6	17.4	0.3						
D08	dorsal spine	cf. *Triodus* sp.	Buxières-les-Mines	Asselian-Sakmarian	7 (5)	18.1	0.4	21.7	0.2	3.9	0.2		
BX23-1	dorsal spine	cf. *Triodus* sp.	Buxières-les-Mines	Asselian-Sakmarian	3	16.3	0.0						
BX23-2	dorsal spine	cf. *Triodus* sp.	Buxières-les-Mines	Asselian-Sakmarian	3	16.3	0.4						
D-11-11-96 21	dorsal spine	cf. *Triodus* sp.	Buxières-les-Mines	Asselian-Sakmarian	14	17.3	0.4						
D-13-06-98 5	dorsal spine	cf. *Orthacanthus* sp.	Buxières-les-Mines	Asselian-Sakmarian	12	17.6	0.2						
BX04	dorsal spine	cf. *Orthacanthus* sp.	Buxières-les-Mines	Asselian-Sakmarian	19	16.7	0.3	20.9	0.2	1.2	0.1	-1.7	3.1
D17	dorsal spine	cf. *Orthacanthus* sp.	Buxières-les-Mines	Asselian-Sakmarian	6(3)	16.4	0.1	20.6	0.2	0.6	0.1	1.3	0.1
BXR1	Bone	Temnospondyli indet.	Buxières-les-Mines	Asselian-Sakmarian	1	15.7		20.1		-2.6		-20.3	
BXR2	Bone	Temnospondyli indet.	Buxières-les-Mines	Asselian-Sakmarian	1	15.5		20.0		-2.7		5.5	
BXR3	Bone	Temnospondyli indet.	Buxières-les-Mines	Asselian-Sakmarian	1	15.4		19.9		-2.5		1.1	
BXR4	Bone	Temnospondyli indet.	Buxières-les-Mines	Asselian-Sakmarian	1	15.5		20.1		-2.4		7.2	
BXR5	Bone	Temnospondyli indet.	Buxières-les-Mines	Asselian-Sakmarian	1	15.5		20.1		-2.6		5.5	
BXR6	Bone	Temnospondyli indet.	Buxières-les-Mines	Asselian-Sakmarian	1	14.0		20.1		-2.7		5.8	
BXR7	Bone	Temnospondyli indet.	Buxières-les-Mines	Asselian-Sakmarian	1	14.9		19.7		-2.6		6.2	
BXR8	Bone	Temnospondyli indet.	Buxières-les-Mines	Asselian-Sakmarian	1	14.6						7.9	

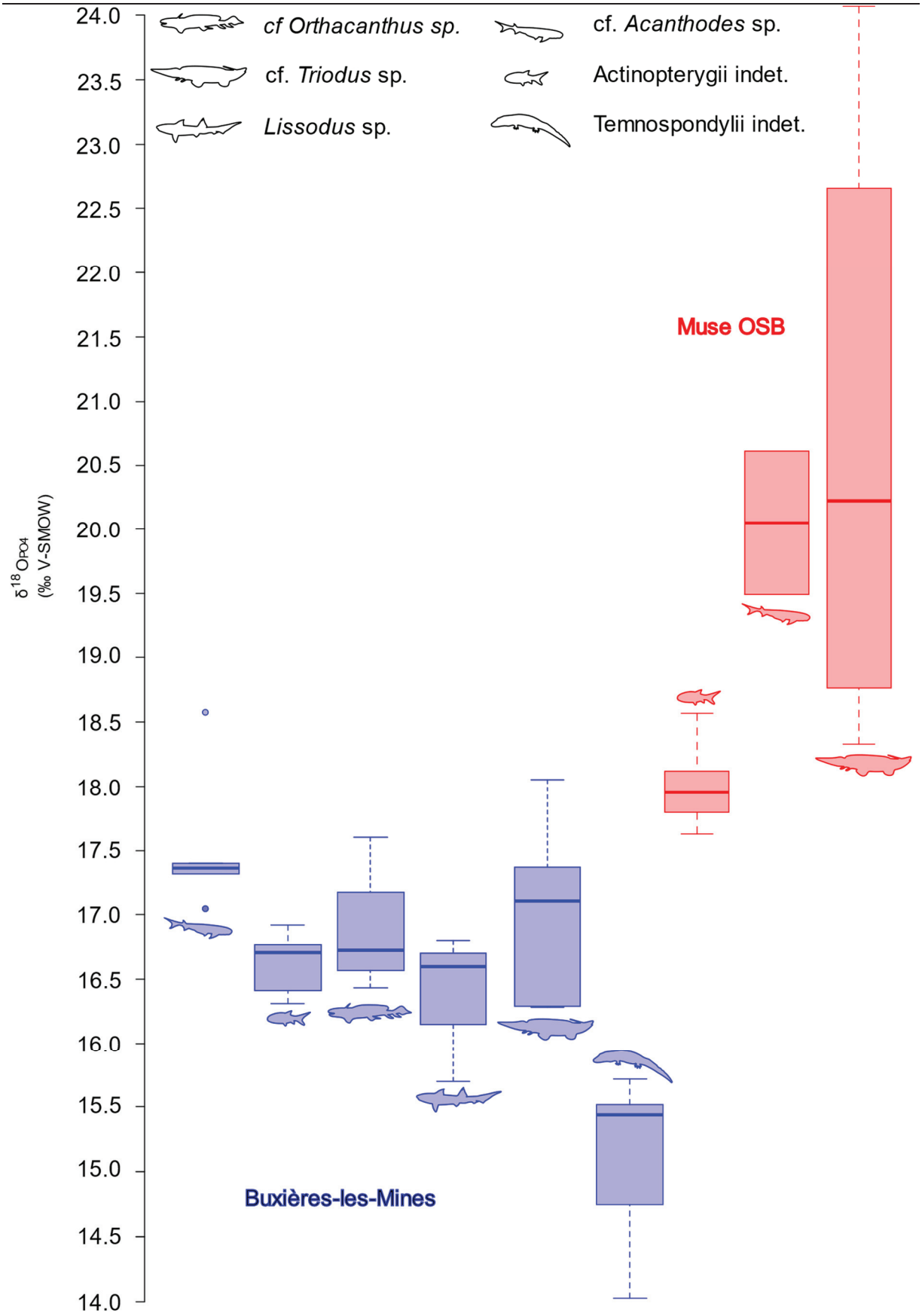

Figure 79. Boxplot of the $\delta^{18}O_p$ values of the vertebrate faunas from the Muse OSB and Buxières-les-Mines. Data for the boxplot of *Lissodus* sp. are from Fischer *et al.* (2013).

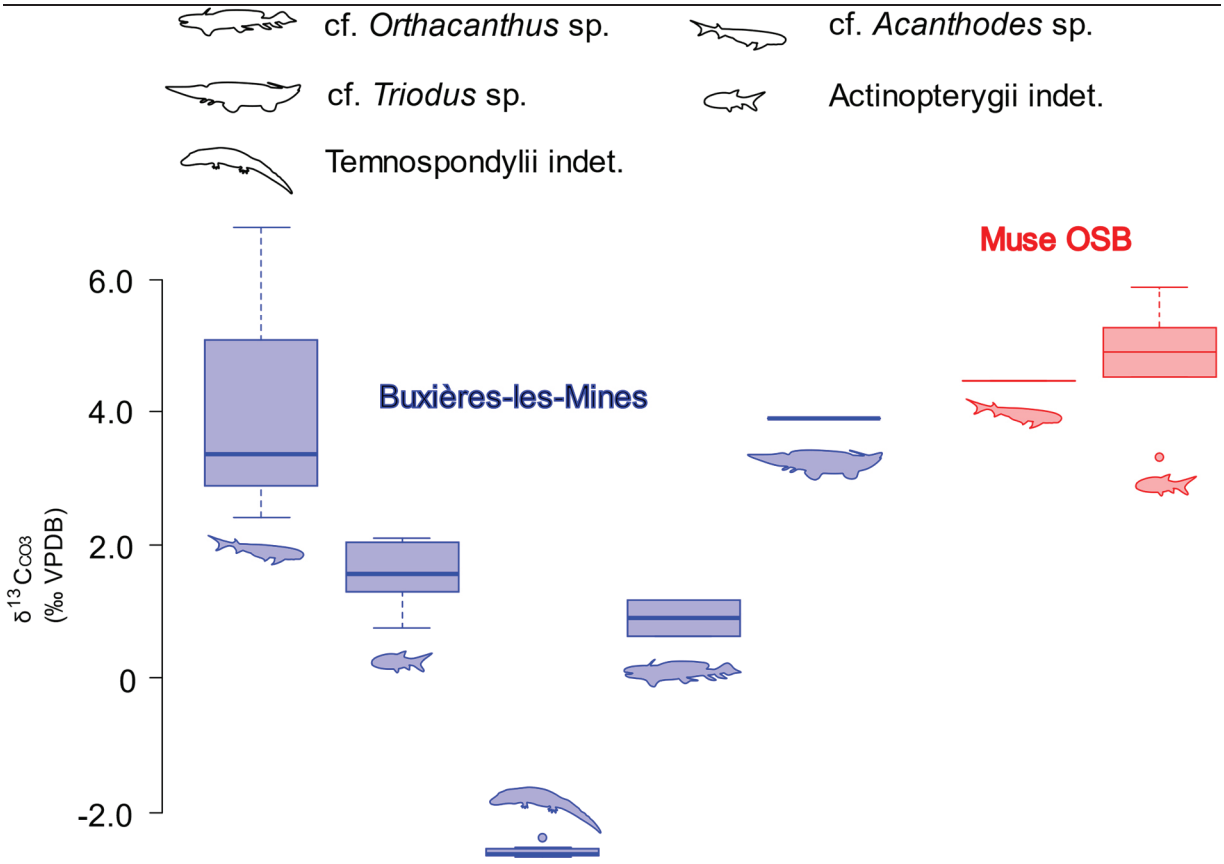

Figure 80. Boxplot of the $\delta^{13}C_c$ values of the vertebrate faunas from the Muse OSB and Buxières-les-Mines.

943 shows an increase of in $\delta^{18}O_p$ values of almost 2‰ whereas specimens 326 and 907b exhibit an increase of more than 4‰. For the two diplodoselachid dorsal spine from Buxières-les-Mines (Fig. 84), $\delta^{18}O_p$ values range from 17.2‰ to 18.0‰ (D13) and from 16.2‰ to 17.1‰ (BX04). The $\delta^{18}O_p$ values tend to decrease from the apex to the base with a distinct fall on the two dorsal spines, but they never reach more than 18‰ and there is less than 1‰ difference between the highest and the lowest values. $\delta^{18}O_p$ values of xenacanthid from Buxières-les-Mines (Fig. 84) range from 15.9‰ to 18.5‰. Despite apparent tendencies to increase (BX28) or to decrease

$\delta^{18}O_p$ values of xenacanthid dorsal spines from the Muse OSB range from 17.3‰ to 25.1‰ (Fig. 84). There are different observed tendencies in the $\delta^{18}O_p$ values along the dorsal spine. One dorsal spine (965a) shows no significative evolution in the $\delta^{18}O_p$ values. For the other three ones, there is an increase in $\delta^{18}O_p$ values between the apex and the base. Specimen 943 shows an increase of in $\delta^{18}O_p$ values of almost 2‰ whereas specimens 326 and 907b exhibit an increase of more than 4‰. For the two diplodoselachid dorsal spine from Buxières-les-Mines (Fig. 84), $\delta^{18}O_p$ values range from 17.2‰ to 18.0‰ (D13) and from 16.2‰ to 17.1‰ (BX04).

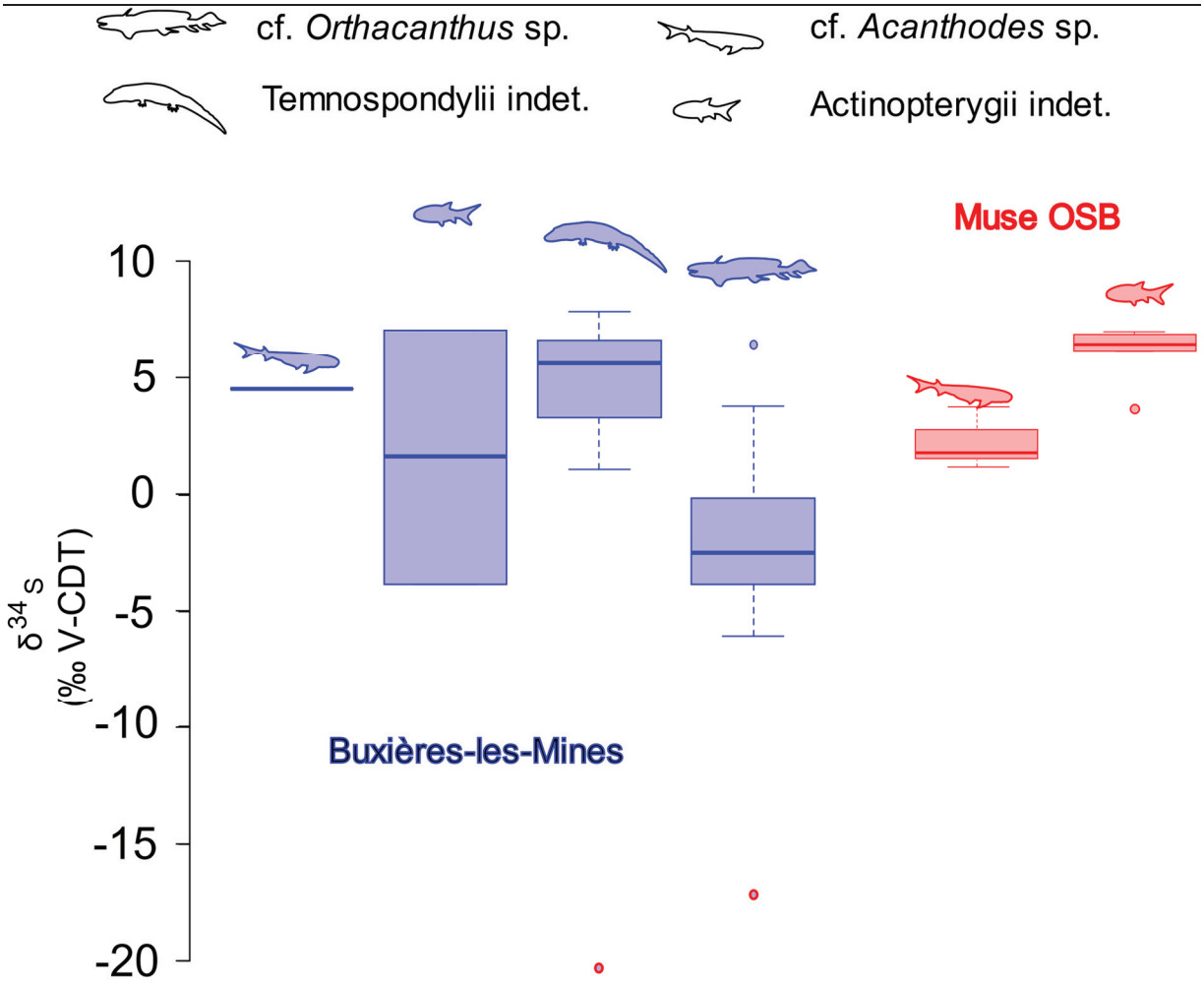

Figure 81. Boxplot of the $\delta^{34}S$ values of the vertebrate faunas from the Muse OSB and Buxières-les-Mines. Red points are diagenetic altered samples in Buxières-les-Mines.

The $\delta^{18}O_p$ values tend to decrease from the apex to the base with a distinct fall on the two dorsal spines, but they never reach more than 18‰ and there is less than 1‰ difference between the highest and the lowest values. $\delta^{18}O_p$ values of xenacanthid from Buxières-les-Mines (Fig. 84) range from 15.9‰ to 18.5‰. Despite apparent tendencies to increase (BX28) or to decrease (D08), the $\delta^{18}O_p$ values within each dorsal spine do not vary more than 1‰ between the apex and the base.

In Buxières-les-Mines, $\delta^{13}C_c$ (Fig. 82) values of BX04 range from 0.9‰ to 1.9‰ with exception of the most proximal point (base of the dorsal spine) at 0‰. The variation seems to be cyclical. $\delta^{18}C_c$ values of D08 continuously decrease from the apex to the base from 5.2‰ to 2.7‰. The $\delta^{34}S$ values of BX04 (Fig. 83) range from -6.0‰ to 3.8‰ and seem to follow

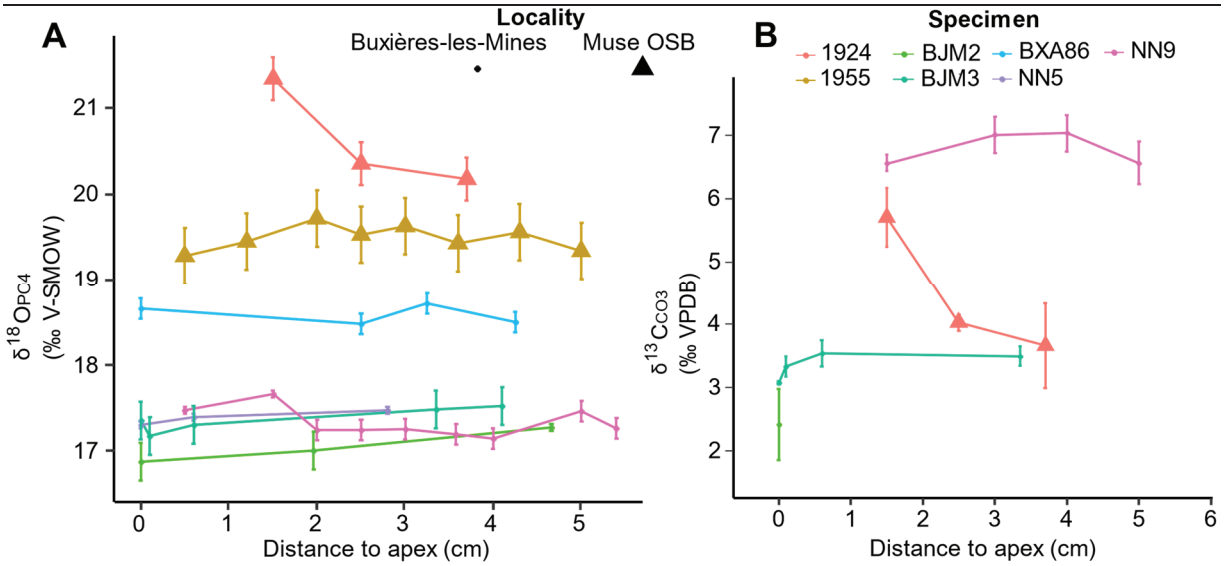

Figure 82. Evolution of the $\delta^{18}O_p$ (**A**) and $\delta^{13}C_c$ (**B**) values along the acanthodian fin spines.

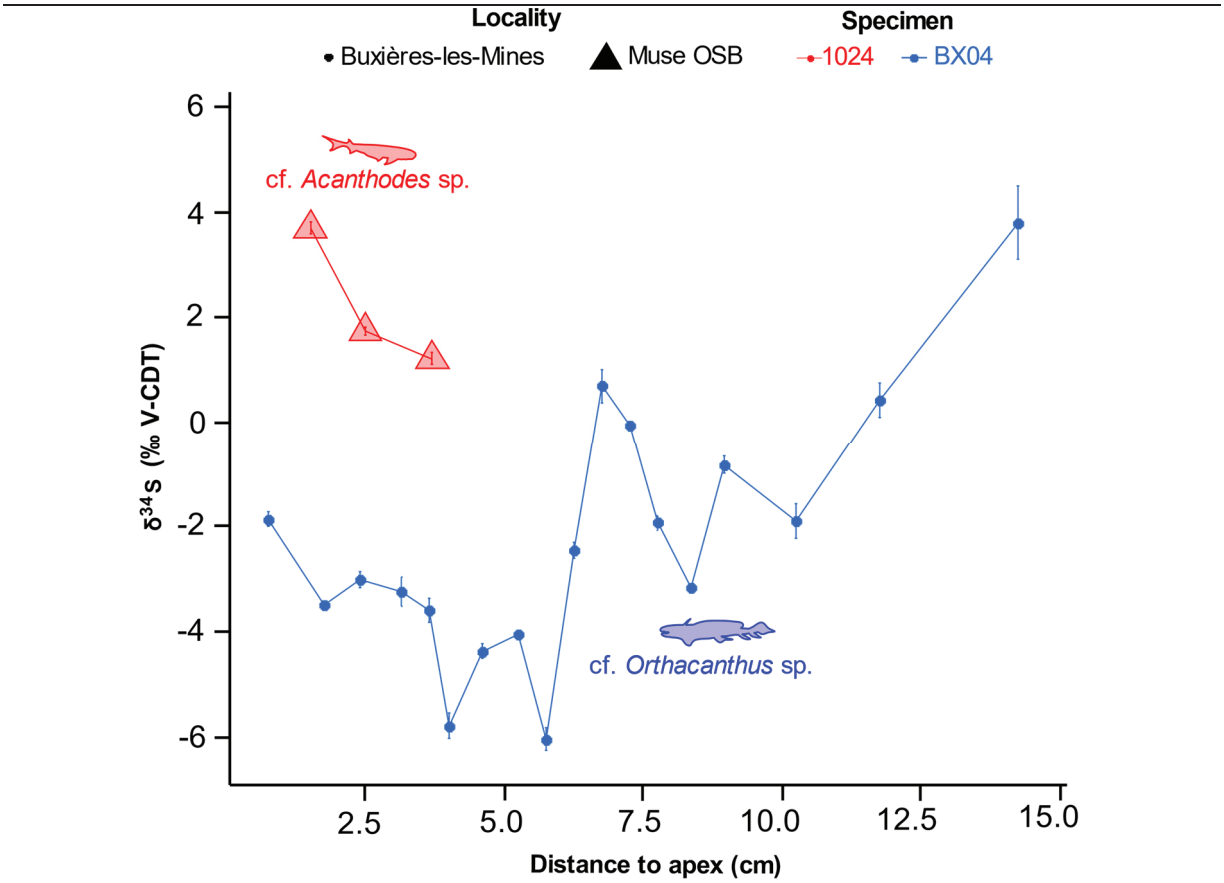

Figure 83. Evolution of the $\delta^{34}S$ values along the acanthodian and xenacanthiform spines.

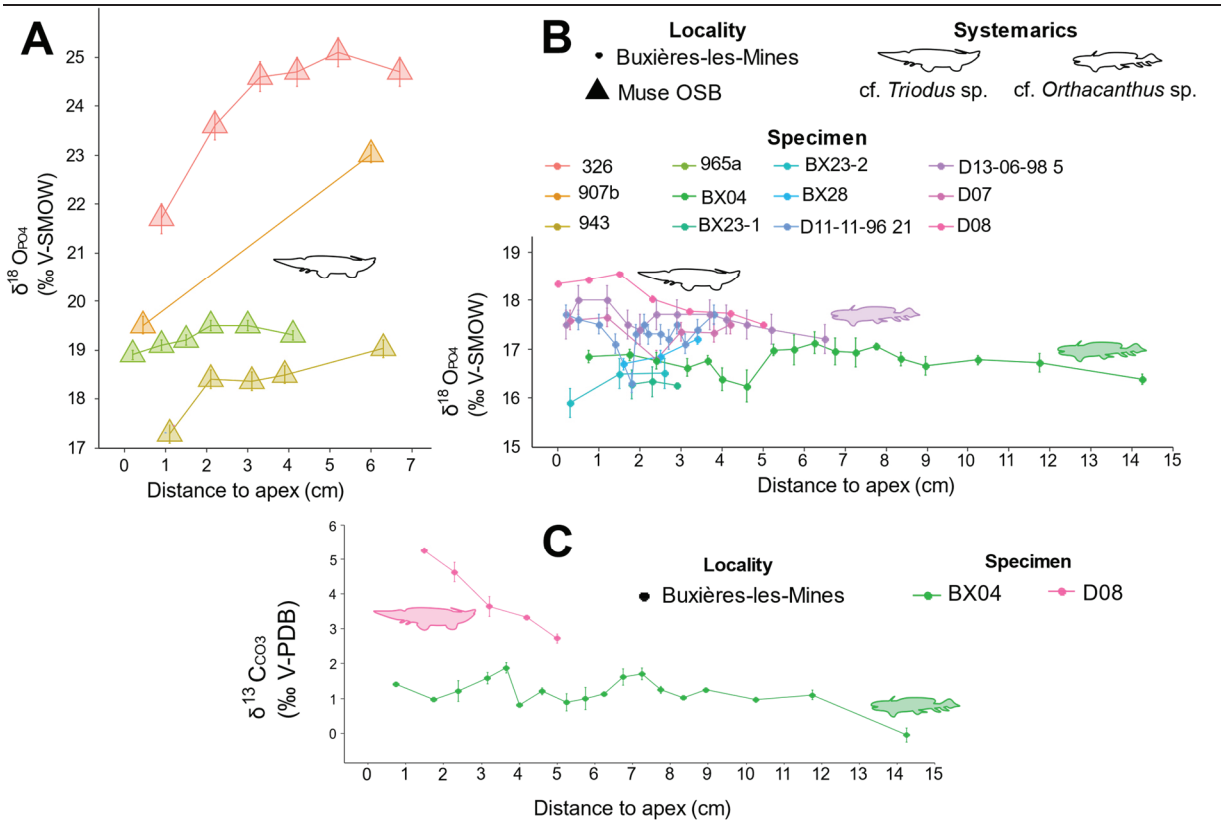

Figure 84. Evolution of the $\delta^{18}O_p$ (**A–B**) and $\delta^{13}C_c$ (**C**) values along the xenacanthiform dorsal spines.

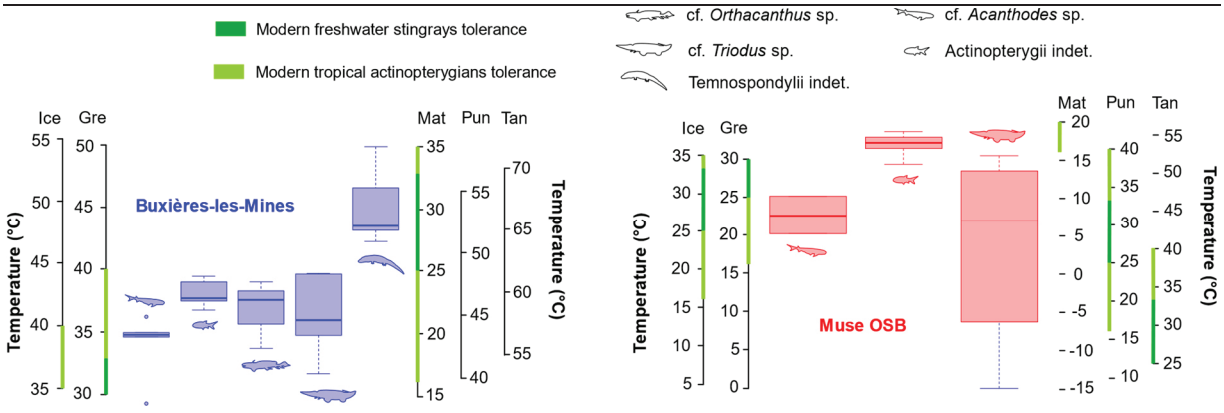

Figure 85. Reconstruction of the palaeotemperatures in Buxières-les-Mines and the Muse OSB. **Abbreviations: Ice,** icehouse Earth; **Gre,** greenhouse Earth; **Mat,** Lake Matano; **Pun,** Lake Punta Laguna; **Tan,** Lake Tanganyika.

irregular cycles of decreases and increases with the highest values at the base of the dorsal spine.

Reconstruction of the palaeotemperature

The viable environmental temperatures of current tropical actinopterygians range from 16°C to 40°C (Pandian & Vivekanandan 1985) and those of freshwater stingrays from 25°C to 33°C (Almeida *et al.* 2009) We reconstruct the palaeotemperatures (Fig. 85) based on four different modern aquatic environments with the corresponding $\delta^{18}O_w$ (see Table S4): seawater with (0‰) and without (-1‰) glaciation (Shackleton 1975), Lake Matano (-4.3‰) (Katsev *et al.* 2010), Lake Punta Laguna (0.93‰) (Curtis & Hodell 1996) and Lake Tanganyika (3.85‰) (Casanova & Hilaire-Marcel 1992) in order to find the most theoretically viable one.

For Buxières-les-Mines, only the Lake Matano model proposes viable temperatures for the investigated fauna. The greenhouse Earth model could be viable for the highest $\delta^{18}O_p$ values. For the Muse OSB, no model is entirely viable for the calculated temperature range. The Lake Punta Laguna, icehouse and greenhouse Earth models could be viable for the lowest $\delta^{18}O_p$ values and the Lake Tanganyika model could be viable for the highest $\delta^{18}O_p$ values.

Discussion

Preservation of the original isotopic compositions of fossil bioapatites

No method is available to formally demonstrate that the original isotopic compositions of the $\delta^{18}O_p$ are preserved in fossil bioapatites. However, several tests have been proposed. In modern vertebrate skeletal tissues, and supposedly in fossil ones, phosphates and carbonates of the bioapatite both precipitates following an equilibrium with body water. Consequently, $\delta^{18}O_p$ and $\delta^{18}O_c$ are positively correlated. Re-equilibration of water phosphates and carbonates is not expected because both have different isotopic exchanges. Moreover, it is expected that the $\delta^{18}O_p$ and $\delta^{18}O_c$ values of fossil fishes and sharks follow those of modern vertebrates (e.g. Kolodny & Luz 1991; Bryant *et al.* 1996; Iacumin *et al.* 1996; Vennemann *et al.* 2001; Lécuyer *et al.* 2003). $\delta^{18}O_p$ and $\delta^{18}O_c$ values of vertebrates from Buxières-les-Mines and the Muse OSB (Fig. 86) follow the distribution of modern and fossil sharks. Another evidence in favour of an original preservation of the isotopic compositions is the difference of almost 1.5‰ between exclusive aquatic and semi-aquatic vertebrates in Buxières-les-Mines. As they have different physiology and ecology, a difference is expected. For these reasons, we can consider that the original oxygen isotopic signal is preserved.

We compare the oxygen isotope compositions of the $\delta^{18}O_p$ and the $\delta^{18}O_c$ values with the carbonate content (CO_3^{2-} wt%) of each sample (Fig. 87). In modern mammals, the $\delta^{18}O_p$ values are between 7 and 9‰ lower than the $\delta^{18}O_c$ values (Iacumin *et al.* 1996), but this difference can

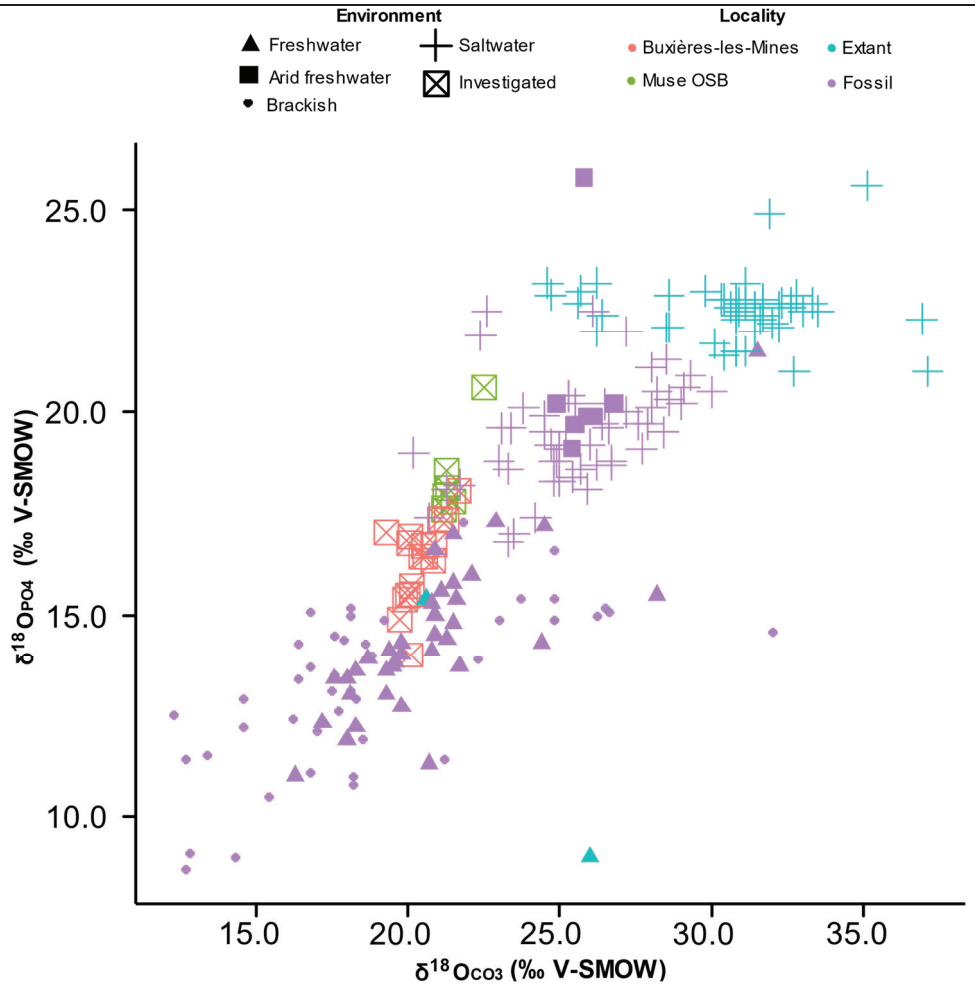

Figure 86. Oxygen isotope compositions of bioapatite ($\delta^{18}O_p$) from studied vertebrate taxa plotted against their corresponding oxygen isotope composition of carbonate ($\delta^{18}O_c$). Other points are extant and fossil referent samples from different aquatic environments. Additional extant data are from Iacumin *et al.* (1996) and Vennemann *et al.* (2001) and fossil data are from Kolodny & Luz (1991); Fricke *et al.* (1998); Lécuyer *et al.* (2003a); Amiot *et al.* (2010); Goedert *et al.* (2018).

increase to 14.7‰ in modern sharks (Vennemann *et al.* 2001). Microbially induced diagenetic alteration has previously been shown to increase the offset between $\delta^{18}O_p$ and $\delta^{18}O_c$ values. The CO_3^{2-} wt% values of teeth and bones of modern vertebrates range from 2.0 to 13.4 wt% (Brudefold & Soremark 1967; Rink & Schwarcz 1995; Vennemann *et al.* 2001). The sample from Buxières-les-Mines and Muse have $\delta^{18}O_c$-$\delta^{18}O_p$ and CO_3^{2-} wt% values out of the supposed diagenetic area, except two samples. So, we assume that the oxygen and carbon content of the carbonate has preserved the original isotopic signal of the global sampled data set.

Concerning the $\delta^{34}S$ values, secondary sulfur-bearing minerals can precipitate at the surface or within the bones during fossilisation and they would tend to increase the sulfur

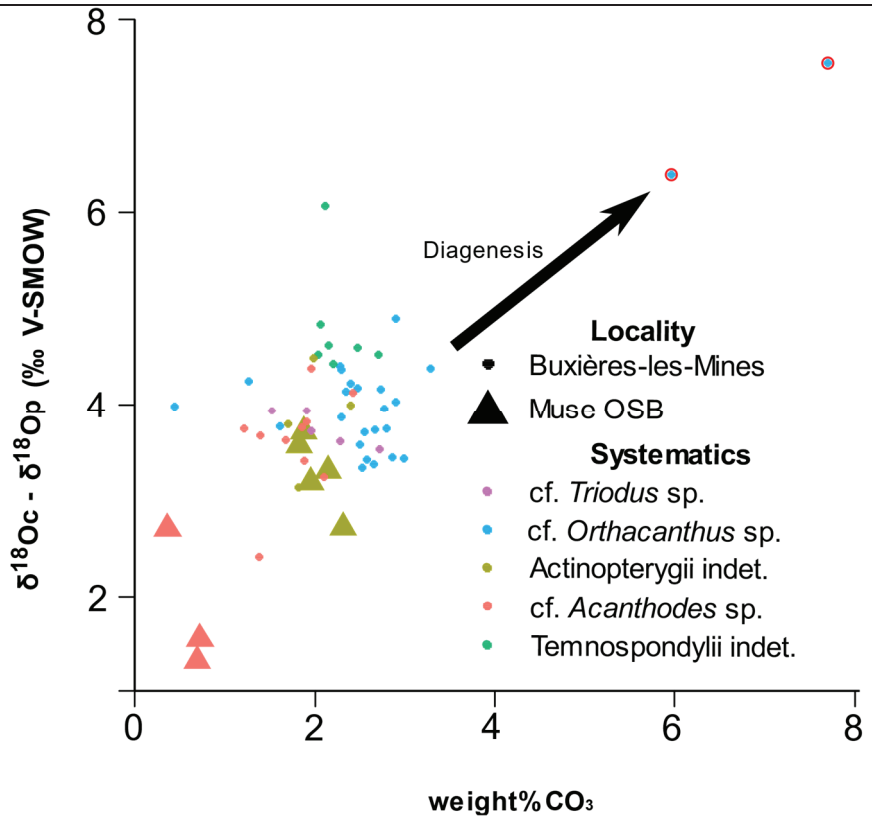

Figure 87. Difference between the oxygen isotope compositions of bioapatite carbonate ($\delta^{18}O_c$) and phosphate ($\delta^{18}O_p$) plotted against the carbonate concentration.

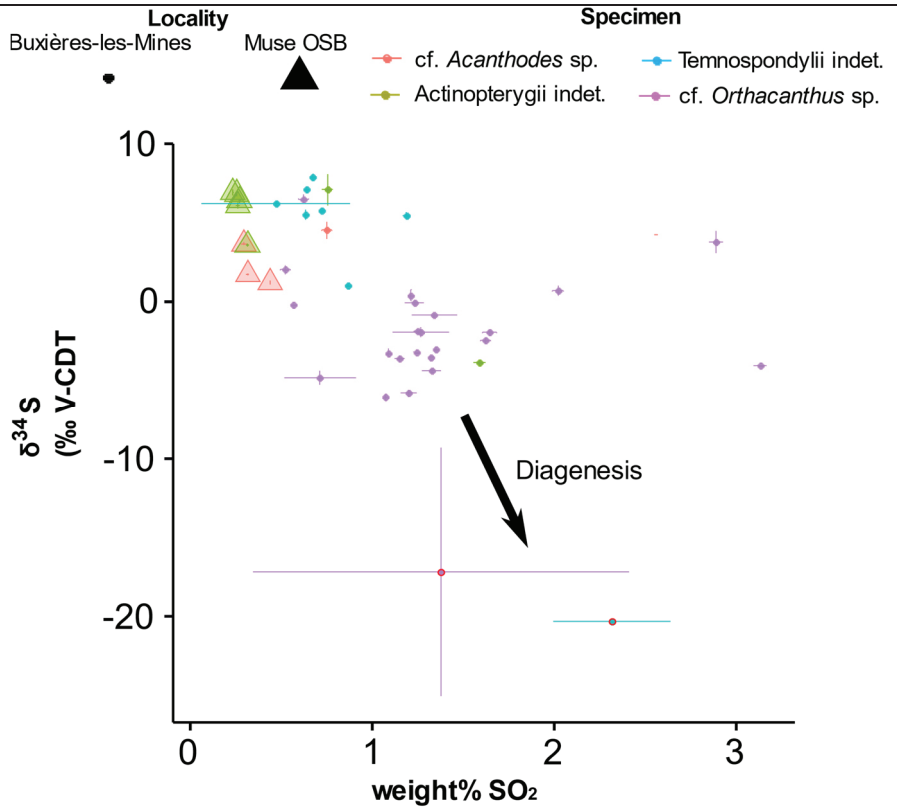

Figure 88. The sulfur isotope composition ($\delta^{34}S$) plotted against the sulfur content (weight% SO_2).

content of bones, which is lower than 0.6 weight% SO_2 (wt%) in modern bioapatites (e.g. Goedert *et al.* 2018). The Muse OSB samples show lower wt% (from 0.2 wt% to 0.4 wt%) than those of Buxières-les-Mines (from 0.5 wt% to 3.1 wt%; Fig. 88). In the Muse OS, Acanthodians and Actinopterygians have similar $\delta^{34}S$ and sulfur content values that vary little within taxonomic groups. The $\delta^{34}S$ values can be interpreted as biogenic. The sample size at Buxières-les-Mines being more important than that of the Muse OSB, the variability of the $\delta^{34}S$ and wt% is higher within taxonomic groups. However, the majority is comprised between −10‰ and 10‰ for the $\delta^{34}S$ and between 0 wt% and 2 wt% for the sulfur content. Within taxonomic groups, a few points show low $\delta^{34}S$ values for slightly higher wt%. Consequently, these few samples are interpreted as diagenetically altered and the global $\delta^{34}S$ measurements of Buxières-les-Mines could be seen as biogenic.

$\delta^{18}O_p$ values

Buxières-les-Mines

The oxygen isotope composition is more likely to be well preserved in conodonts than in brachiopods (Joachimski *et al.* 2004, 2006, 2009; Wenzel *et al.* 2008; Chen *et al.* 2013), so $\delta^{18}O_p$ from conodonts can be used as a marine reference. Bioapatite $\delta^{18}O_p$ values of Moscovian-Gzhelian tropical marine conodonts range from 18.2‰ to 21.5‰ and those of tropical marine vertebrates from 18.7‰ to 21.2‰ from the late early Carboniferous (Joachimski *et al.* 2006) and around 21.6‰ for the tropical marine conodonts from the early late Carboniferous (Fischer *et al.* 2013). Even if the early Permian bioapatite $\delta^{18}O_p$ values are not available, those of intertropical to temperate marine Triassic range from 17.8‰ to 22.3‰ (Fischer *et al.* 2012). Consequently, we can consider that $\delta^{18}O_p$ values of early Permian marine setting is between 18‰ and 22‰.

Except for the temnospondyls which have $\delta^{18}O_p$ values between 14.0‰ and 15.7‰, the whole aquatic vertebrate fauna, i.e. actinopterygians, acanthodians and xenacanthiforms, shows $\delta^{18}O_p$ values between 16.2‰ and 18.7‰ (Fig. 79). These values suggest a freshwater environment as already recorded in other early European Permian localities. The fact that all the strict aquatic vertebrates which are supposed to live within a same food web (Kriwet *et al.* 2008) have similar $\delta^{18}O_p$ is expected. Temnospondyls exhibit lower $\delta^{18}O_p$ values by almost 2‰. This is congruent with an ecological partitioning due to their semi-terrestrial behaviour. Palynomorph assemblages indicate coal-swamp to mesoxerophytic environment, including significant humidity (Paquette *et al.* 1980; Steyer *et al.* 2000). So, temnospondyls could partly live in humid terrestrial environment, which was little subject to evaporation relative to the lake

water, leading to lower $\delta^{18}O_p$ values. The $\delta^{18}O_p$ depletion could also represent physiological effect not yet understood in temnospondyls.

The variation of the $\delta^{18}O_p$ along the xenacanthiform and acanthodian spines is negligible (Figs. 82-84). The variation between the spine apex and base does not reach more than 1‰: this could correspond to physiological variation little influenced by environmental changes. Consequently, the living environment of xenacanthiformss and acanthodians seems to be rather stable all along their lifespan.

According to the viable temperature range recorded in modern tropical freshwater fishes (16°C to 40°C; Pandian & Vivekanandan 1985), the most viable palaeotemperature model, i.e. with temperature between 14°C to 35°C, for Buxières-les-Mine is the Lake Matano, a tropical freshwater lake with a significant depth (several hundred meters; Fig. 85). The Lake Matano is submitted to monsoon-like condition, so with an alternation of dry and wet season, and aridity events have been proposed in Buxières-les-Mines based on sedimentological evidence (Kaulfuß 2003). Following these results, this locality, as already supposed, is a palaeo-lake with significative depth under tropical hydrological conditions with wet and dry periods. This assumption agrees with the faunal list of vertebrates reported: they are distributed from small actinopterygians to large *Orthacanthus* and temnospondyls (e.g. Steyer *et al.* 2000). A fauna with this diversity could not be present in small hydrological systems and needs large environment like open lake to develop (Salzburger *et al.* 2014).

Muse OSB

The $\delta^{18}O_p$ values range from 17.29‰ to 25.10‰ for xenacanthiforms, from 19.28‰ to 21.34‰ for acanthodians and from 17.61‰ to 18.56‰ for actinopterygians (Fig. 79). As for Buxières-les-Mines, most of them, lower or close to 18‰, can be interpreted as freshwater markers. However, the mean $\delta^{18}O_p$ value in the Muse OSB is higher (19.36‰) than that of Buxières-les-Mines (16.47‰) and numerous $\delta^{18}O_p$ values, especially in xenacanthiforms and acanthodians, are higher than 18‰ and up to 25.1‰. The typical early Permian seawater $\delta^{18}O_p$ is between 18‰ and 22‰ and can correspond to several $\delta^{18}O_p$ values recorded in the Muse OSB. However, $\delta^{18}O_p$ increases can be produced by evaporation events that can also exceed those in the marine setting. Such mechanisms can be favoured by monsoonal climate which can be supposed to occur in these low latitude tropical basins (Roscher & Schneider 2006). Shallow tropical waters, such as swamps, can produce, due to high difference of water inputs between wet and dry season, $\delta^{18}O_p$ differences of up to 5‰ (Otero *et al.* 2010) which are in the range of the highest $\delta^{18}O_p$ values compared to the lowest ones. As the highest $\delta^{18}O_p$ values are higher

than those of the contemporaneous marine vertebrates and no sedimentological or palaeogeographical evidence agrees with a potential connection between the French Massif central basins and the marine setting, the Muse OSB could be a shallow freshwater environment recording intense drying up events.

The $\delta^{18}O_p$ variation along the acanthodians fin spines is negligible (sd=0.1) for one spine (1955) and more variable in another one (1024) with a significant decrease from the apex to the base (Fig. 82). The more stable fin spine has values between 19‰ and 20‰ and the most variable from 20‰ to more than 21‰. These $\delta^{18}O_p$ values show that the acanthodians could live in variable environments and were able to endure dry periods. This agrees with the already known acanthodian environmental tolerance in various freshwater habitats (e.g. Schultze 2009). The same thing could be proposed for the xenacanthiforms. The dorsal spines with the most variable $\delta^{18}O_p$ values are also those with the highest $\delta^{18}O_p$ values (Fig. 84). This could be evidence for the ability of xenacanthiforms to live in shallow freshwater environments submitted to high hydrological variations. The hypothesis that Xenacanthiformes could be air-breathing organisms is not supported by the high values of $\delta^{18}O_p$ recorded in the Muse OSB. Indeed, the $\delta^{18}O_p$ values of Temnospondyls which are clearly air-breathing animals are lower than those of contemporary xenacanthiformes, acanthodians or actinopterygians. If these groups exhibited air-breathing ability, $\delta^{18}O_p$ values might be closer to those of temnospondyls. In the present case, the highest $\delta^{18}O_p$ values could correspond to period of drying up with shallow low-oxygenised waters. This ability to live in such environment was already proposed for xenacanthiforms based on morphological arguments (e.g. Compagno 1990).

$\delta^{13}C_c$ values

Buxières-les-Mines

The late Carboniferous and early Permian are characterised by a $\delta^{13}C$ of marine carbonate of 2‰ compared to the current one at 0‰ (e.g. Saltzman *et al.* 2012). This positive shift is also recorded in the $\delta^{13}C_c$ of brachiopod calcite shells which is between 4‰ and 6‰ compared to the current ones at 2‰ (e.g. Berner 2006). This time interval records a $\delta^{13}C$ positive shift of 2‰ to 4‰ compared to the modern conditions.

The $\delta^{13}C_c$ values of strict aquatic vertebrates range from -0.80‰ to 7.02‰ (Fig. 80). Modern marine shark teeth have $\delta^{13}C_c$ values between -6.8‰ and 4.8‰ (Vennemann *et al.* 2001). The very high values of Buxières-les-Mines fauna could be interpreted as a combination of the positive shift of the $\delta^{13}C$ in the Carboniferous-Permian record and an intense primary production. This locality is in intra-mountainous context, so subject to intense detrital products

that bring nutritional elements from the erosion of the Hercynian Mountains. Consequently, the detrital effect could be more important than the environmental one, so, in this case, the $\delta^{13}C_c$ is not the most efficient proxy for palaeoenvironmental reconstructions.

$\delta^{13}C_c$ of temnospondyls are low, compared to strict aquatic taxa (Fig. 80). They average -2.57‰ with low variability (sd = 0.1). Again, these values could be interpreted as ecological partitioning due to their semi-terrestrial way of life. The terrestrial primary producers have lower $\delta^{13}C$ values than aquatic ones (Clementz & Koch 2001), so it is expected that a semi-aquatic taxon has lower $\delta^{13}C_c$ values than strict aquatic taxa.

Even if it is not as intense as between primary producers and primary consumers (e.g. Cerling & Harris 1999), the $\delta^{13}C_c$ difference between preys and predators which are secondary or tertiary consumers can be up to +1pmil for predators. This assumption agrees with the $\delta^{13}C_c$ of acanthodians, actinopterygians and the small xenacanthid *Triodus.* It is therefore surprising that the large diplodoselachid *Orthacanthus* exhibits such low $\delta^{13}C_c$ values (from -0.4‰ to 1.88‰). Boy & Schindler (2000) and Kriwet *et al.* (2008) proposed that large *Orthacanthus* were the apex predator of their ecosystem, feeding on all the other smaller predators such as *Triodus* and large temnospondyls. Indirect evidence of consumptions of *Triodus* by *Orthacanthus* in the Puertollano Basin (Gzhelian of Spain) were reported by Soler-Gijón (1995) and temnospondyl mandibule with *Orthacanthus* tooth stuck in it is reported in Buxières-les-Mines (Fig. 89). So, it is probable that, in Buxières-les-Mines, *Orthacanthus* feeds on *Triodus* and temnospondyls too. The *Orthacanthus* $\delta^{13}C_c$ values are intermediate between those of *Triodus* and temnospondyls (Fig. 80). If *Orthacanthus* feeds on these two taxa, these intermediate values are expected because they reflect the diversity of its preys: *Triodus* evolving in strict aquatic environment and temnospondyls evolving in semi-terrestrial one.

Along the *Orthacanthus* dorsal spine, $\delta^{13}C_c$ values seem to vary cyclically but they are also characterised by low $\delta^{13}C_c$ values at the base (Fig. 84). Modern elasmobranchs are characterised by a rapid growth during their early life stages and by a slow growth when they reach their adult stage (e.g. Tovar-Ávila *et al.* 2009). The dorsal spines of modern elasmobranchs grow following the same pattern (Irvine *et al.* 2006). Consequently, we can estimate that the xenacanthiform dorsal spine grows faster during their early life stages than during their late life stages because this structure is homologous with that of modern chondrichthyans (e.g. Soler-Gijón 1999). As the sampling was made by cutting small spine sections along the length, the lower $\delta^{13}C_c$ values at the base could reflect the variation of the growth rate of the dorsal spine during the xenacanthiform lifespan. The measured $\delta^{13}C_c$ values correspond to a mean value of the entire investigated spine section. Furthermore, they

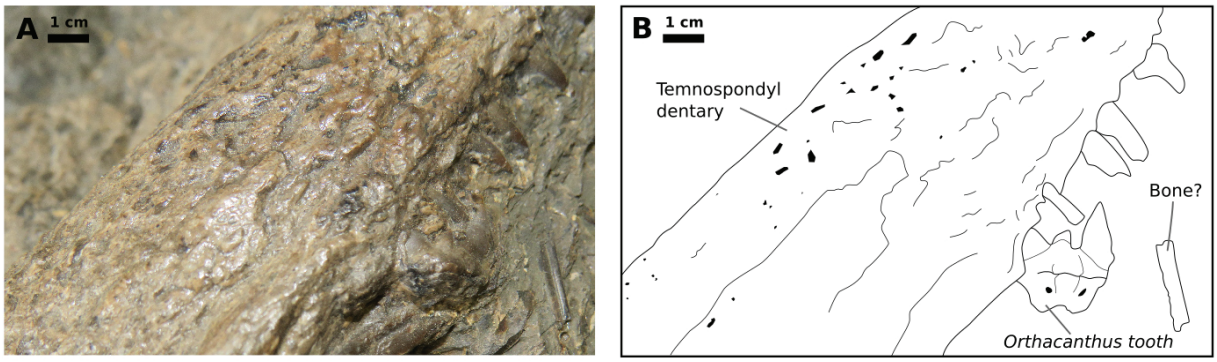

Figure 89: Stuck *Orthacanthus* tooth in a temnospondyl dentary in Buxières-les-Mines. **A**, Photograph. **B**, interpretation drawing.

correspond to a short time at the apex and to a long time at the base. So, the $\delta^{13}C_c$ values at the base could record more variations than those at the apex, resulting in a different value compared to the rest of the dorsal spine.

Muse OSB

The actinopterygians from the Muse OSB exhibit high $\delta^{13}C_c$ values that range from 3.31‰ to 5.88‰ and the sole available acanthodian fin spine is at 4.45‰ (Fig. 80). As this locality is also located in intra-mountainous context, these values could also correspond to the positive shift of the $\delta^{13}C$ in the Carboniferous-Permian record and the intense primary production due to detrital inputs like in Buxières-les-Mines.

$\delta^{34}S$ values

The seawater $\delta^{34}S$ values was of about 12‰ during the Carboniferous-Permian transition, contrary to the current one which is of about 21‰ (e.g. Paytan *et al.* 2020). Based on recent investigations on modern and fossil vertebrates from a broad phylogenetic context (Goedert 2017; Goedert *et al.* 2018, 2020), the $\delta^{34}S$ of vertebrate bioapatite is supposed to be close to that of their living environment without significant fractionation process.

The taxonomic groups from Buxières-les-Mines exhibit $\delta^{34}S$ values lower than 12‰ with a mean of 1.81‰ and variations from -6.02‰ to 7.94‰ for unaltered samples (Fig. 81). The $\delta^{34}S$ values from the Muse OSB have a mean of 4.58‰ and range from 1.27‰ to 6.95‰ (Fig. 81). These $\delta^{34}S$ values are less positive, at least, by 3‰ and on average by 10‰ compared to the seawater $\delta^{34}S$. This means that their sulfur content is not derived from seawater sulfate. In the light of the bioapatite $\delta^{34}S$, the environment of Buxières-les-Mines and the Muse OSB

does not seems to be submitted to marine influences contrary to what was assumed in previous studies (e.g. Schultze & Soler-Gijón 2004; Schultze 2009).

The variations of the $\delta^{34}S$ along the dorsal spine length of *Orthacanthus* (BX04) from Buxières-les-Mines show high values at its base (Fig. 83). The same explanation as for the $\delta^{13}C_c$ could be proposed for the $\delta^{34}S$: the base records longer time than the apex, so it records potentially more $\delta^{34}S$ variations, resulting in a higher $\delta^{34}S$ mean within the investigated spine section. The observed variations of the dorsal spine seem irregular, so not derived from potential environmental cycles. The $\delta^{34}S$ variation do not seem to be related to the other isotopic variations. *A contrario* the constant decrease of the $\delta^{34}S$ values in the acanthodian fin spine (1024) from the Muse OSB (Fig. 83) seems to be related to the global decrease of isotopic values in this specimen (Fig. 82).

Environmental reconstruction of the early Permian basins from the French Massif central

The interpretation of Buxères-les-Mines as a full freshwater environment without marine influence agrees with Fischer's *et al.* (2013) geochemical study on chondrichthyan teeth from numerous Carboniferous-Permian intra-mountainous basins. Our environmental interpretation does not agree with a marine influences in European basins as proposed by Schultze & Soler-Gijón (2004) and Schultze (2009).

In the Muse OSB, plant inventory (Van Waveren *et al.* 2012) supports a shallow tropical lake submitted to drying up events. The presence of roots and rhizomes of *Calamites* indicate a shallow environment close to the coastlines. The presence of hydrophile to mesophile plants (Van Waveren *et al.* 2012) indicates a fluctuant water level in agreement with significant variations of the observed $\delta^{18}O_p$. Moreover, ferns are abundant and present under succulent form that could result to potential hybridisations due to a reduced population caused by drying up periods.

The strong variability of the Muse OSB $\delta^{18}Op$ values (Fig. 79) is more likely to happen in a freshwater environment than in marine setting. In fact, the variations of the seawater $\delta^{18}O$ at tropical latitudes are mainly caused by both evaporations and freshwater inputs from river mouths. The variations of the superficial waters are around 1‰ (e.g. LeGrande & Schmidt 2006). They are less important than the observed variation of the $\delta^{18}O_p$ in the Muse OSB. Such variations are more likely to occur in fresh waters submitted to monsoon rains or a drying up as it already was reported for the tropical Lake Tanganyika (Otero *et al.* 2010).

Some studies (e.g. Becq-Giraudon *et al.* 1996) have argued for a significant altitude, like those in the modern Himalaya Mountain, for the basins from the French Massif central.

The $\delta^{18}O_p$ values of the aquatic fauna disagree with such an interpretation. The $\delta^{18}O$ decreases of 0.28‰ when the altitude increases of 100 m (e.g. Dansgaard 1964; Rozanski *et al.* 1993; Poage & Chamberlain 2001). If the Muse OSB records high altitudes, the $\delta^{18}O_p$ values must be lower than typical Carboniferous-Permian freshwater values, so lower than 14‰ (upper limit of diagenetic samples in Fischer *et al.* [2013]). However, this is not the case: the measured $\delta^{18}O_p$ values (Fig. 79) are too high to correspond to such environment.

The faunal composition of the investigated localities agrees with the two proposed environmental interpretations (Fig. 89). In Buxières-les-Mines, many components of the Carboniferous-Permian freshwater fauna were already reported in other basins like the Saar-Nahe Basin and its large lacustrine system (e.g. Kriwet *et al.* 2008). This similarity agrees with an open, large and deep lake in which all the food web is represented: large predators (*Orthacanthus* and temnospondyls), small predators (*Triodus*) and preys or small consumers (acanthodians and actinopterygians). In the Muse OSB, the food web is mainly limited to small consumers (acanthodians and actinopterygians) and small predators (*Triodus*). The systematic revision has shown that the genus *Orthacanthus* was present in the Muse OSB with *O.* cf. *kounoviensis* (Luccisano *et al.* 2022). The only reported lateral tooth does not reach the size of the large adult teeth of *O. kounoviensis* from Buxières-les-Mines, so it could correspond to a medium-sized animal different from the large *Orthacanthus* from Buxières-les-Mines or to a late juvenile to sub-adult. Consequently, it could be able to live in shallow as well as large lakes. Furthermore, the presence of this single tooth in the Muse OSB could be questioned because its stratigraphic origin is unclear. Even if it is supposed to come from the base of the Muse OSB (Luccisano *et al.* 2022), no *Orthacanthus* material was found during the recent excavation campaigns (Gand *et al.* 2011, 2015 and during the last campaign in 2021). As the Muse OSB presents a distinct East-oriented dip and the provenance of the tooth is unclear (Heyler 1969), this tooth could come from a different stratigraphic levels older or younger than the analysed material, so not from the Muse OSB as it is currently known. In the light of our results, the Muse OSB fauna is more likely to occur in a small and shallow aquatic environment than in open and large lakes or river-channels.

The reconstructed environmental temperatures of the Muse OSB and Buxières-les-Mines also indicate two different environments. For Buxières-les-Mines, the palaeotemperatures range from 34°C to 54°C and from 29°C to 50°C for the seawater models with and without glaciation respectively, from 14°C to 35°C for the Lake Matano model, from 40°C to 59°C for the Lake Punta Laguna model and from 51°C to 72°C for the Lake Tanganyika model. For the Muse OSB, the palaeotemperatures range from 4°C to 38°C and from 0°C to

34°C for the seawater models with and without glaciation respectively, from -15°C to 19°C for the Lake Matano model, from 9°C to 42°C for the Lake Punta Laguna model and from 22°C to 55°C for the Lake Tanganyika model.

For Buxières-les-Mines, the most probable environment, i.e. the one for which the calculated temperatures are the most viable, is similar to the Lake Matano model (Fig. 85), a deep and large freshwater lake. For the Muse OSB, the lowest $\delta^{18}O_p$ values agrees with viable temperature in a model similar to the Lake Punta Laguna model (shallow freshwater lake) whereas the highest values correspond better with a Lake Tanganyika model (tropical freshwater lake with strong variations of the water inputs and occurrence of drying up periods; Fig. 85). It must be noted that in both localities the seawater model indicates viable temperature. However, the $\delta^{34}S$ values (Fig. 81) disagrees with a significant salinity, so with marine or marine influenced environment.

Palaeoecological implications

In the light of the investigated specimens from the Autun and Bourbon-l'Archambault basins, several assumptions can be made on the palaeoecology of the early Permian Xenacanthiformes from the French Massif central. Firstly, the $\delta^{18}O_p$ and $\delta^{34}S$ values of their dorsal spines (Figs. 83-84) do not show any euryhaline ecology and indicate a full freshwater one contrary to many studies (e.g. Schultze & Soler-Gijón 2004; Schultze 2009; Beck *et al.* 2016) which argued for an euryhaline or brackish ecology.

Consequently, the hypothesis of migration patterns between the freshwater and marine settings is not supported by our analyses, contrary to the opinion of Beck's *et al.* (2016) for the lower Permian American Xenacanthiformes. The apparent stability of the isotopic compositions along the dorsal spine length suggests that Xenacanthiformes lived in freshwater environments. However, the specimens from the Muse OSB indicate that they were able to adapt to endure strong variations of their freshwater environment such as a decrease of water level and oxygenation. This result confirms previous assumptions of the physiological tolerance of this group (e.g. Compagno 1990).

The carbon composition of the fauna of the investigated localities (Fig. 80) confirms the previous global organisation of food webs in the European Carboniferous-Permian basins (e.g. Boy & Schindler 2000; Kriwet *et al.* 2008). The large *Orthacanthus* was the top predator, feeding on other large vertebrates like temnospondyls and smaller xenacanthiforms. The $\delta^{13}C_c$ values of temnospondyls of Buxières-les-Mines is significantly lower than those of the fully

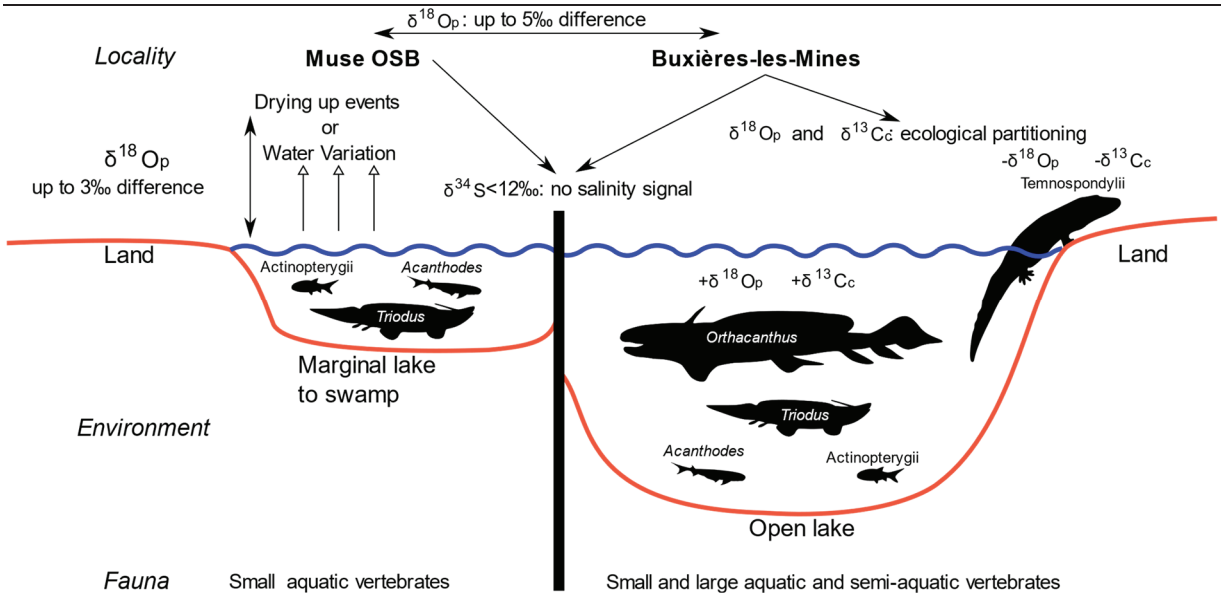

Figure 90. Environmental reconstruction of the Muse OSB and Buxières-les-Mines.

aquatic vertebrates (Fig. 80). It could indicate that they fed more frequently in terrestrial environment than in the aquatic one.

Our analyses also show a differential environmental adaptiveness among the Xenacanthiformes. The large Diplodoselachidae were restricted to large and deep lakes and river systems like Buxières-les-Mines in France whereas the small Xenacanthidae were able to colonise more diversified environments, from large lakes to shallow swamps like in the Muse OSB (Fig. 89). The observed different ecologies agree with the current known palaeobiogeography of the Carboniferous-Permian Xenacanthiformes from Europe. The large xenacanthiforms like *Orthacanthus* are almost restricted to the upper Carboniferous in which large freshwater basins in connection with each other were reported (e.g. Luccisano *et al.* 2022). At the Carboniferous-Permian transition, the Franconian tectonic movements have suppressed the connections between large basins containing large and deep lakes like Buxières-les-Mines (e.g. Schneider 1996). The resulting isolated basins could be of smaller size and could contain smaller lacustrine systems like the Muse OSB. In such shallow lakes, only small xenacanthiforms like *Triodus* can survive and this agrees with the apparent diversification of the latter in the early Permian. The large xenacanthiforms survived in a few places like Buxières-les-Mines or the Saar-Nahe Basin in which large and deep lakes still occurred.

Conclusions

The analyses of the oxygen, carbon and sulfur compositions of the bioapatite of the aquatic vertebrates from two early Permian localities of the French Massif central allow to reconstruct their palaeoenvironment. The non-contemporaneous localities of the Muse OSB and Buxières-les-Mines represents two different environments. Buxières-les-Mines is a large, open and deep freshwater lake containing a diversified vertebrate fauna, from large xenacanthiforms to small actinopterygians. *A contrario*, the Muse OSB has a less diversified fauna with only small sized vertebrates and characterised by a shallow freshwater environment submitted to drying up events. These localities well illustrate the environmental changes of the aquatic setting of the early Permian intra-mountainous basins of the European Hercynian Mountain. Buxières-les-Mines is remnant of the large lake and river systems of the upper Carboniferous in which diversified aquatic vertebrates evolved. It represents one of the last large lacustrine systems in the European early Permian. The Muse OSB characterises the most common intra-mountainous freshwater ecosystems occurring in the early Permian. It contains a less diversified fauna of small size evolving in a shallow lakes or swamps and it could be submitted to significant drying up events. However, this study agrees with previous analyses that postulated for no marine influence on these intra-mountainous basins in the lower Permian.

Permian Xenacanthiformes from France appear to live in a constant freshwater environment without apparent marine influences or migrations into marine settings. However, small xenacanthiforms appear to be able to adapt to stressing setting like drying up events or low oxygenised waters. This adaptation could explain their diversification in the early Permian. These palaeoecological assumptions disagree with previous ones on American species. New studies for a larger temporal and geographic scale are needed to assess the different adaptative strategies of this group along their evolutionary history and to explain their global occurrence in the late Palaeozoic.

Acknowledgements

The authors thank the Rhinopolis Association, the Gannat Town hall and the Conseil Départemental de l'Allier for the funding of the excavation campaigns in Buxières-les-Mines during which the studied specimens were found, and for providing storage space in which the Buxières-les-Mines fossils are housed. They also thank the Muséum d'Histoire Naturel d'Autun

(MHNA) and its curator Dominique Chabard for access to the Muse OSB specimens. Specimens from the Muse OSB were found during several excavation campaigns (2010-2014 and 2021) and the authors thank for their valuable help D. Beaudoin, F. Beaudoin, R. Pillon, G. Barnay, P. Baudinaud, N. Pégon, B. Arnoult (SHNA), D. Chabard, E. Chabard, A. Margueron (MHNA), the Gevrey, Barnay, and Jacquemard families, G. Grillot, S. Kunz (Dracy-Saint-Loup Municipality) B. Blanc (Marine), E. Chenal (Éducation Nationale), C. Delhaye (CNRS), I. van Waveren and her students (Naturalis, Leiden), J. Fortuny (ICP, Barcelona), S. Hervet (PaléOvergne), J. Galtier (Montpellier), A. Bercovici (Manchester University), F. Prost (Dijon University), S. Giner (Var Département), K. Rey (ex-BPI), and J.-S. Steyer, O. Béthoux, G. Cousin, G. Odin, L. Anseaume, J. Barbier, M. Sanders, D. Perez, J. Falconnet, D. Germain and V. Rouchon (MNHN). The first author was funded by the Doctoral School ED 341 - E2M2 Évolution Écosystème Microbiologie Modélisation, Université Claude Bernard Lyon 1, France.

Supplementary material

Table S3. Evolution of the oxygen, carbon and sulfur isotope compositions along the acanthodian and xenacanthiform spines length. **Abbreviations**: **Aca**, acanthodian; **d**, distance to apex; **Ort**, *Orthacanthus*; **sd**, standard error; **Sp.**, specimen; **Syst**, Systematics; **Tri**, *Triodus*.

Sample	Sp.	Syst	d (cm)	$\delta^{18}O_p$ (‰V-SMOW)	sd	$\delta^{18}O_c$ (‰V-SMOW)	sd	$\delta^{13}C_c$ (‰V-PDB)	sd	$\delta^{34}S$ (‰V-CDT)	sd
1955-1	1955	Aca	5.0	19.34	0.3						
1955-2	1955	Aca	4.3	19.56	0.3						
1955-3	1955	Aca	3.6	19.43	0.3						
1955-4	1955	Aca	3.0	19.63	0.3						
1955-5	1955	Aca	2.5	19.53	0.3						
1955-6	1955	Aca	2.0	19.72	0.3						
1955-7	1955	Aca	1.2	19.45	0.3						
1955-8	1955	Aca	0.5	19.28	0.3						
1924-1	1924	Aca	1.5	21.34	0.3	22.91	0.4	5.70	0.5	3.70	0.1
1924-2	1924	Aca	2.5	20.35	0.3	23.06	1.0	4.02	0.1	1.75	0.1
1924-3	1924	Aca	3.7	20.18	0.3	21.52	0.7	3.66	0.7	1.23	0.1
943-1	943	Tri	6.3	19.03	0.2						
943-4	943	Tri	3.9	18.49	0.2						
943-5	943	Tri	3.1	18.36	0.2						
943-6	943	Tri	2.1	18.41	0.2						
943-7	943	Tri	1.1	17.29	0.2						
907b-12	907b	Tri	6.0	23.02	0.2						
907b-13	907b	Tri	0.5	19.50	0.2						
965a-1	965a	Tri	0.2	18.94	0.1						
965a-2	965a	Tri	0.9	19.05	0.1						
965a-3	965a	Tri	1.5	19.18	0.1						
965a-4	965a	Tri	2.1	19.45	0.1						
965a-5	965a	Tri	3.0	19.46	0.1						
965a-6	965a	Tri	4.1	19.28	0.1						
326a-1	326a/326b	Tri	0.9	21.66	0.3						
326a-2	326a/326b	Tri	2.2	23.59	0.3						
326a-3	326a/326b	Tri	3.3	24.64	0.3						
326a-4	326a/326b	Tri	4.2	24.70	0.3						
326a-5	326a/326b	Tri	5.2	25.14	0.3						
326a-6	326a/326b	Tri	6.7	24.67	0.3						
NN5-1	NN5	Aca	0.0	17.30	0.0						
NN5-2	NN5	Aca	0.6	17.39	0.0						
NN5-3	NN5	Aca	2.8	17.47	0.0						
NN9-1	NN9	Aca	5.4	17.26	0.1						
NN9-2	NN9	Aca	5.0	17.46	0.1	21.22	0.3	6.56	0.3		
NN9-3	NN9	Aca	4.0	17.14	0.1	21.27	0.5	7.03	0.3		
NN9-4	NN9	Aca	3.6	17.19	0.1						

Sample	Sp.	Syst	d (cm)	$\delta^{18}O_p$ (‰V-SMOW)	sd	$\delta^{18}O_c$ (‰V-SMOW)	sd	$\delta^{13}C_c$ (‰V-PDB)	sd	$\delta^{34}S$ (‰V-CDT)	sd
NN9-5	NN9	Aca	3.0	17.25	0.1	21.64	0.0	7.00	0.3		
NN9-6	NN9	Aca	2.5	17.24	0.1						
NN9-7	NN9	Aca	2.0	17.24	0.1						
NN9-8	NN9	Aca	1.5	17.66	0.0	20.91	0.3	6.56	0.1		
NN9-9	NN9	Aca	0.5	17.47	0.0						
BJM2-1	BJM2	Aca	4.7	17.27	0.0						
BJM2-3	BJM2	Aca	2.0	17.00	0.2						
BJM2-4	BJM2	Aca	0.0	16.87	0.2	19.30	1.0	2.41	0.6		
BJM3-1	BJM3	Aca	4.1	17.52	0.2						
BJM3-2	BJM3	Aca	3.4	17.48	0.2	21.11	0.2	3.49	0.2		
BJM3-3	BJM3	Aca	0.6	17.30	0.2	20.98	0.2	3.54	0.2		
BJM3-4	BJM3	Aca	0.1	17.17	0.2	20.92	0.2	3.33	0.2		
BJM3-5	BJM3	Aca	0.0	17.35	0.2	21.18	0.3	3.07	0.0		
BXA86-1	BXA86	Aca	4.3	18.49	0.1						
BXA86-2	BXA86	Aca	3.3	18.71	0.1						
BXA86-3	BXA86	Aca	2.5	18.47	0.1						
BXA86-4	BXA86	Aca	0.0	18.65	0.1						
BX28-1	BX28	Tri	3.4	17.21	0.1						
BX28-2	BX28	Tri	2.5	16.84	0.1						
BX28-3	BX28	Tri	1.6	16.69	0.1						
D07-1	D07	Tri	4.2	17.49	0.2						
D07-2	D07	Tri	3.8	17.33	0.2						
D07-3/4	D07	Tri	3.0	17.35	0.2						
D07-4	D07	Tri	2.4	16.78	0.2						
D07-5	D07	Tri	1.2	17.65	0.2						
D07-6	D07	Tri	0.3	17.59	0.2						
D08-1	D08	Tri	5.0	17.49	0.1	21.22	0.3	2.72	0.1		
D08-2	D08	Tri	4.2	17.72	0.1	21.67	0.1	3.32	0.0		
D08-3	D08	Tri	3.2	17.77	0.1	21.39	0.3	3.63	0.3		
D08-4	D08	Tri	2.3	18.03	0.1	21.97	0.1	4.63	0.3		
D08-5	D08	Tri	1.5	18.55	0.1	22.10	0.1	5.25	0.1		
D08-6	D08	Tri	0.8	18.42	0.1						
D08-7	D08	Tri	0.0	18.34	0.1						
BX23-11	BX23-1	Tri	2.9	16.25	0.1						

Sample	Sp.	Syst	d (cm)	$\delta^{18}O_p$ (‰V-SMOW)	sd	$\delta^{18}O_c$ (‰V-SMOW)	sd	$\delta^{13}C_c$ (‰V-PDB)	sd	$\delta^{34}S$ (‰V-CDT)	sd
BX23-12	BX23-1	Tri	2.3	16.33	0.3						
BX23-13	BX23-1	Tri	1.8	16.27	0.3						
BX23-2122	BX23-2	Tri	2.6	16.50	0.3						
BX23-2324	BX23-2	Tri	1.5	16.49	0.3						
BX23-2526	BX23-2	Tri	0.3	15.89	0.3						
X1-1	D-11-11-96 21	Tri	0.2	17.70	0.2						
X1-2	D-11-11-96 21	Tri	0.5	17.63	0.2						
X1-3	D-11-11-96 21	Tri	1.0	17.49	0.2						
X1-4	D-11-11-96 21	Tri	1.4	17.08	0.2						
X1-5	D-11-11-96 21	Tri	1.8	16.27	0.2						
X1-6	D-11-11-96 21	Tri	1.9	17.28	0.2						
X1-7	D-11-11-96 21	Tri	2.1	17.49	0.2						
X1-8	D-11-11-96 21	Tri	2.2	17.26	0.2						
X1-9	D-11-11-96 21	Tri	2.5	17.28	0.2						
X1-10	D-11-11-96 21	Tri	2.7	17.19	0.2						
X1-11	D-11-11-96 21	Tri	2.9	17.51	0.2						
X1-12	D-11-11-96 21	Tri	3.1	17.13	0.2						
X1-13	D-11-11-96 21	Tri	3.4	17.42	0.2						
X1-14	D-11-11-96 21	Tri	3.8	17.71	0.2						
X2-1	D-13-06-98 5	Ort	0.2	17.49	0.3						
X2-2	D-13-06-98 5	Ort	0.5	17.96	0.3						
X2-3	D-13-06-98 5	Ort	1.2	18.00	0.3						
X2-4	D-13-06-98 5	Ort	1.7	17.47	0.3						
X2-5	D-13-06-98 5	Ort	2.0	17.44	0.3						
X2-6	D-13-06-98 5	Ort	2.4	17.72	0.3						
X2-7	D-13-06-98 5	Ort	2.9	17.65	0.3						
X2-8	D-13-06-98 5	Ort	3.7	17.70	0.3						
X2-9	D-13-06-98 5	Ort	4.1	17.59	0.3						

Sample	Sp.	Syst	d (cm)	$\delta^{18}O_p$ (‰V-SMOW)	sd	$\delta^{18}O_c$ (‰V-SMOW)	sd	$\delta^{13}C_c$ (‰V-PDB)	sd	$\delta^{34}S$ (‰V-CDT)	sd
X2-10	D-13-06-98 5	Ort	4.6	17.50	0.3						
X2-11	D-13-06-98 5	Ort	5.2	17.35	0.3						
X2-12	D-13-06-98 5	Ort	6.5	17.19	0.3						
BX04-1	BX04	Ort	0.8	16.85	0.1	20.48	0.2	1.41	0.1	-1.87	0.1
BX04-2	BX04	Ort	1.8	16.88	0.1	23.20	0.2	0.97	0.0	-3.50	0.1
BX04-3	BX04	Ort	2.4	16.75	0.2	21.05	0.7	1.21	0.3	-3.00	0.2
BX04-4	BX04	Ort	3.2	16.62	0.2	20.73	0.1	1.58	0.2	-3.23	0.3
BX04-51	BX04	Ort	3.7	16.76	0.1	20.72	0.3	1.88	0.1	-3.59	0.2
BX04-52	BX04	Ort		16.35	0.3	20.53	0.2	1.49	0.2	-0.18	0.1
BX04-6	BX04	Ort	4.0	16.38	0.2	23.85	0.1	0.81	0.0	-5.78	0.2
BX04-7	BX04	Ort	4.6	16.24	0.3	21.07	0.1	1.21	0.1	-4.37	0.1
BX04-8	BX04	Ort	5.3	16.97	0.1	20.28	0.2	0.89	0.2	-4.04	0.0
BX04-9	BX04	Ort	5.8	16.98	0.3	20.38	0.3	1.00	0.3	-6.03	0.2
BX04-10	BX04	Ort	6.3	17.12	0.2	20.52	0.3	1.14	0.1	-2.45	0.1
BX04-11	BX04	Ort	6.8	16.95	0.3	20.30	0.1	1.62	0.2	0.70	0.3
BX04-12	BX04	Ort	7.3	16.93	0.3	20.34	0.0	1.71	0.2	-0.06	0.1
BX04-13	BX04	Ort	7.8	17.06	0.1	20.60	0.1	1.25	0.1	-1.93	0.1
BX04-14	BX04	Ort	8.4	16.80	0.1	20.50	0.2	1.02	0.1	-3.16	0.0
BX04-15	BX04	Ort	9.0	16.65	0.2	20.58	0.2	1.26	0.1	-0.82	0.2
BX04-16	BX04	Ort	10.3	16.77	0.1	20.76	0.1	0.97	0.1	-1.90	0.3
BX04-17	BX04	Ort	11.8	16.72	0.2	20.32	0.5	1.10	0.1	0.43	0.3
BX04-18	BX04	Ort	14.3	16.38	0.1	20.20	0.3	-0.05	0.2	3.81	0.7
D17-1	D17	Ort		15.74	0.1	20.13	0.1	-0.40	0.0	2.05	0.3
D17-2	D17	Ort		16.64	0.1	21.05	0.2	1.69	0.1	6.53	0.3
D17-3	D17	Ort		15.91	0.1	20.14	0.4	-0.82	0.1	-17.20	7.9
D17-4	D17	Ort		16.57	0.1	20.72	0.1	1.32	0.2	-4.79	0.5
D17-5	D17	Ort		16.50	0.1	20.38	0.2	0.38	0.2		
D17-6	D17	Ort		17.22	0.1	20.97	0.1	1.61	0.0		

Table S4. Carbonate and sulfate concentration for assessing the diagenesis in the analysed dataset. **Abbreviations**: **Aca**, acanthodian; **Act**, actinopterygian; **O**rt, *Orthacanthus*; **Tem**, temnospondyl; **Tri**, *Triodus*; **Syst**, systematics.

Sample	**Syst**	**$\delta^{18}O_p$ (%V-SMOW)**	**$\delta^{18}O_c$ (%V-SMOW)**	**$d^{18}O_c$-$d^{18}O_p$**	**CO_3 %**	**sd**	**$\delta^{34}S$ (%V-CDT)**	**sd**	**SO_2 %**	**sd**
BXT	Act	16.33	20.83	4.50	1.98	0.16	-3.83	0.19	1.59	0.03
BX39	Act	16.72	20.52	3.80	1.70	0.09				
D062	Act	16.92	20.07	3.15	1.81	0.16				
D20-1	Act	16.77	20.06	3.29	2.16	0.07				
D20-2	Act	16.43	20.43	4.00	2.39	0.23				
0-20-04-97-2	Act						7.13	0.98	0.76	0.03
BX-12-03-96-2	Aca						4.55	0.52	0.75	0.03
BJMP3-2	Aca	17.48	21.11	3.63	1.67	0.06				
BJMP3-3	Aca	17.30	20.98	3.68	1.39	0.04				
BJMP3-4	Aca	17.17	20.92	3.75	1.21	0.08				
BJMP3-5	Aca	17.35	21.18	3.83	1.90	0.10				
NN9-2	Aca	17.46	21.22	3.77	1.86	0.04				
NN9-3	Aca	17.14	21.27	4.13	2.42	0.20				
NN9-5	Aca	17.25	21.64	4.39	1.95	0.09				
NN9-8	Aca	17.66	20.91	3.25	2.09	0.20				
BJMP2-4	Aca	16.87	19.30	2.43	1.37	0.08				
BJMP3-1	Aca	17.52	20.94	3.42	1.88	0.07				
D08-1	Tri	17.49	21.22	3.73	1.95	0.14				
D08-2	Tri	17.72	21.67	3.95	1.52	0.09				
D08-3	Tri	17.77	21.39	3.62	2.28	0.22				
D08-4	Tri	18.03	21.97	3.95	1.90	0.13				
D08-5	Tri	18.55	22.10	3.54	2.71	0.05				
BX04-1	Ort	16.77	20.48	3.71	2.55	0.22	-1.87	0.14	1.25	0.02
BX04-2	Ort	16.80	23.20	6.40	5.96	0.33	-3.50	0.06	1.33	0.02
BX04-3	Ort	16.67	21.05	4.38	2.28	0.10	-3.00	0.15	1.35	0.01
BX04-4	Ort	16.54	20.73	4.19	2.47	0.28	-3.23	0.27	1.09	0.01
BX04-51	Ort	16.68	20.72	4.04	2.89	0.39	-3.59	0.22	1.15	0.03
BX04-52	Ort	16.27	20.53	4.26	1.26	0.08	-0.18	0.10	0.57	0.00
BX04-6	Ort	16.30	23.85	7.55	7.69	0.17	-5.78	0.24	1.20	0.05
BX04-7	Ort	16.16	21.07	4.91	2.90	0.10	-4.37	0.14	1.33	0.05
BX04-8	Ort	16.93	20.28	3.34	2.52	0.33	-4.04	0.01	3.13	0.04

Sample	**Syst**	**$\delta^{18}O_p$ (‰V-SMOW)**	**$\delta^{18}O_c$ (‰V-SMOW)**	**$d^{18}O_c$-$d^{18}O_p$**	**CO_3 %**	**sd**	**$\delta^{34}S$ (‰V-CDT)**	**sd**	**SO_2 %**	**sd**
BX04-9	Ort	16.94	20.38	3.44	2.98	0.20	-6.03	0.22	1.08	0.01
BX04-10	Ort	17.08	20.52	3.43	2.57	0.12	-2.45	0.14	1.62	0.03
BX04-11	Ort	16.91	20.30	3.38	2.65	0.05	0.70	0.32	2.02	0.03
BX04-12	Ort	16.89	20.34	3.45	2.86	0.25	-0.06	0.09	1.23	0.05
BX04-13	Ort	17.02	20.60	3.59	2.50	0.03	-1.93	0.15	1.65	0.04
BX04-14	Ort	16.76	20.50	3.75	2.66	0.22	-3.16	0.02	1.25	0.01
BX04-15	Ort	16.61	20.58	3.97	2.76	0.39	-0.82	0.15	1.34	0.12
BX04-16	Ort	16.60	20.76	4.17	2.72	0.24	-1.90	0.32	1.27	0.16
BX04-17	Ort	16.54	20.32	3.78	1.61	0.06	0.43	0.33	1.22	0.02
BX04-18	Ort	16.20	20.20	4.00	0.44	0.05	3.81	0.70	2.89	0.04
D17-1	Ort	15.74	20.13	4.39	3.28	0.30	2.05	0.26	0.52	0.03
D17-2	Ort	16.64	21.05	4.41	2.27	0.11	6.53	0.30	0.62	0.03
D17-3	Ort	15.91	20.14	4.23	2.40	0.33	-17.20	7.90	1.38	1.03
D17-4	Ort	16.57	20.72	4.15	2.34	0.16	-4.79	0.46	0.72	0.20
D17-5	Ort	16.50	20.38	3.87	2.29	0.11				
D17-6	Ort	17.22	20.97	3.76	2.79	0.23				
BXR-1	Tem	15.71	20.15	4.44	2.20	0.14	-20.32	0.03	2.32	0.32
BXR-2	Tem	15.48	20.02	4.53	2.03	0.04	5.54	0.34	0.64	0.02
BXR-3	Tem	15.38	19.91	4.53	2.70	0.16	1.07	0.08	0.87	0.02
BXR-4	Tem	15.51	20.13	4.63	2.14	0.18	7.15	0.14	0.64	0.01
BXR-5	Tem	15.52	20.12	4.60	2.47	0.31	5.49	0.16	1.19	0.02
BXR-6	Tem	14.01	20.07	6.07	2.11	0.19	5.77	0.12	0.73	0.01
BXR-7	Tem	14.87	19.72	4.84	2.06	0.07	6.24	0.13	0.47	0.41
BXR-8	Tem	14.59	0.31				7.94	0.16	0.68	0.01
MU-1	Act	17.94	21.25	3.31	2.14	0.17	6.41	0.09	0.27	0.01
MU-2	Act	17.78	21.50	3.72	1.88	0.22	6.14	0.19	0.26	0.01
MU-3	Act	17.61	21.19	3.58	1.83	0.04	3.60	0.06	0.32	0.01
MU-4	Act	18.12	21.31	3.19	1.95	0.08	6.86	0.14	0.26	0.00
MU-5	Act	18.57	21.29	2.73	2.31	0.14	6.95	0.22	0.24	0.00
1924-1	Aca	21.34	22.91	1.57	0.72	0.04	3.70	0.11	0.30	0.02
1924-2	Aca	20.35	23.06	2.71	0.36	0.02	1.75	0.07	0.32	0.01
1924-3	Aca	20.18	21.52	1.34	0.69	0.04	1.23	0.11	0.44	0.00

Table S5. Reconstructed water palaeotemperature in Buxières-les-Mines and in the Muse OSB using water oxygen isotope composition ($\delta^{18}O_w$) from different modern aquatic settings.

Specimen	Systematics	Locality name	n	δ18Op (%V-SMOW)	sd (δ18Op)	Saltwater model (deglaciation) (°C)	Saltwater model (glaciation) (°C)	Lake Matano model (°C)	Lake Punta Laguna model (°C)	Lake Tanganyika model (°C)	sd (Temperature)
MU1	Actinopterygii indet.	Muse OSB	1	17.94	0.03	32.17	36.67	17.32	40.85	53.99	0.16
MU2	Actinopterygii indet.	Muse OSB	1	17.78	0.03	32.87	37.37	18.02	41.56	54.70	0.16
MU3	Actinopterygii indet.	Muse OSB	1	17.61	0.03	33.64	38.14	18.79	42.32	55.46	0.16
MU4	Actinopterygii indet.	Muse OSB	1	18.12	0.03	31.37	35.87	16.52	40.06	53.20	0.16
MU5	Actinopterygii indet.	Muse OSB	1	18.57	0.03	29.36	33.86	14.51	38.04	51.18	0.16
1924	Acanthodii (cf. Acanthodes sp.)	Muse OSB	3	20.62	0.63	20.10	24.60	5.25	28.79	41.93	2.82
1955	Acanthodii (cf. Acanthodes sp.)	Muse OSB	8	19.49	0.15	25.20	29.70	10.35	33.88	47.02	0.68
943	Xenacanthidae (cf. Triodus sp.)	Muse OSB	5	18.32	0.63	30.46	34.96	15.61	39.15	52.29	2.84
907b	Xenacanthidae (cf. Triodus sp.)	Muse OSB	2	21.26	2.49	17.23	21.73	2.38	25.92	39.06	11.21
965a	Xenacanthidae (cf. Triodus sp.)	Muse OSB	6	19.20	0.21	26.50	31.00	11.65	35.19	48.33	0.95
326a/326b	Xenacanthidae (cf. Triodus sp.)	Muse OSB	6	25.10	1.29	-0.05	4.45	-14.90	8.63	21.78	5.81
BXT	Actinopterygii indet.	Buxières-les-Mines	1	16.33	0.07	39.43	43.93	24.58	48.11	61.25	0.33
BX39	Actinopterygii indet.	Buxières-les-Mines	1	16.72	0.07	37.67	42.17	22.82	46.36	59.50	0.33
D062	Actinopterygii indet.	Buxières-les-Mines	1	16.92	0.03	36.74	41.24	21.89	45.43	58.57	0.16
D20-1	Actinopterygii indet.	Buxières-les-Mines	1	16.77	0.03	37.44	41.94	22.59	46.12	59.26	0.16
D20-2	Actinopterygii indet.	Buxières-les-Mines	1	16.43	0.03	38.97	43.47	24.12	47.65	60.79	0.16
NN5	Acanthodii (cf. Acanthodes sp.)	Buxières-les-Mines	3	17.40	0.10	34.60	39.10	19.75	43.29	56.43	0.45
NN9	Acanthodii (cf. Acanthodes sp.)	Buxières-les-Mines	9 (4)	17.32	0.17	34.96	39.46	20.11	43.65	56.79	0.77
BJM2	Acanthodii (cf. Acanthodes sp.)	Buxières-les-Mines	3 (1)	17.05	0.20	36.18	40.68	21.33	44.86	58.00	0.90
BJM3	Acanthodii (cf. Acanthodes sp.)	Buxières-les-Mines	5 (4)	17.36	0.14	34.78	39.28	19.93	43.47	56.61	0.63
BXA86	Acanthodii (cf. Acanthodes sp.)	Buxières-les-Mines	4	18.58	0.12	29.29	33.79	14.44	37.98	51.12	0.54
BX28	Xenacanthidae (cf. Triodus sp.)	Buxières-les-Mines	3	16.91	0.27	36.81	41.31	21.96	45.49	58.63	1.22
D07	Xenacanthidae (cf. Triodus sp.)	Buxières-les-Mines	6	17.37	0.31	34.74	39.24	19.89	43.42	56.56	1.40
D08	Xenacanthidae (cf. Triodus sp.)	Buxières-les-Mines	7 (5)	18.05	0.40	31.68	36.18	16.83	40.36	53.50	1.80
BX23-1	Xenacanthidae (cf. Triodus sp.)	Buxières-les-Mines	3	16.28	0.04	39.64	44.14	24.79	48.33	61.47	0.18
BX23-2	Xenacanthidae (cf. Triodus sp.)	Buxières-les-Mines	3	16.29	0.35	39.60	44.10	24.75	48.28	61.42	1.58
D-11-11-96 21	Xenacanthidae (cf. Triodus sp.)	Buxières-les-Mines	14	17.30	0.36	35.05	39.55	20.20	43.74	56.88	1.62
D-13-06-98 5	Diplodoselachidae (cf. Orthacanthus sp.)	Buxières-les-Mines	12	17.60	0.24	33.70	38.20	18.85	42.39	55.53	1.08
BX04	Diplodoselachidae (cf. Orthacanthus sp.)	Buxières-les-Mines	19	16.75	0.25	37.55	42.05	22.70	46.23	59.37	1.14
D17	Diplodoselachidae (cf. Orthacanthus sp.)	Buxières-les-Mines	6	16.43	0.07	38.97	43.47	24.12	47.65	60.79	0.33
BXR1	Temnospondyli indet.	Buxières-les-Mines	1	15.71	0.31	42.21	46.71	27.36	50.90	64.04	1.41
BXR2	Temnospondyli indet.	Buxières-les-Mines	1	15.48	0.31	43.23	47.73	28.38	51.92	65.06	1.41
BXR3	Temnospondyli indet.	Buxières-les-Mines	1	15.38	0.31	43.69	48.19	28.84	52.37	65.51	1.41
BXR4	Temnospondyli indet.	Buxières-les-Mines	1	15.51	0.31	43.12	47.62	28.27	51.81	64.95	1.41
BXR5	Temnospondyli indet.	Buxières-les-Mines	1	15.52	0.31	43.08	47.58	28.23	51.76	64.90	1.41
BXR6	Temnospondyli indet.	Buxières-les-Mines	1	14.01	0.31	49.88	54.38	35.03	58.56	71.70	1.41
BXR7	Temnospondyli indet.	Buxières-les-Mines	1	14.87	0.31	45.97	50.47	31.12	54.65	67.79	1.41
BXR8	Temnospondyli indet.	Buxières-les-Mines	1	14.59	0.31	47.24	51.74	32.39	55.92	69.06	1.41

Chapter VI – General discussion and perspectives

1. Diversity dynamics of the European Carboniferous-Permian Xenacanthiformes

The present study updates the systematics and the palaeocology of the xenacanthiform faunas from the French Northern Massif central. Removing ambiguous systematic attributions allow to better compare the French fossil record to the other European Carboniferous-Permian basins in order to better understand the diversity dynamics of this group.

1.1. Diversity of the Xenacanthiformes in the early Permian of the Northern Massif central

The problematic genus '*Expleuracanthus*' was erected to replace the invalid genus '*Pleuracanthus'*, preoccupied by a coleopteran. However, the change of name did not solve the systematic issue. In fact, '*Expleuracanthus*' appears to be a catch-all name to many xenacanthid remains. It represents two distinct genera. For example, '*E.*' *laevissimus* (Davis, 1880) and '*E.*' *serratus* Davis, 1892 are currently related to *Xenacanthus laevissimus* and *Triodus serratus* (Hampe 2003). Regarding the Muse OSB material, the results of the systematic revision of the '*Expleuracanthus*' material does not support the validity of this genus. The species '*E*'. *frossardi* is a *nomen dubium* and could be related to the genus *Triodus*. '*E.*' *bonnardi* is still in need of a revision but was considered as a synonym of '*E.*' *frossardi* (Sauvage, 1893). These French representatives could all be related to the genus *Triodus*.

The new faunal list confirms that the genera *Plicatodus* and *Lebachacanthus* are not present in the Massif central, so not widely distributed, and *Triodus* and *Orthacanthus* are among the most diversified genera in the European Carboniferous-Permian basins. The genus *Xenacanthus* is not recovered in the Autun and Bourbon-l'Archambault basins whereas it is present in the late Carboniferous Commentry Basin (Allier, France) with *X. gaudryi* and it is also present in the British, German, Czech and maybe Ukrainian late Carboniferous basins and in the German and Czech early Permian basins. *A contrario,* the genus *Orthacanthus* is widely distributed in the late Carboniferous, from Spain to the Czech Republic and maybe Ukraine,

but it has not been recovered from the French late Carboniferous. It is represented in the early Permian of France with *O. kounoviensis* and *O. buxieri* in the Bourbon-l'Archambault Basin and maybe in the Autun Basin. The largest *Xenacanthus* species are supposed to reach up to 2 m (Soler-Gijón 2004) and the largest *Orthacanthus* exceeds 3 m. The presence of *Xenacanthus* in the late Carboniferous of the Massif central could be related to the absence of *Orthacanthus* that usually occupies the top predator ecological niche (e.g. Kriwet *et al.* 2008). In fact, *X. gaudryi* could reach more than 1 m (Brongniart & Sauvage 1888), and without *Orthacanthus*, *Xenacanthus* could occupy this latter niche, The migration of *Orthacanthus* in the French Massif central in the early Permian could be the cause of the extinction of *Xenacanthus*. For example, in the Saar-Nahe Basin, the most complete trophic structure includes large *Orthacanthus* or *Lebachacanthus* as top predators, small *Triodus* as secondary consumers but never the intermediate-sized *Xenacanthus*.

1.2. Palaeobiogeographical patterns

The study of the Muse OSB in the Autun Basin confirms that *Triodus* displays a diversification event in the early Permian. This genus is present since the late Bashkirian in British, Russian, Austrian, and German basins with one species in each basin. At the Carboniferous-Permian transition, when Franconian tectonic movements affecting the distribution of the freshwater chondrichthyans occurred (Schneider 1996), it disappears from British, Russian, Austrian basins but it is also recovered in the Czech, French and German basins. Above all, the number of species increases with one in Bohemia, two in the Autun Basin (*T. aeduorum* and *Triodus* sp.) and four in the Saar-Nahe Basins against four species in the late Carboniferous. The supposed environmental fractionation restricted its geographical distribution but not its specific diversity. Furthermore, is it interesting to note that the Muse OSB (2 species, maybe three if the ambiguous *'Expleuracanthus' bonnardi* is included) and the Saar-Nahe Basin (4 species), the most diversified localities, are interpreted as freshwater environment with evaporative events (Fischer *et al.* 2013). The diversification of *Triodus* could therefore be a successful adaptation to shallow freshwater lake submitted to drying up periods.

This work confirms the presence of the genus *Orthacanthus* in Buxières-les-Mines (Bourbon-l'Archambault Basin) and in the Muse OSB (Autun Basin). This implies several revisions of the palaeobiogeography of this genus in Europe at the Carboniferous-Permian transition. Firstly, the presence of *O. kounoviensis* in Buxières-les-Mines and *O.* cf. *kounoviensis* in the Muse OSB is the first palaeontological evidence for a connection between these two basins. Furthermore, the presence of *O. kounoviensis* in the Massif central supposes

different palaeobiogeographical strategies between the European xenacanthiforms. *O. kounoviensis* is also present in the late Carboniferous of Bohemia and the Saar-Nahe Basin (Germany) and maybe in the United Kingdom with *O.* cf. *kounoviensis*. Another species, *O. gracilis*, is present in the late Carboniferous of the Saar-Nahe Basin and *O.* cf. *gracilis* in the United Kingdom. *A contrario*, the genus *Triodus*, during the late Carboniferous and the early Permian, is represented by species which are not present in more than one basin.

These different distribution patterns could explain the survival differences between the large *Orthacanthus* and the small *Triodus* at the Carboniferous-Permian transition. The diversity of *Orthacanthus* decreases sharply with the sole species *O. kounoviensis* (two species if the putative *O. buxieri* is valid) present in the early Permian of the Massif central. It is interesting to note that it is the same species which is widely present in the European late Carboniferous that passed through this boundary. The specific diversity of *Triodus* increases in the early Permian with 7 species instead of 4 in the late Carboniferous. Another major difference with *Orthacanthus* is that *Triodus* is not present in the same basins between the Permian and the Carboniferous (with the exception of the Saar-Nahe Basin) and no species passes through this boundary. The survival strategy of *Triodus* appears therefore more efficient than that of *Orthacanthus* with speciation events associated to occupancy of new environments (shallow freshwater lake) whereas *Orthacanthus* only survived with a still widely distributed species. This observed difference in distribution is expected because the environmental fractionation by the Franconian movement is more likely to impact large organisms than smaller ones. *Orthacanthus* is restricted to large freshwater systems like in Buxières-les-Mines.

The systematic study demonstrated for the first time the presence of the genus *Orthacanthus* in the Muse OSB and therefore in the Autun Basin. Regarding the proposed palaeoenvironmental reconstructions of the Muse OSB and the observed palaeobiogeography of this genus in Europe, its presence is not expected in this locality. In fact, it is the first time that Permian *Orthacanthus* individuals are found in a shallow environment contrary to the large open lake of Buxières-les-Mines in France or the Saar-Nahe Basin in Germany. However, it must be noted that the fossil record from the Muse OSB is made of a single tooth. Its size does not reach that of large *Orthacanthus kounoviensis* teeth observed in Buxères-les-Mines: it could correspond to a late juvenile or sub-adult specimen. Consequently, its ecology could be different from adult *Orthacanthus* and more related to that of *Triodus*. Late juvenile to sub-adult *Orthacanthus* could be able to live in more various environment, i.e. not restricted to open and large lakes. However, this hypothesis seems difficult to support. If it is the case, why were adults restricted to large lakes and how juveniles/sub-adults could migrate to shallower

environment? Additionally, the distinct East-oriented in the Muse OSB and the inaccuracies about the stratigraphic provenance of the single tooth could question the presence of *Orthacanthus* in the Muse OSB as it is currently known. New investigations are needed to clarify the stratigraphic position, the systematics and the ontogeny of *Orthacanthus* from the Muse OSB in order to understand its presence in this shallow lake.

1.3. Palaeoecological implication on the survival of European Permian Xenacanthiformes

The environmental reconstruction of the Muse OSB and Buxières-les-Mines localities confirms that the European Carboniferous-Permian Xenacanthiformes lived in freshwater setting, as it has previously been proposed (Fischer *et al.* 2013). During the late Carboniferous and early Permian, the global climate changed from a wet icehouse to a dry greenhouse setting. This transition was not abrupt, and several glaciation-deglaciation events occurred at the Carboniferous-Permian transition, limiting the aridification. These cycles ended during the late Artinskian. The latest European Permian Xenacanthiformes went extinct in the late Artinskian. As it has been demonstrated (e.g. Tedesco *et al.* 2013) that modern freshwater fishes are particularly sensitive to aridification and water losses. The aridity increases in the late lower Permian and could therefore explain this extinction: the latest xenacanthiform, i.e. small *Triodus* and *Xenacanthus*, that survived the environmental fractionations of the Carboniferous-Permian transition under a global wet climate did not survive the aridification.

2. Comparisons with the American Xenacanthiformes fossil record

Even if the first report of Xenacanthiformes dates from the 19th century (Cope 1888), it was only since the 1980s that the American fossil record was intensively investigated (e.g. Johnson 1980, 1984, 1995, 1996, 1999; Schaeffer 1981; Zidek 1992, 1993). Consequently, these authors compared the American specimens to the known European species. North America was situated at Pangea western margin whereas Europe was at its Eastern margin. The presence of the same genera (*Orthacanthus*, *Xenacanthus*, *Triodus*) and even of common species (*X. remigiusbergensis* and maybe *O. compressus*) from both Pangea extremities questions the actual systematics of American specimens.

The xenacanthiform fossil record in North America dates from the Visean with *Dicentrodus*. Among the common species with Europe, there are *Triodus elpia* from the Bashkirian, *Xenacanthus remigiusbergensis* from the Gzhelian, *X. slaughteri* from the

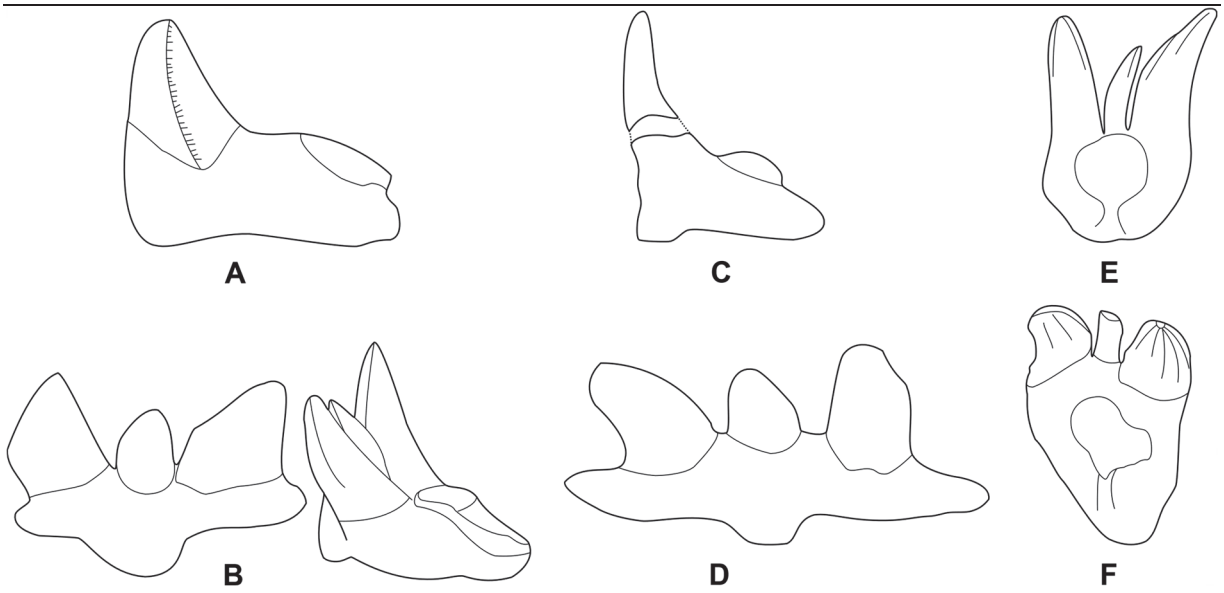

Figure 91. Anatomical comparisons between European (top) and American (bottom) xenacanthiforms. **A–B**, *Orthacanthus* with *O. gracilis* (**A**) and *O. donnelljohnsi* (**B**). **C–D**, *Xenacanthus* with *X. laevissimus* (**C**) and *X. slaughteri* (**D**). **E–F**, *Triodus* with *T. serratus* (**E**) and *T. elpia* (**F**) (modified from Hampe 1994, 2003; Johnson 1999; Johnson & Thayer 2009). The teeth are not in scale.

Sakmarian and the five *Orthacanthus* species known from the Bashkirian to the Sakmarian. The oldest European representatives of these genera date from almost the same stages.

The anatomical comparisons (Fig. 90) between American and European species clearly allow distinguishing them. For *Orthacanthus*, the American species are characterised by thin tooth base and lateral cusps without (smooth) or with slightly developed serration. The European species present thick tooth base and developed serrations on the lateral cutting edges which can be complex in *O. kounoviensis*. Only the early Permian *O. texensis* resembles the European species. Almost the same thing can be observed for *Xenacanthus*: *X. slaughteri* is characterised by extremely reduced tooth base contrary to the European species, excepted *X. remigiusbergensis* that is also reported in North America even if firstly attributed to another species (?*X. ossiani*; Johnson 1999). For *Triodus*, the American *T. elpia* is clearly different from the European species by its asymmetric tooth base, a rare character within the Xenacanthiformes. These anatomical differences could be phylogenetic signals and imply that the American and European Xenacanthiformes were isolated from each other as early as the late Mississippian.

In order to test this hypothesis, a similarity analysis using the Jaccard similarity index was performed with PAST (Hammer *et al.* 2001). The comparison matrix includes the 14 known xenacanthiform genera (Table 11). The geographic areas are divided into North

Table 11. Occurrence of the xenacanthiform genera. **X**, presence. **1**, Mississippian. **2**, Pennsylvanian. **3**, Cisuralian. **4**, Guadalupian. **5**, Triassic.

	Orthacanthus	***Lebachacanthus***	***Triodus***	***Xenacanthus***	***Plicatodus***	***Diplodoselache***
North America1						
Australia1						
United Kingdom1				X		X
Russia1						X
North America2	X		X	X		
United Kingdom2	X		X	X		
France2			X	X		
Germany2	X	X	X	X		
Czech Republic2	X			X	X	
Russia2			X			
Austria2			X			
Espagne2	X		X			
Ukraine2	X		X	X		
North America3	X			X		
Brazil3				X		
France3	X		X			
Germany3		X	X	X	X	
Czech Republic3			X	X		
Italy3	X		X	X		
Brazil4			X	X		
North America5						
Australia5						
India5						
United Kingdom5						
Germany5						

	Dicentrodus	***Wurdigneria***	***Mooreodontus***	***Tikiodontus***	***Reginaselache***	***Hokomata***
North America1	X					
Australia1					X	
United Kingdom1	X					
Russia1						
North America2						X
United Kingdom2						
France2						
Germany2						
Czech Republic2						
Russia2						
Austria2						
Espagne2						
Ukraine2						

	Dicentrodus	*Wurdigneria*	*Mooreodontus*	*Tikiodontus*	*Reginaselache*	*Hokomata*
North America3						
Brazil3		X				
France3						
Germany3						
Czech Republic3						
Italy3						
Brazil4		X				
North America5			X			
Australia5			X			
India5			X	X		
United Kingdom5			X			
Germany5			X			

	Taquaralodus	*Hagenoselache*
North America1		
Australia1		
United Kingdom1		
Russia1		
North America2		
United Kingdom2		
France2		
Germany2		X
Czech Republic2		
Russia2		
Austria2		
Espagne2		
Ukraine2		
North America3		
Brazil3	X	
France3		
Germany3		
Czech Republic3		
Italy3		
Brazil4		
North America5		
Australia5		
India5		
United Kingdom5		
Germany5		

Table 12. Jaccard similarity coefficients for the xenacanthiform assemblages. **1**, Mississippian. **2**, Pennsylvanian. **3**, Cisuralian. **4**, Guadalupian. **5**, Triassic.

	North America1	**Australia1**	**United Kingdom1**	**Russia1**	**North America2**	**United Kingdom2**
North America1	1	0	0	0	0	0
Australia1	0	1	0	0	0	0
United Kingdom1	0,33333333	0	1	0,33333333	0,16666667	0,2
Russia1	0	0	0,33333333	1	0	0
North America2	0	0	0,16666667	0	1	0,75
United Kingdom2	0	0	0,2	0	0,75	1
France2	0	0	0,25	0	0,5	0,66666667
Germany2	0	0	0,14285714	0	0,5	0,6
Czech Republic2	0	0	0,2	0	0,4	0,5
Russia2	0	0	0	0	0,25	0,33333333
Austria2	0	0	0	0	0,25	0,33333333
Espagne2	0	0	0	0	0,5	0,66666667
Ukraine2	0	0	0,2	0	0,75	1
North America3	0	0	0	0	0,5	0,66666667
Brazil3	0	0	0,2	0	0,16666667	0,2
France3	0	0	0	0	0,5	0,66666667
Germany3	0	0	0,16666667	0	0,33333333	0,4
Czech Republic3	0	0	0,25	0	0,5	0,66666667
Italy3	0	0	0,2	0	0,75	1
Brazil4	0	0	0,2	0	0,4	0,5
North America5	0	0	0	0	0	0
Australia5	0	0	0	0	0	0
India5	0	0	0	0	0	0
United Kingdom5	0	0	0	0	0	0
Germany5	0	0	0	0	0	0

	France2	**Germany2**	**Czech Republic2**	**Russia2**	**Austria2**	**Espagne2**
North America1	0	0	0	0	0	0
Australia1	0	0	0	0	0	0
United Kingdom1	0,25	0,14285714	0,2	0	0	0
Russia1	0	0	0	0	0	0
North America2	0,5	0,5	0,4	0,25	0,25	0,5
United Kingdom2	0,66666667	0,6	0,5	0,33333333	0,33333333	0,66666667
France2	1	0,4	0,25	0,5	0,5	0,33333333
Germany2	0,4	1	0,33333333	0,2	0,2	0,4
Czech Republic2	0,25	0,33333333	1	0	0	0,25
Russia2	0,5	0,2	0	1	1	0,5
Austria2	0,5	0,2	0	1	1	0,5
Espagne2	0,33333333	0,4	0,25	0,5	0,5	1
Ukraine2	0,66666667	0,6	0,5	0,33333333	0,33333333	0,66666667
North America3	0,33333333	0,4	0,66666667	0	0	0,33333333

	France2	**Germany2**	**Czech Republic2**	**Russia2**	**Austria2**	**Espagne2**
Brazil3	0,25	0,14285714	0,2	0	0	0
France3	0,33333333	0,4	0,25	0,5	0,5	1
Germany3	0,5	0,5	0,4	0,25	0,25	0,2
Czech Republic3	1	0,4	0,25	0,5	0,5	0,33333333
Italy3	0,66666667	0,6	0,5	0,33333333	0,33333333	0,66666667
Brazil4	0,66666667	0,33333333	0,2	0,33333333	0,33333333	0,25
North America5	0	0	0	0	0	0
Australia5	0	0	0	0	0	0
India5	0	0	0	0	0	0
United Kingdom5	0	0	0	0	0	0
Germany5	0	0	0	0	0	0

	Ukraine2	**North America3**	**Brazil3**	**France3**	**Germany3**	**Czech Republic3**
North America1	0	0	0	0	0	0
Australia1	0	0	0	0	0	0
United Kingdom1	0,2	0,25	0,2	0	0,16666667	0,25
Russia1	0	0	0	0	0	0
North America2	0,75	0,5	0,16666667	0,5	0,33333333	0,5
United Kingdom2	1	0,66666667	0,2	0,4	0,33333333	0,66666667
France2	0,66666667	0,33333333	0,25	0,33333333	0,5	1
Germany2	0,6	0,4	0,14285714	0,4	0,28571429	0,4
Czech Republic2	0,5	0,66666667	0,2	0,25	0,4	0,25
Russia2	0,33333333	0	0	0,5	0,25	0,5
Austria2	0,33333333	0	0	0,5	0,25	0,5
Espagne2	0,66666667	0,33333333	0	1	0,2	0,33333333
Ukraine2	1	0,66666667	0,2	0,4	0,33333333	0,66666667
North America3	0,66666667	1	0,25	0,33333333	0,2	0,33333333
Brazil3	0,2	0,25	1	0	0,16666667	0,25
France3	0,66666667	0,33333333	0	1	0,2	0,33333333
Germany3	0,4	0,2	0,16666667	0,2	1	0,5
Czech Republic3	0,66666667	0,33333333	0,25	0,33333333	0,5	1
Italy3	1	0,66666667	0,2	0,4	0,33333333	0,66666667
Brazil4	0,5	0,25	0,5	0,25	0,4	0,66666667
North America5	0	0	0	0	0	0
Australia5	0	0	0	0	0	0
India5	0	0	0	0	0	0
United Kingdom5	0	0	0	0	0	0
Germany5	0	0	0	0	0	0

	Italy3	**Brazil4**	**North America5**	**Australia5**	**India5**	**United Kingdom5**
North America1	0	0	0	0	0	0
Australia1	0	0	0	0	0	0
United Kingdom1	0,2	0,2	0	0	0	0

	Italy3	Brazil4	North America5	Australia5	India5	United Kingdom5
	0	0	0	0	0	0
Russia1	0,75	0,4	0	0	0	0
North America2	1	0,5	0	0	0	0
United Kingdom2	0,66666667	0,66666667	0	0	0	0
France2	0,6	0,33333333	0	0	0	0
Germany2	0,5	0,2	0	0	0	0
Czech Republic2	0,33333333	0,33333333	0	0	0	0
Russia2	0,33333333	0,33333333	0	0	0	0
Austria2	0,66666667	0,25	0	0	0	0
Espagne2	1	0,5	0	0	0	0
Ukraine2	0,66666667	0,25	0	0	0	0
North America3	0,2	0,5	0	0	0	0
Brazil3	0,66666667	0,25	0	0	0	0
France3	0,4	0,4	0	0	0	0
Germany3	0,66666667	0,66666667	0	0	0	0
Czech Republic3	1	0,5	0	0	0	0
Italy3	0,5	1	0	0	0	0
Brazil4	0	0	1	1	0,5	1
North America5	0	0	1	1	0,5	1
Australia5	0	0	0,5	0,5	1	0,5
India5	0	0	1	1	0,5	1
United Kingdom5	0	0	1	1	0,5	1
Germany5	0	0	1	1	0.5	1

	Germany5
North America1	0
Australia1	0
United Kingdom1	0
Russia1	0
North America2	0
United Kingdom2	0
France2	0
Germany2	0
Czech Republic2	0
Russia2	0
Austria2	0
Espagne2	0
Ukraine2	0
North America3	0
Brazil3	0
France3	0
Germany3	0

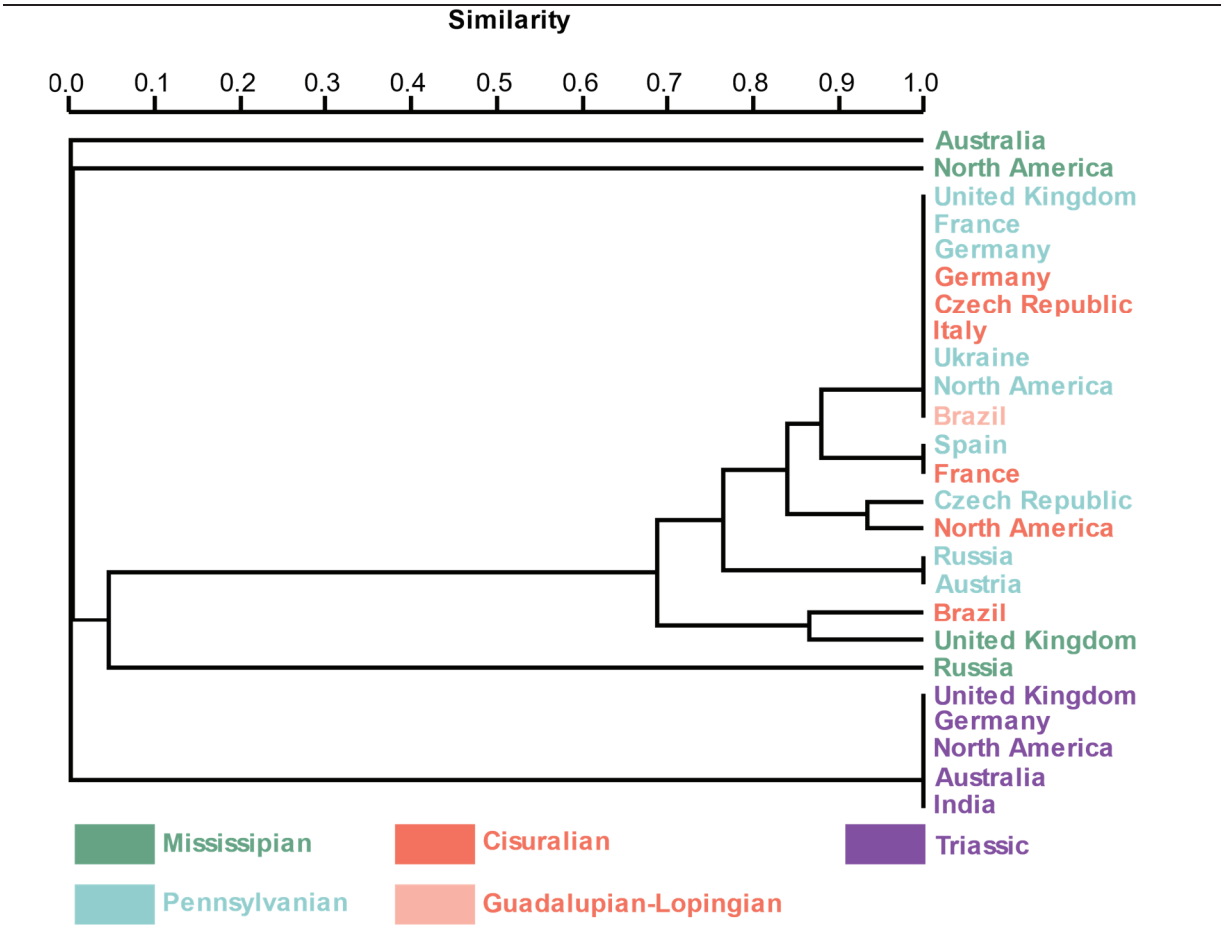

Figure 92. Dendrogram of the similarity of the xenacanth assemblages of the world.

America, Brazil, Australia, India and nine European areas (United Kingdom, Russia, France, Germany, Czech Republic, Austria, Spain, Italy, Ukraine). Each area is divided into five temporal ranges (Mississippian, Pennsylvanian, Cisuralian, Guadalupian-Lopingian and Triassic).

The main result of the calculation of the Jaccard index (Fig. 91, Table 12) is that the American and European areas are not discernible whatever the considered period. This result can be interpreted in different ways. It could correspond to active faunal exchanges between North America and European as late as the early Permian. However, this hypothesis seems difficult to support because of the apparent strict freshwater ecology of Carboniferous-Permian European xenacanthiforms (this work; Fischer *et al.* 2013) and of Sakmarian-Kungurian American ones (Fischer *et al.* 2014b) Another hypothesis could be that the observed similarities are convergences. The xenacanth teeth, like modern elasmobranchs, could be highly dedicated to them. So, the original phylogenetic signals cannot be recovered, and the American and European areas appear similar in this analysis. The small observed dental differences could be local adaptations to environmental conditions. Even if Fischer *et al.* (2014b) plead for a strict

freshwater ecology, Soler-Gijón (1999) and Beck *et al.* (2016) argued for a marine tolerance in American *Orthacanthus*. The ecology of American xenacanthiform could be more related to the marine setting and, consequently, has produced different dental adaptations. Another explanation could be that high resemblances between two distant (thousands of kilometres) geographic areas are not possible and American specimens represents different genera than the European ones. The observed resemblances represent therefore ecological convergences related to a similar freshwater environment (Fischer *et al.* 2014b).

The analysis of the relationships between American and European is out of the scope of this Ph.D. work. However, in the light of this preliminary attempt, it seems obvious that this problem needs more investigations including detailed anatomical comparisons and distribution patterns.

3. How to explain the distribution pattern of the Xenacanthiformes at the global scale?

This work and previous studies (e.g. Fischer *et al.* 2013, 2014b) support the main freshwater adaptation of the Xenacanthiformes. Following this interpretation, several questions can be raised, including how did they colonise numerous localities from North America to Australia? It seems unlikely that this distribution can only be explained by considering river-channel systems only. Furthermore, the Xenacanthiformes are widely distributed all around the world since the beginning of their evolutionary history. However, no geochemical analysis has found evidence for a marine living environment and the results of histological studies (Soler-Gijón 1999; Beck *et al.* 2016) of their dorsal spines can be discussed. Until now, only late Carboniferous and early Permian Xenacanthiformes were investigated. it could be interesting to consider older fossil records and to attempt geochemical analyses on Mississippian specimens, e.g. *Diplodoselache* or *Dicentrodus*. If a clear marine tolerance is found in these genera, the wide distribution of the group could be more understandable, and the observed strict freshwater ecology could be a secondary adaptation of more derived forms.

Another way to explore the origin of their distribution could be to investigate the ecology of the closest related groups like the order Bransonelliformes or supposed stem-xenacanth like ‘Ctenacanthiformes’, Phoebodontiformes or Antarctilamniformes. None has ever been found in freshwater deposits, but they could have had freshwater tolerance. Again, investigating these groups from a geochemical point of view could be a way to understand why the xenacanthiforms seem to be exclusively adapted to freshwater.

Conclusion

This Ph.D. project aimed to revise the systematics of the presumed freshwater ecology of the early Permian chondrichthyans of intra-mountainous basins of the French Massif central. The systematic revision provided numerous updates on the chondrichthyan faunas, and especially on Xenacanthiformes, from the Muse OSB in the Autun Basin and from Buxières-les-Mines in the Bourbon-l'Archambault Basin.

The main results are the taxonomic invalidity of some historical species from the Autun Basin ('*Expleuracanthus*' *frossardi*, *Triodus* ?*frossardi*, *Bibractopiscis niger*, *Orthacanthus commailli*) and justified doubts on the validity of *Orthacanthus buxieri* from Buxières-les-Mines in the Bourbon-l'Archambault Basin. However, new species in the Muse OSB (*T. aeduorum*) and first reports of already known species in Buxières-les-Mines (*O. kounoviensis*) or new forms in the Autun Basin (*O.* cf. *kounoviensis*, 'Ctenacanthiformes' indet. and ?Xenacanthimorpha) in the late Carboniferous-early Permian of France were also noted. This new faunal list allows to better understand the diversity of the Carboniferous-Permian chondrichthyans from the Massif central: they were dominated by the Xenacanthiformes even if some closely related forms could also be present. This faunal list also allows to compare these two basins and to propose a first palaeontological argument for their connection at the Carboniferous-Permian transition based on the presence of *O. kounoviensis* and the closely related form *O.* cf. *kounoviensis* in these two basins.

This work also allows discussing the global evolutionary history of the European Xenacanthiformes. New phylogenetic hypothesis was proposed based on the detailed description of their neurocranial anatomy and that of closely related forms. The Xenacanthiformes could be more closely related to Ctenacanthiformes than to Phoebodontiformes but other forms like ?Xenacanthimorpha are their closest relatives. This result, reinforced by a first geometric morphometric attempt on their neurocranial shape, highlights the need to investigate their sister-group, i.e. Bransonelliformes, in order to stabilise their relationships among the global chondrichthyan phylogeny. This needs new excavation campaigns in order to find new cranial and post-cranial elements.

The early French Permian fossil record allows discussing the global palaeobiogeography of the Xenacanthiformes at the Carboniferous-Permian transition and to tentatively explain the observed systematic turn-over. Buxières-les-Mines is the latest record of

the large top predator *Orthacanthus* with the survival of *O. kounoviensis*, and maybe *O. buxieri*. *O.* cf. *kounoviensis* is also present in the Autun Basin. Its presence in the early Permian of France is unexpected in the light of its fossil record in other European basins in which it is restricted to the late Carboniferous. The Northern Massif central is thus a refuge area for the large xenacanthiform after a global change in the geometry of the basins due to tectonic movements. At the same time, the record of the new species *Triodus aeduorum* which is unknown in other European basins questions its evolutionary model. *Triodus* seems to perform rapid speciation events with numerous endemic species to their respective basins. Furthermore, it is more diversified in the early Permian than in the late Carboniferous. This distribution pattern is completely different from that of *Orthacanthus*.

Consequently, how can this palaeobiogeography be explained? What are its control factors? In a time of environmental changes like during the Carboniferous-Permian transition, a potential answer could be related to the environment. In fact, the palaeoenvironment and palaeoecology of the Xenacanthiformes are highly debated, and another research axis of this Ph.D. project was to reassess them based on the oxygen, carbon and sulfur isotope compositions of the bioapatite of their dorsal spines. This axis confirms the freshwater ecology of the early Permian Xenacanthiformes from the Northern Massif central. It also contradicts hypotheses on potential marine influences which are not supported in the Muse OSB and in Buxières-les-Mines. This result is reinforced by the same analyses on the associated vertebrate fauna that show the same conclusions. The geochemical analyses also confirm the top predator position of *Orthacanthus* in Carboniferous-Permian freshwater basins. Another update is to invalid the migration hypothesis. Oxygen isotope compositions along the growth axis of the dorsal spines are constant, indicating none significant environmental changes during the lifespan of Xenacanthiformes and also of acanthodians.

The apparent stable freshwater ecology of the early Permian Xenacanthiformes from the Northern Massif central does not mean that all of them have the same ecological tolerances. The geochemical analyses show two patterns: *Orthacanthus* from the large and deep Buxières-les-Mines lake lived in a very constant environment, not submitted to significant environmental variations. On the contrary, *Triodus* from the Muse OSB lived in an environment where the oxygen isotope variations imply strong environmental variations. The small xenacanthiforms could therefore be able to adapt to settings influenced by environmental stresses like drying up events and/or low-oxygenised waters. This difference could explain the palaeobiogeography of the group at a more global scale in Europe during the Carboniferous-Permian transition. The large xenacanthiform like *Orthacanthus* lived in large freshwater lakes or river-channels which

were abundant in the late Carboniferous and restricted to a few localities in the early Permian, explaining their low diversity in the early Permian, whereas small xenacanthiforms were able to live in more various environments from large lakes to shallow swamps. They were more diversified in the early Permian during which the shallow freshwater settings were more abundant due to the fractionation of large lakes at the Carboniferous-Permian transition by tectonic movements.

These studies open the way for additional works on the evolutionary history of the Xenacanthiformes. The fossil record of the intra-mountainous basins of the Northern Massif central could not be entirely revised. Some species like *'Expleuracanthus' bonnardi* from the Muse OSB and *Orthacanthus buxieri* from Buxières-les-Mines are still highly questionable. Unfortunately, these specimens are too badly preserved and/or cannot be mechanically prepared to allow a satisfactory revision. Use of new technology like 2D chemical imaging, e.g. X-ray fluorescence mapping, or new X-ray computed microtomographic scan could allow to assess their systematic status. The present palaeoenvironmental and palaeoecological reconstructions are only valid for the investigated basins and localities. The Xenacanthiformes being a globally distributed taxon from the early Carboniferous to the upper Triassic, new investigations on their diversity and disparity pattern as well as on their environmental adaptations along their stratigraphic occurrences are needed to fully understand their evolutionary history.

References

Aarestrup, K., Okland, F., Hansen, M. M., Righton, D., Gargan, P., Castonguay, M., Bernatchez, L., Howey, P., Sparholt, H., Pedersen, M. I. & McKinley, R. S. 2009. Oceanic Spawning Migration of the European Eel (*Anguilla anguilla*). *Science*, 325, 1660.

Adams, D. C. & Otarola-Castillo, E. 2013. geomorph: Software for geometric morphometric analyses. R package version 3.3.1. *Methods in Ecology and Evolution*, 4, 393–399.

Agassiz, L. 1833. *Recherches Sur Les Poissons Fossiles 2. Contenant l'Histoire de l'Ordre Des Ganoïdes*. Petitpierre, Neuchâtel, 336 pp.

Agassiz, L. 1837a. *Recherches Sur Les Poissons Fossiles. Vol. 3, Contenant l'Histoire de l'Ordre Des Placoïdes*. Petitpierre, Neuchâtel, 1–72 pp.

Agassiz, L. 1837b. *Recherches Sur Les Poissons Fossiles. Vol. 3, Contenant l'Histoire de l'Ordre Des Placoïdes*. Petitpierre, Neuchâtel, 157–390 pp.

Agassiz, L. 1838. *Recherches Sur Les Poissons Fossiles. Tome III (Livr. 11)*. Imprimérie de Petitpierre, Neuchatel, 73–140 pp.

Agassiz, L. 1843. *Recherches Sur Les Poissons Fossiles. Vol. 3, Contenant l'Histoire de l'Ordre Des Placoïdes*. Petitpierre, Neuchâtel, 157–390 pp.

Almeida, M. P. D., Barthem, R. B., Viana, A. D. S. & Charvet-Almeida, P. 2009. Factors affecting the distribution and abundance of freshwater stingrays (Chondrichthyes: Potamotrygonidae) at Marajó Island, mouth of the Amazon River. *Pan-American Journal of Aquatic Sciences*, 4, 1–11.

Ambrose, S. H. & Norr, L. 1993. Experimental Evidence for the Relationship of the Carbon Isotope Ratios of Whole Diet and Dietary Protein to Those of Bone Collagen and Carbonate. *In*: *Prehistoric Human Bone*. Springer, Berlin, Heidelberg, 1–37.

Amiot, R., Lécuyer, C., Buffetaut, É., Fluteau, F., Legendre, S. & Martineau, F. 2004. Latitudinal temperature gradient during the Cretaceous Upper Campanian–Middle Maastrichtian: $\delta^{18}O$ record of continental vertebrates. *Earth and Planetary Science Letters*, 226, 255–272.

Amiot, R., Lécuyer, C., Escarguel, G., Billon-Bruyat, J.-P., Buffetaut, É., Langlois, C., Martin, S., Martineau, F. & Mazin, J.-M. 2007. Oxygen isotope fractionation between crocodilian phosphate and water. *Palaeogeography, Palaeoclimatology, Palaeoecology*, 243, 412–420.

Amiot, R., Wang, X., Lécuyer, C., Buffetaut, É., Boudad, L., Cavin, L., Ding, Z., Fluteau, F., Kellner, A. W. A., Tong, H. & Zhang, F. 2010. Oxygen and carbon isotope compositions of middle Cretaceous vertebrates from North Africa and Brazil: Ecological and environmental significance. *Palaeogeography, Palaeoclimatology, Palaeoecology*, 297, 439–451.

Angst, D. 2014. *Successeurs Des Dinosaures ? Paléobiologie et Paléoécologie d'un Oiseau Géant Terrestre Du Paléogène*. Unpublished Ph. D. thesis, Université Claude Bernard Lyon 1, 246 pp.

Angst, D., Lécuyer, C., Amiot, R., Buffetaut, É., Fourel, F., Martineau, F., Legendre, S., Abourachid, A. & Herrel, A. 2014. Isotopic and anatomical evidence of an herbivorous diet in the Early Tertiary giant bird *Gastornis*. Implications for the structure of Paleocene terrestrial ecosystems. *Naturwissenschaften*, 101, 313–322.

Ayliffe, L. K., Lister, A. M. & Chivas, A. R. 1992. The preservation of glacial-interglacial climatic signatures in the oxygen isotopes of elephant skeletal phosphate. *Palaeogeography, Palaeoclimatology, Palaeoecology*, 99, 179–191.

Baertschi, P. 1976. Absolute ^{18}O content of standard mean ocean water. *Earth and Planetary Science Letters*, 31, 341–344.

Baptiste, J. 2016. *Cartographie Structurale et Lithologique Du Substratum Du Bassin Parisien et Sa Place Dans La Chaîne Varisque de l'Europe de l'Ouest : Approches Combinées Géophysiques, Pétrophysiques, Géochronologiques et Modélisations 2D*. Unpublished Ph. D. thesis, Université d'Orléans, 367 pp.

Barkas, T. P. 1873. *Illustrated Guide to the Fish, Amphibian, Reptilian, and Supposed Mammalian Remains of the Northumberland Carboniferous Strata*. Hutchings, London, 138 pp.

Barkas, T. P. 1874. On the microscopical structure of fossil fishes from the Northumberland True Coal Measures. Chapter II. *The Monthly Review of Dental Surgery*, 2, 9–344.

Barnett, L. A. K., Ebert, D. A. & Cailliet, G. M. 2009. Assessment of the dorsal fin spine for chimaeroid (Holocephali: Chimaeriformes) age estimation. *Journal of Fish Biology*, 75, 1258–1270.

Barrick, J. E., Fischer, A. G. & Showers, W. J. 1999. Oxygen isotopes from turtle bone: applications for terrestrial paleoclimates?. *PALAIOS*, 186–191.

Beck, K. G., Soler-Gijón, R., Carlucci, J. R. & Willis, R. E. 2016. Morphology and histology of dorsal spines of the xenacanthid shark *Orthacanthus platypternus* from the Lower Permian of Texas, USA: Palaeobiological and palaeoenvironmental implications. *Acta Palaeontologica Polonica*, 61, 97–117.

Becker, M. A., Chamberlain Jr, J. A. & Stoffer, P. W. 2000. Pathologic tooth deformities in modern and fossil chondrichthians: a consequence of feeding-related injury. *Lethaia*, 33, 103–118.

Becq-Giraudon, J. F., Montenat, C. & Van Den Driessche, J. 1996. Hercynian high-altitude phenomena in the French Massif Central: tectonic implications. *Palaeogeography, Palaeoclimatology, Palaeoecology*, 122, 227–241.

Bengtson, P. 1988. Open Nomenclature. *Palaeontology*, 31, 223–227.

Benner, R., Biddanda, B., Black, B. & McCarthy, M. 1997. Abundance, size distribution, and stable carbon and nitrogen isotopic compositions of marine organic matter isolated by tangential-flow ultrafiltration. *Marine chemistry*, 57, 243–263.

Benzer, P. 1944. Morphology of calcification in *Squalus acanthias*. *Copeia*, 1944, 217–224.

Bercovici, A. 2009. *Reconstitutions Paléoenvironnementales Du Domaine Ouest Téthysien à La Transition Permien-Trias : Impacts Relatifs Du Climat, de La Ré-Organisation de La Biosphère Continentale et Des Topographies Sur La Préservation Des Systèmes Sédimentaires Continentaux*. Unpublished Ph. D. thesis, Université de Rennes 1, 345 pp.

Berg, L. S. 1937. A classification of fish-like vertebrates. *Bulletin de l'Académie des Sciences de l'URSS*, 4, 1277–1280.

Berg, L. S. 1940. Sistema ryboobraznykh i ryb, nyne zhivushchikh i ickopaemykh. *Trudy Zoologicheckogo instituta Akademii nauk SSSR*, 5, 87–345.

Berner, R. A. 2006. GEOCARBSULF: a combined model for Phanerozoic atmospheric O_2 and CO_2. *Geochimica et Cosmochimica Acta*, 70, 5653–5664.

Berner, R. A. & Kothavala, Z. 2001. GEOCARB III: a revised model of atmospheric CO_2 over Phanerozoic time. *American Journal of Science*, 301, 182–204.

Berthoumieu, J.-J. 1903. *Flore Carbonifere et Permienne Du Centre de La France*. Auclair, Moulis, 56 pp.

Beyrich, E. 1848. Über *Xenacanthus decheni* und *Holacanthus gracilis*, zwei Fische aus der Formation des Rothliegenden in Norddeutschland. *Berichte der Königlich-Preussischen Akademie der Wissenschaften*, 1848, 24–33.

Beznosov, P. 2009. A redescription of the Early Carboniferous acanthodian *Acanthodes lopatini* Rohon, 1889. *Acta Zoologica*, 90, 183–193.

Bhat, M. S., Ray, S. & Datta, P. M. 2018. A new assemblage of freshwater sharks (Chondrichthyes: Elasmobranchii) from the Upper Triassic of India. *Geobios*, 51, 269–283.

Biddle, K. T. & Christie-Blick, N. 1985. Strike-slip deformation, basin formation, and sedimentation. *Society of Economic Paleontologists and Mineralogists*, 37, 1–34.

Binney, E. W. 1840. On the fossil fishes of the Pendleton Coal Field. *Transactions of the Geological Society of Manchester*, 1840, 153–178.

Bishop, J. W., Montañez, I. P. & Osleger, D. A. 2010. Dynamic Carboniferous climate change, Arrow Canyon, Nevada. *Geosphere*, 6, 1–34.

Bocherens, H., Koch, P. L., Mariotti, A., Geraads, D. & Jaeger, J.-J. 1996. Isotopic biogeochemistry (^{13}C, ^{18}O) of mammalian enamel from African Pleistocene hominid sites. *PALAIOS*, 306–318.

Böttcher, M. E., Brumsack, H. J. & Dürselen, C. D. 2007. The isotopic composition of modern seawater sulfate: I. Coastal waters with special regard to the North Sea. *Journal of Marine Systems*, 67, 73–82.

Bottrell, S. H. & Newton, R. J. 2006. Reconstruction of changes in global sulfur cycling from marine sulfate isotopes. *Earth-Science Reviews*, 75, 59–83.

Bougnieres, L. 1961. Le bassin de l'Aumance. *Comptes Rendus de l'Académie des Sciences de Paris, D*, 252, 2901–2903.

Boule, M. & Glangeaud, P. 1893. Le *Callibrachion gaudryi*, nouveau Reptile fossile du Permien d'Autun. *Bulletin de la Société d'Histoire Naturelle et des Amis du Musée d'Autun*, 6, 199–215.

Bourquin, S., Bercovici, A., López-Gómez, J., Diez, J. B., Broutin, J., Ronchi, A., Durand, M., Arché, A., Linol, B. & Amour, F. 2011. The Permian–Triassic transition and the onset of Mesozoic sedimentation at the northwestern peri-Tethyan domain scale: palaeogeographic maps and geodynamic implications. *Palaeogeography, Palaeoclimatology, Palaeoecology*, 299, 265–28.

Bouttes, N., Paillard, D., Roche, D. M., Brovkin, V. & Bopp, L. 2011. Last Glacial Maximum CO_2 and $\delta^{13}C$ successfully reconciled. *Geophysical Research Letters*, 38, L02705.

Boy, J. A. & Schindler, T. 2000. Ökostratigraphische Bioevents im Grenzbereich Stephanium/Autunium (höchstes Karbon) des Saar-Nahe-Beckens (SW-Deutchland) und benachbarter Gebiete. *Neues Jahrbuch für Geologie und Paläontologie Abhandlungen*, 216, 89–152.

Brazeau, M. D. 2009. The braincase and jaws of a Devonian 'acanthodian' and modern gnathostome origins. *Nature*, 457, 305–308.

Brazeau, M. D. & de Winter, V. 2015. The hyoid arch and braincase anatomy of *Acanthodes* support chondrichthyan affinity of 'acanthodians'. *Proceedings of the Royal Society B: Biological Sciences*, 282, 20152210.

Brazeau, M. D. & Friedman, M. 2014. The characters of Palaeozoic jawed vertebrates. *Zoological Journal of the Linnean Society*, 779–821.

Brazeau, M. D., Giles, S., Dearden, R. P., Jerve, A., Ariunchimeg, Y. A., Zorig, E., Sansom, R., Guillerme, T. & Castiello, M. 2020. Endochondral bone in an Early Devonian 'placoderm' from Mongolia. *Nature Ecology & Evolution*, 4, 1477–1484, doi: 10.1101/2020.06.09.132027.

Brignon, A. 2014. Les recherches paléoichthyologiques et géologiques sur le gisement permien de Muse près d'Autun (Saône-et-Loire) au début du XIXe siècle. *Bulletin de la Société géolologique de France*, 185, 233–252.

Brito, P. M. & Ferreira, P. L. N. 1989. The first hybodont shark, *Tribodus limae* n. g., n. sp., from the Lower Cretaceous of Chapada do Araripe (north-east Brazil). *Anais da Academia Brasileira de Ciências*, 61, 53–57.

Brongniart, C. & Sauvage, H. É. 1888. Faunes ichthyologique et entomologique. *Bulletin de la Société de l'Insdustrie minérale, 3ème série*, 2, 1–120.

Browne, R. K., Li, H., Wang, Z., Okada, S., Hime, P., McMillan, A., Wu, M., Diaz, R., McGinnity, D. & Briggler, J. T. 2014. The giant salamanders (Cryptobranchidae): Part B. Biogeography, ecology and reproduction. *Amphibian and Reptile Conservation*, 5, 30–50.

Brudefold, F. & Soremark, R. 1967. Chemistry of the mineral phase of enamel—Crystalline organization of dental mineral. *Structural and Chemical Organization of Teeth*, 247–277.

Bryant, J. D. & Froelich, P. N. 1995. A model of oxygen isotope fractionation in body water of large mammals. *Geochimica et Cosmochimica Acta*, 59, 4523–4537.

Bryant, J. D., Luz, B. & Froelich, P. N. 1994. Oxygen isotopic composition of fossil horse tooth phosphate as a record of continental paleoclimate. *Palaeogeography, Palaeoclimatology, Palaeoecology*, 107, 303–316.

Bryant, J. D., Froelich, P. N., Showers, W. J. & Genna, B. J. 1996. Biologic and climatic signals in the oxygen isotopic composition of Eocene-Oligocene equid enamel phosphate. *Palaeogeography, Palaeoclimatology, Palaeoecology*, 126, 75–78.

Burrow, C. J., Davidson, R. G., Den Blaauwen, J. L. & Newman, M. J. 2015. Revision of *Climatius reticulatus* Agassiz, 1844 (Acanthodii, Climatiidae), from the Lower Devonian of Scotland, based on new histological and morphological data. *Journal of Vertebrate Paleontology*, 35, e913421.

Burrow, C. J., den Blaauwen, J., Newman, M. & Davidson, R. 2016. The diplacanthid fishes (Acanthodii, Diplacanthiformes, Diplacanthidae) from the Middle Devonian of Scotland. *Palaeontologia Electronica*, 19, 1–83.

Carpenter, D., Falcon-Lang, H. J., Benton, M. J. & Nelson, J. W. 2011. Fishes and tetrapods in the Upper Pennsylvanian (Kasimovian) Cohn coal member of the Mattoon formation of Illinois, United States: systematics, paleoecology, and paleoenvironments. *PALAIOS*, 26, 619–657.

Casanova, J. & Hilaire-Marcel, C. 1992. Late Holocene hydrological history of Lake Tanganyika, East Africa, from isotopic data on fossil stromatolites. *Palaeogeography, Palaeoclimatology, Palaeoecology*, 91, 35–48.

Cerling, T. E. & Harris, J. M. 1999. Carbon isotope fractionation between diet and bioapatite in ungulate mammals and implications for ecological and paleoecological studies. *Oecologia*, 120, 347–363.

Chahud, A., Fairchild, T. R. & Petri, S. 2010. Chondrichthyans from the base of the Irati Formation (Early Permian, Parána Basin), São Paulo, Brazil. *Gondwana Research*, 18, 528–537.

Châteauneuf, J. J. 1980. Synthèse géologique des bassins permiens français. *Rapport du Bureau de Recherches Géologiques et Minières*, 82, 124.

Châteauneuf, J. J. & Farjanel, G. 1989. Synthèse géologique des bassins permiens français. *Mémoires du Bureau de Recherches Géologiques Minières*, 1–128.

Châteauneuf, J. J., Farjanel, G., Pacaud, G. & Broutin, J. 1992. The Autun permian basin, the autunian startotype. *Cahiers de Micropaléontologie*, 7, 123–139.

Chen, B., Joachimski, M. M., Shen, S.-Z., Lambert, L. L., Lai, X. L., Wang, X.-D., Chen, J. & Yuan, D. X. 2013. Permian ice volume and palaeoclimate history: Oxygen isotope proxies revisited. *Gondwana Research*, 24, 77–89.

Chillón, B. S., Alberdi, M. T., Leone, G., Bonadonna, F. P., Stenni, B. & Longinelli, A. 1994. Oxygen isotopic composition of fossil equid tooth and bone phosphate: an archive of difficult interpretation. *Palaeogeography, Palaeoclimatology, Palaeoecology*, 107, 317–328.

Choulet, F., Faure, M., Fabbri, O. & Monié, P. 2012. Relationships between magmatism and extension along the Autun–La Serre fault system in the Variscan Belt of the eastern French Massif Central. *International Journal of Earth Sciences*, 101, 393–413.

Clarke, M. W., Connolly, P. L. & Bracken, J. J. 2002. Age estimation of the exploited deepwater shark *Centrophorus squamosus* from the continental slopes of the Rockall Trough and Porcupine Bank. *Journal of Fish Biology*, 60, 501–514.

Claude, J. 2008. *Morphometric with R*. Springer, New York, 316 pp.

Claypool, G. E., Holser, W. T., Kaplan, I. R., Sakai, H. & Zak, I. 1980. The age curves of sulfur and oxygen isotopes in marine sulfate and their mutual interpretation. *Chemical geology*, 28, 199–260.

Cleal, C. J. & Thomas, B. A. 2005. Palaeozoic tropical rainforests and their effect on global climates: is the past the key to the present? *Geobiology*, 3, 13–31.

Clementz, M. T. & Koch, K. L. 2001. Differentiating aquatic mammal habitat and foraging ecology with stable isotopes in tooth enamel. *Oecologia*, 129, 461–472.

Coates, M. I. & Sequeira, S. E. K. 1998. The braincase of a primitive shark. *Transactions of the Royal Society of Edinburgh: Earth Sciences*, 89, 63–85.

Coates, M. I. & Sequeira, S. E. K. 2001a. Early sharks and primitive gnathostome interrelationships. *Systematics Association special volume*, 61, 241–262.

Coates, M. I. & Sequeira, S. E. K. 2001b. A new stethacanthid chondrichthyan from the Lower Carboniferous of Bearsden, Scotland. *Journal of Vertebrate Paleontology*, 21, 438–459.

Coates, M. I. & Tietjen, K. 2018. The neurocranium of the Lower Carboniferous shark *Tristychius arcuatus* (Agassiz, 1837). *Earth and Environmental Science Transactions of the Royal Society of Edinburgh*, 108, 19–35.

Coates, M. I., Gess, R. W., Finarelli, J. A., Criswell, K. E. & Tietjen, K. 2017. A symmoriiform chondrichthyan braincase and the origin of chimaeroid fishes. *Nature*, 541, 208–211.

Coates, M. I., Finarelli, J. A., Sansom, I. J., Andreev, P. S., Criswell, K. E., Tietjen, K., Rivers, M. L. & La Riviere, P. J. 2018. An early chondrichthyan and the evolutionary assembly of a shark body plan. *Proceedings of the Royal Society B: Biological Sciences*, 285, 1–10.

Colorado Plateau Geosystems, Inc. 2020. DeepTimeMaps™. https://deeptimemaps.com/

Compagno, L. J. V. 1990. Alternative life-history styles of cartilaginous fishes in time and space. *Environmental Biology of Fishes*, 28, 33–75.

Cope, E. D. 1884. On the Structure of the Skull in the Elasmobranch Genus *Didymodus*. *Proceedings of the American Philosophical Society*, 21, 572–590.

Cope, E. D. 1888. Systematic catalogue of the species of Vertebrata found in the beds of the Permian epoch in North America with notes and descriptions. *Transactions of the American Philosophical Society*, 26, 285–297.

Coplen, T. B. 2001. Atomic Weights of the Elements 1999. *Journal of Physical and Chemical Reference Data*, 30, 1.

Coplen, T. B., Böhlke, J. K., De Bievre, P., Ding, T., Holden, N. E., Hopple, J. A., Krouse, H. R., Lamberty, A., Peiser, H. S., Revesz, K., Rieder, S. E., Rosman, K. J. R., Roth, E., Taylor, P. D. P., Vocke, R. D. & Xiao, Y. K. 2002. Isotope-abundance variations of selected elements (IUPAC Technical Report). *Pure and applied chemistry*, 74, 1987–2017.

Craig, H. 1957. Isotopic standards for carbon and oxygen and correction factors for massspectrometric analysis of carbon dioxide. *Geochimica et Cosmochimica Acta*, 12, 133–149.

Craig, H. 1961. Isotopic variations in meteoric waters. *Science*, 133, 1702–1703.

Criss, R. E. 1999. *Principles of Stable Isotope Distribution*. Oxford University Press, Oxford, 265 pp.

Crowell, J. C. 1978. Gondwanan glaciation, cyclothems, continental positioning, and climate change. *American Journal of Science*, 278, 1345–1372.

Crowson, R. A., Showers, W. J., Wright, E. K. & Hoering, T. C. 1991. Preparation of Phosphate Samples for Oxygen Isotope Analysis. *Analytical chemistry*, 63, 2397–2400.

Curtis, J. H. & Hodell, D. A. 1996. Climate variability on the Yucatan Peninsula (Mexico) during the past 3500 years, and implications for Maya cultural evolution. *Quaternary Research*, 46, 37–47.

d'Angela, D. & Longinelli, A. 1990. Oxygen isotopes in living mammal's bone phosphate: further results. *Chemical Geology: Isotope Geoscience section*, 86, 75–82.

Dansgaard, W. 1964. Stable isotopes in precipitation. *Tellus*, 16, 436–468.

Daux, V., Lécuyer, C., Héran, M.-A., Amiot, R., Simon, L., Fourel, F., Martineau, F., Lynnerup, N., Reychler, H. & Escarguel, G. 2008. Oxygen isotope fractionation between human phosphate and water revisited. *Journal of human evolution*, 55, 1138–1147.

Davis, J. W. 1880. On the Genus *Pleuracanthus*, Agass., including the Genera *Orthacanthus*, Agass. and Goldf., *Diplodus* Agass., and *Xenacanthus*, Beyr. *Quaterly Journal of the Geological Society*, 36, 321–336.

Davis, J. W. 1881. On *Anodontacanthus*, a new genus of fossil fishes from the Coal-Measures; with descriptions of three new species. *Quarterly Journal of the Geological Society of London*, 37, 427–429.

Davis, J. W. 1892. *On the Fossil Fish Remains of the Coal Measures of the British Islands. Part I - Pleuracanthidae*. Royal Dublin Society, London, 703–782 pp.

Davis, S. P. 2002. *Comparative Anatomy and Relationships of the Acanthodian Fishes*. Unpublished PhD thesis, University of London, 318 pp.

Davis, S. P., Finarelli, J. A. & Coates, M. I. 2012. *Acanthodes* and shark-like conditions in the last common ancestor of modern gnathostomes. *Nature*, 486, 247–250.

Dawson, T. E. & Ehleringer, J. R. 1993. Isotopic enrichment of water in the "woody" tissues of plants: implications for plant water source, water uptake, and other studies which use the stable isotopic composition of cellulose. *Geochimica et Cosmochimica Acta*, 57, 3487-3492.

de F. L. Viana, S. E. T., Lisher, M. W. & de Carvalho, M. R. 2018. Two new species of short-snouted dogfish sharks of the genus *Squalus* Linnaeus, 1758, from southern Africa (Chondrichthyes: Squaliformes: Squalidae). *Marine Biodiversity,* 48, 1787–1814.

de Launay, L. D. 1888. Étude sur le terrain permien de l'Allier. *Bulletin de la Société Géologique de France*, 3, 298–337.

Debriette, P. 1992. Le bassin de Bourbon-l'Archambault et le sillon houillier (Allier, France). Présentation et itinéraire géologique. *Bulletin trimestriel de la Société d'Histoire Naturelle et des Amis du Muséum d'Autun*, 144, 13–34.

Delafond, F. 1889. *Bassin Houiller et Permien d'Autun et d'Epinac: Stratigraphie. Étude de Gîtes Minéraux de La France*. Maison Quantin, 112 pp.

Denison, R. H. 1979. *Handbook of Paleoichthyology - Chondrichthyes V - Acanthodii*. Schultze, H.-P. & Oskar, K. Gustav Fischer Verlag, Stuttgart, 62 pp.

Diana, J. S. 1980. Diel Activity Pattern and Swimming Speeds of Northern Pike (*Esox lucius*) in Lac Ste. Anne, Alberta. *Canadian Journal of Fisheries and Aquatic Sciences*, 37, 1454–1458.

Dick, J. R. F. 1981. *Diplodoselache woodi* gen. et sp. nov., an early Carboniferous shark from the Midland Valley of Scotland. *Transactions of the Royal Society of Edinburgh: Earth Sciences*, 72, 99–113.

DiMichele, W. A. & Phillips, T. L. 1996. Climate change, plant extinction and vegetational recovery during the Middle-Late Pennsylvanian transition: the case of tropical case-forming environments in North America. *Geological Society, London, Special Publications*, 102, 201–221.

Donelan, C. & Johnson, G. D. 1997. *Orthacanthus platypternus* (Chondrichthyes: Xenacanthida) occipital spines from the Lower Permian Craddock Bonebed, Baylor County, Texas. *Journal of Vertebrate Paleontology*, 17, 43A.

Ducassou, C., Bourquin, S., Pellenard, P., Beccaletto, L., Mercuzot, M., Rossignol, C., Poujol, M., Hallot, E., Pierson-Wickmann, A.-C. & Gand, G. 2018. *Caractérisation Pétro-*

Géochimique et Datation U/Pb Du Volcanisme Contemporain Des Bassins d'âge Fini-Carbonifère à Permien Du Nord Du Massif Central. 26ème Réunion des Sciences de la Terre, Lille.

Duffin, C. J. & Ginter, M. 2006. Comments on the Selachian genus *Cladodus* Agassiz, 1843. *Journal of Vertebrate Paleontology*, 26, 253–266.

Eastman, C. R. 1897. *Tamiobatis vetustus*; a new form of fossil skate. *American Journal of Science*, s4-4, 85–90.

Egerton, P. M. G. 1845. Description of *Hybodus* found by Mr. Boscawen Ibbetson in the Isle of Wight. Quart. *Journal of the Geological Society, London*, 1, 197–199.

Elsass Damon, F. 1977. *Les «schistes Bitumineux» Du Bassin d'Autun: Pétrographie, Minéralogie, Cristallochimie, Pyrolise*. Unpublished Ph. D. thesis, Université Pierre et Marie Curie, 93 pp.

Falcon-Lang, H. J., Benton, M. J., Braddy, S. J. & Davies, S. J. 2006. The Pennsylvanian tropical biome reconstructed from the Joggins Formation of Canada. *Journal of the Geological Society of London*, 163, 561–576.

Falconnet, J. 2014. An evaluation of French amniote diversity through the Pennsylvanian-Cisuralian boundary. *Annales de Paléontologie*, 100, 119–130.

Falconnet, J. 2015. The sphenacodontid synapsid *Neosaurus cynodus*, and related material, from the Permo-Carboniferous of France. *Acta Palaeontologica Polonica*, 60, 169–182.

Faure, M., Mézème, E. B., Duguet, M., Cartier, C. & Talbot, J. Y. 2005. Paleozoic tectonic evolution of medio-Europa from the example of the French Massif Central and Massif Armoricain. *Journal of the virtual Explorer*, 19, 1–25.

Fielding, C. R., Frank, T. D., Birgenheier, L. P., Rygel, M. C., Jones, A. T. & Roberts, J. 2008. Stratigraphic imprint of the Late Palaeozoic Ice Age in eastern Australia: a record of alternating glacial and nonglacial climate regime. *Journal of the Geological Society*, 165, 129–140.

Finarelli, J. A. & Coates, M. I. 2014. *Chondrenchelys problematica* (Traquair, 1888) redescribed: a Lower Carboniferous, eel-like holocephalan from Scotland. *Earth and Environmental Science Transactions of the Royal Society of Edinburgh*, 105, 35–59.

Fischer, J. & Kogan, I. 2008. Elasmobranch egg capsules *Palaeoxyris*, *Fayolia* and *Vetacapsula* as subject of palaeontological research – an annotated bibliography. *Freiberger Forschungshefte*, C528, 75–91.

Fischer, J., Voigt, Sebastian, Schneider, J. W., Buchwitz, M. & Voigt, Silke. 2011. A selachian freshwater fauna from the Triassic of Kyrgyzstan and its implication for Mesozoic shark nurseries. *Journal of Vertebrate Paleontology*, 31, 937–953.

Fischer, J., Voigt, S., Franz, M., Schneider, J. W., Joachimski, M. M., Tichomirowa, M., Götze, J. & Furrer, H. 2012. Palaeoenvironments of the late Triassic Rhaetian Sea: Implications from oxygen and strontium isotopes of hybodont shark teeth. *Palaeogeography, Palaeoclimatology, Palaeoecology*, 353–355, 60–72.

Fischer, J., Schneider, J. W., Voigt, S., Joachimski, M. M., Tichomirowa, M., Tütken, T., Götze, J. & Berner, U. 2013. Oxygen and strontium isotopes from fossil shark teeth: Environmental and ecological implications for Late Palaeozoic European basin. *Chemical Geology*, 342, 44–62.

Fischer, J., Licht, M., Kriwet, J., Schneider, J. W., Bushwitz, M. & Bartsch, M. 2014a. Egg capsule morphology provides new information about the interrelationships of chondrichthyan fishes. *Journal of Systematic Palaeontology*, 12, 389–399.

Fischer, J., Schneider, J. W., Hodnett, J.-P. M., Elliott, D. K., Johnson, G. D., Voigt, S., Joachimski, M. M., Tichomirowa, M. & Götze, J. 2014b. Stable and radiogenic isotope analyses on shark teeth from the Early to the Middle Permian (Sakmarian–Roadian) of the southwestern USA. *Historical Biology*, 26, 710–727.

Foley, J. D., Van, F. D., Van Dam, A., Feiner, S. K., Hughes, J. F. & Hughes, J. 1996. *Computer Graphics: Principles and Practice*. Addison-Wesley Professional, Boston, 1264 pp.

Forel, F. A. 1901. *Handbuch Der Seenkunde. Allgemeine Limnologie*. Verlag Von J. Engelhorn, Stuttgart, 249 pp.

Foster, G. L., Royer, D. L. & Lunt, D. J. 2017. Future climate forcing potentially without precedent in the last 420 million years. *Nature communications*, 8, 1–8.

Fourel, F., Martineau, F., Lécuyer, C., Kupka, H. J., Lange, L., Ojeimi, C. & Seed, M. 2011. $^{18}O/^{16}O$ ratio measurements of inorganic and organic materials by elemental analysis–pyrolysis–isotope ratio mass spectrometry continuous-flow technique. *Rapid Communications in Mass Spectrometry*, 25, 2691–2696.

Fourel, F., Martineau, F., Seris, M. & Lécuyer, C. 2014. Measurement of $^{34}S/^{32}S$ Ratios of NBS 120c and BCR 32 Phosphorites Using Purge and Trap EA-IRMS Technology. *Geostandards and Geoanalytical Research*, 39, 47–53.

Fourel, F., Lécuyer, C. & Balter, V. 2015. New frontiers for sulfur isotopic analyses. *Procedia Earth and Planetary Science*, 13, 232–239.

Fourel, F., Martineau, F., Tóth, E. E., Görög, A., Escarguel, G. & Lécuyer, C. 2016. Carbon and oxygen isotope variability among foraminifera and ostracod carbonated shells. *Annales Universitatis Mariae Curie-Sklodowska, sectio AAA–Physica*, 70, 133.

Fouts, W. R. & Nelson, D. R. 1999. Prey Capture by the Pacific Angel Shark, *Squatina californica*: Visually Mediated Strikes and Ambush-Site Characteristics. *Copeia*, 2, 304–312.

Frakes, L. A., Francis, J. E. & Syktus, I. 1992. *Climate Modes of the Phanerozoic*. Cambridge University Pres, Cambridge, 286 pp.

Francillon-Vieillot, H., de Buffrénil, V., Castanet, J., Géraudie, J., Meunier, F. L., Sire, J.-Y., Zylberberg, L. & de Ricqlès, A. 2009. Microstructure and mineralization of vertebrate skeletal tissues. *In*: *Skeletal Biomineralization: Patterns, Processes and Evolutionary Trends*. Van Nostrand Reinhold, New York, 471–530.

Franke, W. 2000. The mid-European segment of the Variscides: tectonostratigraphic units, terrane boundaries and plate tectonic evolution. *Geological Society, London, Special Publications*, 179, 35–61.

Franke, W., Cocks, L. R. M. & Torsvik, T. H. 2017. The palaeozoic variscan oceans revisited. *Gondwana research*, 48, 257–284.

Frey, L., Coates, M., Ginter, M., Hairapetian, V., Rücklin, M., Jerjen, I. & Klug, C. 2019. The early elasmobranch *Phoebodus*: phylogenetic relationships, ecomorphology and a new time-scale for shark evolution. *Proceedings of the Royal Society B: Biological Sciences*, 286, 1–10.

Frey, L., Coates, M. I., Tietjen, K., Rücklin, M. & Klug, C. 2020. A symmoriiform from the Late Devonian of Morocco demonstrates a derived jaw function in ancient chondrichthyans. *Communications biology*, 3, 1–10.

Fricke, H. C. & O'Neil, J. R. 1999. The correlation between $^{18}O/^{16}O$ ratios of meteoric water and surface temperature: its use in investigating terrestrial climate change over geologic time. *Earth and Planetary Science Letters*, 170, 181–196.

Fricke, H. C., Clyde, W. C., O'Neil, J. R. & Gingerich, P. D. 1998. Evidence for rapid climate change in North America during the latest Paleocene thermal maximum: oxygen isotope compositions of biogenic phosphate from the Bighorn Basin (Wyoming). *Earth and Planetary Science Letters*, 160, 193–208.

Fritsch, A. 1879. *Fauna Der Gaskohle Und Der Kalksteine Der Permoformation Böhmens*. Selbstverlag Fr. Rivnac, Prague, 92 pp.

Fritsch, A. 1889. *Fauna Der Geskohle Und Der Kalksteine Der Permformation Böhmens. 2. Stegocephali (Schluss)-Dipnoi. Selachii (Anfang)*. Selbstverlag Fr. Rivnac, Prague, 114 pp.

Fritsch, A. 1890. *Fauna Der Gaskohle Und Der Kalksteine Der Permformation Böhmens. Vol. 3. Heft 1. Selachii (*Pleuraanthus*,* Xenacanthus*)*. Selbstverlag Fr. Rivnac, Prague, 132 pp.

Fry, B. & Sherr, E. B. 1989. $\delta^{13}C$ Measurements as Indicators of Carbon Flow in Marine and Freshwater Ecosystems. *In*: *Stable Isotopes in Ecological Research. Ecological Studies*. Springer, New York, 196–229.

Fry, B. & Wainright, S. C. 1991. Diatom sources of ^{13}C-rich carbon in marine food webs. *Marine Ecology Progress Series*, 149–157.

Gaida, I. H. 1997. Population Structure of the Pacific Angel Shark, *Squatina californica* (Squatiniformes: Squatinidae), around the California Channel Islands. *Copeia*, 4, 738–744.

Gand, G., Garric, J. & Lapeyrie, J. 1997a. Biocénoses à Tripsidés (Crustacea, Branchiopoda) du Permien du bassin de Lodève (France). *Geobios*, 30, 673–700.

Gand, G., Lapeyrie, J., Garric, J., Nel, A., Schneider, J. W. & Walter, H. 1997b. Découverte d'arthropodes et de bivalves inédits dans le Permien continental (Lodévois, France). *Comptes Rendus de l'Académie des Sciences de Paris*, 325, 891–898.

Gand, G., Châteauneuf, J.-J., Durand, M., Chabard, D. & Passaqui, J.-P. 2007. *Early Permian Continental Environnements in the Autun Basin*. Association de Sédimentologistes française, Autun, 35 pp.

Gand, G., Steyer, J.-S. & Chabard, D. 2011. Reprise de fouilles paléontologiques dans un gîte bourgignon célèbre : les 'schistes bitumineux' de l'Autunien de Muse (Bassin d'Autun) Bilan 2010 et perspectives. *Revue Scientifique Bourgogne-Nature*, 12, 10–29.

Gand, G., Steyer, J. S., Pellenard, P., Béthoux, O., Odin, G., Rouchon, V., Van Waveren, I., de Ploeg, G. & Chabard, D. 2015. Le stratotype autunien (Permien) du bassin d'Autun: résultats préliminaires des travaux réalisés en 2014 sur les niveaux de la couche de Muse (Saône-et-Loire, France). *Bulletin de la Société d'Histoire Naturelle et des Amis du Musée d'Autun*, 207, 12–31.

Gand, G., Pellenard, P., Galtier, J., Broutin, J. & Steyer, J.-S. 2017. Le stratotype autunien du bassin d'Autun (Bourgogne-France) : évolution de la stratigraphie et des âges. *Bulletin de la Société d'Histoire Naturelle et des Amis du Musée d'Autun*, 211, 19–36.

Gaudry, A. 1867. Mémoire sur le reptile découvert par M. Frossard à Muse (Saône-et-Loire). *Nouvelles Archives du Muséum d'Histoire Naturelle*, 3, 21–40.

Gaudry, A. 1883. *Les Enchaînements Du Monde Animal Dans Les Temps Géologiques. Fossiles Primaires*. Librairie F. Savy, Paris, 317 pp.

Gaudry, A. 1886. Sur un nouveau genre de reptile trouvé dans le terrain permien. *Bulletin de la Société Géologique de France*, 14, 430–433.

Giebel, C. G. 1848. *Gaea Excursoria Germanica: Deutschlands Geologie, Geognosie Und Paläontologie Als Unentbehrlicher Leitfaden Auf Excursionen Und Beim Selbststudium*. Brockhaus, Leipzig, 467 pp.

Ginter, M. 2004. Devonian sharks and the origin of Xenacanthiformes. *In*: *Recent Advances in the Origin and Early Radiation of Vertebrates*. Verlag Dr. Friedrich Pfeil, Munich, 473–468.

Ginter, M. & Maisey, J. G. 2007. The braincase and jaws of *Cladodus* from the Lower Carboniferous of Scotland. *Palaeontology*, 50, 305–322.

Ginter, M., Hampe, O. & Duffin, C. J. 2010. *Handbook of Paleoichthylology - Volume 3D-Chondrichtyes - Paleozoic Elasmobranchii: Teeth*. Schultze, H.-P. & Kuhn, O. Verlag Dr. Friedrich Pfeil, Munich, 168 pp.

Goddéris, Y., Donnadieu, Y., Carretier, S., Aretz, M., Dera, G., Macouin, M. & Regard, V. 2017. Onset and ending of the late Palaeozoic ice age triggered by tectonically paced rock weathering. *Nature Geoscience*, 10, 382–386.

Goedert, J. 2017. *Écologie Des Premiers Tétrapodes Dévoilée Par La Composition Isotopique Du Soufre ($^{34}S/^{32}S$) de Leurs Squelettes*. Unpublished Ph. D. thesis, Université Claude Bernard Lyon 1, 239 pp.

Goedert, J., Fourel, F., Amiot, R., Simon, L. & Lécuyer, C. 2016. High-precision $^{34}S/^{32}S$ measurements in vertebrate bioapatites using purge-and-trap elemental analyser/isotope ratio mass spectrometry technology. *Rapid Communications in Mass Spectrometry*, 30, 2002–2008.

Goedert, J., Lécuyer, C., Amiot, R., Arnaud-Godet, F., Wang, X., Cui, L., Cuny, G., Douay, G., Fourel, F., Panczer, G., Simon, L., Steyer, J.-S. & Zhu, M. 2018. Euryhaline ecology of early tetrapods revealed by stable isotopes. *Nature*, 558, 68–72.

Goedert, J., Amiot, R., Berthet, D., Fourel, F., Simon, L. & Lécuyer, C. 2020. Combined oxygen and sulphur isotope analysis—a new tool to unravel vertebrate (paleo)-ecology. *The Science of Nature*, 107, 1–9.

Gonfiantini, R., Stichler, W. & Rozanski, K. 1995. Standards and intercomparison materials distributed by the International Atomic Energy Agency for stable isotope measurements. *Intercomparison materials for stable isotopes of light elements*, 825, 13–29.

Goujet, D. 1975. *Dicksonosteus*, un nouvel arthrodire du Dévonien du Spitsberg remarques sur le squelette visceral des Dolichothoraci. *Colloques Internationaux du Centre National de la Recherche Scientifique*, 218, 81–99.

Goujet, D. 1984. *Les Poissons Placodermes Du Spitsberg*. Muséum national d'Histoire naturelle, Paris, Paris, 316 pp.

Gray, J. 1988. Evolution of the freshwater ecosystem: the fossil record. *Palaeogeography, Palaeoclimatology, Palaeoecology*, 62, 1–214.

Grey, M., Pufahl, P. K. & Azziz, A. A. 2011. Using multiple environmental proxies to determine degree of marine influence and paleogeographic position of the Joggins Fossil Cliffs, UNESCO World Heritage Site. *PALAIOS*, 26, 263–265.

Griffith, E., Pidgeon, E. & Gray, G. 1832. The class Insecta arranged by the Baron Cuvier with supplementary additions to each order. *In*: *The Animal Kingdom Arranged in Conformity with Its Organization, by the Baron Cuvier, Member of the Institute of France, &c. &c. &c. with Supplementary Additions to Each Order*. Whittaker, Treacher, and Co, London, 1–793.

Gross, W. 1937. Das Kopfskelett von *Cladodus wildungensis* Jaekel. 1. Teil. *Endocranium* und *Palatoquadratum*. *Senckenbergiana*, 19, 80–107.

Gross, W. 1971. Downtonische und dittonische Acanthodier-Reste des Ostseegebietes. *Palaeontographica A*, 136, 1–82.

Guillot, L. 1958. Compte-rendu de la réunion du 26 juin 1958. *Revue Scientifique du Bourbonnais et du Centre de la France*, 58, 53–54.

Halas, S. & Szaran, J. 2001. Improved thermal decomposition of sulfates to SO_2 and mass spectrometric determination of $\delta^{34}S$ of IAEA SO-5, IAEA SO-6 and NBS-127 sulfate standards. *Rapid Communications in Mass Spectrometry*, 15, 1618–1620.

Hammer, Ø., Harper, D. A. & Ryan, P. D. 2001. PAST: Paleontological statistics software package for education and data analysis. *Palaeontologia electronica*, 4, 9.

Hampe, O. 1988a. Über die Bezahnung des *Orthacanthus* (Chondrichthyes: Xenacanthida; Oberkarbon - Unterperm). *Paläontologische Zeitschrift*, 62, 285–296.

Hampe, O. 1988b. Über die Bezahnung des *Xenacanthus* (Chondrichthyes: Xenacanthida; Unterperm, SW-Deutschland). *Neues Jahrbuch für Geologie und Paläontologie-Monatshefte*, 1988, 743–756.

Hampe, O. 1989. Revision der *Triodus*-Arten (Chondrichthyes: Xenacanthida) aus dem saarpf~ilzischen Rotliegenden (Oberkarbon - Perm, SW-Deutschland) aufgrund ihrer Bezahnung. *Paläontologische Zeitschrift*, 63, 79–101.

Hampe, O. 1991. Histologische Untersuchungen an fossilen Zähnen der Haifisch-Ordnung Xenacanthida (Chondrichthyes: Elasmobranchii) mit Hilfe der Fluoreszenzmikroskopie. *Leica Mitteilungen für Wissenschaft und Technik*, 10, 17–27.

Hampe, O. 1993. Variation of xenacanthid teeth in the Permo-Carboniferous deposits of the Saar-Nahe Basin (SW-Germany). *In*: *New Research on Permo-Carboniferous Faunas*. POLLICHIA-Buch, 37–51.

Hampe, O. 1994. Neue Erkenntnisse zur permokarbonischen Xenacanthiden-Fauna (Chondrichthyes: Elasmobranchii) und deren Verbreitung im südwestdeutschen Saar-Nahe-Becken. *Neues Jahrbuch für Geologie und Paläontologie Abhandlungen*, 192, 53–87.

Hampe, O. 1995. *Plicatodus jordani* ng, n. sp., a new xenacanthid shark from the Lower Permian of Europe (Saar-Nahe Basin, Germany). *Bulletin du Muséum national*

d'Histoire naturelle, 4ème série–section C–Sciences de la Terre, Paléontologie, Géologie, Minéralogie, 17, 209–226.

Hampe, O. 1997a. Dental growth anomalies and morphological changes in teeth of the Xenacanthida (Lower Permian; SaarNahe basin, SW-Germany). *Modern Geology*, 21, 121–135.

Hampe, O. 1997b. Zur funktionellen Deutung des Dorsalstachels und der Placoidschuppen der Xenacanthida (Chondrichthyes: Elasmobranchii; Unterperm). *Neues Jahrbuch für Geologie und Paläontologie. Abhandlungen*, 206, 29–51.

Hampe, O. 2003. Revision of the Xenacanthida (Chondrichthyes: Elasmobranchii) from the Carboniferous of the British Isles. *Transactions of the Royal Society of Edinburgh: Earth Sciences*, 93, 191–237.

Hampe, O. & Heidtke, U. H. J. 1997. *Hagenoselache sippeli* n. gen. n. sp., ein früher xenacanthider Elasmobranchier aus dem Oberkarbon (Namurium 8) von Hagen-Vorhalle (NW-Sauerland/Deutschland). *Geologie und Paläontologie in Westfalen*, 47, 5–42.

Hampe, O. & Ivanov, A. 2007a. Bransonelliformes — a new order of the Xenacanthimorpha (Chondrichthyes, Elasmobranchii). *Fossil Record*, 10, 190–194.

Hampe, O. & Ivanov, A. 2007b. First xenacanthid shark from the Pennsylvanian (Moscovian) of the Northern Caucasus (Russia). *Fossil Record*, 10, 179–189.

Hampe, O., Johnson, G. D. & Turner, S. 2006. *Dicentrodus* (Chondrichthyes: Xenacanthida) from the Early Carboniferous (Visean: upper St Louis Formation) of Iowa, USA. *Geological Magazine*, 143, 545–549.

Hare, P. E. 1980. Organic geochemistry of bone and its relation to the survival of bone in the natural environment. *In*: *Fossils in the Making. Vertebrate Taphonomy and Paleoecology*. University Chicago Press, Chicago, 208-219.

Harper, D. G. & Blake, R. W. 1990. Fast-start performance of rainbow trout *Salmo gairdneri* and northern pike *Esox lucius*. *Journal of Experimental Biology*, 150, 321–342.

Hedges, R. E. 2002. Bone diagenesis: an overview of processes. *Archaeometry*, 44, 319–328.

Heidtke, U. H. J. 1982. Der Xenacantiüde *Orthacanthus senckenbergianus* aus dem pfälzischen Rodiegenden (Unter-Perm). *Mitteilungen der POLLICHIA*, 70, 65–86.

Heidtke, U. H. J. 1998. Revision der Gattung *Orthacanthus* Agassiz 1843 (Chondrichthyes: Xenacanthida). *Paläontologische Zeitschrift*, 72, 135–147.

Heidtke, U. H. J. 1999. *Orthacanthus* (*Lebachacanthus*) *senckenbergianus* Fritsch 1889 (Xenacanthida: Chondrichthyes): Revision, Organisation und Phylogenie. *Freiberger Forschungshefte*, C481, 63–106.

Heidtke, U. H. J. 2003. Neue Rekonstruktionen xenacanthider Haie aus dem Permokarbon des Saar-Nahe-Beckens (SW-Deutschland). *Mitteilungen der POLLICHIA*, 90, 19–28.

Heidtke, U. H. J. 2007. Neue Erkenntnisse über *Lebachacanthus* (Chondrichthyes: Xenacanthida) aus dem Unteren Rotliegend des südwestdeutschen Saar-Nahe-Beckens. *Mitteilungen der POLLICHIA*, 93, 7–14.

Heidtke, U. H. J. & Dürkheim, B. 1996. *Acanthodes bourbonensis* n. sp., ein neuer Acanthodier (Acanthodii:Pisces) aus dem Autunium (Unterperm) von Bourbon-l'Archambault (Allier, Frankreich). *Paläontologische Zeitschrift*, 70, 497–504.

Heidtke, U. H. J. & Krätschmer, K. 2001. *Gladbachus adentatus* nov. gen. et sp., ein primitiver Hai aus dem Oberen Givetium (Oberes Mitteldevon) der Bergisch Gladbach-Paffrath-Mulde (Rheinisches Schiefergebirge). *Mainzer Geowissenschaftliche Mitteilungen*, 30, 105–122.

Heidtke, U. H. J. & Schwind, C. 2004. Über die Organisation des Skelettes der Gattung *Xenacanthus* (Elasmobranchii: Xenacanthida) aus dem Unterperm de südwestdeutschen Saar-Nahe-Beckens. *Neues Jahrbuch für Geologie und Paläontologie Abhandlungen*, 231, 85–117.

Heidtke, U. H. J., Schwind, C. & Krätschmer, K. 2004. Über die Organisation des Skelettes und die verwandschaftlichen Beziehunger der Gattung *Triodus* JORDAN 1849 (Elasmobranchii: Xenacanthida). *Mainzer geowissenschaftliche Mitteilungen*, 32, 9–54.

Helfman, G. S., Collette, B. B. & Facey, D. E. 1997. *The Diversity of Fishes*. Blackwell Science, Malden MA, 528 pp.

Hemminga, M. A. & Mateo, M. A. 1996. Stable carbon isotopes in seagrasses: variability in ratios and use in ecological studies. *Marine Ecology Progress Series*, 140, 285–298.

Heyler & Poplin, C. 1990. Les Vertébrés autuniens de Buxières-lesMines (Allier, France). *Bulletin du Muséum National d'Histoire Naturelle, 4e série, Section C*, 12, 39–225.

Heyler, D. 1969. *Vertébrés de l'Autunien de France*. Centre National de la Recherche Scientifique. Paris, Cahiers de Paléontologie, 259 pp.

Heyler, D. 1984. Faune fossile du Permien de l'Allier. *Revue scientifique du Bourbonnais*, 84, 103–122.

Heyler, D. 1987. Vertébrés des bassins stéphaniens et autuniens du Massif Central français; paléobiogéographie et paléoenvironnements. *Annales de la Société Géologique du Nord*, 123–130.

Heyler, D. 2000. Les actinoptérygiens stéphaniens et autuniens du Massif central (France) dans les collections du MNHN (Paris) et du Muséum d'Autun: compléments, mises au point, bilan. *Bulletin de la Société d'Histoire Naturelle et des Amis du Musée d'Autun*, 169, 7–44.

Heyler, D. & Debriette, P. 1986. Sur les xénacanthiformes (poissons, élasmobranches) à la lumière de découvertes récentes ans le permo-carbonifère de France. *In*: III° congrès national des sociétés savantes. Minitère de l'Éducation Nationale Comité des Travaux Historiques et Scientifiques ou CTHS, Poitiers, 89–109.

Heyler, D. & Pacaud, G. 1978. Nouveautés paléontologiques et géologiques dans l'Autunien du Bassin d'Autun. *Bulletin de la Société d'Histoire Naturelle et des Amis du Musée d'Autun*, 85, 12–23.

Heyler, D. & Poplin, C. 1982. Sur quelques neurocrânes d'Élasmobranches du Permien du bassin d'Autun (Saône-et-Loire, France). *Annales de Paléontologie*, 68, 15–32.

Heyler, D. & Poplin, C. 1989. Systematics and relationships among the Xenacanthiformes (Pisces, Chondrichthyes) in the light of Carboniferous and Permian French material. *Acta Musei Reginaehradecensis S. A. Scientiae Naturales*, XXII, 69–78.

Hodnett, J.-P. M. & Elliott, D. K. 2018. Carboniferous chondrichthyan assemblages from the Surprise Canyon and Watahomigi formations (latest Mississippian–Early Pennsylvanian) of the western Grand Canyon, Northern Arizona. *Journal of Paleontology*, 92, 1–33.

Hodnett, J.-P. M., Elliott, D. K., Olson, T. J. & Wittke, J. H. 2012. Ctenacanthiform sharks from the Permian Kaibab Formation, northern Arizona. *Historical Biology*, 1, 1–15.

Hodnett, J.-P. M., Grogan, E. D., Lund, R., Lucas, S. G., Suazo, T., Elliott, D. K. & Pruitt, J. 2021. Ctenacanthiform sharks from the Late Pennsylvanian (Missourian) Tinajas

Member of the Atrasado Formation, central New Mexico. *New Mexico Museum of Natural History and Science Bulletin*, 84, 391–424.

Hoefs, J. 2009. *Stable Isotope Geochemistry 6th Edition*. Springer, Berlin, 385 pp.

Hota, A. K. 1994. Growth in amphibians. *Gerontology*, 40, 160.

Hut, G. 1987. Stable Isotope Reference Samples for Geochemical and Hydrological Investigations. International Atomic Energy Agency, Vienna.

Hutchinson, E. 1957. *A Treatise on Limnology. I, Geography, Physics and Chemistry*. John Wiley & Sons, New York, 1044 pp.

Huxley, T. H. 1880. On the application of the laws of evolution to the arrangement of the Vertebrata, and more particularly of the Mammalia. *Proceedings of the Scientific Meetings of the Zoological Society of London*, 1880, 649–662.

Hyde, W. T., Crowley, T. J., Tarasov, L. & Peltier, W. R. 1999. The Pangean ice age: Studies with a coupled climate-ice sheet model. *Climate Dynamics*, 15, 619–629.

Iacumin, P. & Longinelli, A. 2002. Relationship between $\delta^{18}O$ values for skeletal apatite from reindeer and foxes and yearly mean $\delta^{18}O$ values of environmental water. *Earth and Planetary Science Letters*, 201, 213–219.

Iacumin, P., Bocherens, H., Mariotti, A. & Longinelli, A. 1996. Oxygen isotope analyses of co-existing carbonate and phosphate in biogenic apatite: a way to monitor diagenetic alteration of bone phosphate? *Earth and Planetary Science Letters*, 142, 1–6.

IAEA. 2020. *Global Network of Isotopes in Precipitation. The GNIP Database. [WWW Document] Https://Nucleus.Iaea.Org/Sites/ReferenceMaterials/Pages/Stable-Isotopes.Aspx*.

Irvine, S. B., Stevens, J. D. & Laurenson, L. J. B. 2006. Comparing external and internal dorsal spine bands to interpret the age and growth of the giant lantern shark, *Etmopterus baxteri* (Squaliformes: Etmopteridae). *Environmental Biology of Fishes*, 77, 253–264.

Isbell, J. L., Lenaker, P. A., Askin, R. A., Miller, M. F. & Babcock, L. E. 2003. Reevaluation of the timing and extent of late Paleozoic glaciation in Gondwana: Role of the Transantarctic Mountains. *Geology*, 31, 977–980.

Isbell, J. L., Cole, D. I., Catuneanu, O., Fielding, C. R. & Frank, T. D. 2008. Carboniferous-Permian glaciation in the main Karoo Basin, South Africa: Stratigraphy, depositional

controls, and glacial dynamics. *Geological Society of America Special Paper*, 441, 71–82.

Isbell, J. L., Henry, L. C., Gulbranson, E. L., Limarino, C. O., Fraiser, M. L., Koch, Z. J., Ciccioli, P. L. & Dineen, A. A. 2012. Glacial paradoxes during the late Paleozoic ice age: Evaluating the equilibrium line altitude as a control on glaciation. *Gondwana Research*, 22, 1–19.

Jaekel, O. 1895. Über die Organisation der Pleuracanthiden. *Sitzungsberichte der Gesellschaft der Naturforschenden Freunde*, 1895, 69–86.

Jaekel, O. 1906. Neue Rekonstruktionen von *Pleuracanthus sessilis* und von *Polyacrodus* (*Hybodus*) *Hauffianus*. *Sitzungsberichte der Gesellschaft der Naturforschenden Freunde*, 1906, 9–155.

Jaekel, O. 1921. Die Stellung der Paläontologie zu einigen Problemen der Biologie und Phylogenie. 2. Schädelprobleme. *Paläontologische Zeitschrift*, 3, 213–239.

Janvier, P. 1996. *Early Vertebrates*. Oxford University Press, Oxford, 406 pp.

Jarvik, E. 1980. *Basic Structure and Evolution of Vertebrates*. Academic Press, London, 576 pp.

Jerve, A. 2016. *Development and Threedimensional Histology of Vertebrate Dermal Fin Spines*. Unpublished Ph. D. thesis, Acta Universitatis Upsaliensis, 53 pp.

Jerve, A., Bremer, O., Sanchez, S. & Ahlberg, P. E. 2017. Morphology and histology of acanthodian fin spines from the late Silurian Ramsåsa E locality, Skåne, Sweden. *Palaeontologia Electronica*, 20.3.56A, 1–19.

Joachimski, M. M., Van Geldern, R., Breisig, S., Buggisch, W. & Day, J. 2004. Oxygen isotope evolution of biogenic calcite and apatite during the Middle and Late Devonian. *International Journal of Earth Sciences*, 93, 542–553.

Joachimski, M. M., von Bitter, P. H. & Buggisch, W. 2006. Constraints on Pennsylvanian glacioeustatic sea-level changes using oxygen isotopes of conodont apatite. *Geology*, 34, 277–280.

Joachimski, M. M., Breisig, S., Buggisch, W., Talent, J. A., Mawson, R., Gereke, M., Morrow, J. R., Day, J. & Weddige, K. 2009. Devonian climate and reef evolution: insights from oxygen isotopes in apatite. *Earth and Planetary Science Letters*, 284, 599–609.

Johnson, B. J., Fogel, M. L. & Miller, G. H. 1998. Stable isotopes in modern ostrich eggshell: a calibration for paleoenvironmental applications in semi-arid regions of southern Africa. *Geochimica et Cosmochimica Acta*, 62, 2451–2461.

Johnson, G. D. 1979. *Early Permian Vertebrates from Texas: Actinopterygii (Schaefferichthys), Chondrichthyes (Including North American Pennsylvanian and Triassic Xenacanthodii), and Acanthodii*. Unpublished Ph. D. thesis, Southern Mathodist University, 76–289 pp.

Johnson, G. D. 1980. Xenacanthodii (Chondrichthyes) from the Tecovas Formation (Late Triassic) of West Texas. *Journal of Paleontology*, 923–932.

Johnson, G. D. 1984. A new species of Xenacanthodii (Chondrichthyes, Elasmobranchii) from the late Pennsylvanian of Nebraska. *Special Publication Carnegie Museum of Natural History*, 9, 178–1986.

Johnson, G. D. 1995. Does *Xenacanthus* (Chondrichthyes: Xenacanthiformes) occur in the Upper Paleozoic of North America?. *Journal of Vertebrate Paleontology*, 15, 38A.

Johnson, G. D. 1996. Vertebrate microfossils from the Lueders Formation, Albany Group, and the faunal transition from the Wichita Group into the Clear Fork Group, Lower Permian of Texas. *Modern Geology*, 20, 371–382.

Johnson, G. D. 1999. Dentitions of Late Palaeozoic *Orthacanthus* species and new species of ?*Xenacanthus* (Chondrichthyes: Xenacanthiformes) from North America. *Acta Geologica Polonica*, 49, 215–266.

Johnson, G. D. 2012. Possible origin of the xenacanth sharks *Orthacanthus texensis* and *Orthacanthus platypternus* in the Lower Permian of Texas, USA. *Historical Biology*, 24, 369–379.

Johnson, G. D. 2018. *Orthacanthus platypternus* (Cope, 1883) (Chondrichthyes: Xenacanthiformes) teeth and other isolated vertebrate remains from a single horizon in the early Permian (Artinskian) Craddock Bonebed, lower Clear Fork Group, Baylor County, Texas, USA. *Acta Palaeontologica Polonica*, 68, 421–436.

Johnson, G. D. & Thayer, D. W. 2009. Early Pennsylvanian xenacanth chondrichthyans from the Swisshelm Mountains, Arizona, USA. *Acta Palaeontologica Polonica*, 54, 649–668.

Johnson, T. & Muller, K. 1978. Migration of pike, *Essox lucius* L., from a coastal stream to the Northern Part of the Bothnian Sea. *Aquilo Serie Zoologica*, 18, 57–61.

Jones, M. T., Jerram, D. A., Svensen, H. H. & Grove, C. 2016. The effects of large igneous provinces on the global carbon and sulphur cycles. *Palaeogeography, Palaeoclimatology, Palaeoecology*, 441, 4–21.

Jordan, H. 1849. *Triodus sessilis*, ein neuer Fisch der Kohlenformation von Lebach. *Neues Jahrbuch für Mineralogie, Geologie und Paläontologie*, 1–843.

Juanes, F., Buckel, J. A. & Scharf, F. S. 2002. 12 Feeding Ecology of Piscivorous Fishes. *In*: *Handbook of Fish Biology and Fisheries: Fish Biology*. Blackwell Publishing, Oxford, 267–283.

Kampschulte, A. & Strauss, H. 2004. The sulfur isotopic evolution of Phanerozoic seawater based on the analysis of structurally substituted sulfate in carbonates. *Chemical Geology*, 204, 255–286.

Kampschulte, A., Bruckschen, P. & Strauss, H. 2001. The sulphur isotopic composition of trace sulphates in Carboniferous brachiopods: implications for coeval seawater, correlation with other geochemical cycles and isotope stratigraphy. *Chemical Geology*, 175, 149–173.

Kaplan, I. R. 1983. Stable isotopes of sulfur, nitrogen and deuterium in recent marine environments. *In*: *Stable Isotopes in Sedimentary Geology*. Society of Economic Paleontologists and Mineralogists Short Course, Dallas, 2.1-2.108.

Karas, P. & Lehtonen, H. 1993. Patterns of Movement and Migration of Pike (.*Esox lucius* L.) in the Baltic Sea. *Nordic journal of freshwater research*, 68, 72–79.

Katsev, S., Crowe, S. A., Mucci, A., Sundby, B., Nomosatryo, S., Haffner, D. G. & Fowlef, D. A. 2010. Mixing and its effects on biogeochemistry in the persistently stratified, deep, tropical Lake Matano, Indonesia. *Limnology and Oceanography*, 55, 763–776.

Katz, M. E., Wright, J. D., Miller, K. G., Cramer, B. S., Fennel, K. & Falkowski, P. G. 2005. Biological overprint of the geological carbon cycle. *Marine Geology*, 217, 323–338.

Kaulfuß, U. 2003. *Lithofazies, Genese Und Stratigraphie Des Permokarbon Im Becken von Bourbon-L`Archambault (Massif Central) – Fallstudie Buxières-Les-Mines*. Unpublished Master thesis, Bergakademie Freiberg Technische Universität, 82 pp.

Kelly, J. F. 2000. Stable isotopes of carbon and nitrogen in the study of avian and mammalian trophic ecology. *Canadian journal of zoology*, 78, 1–27.

Kelts, K. 1988. Environments of deposition of lacustrine petroleum source rocks: an introduction. *Geological Society, London, Special Publications*, 40, 3–26.

Kner, R. 1867. Über *Orthacanthus dechenii* Goldf. oder *Xenacanthus dechenii* Beyr. *Sitzungsberichte der Mathematisch-Naturwissenschaftlichen Classe der Kaiserlichen Akademie der Wissenschaften*, 55, 84–540.

Koch, P. L. 1998. Isotopic reconstruction of past continental environments. *Annual Review of Earth and Planetary Sciences*, 26, 573–613.

Koch, P. L., Tuross, N. & Fogel, M. L. 1997. The Effects of Sample Treatment and Diagenesis on the Isotopic Integrity of Carbonate in Biogenic Hydroxylapatite. *Journal of Archaeological Science*, 24, 417–429.

Koch, P. L., Michener, R. & Lajtha, K. 2007. Isotopic study of the biology of modern and fossil vertebrates. *In*: *Stable Isotopes in Ecology and Environmental Science*. Blackwell Scientific, London, 99–154.

Kohn, M. J. 1996. Predicting animal $\delta^{18}O$: accounting for diet and physiological adaptation. *Geochimica et Cosmochimica Acta*, 60, 4811–4829.

Kohn, M. J. 2010. Carbon isotope compositions of terrestrial C^3 plants as indicators of (paleo) ecology and (paleo) climate. *Proceedings of the National Academy of Sciences*, 107, 19691–19695.

Koken, E. 1889. Über *Pleuracanthus* Ag. oder *Xenacanthus* Beyr. *Sitzungsberichte der Gesellschaft der Naturforschenden Freunde*, 1889, 77–94.

Kolodny, Y. & Luz, B. 1991. The isotopic record of oxygen in phosphates of fossil fish-Devonian to Recent. *Stable isotope geochemistry: A tribute to Samuel Epstein. The Geochemical Society, Special Publication.*, 3, 105–119.

Kolodny, Y., Luz, B. & Navon, O. 1983. Oxygen isotope variations in phosphate of biogenic apatites, I. Fish bone apatite—rechecking the rules of the game. *Earth and Planetary Science Letters*, 64, 398–404.

Korte, C., Kozur, H. W. & Veizer, J. 2005. $\delta^{13}C$ and $\delta^{18}O$ values of Triassic brachiopods and carbonate rocks as proxies for coeval seawater and palaeotemperature. *Palaeogeography, Palaeoclimatology, Palaeoecology*, 226, 287–306.

Krätschmer, K. & Forst, M. H. 2005. Ein Neufund von assoziierten Skelettelementen von *Sphenacanthus* cf. *carbonarius* (Giebel 1848) aus dem Top Oberkarbon (Breitenbach-

Fm., Stefan C) des Saar–Nahe Beckens (SW-Deutschland) mit Anmerkungen zur Paläoökologie der Vertebraten-Lokalitäten von Altenkirchen. *Geowissenschaftliche Beiträge zum Saarpfälzischen Rotliegenden*, 3, 29–37.

Kriwet, J., Witzmann, F., Klug, S. & Heidtke, U. H. J. 2008. First direct evidence of a vertebrate three-level trophic chain in the fossil record. *Proceedings of the Royal Society B: Biological Sciences*, 275, 181–186.

Krouse, H. R. 1980. Ch. 11. Sulphur isotopes in our environment. *In*: *Handbook of Environmental Isotope Geochemistry*. Elsevier, Amsterdam, 435−471.

Krouse, H. R. 1989. Sulfur Isotope Studies of the Pedosphere and Biosphere. *In*: *Stable Isotopes in Ecological Research. Ecological Studies*. Springer, New York, 424–444.

Kumbar, S. M. & Pancharatna, K. 2004. Annual formation of growth marks in a tropical amphibian. *Herpetological Review*, 35, 35–37.

Kurita, N., Ichiyanagi, K., Matsumoto, J., Yamanaka, M. D. & Ohata, T. 2009. The relationship between the isotopic content of precipitation and the precipitation amount in tropical regions. *Journal of Geochemical Exploration*, 102, 113–122.

Kutzbach, J. E. & Street-Perrott, F. A. 1985. Milankovitch forcing of fluctuations in the level of tropical lakes from 18 to 0 kyr BP. *Nature*, 317, 130–134.

Landis, E. N. & Keane, D. T. 2010. X-ray microtomography. *Materials characterization*, 61, 1305–1316.

Lane, J. A. 2010. Morphology of the Braincase in the Cretaceous Hybodont Shark *Tribodus limae* (Chondrichthyes: Elasmobranchii), Based on CT Scanning. *American Museum Novitates*, 3681, 1–70.

Langlois, C., Simon, L. & Lécuyer, C. 2003. Box-modeling of bone and tooth phosphate oxygen isotope compositions as a function of environmental and physiological parameters. *Isotopes in Environmental and Health Studies*, 39, 259–272.

Laurin, M. & Soler-Gijón, R. 2006. The oldest known stegocephalian (Sarcopterygii: Temnospondyli) from Spain. *Journal of Vertebrate Paleontology*, 26, 284–299.

Laurin, M. & Soler-Gijón, R. 2010. Osmotic tolerance and habitat of early stegocephalians: indirect evidence from parsimony, taphonomy, palaeobiogeography, physiology and morphology. *Geological Society, London, Special Publications*, 339, 151–179.

Lebedev, O. A. 1996. Fish assemblages in the Tournaisian-Viséan environments of the East European Platform. *Geological Society, London, Special Publications*, 107, 387–415.

Lécuyer, C., Grandjean, P., O'Neil, J. R., Cappetta, H. & Martineau, F. 1993. Thermal excursions in the ocean at the Cretaceous-Tertiary boundary (northern Morocco): $\delta^{18}O$ record of phosphatic fish debris. *Palaeogeography, Palaeoclimatology, Palaeoecology*, 105, 235–243.

Lécuyer, C., Picard, S., Garcia, J. P., Sheppard, S. M., Grandjean, P. & Dromart, G. 2003a. Thermal evolution of Tethyan surface waters during the Middle-Late Jurassic: Evidence from $\delta^{18}O$ values of marine fish teeth. *Paleoceanography*, 18, 1076.

Lécuyer, C., Bogey, C., Garcia, J. P., Grandjean, P., Barrat, J. A., Floquet, M., Bardet, N. & Pereda-Superbiola, X. 2003b. Stable isotope composition and rare earth element content of vertebrate remains from the Late Cretaceous of northern Spain (Laño): did the environmental record survive? *Palaeogeography, Palaeoclimatology, Palaeoecology*, 193, 457–471.

Lécuyer, C., Fourel, F., Martineau, F., Amiot, R., Bernard, A., Daux, V., Escarguel, G. & Morrison, J. 2007. High-precision determination of $^{18}O/^{16}O$ ratios of silver phosphate by EA-pyrolysis-IRMS continuous flow technique. *Journal of Mass Spectrometry*, 42, 36–41.

Lécuyer, C., Amiot, R., Touzeau, A. & Trotter, J. 2013. Calibration of the phosphate $\delta^{18}O$ thermometer with carbonate–water oxygen isotope fractionation equations. *Chemical Geology*, 347, 217–226.

Lee-Thorp, J. A., Sealy, J. C. & Van Der Merwe, N. J. 1989. Stable carbon isotope ratio differences between bone collagen and bone apatite, and their relationship to diet. *Journal of Archaeological Science*, 16, 585–599.

LeGrande, A. N. & Schmidt, G. A. 2006. Global gridded data set of the oxygen isotopic composition in seawater. *Geophysical research letters*, 33.

Letourneur, J. 1953. Le grand Sillon Houiller du plateau central français. *Bulletin de la Carte Geologique de France*, 238, 1–236.

Levinson, A. A., Luz, B. & Kolodny, Y. 1987. Variations in oxygen isotopic compositions of human teeth and urinary stones. *Applied Geochemistry*, 2–4, 367–371.

Lewis Jr, W. M. 1987. Tropical limnology. *Annual review of ecology and systematics*, 18, 159–184.

Li, W., Ni, B., Jin, D. & Zhang, Q. 1988. Measurement of the absolute abundance of oxygen-17 in VSMOW. *Kexue Tongbao/Chinese Science Bulletin*, 33, 1610–1613.

Lin, G. & Sternberg, L. 1993. Hydrogen isotopic fractionation by plant roots during water uptake in coastal wetland plants. *In*: *Stable Isotopes and Plant Carbon-Water Relations*. Academic Press Inc., San Diego, 497–510.

Linnaeus, C. 1758. *Systema Naturae per Regna Tria Naturae, Secundum Classes, Ordines, Genera, Species, Cum Characteribus, Differentiis, Synonymis, Locis. Ed 10, Tomus 1*. L. Salvii. Stockholm, 823 pp.

Long, J. A. & Young, G. C. 1995. Sharks from the Middle-Late Devonian Aztec Siltstone, southern Victoria Land, Antarctica, and southeastern Australia. *Records-Western Australian Museum*, 17, 287–308.

Longinelli, A. 1984. Oxygen isotopes in mammal bone phosphate: a new tool for paleohydrological and paleoclimatological research? *Geochimica et Cosmochimica Acta*, 48, 385–390.

Longinelli, A. & Nuti, S. 1973. Revised phosphate-water isotopic temperature scale. *Earth and Planetary Science Letters*, 19, 373–376.

Longinelli, A., Iacumin, P., Davanzo, S. & Nikolaev, V. 2003. Modern reindeer and mice: revised phosphate–water isotope equations. *Earth and Planetary Science Letters*, 214, 491–498.

Luccisano, V., Pradel, A., Amiot, R., Gand, G., Steyer, J.-S. & Cuny, G. 2021a. A new *Triodus* shark species (Xenacanthidae, Xenacanthiformes) from the lowermost Permian of France and its paleobiogeographic implications. *Journal of Vertebrate Paleontology*, 41, e1926470.

Luccisano, V., Rambert-Natsuaki, M., Cuny, G., Amiot, R., Pouillon, J.-M. & Pradel, A. 2021b. 3D models related to the publication: Phylogenetic implications of the systematic reassessment of Xenacanthiformes and ‘Ctenacanthiformes’ (Chondrichthyes) neurocrania from the Carboniferous-Permian Autun Basin (France). *MorphoMuseumM*, 7, 155.

Luccisano, V., Rambert-Natsuaki, M., Cuny, G., Amiot, R., Pouillon, J.-M. & Pradel, A. 2021c. Phylogenetic implications of the systematic reassessment of Xenacanthiformes and 'Ctenacanthiformes'(Chondrichthyes) neurocrania from the Carboniferous–Permian Autun Basin (France). *Journal of Systematic Palaeontology*, 19, 1623–1642.

Luccisano, V., Pradel, P., Amiot, R., Pouillon, J.-M., Kindlimann, R., Steyer, J.-S. & Cuny, G. 2022. Systematics, ontogeny and palaeobiogeography of the genus *Orthacanthus* (Diplodoselachidae, Xenacanthiformes) from the lower Permian of France. *Papers in Palaeontology*, 8, e1470.

Lund, R. & Grogan, E. D. 1997. Relationships of the Chimaeriformes and the basal radiation of the Chondrichthyes. *Reviews in Fish Biology and Fisheries*, 7, 65–123.

Luz, B. & Kolodny, Y. 1985. Oxygen isotope variations in phosphate of biogenic apatites, IV. Mammal teeth and bones. *Earth and Planetary Science Letters*, 75, 29–36.

Luz, B., Kolodny, Y. & Horowitz, M. 1984. Fractionation of oxygen isotopes between mammalian bone-phosphate and environmental drinking water. *Geochimica et Cosmochimica Acta*, 48, 1689–1693.

MacLeod, N. A. & Barton, D. R. 1998. Effects of light intensity, water velocity, and species composition on carbon and nitrogen stable isotope ratios in periphyton. *Canadian Journal of Fisheries and Aquatic Sciences*, 55, 1919–1925.

MacNamara, J. & Thode, H. G. 1950. Comparison of the isotopic constitution of terrestrial and meteoritic sulfur. *Physical Review*, 78, 307.

Mader, H. 1986. Schuppen und Zähne von Acanthodiern und Elasmobranchiern aus dem Unter-Devon Spaniens (Pisces). *Göttinger Arbeiten zur Geologie und Paläontologie*, 28, 1–59.

Maisey, J., Miller, R. & Turner, S. 2009. The braincase of the chondrichthyan *Doliodus* from the Lower Devonian Campbellton Formation of New Brunswick, Canada. *Acta Zoologica (Stockholm)*, 90, 109–122.

Maisey, J. G. 1978. Growth and Form of finspines in Hybodont sharks. *Palaeontology*, 21, 657–666.

Maisey, J. G. 1979. Finspine morphogenesis in squalid and heterodontid sharks. *Zoological Journal of the Linnean Society*, 66, 161–183.

Maisey, J. G. 1982. Studies on the Paleozoic selachian genus *Ctenacanthus* Agassiz. No. 2, *Bythiacanthus* St. John and Worthen, *Amelacanthus*, new genus, *Eunemacanthus* St. John and Worthen, *Sphenacanthus* Agassiz, and Wodnika Münster. *American Museum Novitates*, 2722, 1–24.

Maisey, J. G. 1983. Cranial Anatomy of *Hybodus basanus* Egerton from the Lower Cretaceous of England. *American Museum Novitates*, 2758, 1–64.

Maisey, J. G. 1984. Chondrichthyan phylogeny: a look at the evidence. *Journal of Vertebrate Paleontology*, 4, 359–371.

Maisey, J. G. 1985. Cranial Morphology of the Fossil Elasmobranch *Synechodus dubrisiensis*. *American Museum Novitates*, 2804, 1–28.

Maisey, J. G. 1987. Cranial Anatomy of the Lower Jurassic Shark *Hybodus reticulatus* (Chondrichthyes: Elasmobranchii), with Comments on Hybodontid Systematics. *American Museum Novitates*, 2878, 1–39.

Maisey, J. G. 2001. CT-scan reveals new cranial features in Devonian chondrichthyan "*Cladodus*" *wildungensis*. *Journal of Vertebrate Paleontology*, 21, 807–810.

Maisey, J. G. 2005. Braincase of the Upper Devonian shark *Cladodoides wildungensis* (Chondrichthyes, Elasmobranchii), with observations on the braincase in early chondrichthyans. *Bulletin of the American Museum of Natural History*, 288, 1–103.

Maisey, J. G. 2007. The braincase in Paleozoic symmoriiform and cladoselachian sharks. *Bulletin of the American Museum of Natural History*, 307, 1–122.

Maisey, J. G. 2009. The spine-brush complex in symmoriiform sharks (Chondrichthyes; Symmoriiformes), with comments on dorsal fin modularit. *Journal of Vertebrate Paleontology*, 29, 14–24.

Maisey, J. G., Denton, J. S. S., Burrow, C. J. & Pradel, A. 2020. Architectural and ultrastructural features of tessellated calcified cartilage in modern and extinct chondrichthyan fishes. *Journal of Fish Biology*, 1–23.

Manès, W. 1844. *Mémoire Sur Les Bassins Houillers de Saone-et-Loire*. Imprimerie de Vve Dondey-Dupré, Paris, 21 pp.

Manès, W. 1847. *Statistique Minéralogique, Géologique et Minéralurgique Du Département de Saône et Loire*. mprimerie de Dejussieu, Mâcon, 242 pp.

Marshak, S. & Werner, J. 2013. *Essentials of Geology*. W. W. Norton & Compagny, New York, 188 pp.

Marshall, J. D., Brooks, J. R. & Lajtha, K. 2007. Sources of variation in the stable isotopic composition of plants. *Stable isotopes in ecology and environmental science*, 2, 22–60.

Marteau, P. 1983. *Le Bassin Permo Carbonifère d'Autun: Stratigraphie, Sédimentologie et Aspects Structuraux*. Unpublished Ph.D. Thesis, Université de Dijon, 183 pp.

Martin, R. A. 2005. Conservation of freshwater and euryhaline elasmobranchs. *Journal of the Marine Biology Association*, 85, 1049–1073.

Mathis, V. & Brulhet, J. 1990. Les gisements uranifères du bassin permien de Bourbon-l'Archambault (nord du Massif central français). *Chronique de la recherche minière*, 499, 19–30.

Matte, P. 2001. The Variscan collage and orogeny (480–290 Ma) and the tectonic definition of the Armorica microplate: a review. *Terra nova*, 13, 122–128.

McCann, T. 2008. *The Geology of Central Europe, Vol. 1, Precambrian and Palaeozoic*. Geological Society of London, London, 784 pp.

McKinney, C. R., McCrea, J. M., Epstein, S., Allen, H. A. & Urey, H. C. 1950. Improvements in mass spectrometers for the measurement of small differences in isotope abundance ratios. *Review of Scientific Instruments*, 21, 724–730.

Mercuzot, M. 2020. *Reconstitutions Paléoenvironnementales et Paléoclimatiques En Contexte Tardi-Orogénique : Cas Des Bassins Fini Carbonifères à Permiens Du Nord-Est Du Massif Central, France*. Université de Rennes 1, 551 pp.

Mercuzot, M., Bourquin, S., Pellenard, P., Beccaletto, L., Schnyder, J., Baudin, F., Ducassou, C., Garel, S. & Gand, G. 2022. Reconsidering Carboniferous–Permian continental paleoenvironments in eastern equatorial Pangea: facies and sequence stratigraphy investigations in the Autun Basin (France). *International Journal of Earth Sciences*, 111, 1663–1696.

Miller, R. F., Cloutier, R. & Turner, S. 2003. The oldest articulated chondrichthyan from the Early Devonian period. *Nature*, 425, 501–504.

Monaghan, J. M., Scrimgeour, C. M., Stein, W. M., Zhao, F. J. & Evans, E. J. 1999. Sulphur accumulation and redistribution in wheat (*Triticum aestivum*): a study using stable sulphur isotope ratios as a tracer system. *Plant, Cell & Environment,* 22, 831–839.

Montañez, I. P. & Poulsen, C. J. 2013. The Late Paleozoic ice age: an evolving paradigm. *Annual Review of Earth and Planetary Sciences*, 41, 629–656.

Moreau, J.-D. 2017. *Imagerie de Plantes Fossiles Par La Tomographie Synchrotron : Cas de Préservations Exceptionnelles et de Fleurs Du Cénomanien de Charente-Maritime et Du Gard*. Unpublished Ph. D. thesis, Université de Rennes 1, 310 pp.

Morris, A. W. & Riley, J. P. 1966. The bromide/chlorinity and sulphate/chlorinity ratio in sea water. *Deep sea research and oceanographic Abstracts*, 13, 699–705.

Moy-Thomas, J. A. 1936. On the structure and Affinities of the Carboniferous Cochliodont *Helodus simplex*. *Geological Magazine*, 73, 488–503.

Müller, U. K., Smit, J., Stamhuis, E. J. & Videler, J. J. 2001. How the body contributes to the wake in undulatory fish swimming: flow fields of a swimming eel (*Anguilla anguilla*). *Journal of Experimental Biology*, 204, 2751–2762.

Navarro, N., Lécuyer, C., Montuire, S., Langlois, C. & Martineau, F. 2004. Oxygen isotope compositions of phosphate from arvicoline teeth and Quaternary climatic changes, Gigny, French Jura. *Quaternary Research*, 62, 172–182.

Nehlich, O. 2015. The application of sulphur isotope analyses in archaeological research: A review. *Earth-Science Reviews*, 142, 1–17.

Newberry, J. S. 1856. Description of several new genera and species of fossil fishes, from the Carboniferous strata of Ohio. *Proceedings of the Academical Natural Society of Philadelphia*, 8, 96–100.

Newberry, J. S. 1889. *The Paleozoic Fishes of North America*. Government Printing Office, Washigton, 340 pp.

Oduro, H., Van Alstyne, K. L. & Farquhar, J. 2012. Sulfur isotope variability of oceanic DMSP generation and its contributions to marine biogenic sulfur emissions. *Proceedings of the National Academy of Sciences*, 109, 9012–9016.

Oelofsen, B. W. 1986. A fossil shark neurocranium from the Permo-Carboniferous (lowermost Ecca Formation) of South Africa. *In*: *Proceedings of the Second International Conference on Indo-Pacific Fishes*. Ichthyological Society of Japan, Tokyo, 107–124.

Ohkouchi, N., Kawamura, K., Kajiwara, Y., Wada, E., Okada, M., Kanamatsu, T. & Taira, A. 1999. Sulfur isotope records around Livello Bonarelli (northern Apennines, Italy) black shale at the Cenomanian-Turonian boundary. *Geology*, 27, 535–538.

Olson, E. C. 1989. The Arroyo Formation (Leonardian, Lower Permian) and its vertebrate fossils. *Texas Memorial Museum Bulletin*, 33, 1–25.

Osborne, C. P. & Beerling, D. J. 2006. Nature's green revolution: the remarkable evolutionary rise of C_4 plants. *Philosophical Transactions of the Royal Society B: Biological Sciences*, 361, 173–194.

Osmond, C. B., Valaane, N., Haslam, S. M., Uotila, P. & Roksandic, Z. 1981. Comparisons of $\delta^{13}C$ values in leaves of aquatic macrophytes from different habitats in Britain and Finland; some implications for photosynthetic processes in aquatic plants. *Oecologia*, 50, 117–124.

Otero, O., Lécuyer, C., Fourel, F., Martineau, F., Mackaye, H. T., Vignaud, P. & Brunet, M. 2010. Freshwater fish $\delta^{18}O$ indicates a Messinian change of the precipitation regime in Central Africa. *Geology*, 39, 435–438.

Owen, R. 1867. On the dental characters of genera and species, chiefly of fishes, from the Low Main Seam and shales of coal, Northumberland. *Transactions of the OdontologicalSociety of Great Britain*, 5, 92–323.

Pan, Y. & Fleet, M. E. 2002. Compositions of the apatite-group minerals: substitution mechanisms and controlling factors. *Reviews in mineralogy and geochemistry*, 48, 13–49.

Pandian, T. J. & Vivekanandan, E. 1985. Energetics of Feeding and Digestion. *In*: *Fish Energetics*. Springer, Dordrecht, 99–124.

Paquette, Y. 1980. *Le Bassin Autunien de l'Aumance (Allier, France). Sédimentologie, Charbon, Cinérites. Tectonique Syndiagénétique*. Unpublished Ph. D. thesis, Université de Bourgogne, 277 pp.

Paquette, Y., Doubinger, J. & Courel, L. 1980. Étude palynologique de la couche du toit du bassin autunien de l'Aumance (assise de Buxières): liaison avec les milieux sédimentaires. *Bulletin de la Société d'Histoire Naturelle et des Amis du Musée d'Autun*, 95, 85–101.

Passey, B. H., Robinson, T. F., Ayliffe, L. K., Cerling, T. E., Sponheimer, M., Dearing, M. D., Roeder, B. L. & Ehleringer, J. R. 2005. Carbon isotope fractionation between diet, breath CO_2, and bioapatite in different mammals. *Journal of Archaeological Science*, 32, 1459–1470.

Passey, B. H., Cerling, T. E. & Levin, N. E. 2007. Temperature dependence of oxygen isotope acid fractionation for modern and fossil tooth enamels. *Rapid Communications in Mass Spectrometry*, 21, 2853–2859.

Pasteris, J. D., Wopenka, B. & Valsami-Jones, E. 2008. Bone and tooth mineralization: why apatite? *Elements*, 4, 97–104.

Pauliv, V. E., Martinelli, A. G., Francischini, H., Dentzen-Dias, P., Soares, M., Schultz, C. L. & Ribeiro, A. M. 2017. The first Western Gondwanan species of *Triodus* Jordan 1849: A new Xenacanthiformes (Chondrichthyes) from the late Paleozoic of Southern Brazil. *Journal of South American Earth Sciences*, 80, 482–493.

Paytan, A., Kastner, M., Campbell, D. & Thiemens, M. H. 1998. Sulfur isotopic composition of Cenozoic seawater sulfate. *Science*, 282, 1459–1462.

Paytan, A., Kastner, M., Campbell, D. & Thiemens, M. H. 2004. Seawater sulfur isotope fluctuations in the Cretaceous. *Science*, 304, 1663–1665.

Paytan, A., Yao, W., Faul, K. L. & Gray, E. T. 2020. Application of sulphur isotopes for stratigraphic correlation. *Geologic Time Scale 2020*, 1, 259–278.

Pellenard, P., Gand, G., Schmitz, M., Galtier, J., Broutin, J. & Steyer, J.-S. 2017. High-precision U-Pb zircon ages for explosive volcanism calibrating the NW European continental Autunian stratotype. *Gondwana Research*, 51, 118–136.

Poage, M. A. & Chamberlain, C. P. 2001. Empirical relationships between elevation and the stable isotope composition of precipitation and surface waters: considerations for studies of paleoelevation change. *American Journal of Science*, 301, 1–15.

Poplin, C. 1999. Un paléoniscoïde (Pisces, Actinopterygii) de Buxières-les-Mines, témoin des affinités fauniques entre Massif central et Bohême au passage Carbonifère-Permien. *Geodiversitas*, 21, 147–155.

Poplin, C. & Dutheil, D. B. 2005. Les Aeduellidae (Pisces, Actinopterygii) carbonifères et permiens: systématique et étude phylogénétique préliminaire. *Geodiversitas*, 27, 17–33.

Poplin, C. & Heyler, D. 1989. Évolution et phylogénie des Xenacanthiformes (=Pleuracanthiformes) (Pisces, Chondrichthyes). *Annales de Paléontolgie*, 75, 187–222.

Poplin, C., Sotty, D. & Janvier, P. 2001. Un Myxinoïde (Craniata, Hyperotreti) dans le Konservat-Lagerstätte Carbonifere supérieur de Montceau-les-Mines (Allier, France).

Comptes Rendus de l'Académie des Sciences-Series IIA-Earth and Planetary Science, 332, 345–35.

Pradel, A. 2010. Skull and brain anatomy of Late Carboniferous Sibyrhynchidae (Chondrichthyes, Iniopterygia) from Kansas and Oklahoma (USA). *Geodiversitas*, 32, 595–661.

Pradel, A., Langer, M., Maisey, J. G., Geffard-Kuriyama, D., Cloetens, P., Janvier, P. & Tafforeau, P. 2009. Skull and brain of a 300-million-year-old chimaeroid fish revealed by synchrotron holotomography. *Proceedings of the National Academy of Sciences of the United States of America*, 106, 5224–5228.

Pradel, A., Tafforeau, P. & Janvier, P. 2010. Study of the pectoral girdle and fins of the Late Carboniferous sibyrhynchid iniopterygians (Vertebrata, Chondrichthyes, Iniopterygia) from Kansas and Oklahoma (USA) by means of microtomography, with comments on iniopterygian relationships. *Comptes Rendus Palevol*, 9, 377–387.

Pradel, A., Tafforeau, P., Maisey, J. G. & Janvier, P. 2011. A New Paleozoic Symmoriiformes (Chondrichthyes) from the Late Carboniferous of Kansas (USA) and Cladistic Analysis of Early Chondrichthyans. *PLoS ONE*, 6, e24938.

Pruvost, P. 1919. *Introduction à l'étude Du Terrain Houiller Du Nord et Du Pas-de-Calais: La Faune Continentale Du Terrain Houiller Du Nord de La France Mémoires Pour Servir à l'explication de La Carte Géologique Détaillée de La France*. Imprimerie Nationale, Paris, 439–453 pp.

Pruvost, P. 1930. La faune continentale du terrain houiller de la Belgique. *Mémoires du Musée Royal d'Histoire Naturelle de Belgique*, 44, 133–141.

Pruvost, P. 1942. *Étude Géologique Du Bassin Permo-Carbonifère d'Autun*. BRGM, Orléans-la-Source, 23 pp.

R Core Team. 2020. R: A language and environment for statistical computing. R Foundation for Statistical Computing.

Rafinesque-Schmaltz, C. S. 1810. *Indice d'Ittiologia Siciliana Ossia Catalogo Metodico Dei Nomi Latini Italiani, e Siciliani Dei Pesci, Che Si Rinvengono in Sicilia Disposti Secondo Un Metodo Naturale e Seguito Da Un Appendice Che Contiene La Descrizione Di Alcuni Nuovi Pesci Siciliani Illustrato Da Due Piance*. Giovanni del Nobold. Messina, 70 pp.

Ragonha, E. W. 1984. *Taxionomia de Dentes e Espinhos Isolados de Xenacanthodii (Chondrichthyes, Elasmobranchii) Da Formação Corumbataí: Considerações Cronológicas e Paleoambientais*. Unpublished Ph. D. thesis, Universidade de São Paulo, 166 pp.

Ramos, R. Ø. 2007. *Age and Growth Estimates for the Port Jackson Shark, Heterodontus Portusjacksoni,(Mayer, 1793) from New South Wales, Australia*. Unpublished Ph. D. thesis, University of Newcastle, 222 pp.

Rasband, W. S. 1997-2020. ImageJ. U. S. National Institutes of Health, Bethesda, Maryland, USA.

Rau, G. H., Chavez, F. P. & Friederich, G. E. 2001. Plankton $^{13}C/^{12}C$ variations in Monterey Bay, California: evidence of non-diffusive inorganic carbon uptake by phytoplankton in an upwelling environment. *Deep Sea Research Part I: Oceanographic Research Paper*, 48, 79–94.

Rees, C. E., Jenkins, W. J. & Monster, J. 1978. The sulphur isotopic composition of ocean water sulphate. *Geochimica et Cosmochimica Acta*, 42, 377–381.

Reif, W.-E. 1976. Morphogenesis, Pattern Formation and Function of the Dentition of *Heterodontus* (Selachii). *Zoomorphologie*, 83, 1–47.

Reif, W.-E. 1978. Types of morphogenesis of the dermal skeleton in fossil sharks. *Paläontologische Zeitschrift*, 52, 110–128.

Renault, B. & Zeiller, R. 1888. Sur l'attribution des genres *Fayolia* et *Palaeoxyris*. *Comptes rendus hebdomadaires des séances de l'Académie des sciences*, 107, 1022–1025.

Rey, K., Amiot, R., Fourel, F., Abdala, F., Day, M. O., Fernandez, V., Fluteau, F., France-Lanord, C., Rubidge, B. S., Smith, R. N., Viglietti, P. A., Zipfel, F. & Lécuyer, C. 2016. Global climate perturbations during the Permo-Triassic mass extinctions recorded by continental tetrapods from South Africa. *Gondwana Research*, 37, 384–396.

Richter, M. 2005. A new xenacanthid shark (Chondrichthyes) from the Teresina Formation, Permian of the Paraná Basin, southern Brazil. *Revista Brasileira de Paleontologia*, 8, 149–158.

Rink, W. J. & Schwarcz, H. P. 1995. Tests for diagenesis in tooth enamel: ESR dating signals and carbonate contents. *Journal of Archaeological Science*, 22, 251–255.

Roche, E. 1881. Sur les fossiles du terrain permien d'Autun (Saône-et-Loire). *Bulletin de la Société Géologique de France*, 3, 78–83.

Romer, A.-S. 1964. The braincase of the Paleozoic elasmobranch *Tamiobatis*. *Bulletin of the Museum of Comparative Zoology*, 131, 87–105.

Röntgen, W. K. 1896. A New Form of Radiation. *Science*, 3, 726–729.

Roscher, M. & Schneider, J. W. 2006. Permo-Carboniferous climate: Early Pennsylvanian to Late Permian climate development of central Europe in a regional and global context. *Geological Society, London, Special Publications*, 265, 95–136.

Rosell, R. S. & MacOscar, K. C. 2002. Movements of pike, *Esox lucius*, in Lower Lough Erne, determined by mark-recapture between 1994 and 2000. *Fisheries Management and Ecology*, 9, 189–196.

Rowe, T., Carlson, W. & Bottorff, W. W. 1992. *Thrinaxodon: Digital Atlas of the Skull, a Compact Disc*. University of Texas Press, Austin pp.

Royer, A., Lécuyer, C., Montuire, S., Amiot, R., Legendre, S., Cuenca-Bescós, G., Jeannet, M. & Martineau, F. 2013. What does the oxygen isotope composition of rodent teeth record? *Earth and Planetary Science Letters*, 361, 258–271.

Rozanski, K., Araguas-Araguas, L. & Gonfiantini, R. 1993. Isotopic Patterns in Modern Global Precipitation. *Climate change in continental isotopic records*, 78, 1–36.

Saito, K. 2004. Sulfur assimilatory metabolism. The long and smelling road. *Plant Physiology*, 136, 2443–2450.

Saltzman, M. R., Thomas, E., Gradstein, F. M. & Ogg, J. G. 2012. Carbon isotope stratigraphy. *The Geologic Time Scale*, 1, 207–232.

Salzburger, W., Van Bocxlaer, B. & Cohen, A. S. 2014. Ecology and evolution of the African Great Lakes and their faunas. *Annual Review of Ecology, Evolution, and Systematics*, 45, 519–545.

Sand-Jensen, J., Revsbech, N. P. & Barker Jörgensen, B. 1985. Microprofiles of oxygen in epiphyte communities on submerged macrophytes. *Marine Biology*, 89, 55–62.

Sasagawa, I., Ishiyama, M., Yokosuka, H. & Mikami, M. 2013. Teeth and ganoid scales in *Polypterus* and *Lepisosteus*, the basic actinopterygian fish: an approach to understand the origin of the tooth enamel. *Journal of Oral Biosciences*, 55, 76–84.

Sauvage, H. É. 1893. *Bassin Houiller et Permien d'Autun et d'Épinac: Poissons Fossiles. Fascicule V*. Imprimerie Nationale, Paris, 34 pp.

Schaeffer, B. 1981. The xenacanth shark neurocranium, with comments on elasmobranch monophyly. *Bulletin of the American Museum of Natural History*, 169, 1–66.

Schindler, T. & Hampe, O. 1996. Eine erste Fischfauna (Chondrichthyes, Acanthodii, Osteichthyes) aus dem Permokarbon Niederösterreichs (Zöbing, NE Krems) mit paläoökologischen und biostratigraphischen Anmerkungen. *Beiträge zur Paläontologie*, 21, 93–103.

Schneider, J. W. 1985. Elasmobranchier-Zahntypen (Pisces, Chondrichthyes) und ihre stratigraphische Verbreitung im Karbon und Perm der Saale-Senke (DDR). *Freiberger Forschungshefte*, C400, 90–100.

Schneider, J. W. 1988. Grundlagen der Morphogenie, Taxonomie und Biostratigraphie isolierter Xenacanthodier-ZaÈ hne (Elasmobranchii). *Freiberger Forschungshefte*, C419, 71–80.

Schneider, J. W. 1996. Xenacanth teeth - a key for taxonomy and biostratigraphy. *Modern Geology*, 20, 321–340.

Schneider, J. W. & Werneburg, R. 2006. Insect biostratigraphy of the Euramerican continental late Pennsylvanian and early Permian. *Geological Society, London, Special Publications*, 265, 325–336.

Schneider, J. W. & Zajíc, J. 1994. Xenacanthiden (Pisces, Chondrichtyes) des mitteleuropäischen Oberkarbon und Perm. *Freiberger Forschungshefte*, C452, 101–151.

Schneider, J. W., Hampe, O. & Soler-Gijón, R. 2000. The Late Carboniferous and Permian: Aquatic vertebrate zonation in southern Spain and German basins. *Courier-Forschungsinstitut Senckenberg*, 223, 543–561.

Schoch, R. R. 1992. Comparative ontogeny of Early Permian brachiosaurid amphibians from southwestern Germany. Developmental stages. *Palaeontographica. Abteilung A, Paläozoologie, Stratigraphie*, 222, 43–83.

Schoeller, D. A., Leitch, C. A. & Brown, C. H. R. I. 1986. Doubly labeled water method: in vivo oxygen and hydrogen isotope fractionation. *American Journal of Physiology-Regulatory, Integrative and Comparative Physiology*, 251, 1137–1143.

Schultze, H.-P. 1985. Marine to onshore vertebrates in the Lower Permian of Kansas and their paleoenvironmental implications. *University of Kansas Paleontological Contributions*, 113, 1–18.

Schultze, H.-P. 1995. Terrestrial biota in coastal marine deposits: Fossil-lagerstätten in the Pennsylvanian of Kansas, USA. *Palaeogeography, Palaeoclimatology, Palaeoecology*, 119, 255–273.

Schultze, H.-P. 1998. The Fossil Record of the Intertidal Zone. *In*: *Intertidal Fishes. Life in Two Worlds*. Academic Press, San Diego, 373–392.

Schultze, H.-P. 2009. Interpretation of marine and freshwater paleoenvironments in Permo–Carboniferous deposits. *Palaeogeography, Palaeoclimatology, Palaeoecology*, 281, 126–136.

Schultze, H.-P. 2013. The palaeoenvironments at the transition from piscine to tetrapod sarcopterygians. *New Mexico Museum of Natural History and Science Bulletin*, 60, 373–397.

Schultze, H.-P. 2018. Hard tissues in fish evolution: history and current issues. *Cybium*, 42, 29–39.

Schultze, H.-P. & Soler-Gijón, R. 2004. A xenacanth clasper from the ?uppermost Carboniferous - Lower Permian of Buxières-ls-Mines (Massif Central, France) and the palaeoecology of the European Permo-Carboniferous basins. *Neues Jahrbuch für Geologie und Paläontologie Abhandlungen*, 232, 325–363.

Schwind, C. 1991. *Zur Organisation Und Zur Phylogenie Der Beiden Gattungen* Triodus *Und* Xenacanthus. Unpublished Ph. D. thesis, University of Mainz, 201 pp.

Scotese, C. R. 2002. 3D paleogeographic and plate tectonic reconstructions: The PALEOMAP Project is back in town. http://www.scotese.com/

Scotese, C. R., Boucot, A. G. & McKerrow, W. S. 1999. Gondwanan palaeogeography and palaeoclimatology. *Journal of African Earth Sciences*, 28, 99–114.

Séon, N., Amiot, R., Martin, J. E., Young, M. T., Middleton, H., Fourel, F., Picot, L., Valentin, X. & Lécuyer, C. 2020. Thermophysiologies of Jurassic marine crocodylomorphs inferred from the oxygen isotope composition of their tooth apatite. *Proceedings of the Royal Society B: Biological Sciences*, 375, 20190139.

Shackleton, N. J. 1975. Paleotemperature history of the Cenozoic and the initiation of Antarctic glaciation: oxygen and carbon isotope analyses in DSDP sites 277, 279 and 281. *Initial Reports of the DSDP*, 29, 743–755.

Sharp, Z. 2007. *Principles of Stable Isotope Geochemistry*. Pearson education, Upper Saddle River, 359 pp.

Sillen, A. & Lee-Thorp, J. A. 1994. Trace element and isotopic aspects of predator-prey relationships in terrestrial foodwebs. *Palaeogeography, Palaeoclimatology, Palaeoecology*, 107, 243–255.

Simenstad, C. A. & Wissmar, R. C. 1985. $\delta^{13}C$ evidence of the origins and fates of organic carbon in estuarine and nearshore food webs. *Marine Ecology Progress Series*, 22, 141–152.

Sire, J. Y. 1994. Light and TEM study of nonregenerated and experimentally regenerated scales of *Lepisosteus oculatus* (Holostei) with particular attention to ganoine formation. *The Anatomical Record,* 240, 189–207.

Sire, J. Y., Géraudie, J., Meunier, F. J. & Zylberberg, L. 1986. Participation des cellules épidermiques à la formation de la ganoïne au cours de la régénération expérimentale des écailles de *Calamoichthys calabaricus* (Smith, 1886) (Polypteridae, Osteichthyeus). *Comptes rendus de l'Académie des sciences. Série 3, Sciences de la vie*, 303, 625–628.

Sire, J. Y., Géraudie, J., Meunter, F. J. & Zylberberg, L. 1987. On the origin of ganoine: Histological and ultrastructural data on the experimental regeneration of the scales of *Calamolchthys calabaricus* (osteichthyes, brachyopterygii, polypteridae). *American Journal of Anatomy*, 180, 391–402.

Soler-Gijón, R. 1993a. *Estudios de Los Vertebrados Fósiles Del Carbonifero Superior de Puertollano, Ciudad Real*. Unpublished Ph. D. thesis, Unoversidad Complutense de Madrid, 293 pp.

Soler-Gijón, R. 1993b. The xenacanth sharks from the Upper Stephanian of the Puertollano basin (Spain). *Journal of Vertebrate Paleontology*, 13, 58A.

Soler-Gijón, R. 1994. Los Vertebrados de la cuenca carbonifera de Puertollano. *Communicaciones de las X Jornadas de Paleontologia*, Excursión A, 212–220.

Soler-Gijón, R. 1995. Evidence of predator-prey relationship in xenacanth sharks of the Upper Carboniferous (Stephanian C) from Puertollano, Spain. *Geobios*, 28, 151–156.

Soler-Gijón, R. 1997a. New discoveries of xenncanth sharks from the Late Carboniferous of Spain (Puertollano Basin) and Early Permian of Germany (Saar-Nahe Basin): Implications for the phylogeny of xenacanthiform and anacanthous sharks. *Neues Jahrbuch für Geologie und Paläontologie Abhandlungen*, 205, 1–31.

Soler-Gijón, R. 1997b. *Orthacanthus meridianalis*, a new xenacanth shark (Elasmobranchii) from the Upper Carboniferous of the Puertollano basin, Spain. *Neues Jahrbuch für Geologie und Paläontologie Abhandlungen*, 204, 141–169.

Soler-Gijón, R. 1999. Occipital Spine of *Orthacanthus* (Xenacanthidae, Elasmobranchii): Structure and Growth. *Journal of Morphology*, 242, 1–45.

Soler-Gijón, R. 2000. Phylogenetic relationships of Lebachacanthidae Soler-Gijón 1997 (Xenacanthiformes; Elasmobranchii). *Paläontologische Zeitschrift*, 74, 363–377.

Soler-Gijón, R. 2004. Development and growth in xenacanth sharks: new data from Upper Carboniferous of Bohemia. *In*: *Recent Advances in the Origin and Early Radiation of Vertebrates*. Verlag Dr. Friedrich Pfeil, München, Germany, 533–562.

Soler-Gijón, R. & Hampe, O. 1998. Evidence of *Triodus* JORDAN 1849 (Elasmobranchii: Xenacanthidae) in the Lower Permian of the Autun basin (Muse, France). *Neues Jahrbuch für Geologie und Paläontologie-Monatshefte*, 1998, 335–348.

Soler-Gijón, R. & Moratalla, J. J. 2001. Fish and tetrapod trace fossils from the Upper Carboniferous of Puertollano, Spain. *Palaeogeography, Palaeoclimatology, Palaeoecology*, 171, 1–28.

Štamberg, S. 1998. Preliminary results of the study of Permian actinopterygian fishes from Buxières-les-Mines (Allier, France). *Acta Musei Reginaehradecensis S. A. Scientiae Naturales*, 26, 173–178.

Štamberg, S. 2018. Actinopterygians of The Permian Locality Buxières-Les-Mines (Bourbonl'archambault Basin, France) and Their Relationship to Other Early Actinopterygians. *Fossil Imprint*, 74, 245–291.

Štamberg, S. & Steyer, J.-S. 2021. New actinopterygians from the Permian of the Brive Basin, and the ichthyofaunas of the French Massif Central. *Fossil Imprint*, 77, 145–165.

Štamberg, S., Schneider, J. W. & Werneburg, R. 2016. Fossil fauna and flora of a re-discovered locality in the Late Carboniferous Ploužnice Horizon of the Krkonoše Piedmont Basin, Bohemian Massif. *Fossil Imprint*, 72, 215–224.

Stanton, K. J. 2006. *Stable Oxygen and Carbon Isotope Analyses of Extinct Archosaurs (Dinosauria) and Their Closest Extant Relatives, Ratite Birds and Crocodylians*. Unpublished Ph. D. thesis, University of California, 164 pp.

Stensiö, E. A. 1927. The Devonian and Downtonian vertebrates of Spitsbergen. 1. Family Cephalaspidae. *Skrifier om Svalbard og Ishavet*, 12, 1–391.

Steyer, J.-S. 2000. Are European Paleozoic amphibians good stratigraphic markers?. *Bulletin de la Société Géologique de France*, 171, 127–135.

Steyer, J.-S. 2002. The first articulated trematosaur 'amphibian'from the Lower Triassic of Madagascar: implications for the phylogeny of the group. *Palaeontology*, 45, 771–793.

Steyer, J.-S. 2014. The salt of life: euryhalinity and halotolerance in Temnospondyls. *Journal of Vertebrate Paleontology*, 74, 235A.

Steyer, J.-S. & Escuillié, F. 1997. Le chantier de fouilles paléontologiques dans le permien inférieur de Buxières-les-Mines (Allier, France) en août 1996 : Compte rendu préliminaire et perspectives. *Revue Scientifique Bourbonnais*, 95, 11–18.

Steyer, J.-S., Gand, G. & Pouillon, J. M. 1997. Les amphibiens du Paléozoïques et du Trias français : historique et inventaire. *Bulletin de la Société d'Histoire Naturelle et des Amis du Musée d'Autun*, 162, 23–40.

Steyer, J.-S., Escuillié, F., Pouillon, J.-M., Broutin, J., Debriette, P., Freytet, P., Gand, G., Poplin, C., Rage, J.-C., Rival, J., Schneider, J. W., Štamberg, S., Werneburg, R. & Cuny, G. 2000. New data on the flora and fauna from the ?uppermost Carboniferous-Lower Permian of Buxières-les-Mines, Bourbon-l'Archambault Basin (Allier, France). preliminary report. *Bulletin de la Société Géologique de France*, 171, 239–249.

Steyer, J.-S., Laurin, M., Castanet, J. & De Ricqlès, A. 2004. First histological and skeletochronological data on temnospondyl growth: palaeoecological and palaeoclimatological implications. *Palaeogeography, Palaeoclimatology, Palaeoecology*, 206, 193–201.

Steyer, J.-S., Sanchez, S., Debriette, P., Valli, A. M. F., Escuillié, F., Pohl, B., Dechambre, R.-P., Vacant, R., Spence, C. & de Ploeg, G. 2012. A new vertebrate Lagerstätte from the Lower Permian of France (Franchesse, Massif Central): palaeoenvironmental implications for the Bourbon-l'Archambault basin. *Bulletin de la Société Géologique de France*, 183, 509–515.

Stock, T. 1880. On a spine (*Lophacanthus Taylori*, mihi, nov. gen. et spec.) from the Coal-Measures of Northumberland. *The Annals and Magazine of Natural History*, 5, 20–217.

Strauss, H. 1993. The sulfur isotopic record of Precambrian sulfates: new data and a critical evaluation of the existing record. *Precambrian research*, 63, 225–246.

Street-Perrott, F. A. & Harrison, S. P. 1984. Temporal variations in lake levels since 30,000 yr BP—an index of the global hydrological cycle. *Climate processes and climate sensitivity*, 29, 118–129.

Sur, S., Owens, J. D., Soreghan, G. S., Lyons, T. W., Raiswell, R., Heavens, N. G. & Mahowald, N. M. 2015. Extreme eolian delivery of reactive iron to late Paleozoic icehouse seas. *Geology*, 43, 1099–1102.

Sweet, W. C. & Donoghue, P. J. 2001. Conodonts: past, present, future. *Journal of Paleontology*, 75, 1174–1184.

Swofford, D. L. 2003. PAUP*. Phylogenetic analysis using parsimony (* and other methods). Sinauer Associates, Sunderland.

Tabor, N. J. & Poulsen, C. J. 2008. Palaeoclimate across the Late Pennsylvanian–Early Permian tropical palaeolatitudes: a review of climate indicators, their distribution, and relation to palaeophysiographic climate factors. *Palaeogeography, Palaeoclimatology, Palaeoecology*, 268, 293–310.

Tcherkez, G. & Tea, I. 2013. $^{32}S/^{34}S$ isotope fractionation in plant sulphur metabolism. *New Phytologist*, 200, 44–53.

Tedesco, P. A., Oberdorff, T., Cornu, J. F., Beauchard, O., Brosse, S., Dürr, H. H., Grenouillet, G., Leprieur, F., Tisseuil, C., Zaiss, R. & Hugueny, B. 2013. A scenario for impacts of water availability loss due to climate change on riverine fish extinction rates. *Journal of Applied Ecology*, 50, 1105–1115.

Tieszen, L. L. & Fagre, T. 1993. Effect of Diet Quality and Composition on the Isotopic Composition of Respiratory CO_2, Bone Collagen, Bioapatite, and Soft Tissues. *In*: *Prehistoric Human Bone*. Springer, Berlin, Heidelberg, 121–155.

Touchard, L. 2000. *Les Lacs, Origine et Morphologie*. L'Harmattan, Paris, 210 pp.

Tovar-Ávila, J., Izzo, C., Walker, T. I., Braccini, J. M. & Day, R. W. 2008. Dorsal-fin spine growth of *Heterodontus portusjacksoni*: a general model that applies to dorsal-fin spines of chondrichthyans? *Canadian Journal of Fisheries and Aquatic Sciences*, 65, 74–82.

Tovar-Ávila, J., Troynikov, V. S., Walker, T. I. & Day, R. W. 2009. Use of stochastic models to estimate the growth of the Port Jackson shark, *Heterodontus portusjacksoni*, off eastern Victoria, Australia. *Fishries Research*, 95, 230–235.

Traquair, R. H. 1881. Notice of new fish remainsfrom the Blackband Ironstone of Borough Lee near Edinburgh. *Geological Magazine Decade II*, 8, 7–34.

Traquair, R. H. 1882. Notice of new fish remains from the Blackband Ironstone of Borough Lee, near Edinburgh. No. III. *Geological Magazine Decade II*, 9, 6–540.

Traquair, R. H. 1888. Further notes on Carboniferous Selachii. *Proceedings of the Royal Physical Society of Edinburgh*, 9, 421–426.

Traquair, R. H. 1903. On the distribution of fossil fish-remains in the Carboniferous rocks of the Edinburgh district. *Transactions of the Royal Society of Edinburgh: Earth Sciences*, 40, 687–707.

Trust, B. A. & Fry, B. 1992. Stable sulphur isotopes in plants: a review. *Plant, Cell & Environment*, 15, 1105–1110.

Turner, S. 1982. Middle Palaeozoic elasmobranch remains from Australia. *Journal of Vertebrate Paleontology*, 2, 117–137.

Turner, S. & Burrow, C. J. 2011. A Lower Carboniferous xenacanthiform shark from Australia. *Journal of Vertebrate Paleontology*, 31, 241–257.

UNEP. 1990. GEMS/Water data summary 1985–1987. Burlington, Ontario, Canada Centre for Inland Waters; United Nations Environment Programme, Global Environment Monitoring System, GEMS/Water Programme Office.

Urey, H. C. 1947. The thermodynamic properties of isotopic substances. *Journal of the Chemical Society (Resumed)*, 562–581.

Van Waveren, I., Gand, G., Steyer, J. S., Barbier, J., Auseaume, L., Hervet, S. & Chabard, D. 2012. Inventaire de la paléoflore découverte dans la partie supérieure de la formation de Muse au cours des fouilles paléontologiques de 2011. *Bulletin de la Société d'Histoire Naturelle et des Amis du Musée d'Autun*, 44–52.

Veevers, J. J. 1994. Case for the Gamburtsev Subglacial Mountains of East Antarctica originating by mid-Carboniferous shortening of an intracratonic basin. *Geology*, 22, 593–596.

Veizer, J. & Prokoph, A. 2015. Temperatures and oxygen isotopic composition of Phanerozoic oceans. *Earth-Science Reviews*, 146, 92–104.

Vennemann, T. W., Hegner, E., Cliff, G. & Benz, G. W. 2001. Isotopic composition of recent shark teeth as a proxy for environmental conditions. *Geochimica et Cosmochimica Acta*, 65, 1583–1599.

Voigt, S., Schindler, T., Thum, H. & Fischer, J. 2019. Field trip C2: Pennsylvanian-Permian of the Saar-Nahe Basin, SW Germany. *In*: *Proceedings of the 19th International Congress on the Carboniferous and Permian*. Kölner Forum für Geologie und Paläontologie, Cologne, 217–250.

von Grafenstein, U. V., Erlenkeuser, H., Müller, J., Trimborn, P. & Alefs, J. 1996. A 200 year mid-European air temperature record preserved in lake sediments: An extension of the $\delta^{18}O_p$-air temperature relation into the past. *Geochimica et Cosmochimica Acta*, 60, 4025–4036.

Walsh, J. H. & Ebert, D. A. 2007. A review of the systematics of western North Pacific angel sharks, genus *Squatina*, with redescriptions of *Squatina formosa*, *S. japonica*, and *S. nebulosa* (Chondrichthyes: Squatiniformes, Squatinidae). *Zootaxa*, 1551, 31–47.

Ward, J. 1890. The geological features of the North Staffordshire Coal Fields, their organic remains, their range and distribution; with a catalogue of the fossils of the Carboniferous system of North Staffordshire. *Transactions of the North Staffordshire Institute of Mining and Mechanical Engineers*, 10, 1–189.

Wass, R. C. 1973. Size, growth, and reproduction of the sandbar shark, *Carcharhinus milberti*, in Hawaii. *Pacific Science*, 27, 305–318.

Wenzel, B., Lécuyer, C. & Joachimski, M. M. 2008. Comparing oxygen isotope records of Silurian calcite and phosphate—$\delta^{18}O$ compositions of brachiopods and conodonts. *Geochimica et Cosmochimica Acta*, 64, 1859–1872.

Werneburg, R. 1997. Der Eryopide *Onchiodon* (Amphibia) aus dem Rotliegend des Beckens von Autun (Frankreich). *Freiberger Forschungshefte*, C466, 167–181.

Werneburg, R. & Steyer, J.-S. 1999. Redescription of the holotype of *Actinodon frossardi* (Amphibia, Temnospondyli) from the Lower Permian of the Autun Basin (France). *Geobios*, 32, 599–607.

Wetzel, R. 1983. *Limnology*. Saunders College Publication, Philadelphia, 767 pp.

Williams, M. E. 1985. The 'Cladodont level' sharks of the Pennsylvanian black shales of central North America. *Palaeontographica A*, 190, 83–158.

Williams, M. E. 1998. A new specimen of *Tamiobatis vetustus* (Chondrichthyes, Ctenacanthoidea) from the late Devonian Cleveland Shale of Ohio. *Journal of Vertebrate Paleontology*, 18, 251–260.

Wils, P. 2020. Analyses non destructives par tomographie à rayons X. *Les nouvelles de l'archéologie*, 159, 13–19.

Wilson, J. P., Montañez, I. P., White, J. D., DiMichele, W. A., McElwain, J. C., Poulsen, C. J. & Hren, M. T. 2017. Dynamic Carboniferous tropical forests: new views of plant function and potential for physiological forcing of climate. *New Phytologist*, 215, 1333–1353.

Wong, W. W., Cochran, W. J., Klish, W. J., Smith, E. O., Lee, L. S. & Klein, P. D. 1988. In vivo isotope-fractionation factors and the measurement of deuterium-and oxygen-18-dilution spaces from plasma, urine, saliva, respiratory water vapor, and carbon dioxide. *The American journal of clinical nutrition*, 47, 1–6.

Woodward, A. S. 1889. Palaeichthyological notes. 2. On *Diplodus Moorei*, sp. nov., from the Keuper of Somersetshire. *The Annals and Magazine of Natural History*, 3, 297–302.

Woodward, A. S. 1891. Dr. Anton Fritsch on Palaeozoic elasmobranch fishes. *Geological Magazine8*, 3, 78–375.

Woodward, A. S. 1892. On the Lower Devonian fish-fauna of Campbellton, New Brunswick. *Geological Magazine*, 16, 1–6.

Woodward, A. S. & Sherborn, C. D. 1890. *A Catalogue of British Fossil Vertebrata*. Dulau & Co, London, 396 pp.

Würdig-Maciel, N. L. 1975. Ichtiodontes e Ichtiodorulitos (Pisces) da Formação Estrada Nova e Sua Aplicação na Estratigrafia do Grupo Passa Dois. *Pesquisas em Geociências*, 5, 7–166.

Young, G. C. 1982. Devonian sharks from South-Eastern Australia and Antarctica. *Palaeontology*, 25, 817–843.

Zajíc, J. 1985. New finds of acanthodians (Acanthodii) from the Kounov Member (Stephanian B, central Bohemia). *Věstník Ústředního ústavu geologického*, 60, 277–284.

Zajíc, J. 1998. Acanthodians of the Bohemian limnic Stephanian. *Czech Geological Survey Special Papers*, 10, 1–45.

Zangerl, R. 1981. *Handbook of Paleoichthyology - Chondrichthyes I - Paleozoic Elasmobranchii*. Schultze, H.-P. & Kuhn, O. Gustav Fischer Verlag, Stuttgart, 115 pp.

Zazzo, A., Lécuyer, C., Sheppard, S. M., Grandjean, P. & Mariotti, A. 2004. Diagenesis and the reconstruction of paleoenvironments: a method to restore original $\delta^{18}O$ values of carbonate and phosphate from fossil tooth enamel. *Geochimica et Cosmochimica Acta*, 68, 2245–2258.

Zheng, H. & Wang, X. 2010. Telemetric Data Reveals Ecologically Adaptive Behavior of Captive Raised Chinese Giant Salamanders When Reintroduced into Their Native Habitat. *Asian Herpetological Research*, 1, 31–35.

Zhu, M., Yu, X., Ahlberg, P. E., Choo, B., Lu, J., Qiao, Q., Zhao, L. J., Blom, H. & Zhu, Y. A. 2013. Silurian placoderm with osteichthyan-like marginal jaw bones. *Nature*, 502, 188–193.

Zidek, J. 1992. Late Pennsylvanian Chondrichthyes, Acanthodii, and deep-bodied Actinopterygii from the Kinney Quarry, Manzanita Mountains, New Mexico. *New Mexico Bureau of Mines and Mineral Resources Bulletin*, 138, 145–182.

Zidek, J. 1993. Xenacanthid genera: How many and how to tell them apart? *In*: *New Reseach on Permo-Carboniferous Faunas*. Pollichia-Buch, Bad Dürkheim, 23–35.

Zidek, J., Johnson, G. D., May, W. & Claborn, A. 2003. New specimens of xenacanth and hybodont sharks from the Lower Permian of Southwestern Oklahoma. *Oklahoma Geology Notes*, 63, 136–147.

Ziegler, M. 1996. Permian world topography and climate. *Late glacial and postgracial environmental changes-Quaternary, Carboniferous-Permian and Proterozoic*, 1–37.

Zoehfeld, K. W., Mossbrucker, M. T., Bakker, R. T. & Fils, C. J. 2014. *Dimetrodon* feeding on sharks and sharks feeding on *Dimetrodon*: Texas Early Permian food webs based on aquatic predation. *In*: 2014 GSA Annual Meeting. Geological Society of America Abstract with Programs, Vancouver, 332.